DOCTORAL THESIS

VALORISATION OF RICE STRAW BY OBTAINING ACTIVE COMPOUNDS AND CELLULOSIC MATERIALS FOR THE DEVELOPMENT OF BIODEGRADABLE FOOD PACKAGING SYSTEMS

UNIVERSITAT POLITÈCNICA DE VALÈNCIA

Instituto Universitario de Ingeniería de Alimentos para el Desarrollo

Pedro Augusto Vieira de Freitas

Supervisors:

Amparo Chiralt Boix
Chelo González-Martínez

Valencia, November 2022

A mi madre Maria do Carmo,
a mis hermanos Flávia y Phillipe
y a mi sobrina Helena

ACKNOWLEDGEMENTS

Profesora **Amparo Chiralt**, gracias por haberme dado la oportunidad de formar parte de este grupo de investigación tan reconocido. Gracias sobre todo por compartir tantos conocimientos y demostrarme que cuando se hace algo con dedicación, paciencia y pasión, los obstáculos se convierten en el camino. Gracias, Profesora **Chelo**, por todo apoyo, dedicación y confianza que me brindaste en todo momento. Tu inteligencia, paciencia, claridad y alegría fueron determinantes durante esta etapa.

Gracias al **Gobierno español** y a la **Agencia Estatal de Investigación** por la inversión y financiación de proyectos de investigación concedidos al laboratorio. Gracias también a la **Generalitat Valenciana** por el contrato predoctoral Santiago Grisolía.

Gracias, **Carol**, por todas las palabras, consejos, amistad y gran ayuda a lo largo de mi trayectoria investigadora en el laboratorio. Gracias a mis compañeros de laboratorio **Eva H.**, **Ramón**, **Johana**, **Eva M.** y **Marta** por todos los momentos que hemos compartido en el laboratorio. Gracias, **Nuria**, **Julián**, **Laia**, **Silvia**, **María**, **Paula**, **Laura**, **Clara**, **Héctor** y **Pere**, por la oportunidad de trabajar/orientar vuestro trabajo de fin de grado o de máster y por haber aprendido mucho con y de vosotros.

La distancia y las dificultades no son nada para quienes están siempre juntos. Gracias, mis hermanos, **Flávia** y **Phillipe**, por el apoyo, las oraciones y todos los momentos que hemos vividos. Vuestras victorias serán siempre las mías. **Helena**, aunque seas tan pequeña, eres mi fuerza y mi inspiración cada día; algún día te enterarás de todo el bien que nos ha hecho tu llegada. Gracias mis abuelos, **Isabel** y **Benedito**, por el ejemplo de vida y protección; sois lo que un día deseo llegar a ser. **Madre**, eres la razón de lo que soy, de lo que hago y de lo que aún deseo hacer. Gracias por toda valentía, dedicación, amor, cuidado y lo que pasaste por nosotros tres; somos muy afortunados de poder compartir esta vida contigo.

“Desde que me cansé de buscar, aprendí a encontrar. Desde que un viento se me opuso, navego con todos los vientos.”. (*Friedrich Nietzsche).*

ABSTRACT

Different approaches are needed to minimise the environmental problem of plastics, including the use of biodegradable materials for food packaging, due to the large contribution of single-use packaging to the consumption of plastics. Due to their compatibility for food contact, poly (lactic acid) (PLA) and starch are bio-based and biodegradable polymers with great potential in this field. However, the properties of these biopolymers need to be improved to meet food packaging requirements while adding value to these materials would offset their higher cost in the plastics market. On the other hand, lignocellulosic agricultural residues, such as rice straw (RS), could be valorised into cellulosic fractions and active extracts which can be used to improve the performance of biodegradable packaging materials, thus also contributing to the circular economy.

This Doctoral thesis focused on obtaining cellulosic fractions and bioactive extracts from RS by applying different extraction and purification techniques, using water as a green solvent. These fractions were incorporated into starch and PLA-based films, as well as into starch-PLA bilayers, to obtain active packaging materials useful for extending the shelf life of different food matrices.

The combined ultrasound-reflux heating method (USHT) and subcritical water extraction (SWE) (at 160 °C, 7 bars (SWE-160) and 180 °C, 11 bars (SWE-180)) were highly effective at obtaining active aqueous extracts from rice straw. The extracts exhibited high phenolic content (37, 51, 83 mg GAE.g^{-1} dry extract, respectively) and antioxidant activity (6.3, 2.0, and 1.2 mg dry extract.mg^{-1} DPPH, respectively). The SWE extracts showed antibacterial activity against *L. innocua* (MIC_{SWE160}: 50; MIC_{SWE180}: 30 mg dry extract.mL^{-1}) and *E. coli* (MIC_{SWE180}: 182 mg dry extract.mL^{-1}). Cellulose fibres (CF) were isolated from the extraction insoluble fractions and compared with those obtained from the traditional alkaline method. Despite slight differences in the degree of purification, the new methods gave rise to CFs with higher yields than the alkaline method (35-39 % *vs.* 29 %), with similar crystallinity (60-69 %), thermal behaviour, and aspect ratios (20-60).

CFs obtained by USHT and alkaline methods were incorporated into methylcellulose/ gum Arabic blend films and exhibited similar reinforcing behaviour, increasing the films' resistance to break and stiffness. Likewise, USHT fibres were also incorporated at 1, 3, and 5 % wt. into corn starch, and corn starch-modified by heat treatment, obtained by melt blending and compression moulding. The incorporation of CF at 3 % gave rise to films more resistant to break (~100 %), stiffer (~215 %), less extensible (~53 %), and with improved oxygen (~30 %) and water vapour (~15 %) barrier capacity. When active extracts were incorporated at different ratios (4, 6, and 8 % wt.) into the starch matrix, with or without CF (3 %), the films were more stretchable and less resistant, but with higher oxygen barrier capacity. Likewise,

mono-dose bags of these active and reinforced films effectively reduced the oxidation of packed sunflower oil.

Active, PEG1000-plasticised PLA films were produced, incorporating different ratios (2, 4, and 6 % wt.) of the USHT extract, by melt blending and compression moulding. The presence of extract coloured the films and slightly reduced their resistance to break, stretchability, water vapour barrier capacity and thermostability, but enhanced their oxygen barrier capacity. The release kinetics of the incorporated antioxidant compounds in food simulants of different polarity (A: aqueous products; and D1: oil-in-water systems) showed that films containing 6 % of extract, delivered similar antioxidant capacity regardless of the food simulant polarity.

Biodegradable bilayers were obtained by laminating PEG1000-plasticised PLA, with and without USHT extract (6 %), and thermoplastic starch sheets, with or without USHT CFs (3 %). The bilayers exhibited improved overall barrier capacity to oxygen and water vapour with respect to the monolayers. However, the interlayer compound migration led to less stiff and resistant films with respect to that expected from the PLA film contribution. Likewise, the active and reinforced bilayers were able to inhibit the oxidation, bacterial growth, and colour changes of the packed pork meat during cold storage.

In order to compare the bioactive properties of the different extracts (USHT, SWE-160, and SWE-180) when incorporated into polymer matrices, PLA films with 6 % wt. of each extract were produced, by melt blending and compression moulding. All extracts weakened the PLA matrix, decreasing its tensile strength (~15-18 %) and stretchability (~32-36 %) and its water vapour barrier capacity (~30 %). Nonetheless, the films exhibited improved oxygen barrier capacity (~16-25 %) and an intense UV light-blocking effect. Furthermore, the active PLA films, especially those with SWE-180 extract, extended the shelf life of packed pork meat since the legal limits of microbial count and oxidation were not reached in the 16 days of cold storage.

The CFs obtained with the different purification methods were also used to produce cellulose aerogels, superabsorbent biodegradable materials with potential applications in different fields. The differences in the chemical composition of the CFs affected the microstructure of aerogels. Specifically, the SWE-180 CF, with the lowest hemicellulose content and high silica ratio, gave rise to a less cohesive matrix, with lower porosity. The water absorption and retention capacity of the aerogels were within the previously reported ranges for this type of material.

Thus, it was possible to obtain valorised fractions of rice straw, active extracts and cellulosic fibres, useful in the development of active biodegradable materials based on starch and PLA. Further studies are needed to validate the food safety of the materials, as well as for developing other applications in the food or pharmaceutical industry.

RESUMEN

Para minimizar el problema medioambiental que suponen los plásticos son necesarios diferentes enfoques y, entre ellos, está el uso de materiales biodegradables para el envasado de alimentos, debido a la gran contribución de los envases de un solo uso al consumo de plásticos. Debido a su compatibilidad para el contacto con los alimentos, el poli (ácido láctico) (PLA) y el almidón son polímeros de base biológica y biodegradables con gran potencial en este campo. No obstante, es necesario mejorar las propiedades de estos biopolímeros para cumplir con los requisitos de envasado alimentario, a la vez que la incorporación de valor añadido a estos materiales permitiría compensar su mayor coste en el mercado del plástico. Por otro lado, los residuos agrícolas lignocelulósicos, como la paja de arroz (RS), podrían ser valorizados en fracciones celulósicas y extractos activos que pueden ser utilizados para mejorar el rendimiento de los materiales de envasado biodegradables, contribuyendo así también a la economía circular.

Esta tesis doctoral se centró en la obtención de fracciones celulósicas y extractos bioactivos de paja de arroz mediante la aplicación de diferentes técnicas de extracción y purificación, utilizando agua como disolvente. Estas fracciones se incorporaron a películas basadas en almidón y PLA, así como a bicapas de almidón-PLA, para obtener materiales de envasado activos útiles para alargar la vida útil de diferentes matrices alimentarias.

El método de aplicación combinada de ultrasonidos y calentamiento a reflujo (USHT) y la extracción con agua subcrítica (SWE) (a 160 °C, 7 bares (SWE-160) y 180 °C, 11 bares (SWE-180)) fueron muy eficaces para obtener extractos acuosos activos de la paja de arroz. Los extractos mostraron un alto contenido fenólico (37, 51 y 83 mg GAE.g^{-1} de extracto seco, respectivamente) y actividad antioxidante (6,3, 2,0 y 1,2 mg de extracto seco.mg^{-1} DPPH, respectivamente). Los extractos SWE mostraron actividad antibacteriana contra *L. innocua* (MIC_{SWE160}: 50 mg extracto seco.mL^{-1}; MIC_{SWE180}: 30 mg extracto seco.mL^{-1}) y *E. coli* (MIC_{SWE180}: 182 mg extracto seco.mL^{-1}). Se aislaron fibras de celulosa (FC) de las fracciones insolubles de la extracción y se compararon con las obtenidas con el método alcalino tradicional. A pesar de las ligeras diferencias en el grado de purificación, los nuevos métodos dieron lugar a FCs con rendimientos más elevados que el método alcalino (35-39 % frente al 29 %), con cristalinidad (60-69 %), comportamiento térmico y relación de aspecto (20-60) similares.

Las FC obtenidas por el método USHT y alcalino se incorporaron a películas de mezclas de metilcelulosa y goma arábiga y mostraron un comportamiento de refuerzo similar, aumentando la resistencia a la rotura y la rigidez de las películas. Asimismo, también se incorporaron fibras USHT al 1, 3 y 5 % (p/p) en películas de almidón de maíz, y de almidón de maíz modificado por tratamiento térmico, obtenidas por mezclado en fundido y moldeo por compresión. La incorporación de FC al 3 % dio lugar a películas más resistentes a la rotura

(~100 %), más rígidas (~215 %), menos extensibles (~53 %) y con mayor capacidad de barrera al oxígeno (~30 %) y al vapor de agua (~15 %). Cuando los extractos activos se incorporaron en diferentes proporciones (4, 6 y 8 % en peso) a la matriz de almidón, con o sin CF (3 %), las películas fueron más extensibles y menos resistentes, pero con mayor capacidad de barrera al oxígeno. Asimismo, las bolsas monodosis de estas películas activas y reforzadas redujeron eficazmente la oxidación del aceite de girasol envasado.

Se obtuvieron películas activas de PLA plastificado con PEG1000, incorporando diferentes proporciones (2, 4 y 6 % p/p) del extracto USHT, mediante mezclado en fundido y moldeo por compresión. La presencia del extracto coloreó las películas y redujo ligeramente su resistencia a la rotura, su extensibilidad, su capacidad de barrera al vapor de agua y su termoestabilidad, pero aumentó su capacidad de barrera al oxígeno. La cinética de liberación de los compuestos antioxidantes incorporados, en simulantes alimentarios de diferente polaridad (A: productos acuosos; y D1: sistemas de aceite en agua), mostró que las películas con un 6% de extracto, desarrollaron una capacidad antioxidante similar, independientemente de la polaridad del simulante alimentario.

Se obtuvieron bicapas biodegradables laminando PLA plastificado con PEG1000, con y sin extracto USHT (6 %), y láminas de almidón termoplástico, con o sin FC USHT (3 %). Las bicapas mostraron una mejor capacidad de barrera global al oxígeno y al vapor de agua con respecto a las monocapas. Sin embargo, la migración de compuestos entre capas dio lugar a películas menos rígidas y resistentes respecto a lo esperado de la contribución de la película de PLA. Asimismo, las bicapas activas y reforzadas fueron capaces de inhibir la oxidación, el crecimiento bacteriano y los cambios de color de la carne de cerdo envasada durante el almacenamiento en frío.

Con el fin de comparar las propiedades bioactivas de los diferentes extractos (USHT, SWE-160 y SWE-180) cuando se incorporan a matrices poliméricas, se obtuvieron películas de PLA con un 6 % (p/p) de cada extracto, mediante mezclado en fundido y moldeo por compresión. Todos los extractos debilitaron la matriz de PLA, disminuyendo su resistencia a la rotura (~15-18 %), su extensibilidad (~32-36 %) y su capacidad de barrera al vapor de agua (~30 %). Sin embargo, las películas mostraron una mayor capacidad de barrera al oxígeno (~16-25 %) y un intenso efecto de bloqueo de la luz UV. Además, las películas de PLA activo, especialmente las que contenían el extracto SWE-180, prolongaron la vida útil de la carne de cerdo envasada, ya que no se alcanzaron los límites legales de recuento microbiano y oxidación en los 16 días de almacenamiento en frío.

Las FCs obtenidas con los diferentes métodos de purificación también se utilizaron para producir aerogeles de celulosa, materiales biodegradables superabsorbentes con potencial aplicación en diferentes campos. Las diferencias en la composición química de las FCs afectaron a la microestructura de los aerogeles. En concreto, el aerogel SWE-180, con el menor contenido en hemicelulosa y alta proporción de sílice, dio lugar a una matriz menos

cohesionada, con menor porosidad. La capacidad de absorción y de retención de agua de los aerogeles estuvo dentro de los rangos previamente descritos para este tipo de materiales.

Por tanto, fue posible obtener fracciones valorizadas de la paja de arroz, extractos activos y fibras celulósicas, útiles en el desarrollo de materiales biodegradables activos a base de almidón y PLA. Son necesarios más estudios para validar la seguridad alimentaria de los materiales, así como para el desarrollo de otras aplicaciones en el campo de la industria alimentaria o farmacéutica.

RESUM

Per minimitzar el problema mediambiental que suposen els plàstics són necessaris diferents enfocaments i, entre ells, hi ha l'ús de materials biodegradables per a l'envasament d'aliments, a causa de la gran contribució dels envasos d'un sol ús al consum de plàstics. Per la seva compatibilitat per al contacte amb els aliments, el poli (àcid làctic) (PLA) i el midó són polímers de base biològica i biodegradables amb gran potencial en aquest camp. No obstant això, és necessari millorar les propietats d'aquests biopolímers per complir amb els requisits d'envasament alimentari, i l'addició de valor afegit a aquests materials permetria compensar el seu major cost en el mercat del plàstic. D'altra banda, els residus agrícoles lignocel·lulòsics, com la palla d'arròs (RS), podrien ser valoritzats en fraccions cel·lulòsiques i extractes actius que poden ser utilitzats per millorar les propietats dels materials d'envasament biodegradables, contribuint així també a l'economia circular.

Aquesta tesi doctoral es va centrar en l' obtenció de fraccions cel·lulòsiques i extractes bioactius de palla d' arròs mitjançant l'aplicació de diferents tècniques d'extracció i purificació, utilitzant aigua com a dissolvent. Aquestes fraccions es van incorporar a pel·lícules basades en midó i PLA, així com a bicapes de midó-PLA, per obtenir materials d'envasament actius útils per allargar la vida útil de diferents matrius alimentàries.

El mètode d'aplicació combinada d'ultrasons i escalfament a reflux (USHT) i l'extracció amb aigua subcrítica (SWE) (a 160 °C, 7 bars (SWE-160) i 180 °C, 11 bars (SWE-180)) van ser molt eficaços per obtenir extractes aquosos actius de la palla d'arròs. Els extractes van mostrar un alt contingut fenòlic (37, 51 i 83 mg GAE.g^{-1} d'extracte sec, respectivament) i activitat antioxidant (6,3, 2,0 i 1,2 mg d'extracte sec.mg^{-1} DPPH, respectivament). Els extractes SWE van mostrar activitat antibacteriana contra *L. innocua* (MIC_{SWE160}: 50 mg extracte sec.mL^{-1}; MICSWE180: 30 mg extracte sec.mL^{-1}) i *E. coli* (MIC_{SWE180}: 182 mg extracte sec.mL^{-1}). Es van aïllar fibres de cel·lulosa (FC) de les fraccions insolubles de l'extracció i es van comparar amb les obtingudes amb el mètode alcalí tradicional. Malgrat les lleugeres diferències en el grau de purificació, els nous mètodes van donar lloc a FCs amb rendiments més elevats que el mètode alcalí (35-39 % enfront del 29 %), amb cristal·linitat (60-69 %), comportament tèrmic i relació d'aspecte (20-60) similars.

Les FC obtingudes pel mètode USHT i alcalí es van incorporar a pel·lícules de mescles de metilcel·lulosa i goma aràbiga i van mostrar un comportament de reforç similar, augmentant la resistència al trencament i la rigidesa de les pel·lícules. Així mateix, també es van incorporar fibres USHT a l'1, 3 i 5 % (p/p) en pel·lícules de midó de dacsa, i de midó de dacsa modificat per tractament tèrmic, obtingudes per barrejat en fos i emmotllament per compressió. La incorporació de FC al 3 % va donar lloc a pel·lícules més resistents al trencament (~100 %), més rígides (~215 %), menys extensibles (~53 %) i amb més capacitat de barrera a l'oxigen

(~30 %) i al vapor d'aigua (~15 %). Quan els extractes actius es van incorporar en diferents proporcions (4, 6 i 8 % en pes) a la matriu de midó, amb o sense CF (3 %), les pel·lícules van ser més extensibles i menys resistents, però amb més capacitat de barrera a l'oxigen. Així mateix, les bosses monodosi d'aquestes pel·lícules actives i reforçades van reduir eficaçment l'oxidació de l'oli de gira-sol envasat.

Es van obtenir pel·lícules actives de PLA plastificat amb PEG1000, incorporant diferents proporcions (2, 4 i 6 % p/p) de l'extracte USHT, mitjançant barrejat en fos i emmotllament per compressió. La presència de l'extracte va acolorir les pel·lícules i va reduir lleugerament la seva resistència al trencament, la extensibilitat, la capacitat de barrera al vapor d'aigua i la termoestabilitat, però va augmentar la seva capacitat de barrera a l'oxigen. La cinètica d'alliberament dels compostos antioxidants incorporats, en simulants alimentaris de diferent polaritat (A: productes aquosos; i D1: sistemes d'oli en aigua), va mostrar que les pel·lícules amb un 6% d'extracte, van desenvolupar una capacitat antioxidant similar, independentment de la polaritat del simulant alimentari.

Es van obtenir bicapes biodegradables laminant PLA plastificat amb PEG1000, amb i sense extracte USHT (6 %), i làmines de midó termoplàstic, amb o sense FC USHT (3 %). Les bicapes van mostrar una millor capacitat de barrera global a l'oxigen i al vapor d'aigua respecte a les monocapes. No obstant això, la migració de compostos entre capes va donar lloc a pel·lícules menys rígides i resistents respecte a l'esperat de la contribució de la pel·lícula de PLA. Així mateix, les bicapes actives i reforçades van ser capaces d'inhibir l'oxidació, el creixement bacterià i els canvis de color de la carn de porc envasada durant l'emmagatzematge en fred.

Per tal de comparar les propietats bioactives dels diferents extractes (USHT, SWE-160 i SWE-180) quan s'incorporen a matrius polimèriques, es van obtenir pel·lícules de PLA amb un 6 % (p/p) de cada extracte, mitjançant barrejat en fos i emmotllat per compressió. Tots els extractes van debilitar la matriu de PLA, disminuint la seva resistència al trencament (~15-18 %), la extensibilitat (~32-36 %) i la capacitat de barrera al vapor d'aigua (~30 %). No obstant això, les pel·lícules van mostrar una major capacitat de barrera a l'oxigen (~16-25 %) i un intens efecte de bloqueig de la llum UV. A més, les pel·lícules de PLA actiu, especialment les que contenien l'extracte SWE180, van prolongar la vida útil de la carn de porc envasada, ja que no es van assolir els límits legals de recompte microbià i oxidació en els 16 dies d'emmagatzematge en fred.

Les FCs obtingudes amb els diferents mètodes de purificació també es van utilitzar per produir aerogels de cel·lulosa, materials biodegradables superabsorbents amb potencial aplicació en diferents camps. Les diferències en la composició química de les FCs van afectar la microestructura dels aerogels. En concret, l'aerogel SWE-180, amb el menor contingut en hemicel·lulosa i alta proporció de sílice, va donar lloc a una matriu menys cohesionada amb menor porositat. La capacitat d' absorció i de retenció d'aigua dels aerogels va estar dins dels rangs prèviament descrits per a aquest tipus de materials.

Per tant, va ser possible obtenir fraccions valoritzades de la palla d' arròs, extractes actius i fibres cel·lulòsiques, útils en el desenvolupament de materials biodegradables actius a base de midó i PLA. Són necessaris més estudis per validar la seguretat alimentària dels materials, així com per al desenvolupament d' altres aplicacions en el camp de la indústria alimentària o farmacèutica.

PREFACE

DISSERTATION OUTLINE

This Doctoral Thesis was structured in five sections, as summarized in **Figure 1**: **Introduction**, **Objectives**, **Chapters**, **General Discussion**, and **Conclusions**.

The **Introduction** section outlines the potential use of biopolymers to produce food packaging, focusing on different strategies to improve their functionality. The assembling of biopolymers with complementary properties to obtain multilayer systems, as well as the incorporation of natural active substances into the packaging material were discussed. Likewise, the state of the art regarding the extraction and use of cellulosic reinforcing agents and active compounds from agro-industrial waste, such as rice straw, was also discussed. Subsequently, the **Objective** section presents the general and specific objectives of this Doctoral Thesis.

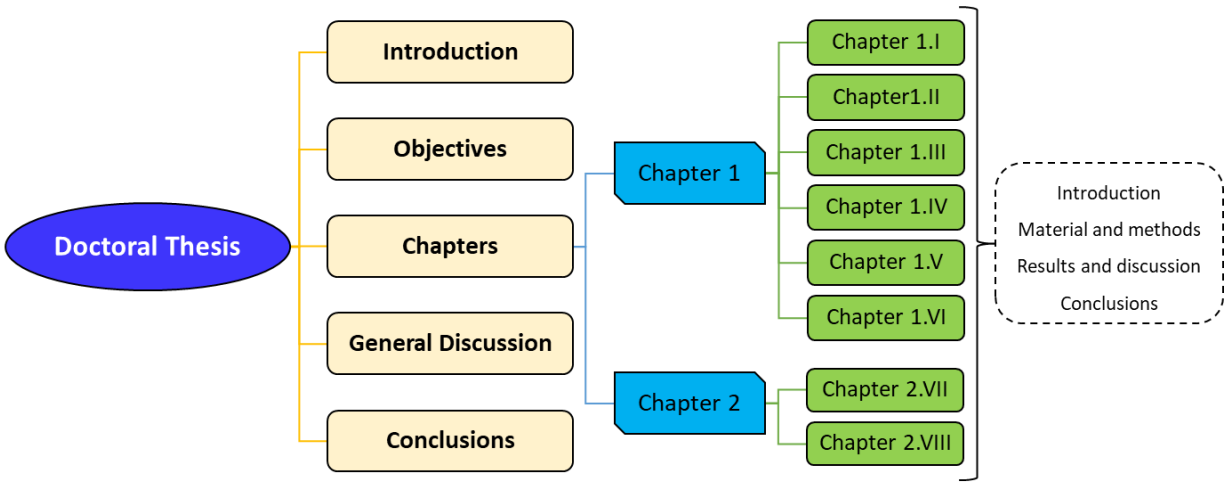

Figure 1. Structure of the present Doctoral Thesis.

The results obtained throughout this Doctoral Thesis were presented and discussed in the different **Chapters**, corresponding to eight scientific publications with the usual sections: *Introduction*, *Material and Methods*, *Results and Discussion*, and *Conclusions*.

Chapter 1 comprises the studies focused on the isolation and characterisation of cellulose fibres and bioactive extracts from rice straw by applying ultrasound-assisted extraction. Once these valorised fractions were obtained, their effectiveness to improve the functional and bioactive properties of different biopolymer matrices was investigated. In this way, **Chapter 1.I** entitled "*Application of ultrasound pre-treatment for enhancing the extraction of bioactive compounds from rice straw*" investigates different green extraction techniques to improve the aqueous extraction of bioactive compounds from rice straw. Ultrasound-assisted extraction was studied as a pre-treatment, in combination with other methods. The physical

modifications induced in the plant tissue, the release kinetics of phenolic compounds, as well as the phenolic richness and antioxidant and antibacterial capacities of the obtained extracts, are described. Of the tested methods, the combination of ultrasound with reflux heating is recommended to obtain an active extract with potential application in food packaging materials.

To fully valorise rice straw, **Chapter 1.II** entitled "*Applying ultrasound-assisted processing to obtain cellulose fibres from rice straw to be used as reinforcing agents*" studies the isolation of cellulose fibres from the solid residue obtained after extraction by applying the combined ultrasound-reflux heating method. The morphogeometric and thermal properties, micro- and nanostructural characteristics, as well as the reinforcing capacity of the cellulose fibres in methylcellulose/gum arabic blended films were investigated. The characteristics and properties of the cellulose fibres obtained with the new method are compared to those from the conventional alkaline extraction method. The results show that the proposed greener method yields cellulose fibres with potential application as reinforcing agents in biopolymers.

Chapter 1.III entitled "*Valorization of rice straw into cellulose microfibers for the reinforcement of thermoplastic corn starch films*" compares the changes induced by the incorporation of different ratios of cellulose fibres from rice straw into thermoplastic starch films with and without starch dry heating pre-treatment. The control and composite films were characterised as to their morphological, thermal, tensile and barrier properties, water solubility and water uptake capacity. The results reveal that the obtained cellulose fibres applying the combined ultrasound-reflux heating method can be used to improve the functional properties of both types of thermoplastic starch films.

Chapter 1.IV entitled "*Antioxidant poly (lactic acid) films with rice straw extract for food packaging applications*" studies the obtention of active films based on PLA incorporating the active extract from rice straw obtained by the ultrasound-reflux heating method. The effect of the extract ratio on the functional properties of the films and the release kinetics of phenolic compounds in food simulants of different polarities is analysed. The results show that active PLA films are successfully obtained with slightly modified properties and different phenolic release rates and ratios depending on the polarity of the food simulant.

In **Chapter 1.V**, entitled "*Using rice straw fractions to develop reinforced, active PLA-starch bilayers for meat preservation*", bilayer films are obtained by combining cellulose fibre reinforced-starch films and PLA films with active extract, using the previously optimised ratio of fibres and active extract. The functional properties of the bilayers as packaging materials are evaluated, as well as their effectiveness as active packaging by analysing their capacity to extend shelf life of cold stored fresh pork meat.

In **Chapter 1.VI** entitled "*Antioxidant starch composite films containing rice straw extract and cellulose fibres*", both valorised rice straw fractions, active extract and cellulose fibres, are used to develop thermoplastic starch-based films. The effect of different extract ratios, with or without cellulose fibres, on the functional properties of the films is investigated. Likewise, the active properties of the films are validated in mono-dose sunflower oil bags submitted to an accelerated oxidation test.

Chapter 2 analyses the potential of also green subcritical water extraction to obtain active extracts and cellulose fibres from rice straw for its valorisation. Thus, **Chapter 2.VII** entitled "*Active poly (lactic acid) films with rice straw aqueous extracts for meat preservation*" explores the obtention and characterisation of bioactive extracts from rice straw by applying subcritical water extraction. The yields and bioactive properties of the extracts were evaluated and compared with that obtained with the combined ultrasound-reflux heating method. Additionally, the chapter studies the incorporation of the extracts into PLA films and their effect on the films' functional properties and their capacity to extend the shelf life of cold storage pork meat.

In **Chapter 2.VIII** entitled "*Cellulose aerogels obtained from rice straw. Influence of the cellulose purification process*", cellulose fibres are isolated from the solid residues of the and characterised, in comparison with those obtained from the conventional alkaline extraction and combined ultrasound-reflux heating method. Likewise, aerogels are obtained with different fibres and compared in their typical properties, such as microstructure, porosity, water sorption and absorption capacity. The results indicate that the cellulose purification process affects the final composition of the fibres and the three-dimensional network arrangement of the aerogels.

The most relevant results in each chapter are discussed in the **General Discussion** section, which brings an overview of the lignocellulosic fractions obtained as well as the effect that their incorporation has on the polymer matrices studied. Finally, the **Conclusions** section presents the main findings of this Doctoral Thesis.

DISSEMINATION OF RESULTS

INTERNATIONAL JOURNALS JCR

- ***Published***

"Application of ultrasound pre-treatment for enhancing the extraction of bioactive compounds from rice straw". Pedro A. V. Freitas, Chelo González-Martínez, Amparo Chiralt. *Foods* (2020), 9(11), 1-15.

"Applying ultrasound-assisted processing to obtain cellulose fibres from rice straw to be used as reinforcing agents". Pedro A. V. Freitas, Chelo González-Martínez, Amparo Chiralt. *Innovative Food Science & Emerging Technologies* (2022), 76, 102932.

"Valorization of rice straw into cellulose microfibers for the reinforcement of thermoplastic corn starch films". Pedro A. V. Freitas, Carla I. La Fuente Arias, Sergio Torres-Giner, Chelo González-Martínez, and Amparo Chiralt. *Applied Sciences* (2021), 11, 8433.

"Antioxidant starch composite films containing rice straw extract and cellulose fibres". Pedro A. V. Freitas, Chelo González-Martínez, Amparo Chiralt. *Food Chemistry* (2022), 400, 134073.

- ***Submitted***

"Antioxidant poly (lactic acid) films with rice straw extract for food packaging applications". Pedro A. V. Freitas, Nuria J. B. Gil, Chelo González-Martínez, Amparo Chiralt. *Food Packaging and Shelf Life*.

"Using rice straw fractions to develop reinforced, active PLA-starch bilayers for meat preservation". Pedro A. V. Freitas, Chelo González-Martínez, Amparo Chiralt. *Food Chemistry*.

"Influence of the cellulose purification process on the properties of aerogels obtained from rice straw". Pedro A. V. Freitas, Chelo González-Martínez, Amparo Chiralt. *Food Hydrocolloids.*

"Active poly (lactic acid) films with rice straw aqueous extracts for meat preservation". Pedro A. V. Freitas, Chelo González-Martínez, Amparo Chiralt. *Food Packaging and Shelf Life.*

COMMUNICATIONS IN INTERNATIONAL CONGRESSES

Poster: **"Antioxidant PLA films containing rice straw extracts for food packaging applications"**. Pedro A. V. Freitas, Nuria J. B. Gil, Chelo González-Martínez, Amparo Chiralt. 6th International ISEKI Food Conference (ISEKI_FOOD 2021). Online (2021).

Poster: **"Antioxidant starch films to obtain mono-dose bags of sunflower oil using extract and cellulosic reinforcements from rice straw"**. XI Congreso Nacional de Ciencia y Tecnología de los Alimentos (CyTA/CESIA 2022). Zaragoza, Spain (2022).

Poster: "**Obtaining cellulose aerogels from rice straw pre-treated with subcritical water extraction**". 8th International Conference on Biobased and Biodegradable Polymers (BIOPOL-2022). Alicante, Spain (2022).

Poster: **"Valorising rice straw fractions into active polyester-starch bilayers for meat preservation"**. 10th Shelf Life International Meeting. Bogotá, Colombia (2022).

Poster: **"Active aqueous extracts from rice straw to improve the PLA capacity to preserve pork meat"**. 10th Shelf Life International Meeting. Bogotá, Colombia (2022).

COMMUNICATIONS IN SCIENTIFIC EVENTS

Valorización de la paja de arroz mediante la obtención de compuestos activos y materiales celulósicos aplicables en films biodegradables para el envasado de alimentos. Jornada de Investigación en Ciencia y Tecnología de Alimentos. Valencia (2021).

Embalagens Ativas e Inteligentes: Conceitos, Avanços e Perspectivas na Indústria de Alimentos. Congresso Brasileiro Online de Ciência e Tecnologia de Alimentos. Online (2021).

Valorización de la paja de arroz mediante la obtención de fracciones activas y celulósicas aplicables en films biodegradables. I Jornadas de Investigación: Doctorado en Ciencia, Tecnología y Gestión Alimentaria. Valencia (2022).

Films laminados biodegradables activos para la conservación de alimentos, utilizando fracciones valorizadas de residuos agroalimentarios. Segundas Jornadas Iberoamericanas sobre herramientas clave para implementar economías circulares en procesos agroindustriales. Online (2022).

CO-SUPERVISION OF FINAL DEGREE OR MASTER'S PROJECTS

Extracción de antioxidantes de la paja de arroz. Aplicación de ultrasonidos con tratamiento térmico. Paula, J. Tomas (2020). *Grado en Ingeniería Agronómica y del Medio Natural (Universitat Politècnica de València).*

Antioxidant poly (lactic acid) (PLA) films containing rice straw extract for active food packaging applications. Nuria, J. B. Gil (2021). *Grado en Biotecnolgía (Universidad Católica de Valencia).*

Extractos activos de la paja de arroz obtenidos por extracción acuosa en condiciones subcríticas. Laura Ivars (2022). *Grado en Ciencia y Tecnología de los Alimentos (Universitat Politècnica de València).*

Propiedades físicas y estabilidad de films bicapa almidón-PLA con extracto activo y fibras celulósicas de paja de arroz. Pere Aguado (2022). *Grado en Ciencia y Tecnología de los Alimentos (Universitat Politècnica de València).*

Absorbedores celulósicos obtenidos de la paja de arroz. Influencia del proceso de separación de la celulosa. María Molinero (2022). *Máster en Ciencia e Ingeniería de los Alimentos (Universitat Politècnica de València)*.

Bolsas monodosis de almidón con extracto activo y microfibras celulósicas de paja de arroz para la conservación de aceite de girasol. Julián Manzanares (2022). *Máster en Gestión de la Seguridad y Calidad Alimentaria (Universitat Politècnica de València)*.

Extractos acuosos activos de la paja de arroz para mejorar la capacidad de conservación del PLA en carne de cerdo. Nuria, J. B. Gil (2022). *Máster en Gestión de la Seguridad y Calidad Alimentaria (Universitat Politècnica de València)*.

Valorization of Wine Making Residues by Using Subcritical Water Extraction: Obtaining Polyphenol Extracts, Useful in Developing Active and Biodegradable Food Packaging Materials. Silvia Meyer (2022). *Master Thesis in the Field of Food Science (ETH Zurich / Universitat Politècnica de València*

TABLE OF CONTENTS

NOMENCLATURE

AARD: average absolute relative deviation

Abs: absorbance

ABTS: 2,2'-Azino-bis (3-ethylbenzothiazoline- 6 -sulfonic acid) diammonium salt

ASTM: American Society for Testing and Materials

ALK: alkaline treatment

ANOVA: analysis of variance

a^*: redness-greenness

b^*: yellowness-blueness

BHA: 3-tert-Butyl-4-hydroxyanisole

BHT: 2,6-bis(1,1-dimethylethyl)-4-methylphenol

C_{ab}^*: chroma

C_e: equilibrium concentration of pseudo-second-order rate law

C_o: initial concentration of pseudo-second-order rate law

C_t: concentration at any time t of pseudo-second-order rate law

CF: cellulose fibres

CI: crystallinity index

CMF: cellulose microfibres

CNC: cellulose nanocrystals

CFU: colony forming unit

CH_4: methane

CO_2: carbon dioxide

DH: dry heating

DPPH: 2,2-Diphenyl-1-pikryl-hydrazyl

DSC: differential scanning calorimetry

DTGA: thermal weight loss derivative

E: elongation at break

EC_{50}: half maximal effective concentration

EM: elastic modulus

EV: equilibrium value

es: extract solid

ε: relative elongation

FAO: Food and Agriculture Organization of the United Nations

FESEM: field emission scanning electron microscopy

FT: freeze-thawing

FTIR: Fourier transform infrared spectroscopy

GA: gum arabic

GAE: gallic acid equivalent

Gly: glycerol

h_{ab}^*: hue angle

h: initial extraction rate of pseudo-second-order rate law

HPLC: high-performance liquid chromatography

HPMC: hydroxypropilmethylcellulose

HT: heating treatment

HSD: honestly significant difference

H_2SO_4: sulfuric acid

KOH: potassium hydroxide

k: second-order extraction rate constant / rate constant of Korsmeyer-Peppas model

k_1: kinetic constant of Peleg model

k_2: constant of Peleg model

*L**: lightness

LA: lactic acid bacteria

LDPE: low-density polyethylene

MC: methylcellulose

MCC: microcrystalline cellulose

MDA: malondialdehyde

$Mg(NO_3)_2$: magnesium nitrate

MIC: minimal inhibitory concentration

MRS: Man, Rogosaand Sharpe agar

M_t: total phenolic content incorporated

M_∞: Amount of active compound released at equilibrium

NaOH: sodium hydroxide

Na_2CO_3: sodium carbonate

N_2O: nitrous oxide

NCC: nano-crystalline cellulose

NREL: National Renewable Energy Laboratory

n: Diffusional exponent of Korsmeyer-Peppas model

OP: oxygen permeability

OTR: oxygen transmission rate

p: p-value

PB: psychrotrophic bacteria

PBAT: Polybutylene adipate-*co*-terephthalate

PBS: Polybutylene succinate

PCL: Poly(ε-caprolactone)

PE: polyethylene

PEG1000: polyethylene glycol 1000 Da

PET: polyethylene terephthalate

PHA: Polyhydroxyalkanoates

PHB: Poly-β-hydroxybutyrate

PHBV: Poly(3-hydroxybutyrate)-co-(3-hydroxyvalerate)

PHV: poly (3-hydroxy valerate)

PLA: poly (lactic acid)

PP: polypropylene

PS: polystyrene

PV: peroxide value

PVA: poly (vivyl alchohol)

PVAc: polyvinyl acetate

P_2O_5: di-phosphorus pentoxide

R: reflection spectra

R_g: white background

RH: relative humidity

R_o: black background

RS: rice straw

R^2: determination coefficient

R_∞: infinite reflectance

SEM: scanning electron microscopy

SiO_2: amorphous silica

ST: stirring method

SWE: subcritical water extraction

t: time

TBARS: 2-thiobarbituric acid reactive substances

TEAC: Trolox equivalent antioxidant capacity

T_f: final temperature

TGA: thermogravimetric analysis

T_g: glass transition temperature

T_i: internal transmittance

TiO_2: titanium oxide

T_{on}: onset temperature

T_p: peak temperature

TC: total coliform counts

TPC: total phenolic content

TPS: thermoplastic starch

TS: tensile strength at break

TSA: tryptic soy agar

TSB: tryptic soy broth

TSY: total solid yield

TV: total viable count

UAE: ultrasound-assisted extraction

US: ultrasound

USHT: combined ultrasound-reflux heating method

USST: combined ultrasound-stirring method

UV: ultraviolet

UV-vis: ultraviolet-visible

VRB: Violet red bile agar

WAC: water absorption capacity

WI: whiteness index

WVP: water vapour permeability

WVTR: water vapour transmission rate

WRC: water retention capacity

XRD: X-ray diffraction

ZnO: zinc oxide

ΔE^*: total colour difference

ΔH_{relax}: relaxation enthalpy

Δm: mass variation

α: significance level

Ø: diameter

INTRODUCTION

1. Trends and advances in the development of biodegradable active packaging materials for food preservation

Since the 1940s, conventional plastics have been widely used in several fields due to their cheapness, excellent mechanical and water vapour and gas barrier properties, easy processing, lightweight, good chemical resistance, and potential reusability (Shlush & Davidovich-Pinhas, 2022; Thakur et al., 2018). Conventional plastics, however, are petroleum-derived synthetic polymers that exhibit high durability and stability over time. Combined with the dependence on plastics by modern society, conventional plastics have been highly accumulating in the environment and contributing to the pollution of seas, freshwater systems, cities, and landfills. Likewise, large amounts of carbon dioxide (CO_2) and other greenhouse gases (CH_4, N_2O) have been emitted into the atmosphere when they are incinerated (Hong et al., 2021). In 2020, plastics production reached 367 Mt, of which 40 % corresponds to the packaging sector, followed by building (20 %), automotive (9 %), electronics (6 %), household (4 %), agriculture (3 %), and other segments (17 %) (Plastics Europe, 2021). According to Geyer et al. (2017), if primary plastics production exhibits steady growth as observed in recent decades, 26,000 Mt of plastic resins will have been produced by the end of 2050, of which 9,000 Mt will have been recycled, 12,000 Mt incinerated, and 12,000 Mt disposed of in landfills or in the environment. Since most plastics commonly used in food packaging are not biodegradable (PE, PP, PS, PVC, and PET), the only way to permanently dispose of them is through destructive thermal treatments, such as combustion or pyrolysis (Geyer et al., 2017). Nonetheless, this option of plastic waste management has become less and less suitable, as the burning of 1 kg of plastic is associated with 2.8 kg of CO_2 emissions (Thakur et al., 2018). In this sense, efforts have been made towards minimising the environmental impact caused by conventional plastics, including recycling, or developing new sustainable materials, such as biodegradable bioplastics, in order to replace petrochemical-based plastic packaging.

Biopolymers are defined as materials that are biodegradable, bio-based, or both. According to the source, they can be classified as bio-based biodegradable or non-biodegradable; or even fossil-based biodegradable. The production of biopolymers has been growing progressively in the last years, reaching 2.42 Mt in the year 2021 and projected to reach 7.6 Mt in 2026 (Figure 1). Of the total production in 2021, 64.2 % corresponds to biodegradable biopolymers, the main ones being PBAT, PLA, and starch blends. Furthermore, approximately 48 % of biopolymer production is associated with rigid and flexible packaging (European Bioplastics, 2021).

In general, food packaging is composed of several layers of different polymers, which have complementary functional properties to provide adequate protection to maintain the quality of the food during transportation and storage. Due to technological limitations, high costs,

and complexity to separate such materials, recycling of food packaging becomes a difficult or unfeasible task. In this way, biopolymers, especially biodegradable ones, are undoubted alternatives to produce multilayer food packaging materials or food coatings with environmentally-friendly approach.

Currently, the use of biopolymers for food packaging purposes is still limited due to their high cost and poor functional properties compared to petrochemical-based polymers, including water vapour and gas barrier properties, processability, mechanical performance and thermal stability. Thus, different alternatives and approaches have been proposed towards improving the performance of these biopolymers. Strategies such as incorporation of fillers, compatibilising agents, plasticisers, polymer functionalization, use of polymer blends and biodegradable multilayer systems have been successfully studied. Also, the incorporation of bioactive substances into the packaging material provides new functionalities to the food packaging. The production of this active packaging has been shown to play an important role in extending shelf-life of foods and maintaining their quality until consumption. Essential oils, enzymes, bacteriocins and active extracts obtained from agro-industrial wastes have been investigated as bioactive substances with a high potential application in the biodegradable food packaging sector.

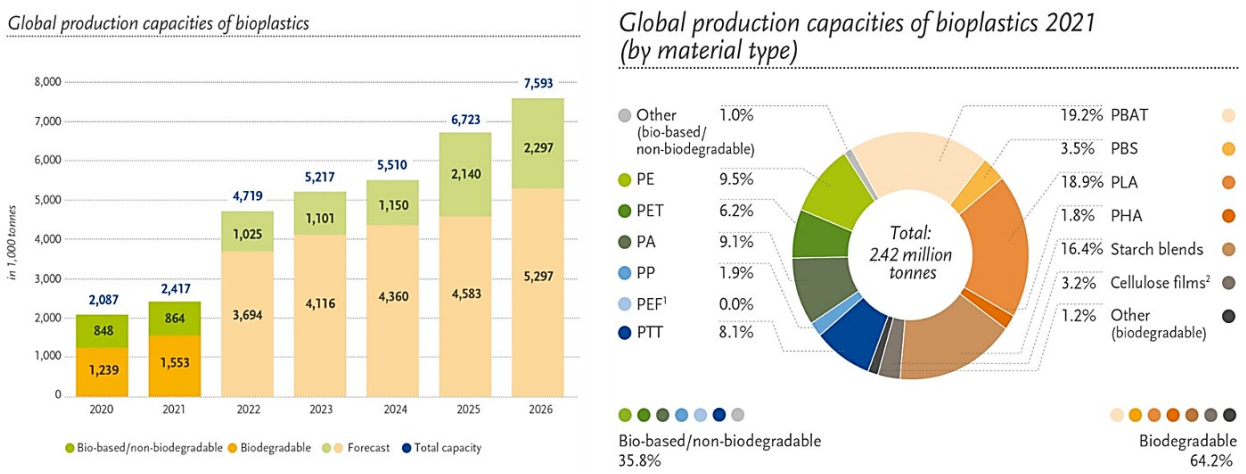

Figure 1. Global production (2020 and 2021) and production estimation of bioplastics (2022-2026); and global production by material type in 2021 (European Bioplastics, 2021).

1.1 Bioplastics for food packaging applications

Bioplastics are considered as a friendly alternative to the environmental problems and the limited sources of petroleum-based materials (Byun & Kim, 2014; Hong et al., 2021). Bioplastics can be defined as plastics that can be bio-based, biodegradable or both (Shlush & Davidovich-Pinhas, 2022). Figure 2 shows the classification of the plastics based on their origin,

source, and biodegradable or non-biodegradable nature. Likewise, the biopolymers can be divided into four groups as regarding chemical composition, origin and synthesis method: polymers obtained directly from biomass (starch, cellulose, chitosan, proteins); polymers produced by chemical synthesis from bio-based monomers (poly (lactic acid) (PLA), bio-based polyethylene); polymers obtained by microbial fermentation (polyhydroxyalkanoates (PHAs)); and polymers produced by chemical synthesis from both bio-based monomers and petroleum-based monomers (poly (butylene succinate), poly (trimethylene terephthalate)) (Byun & Kim, 2014).

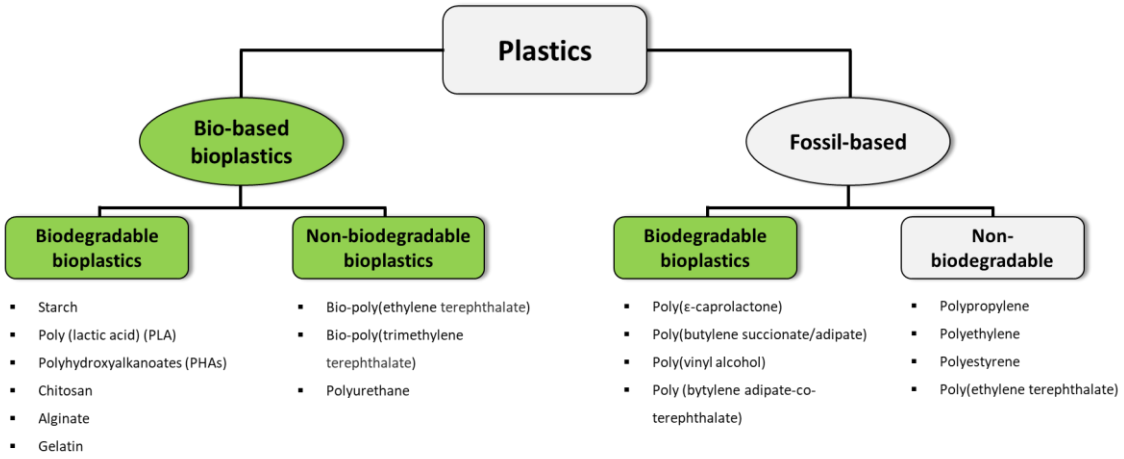

Figure 2. Classification of plastics based on the origin, source, and biodegradable or non-biodegradable nature.

Several biopolymers obtained from biomass have been studied for food packaging applications, including polysaccharides and proteins (Figure 3). Starch, for example, is a semi-crystalline biopolymer found in many plant sources, such as corn, potatoes, sweet potatoes, and rice. It is widely studied as a potential packaging material due to its low cost, availability, renewability and biocompatibility (Carvalho, 2008; González et al., 2015). As shown in Figure 3, starch consists of two fractions, known as amylose and amylopectin, composed of D-glycopyranose units organized into linear and branched chains, respectively (Galdeano et al., 2009). Starch, in its native state, presents its fractions organized in starch granules, which can be processed with plasticizers in an extruder, giving rise to a thermoplastic material with excellent capacity to form films with high barrier to oxygen, lipids and carbon dioxide (Carvalho, 2008). Chitosan, a deacetylated derivative of chitin mainly composed of (1-4)-linked 2-amino-2-deoxy-β-D-glucose monomers, is another example of a highly available biopolymer in nature with interesting properties, including antimicrobial activity, solubility, film forming and ion biding capacity and viscosity (Priyadarshi & Rhim, 2020; Wang et al., 2018). Cellulose is a highly abundant biopolymer in nature formed by linkages of D-glucose with 1,4- β-glycosidic bonds (Sticklen, 2008). Due to its biocompatibility, thermal stability,

biodegradability, availability, high porosity, stiffness and chemical stability, cellulose can be used as environmentally friendly products with several industrial applications as follows: (1) cellulose fibres, microfibres, or nanofibres applied as reinforcing agents in polymer matrices; (2) cellulose films and membranes; (3) cellulose hydrogels; (4) cellulose aerogels; (5) cellulose microspheres and beads; (6) cellulose-based composites; among others (Long et al., 2021; Wang et al., 2016). Proteins such as gelatin and dairy derivatives are also interesting sources of biomass that can be used as food packaging materials. Being obtained from the hydrolysis of collagen present in animal skins and bones, gelatin is a versatile polymer for packaging purposes, edible films, or coatings due to its biodegradability, biocompatibility, and low price. However, due to its poor mechanical properties and water resistance, gelatin-based matrices are usually blended with active agents, compatibilizers, and fillers to improve their functional characteristics (Lu et al., 2022).

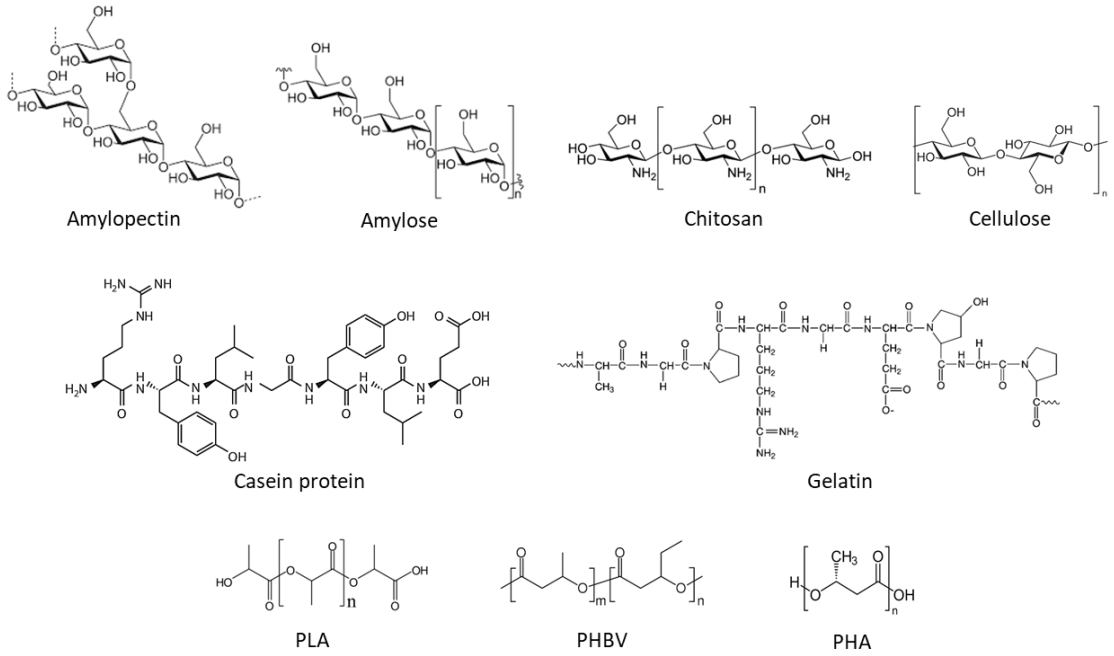

Figure 3. Chemical structures of different biopolymers used as food packaging materials.

Biopolymers produced by chemical synthesis can be obtained from bio-based (e. g., PLA) or fossil-based (e. g., Poly(ε-caprolactone) (PCL), poly (vinyl alcohol) (PVA)) monomers. PLA is a thermoplastic, compostable, and aliphatic polyester, classified as GRAS, derived from renewable sources such as corn, potato starch, and sugar beets (Kale et al., 2006). Due to its low environmental impact, PLA is considered as a potential substitute for petroleum-based polymers, especially for food packaging material applications (Harnkarnsujarit et al., 2021; Rocca-Smith et al., 2019). Among the chemical routes to obtain PLA, the ring-opening polymerisation of cyclic lactide is the most common to give rise to high molecular mass PLA

with suitable properties (Harnkarnsujarit et al., 2021). The ratio of L-lactide to D-lactide, the precursor molecules of PLA, determines the degree of crystallinity of the polymer and consequently, its properties, such as mechanical, barrier, compatibility, hydrophobicity, machinability, and thermoprocessing properties. Although increasing the D-lactide stereoisomer concentration in the PLA molecule increases its crystallinity, the production cost increases remarkably, not being economically viable (Byun & Kim, 2014). In general, PLA-based films for food packaging purposes show excellent water vapour barrier properties and mechanical performance, although its hydrophobic characteristic worsens its barrier properties to gases such as oxygen. Among biopolymers from fossil-based sources, PCL is a biodegradable polymer obtained from the ring-opening polymerisation of ε-caprolactone monomers, which give rise to a hydrophobic semi-crystalline polyester. It is a polymer that is highly flexible, mechanically tough, processable and hydrolysable under physiological conditions, leading to its extensive use and study as medical and food contact materials (Harnkarnsujarit et al., 2021). PVA is another example of fossil-based semi-crystalline biopolymer, which is synthesised through alkaline hydrolysis of polyvinyl acetate (PVAc). It is a water-soluble polymer with interesting properties for packaging material purposes, such as good tensile strength, flexibility, transparency, heat sealability and gas barrier capacity (Singh et al., 2021).

Another category of biopolymers that have been widely studied are those synthesized via bacterial fermentation, such as the so-called polyhydroxyalkanoates (PHAs). The PHAs are linear polyesters comprised of the homo- or copolymers of hydroxybutyric acid and hydroxyvaleric acid. They are produced as a result of bacterial metabolism of sugars, glucose, and vegetable oils found in plant derivatives or agro-industrial wastes (Bera et al., 2015). Poly(D-3-hydroxybutyrate) (PHB), for example, is stiff and brittle, while poly (3-hydroxy valerate) (PHV) is more flexible and less crystalline than PHB. When PHB is co-polymerised with PHV, the result is poly(3-hydroxybutyrate-*co*-3-hydroxy valerate) or PHBV, being more stretchable, less rigid and less crystalline than PHB (Ross et al., 2017). These polymers have good functional properties to be used as food packaging materials.

1.2 Using natural and active compounds to obtain biodegradable active packaging materials

Food packaging represents an essential tool in maintaining food quality and safety, extending the shelf-life and protecting food against oxygen, moisture, mechanical shocks, spoilage, contamination and ultraviolet light (Topuz & Uyar, 2020). Nevertheless, technological innovations in packaging systems have been improved in line with the demands of consumers and industry towards safer, synthetics-free and environmentally-friendly foodstuffs and technologies (Ahmed et al., 2017). In this sense, the use of biopolymers incorporating active

compounds to produce active food packaging materials represents an interesting and challenging approach for this packaging sector.

Active packaging systems consist of incorporating additives, known as active compounds, within packaging materials to positively interact with the headspace or packaged food, improving or preserving their nutritional quality and safety throughout storage and transportation (Baghi et al., 2022; García Ibarra et al., 2016). The active character of a packaging can also be achieved by incorporating the active compound within pads or sachets, which are placed inside the package containing the food (Ahmed et al., 2017). There are several categories of active systems for food packaging, based on absorbing systems and releasing systems. Absorbing or scavenging systems are designed to absorb substances from the food or its metabolism or from the packaging headspace, such as absorbers/scavengers of oxygen, radicals, moisture, gases, odours, ethylene, and volatile compounds. Releasing systems are designed to release active substances into the headspace or onto the surface of the food to improve, preserve or extend their shelf-life.

Releasing approaches can be obtained with antimicrobial, antioxidant, flavouring and preservative agents. The strategy of these releasing systems is to incorporate the active substances into the packaging material rather than adding them directly to the food. Thus, the packaging displays a controlled release of the additives from the packaging material to the environment surrounding the food or its surface. This release over time presents some advantages: there are not high amounts of the active compounds incorporated in the food, which would be ingested by the consumers; there is not an undesirable impact on food properties (appearance, taste, texture, and odour) due to the presence of additives or preservatives; less active compound is needed than if it were incorporated into the food composition; and the active substances released are more effective since there are less interactions with the food components.

Several types of active compounds have been described for antimicrobial and/or antioxidant food packaging purposes, including metal ions (e.g., silver, platinum), metal oxides (e.g., ZnO, Ti_2O), sulphites, synthetic antimicrobial agents (e.g., quaternary ammonium salts, ethylenediaminetetraacetic acid), and synthetic antioxidants (e.g., 2 and 3-tert-Butyl-4-hydroxyanisole (BHA), 2,6-bis(1,1-dimethylethyl)-4-methylphenol (BHT)) (Vilela et al., 2018). Nonetheless, the current and continuous consumer demand for natural substances stimulates the use of those from natural sources. In this sense, bacteriocins, essential oils, phenolic compounds, plant extracts, and their derivatives can be used as active substances in food packaging materials with antimicrobial and antioxidant capacities. Table 1 gathers some recent studies based on the use of natural compounds as antioxidant and/or antimicrobial agents incorporated into biopolymer matrices.

Essential oils have been extensively studied for their potential application in antimicrobial and/or antioxidant food packaging. Essential oils are organic substances composed of mixtures of low molecular weight aromatic compounds, such as flavonoids, monoterpenes, phenolic compounds, and phenolic acids. Being products of plant cellular metabolism, essential oils are extracted from various sources such as seeds, leaves, stems, etc. (Roy & Rhim, 2021b). Several essential oils have proven antimicrobial and antioxidant activities and have been used as active compounds, such as those from clove, oregano, rosemary, cinnamon, thyme, and coriander. Likewise, their derivatives are made up of isolated components that can also be exploited, including eugenol, thymol, and carvacrol. For example, Sharma et al. (2022) used essential oil from thyme to produce active P(3H-*co*-4HB)-based polyester films for bread preservation. The films were produced by solvent casting method using chloroform and incorporated 10, 20, and 30 % thyme oil. Besides promoting plasticizer effect on P(3H-*co*-4HB) matrix, the incorporation of thyme essential oil inhibited the growth of molds on the packed bread and extended its shelf life at least 5 days compared to the control.

Despite their excellent antimicrobial and antioxidant properties, the use of essential oils may be limited due to their high volatility, low water solubility, and sensitivity to oxidation. In this sense, strategies such as encapsulation and emulsion techniques can be applied to overcome these application drawbacks (Xu et al., 2020). This was proposed by Roy & Rhim (2021a) producing Pickering nanoemulsion of clove essential oil stabilized with cellulose nanofibers and incorporating them in gelatin/ agar blends by solvent casting technique. The incorporation of the emulsion was compatible with the polymer matrix, improved the mechanical properties (tensile strength) and water vapour barrier, while films showed antioxidant activity (DPPH and ABTS assays). In general, large amounts of essential oil must be incorporated into the food or packaging material to achieve the necessary antimicrobial or antioxidant effect, thereby altering its sensory characteristics. Thus, the combination of active compounds with essential oils may be attractive from a practical point of view, in order to limit its sensory impact. Roy & Rhim, (2021b) proposed the combination of cinnamon essential oil and rutin, which exhibited a synergistic effect, to manufacture antimicrobial gelatin/ chitosan-based films. Nevertheless, some essential oils, such as that obtained from the torch ginger inflorescence, can be added to starch based active films with proven antimicrobial and antioxidant actions, thus not affecting the organoleptic characteristics of the packaged meat (Marzlan et al. 2022).

Bacteriocins are another category of natural compounds that can be used as active substances. They are thermostable, low molecular weight ribosomal peptides produced by many species of microorganisms. Bacteriocins, such as nisin and lactoferrin, can display antimicrobial activity against some pathogenic bacteria and fungi, thus showing interest from the food industry (Chen et al., 2014; Verma et al., 2022). For instance, Correa et al. (2017) adsorbed nisin, the only commercial bacteriocin approved for food applications, onto

reinforced Polyhydroxybutyrate/ Poly(ε-caprolactone) films. The authors optimised the adsorption conditions of nisin on the surface of the films by studying the nisin concentration (4000, 2000, 500, 200, 100, and 50 IU.cm^{-3}), contact time (1, 5, 10, 15, 30, 60, and 120 min) and solution temperature (20, 30, and 40 °C). The optimised film (4000 IU.cm^{-3}, 40 °C, and 10 min) exhibited antimicrobial activity against *L. plantarum* CRL691 inoculated into sliced ham, showing potential application to extend the shelf life of processed meat.

Currently, considerable interest has arisen in bioactive compounds obtained from plant extracts. Generally, these materials or their derivatives, are extracted from a wide range of plants or agro-industrial residues, such as green tea, algae and microalgae, coffee husk, grape seed, pink pepper, rice straw, rice husk, hops, among others. Plant extracts are composed of a set of compounds, such as organic acids, flavonoids, phenolic compounds, sugars, tannins, and proteins, which can present excellent antioxidant and antimicrobial properties. This compositional diversity of the extracts, coupled with the possible interactions between their components and the polymer matrix, can give rise to materials with improved functional properties, such as gas and water vapour barrier, film stiffness, and ultraviolet light barrier. In this sense, the development of biodegradable food packaging materials with these active extracts represents a promising area for the food sector. Vilarinho et al. (2021) incorporated green tea extract in a PLA matrix reinforced with cellulose nanocrystals (CNC) by melting blending and compression moulding. The authors reported that PLA films with 2 % CNC and 1 % green tea extract exhibited improved water vapour and oxygen barrier properties and effectively retarded the lipid oxidation of sliced salami. Likewise, Luzi et al. (2022) used aqueous extracts from Lemma minor, a floating plant, to obtain poly(vinyl alcohol) (PVA) based active films by solvent casting. The active extract was added at 1, 5, 10, and 20 % wt. (with respect to the polymer mass) and the films were characterised as to their optical, morphological, *in vitro* antioxidant properties and used for avocado packaging. The authors reported that the active PVA films showed antioxidant, antibacterial and antifungal activity when in contact with avocado, which demonstrates the great potential of its application as active packaging.

Ficus carica L. leaves have excellent properties, including antioxidant, antifungal and antibacterial, antidiabetic, and anti-inflammatory properties. In this regard, Yilmaz et al. (2022) incorporated an active extract from *Ficus carica L.* leaves in chitosan-based films at different concentrations (2-6 % wt.). The authors reported homogeneous dispersion of the extract into the polymer matrix, which led to slightly worsened mechanical properties. Nevertheless, the incorporation of this active extract significantly improved the antioxidant and biodegradability properties of the films.

It is worth mentioning that the type of plant material, the method of extraction and its processing conditions, the composition and purification process of the obtained extracts, the

type of biopolymer matrix and film processing method, and the degree of interaction between the extract components and the polymer network, are key factors to be considered when manufacturing active packaging using plant extracts. Furthermore, extracts obtained from agro-industrial wastes and by-products represents an environmentally-friendly approach, since it produces value-added materials, reduces food losses, contributes to waste management and boosts the circular bioeconomy (Ng et al., 2015). A comprehensive study on active extracts obtained from agro-industrial wastes will be discussed in more detail in the subsection 2.3.

Table 1. Recent studies based on the use of antioxidant and antimicrobial agents incorporated into biopolymer matrices.

Source/ Active compound	Main component	Polymer matrix	Processing method	Bioactive effect	Reference
Essential oil					
Thyme	Thymol, p-cymene, γ-terpinene, carvacrol	Poly (3-hydroxybutyrate-co-4-hydroxybutyrate) (P(3H-co-4HB))	Solvent casting (chloroform)	Antimicrobial activity against total bread molds	Sharma et al. (2022)
Clove	Eugenol, phenylpropanoid, monoterpene ester, and caryophyllene	Gelatin/agar	Solvent casting (water)	Antioxidant activity using DPPH and ABTS radical scavenging assays	Roy and Rhim (2021)
Cinnamon (combined with rutin)	Cinnamaldehyde and eugenol	Gelatin/chitosan	Solvent casting	Antimicrobial activity against *E. coli* and *L. monocytogenes* / Antioxidant activity by DPPH and ABTS assays	Roy and Rhim (2021)
Torch ginger inflorescence	Bioactive compounds, 1-dodecanol, dodecanal	Starch	Solvent casting	Antimicrobial and antioxidant activities in chicken meat	Marzlan et al. (2022)
Bacteriocin					
Nisin	-	Polyhydroxybutyrate/ Poly(ε-caprolactone)	Melting blending and compression moulding	Antimicrobial activity against *Lactobacillus* inoculated in ham	Correa et al. (2017)
Phenolic compounds and plant extracts					
Ferulic, *p*-coumaric, protocatechuic acids	Phenolic compounds	Starch/gellan gum	Melting blending and compression moulding	Antimicrobial and antioxidant activities in pork meat	Hernández-García et al. (2022)

Table 1. (Continued)

Source/ Active compound	Main component	Polymer matrix	Processing method	Bioactive effect	Reference
Green tea extract	Benzoic, gallic acid, and flavanols such as epigallocatechin-3-gallate and epicatechin-3-gallate	Poly(lactic acid) (PLA)	Melting blending and compression moulding	Antioxidant activity in sliced salami	Vilarinho et al. (2021)
Lemna minor aqueous extract	low molecular weight phenols, phenolic acids and flavonoids	Poly (vinyl alcohol) (PVA)	Solvent casting	Antioxidant, antibacterial and antifungal actives in avocado fruit	Luzi et al. (2022)
Ficus carica Linn leaves extract	hydroxybenzoic acids, hydroxycinnamic acids, flavonoids and coumarins	Chitosan	Solvent casting	Antioxidant activity using DPPH radical scavenging assay	Yilmaz and Demirhan (2022)

1.3 Biodegradable multilayer systems for food active packaging applications

Biopolymers generally have worsened functional properties when compared to petroleum-based packaging materials, including gas and water vapour barrier, mechanical, and thermal properties. In this sense, researchers and industries have made efforts to overcome these drawbacks, such as the incorporation of plasticisers, crosslinkers, fillers and reinforcing agents, as well as the fabrication of multilayer polymeric systems (Wang et al., 2022). The use of one or more of these strategies to produce enhanced biodegradable packaging systems aims to further protect foodstuffs, thus preserving them from contamination and/or delaying their spoilage during storage and transportation.

Among the different approaches proposed to improve the functional properties of biopolymers, biodegradable multilayer systems have been gaining interest in research and the food sector. These multilayer packaging materials combine two or more polymer layers with different and complementary performances. The obtained material usually exhibits better functional properties than their respective individual monolayers. These multilayer systems can be designed to improve or modify packaging performance, such as food preservation and protection properties (moisture, light, gas, and odour barriers), mechanical performance, machinability, sealabillity, convenience, and promotion (Anukiruthika et al., 2020; Kaiser et al., 2017). Furthermore, the incorporation of active substances to one of the layers can bring new functionalities to the packaging system, such as antioxidant and antimicrobial properties, leading to the preservation and extension of the shelf life of packaged foods.

The multilayer manufacturing techniques can be divided into two groups: conventional techniques and techniques based on nanostructured multilayer films. Of the nanostructured multilayer techniques, the most common are layer-by-layer nanoassembly and electrohydrodynamic processing. Among the conventional techniques, the most common are (Anukiruthika et al., 2020; Kim et al., 2016):

- **Coextrusion**: is the most used method to manufacture multilayer systems, where two or more polymers are first extruded and melted separately. Then, the melted materials are combined to obtain a single material with several assembled layers.
- **Lamination**: combination of two or more layers of polymeric or non-polymeric materials (e.g., paper) using melted polymers, waxes, or adhesives between the layers. The films produced have better stability, appearance, strength, and functional properties.
- **Coating**: several coating techniques can be applied, such as extrusion coating, solvent-based coating, aqueous dispersion, waxing and hot melt coating. In general, a material is coated on the surface of another and a drying or curing step is performed on the deposited material to obtain the multilayer.

- **Thermocompression or hot-pressing:** this process is performed by compressing two or more layers of films under conditions of suitable temperature and pressure to promote good adhesion between them.

The selection of the multilayer manufacturing technique is determined considering factors, such as type and polarity of the biopolymers, adhesiveness between the layers, costs and production scalability, machinability, the desired functional performance, polymer glass transition temperatures, crystallinity, the type of food to be packaged, biodegradability, recyclability and reusability, as well as the possible changes that occur in the biopolymer layers throughout the manufacture process, storage and transport (Anukiruthika et al., 2020; Wang et al., 2022). Likewise, many aspects related to the active substances added in active multilayers must also be taken into account, including the nature of the active substance and polymer matrix, the existence of active-polymer network interaction, the profile and migration rate of the active compounds, the nature of the packaged food, manufacturing costs, combination strategies (e.g., use of fillers, plasticisers), and regulatory and legislative requirements. Table 2 shows some recent studies that have developed active multilayer systems by different manufacturing techniques and different food packaging purposes.

As commented on above, the combination of monolayers of biopolymers with complementary characteristics is the basis of multilayer manufacturing. As an example, hydrophilic biopolymers, which exhibit barrier to gases such as oxygen, can be combined with those of hydrophobic character, which generally are excellent barrier to water vapour. Furthermore, depending on the type of food to be packaged, the incorporation of the active compounds is usually carried out in the most hydrophobic matrix, since hydrophilic monolayers can dissolve on the surface of a moist food. Thus, Hernández-García et al. (2022), obtained bilayers based on thermoplastic starch containing gellan gum and a PLA:PBHV blends incorporating ferulic, *p*-coumaric, and protocatechuic acids. The respective monolayers were obtained by melt blending and compression moulding techniques and adhered via thermocompression in a hydraulic plate press. The authors reported significant improvements in mechanical and barrier properties and the developed bilayer material were effective in reducing lipid oxidation and microbial growth of packaged pork throughout cold storage. Andrade et al. (2022), who reported PLA/PVA/PLA-based three-layer systems incorporating carvacrol or ferulic acid in the PVA interlayer, in which carvacrol was or was not encapsulated in lecithin liposomes due to its volatility and thermal sensitivity. All multilayer treatments showed similar tensile properties to the PLA film and markedly improved barrier properties in comparison with the respective monolayers. The active multilayer bags controlled the microbial growth of beef meat during cold storage. Furthermore, the meat samples packed with the active multilayer bags did not reach the limit for total viable counts for 17 days, while the control samples achieved this limit after three days of storage.

Tampau et al. (2018) used electrohydrodynamic processing technique to electrodeposit electrospun poly-(ε-caprolactone) (PCL) mats incorporating carvacrol on thermoplastic starch (TPS) films to obtain multilayer films (TPS/PCL/TPS) with enhanced properties. PCL fibres with carvacrol were effective at controlling *E. coli* growth and exhibited release of the active compound in less polar food simulants (50 % ethanol and isooctane). Likewise, carvacrol-loaded mats in multilayer films decreased water vapour permeability and showed antimicrobial activity. Jiang et al. (2022) proposed the lamination of myofibrillar protein films incorporated with clove essential oil (at 0, 3, 6, 9 % wt.), as inner layer, and gelatin films, which provides good optical and mechanical properties, as well as moisture resistance. Each film was prepared by solvent casting technique and the adhesion step was conducted by heating the films using a fan oven followed by compression in a physical tester. The functional properties of the obtained bilayers were evaluated in terms of optical, mechanical, structural and release properties in different food simulants. The multilayer films exhibited better barrier properties with respect to monolayers, while they were less extensible as the essential oil was incorporated. Fourier transform infrared analysis revealed the alteration in the characteristic band of amide bonds, suggesting interactions between the protein and the phenolic compounds. Furthermore, the antioxidant capacity was validated, being the release of antioxidant compounds more effective in 50 % ethanol (food simulant of fatty foods).

The adhesiveness between the layers is a mandatory aspect to obtain a multilayer material with potential application in food. In this way, Xia et al. (2019) proposed a blend of zein and gelatin, to produce zein (outer layer)/zein:gelatin (middle layer)/gelatin (inner layer) multilayer films by solvent casting technique. During the polymer dispersion step, tea polyphenol was added to the zein:gelatin and gelatin dissolutions at a mass ratio of 2.5 and 7.5 % wt. The films were characterised in terms of their morphological, optical, water vapour barrier, contact angle, mechanical properties, and release kinetics of phenolic compounds. Finally, the multilayer films were used to package fresh cut fruits, typically kiwifruit, avocado, and banana. These films exhibited excellent interlayer adhesion, improved water vapour barrier, and prolonged phenolic release profile. When in contact with fresh cut fruit, multilayer systems were effective at controlling weight loss, preventing rapid browning, and inhibiting bacterial deterioration.

Table 2. Recent studies based on development of active multilayer systems by different manufacturing techniques.

Multilayer biopolymer matrices	Film preparation method	Active compound	Application/properties	Reference
Starch-PLA:PHBV bilayers	Melt blending and compression moulding / Thermocompression	ferulic, *p*-coumaric or protocatechuic acid	The films showed improved barrier and mechanical properties. The active bilayers exhibited antioxidant and antimicrobial action and extended the shelf life of packed pork meat	Hernández-García et al. (2022)
PLA/PVA/PLA	Melt blending and compression moulding / Thermocompression	Carvacrol or ferulic acid	The multilayers films exhibited mechanical properties similar to the PLA monolayer Barrier capacity was markedly improved The developed multilayers were effective to preserve packaged meat	Andrade et al. (2022)
PLA-starch bilayers	Melt blending and compression moulding / Thermocompression	Cinnamaldehyde (incorporated into PLA layer)	The films exhibited improved mechanical performance and better oxygen and water vapour barrier properties.	Muller et al. (2017)
Starch/PCL/Starch	Electrospun PCL fibre mats encapsulating carvacrol	Carvacrol	The loaded carvacrol-mats were effective at controlling E. coli growth The multilayer films exhibited reduced water vapor permeability and similar release of carvacrol	Tampau et al. (2018)
Zein/Zein-gelatin/gelatin	Solvent casting	Tea polyphenol	The films showed improved mechanical and water barrier capacity. The multilayer films reduced weight loss and inhibited bacterial growth in kiwifruit, avocado and banana	Xia et al. (2019)
Gelatin/myofibrillar proteins	Solvent casting / Thermocompression	Clove essential oil	The bilayer exhibited improved barrier properties Protein-phenolic interactions were elucidated by Fourier transform infrared The active films exhibited controlled release in different food simulants	Jiang et al. (2022)

2. Obtaining lignocellulosic fractions from agro-industrial residues for reinforced and active food packaging purposes

2.1 The problematic generation of agro-industrial wastes and their potential valorisation

Waste consists of any unwanted material that is no longer suitable for its use. Wastes are present in natural ecosystems, including gases (oxygen, carbon dioxide), dead organic matter, as well as products from human activity, such as municipal waste, industrial waste, vegetable residues, and agro-industrial wastes. Due to the world's growing population, the constant demand for food and intensive agricultural practices, large quantities of agro-industrial wastes are produced worldwide. In fact, Shinde et al. (2022) report that world production of crop residues reached more than 5000 Mt in 2020 and 2021. In particular, most agro-industrial residues are improperly disposed of, being burned in the harvest fields or incorrectly left in landfills. This inadequate agro-industrial waste management greatly affects the environment, resulting in severe pollution, greenhouse gas emissions, climate change, economic losses, as well as negatively affecting human and animal health (Sadh et al., 2018; Singh & Brar, 2021). Thus, many waste management alternatives and approaches focused on reducing, reusing, and recycling them have been currently proposed, always aiming to decrease environmental impact and stimulate the circular bioeconomy (Beltrán-Ramírez et al., 2019). As shown in Figure 4, agricultural wastes can be commonly managed as livestock feed, bedding, biochar production, on-farm disposal (*in situ* incorporation and composting), mushroom cultivation, as well as valorisation (Shinde et al., 2022).

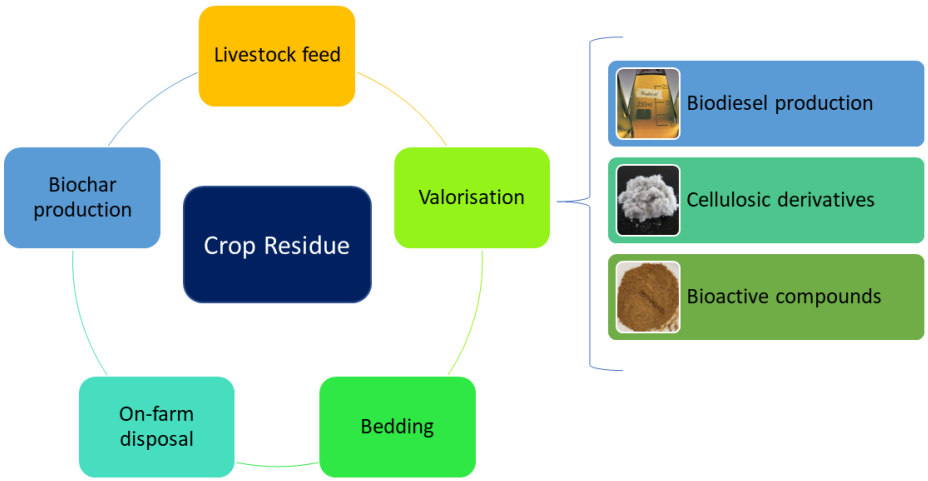

Figure 4. Possibilities for the correct and environmentally-friendly disposal of agro-industrial waste.

Agro-industrial residues are low-cost, highly available, sustainable materials that can be exploited as renewable sources for different purposes. In general, these agro-industrial

residues are composed mainly of lignocellulosic biopolymers, including cellulose, hemicellulose, and lignin. As shown in Figure 5, the lignocellulosic fraction found in these waste biomasses consists of a complex matrix assembled by semicrystalline cellulose microfibrils, as the primary fibre component, linked to a cementing matrix composed of hemicellulose and lignin (Chen et al., 2011). The proportion and properties of each lignocellulosic fraction varies according to the biomass source and its plant variety (Table 3).

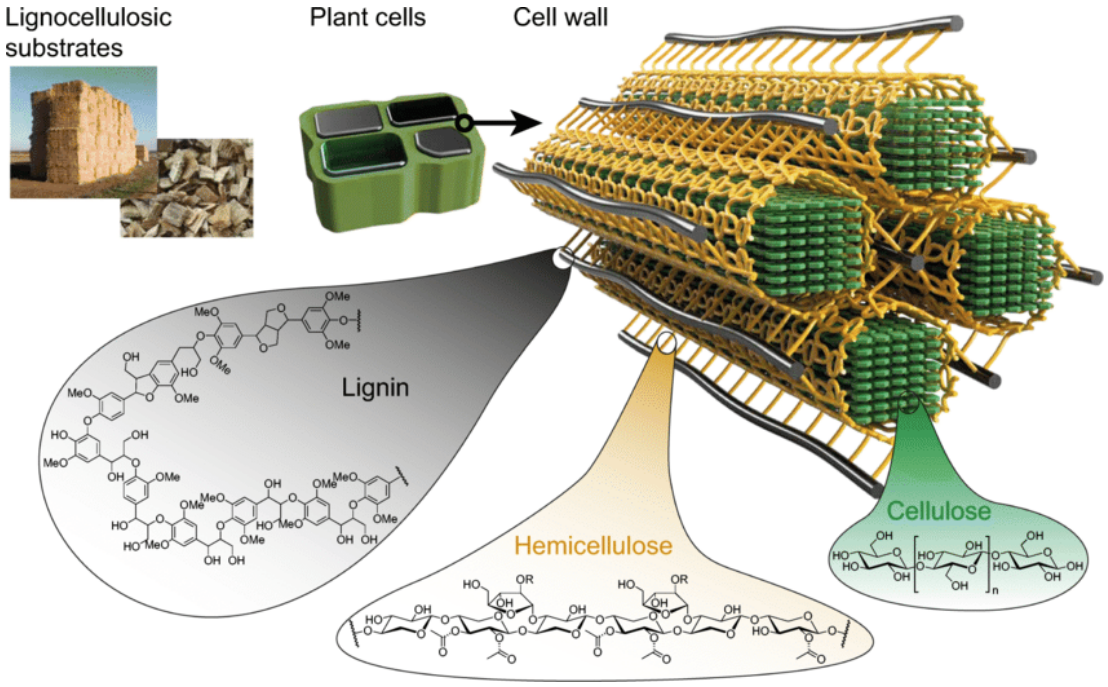

Figure 5. Representative scheme of the lignocellulosic fractions found in plant biomasses (Brethauer et al., 2020).

Table 3. Lignocellulosic composition of different biomass sources.

Source	Cellulose (% wt.)	Hemicellulose (% wt.)	Lignin (% wt.)	Ashes (% wt.)	Reference
Rice straw (*J. Sendra*)	37	19	21	17	Freitas et al. (2022)
Rice straw (*Akitakomachi*)	34	16	11	9	Seo & Sakoda (2014)
Banana peduncle	73	11	15	3	Manimaran et al. (2020)
Jute bast fibres	62	22	14	0.5	Dhali et al. (2021)
Rice husk	34	17	21	16	Collazo-Bigliardi et al. (2018)
Coffee husk	35	18	23	1	
Olive leaves	6	4	40	15	Garcia-Maraver et al. (2013)
Sugarcane bagasse	53	21	25	2	Mkhize et al. (2016)
Corncob of blue corn	28	40	29	2	Toribio-Cuaya et al. (2014)
Corncob of white corn	29	36	26	2	
Water hyacinth	22	23	27	20	
Sugarcane bagasse	44	33	17	5	
Pineapple crown	17	19	24	5	Pereira et al. (2021)

Cellulose is the most abundant polysaccharide in nature, where it is found as a structural constituent in the cell wall of numerous plants and algae, as well as synthesized by several species of bacteria (Sticklen, 2008). Cellulose is considered as a highly promising biopolymer from renewable source due to its high availability in nature, biodegradability, stiffness, and biocompatibility. It is formed by a linear structure with 100-1000 repeating units of D-glucose linked by 1,4-β-glycosidic bonds. Due to their chemical structure, the D-glucose units have strong inter- and intramolecular hydrogen bonds between the hydroxyl groups and the oxygen atoms, which leads to the highly crystalline organisation of the cellulose chains (Singh & Brar, 2021). Nonetheless, the structural configuration of cellulose chains has amorphous regions between the crystalline zones composed of cellulose chain fragments without hydroxyl groups. These amorphous zones are easily hydrolysed by acids to give rise to a highly crystalline material known as cellulose nanocrystals. In general, cellulose is insoluble in polar and most of the apolar solvents as a result of its high crystallinity, which limits its use in some industrial applications, such as thermoforming and dissolution. Nevertheless, different strategies have been proposed to solubilize and/or make cellulose compatible with other materials, such as: use of organic salts known as ionic liquids (imidazolium-based solvents) (Swatloski et al., 2002); chemical modification of cellulose to produce its derivatives (organic and inorganic esters and ethers, silylation, grafting); use of trifluoracetic acid; regeneration of cellulose (rayon, cellophane); preparation of blends with other biodegradable polymers (Gonçalves de Moura et al., 2017; Singh & Brar, 2021).

Hemicellulose is the second most abundant biopolymer in plant biomass after cellulose, which consists of an amorphous heteropolysaccharide with side chains of D-monosaccharides (except L-arabinofuranose), including glucose, galactose, mannose, xylose, arabinose, 4-O-methyl glucuronic acid, and galacturonic acid residues (Brunner, 2014). Hemicelluloses are linear polymers, except for single-sugar side chains and acetyl substituents, and exhibit much smaller and random skeletal structure than cellulose (Bajpai, 2018). Depending on the type of the main sugar in the hemicellulose structure, they can be classified into four general groups, typically xyloglycan (xylan), mannoglycan, xyloglucan, and mixed-linkage β-glucan. The hemicelluloses are associated with each other through covalent and hydrogen bonds, while they are linked via cinnamate ester-acid linkage with the lignin fraction and by extensive hydrogen bonding with cellulose chains (Machmudah et al., 2017). Hemicelluloses is a much more soluble plant fraction than cellulose and can be extracted at temperatures of about 180 °C, by applying alkali treatment (NaOH, KOH), as well as using enzymes (Li et al., 2013). Hemicellulose fractions have aroused great interest of researchers and several industrial areas, such as cosmetic, biomedical, and food packaging applications, due to their rheological properties, film forming capacity, biodegradability, availability, compatibility, as well as their antioxidant and/or antimicrobial potential (Ruthes et al., 2017).

Lignin is a highly branched, amorphous and complex biopolymer. It comprises a high molecular weight fraction that has the adhesive function and structural rigidity to hold the fibres and hemicellulose matrix together (Bajpai, 2018). The chemical structure of lignin contains many methoxyl groups, phenolic hydroxyl groups and terminal aldehyde groups on the side chains. It contains hydroxyphenylpropane units, including trans-*p*-coumaryl alcohol, coniferyl alcohol, and sinapyl alcohol, which are linked by ether and carbon-carbon bonds (Brunner, 2014; Wahyudiono et al., 2013). Lignin has three types of phenylpropanoids linked by several characteristic bonds (β-O-4, β-5, and β-β'), including *p*-hydroxyphenyl, guaiacyl, and syringyl. These structures with aromatic rings can exhibit potent antioxidant and antimicrobial activity, showing commercial interest to be applied as bioactive compounds in food, packaging, and pharmaceutical industry (Zhang & Naebe, 2021).

In this sense, due to the rich composition in lignocellulosic fractions, combined with its renewability, biodegradability, and availability, agro-industrial residues represent an interesting alternative for obtaining value-added materials, such as valorised cellulosic fractions and bioactive compounds. Furthermore, different strategies, techniques and extraction approaches have been proposed, which aim to extract materials with different industrial and research applications, while contributing to circular bioeconomy and environmental impact reduction.

2.2 Isolation of cellulosic fractions from agro-industrial wastes

Cellulosic fractions, such as cellulose fibres (CF), microfibrillated cellulose (MFC), nanofibrillated cellulose (NFC), and cellulose nanocrystals (CNC), can be isolated from many natural sources of agro-industrial residues and by-products, such as rice straw, coffee and rice husks, sugar cane bagasse, cotton, banana stalks, pineapple crown and bast fibres, among others. Regardless of the desired cellulosic fraction, the isolation process is focused on the elimination of non-cellulosic components and/or amorphous regions of the cellulosic fractions, including hemicellulose, lignin, waxes, proteins, sugars and ashes (Boonterm et al., 2016). To this end, different strategies and methods have been proposed to purify natural fibres for various research and industrial purposes.

In general, the processes described in the literature and those used at industrial scale consist of the preparation of cellulosic biomass followed by the purification steps (Figure 6) (Ng et al., 2015; Shen et al., 2022). The type of cellulosic material preparation, as well as the pathway in the purification steps, including pre-treatments, the processing-extraction conditions, and combinations of methods, depend directly on the lignocellulosic source, as well as the type of purified micro- or nanocellulosic material desired.

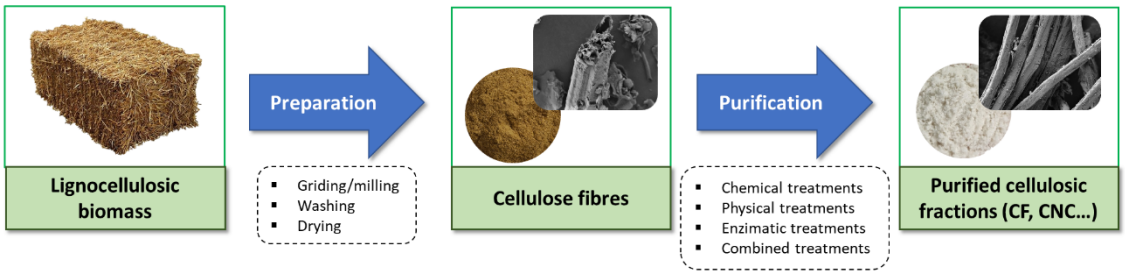

Figure 6. General steps in the isolation of cellulosic fractions from lignocellulosic biomasses.

The preparation of lignocellulosic biomass consists of procedures performed prior to the purification steps. These operations are conducted in order to standardise all the plant material, increase the efficiency of the cellulose extraction, and eliminate interferences in the purification steps. In this sense, the raw biomass can be sieved, ground and cut in suitable equipment, such as grinding machines, vibratory sieving equipment, and cutters (Ng et al., 2015; Thiripura Sundari & Ramesh, 2012). The reduction and uniformity of the particle size of the material promote an increment in the swelling capacity and the contact surface between the chemical reagents/solvents and the non-cellulosic components, thus contributing to improve the purification process. Also, washing the fibre material before purification allows the removal of dirty materials from the biomass surface and water extractable components, which can also hinder the contact between solvent and biomass sample (Ng et al., 2015; Zimmermann et al., 2010).

The next stage in the cellulose extraction process is the purification step, which consists of eliminating the non-cellulosic components of the biomass, such as hemicellulose, lignin, waxes and ashes (Zhang et al., 2014). In general, cellulose purification techniques and strategies can be divided into physical and chemical methods. Physical techniques transfer high amounts of energy in the form of shear, impact, and heat to the plant material, aiming to disintegrate and disrupt the plant particles and tissue by breaking interactions between amorphous components and the cellulose matrix. Physical methods include ball milling, stream explosion, ultrasonication, subcritical water extraction, high pressure steaming, ionized gas (plasma or corona), and laser (Chen et al., 2011; Shen et al., 2022). Chemical methods use chemical reagents in a biomass dispersion to hydrolyse, solubilise and/or oxidise components or amorphous regions of the plant tissue, thus obtaining a more purified material. Usually, one or more steps of chemical treatments are applied, sometimes in combination with the physical methods. This depends on the biomass source, the processing conditions, degree of purification desired and the type of cellulose (micro- or nanoscale). Strategies based on chemical methods can be alkaline treatments (e.g., NaOH, KOH), organosolv treatment (organic solvent combined with strong acids: e.g. acetic acid, acetone, methanol plus hydrochloric or sulfuric acid), acid hydrolysis (e.g., H_2SO_4), oxidative hydrolysis (e.g.., NaClO, 2,2,6,6-Tetramethylpiperidine-1-oxyl (TEMPO), and enzymatic hydrolysis (e.g., endoglucanase, exoglucanase, and β-1,4-glucanase) (Ng et al., 2015; Shen et al., 2022).

Table 4 gathers recent studies obtaining different cellulosic fractions at micro and nanoscale by applying different methods and purification processes, as well as the biomass source or agro-industrial residue, the extraction conditions, and the main characteristics of the cellulosic materials obtained, including particle size, crystallinity index (CI), and aspect ratio. Thus, the most common steps used in the process of obtaining cellulosic fractions (CF, MFC, NFC, CNC) from agro-industrial wastes are: preparation (milling, sieving, washing, dewaxing), alkaline treatment, bleaching step, and acid hydrolysis (Abu-Thabit et al., 2020; Debnath et al., 2021). The alkaline step treats the plant biomass with strong alkaline solution (e.g., NaOH, KOH) to eliminate a substantial fraction of hemicellulose, silica, pectin, and waxes, as well as a part of the lignin present in the cellulosic matrix. This step is performed as many times as necessary, being dependent on each biomass source. After that, the material is washed with water to separate the alkali soluble from the more purified cellulosic fraction (Shen et al., 2022). The next step is bleaching, in which the material previously subjected to alkaline solution is treated with an bleaching solution based on oxidative chemicals, including chlorine-based solutions (NaClO, ClO_2), a piperidine nitroxide radical compound (TEMPO), or an eco-friendlier peroxide-based solution such as hydrogen peroxide (H_2O_2) (Ho et al., 2019; Pongchaiphol et al., 2021). This step oxidises the aromatic rings present in the lignin structure and can hydrolyse a fraction of the remaining hemicellulose, giving rise to a cellulosic material with high whiteness and brightness, the so-called bleached cellulose fibre. In the case of micro- or nano-scale cellulose preparation, a stage of acid hydrolysis is conducted to eliminate the amorphous fractions present in the cellulose, exposing the crystalline zones, or to eliminate remaining fractions of low molecular weight lignin and hemicellulose. After the acid hydrolysis, the insoluble fraction is washed with water to remove the excess of acid and soluble components, and then proceed to the next steps of the process. Subsequent steps in the cellulose purification process can be dialysis, mechanical disintegration, high pressure homogenization, ultrasonication or drying (drying machine, freeze-drying, spray drying). It is worth mentioning that the type of purification techniques and combinations between them, the order of these steps, as well as the process conditions and the chemical reagents used in the pulp purification are directly related to the biomass source, as well as to the desired cellulosic fraction (purity, particle size, degree of crystallinity, mechanical and thermal properties, and degree of stability and chemical reactivity).

As an example, Collazo-Bigliardi et al. (2018) successfully extracted CF and CNC from rice and coffee husks by applying alkaline treatment (2 % wt. NaOH), followed by a bleaching step using $NaClO_2$ under acidic conditions (acetate buffer), and acid hydrolysis (H_2SO_4) step to remove amorphous zones from the cellulose structure. All materials were evaluated as to their thermal properties, crystallinity, morphologies, chemical composition and reinforcing capacity in thermoplastic starch-based films. The authors reported a progressive increase of crystallinity and thermal stability of the cellulosic fractions as the process of amorphous components elimination advanced, corroborating the efficiency of the method employed.

Moreover, these CNC fractions were used to improve the mechanical properties of the starch-based films.

Greener alternative methods to the traditional ones have been proposed in order to reduce the amount of chemical reagents used in the extraction process of cellulosic fractions. In general, physical techniques represent an interesting alternative to replace chemical methods, since they have lower environmental impact, can be industrially scalable, reduce process time, and give rise to materials with industrial application. Among the physical methods, subcritical water extraction (SWE) is a promising technique that uses liquid water under subcritical conditions (temperature above boiling point and pressure higher than atmospheric pressure) to solubilise, hydrolyse, and leach out amorphous components from cellulose matrix. In this regard, Requena et al. (2019) proposed to replace the alkaline treatment by SWE (160 °C, 30 min) to obtaining CF and CNC from rice husk. The results showed that the applied method was as efficient as the conventional alkaline method at eliminating a substantial fraction of hemicellulose present in the lignocellulosic matrix, giving rise to CF and CNC with similar thermal, nano- and microstructural and morphological characteristics.

Thermal steam explosion has also been proposed as a substitute for alkali treatment to obtain purified cellulosic fractions. This method applies steam at high temperatures and pressures, followed by a mechanical breakdown of the material through a powerful explosion in a collection tank, thus thermodegrading amorphous components (lignin and hemicellulose), as well as breaking the cellulose fibre bundles (Iroba et al., 2014). Boonterm et al. (2016) applied steam exploded treatment on rice straw to obtain more purified cellulose fibres in comparison with the alkaline method. The first batch applying steam exploded was performed at 17 bars, 205 °C for 5 min. The second batch was conducted combining different temperature and pressure for 5 min as follows: 13 bar (192 °C), 15 bar (200 °C) and 17 bar (205 °C). The authors reported that the proposed method led to a progressive decrease in the diameter and length of the fibres, with elimination of lignin and hemicellulose from the cellulosic matrix similar to the alkaline method. Although the authors achieved purified cellulose fibres with similar characteristics and properties to those of the alkaline treatment, they pointed out the high energy consumption of the proposed alternative method was the main issue that should be taken into account to obtain cellulose from rice straw.

Table 4. Recent studies for obtaining micro and nano-cellulosic fractions by applying different purification methods.

Source	Fraction cellulosic	Method	Properties	Reference
Rice husk	Cellulose fibres (CF) and cellulose nanocrystals (CNC)	**T1**: Alkaline treatment (4.5 % NaOH) followed by bleaching step (acetate buffer, NaClO2, water), and acid hydrolysis (H2SO4, 64 %) **T2**: Subcritical water extraction (160 °C, 30 min) followed by bleaching step (acetate buffer, $NaClO_2$, water), and acid hydrolysis (H_2SO_4, 64 %)	- Diameter: 2.5-8 nm (both CNCs) - Length: 105-465 nm (CNCs T1); 135-495 nm (CNCs T2) - Aspect ratio: 14-162 (CNCs T1); 50-178 (CNCs T2) - CI: 71 %, 81 % (CF and CNC T1); 68 %, 74 % (CF and CNC T2)	Requena et al. (2019)
Rice straw	CF	**T1**: Alkaline treatment (4.5 % NaOH) followed by bleaching step (acetate buffer, NaClO2, water) **T2**: Combined ultrasound (30 min)-reflux heating (100 °C, 60 min) followed by bleaching step (acetate buffer, $NaClO_2$, water), and acid hydrolysis (H_2SO_4, 64 %)	- Diameter: 100-400 µm for both CF (more than 60% of the particles) - Length: 6-12 µm for both CF (more than 60% of the particles) - Aspect ratio: 5-50 for both CF (more than 60% of the particles) - CI: 69 % (CF T1); 60 % (CF T2)	Freitas et al. (2022)
Rice straw	CF	**T1**: Alkaline treatment (NaOH 1, 5, 10, 15 % NaOH, 30 min) **T2**: thermal steam exploded treatment (first batch: 17 bars (205 °C) for 5 min/ second batch: 13 bars (192 °C), 15 bars (200 °C) and 17 bars (205 °C)	- Diameter: 170 µm (T1); 260, 160, 110 µm (13, 15, 17 bars, 5 min T2) - Length: 26 µm (T1); 36, 31, 8 µm (13, 15, 17 bars, 5 min T2) - Aspect ratio: 150 µm (T1); 140, 200, 73 µm (13, 15, 17 bars, 5 min T2)	Boonterm et al. (2016)
Rice husk and Coffee husk	CF and CNC	Alkaline treatment (2 % NaOH) followed by bleaching step (acetate buffer, $NaClO_2$, water), and acid hydrolysis (H_2SO_4, 64 %)	- Diameter: 10 µm (CF); 310 nm (rice husk CNC); 310 nm (coffee husk CNC) - Length: 60-570 µm (both CF); 39 nm (rice husk CNC); 20 nm (coffee husk CNC) - Aspect ratio: 10-20 (both husk CNC fractions) CI (%): 50%, 90 % (CF and CNC rice husk); 52 %, 92 % (CF and CNC coffee husk)	Collazo-Bigliardi et al. (2019)

Table 4. (Continued)

Source	Fraction cellulosic	Method	Properties	Reference
Walnut shell	CNC	Alkaline treatment (4.5 % NaOH) followed by bleaching step (acetic acid, $NaClO_2$ 1.7 % wt.), and acid hydrolysis (H_2SO_4, 64 %)	- Diameter: 130 nm (equivalent spherical diameter) - CI: 60 %	Hemmati et al. (2018)
Pineapple crown	CF	**T1**: Residue insoluble alcohol (Soxhlet – absolute ethanol, 100 °C, 24h **T2**: Acetosolov extraction (acetic acid 93 % + 0.3 % HCl, 3h, 110 °C) **T3**: Alkaline treatment (AT): NaOH 4 %, 70 °C, 1 h **T4 (1B)**: Bleaching AT fibre (NaOH 4 % + H_2O_2 30 % (v/v)) **T5 (2B)**: Bleaching B1 fibre (NaOH 4 % + H_2O_2 30 % (v/v)) **T6 (2B/KOH)**: Alkaline treatment of 2B fibre KOH 6 %, 80 °C, 1 h	- Diameter: 2.4-6.5 µm (1B, 2B, 2B/KOH fibres) - CI: 78 % (AT), 83 % (1B), 83 (2B), 86 % (2B/KOH).	Pereira et al. (2021)
Jute bast fibre	CF, cellulose nanofibres (CNF), and CNC	**Bleached CF**: Alkaline treatment (10 % NaOH, 50 °C, 4h) + acid treatment (2 M HCl, 80 °C, 2h) followed by bleaching step (acetic acid, NaOH, $NaClO_2$ 1.7 % wt.) **CNF**: mechanical disintegration using a rotor-stator followed by high-pressure homogenization, ultrasonicaton, and freeze-drying **CNC**: acid hydrolysis (H_2SO_4, 64 %, 45 °C, 60 min), dialyzed, and freeze-dried.	- Diameter: 12-15 µm (bleached CF), 6-48 nm (CNF), 10 nm (CNC) - Length: 196 nm (CNC) - CI: 54 % (bleached CF), 67 % (CNF), 76 % (CNC).	Dhali et al. (2021)
Tea stalk	Microcrystalline cellulose (MCC) and nanocellulose crystals (NCC)	H_2O_2 + acid acetic (60 °C, 24 h) followed by acid hydrolysis (65 % H_2SO_4, 40-50 °C, 90-150 min) + Dialysis + ultrasonication	- Diameter: 4-8 nm (NCC) - CI: 61.3 % (MCC), 82 % (NCC)	Guo et al. (2020)

In the last decades, cellulose fractions derived from agro-industrial residues and by-products have been widely exploited in many research and industrial fields, including applications in the polymer, biopolymer and packaging industries (e.g., paper production, reinforcing agents in polymeric composites), environment (e.g., adsorption and flocculation of contaminants, filtration membranes), building and automotive materials, pharmaceutical and biomedical applications (e.g., drug delivery), and other emerging sectors (e.g., cellulose aerogels, catalysts in chemical reactions) (Debnath et al., 2021; Shen et al., 2022). Of the strategies for agro-industrial waste valorisation, the incorporation of its cellulose and derivatives as fillers in biopolymer matrices has been highlighted as an alternative to enhance their properties.

The presence of cellulose in micro or nanoscale as dispersed phase in the biopolymer matrix can markedly improve the functional properties of packaging, such as mechanical, light blocking, gas and water vapour barrier capacity, surface, and thermal properties. The ability to transfer reinforcement from the cellulosic fractions to the polymer network is directly associated with the intensity of fibre entanglement (micro- or nanoscale), the intensity and type of fibre-polymer interactions, as well as the ratio of water adsorption, which promotes material plasticisation (Freitas et al., 2022). As shown in Table 5, a large number of studies have been reported exploiting the potential application of cellulosic fractions from agro-industrial residues, plant sources, and by-products as environmentally-friendly and renewable reinforcing agents in biopolymer matrices.

Due to their high crystallinity and rigidity, cellulosic fractions have demonstrated excellent properties as reinforcements in biopolymer-based films. Furthermore, the large amount of OH groups in the cellulose structure confers extensive hydrophilicity to the cellulosic material, which leads to excellent compatibility and entanglement with more polar and hydrophilic matrices. This was demonstrated by Ilyas et al. (2019), who prepared sugar palm starch-based films incorporated with NFC (0-1.0 % wt.) extracted from sugar palm via solvent casting technique. Microscopy images showed an excellent dispersion of NFC in the starch matrix. Compared to neat starch film, films incorporating 1.0 % wt. of NFC increased water resistance, tensile strength (~120 %) and elastic modulus (~124 %).

In order to optimize the interactions and compatibility between the cellulosic fractions and hydrophobic biopolymer matrices, several alternatives have been proposed. The preparation of polymer blends, incorporation of plasticisers, compatibilisers, as well as the surface modification of cellulose are strategies towards obtaining biodegradable cellulosic fillers with optimised reinforcement properties. As an example, Arrieta et al. (2015) obtained CNC from cotton and proposed a cellulose surface modification using an acid phosphate ester of ethoxylated nonylphenol. The authors compared the reinforcing capacity of the CNC and the modified CNC in a PLA-PHB blend (75:25). The films were characterised in terms of their morphological, crystallinity, FTIR, thermal, mechanical, oxygen barrier, and contact angle

properties. The results showed that the cellulose surface modification led to a polymer matrix better compatibilized with CNC, exhibiting better thermal stability, oxygen barrier capacity and UV-light blocking.

Table 5. Recent studies in the preparation of films based on biopolymers incorporated with different cellulosic fractions as reinforcing agents.

Source	Cellulosic fraction	Biopolymer matrix	Main results	Reference
Sugar palm	Nanofibrillated cellulose (NFC)	Sugar palm (*Arenga pinnata (Wurmb.) Merr*) starch (Solvent casting method)	Excellent compatibility (by microscopy) and extensive hydrogen bonds (by FTIR analysis) between NFC and the starch matrix. The films with 1 % wt. NFC exhibited improved water resistance and an increase in tensile strength and Young' s modulus of 120 % and 124 %, respectively.	Ilyas et al. (2019)
Ramie fibres	Cellulose nanofibres (CNF)	Cassava starch (Solvent casting method)	Starch based films with 10% of CNFs showed the highest tensile strength (13 MPa vs. ~2 MPa control film) and crystallinity index (31 % vs. 18 % control film). The incorporation of CNFs improved the thermal stability of the films.	Syafri et al. (2018)
Rice straw	Cellulose fibres (CF)	Maize starch (TPS) and maize starch modified by dry heating (TPSDH) (Melt blending and compression moulding)	Thermo-compressed films with 3 % wt. CFs were more rigid (~215 % for TPS and ~207 % for the TPSDH), more resistant to break (~100 % for TPS and ~60 % for TPSDH), but also less extensible (~53 % for TPS and ~78 % for TPSDH). The composite films also showed a decrease in water vapor (~15 %), oxygen permeabilities (~30 %), and water solubility.	Freitas et al. (2021)
Rice straw	Cellulose nanocrystals (CNC)	Polyvinyl alcohol/chitosan (Solvent casting method)	The nanocomposite films exhibited similar transparency to the control film, suggesting good CNC and polymer matrix compatibility. The incorporation of CNC increased the tensile strength and thermal stability of the films. Moreover, the films with CNC showed good antifungal and antibacterial activity.	Perumal et al. (2018)
Cotton	CNC and modified CNC (acid phosphate ester of ethoxylated nonylphenol)	Poly(lactic acid) (PLA)-poly(hydroxybutyrate) (PHB) (twin-screw extrusion)	The incorporation of 5% wt. of both CNCs improved the thermal stability of PLA-PHB films. Nevertheless, the modified CNC showed better dispersion and compatibility in the PLA-PHB matrix, leading to an improvement in oxygen permeability, extensibility, and UV light blocking effect.	Arrieta et al. (2015)

Table 5. (Continued)

Source	Cellulosic fraction	Biopolymer matrix	Main results	Reference
Filter paper	Formyl cellulose (FC)	PLA (Solvent casting method)	The PLA films reinforced with FC showed improved compatibility with respect to the control PLA film. The PLA/FC film with 1 % wt. of FC exhibited improved water vapour barrier properties, as well increase in the tensile strength and Young's modulus of about 48 % and 346 %, respectively.	Long et al. (2021)
Rice and coffee husks	CNCs	Maize starch (TPS) (Melt blending and compression moulding)	Both CNCs exhibited good compatibilisation and entanglement with the polymer matrix, leading to a less extensible material. The rice husk and coffee husk CNCs increased the Young's modulus approximately 180 and 120 % with respect to the TPS film.	Collazo-Bigliardi et al. (2018)
Areca nut husk	CNCs	PVA (Solvent casting method)	The PVA/chitosan composite films exhibited good compatibility with the CNCs, which was confirmed by micrographs and transparency of the films. The films incorporated with 3 % wt. CNCs showed increase of tensile strength by about 20 % (with respect to the control film), as well as the films exhibited good antimicrobial activity against foodborne pathogenic bacteria and postharvest pathogenic fungi.	Perumal et al. (2022)
Pea hull	CNCs	Carboxymethyl cellulose (CMC) (Solvent casting method)	The FESEM images of the CMC/CNC-based composite films revealed good dispersion of the CNCs and homogeneity with the polymer matrix up to the limiting concentration of 5 % wt. CNC. The films were mechanically resistant (increase of 50% in tensile strength), UV light barrier, thermal stability, and water vapour barrier (53% reduction). Furthermore, the films were successfully used to decrease the water loss of red pepper throughout storage.	Li et al. (2020)
Coconut shells	CNFs	PVA (incorporated with linseed oil and lemon oil) (Solvent casting method)	The films exhibited improved thermal and mechanical properties compared to control PVA films. The active nanocomposite films showed excellent antioxidant properties and antimicrobial activity against food pathogens, as well as good biodegradability.	Arun et al. (2022)

2.3 Extraction of bioactive compounds from agro-industrial wastes

The agro-industrial residues and wastes represent an interesting source of active compounds at low cost. The bioactive character of the obtained extracts comes from the extensive set of phenolic compounds extracted from the lignin and hemicellulose fraction present in the plant matrix, such as *p*-hydroxybenzoic acid and its derivatives, as well as hydroxycinnamic acids and their derivatives, as shown in Figure 7 (Farhoosh et al., 2016). Likewise, tannins, flavonoids (e.g., flavonols, anthocyanidins, isoflavones, flavonones), and stilbenes are also classes of phenolic compounds that may also be present in high concentrations in the plant matrix.

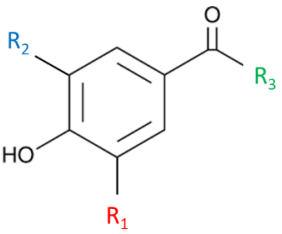

	R_1	R_2	R_3
p-Hydroxybenzoic acid	H	H	OH
Protocathecuic acid	OH	H	OH
Gallic acid	OH	OH	OH
Vanillic acid	OCH_3	H	OH
Ethyl protocatechuate	OH	H	OCH_2CH_3
Syringic acid	OCH_3	OCH_3	OH
Methyl *p*-hydroxybenzoate	H	H	OCH_3
Methyl gallate	OH	OH	OCH_3

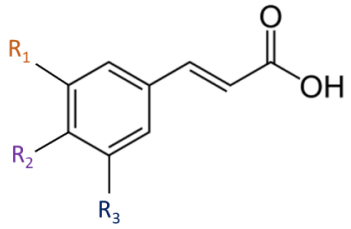

	R_1	R_2	R_3
p-coumaric acid	H	OH	H
Caffeic acid	OH	OH	H
Ferulic acid	OCH_3	OH	H
Sinapic acid	OCH_3	OH	OCH_3

Figure 7. Molecular structure of *p*-hydroxybenzoic acid, hydroxycinnamic acid, and their derivatives.

The powerful antioxidant character of these phenolic compounds is associated with their capacity to donate electrons or hydrogens, reducing, and neutralising the free radicals present in food. Likewise, the phenolic compounds present in plant extracts can act as secondary antioxidants by decomposing the hydroperoxyl radicals formed, thus delaying the initial phase of oxidation. Furthermore, Miklasińska-Majdanik et al. (2018) states that the mechanisms of antibacterial action of phenolic compounds are related to their interaction with the cytoplasmic membrane; ability to inhibit bacterial virulence factors, such as toxins and enzymes; and efficiency in suppressing the formation of bacterial biofilms.

In general, extracts from plants and agro-industrial residues are obtained by applying extraction techniques focused on the maximum leaching out of bioactive compounds. The chosen extraction technique as well as the possible modifications of the process parameters are highly dependent on the plant raw material, the target bioactive components, and possible interferents and contaminants present in the obtained extracts (Alara et al., 2021).

Likewise, processing factors, including type of extraction solvent, pre-treatments, temperature, pressure and extraction times, also affect the extraction efficiency and the composition of bioactive compounds present in the extracts (Herrero et al., 2012).

The extraction methods can be divided into conventional and unconventional techniques. The conventional methods include digestion, infusion, percolation, Soxhlet extraction, decoction, and maceration (Alara et al., 2021). However, conventional techniques may have some drawbacks, such as limitations in extract yield and may require a large deal of energy and time. In this sense, alternative, greener, more scalable, toxic solvent-free and economically profitable methods have been successfully proposed. These methods are based on extraction techniques such as microwave-assisted extraction, ultrasound-assisted extraction, subcritical water extraction, supercritical extraction, high hydrostatic pressure extraction, among others (Alara et al., 2021; Castro-Puyana et al., 2013; Freitas et al., 2020). Table 6 gathers different active extracts obtained from plants and agro-industrial residues, including the extraction method and conditions applied, the main bioactive compounds, and their bioactive effects. The extraction of active components is directly related to the type of solvent, the extraction method, and the process conditions. As an example, Menzel et al. (2020) tested three solvents in obtaining active extract from rice straw by applying the agitation method at room temperature for 1 h. The solvents used were water, ethanol in water (80 %), and methanol in water (80 %). Although the literature generally states that extraction with organic solvents gives rise to extracts with higher yields, these authors reported higher content of total phenolics in the aqueous extract, in which ferulic, *p*-coumaric, and protocatechuic acids were the major components. In line with the higher phenolic extraction, the aqueous extract obtained exhibited higher DPPH radical scavenging capacity than the alcoholic ones.

Ultrasound-assisted extraction (UAE) has been widely studied in the extraction of bioactive compounds from different agro-industrial waste sources. UAE is a green technique that applies intense shear forces to a dispersion to disrupt the primary structure of the plant and extract target components from its matrix. The acoustic cavitation that occurs during extraction is a physical phenomenon characterized by the very rapid and intense formation of zones of rarefaction (forming air or water vapour bubbles) and compression (pressure increase) in the solvent, which leads to the violent explosion of the air or water vapour bubbles and provokes the high shear rates in the dispersion (Cheung & Wu, 2013; Luque-García & Luque de Castro, 2003). UAE allows the extraction of large amounts of target components, can provide a significant decrease in extraction time, is a safe method (room temperatures and atmospheric pressure) and can be used as a pre-treatment in the extraction process (Bendicho et al., 2012; Ojha et al., 2020; Sumere et al., 2018).

Table 6. Recent studies obtaining active extracts from different agro-industrial wastes and by-products.

Source	Extraction method	Main compounds	Bioactive effects	Reference
Açaí seeds	Solvent: percentage of ethanol in water (0, 15, 50, 85, 100 %) Temperature: 25, 36, 62, 89, 100 °C System was stirred and kept for 20 min in a heated batch, followed by sonication for 15 min in an ultrasonic batch.	Procyanidin B1 and B2, catechin, and epicatechin	Antioxidant activity: DPPH (622.81 µmol/g) and ABTS (763.09 µmol TEAC/g) The extract did not improve the oxidative stability of soybean oil submitted to accelerated oxidation tests	Melo et al. (2021)
Rice straw	Solvent: water Extraction methods: stirring (ST) (60 min, 350 rpm, 25 °C) / probe-ultrasound (US) (15, 30, 60 min, 25 °C) / reflux heating (HT) (60 min, 100 °C) / US (30 min) + ST (60 min) / US (30 min) + HT (60 min)	Total phenolic content (TPC) (mg gallic acid equivalent (GAE)/ g dried extract): ST60 (45.7), US15 (49.2), US30 (45.7), US60 (37.4), HT60 (47), USST (42.3), USHT (34.8)	Antioxidant activity: DPPH (EC_{50}): ST60 (11.0), US15 (9.2), US30 (9.35), US60 (9.3), HT60 (7.49), USST (9.39), USHT (6.3) Antibacterial activity: USHT (160 mg/mL) showed a reduction of *Listeria innocua* of 1.7 log cycles	Freitas et al. (2020)
Apple pomace (AP)	Solvent: aqueous ethanol (80 %) Extraction method: bath water with agitation at 70 °C for 1 h.	TPC: 11.42 mg GAE/g AP	Antioxidant activity: DPPH (5.18 mmol Trolox/g); ABTS (402.9 mmol TEAC/g); FRAP (42891 mmol Fe^{2+}/ g)	Carpes et al. (2021)
Orange (O), mandarin (M), and grapefruit (G) by-products	Decoction in methanol:water (50:50 v/v) (pH = 2) + stirring (room temperature, 60 min); followed second extraction with acetone:water (70:30 v/v)	TPC (mg GAE/ g): extractable polyphenols (O: 7.86; M: 8.87; G:19.87); Total flavonoid content (mg rutin equivalent/g): extractable flavonoids (O: 3.66; M: 4.12; G: 6.10); The extracts were rich in hesperidin, naringin, and narirutin flavanones	-	Reynoso-Camacho et al. (2021)
Lemon pomace	Bath ultrasound-assisted aqueous extraction Parameters: particle size (1.40, 2.00 and 2.80 mm), extraction time (10, 20, 30, 40, 50 and 60 min), extraction temperature (ambient (23 °C), 30, 40 and 50 °C), and ultrasonic power (150, 200 and 250 W)	Quantification of hesperidin, *p*-coumaric, chlorogenic, and caffeic acids (highest recovery: 1.40 mm particle size). Highest TPC: size:1.40; temperature: 50 °C; time and power of ultrasound did not affect.	Highest antioxidant activity: DPPH (mg Trolox equivalent/g): size: 1.40 mm; temperature: 50 °C; time and power of ultrasound did not affect.	Papoutsis et al. (2016)

Table 6. (Continued).

Source	Extraction method	Main compounds	Bioactive effects	Reference
Coffee and rice husks	Subcritical water extraction: 180 °C, 60 min, 9.5 bars	TPC (mg GAE/mg dried extract): coffee husk: 65; rice husk: 66	Antioxidant activity: DPPH EC_{50} – mg dried extract/mg DPPH): coffee husk (5.37); rice husk: 5.29 Antibacterial activity: MIC *Listeria innocua* (mg/mL): coffee husk: 34; rice husk: 35 / MIC *Escherichia coli*: coffee husk: 35; rice husk: 45	Collazo-Bigliardi et al. (2019)
Rice husk	Subcritical water extraction: 160 °C; pH 7; time: 5 (E-5), 15 (E-15), 30 (E-30), and 60 (E-60) min	Quantification of main compounds (mg/g extract): ferulic acid (E-5: 1.7; E-15: 3.2; E-30: 3.6; E-60: 4.3) / caffeic acid (E-5: 0.3; E-15: 0.4; E-30: 0.4; E-60: 0.4) / *p*-coumaric acid: (E-5: 0.4; E-15: 0.8; E-30: 1.1; E-60: 0.8)	Antioxidant activity (EC_{50} – mg dried extract/mg DPPH): E-60 (9.6) Antibacterial activity (E-60): MIC *Listeria innocua*: 55 mg/mL; MIC *Escherichia coli*: 95 mg/mL	Requena et al. (2019)
Rice straw	Solvent: water; methanol (Me) in water (80 %); and ethanol (Et) in water (80 %) The systems were stirred at room temperature for 1 h. The same material was subsequently extracted a second and third time.	Quantification of main compounds (mg/g extract): ferulic acid (H_2O: 36; Me: 153; Et: 138) / p-coumaric acid (H_2O: 16; Me: 14; Et: 18.6) / protocatechuic acid (H_2O: 25; Me: 3.2; Et: 4.0) TPC (mg GAE/ g dried extract): H_2O: 225; Me: 153; Et: 138	Antioxidant activity: DPPH (EC_{50} – mg dried extract/mg DPPH): H_2O: 12; Me: 20.3; Et: 19.8 The antioxidant extracts did not show antibacterial activity against *Listeria innocua* and *Escherichia coli*.	Menzel et al. (2019)
Ficus carica leaf	Solvent: water (W) or methanol (Me) Method: intermittent shaking, room temperature, 24 h	Quantification of main compounds: W extract (methoxy-(3.32%), 4-methyl-1,4-heptadiene (6.85%), 1-pentene, 2,3-dimethyl-(2.72%)) / Me extract: 2H-furo[2,3-H]-1-benzopyran-2-one (53.64%), bergapten (19.27%), 9,12,15-octadecatrienoic acid, methyl ester, (Z,Z,Z)-(4.05%) TPC (mg GAE/g): Me extract: 17; W extract: 7.	Antioxidant activity: DPPH (IC_{50} (mg/mL)) – Me extract: 1.45; W extract: 1.83 / ABTS assay (IC_{50} (µg/mL)): Me extract: 559.39; W extract: 428.51 Antibacterial activity (MIC – mg/mL): *E. coli* (W: 2.5; Me: 0.625) / *S. aureus* (W:0.625; Me: 0.156) / *P. aeruginosa* (W: >2.5; Me: >2.5) / *E. faecalis* (W: >2.5; Me: >2.5); *K. pneumoniae* (W: >2.5; Me: >2.5) / *C. albicans* (W: 2.5; Me: 2.5) The Me extract exhibited significant anticancer activity.	Ergül et al. (2019)

The development of biodegradable bioactive packaging incorporating extracts obtained from plants and agro-industrial wastes comprises an interesting alternative to extend the shelf-life and improve the quality and safety of packaged foods. The release of bioactive compounds from the packaging material to the food surface and/or the packaging headspace can minimise or inhibit microbial growth and undesired reactions, such as oxidation of fatty acids, pigments, and vitamins (Han et al., 2018; Nerín et al., 2008). Moreover, the high consumer demand for healthier products, synthetic-free, and that have environmentally friendly claims, boosts the use of active substances obtained from natural and renewable sources. Table 7 shows some recent studies that have been reported developing active packaging systems with active extracts from plant, wastes, or by-products. These studies demonstrate that high value-added materials can be incorporated into biopolymer-based packaging materials to preserve and improve food quality and safety, while boosting the circular economy, the proper management of agro-industrial waste, and decreasing contamination of the global environment.

Table 7. Recent studies incorporating active extracts into biodegradable active films.

Source	Polymer matrix	Processing method	Main results	Reference
Rice (RH) and coffee (CH) husk extracts	Thermoplastic starch	Melting blending and compression moulding (Glycerol: extract ratio of 60:40, 70:30; 80:20)	As the proportion of active extract increased, the films showed increase in elastic modulus of 350 %, water vapour barrier (~50 % for the film with CH extract), and oxygen barrier (50-85 %). Moreover, the films exhibited antioxidant activity by DPPH assay (EC_{50}) (48.4 mg film/ mg DPPH for 60:40 CH film; 84.8 mg film/mg DPPH for 60:40 RH film).	Collazo-Bigliardi et al. (2019)
Green tea extract (GTE)	PLA	Melting blending and compression moulding (2 and 5 % CNC + 1% GTE)	PLA film containing 2 % CNC and 1 % GTE showed marked reduction in water vapour permeability (~33 %) and oxygen permeability (~60 %). This film was effective in retarding salami oxidation within 7-15 days (evaluated by TBARS index), suggesting a rapid release of bioactive compounds from the polymer matrix to the food surface.	Vilarinho et al. (2021)
Rice straw extract	Thermoplastic starch	Melting blending and compression moulding	The incorporation of extract made the films reddish in colour, more brittle, and gave UV light blocking properties. The active extract improved the oxygen barrier properties without significantly affecting the water vapour barrier and thermal properties. Likewise, the films showed good antioxidant activity by DPPH assay.	Menzel et al. (2019)
Pink pepper residue extract	Chitosan	Solvent casting (Extract was added at 0.6 % v/v chitosan suspension)	The control and active films reduced lipid oxidation (evaluated by TBARS index) of the salmon fillets with respect to the control treatment (absorbent pad placed at the top of the polypropylene trays) during 28 days of cold storage. The salmon samples packed in the active films exhibited lower levels of trimethylamine and off-odour score (sensory analysis), as well as in microbial counts (total psychrotrophic and lactic acid bacteria).	Merlo et al. (2019)
Lemma minor aqueous extract	PVA	Solvent casting (Extract at 1, 5, 10, 20 % wt.)	As the extract concentration increased, the films became greenish yellow and exhibited progressive light blocking in the UV region. The films with 1 and 5% wt. of extract did not exhibit antioxidant activity by DPPH assay. Nevertheless, all films with extract prevented fungal growth visible on the avocado surface after 10 days of analysis. The active films were effective in controlling fungal growth (~27 % inhibition) and bacterial growth, especially for the treatment with 5 % active extract.	Luzi et al. (2022)
Hop extract	Chitosan/PVA	Solvent casting (Extract at 10, 20, 40 % wt.)	The incorporation of active extract yielded less resistant (~56), less extensible, more rigid films (~56 % for films with 40 % extract), less resistant to water, more yellowish, and exhibited antioxidant activity (progressive increase as extract was incorporated) by DPPH and ABTS assays.	Almeida et al. (2022)

3. Rice straw: a versatile agro-industrial waste

3.1 Rice production and waste management

Rice (*Oryza sativa* L.) is one of the most important primary crops in the world (Peanparkdee & Iwamoto, 2019). According to the Food and Agriculture Organization of the United Nations (FAO, 2021), despite a 1.5 % reduction in global rice production in 2019 (compared to 2018), the agency reported a slight growth in world rice production in 2020, reaching 756 million tons, with approximately 90 % from the Asian continent (Figure 8). The top 10 rice producing countries include China, India, Indonesia, Bangladesh, Viet Nam, Thailand, Myanmar, Philippines, Brazil, and Japan. In Spain, annual rice production was 739,000 tons in 2020, which represents approximately 20 % of total production in Europe (FAOSTAT, 2021). Among the Spanish autonomous communities, Andalucía is the largest rice producer (~40 % of production), followed by Extremadura (~20 %), Cataluña (~15 %), Comunidad Valenciana (~14 %), and Aragón (~3 %) (MAPA, 2017). It is estimated that the production of rice will continue to grow steadily due to the intense growth of the world population and the demand for food, especially in underdeveloped and emerging countries, since the international prices of this cereal are inexpensive, and its composition provides large amounts of energy to the human body.

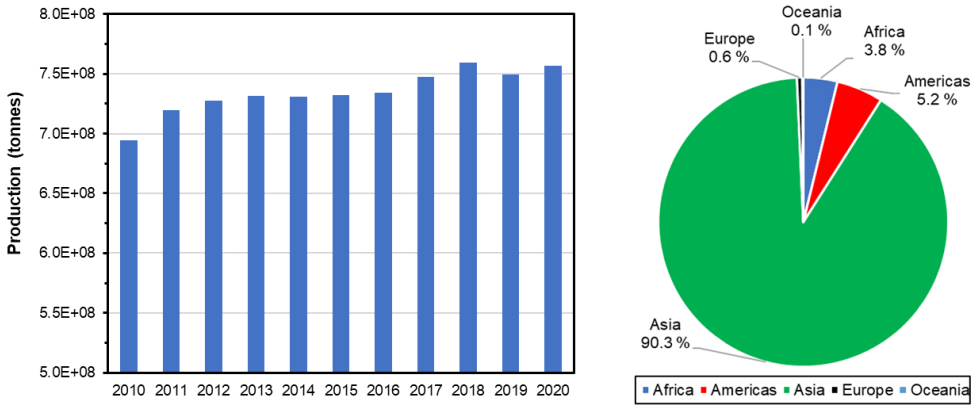

Figure 8. World rice production and percentage of production in each continent.

After rice is cultivated and harvested, large quantities of residues and by-products are obtained, including bran, husk, and straw. Among these agro-wastes, rice straw (RS) represents one of the most generated lignocellulosic residues worldwide, since one kilogram of rice grain provides 1.5 kg of RS (Barana et al., 2016; Peanparkdee & Iwamoto, 2019). RS comprises the leftovers from the rice harvest, including stems, leaf blades, leaf sheaths and the remains of the panicle after threshing. RS is often burned in the paddies, a common practice carried out by farmers with claims of phytosanitary effects, such as reincorporating nutrients into the soil (N, P, and K) and eliminating fungal spores (Sadh et al., 2018).

Nonetheless, the burning of RS represents an incorrect disposal and management of this agro-industrial waste, greatly affecting the environment and the health of the population living near the harvesting fields. Being a highly combustible material, the burning of RS contributes to a continuous increase in air and soil pollution due to the release of harmful dioxins (dibenzofurans and polychlorinated dibenzo-*p*-dioxins), greenhouse gases (CH_4, CO_2), and polycyclic aromatic hydrocarbons, thus resulting in severe and negative environmental impact (Sadh et al., 2018; Singh & Brar, 2021). To overcome these drawbacks, in-depth knowledge of the nature, morphology and composition of RS may be the way to find and propose new alternatives for a greener and more economical management of this agro-waste.

3.2 Structure and composition of rice straw

As shown in Figure 9, the morphological structure of RS comprises a three-dimensional arrangement with vascular bundles in different porous layers composed of the waxy cuticle, silicified epidermis, cortex (collenchyma), highly lignified tissue (sclerenchyma), parenchymatic tissue, and lumen (Seo & Sakoda, 2014). RS has a high content of biogenic silica (~16 %), which is present inside epidermal cells and in vascular tissues mainly in the form of amorphous silica (condensed silicic acid particles), the so-called silica bodies or phytoliths. Silica plays an important role as a physical barrier for plants, protecting them from insects as well as enzymatic degradation when attacked by fungi (Le et al., 2015; Seo & Sakoda, 2014).

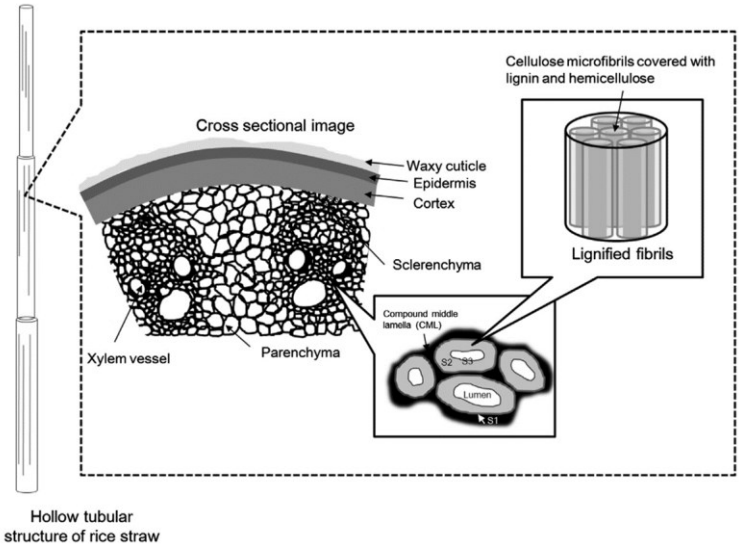

Figure 9. Scheme of the morphological structure of RS (Seo & Sakoda, 2014).

In general, RS is lignocellulosic biomass composed of 70 % dry matter, which is organized into a complex matrix consisting of semicrystalline cellulose nanofibrils embedded in a cementing matrix of hemicellulose and lignin (Barana et al., 2016; Chen et al., 2011) (Figure 5). RS can

present different levels of lignocellulosic components, which is related to plant variety, season, type of tissue, and growing stage. Table 8 gathers the chemical composition of RS from different varieties and references, which range from 31-45 % cellulose, 15-32 % hemicellulose, 11-21 % lignin, and 9-18 % ashes. As regards nutritional values, RS contains a low protein content, ranging from 3.2 to 5 % wt. This protein deficit makes RS not suitable for direct consumption by animals, which require a diet with a minimum of 8 % crude protein. Furthermore, knowledge of the chemical composition of RS is important to control aspects related to the most appropriate management of this waste. For example, high silica content decreases the digestibility of RS when used as animal feed and can promote the erosion in industrial machinery (Le et al., 2015).

Table 8. Lignocellulosic composition of different RS varieties.

Variety	Cellulose (% wt.)	Hemicellulose (% wt.)	Lignin (% wt.)	Ashes (% wt.)	Reference
J. Sendra	37	19	21	17	Freitas et al. (2022)
Akitakomachi	34	16	11	9	Seo and Sakoda (2014)
Akitakomachi	32	29	19	10	Murakami et al. (2012)
Japonica kato	34	20	20	12.4	Gu et al. (2013)
Koshihikari	24-38	12-22	16-20	-	Kahar (2013)
Firozan (stem)	42	25	-	13	Gaceno et al. (2013)
Firozan (sheath)	45	32	-	16	
Sazandegi (stem)	44	26	-	14	
Sazandegi (sheath)	44	32	-	18	
Zayanderrod (stem)	40	24	-	13	
Zayanderrod (sheath)	42	30	-	13	
M-202	33	25	14	11	Liu et al. (2022)

3.3 Sustainable rice straw management

Due to its lignocellulosic-rich composition, RS can have a wide range of potential uses, although nowadays hardly practiced in the industries. The management of RS instead of its burning in the harvest fields is still a constant challenge. There is a need to search alternatives that are economically attractive to farmers, that play an integrated role towards profitable agro-industrial production while obtaining environmentally-friendly products, strategies and processes for society. RS can be reused in the agro-industry and farms themselves, integrally or as part of the diet for animal feed, by means of its incorporation into the soil, composting, mushroom production, as well as for the production of bioenergy and other high value-added materials, such as silica, cellulose fibres, and bioactive substances for industrial purposes (Van Hung et al., 2020). The most common uses of RS, as well as the possibilities of its valorisation

to obtain sustainable and added value materials will be briefly described in the following subsections.

3.3.1 RS as livestock feed

RS is a highly available, easily handled, and cheap biomass, which could be an interesting feed source for ruminants. However, its high lignin and silica content, as well as its poor protein content leads to low digestibility (< 50 %) and affects the growth performance or lactation of animals (Aquino et al., 2020; Singh & Brar, 2021). In this sense, different pre-treatments and techniques have been proposed to improve the nutritional value and nutrient availability of RS for animals. According to Aquino et al. (2020), RS can be submitted to processes to improve its digestibility and availability, including physical treatments (e.g., soaking, grinding, or chopping, pelleting, steaming pressure, and gamma irradiation); chemical treatments (based on sodium hydroxide, urea, and ammonia); and biological treatments (e.g., enzymes, bacteria, and fungi).

3.3.2 RS incorporation into the soil

Due to its high content of nitrogen, potassium, and phosphorus, the incorporation of fresh RS into the soil could reduce the amount of fertiliser required for the following crop. However, the decomposition time of RS is relatively high, which does not achieve the desired fertilising effect and may have negative environmental impacts due to greenhouse gas emissions. Mixing fresh RS with other supplies, such as green manure or animal manure to make compost, improves the decomposition potential of the resulting biomass. It is worth mentioning that compost can be obtained from fresh RS or from mushroom production, but they are not usually applied for rice production, but for growing high value-added crops such as vegetables. Moreover, the incorporation of biochar from RS thermocombustion can be performed to improve the carbon content in the soil (Chivenge et al., 2020).

3.3.3 RS-based composting

Compost production is considered as an effective way of utilising the large quantities of waste generated in an agro-industry during agricultural production. The basis of the composting technique is to safely transform organic waste (by-products, animal waste) into a more decomposed material. When produced properly, compost is used as a soil improver and has the ability to increase both production yields and also soil fertility (Nghi et al., 2020). Composting is defined as the sum of complex metabolic processes carried out by different microorganisms, which in the presence of oxygen in at least some of the phases, use the

nitrogen and carbon present to produce their own biomass. In this process, the microorganisms generate heat and a solid substrate, with less carbon and nitrogen, but more stable and assimilable by plants (Roman et al., 2013). The parameters that must be managed to produce a quality material are factors in the composting process, including temperature, humidity, pH, carbon: nitrogen ratio, and aeration. Control techniques and procedures can be used or combined to obtain an appropriate and quality product. These methods are based on biological (e.g., vermi-composting), chemical (e.g., adjusting the carbon: nitrogen ratio to 20–30), and physical (e.g., mechanized windrow composting) processes (Nghi et al., 2020).

3.3.4 Valorisation of RS

RS and its derivatives have been proposed to be used in different industrial applications. Thus, Table 9 gathers some recent studies valorising and investigating the potential use of RS, integrally or as derivatives with high-added value for different application purposes. These studies highlight the versatility of RS to be applied in different fields, including civil engineering, pharmaceutical and food purposes, food packaging, and biotechnological processes. For example:

- Liu et al. (2022) demonstrated the potential use of RS fibre grafted with nano-SiO_2 as a possible substitute for traditional fibres in concrete. The materials developed with different proportions of modified RS fibre were evaluated as to their mechanical properties (compressive, flexural, and axial compressive tests), microscopic, thermal, as well as large temperature difference dry-wet cycle test. The authors found that the modified fibre exhibited good compatibility with the concrete matrix and exhibited excellent mechanical performance over the analysis time, being possible its use as part of coarse fibre monofilaments.
- Chapla et al. (2013) bioconvert hemicellulose from wheat straw and RS using purified xylanase from *Aspergillus foetidus* MTCC 4898 into xylooligosaccharides, a non-digestible food ingredient used as a prebiotic, i.e., it stimulates the selective growth of some microorganisms present in the gastrointestinal tract, such as *bifidobacteria* and *Lactobacillus*. The obtained xylooligosaccharides were evaluated in terms of their stability in food processing (different pH values, time-temperature binomials) as well as their fermentation *in vitro* using *Bifidobacterium* bacteria. The extracted enzyme yielded high levels of xylooligosaccharides for both agro-industrial sources (7.28 and 4.5 mg/mL for wheat straw and RS, respectively). Furthermore, the xylooligosaccharides exhibited good stability to food processing conditions, as well as excellent fermentability by the bacteria evaluated.
- Menzel et al. (2019) obtained an aqueous extract from RS using a constant stirring method and produced thermoplastic starch-based films by melt blending and compression

moulding. The colour, microscopic, mechanical, thermal, barrier properties as well as the antioxidant potential of the films were evaluated. Micrographs of the films revealed that the extract exhibited excellent compatibilisation with the polymer matrix. Due to its hydrophilic nature, the active extract led to films with improved oxygen barrier properties. Moreover, the bioactive compounds incorporated in the films released from the starch matrix and displayed excellent antioxidant properties.

- Chollakup et al. (2021) used the potential of cellulose fibres from RS to produce paper coated with oxidised starch incorporated with active extract from the Longan (*Dimocarpus longan*) peel. The paper was obtained by applying an alkaline treatment (NaOH 20 % wt., 100 °C, 3 h) followed by disintegration of the cellulose pulp suspension, which was poured on a surface to dry. Oxidized starch films (8 % wt.) were prepared by incorporating the lyophilized active extract at 10, 15, and 20 % wt. (with respect to mass of the polymer) and pouring the forming film solution onto the prepared RS paper. The sheets were evaluated for their mechanical, morphological, water absorption and antibacterial activity against *S. aureus*, *B. cereus*, and *E.* coli. The incorporation of 20 % extract led to a significant improvement in the tensile index by about 13 % when compared with the other active treatments and control films. As the concentration of extract in the films increased, the bilayer was more resistant to water absorption (control bilayer ~250 % vs. bilayer with 20 % extract ~220 %), suggesting that the extract components slightly increased the hydrophobicity of the film. The active films also exhibited antibacterial action against *S. aureus* and *B. cereus* (regardless of extract concentration) but was not effective against *E. coli*.
- Dhali et al. (2022) proposed the valorisation of RS due to its high silica content to cultivate diatom *Navicula* sp. The nanostructured biosilica shells produced by diatoms have multiple applications as they have large surface area, surface charge, nanopores, biocompatibility, and mechanical strength, which characterizes it as an excellent nanocarrier. Likewise, diatoms are widely studied in other research fields, including their potential for biofuel production, as well as sources of several bioactive compounds (polyunsaturated fatty acids, carotenoids, fucoxanthin, eicosapentaenoic acid). In this regard, the authors obtained a hydrolysate from RS and quantified its elemental compositions (carbon, hydrogen, nitrogen, sulphur, and oxygen content % w/w). Based on the nutrient composition, the RS suspension was diluted to different concentrations (10, 30, 50 and 70 % (v/v)) for diatom culture. The growth kinetics of the diatoms was performed every two days of cultivation by counting using Neubauer hemocytometer. The biomass productivity and a scalability study using a 9 L capacity reactor was conducted under the best culture conditions (determined previously). Biochemical composition of the biomass, frustule extraction, and morphological characterisation of the biomass were also performed. The authors found that the best concentration of the RS suspension was 30 %. Likewise, the diatoms showed higher specific growth rates and biomass productivity than the

commercial growth media. The culture exhibited 54 % frustule, 12 % carbohydrates, 19 % lipids, 8 % proteins.

All these studies constitute examples of valorisation of RS residues and its potential to promote the development of profitable products and processes with a low environmental impact, while contributing to the circular economy.

Table 9. Recent studies valorising the RS.

Field	Application	Main results	Reference
Civil engineering	Modified RS fibre reinforced concrete (RSFRC)	The incorporation of 1, 2, and 3 % wt. of modified RS fibre (grafted with Nano-SiO_2) in concrete exhibited progressive increase in compressive strength and flexural strength over time. Micrographs revealed decreased in $Ca(OH)_2$ content for the composite concrete, which suggests higher compatibility of the material compared to concrete without modified fibre.	Liu et al. (2022)
Pharmaceutical / Food / Packaging	Bioactive aqueous extract	The active aqueous RS extracts showed high levels of total phenolics and antioxidant capacity. The combination of ultrasound followed by reflux heating was the best treatment in terms of phenolic yield, antioxidant capacity, and antimicrobial activity (1.7 logarithm reduction of *Listeria innocua*).	Freitas et al. (2022)
	Prebiotics	Xylooligosaccharides were obtained from RS using xylanase (extracted from *Aspergillus foetidus* MTCC 4898) and exhibited a maximum yield of 4.52 mg/mL. The suitability of the obtained xylooligosaccharides as prebiotics was validated by their thermal stability at low pH and *in vitro* fermentation using prebiotic strains.	Chapla et al. (2013)
	Bioactive methanolic extract	Three rice varieties were used to obtain methanolic extracts. All the extracts exhibited gallic acid, pyrogallol, apigeni, and rutin as the main phenolic compounds and flavonoids. The active extract obtained from Hasemi variety showed the highest antioxidant activity through DPPH and nitric oxide free radical scavenging assays.	Karimi et al. (2014)
Food packaging	Bioactive agent	The incorporation of aqueous extract coloured the films, which became more brittle, and showed UV light blocking properties. The active extract improved the films' oxygen barrier properties without significantly affecting the water vapour barrier and thermal properties. Likewise, the films showed good antioxidant activity by DPPH assay.	Menzel et al. (2019)
	Bioactive agent	The PLA films exhibited slightly worsened properties of mechanical strength, water vapour barrier capacity, and thermostability. The phenolic compounds were effectively released from the packaging to the food simulants (10 and 50 % ethanol in water) and exhibited potent antioxidant activity. The release profile depended on the extract concentration, the type of simulant, and the contact time.	Freitas et al. (2022)
	RS paper coated with Longan (*Dimocarpus longan*) peel extract	The RS paper coated with oxidized starch incorporated with active extract showed good adhesion between the layers, as well as improved water resistance. The biodegradable bilayer exhibited marked antimicrobial activity against *S. aureus* and *B. cereus*.	Chollakup et al. (2021)

Table 9. (Continued).

Field	Application	Main results	Reference
Food packaging	Reinforcing agent (Cellulose fibres)	The incorporation of cellulose fibres in the starch films improved the mechanical properties (more resistant to break (~100 %), oxygen barrier (~30 %), and water vapour barrier (~15 %).	Freitas et al. (2021)
Biorefineries	Microbial lipid production (RS hydrolysates)	The purified hydrolysates from RS yielded a high total lipid (8.8 g/L) and lipid yield (0.17 g/g) via fermentation. The authors reported that 2.9 g total lipids would be produced from 1 g of SR and recycled glycerol, with composition similar to soybean oil.	Tang et al. (2020)
	Biogenic silica source (Cultivation of *Navicula* sp.)	The optimum conditions for diatom production were 30 % SR, which led to a doubling time of 1.49 days. The diatoms exhibited higher specific growth rates and biomass productivity than the control treatment (added with modified ASN-III). The culture exhibited 54 % frustule, 12 % carbohydrates, 19 % lipids, 8 % proteins.	Dhali et al. (2022)
	Heterogeneous catalysts (Biodiesel production)	Sodium silicate was obtained from rice straw and used as catalyst in the production of biodiesel using cooking oil. The optimum production parameters were as follows: reaction temperature 65 °C; methanol: oil ratio 15:1; catalyst from RS of 3.5 %; stirring 600 rpm; and reaction time 150 min. The biodiesel conversion rate observed was 93.7 %.	Sahu (2021)
	Bioethanol production	The alkaline treatment of RS resulted in an increase of the fermented sugar content from 56 to 80%. Adequate saccharification of RS was achieved with the combination of three commercial enzymes, which yielded a material with 75 g/L fermentable sugar (94 % hydrolysis efficiency). Under aerobic conditions and after 36 h of process, M. circinelloides resulted in 30.5 g/L of ethanol.	Takano & Hoshino, (2018))

4. References

Abu-Thabit, N. Y., Judeh, A. A., Hakeem, A. S., Ul-Hamid, A., Umar, Y., & Ahmad, A. (2020). Isolation and characterization of microcrystalline cellulose from date seeds (Phoenix dactylifera L.). *International Journal of Biological Macromolecules*, 155, 730–739. https://doi.org/10.1016/j.ijbiomac.2020.03.255

Ahmed, I., Lin, H., Zou, L., Brody, A. L., Li, Z., Qazi, I. M., Pavase, T. R., Lv, L (2017). A comprehensive review on the application of active pakaging technologies to muscle foods. *Food Control*, 82, p. 163-178.

Alara, O. R., Abdurahman, N. H., & Ukaegbu, C. I. (2021). Extraction of phenolic compounds: A review. *Current Research in Food Science*, 4, 200–214. https://doi.org/10.1016/j.crfs.2021.03.011

Almeida, A. da R., Brisola Maciel, M. V. de O., Machado, M. H., Sganzerla, W. G., Teixeira, G. L., da Rosa, C. G., Block, J. M., Nunes, M. R., & Barreto, P. L. M. (2022). Production of chitosan and poly (vinyl alcohol) films functionalized with hop extract (Humulus lupulu L. var. Cascade) for food packaging application. *Food Packaging and Shelf Life*, 32, 100833. https://doi.org/10.1016/j.fpsl.2022.100833

Andrade, J., González-Martínez, C., & Chiralt, A. (2022). Antimicrobial PLA-PVA multilayer films containing phenolic compounds. *Food Chemistry*, 375, 131861. https://doi.org/10.1016/j.foodchem.2021.131861

Anukiruthika, T., Sethupathy, P., Wilson, A., Kashampur, K., Moses, J. A., & Anandharamakrishnan, C. (2020). Multilayer packaging: Advances in preparation techniques and emerging food applications. *Comprehensive Reviews in Food Science and Food Safety*, 19(3), 1156–1186. https://doi.org/10.1111/1541-4337.12556

Aquino, D., Del Barrio, A., Trach, N. X., Hai, N. T., Khang, D. N., Toan, N. T., & Van Hung, N. (2020). Rice Straw-Based Fodder for Ruminants. In M. Gummert, N. V. Hung, P. Chivenge, & B. Douthwaite (Eds.), Sustainable Rice Straw Management (pp. 111–129). Springer International Publishing. https://doi.org/10.1007/978-3-030-32373-8_7

Arrieta, M. P., Fortunati, E., Dominici, F., López, J., & Kenny, J. M. (2015). Bionanocomposite films based on plasticized PLA–PHB/cellulose nanocrystal blends. *Carbohydrate Polymers*, 121, 265–275. https://doi.org/10.1016/j.carbpol.2014.12.056

Arun, R., Shruthy, R., Preetha, R., & Sreejit, V. (2022). Biodegradable nano composite reinforced with cellulose nano fiber from coconut industry waste for replacing synthetic

plastic food packaging. *Chemosphere*, 291, 132786. https://doi.org/10.1016/j.chemosphere.2021.132786

Baghi, F., Gharsallaoui, A., Dumas, E., & Ghnimi, S. (2022). Advancements in Biodegradable Active Films for Food Packaging: Effects of Nano/Microcapsule Incorporation. *Foods*, 11(5), 760. https://doi.org/10.3390/foods11050760

Bajpai, P. (2018). Wood and Fiber Fundamentals. In Biermann's Handbook of Pulp and Paper (pp. 19–74). Elsevier. https://doi.org/10.1016/B978-0-12-814240-0.00002-1

Barana, D., Salanti, A., Orlandi, M., Ali, D. S., & Zoia, L. (2016). Biorefinery process for the simultaneous recovery of lignin, hemicelluloses, cellulose nanocrystals and silica from rice husk and Arundo donax. *Industrial Crops and Products*, 86, 31–39. https://doi.org/10.1016/j.indcrop.2016.03.029

Beltrán-Ramírez, F., Orona-Tamayo, D., Cornejo-Corona, I., Luz Nicacio González-Cervantes, J., de Jesús Esparza-Claudio, J., & Quintana-Rodríguez, E. (2019). Agro-Industrial Waste Revalorization: The Growing Biorefinery. In A. El-Fatah Abomohra (Ed.), Biomass for Bioenergy—Recent Trends and Future Challenges. IntechOpen. https://doi.org/10.5772/intechopen.83569

Bendicho, C., De La Calle, I., Pena, F., Costas, M., Cabaleiro, N., & Lavilla, I. (2012). Ultrasound-assisted pretreatment of solid samples in the context of green analytical chemistry. TrAC *Trends in Analytical Chemistry*, 31, 50–60. https://doi.org/10.1016/j.trac.2011.06.018

Bera, A., Dubey, S., Bhayani, K., Mondal, D., Mishra, S., & Ghosh, P. K. (2015). Microbial synthesis of polyhydroxyalkanoate using seaweed-derived crude levulinic acid as co-nutrient. *International Journal of Biological Macromolecules*, 72, 487–494. https://doi.org/10.1016/j.ijbiomac.2014.08.037

Boonterm, M., Sunyadeth, S., Dedpakdee, S., Athichalinthorn, P., Patcharaphun, S., Mungkung, R., & Techapiesancharoenkij, R. (2016). Characterization and comparison of cellulose fiber extraction from rice straw by chemical treatment and thermal steam explosion. *Journal of Cleaner Production*, 134, 592–599. https://doi.org/10.1016/j.jclepro.2015.09.084

Brethauer, S., Shahab, R. L., & Studer, M. H. (2020). Impacts of biofilms on the conversion of cellulose. *Applied Microbiology and Biotechnology*, 104(12), 5201–5212. https://doi.org/10.1007/s00253-020-10595-y

Brunner, G. (2014). Processing of Biomass with Hydrothermal and Supercritical Water. In Supercritical Fluid Science and Technology (Vol. 5, pp. 395–509). Elsevier. https://doi.org/10.1016/B978-0-444-59413-6.00008-X

Byun, Y., & Kim, Y. T. (2014). Bioplastics for Food Packaging. In Innovations in Food Packaging (pp. 353–368). Elsevier. https://doi.org/10.1016/B978-0-12-394601-0.00014-X

Carpes, S. T., Bertotto, C., Bilck, A. P., Yamashita, F., Anjos, O., Bakar Siddique, M. A., Harrison, S. M., & Brunton, N. P. (2021). Bio-based films prepared with apple pomace: Volatiles compound composition and mechanical, antioxidant and antibacterial properties. *LWT*, 144, 111241. https://doi.org/10.1016/j.lwt.2021.111241

Carvalho, A. J. F. (2008). Starch: Major Sources, Properties and Applications as Thermoplastic Materials. In *Monomers, Polymers and Composites from Renewable Resources* (pp. 321–342). Elsevier. https://doi.org/10.1016/B978-0-08-045316-3.00015-6

Castro-Puyana, M., Herrero, M., Mendiola, J. A., & Ibáñez, E. (2013). Subcritical water extraction of bioactive components from algae. In *Functional Ingredients from Algae for Foods and Nutraceuticals* (pp. 534–560). Elsevier. https://doi.org/10.1533/9780857098689.3.534

Chapla, D., Dholakiya, S., Madamwar, D., & Shah, A. (2013). Characterization of purified fungal endoxylanase and its application for production of value added food ingredient from agroresidues. *Food and Bioproducts Processing*, 91(4), 682–692. https://doi.org/10.1016/j.fbp.2013.08.005

Chawla, R., Sivakumar, S., & Kaur, H. (2021). Antimicrobial edible films in food packaging: Current scenario and recent nanotechnological advancements- a review. Carbohydrate *Polymer Technologies and Applications*, 2, 100024. https://doi.org/10.1016/j.carpta.2020.100024

Chen, C., Chen, X., Jiang, M., Rui, X., Li, W., & Dong, M. (2014). A newly discovered bacteriocin from Weissella hellenica D1501 associated with Chinese Dong fermented meat (Nanx Wudl). *Food Control*, 42, 116–124. https://doi.org/10.1016/j.foodcont.2014.01.031

Chen, X., Yu, J., Zhang, Z., & Lu, C. (2011). Study on structure and thermal stability properties of cellulose fibers from rice straw. *Carbohydrate Polymers*, 85(1), 245–250. https://doi.org/10.1016/j.carbpol.2011.02.022

Cheung, Y.-C., & Wu, J.-Y. (2013). Kinetic models and process parameters for ultrasound-assisted extraction of water-soluble components and polysaccharides from a medicinal fungus. *Biochemical Engineering Journal*, 79, 214–220. https://doi.org/10.1016/j.bej.2013.08.009

Chivenge, P., Rubianes, F., Van Chin, D., Van Thach, T., Khang, V. T., Romasanta, R. R., Van Hung, N., & Van Trinh, M. (2020). Rice Straw Incorporation Influences Nutrient Cycling and Soil Organic Matter. In M. Gummert, N. V. Hung, P. Chivenge, & B. Douthwaite (Eds.), *Sustainable*

Rice Straw Management (pp. 131–144). Springer International Publishing. https://doi.org/10.1007/978-3-030-32373-8_8

Chollakup, R., Kongtud, W., Sukatta, U., Premchookiat, M., Piriyasatits, K., Nimitkeatkai, H., & Jarerat, A. (2021). Eco-Friendly Rice Straw Paper Coated with Longan (Dimocarpus longan) Peel Extract as Bio-Based and Antibacterial Packaging. *Polymers*, 13(18), 3096. https://doi.org/10.3390/polym13183096

Circular economy and global secondary material supply chains. (2015). Waste Management & Research: The Journal for a Sustainable Circular Economy, 33(5), 389–391. https://doi.org/10.1177/0734242X15587641

Collazo-Bigliardi, S. Ortega-Toro, R., & Chiralt, A. (2019) (2018). Isolation and characterisation of microcrystalline cellulose and cellulose nanocrystals from coffee husk and comparative study with rice husk. *Carbohydrate Polymers*, 11.

Collazo-Bigliardi, S., Ortega-Toro, R., & Chiralt, A. (2019). Improving properties of thermoplastic starch films by incorporating active extracts and cellulose fibres isolated from rice or coffee husk. *Food Packaging and Shelf Life*, 22, 100383. https://doi.org/10.1016/j.fpsl.2019.100383

Correa, J. P., Molina, V., Sanchez, M., Kainz, C., Eisenberg, P., & Massani, M. B. (2017). Improving ham shelf life with a polyhydroxybutyrate/polycaprolactone biodegradable film activated with nisin. *Food Packaging and Shelf Life*, 11, 31–39. https://doi.org/10.1016/j.fpsl.2016.11.004

Debnath, B., Haldar, D., & Purkait, M. K. (2021). A critical review on the techniques used for the synthesis and applications of crystalline cellulose derived from agricultural wastes and forest residues. *Carbohydrate Polymers*, 273, 118537. https://doi.org/10.1016/j.carbpol.2021.118537

Dhali, K., Daver, F., Cass, P., & Adhikari, B. (2021). Isolation and characterization of cellulose nanomaterials from jute bast fibers. *Journal of Environmental Chemical Engineering*, 9(6), 106447. https://doi.org/10.1016/j.jece.2021.106447

Dhali, S., Jain, R., Malik, A., Sharma, S., & Raliya, R. (2022). Cultivation of Navicula sp. On rice straw hydrolysate for the production of biogenic silica. *Bioresource Technology*, 360, 127577. https://doi.org/10.1016/j.biortech.2022.127577

Ergül, M., Ergül, M., Eruygur, N., Ataş, M., & Uçar, E. (2019). In Vitro Evaluation of the Chemical Composition and Various Biological Activities of Ficus carica Leaf Extracts. *Turkish Journal of Pharmaceutical Sciences*, 16(4), 401–409. https://doi.org/10.4274/tjps.galenos.2018.70037

European bioplastics. Bioplastics marked data. https://www.european-bioplastics.org/market/# . Accessed in August, 2021.

FAOSTAT. (2021). from https://www.fao.org/faostat/en/#data/QCL/visualize

Farhoosh, R., Johnny, S., Asnaashari, M., Molaahmadibahraseman, N., & Sharif, A. (2016). Structure–antioxidant activity relationships of o-hydroxyl, o-methoxy, and alkyl ester derivatives of p-hydroxybenzoic acid. *Food Chemistry*, 194, 128–134. https://doi.org/10.1016/j.foodchem.2015.08.003

Freitas, P. A. V., Arias, C. I. L. F., Torres-Giner, S., González-Martínez, C., & Chiralt, A. (2021). Valorization of Rice Straw into Cellulose Microfibers for the Reinforcement of Thermoplastic Corn Starch Films. *Applied Sciences*, 11(18), 8433. https://doi.org/10.3390/app11188433

Freitas, P. A. V., Gil, N. J. B., & González-Martínez, C. (2022). Antioxidant poly (lactic acid) films with rice straw extract for food packaging applications. *Food Packaging and Shelf Life*. In press.

Freitas, P. A. V., González-Martínez, C., & Chiralt, A. (2020). Application of Ultrasound Pre-Treatment for Enhancing Extraction of Bioactive Compounds from Rice Straw. *Foods*, 9(11), 1657. https://doi.org/10.3390/foods9111657

Freitas, P. A. V., González-Martínez, C., & Chiralt, A. (2022). Applying ultrasound-assisted processing to obtain cellulose fibres from rice straw to be used as reinforcing agents. *Innovative Food Science & Emerging Technologies*, 76, 102932. https://doi.org/10.1016/j.ifset.2022.102932

Galdeano, M. C., Mali, S., Grossmann, M. V. E., Yamashita, F., & García, M. A. (2009). Effects of plasticizers on the properties of oat starch films. *Materials Science and Engineering: C*, 29(2), 532–538. https://doi.org/10.1016/j.msec.2008.09.034

García Ibarra, V., Sendón, R., & Rodríguez-Bernaldo de Quirós, A. (2016). Antimicrobial Food Packaging Based on Biodegradable Materials. In *Antimicrobial Food Packaging* (pp. 363–384). Elsevier. https://doi.org/10.1016/B978-0-12-800723-5.00029-2

Garcia-Maraver, A., Salvachúa, D., Martínez, M. J., Diaz, L. F., & Zamorano, M. (2013). Analysis of the relation between the cellulose, hemicellulose and lignin content and the thermal behavior of residual biomass from olive trees. *Waste Management*, 33(11), 2245–2249. https://doi.org/10.1016/j.wasman.2013.07.010

Geyer, R., Jambeck, J. R., & Law, K. L. (2017). Production, use, and fate of all plastics ever made. *Science Advances*, 3(7), e1700782. https://doi.org/10.1126/sciadv.1700782

Ghasemi, E., Ghorbani, G. R., Khorvash, M., Emami, M. R., & Karimi, K. (2013). Chemical composition, cell wall features and degradability of stem, leaf blade and sheath in untreated and alkali-treated rice straw. *Animal*, 7(7), 1106–1112. https://doi.org/10.1017/S1751731113000256

Gonçalves de Moura, I., Vasconcelos de Sá, A., Lemos Machado Abreu, A. S., & Alves Machado, A. V. (2017). Bioplastics from agro-wastes for food packaging applications. In *Food Packaging* (pp. 223–263). Elsevier. https://doi.org/10.1016/B978-0-12-804302-8.00007-8

González, K., Retegi, A., González, A., Eceiza, A., & Gabilondo, N. (2015). Starch and cellulose nanocrystals together into thermoplastic starch bionanocomposites. *Carbohydrate Polymers*, 117, 83–90. https://doi.org/10.1016/j.carbpol.2014.09.055

Gu, F., Wang, W., Jing, L., & Jin, Y. (2013). Effects of green liquor pretreatment on the chemical composition and enzymatic digestibility of rice straw. *Bioresource Technology*, 149, 375–382. https://doi.org/10.1016/j.biortech.2013.09.064

Guo, Y., Zhang, Y., Zheng, D., Li, M., & Yue, J. (2020). Isolation and characterization of nanocellulose crystals via acid hydrolysis from agricultural waste-tea stalk. International *Journal of Biological Macromolecules*, 163, 927–933. https://doi.org/10.1016/j.ijbiomac.2020.07.009

Han, J. H. (2014). Innovations in food packaging (2nd edition). Academic Press, an imprint of Elsevier.

Han, J.-W., Ruiz-Garcia, L., Qian, J.-P., & Yang, X.-T. (2018). Food Packaging: A Comprehensive Review and Future Trends: Food packaging: Review and future trends…. *Comprehensive Reviews in Food Science and Food Safety*, 17(4), 860–877. https://doi.org/10.1111/1541-4337.12343

Harnkarnsujarit, N. (n.d.). Chapter 7—Bioplastic for Sustainable Food Packaging. 75.

Hemmati, F., Jafari, S. M., Kashaninejad, M., & Barani Motlagh, M. (2018). Synthesis and characterization of cellulose nanocrystals derived from walnut shell agricultural residues. *International Journal of Biological Macromolecules*, 120, 1216–1224. https://doi.org/10.1016/j.ijbiomac.2018.09.012

Hernández-García, E., Vargas, M., & Chiralt, A. (2022). Starch-polyester bilayer films with phenolic acids for pork meat preservation. *Food Chemistry*, 385, 132650. https://doi.org/10.1016/j.foodchem.2022.132650

Herrero, M., Plaza, M., Cifuentes, A., & Ibáñez, E. (2012). Extraction Techniques for the Determination of Phenolic Compounds in Food. *In* Comprehensive Sampling and Sample Preparation (pp. 159–180). Elsevier. https://doi.org/10.1016/B978-0-12-381373-2.00132-0

Ho, M. C., Ong, V. Z., & Wu, T. Y. (2019). Potential use of alkaline hydrogen peroxide in lignocellulosic biomass pretreatment and valorization – A review. *Renewable and Sustainable Energy Reviews*, 112, 75–86. https://doi.org/10.1016/j.rser.2019.04.082

Hong, L. G., Yuhana, N. Y., Zawawi, E. Z. E., Bangi. (2021). Review of bioplastics as food packaging materials. *AIMS Materials Science*, 8(2), 166–184. https://doi.org/10.3934/matersci.2021012

Ilyas, R. A., Sapuan, S. M., Ibrahim, R., Abral, H., Ishak, M. R., Zainudin, E. S., Atikah, M. S. N., Mohd Nurazzi, N., Atiqah, A., Ansari, M. N. M., Syafri, E., Asrofi, M., Sari, N. H., & Jumaidin, R. (2019). Effect of sugar palm nanofibrillated cellulose concentrations on morphological, mechanical and physical properties of biodegradable films based on agro-waste sugar palm (Arenga pinnata (Wurmb.) Merr) starch. *Journal of Materials Research and Technology*, 8(5), 4819–4830. https://doi.org/10.1016/j.jmrt.2019.08.028

Iroba, K. L., Tabil, L. G., Sokhansanj, S., & Dumonceaux, T. (2014). Pretreatment and fractionation of barley straw using steam explosion at low severity factor. *Biomass and Bioenergy*, 66, 286–300. https://doi.org/10.1016/j.biombioe.2014.02.002

Jiang, J., Watowita, P. S. M. S. L., Chen, R., Shi, Y., Geng, J.-T., Takahashi, K., Li, L., & Osako, K. (2022). Multilayer gelatin/myofibrillar films containing clove essential oil: Properties, protein-phenolic interactions, and migration of active compounds. *Food Packaging and Shelf Life*, 32, 100842. https://doi.org/10.1016/j.fpsl.2022.100842

Kahar, P. (2013). Synergistic Effects of Pretreatment Process on Enzymatic Digestion of Rice Straw for Efficient Ethanol Fermentation. In M. Petre (Ed.), Environmental Biotechnology—New Approaches and Prospective Applications. InTech. https://doi.org/10.5772/54949

Kaiser, K., Schmid, M., & Schlummer, M. (2017). Recycling of Polymer-Based Multilayer Packaging: A Review. *Recycling*, 3(1), 1. https://doi.org/10.3390/recycling3010001

Karimi, E., Mehrabanjoubani, P., Keshavarzian, M., Oskoueian, E., Jaafar, H. Z., & Abdolzadeh, A. (2014). Identification and quantification of phenolic and flavonoid components in straw and seed husk of some rice varieties (Oryza sativa L.) and their antioxidant properties: Identification and quantification of phenolic and flavonoid. *Journal of the Science of Food and Agriculture*, 94(11), 2324–2330. https://doi.org/10.1002/jsfa.6567

Kim, H. W., Jeong, J. Y., Seol, K.-H., Seong, P.-N., & Ham, J.-S. (2016). Effects of Edible Films Containing Procyanidin on the Preservation of Pork Meat during Chilled Storage. Korean *Journal for Food Science of Animal Resources*, 36(2), 230–236. https://doi.org/10.5851/kosfa.2016.36.2.230

Le, D. M., Sørensen, H. R., Knudsen, N. O., & Meyer, A. S. (2015). Implications of silica on biorefineries—Interactions with organic material and mineral elements in grasses. *Biofuels, Bioproducts and Biorefining*, 9(1), 109–121. https://doi.org/10.1002/bbb.1511

Li, H., Shi, H., He, Y., Fei, X., & Peng, L. (2020). Preparation and characterization of carboxymethyl cellulose-based composite films reinforced by cellulose nanocrystals derived from pea hull waste for food packaging applications. *International Journal of Biological Macromolecules*, 164, 4104–4112. https://doi.org/10.1016/j.ijbiomac.2020.09.010

Li, L., Rowbotham, J. S., Christopher Greenwell, H., & Dyer, P. W. (2013). An Introduction to Pyrolysis and Catalytic Pyrolysis: Versatile Techniques for Biomass Conversion. In New and Future Developments in Catalysis (pp. 173–208). Elsevier. https://doi.org/10.1016/B978-0-444-53878-9.00009-6

Liu, J., Xie, X., & Li, L. (2022). Experimental study on mechanical properties and durability of grafted nano-SiO2 modified rice straw fiber reinforced concrete. *Construction and Building Materials*, 347, 128575. https://doi.org/10.1016/j.conbuildmat.2022.128575

Long, S., Zhong, L., Lin, X., Chang, X., Wu, F., Wu, R., & Xie, F. (2021). Preparation of formyl cellulose and its enhancement effect on the mechanical and barrier properties of polylactic acid films. *International Journal of Biological Macromolecules*, 172, 82–92. https://doi.org/10.1016/j.ijbiomac.2021.01.029

Lu, Y., Luo, Q., Chu, Y., Tao, N., Deng, S., Wang, L., & Li, L. (2022). Application of Gelatin in Food Packaging: A Review. *Polymers*, 14(3), 436. https://doi.org/10.3390/polym14030436

Luque-García, J. L., & Luque de Castro, M. D. (2003). Ultrasound: A powerful tool for leaching. *TrAC Trends in Analytical Chemistry*, 22(1), 41–47. https://doi.org/10.1016/S0165-9936(03)00102-X

Luzi, F., Del Buono, D., Orfei, B., Moretti, C., Buonaurio, R., Torre, L., & Puglia, D. (2022). Lemna minor aqueous extract as a natural ingredient incorporated in poly (vinyl alcohol)-based films for active food packaging systems. *Food Packaging and Shelf Life*, 32, 100822. https://doi.org/10.1016/j.fpsl.2022.100822

Machmudah, S., Wahyudiono, Kanda, H., & Goto, M. (2017). Hydrolysis of Biopolymers in Near-Critical and Subcritical Water. In Water Extraction of Bioactive Compounds (pp. 69–107). Elsevier. https://doi.org/10.1016/B978-0-12-809380-1.00003-6

Manimaran, P., Pillai, G. P., Vignesh, V., & Prithiviraj, M. (2020). Characterization of natural cellulosic fibers from Nendran Banana Peduncle plants. *International Journal of Biological Macromolecules*, 162, 1807–1815. https://doi.org/10.1016/j.ijbiomac.2020.08.111

MAPA. Ministerio de Agricultura, Pesca y Alimentación. https://www.mapa.gob.es/es/agricultura/temas/producciones-agricolas/dashboardarrozmayo2017_tcm30-380667.pdf . Accessed in Agust 2021.

Marzlan, A. A., Muhialdin, B. J., Zainal Abedin, N. H., Manshoor, N., Ranjith, F. H., Anzian, A., & Meor Hussin, A. S. (2022). Incorporating torch ginger (Etlingera elatior Jack) inflorescence essential oil onto starch-based edible film towards sustainable active packaging for chicken meat. *Industrial Crops and Products*, 184, 115058. https://doi.org/10.1016/j.indcrop.2022.115058

Melo, P. S., Selani, M. M., Gonçalves, R. H., Paulino, J. de O., Massarioli, A. P., & Alencar, S. M. de. (2021). Açaí seeds: An unexplored agro-industrial residue as a potential source of lipids, fibers, and antioxidant phenolic compounds. *Industrial Crops and Products*, 161, 113204. https://doi.org/10.1016/j.indcrop.2020.113204

Menzel, C., González-Martínez, C., Vilaplana, F., Diretto, G., & Chiralt, A. (2020). Incorporation of natural antioxidants from rice straw into renewable starch films. *International Journal of Biological Macromolecules*, 146, 976–986. https://doi.org/10.1016/j.ijbiomac.2019.09.222

Merlo, T. C., Contreras-Castillo, C. J., Saldaña, E., Barancelli, G. V., Dargelio, M. D. B., Yoshida, C. M. P., Ribeiro Junior, E. E., Massarioli, A., & Venturini, A. C. (2019). Incorporation of pink pepper residue extract into chitosan film combined with a modified atmosphere packaging: Effects on the shelf life of salmon fillets. *Food Research International*, 125, 108633. https://doi.org/10.1016/j.foodres.2019.108633

Miklasińska-Majdanik, M., Kępa, M., Wojtyczka, R., Idzik, D., & Wąsik, T. (2018). Phenolic Compounds Diminish Antibiotic Resistance of Staphylococcus Aureus Clinical Strains. *International Journal of Environmental Research and Public Health*, 15(10), 2321. https://doi.org/10.3390/ijerph15102321

Mkhize, T., Mthembu, L. D., Gupta, R., Kaur, A., Kuhad, R. C., Reddy, P., & Deenadayalu, N. (2016). Enzymatic Saccharification of Acid/Alkali Pre-treated, Mill-run, and Depithed Sugarcane Bagasse. *BioResources*, 11(3), 6267–6285. https://doi.org/10.15376/biores.11.3.6267-6285

Muller, J., González-Martínez, C., & Chiralt, A. (2017). Poly(lactic) acid (PLA) and starch bilayer films, containing cinnamaldehyde, obtained by compression moulding. *European Polymer Journal*, 95, 56–70. https://doi.org/10.1016/j.eurpolymj.2017.07.019

Murakami, K., Sato, M., Kato, T., & Sugawara, K. (2012). Influence of difference in chemical compositions of rice straw on hydrogen formation in nickel-catalyzed steam gasification. *Fuel Processing Technology*, 95, 78–83. https://doi.org/10.1016/j.fuproc.2011.11.020

Nerín, C., Tovar, L., & Salafranca, J. (2008). Behaviour of a new antioxidant active film versus oxidizable model compounds. *Journal of Food Engineering*, 84(2), 313–320. https://doi.org/10.1016/j.jfoodeng.2007.05.027

Ng, H.-M., Sin, L. T., Tee, T.-T., Bee, S.-T., Hui, D., Low, C.-Y., & Rahmat, A. R. (2015a). Extraction of cellulose nanocrystals from plant sources for application as reinforcing agent in polymers. *Composites Part B: Engineering*, 75, 176–200. https://doi.org/10.1016/j.compositesb.2015.01.008

Nghi, N. T., Romasanta, R. R., Van Hieu, N., Vinh, L. Q., Du, N. X., Ngan, N. V. C., Chivenge, P., & Van Hung, N. (2020). Rice Straw-Based Composting. In M. Gummert, N. V. Hung, P. Chivenge, & B. Douthwaite (Eds.), Sustainable Rice Straw Management (pp. 33–41). Springer International Publishing. https://doi.org/10.1007/978-3-030-32373-8_3

Ojha, K. S., Aznar, R., O'Donnell, C., & Tiwari, B. K. (2020). Ultrasound technology for the extraction of biologically active molecules from plant, animal and marine sources. *TrAC Trends in Analytical Chemistry*, 122, 115663. https://doi.org/10.1016/j.trac.2019.115663

Oun, A. A., Shin, G. H., & Kim, J. T. (2022). Antimicrobial, antioxidant, and pH-sensitive polyvinyl alcohol/chitosan-based composite films with aronia extract, cellulose nanocrystals, and grapefruit seed extract. *International Journal of Biological Macromolecules*, 213, 381–393. https://doi.org/10.1016/j.ijbiomac.2022.05.180

Papoutsis, K., Pristijono, P., Golding, J. B., Stathopoulos, C. E., Bowyer, M. C., Scarlett, C. J., & Vuong, Q. V. (2016). Optimisation of aqueous extraction conditions for the recovery of phenolic compounds and antioxidants from lemon pomace. *International Journal of Food Science & Technology*, 51(9), 2009–2018. https://doi.org/10.1111/ijfs.13168

Peanparkdee, M., & Iwamoto, S. (2019). Bioactive compounds from by-products of rice cultivation and rice processing: Extraction and application in the food and pharmaceutical industries. *Trends in Food Science & Technology*, 86, 109–117. https://doi.org/10.1016/j.tifs.2019.02.041

Pereira, P. H. F., Ornaghi, H. L., Arantes, V., & Cioffi, M. O. H. (2021). Effect of chemical treatment of pineapple crown fiber in the production, chemical composition, crystalline structure, thermal stability and thermal degradation kinetic properties of cellulosic materials. *Carbohydrate Research*, 499, 108227. https://doi.org/10.1016/j.carres.2020.108227

Perumal, A. B., Nambiar, R. B., Sellamuthu, P. S., Sadiku, E. R., Li, X., & He, Y. (2022). Extraction of cellulose nanocrystals from areca waste and its application in eco-friendly biocomposite film. *Chemosphere*, 287, 132084. https://doi.org/10.1016/j.chemosphere.2021.132084

Perumal, A. B., Sellamuthu, P. S., Nambiar, R. B., & Sadiku, E. R. (2018). Development of polyvinyl alcohol/chitosan bio-nanocomposite films reinforced with cellulose nanocrystals isolated from rice straw. *Applied Surface Science*, 449, 591–602. https://doi.org/10.1016/j.apsusc.2018.01.022

PlascticsEurope. (2021). Plastics-the Facts 2021. An analysis of European plastics production, demand and waste data. https://plasticseurope.org/knowledge-hub/plastics-the-facts-2021/. Accessed August, 2021.

Pongchaiphol, S., Preechakun, T., Raita, M., Champreda, V., & Laosiripojana, N. (2021). Characterization of Cellulose–Chitosan-Based Materials from Different Lignocellulosic Residues Prepared by the Ethanosolv Process and Bleaching Treatment with Hydrogen Peroxide. ACS Omega, 6(35), 22791–22802. https://doi.org/10.1021/acsomega.1c03141

Prasad, P., Kocchar, A. (2014). Active Packaging in Food Industry: A Review. *Journal of Environmental Science, Toxicology and Food Technology*, 8(5), p. 01-07.

Priyadarshi, R., & Rhim, J.-W. (2020). Chitosan-based biodegradable functional films for food packaging applications. *Innovative Food Science & Emerging Technologies*, 62, 102346. https://doi.org/10.1016/j.ifset.2020.102346

Requena, R., Jiménez-Quero, A., Vargas, M., Moriana, R., Chiralt, A., & Vilaplana, F. (2019). Integral Fractionation of Rice Husks into Bioactive Arabinoxylans, Cellulose Nanocrystals, and Silica Particles. *ACS Sustainable Chemistry & Engineering*, 7(6), 6275–6286. https://doi.org/10.1021/acssuschemeng.8b06692

Reynoso-Camacho, R., Rodríguez-Villanueva, L. D., Sotelo-González, A. M., Ramos-Gómez, M., & Pérez-Ramírez, I. F. (2021). Citrus decoction by-product represents a rich source of carotenoid, phytosterol, extractable and non-extractable polyphenols. *Food Chemistry*, 350, 129239. https://doi.org/10.1016/j.foodchem.2021.129239

Rocca-Smith, J. R., Pasquarelli, R., Lagorce-Tachon, A., Rousseau, J., Fontaine, S., Aguié-Béghin, V., Debeaufort, F., & Karbowiak, T. (2019). Toward Sustainable PLA-Based Multilayer

Complexes with Improved Barrier Properties. *ACS Sustainable Chemistry & Engineering*, 7(4), 3759–3771. https://doi.org/10.1021/acssuschemeng.8b04064

Román, P., Martínez, M. M., Pantoja, A. (2013). Manual de compostaje del agricultor experiencias .pdf.

Ross, G., Ross, S., & Tighe, B. J. (2017). Bioplastics. In Brydson's Plastics Materials (pp. 631–652). Elsevier. https://doi.org/10.1016/B978-0-323-35824-8.00023-2

Roy, S., & Rhim, J.-W. (2021a). Fabrication of bioactive binary composite film based on gelatin/chitosan incorporated with cinnamon essential oil and rutin. *Colloids and Surfaces B: Biointerfaces*, 204, 111830. https://doi.org/10.1016/j.colsurfb.2021.111830

Roy, S., & Rhim, J.-W. (2021b). Gelatin/agar-based functional film integrated with Pickering emulsion of clove essential oil stabilized with nanocellulose for active packaging applications. *Colloids and Surfaces A: Physicochemical and Engineering Aspects*, 627, 127220. https://doi.org/10.1016/j.colsurfa.2021.127220

Ruthes, A. C., Martínez-Abad, A., Tan, H., Bulone, V., Vilaplana, F. (2017). Sequential fractionation of feruloylated hemicelluloses and oligosaccharides from wheat bran using subcritical water and xylanolytic enzymes. *Green Chemistry*, 19, 1919-1931. https://doi.org/10.1039/c6gc03473j

Sadh, P. K., Chawla, P., Bhandari, L., & Duhan, J. S. (2018). Bio-enrichment of functional properties of peanut oil cakes by solid state fermentation using Aspergillus oryzae. *Journal of Food Measurement and Characterization*, 12(1), 622–633. https://doi.org/10.1007/s11694-017-9675-2

Sahu, O. (2021). Characterisation and utilization of heterogeneous catalyst from waste rice-straw for biodiesel conversion. *Fuel*, 287, 119543. https://doi.org/10.1016/j.fuel.2020.119543

Seo, D.-J., & Sakoda, A. (2014). Assessment of the structural factors controlling the enzymatic saccharification of rice straw cellulose. *Biomass and Bioenergy*, 71, 47–57. https://doi.org/10.1016/j.biombioe.2014.10.027

Shen, P., Tang, Q., Chen, X., & Li, Z. (2022). Nanocrystalline cellulose extracted from bast fibers: Preparation, characterization, and application. *Carbohydrate Polymers*, 290, 119462. https://doi.org/10.1016/j.carbpol.2022.119462

Shinde, R., Shahi, D. K., Mahapatra, P., Singh, C. S., Naik, S. K., Thombare, N., & Singh, A. K. (2022). Management of crop residues with special reference to the on-farm utilization

methods: A review. *Industrial Crops and Products*, 181, 114772. https://doi.org/10.1016/j.indcrop.2022.114772

Shlush, E., & Davidovich-Pinhas, M. (2022). Bioplastics for food packaging. *Trends in Food Science & Technology*, 125, 66–80. https://doi.org/10.1016/j.tifs.2022.04.026

Singh, L., & Brar, B. S. (2021). A Review on Rice Straw Management Strategies. *Nature Environment and Pollution Technology*, 20(4). https://doi.org/10.46488/NEPT.2021.v20i04.010

Singh, R., Gautam, S., Sharma, B., Jain, P., & Chauhan, K. D. (2021). Biopolymers and their classifications. In Biopolymers and their Industrial Applications (pp. 21–44). Elsevier. https://doi.org/10.1016/B978-0-12-819240-5.00002-X

Sticklen, M. B. (2008). Plant genetic engineering for biofuel production: Towards affordable cellulosic ethanol. *Nature Reviews Genetics*, 9(6), 433–443. https://doi.org/10.1038/nrg2336

Sumere, B. R., de Souza, M. C., dos Santos, M. P., Bezerra, R. M. N., da Cunha, D. T., Martinez, J., & Rostagno, M. A. (2018). Combining pressurized liquids with ultrasound to improve the extraction of phenolic compounds from pomegranate peel (Punica granatum L.). *Ultrasonics Sonochemistry*, 48, 151–162. https://doi.org/10.1016/j.ultsonch.2018.05.028

Swatloski, R. P., Spear, S. K., Holbrey, J. D., & Rogers, R. D. (2002). Dissolution of Cellose with Ionic Liquids. *Journal of the American Chemical Society*, 124(18), 4974–4975. https://doi.org/10.1021/ja025790m

Syafri, E., Kasim, A., Abral, H., Sudirman, Sulungbudi, G. T., Sanjay, M. R., & Sari, N. H. (2018). Synthesis and characterization of cellulose nanofibers (CNF) ramie reinforced cassava starch hybrid composites. *International Journal of Biological Macromolecules*, 120, 578–586. https://doi.org/10.1016/j.ijbiomac.2018.08.134

Takano, M., & Hoshino, K. (2018). Bioethanol production from rice straw by simultaneous saccharification and fermentation with statistical optimized cellulase cocktail and fermenting fungus. *Bioresources and Bioprocessing*, 5(1), 16. https://doi.org/10.1186/s40643-018-0203-y

Tampau, A., González-Martínez, C., & Chiralt, A. (2018). Release kinetics and antimicrobial properties of carvacrol encapsulated in electrospun poly-(ε-caprolactone) nanofibres. Application in starch multilayer films. *Food Hydrocolloids*, 79, 158–169. https://doi.org/10.1016/j.foodhyd.2017.12.021

Tang, S., Dong, Q., Fang, Z., Cong, W., & Zhang, H. (2020). Microbial lipid production from rice straw hydrolysates and recycled pretreated glycerol. *Bioresource Technology*, 312, 123580. https://doi.org/10.1016/j.biortech.2020.123580

Thakur, S., Chaudhary, J., Sharma, B., Verma, A., Tamulevicius, S., & Thakur, V. K. (2018). Sustainability of bioplastics: Opportunities and challenges. *Current Opinion in Green and Sustainable Chemistry*, 13, 68–75. https://doi.org/10.1016/j.cogsc.2018.04.013

Thiripura Sundari, M., & Ramesh, A. (2012). Isolation and characterization of cellulose nanofibers from the aquatic weed water hyacinth—Eichhornia crassipes. *Carbohydrate Polymers*, 87(2), 1701–1705. https://doi.org/10.1016/j.carbpol.2011.09.076

Topuz, F., & Uyar, T. (2020). Antioxidant, antibacterial and antifungal electrospun nanofibers for food packaging applications. *Food Research International*, 130, 108927. https://doi.org/10.1016/j.foodres.2019.108927

Toribio-Cuaya, H., Pedraza-Segura, L., Macías-Bravo, S., Vasquez-Medrano, R., & Favela-Torres, E. (2014). Characterization of Lignocellulosic Biomass Using Five Simple Steps. *Journal of Chemical, Biological and Physical Sciences*, 4(5), 21.

Van Hung, N., Maguyon-Detras, M. C., Migo, M. V., Quilloy, R., Balingbing, C., Chivenge, P., & Gummert, M. (2020). Rice Straw Overview: Availability, Properties, and Management Practices. In M. Gummert, N. V. Hung, P. Chivenge, & B. Douthwaite (Eds.), Sustainable Rice Straw Management (pp. 1–13). Springer International Publishing. https://doi.org/10.1007/978-3-030-32373-8_1

Verma, D. K., Thakur, M., Singh, S., Tripathy, S., Gupta, A. K., Baranwal, D., Patel, A. R., Shah, N., Utama, G. L., Niamah, A. K., Chávez-González, M. L., Gallegos, C. F., Aguilar, C. N., & Srivastav, P. P. (2022). Bacteriocins as antimicrobial and preservative agents in food: Biosynthesis, separation and application. *Food Bioscience*, 46, 101594. https://doi.org/10.1016/j.fbio.2022.101594

Vilarinho, F., Stanzione, M., Buonocore, G. G., Barbosa-Pereira, L., Sendón, R., Vaz, M. F., & Sanches Silva, A. (2021). Green tea extract and nanocellulose embedded into polylactic acid film: Properties and efficiency on retarding the lipid oxidation of a model fatty food. *Food Packaging and Shelf Life*, 27, 100609. https://doi.org/10.1016/j.fpsl.2020.100609

Vilela, C., Kurek, M., Hayouka, Z., Röcker, B., Yildirim, S., Antunes, M. D. C., Nilsen-Nygaard, J., Pettersen, M. K., & Freire, C. S. R. (2018). A concise guide to active agents for active food packaging. *Trends in Food Science & Technology*, 80, 212–222. https://doi.org/10.1016/j.tifs.2018.08.006

Wahyudiono, W., Machmudah, S., & Goto, M. (2013). Utilization of Sub and Supercritical Water Reactions in Resource Recovery of Biomass Wastes. *Engineering Journal*, 17(1), 1–12. https://doi.org/10.4186/ej.2013.17.1.1

Wang, H., Qian, J., & Ding, F. (2018). Emerging Chitosan-Based Films for Food Packaging Applications. *Journal of Agricultural and Food Chemistry*, 66(2), 395–413. https://doi.org/10.1021/acs.jafc.7b04528

Wang, Q., Chen, W., Zhu, W., McClements, D. J., Liu, X., & Liu, F. (2022). A review of multilayer and composite films and coatings for active biodegradable packaging. *Npj Science of Food*, 6(1), 18. https://doi.org/10.1038/s41538-022-00132-8

Wang, S., Lu, A., & Zhang, L. (2016). Recent advances in regenerated cellulose materials. *Progress in Polymer Science*, 53, 169–206. https://doi.org/10.1016/j.progpolymsci.2015.07.003

Xia, C., Wang, W., Wang, L., Liu, H., & Xiao, J. (2019). Multilayer zein/gelatin films with tunable water barrier property and prolonged antioxidant activity. *Food Packaging and Shelf Life*, 19, 76–85. https://doi.org/10.1016/j.fpsl.2018.12.004

Xu, Y., Chu, Y., Feng, X., Gao, C., Wu, D., Cheng, W., Meng, L., Zhang, Y., & Tang, X. (2020). Effects of zein stabilized clove essential oil Pickering emulsion on the structure and properties of chitosan-based edible films. *International Journal of Biological Macromolecules*, 156, 111–119. https://doi.org/10.1016/j.ijbiomac.2020.04.027

Yilmaz, P., Demirhan, E., & Ozbek, B. (2022). Development of Ficus carica Linn leaves extract incorporated chitosan films for active food packaging materials and investigation of their properties. *Food Bioscience*, 46, 101542. https://doi.org/10.1016/j.fbio.2021.101542

Zhang, Y., & Naebe, M. (2021). Lignin: A Review on Structure, Properties, and Applications as a Light-Colored UV Absorber. *ACS Sustainable Chemistry & Engineering*, 9(4), 1427–1442. https://doi.org/10.1021/acssuschemeng.0c06998

Zhang, Z., Smith, C., & Li, W. (2014). Extraction and modification technology of arabinoxylans from cereal by-products: A critical review. *Food Research International*, 14.

Zimmermann, T., Bordeanu, N., & Strub, E. (2010). Properties of nanofibrillated cellulose from different raw materials and its reinforcement potential. *Carbohydrate Polymers*, 79(4), 1086–1093. https://doi.org/10.1016/j.carbpol.2009.10.045

OBJECTIVES

General objective

The **general objective** of this Doctoral Thesis was the valorisation of rice straw by obtaining cellulose fractions and active extracts, with antioxidant and antibacterial activity, for their use in developing biodegradable food packaging materials. To this end, the obtained fractions were incorporated into corn starch and poly (lactic acid) (PLA) matrices, thus obtaining mono and bilayer films with potential application as sustainable packaging for different food matrices.

Specific objectives

I. To obtain active aqueous extracts from rice straw, by applying ultrasound-assisted extraction and combined extraction methods, analysing the effect of the process conditions on the phenolic content and antioxidant and antibacterial capacity of the extracts.

II. To obtain cellulose fibres from the solid residue from the ultrasound combined extraction and characterise them as to their structural properties, thermal behaviour, and reinforcement capacity, in comparison with those obtained by applying the conventional alkaline treatment.

III. To evaluate the reinforcing properties of rice straw cellulose fibres in thermoplastic starch films, as a function of their ratio in the films and the starch pre-treatment, by analysing their tensile, barrier, optical, thermal, and microstructural properties.

IV. To analyse the effect of incorporating the most active extract (obtained by ultrasound combined extraction) from rice straw into PLA films, at different ratios, through the analyses of the films' structural and functional properties, as well as the release kinetics of the extract phenolic compounds in different food simulants.

V. To develop bilayer films with improved barrier capacity, by combining starch films, with and without cellulose fibres, and PLA films, with and without active extract, and evaluation of their capacity to preserve fresh pork meat during cold storage.

VI. To evaluate the effect of incorporating cellulose fibres and active extract into thermoplastic starch films by characterising their microstructural, thermal, barrier, and optical properties, as well as their effectiveness in preventing sunflower oil oxidation under an accelerated oxidation test.

VII. To apply subcritical water extraction to obtain rice straw active extracts and characterise them as to their antioxidant and antibacterial capacity.

VIII. To obtain cellulose fibres from the residue of subcritical water extractions and characterise them as to their structural and thermal properties and the aerogel formation capacity, in comparison with those obtained from the ultrasound combined method and the conventional alkaline treatment.

IX. To study the effect of incorporating different active extracts obtained by subcritical water extraction into PLA films, through the analyses of their microstructure, thermal behaviour and tensile and barrier properties, as well as to their ability to preserve fresh pork meat during cold storage, in comparison with the extracts obtained by the ultrasound combined method.

CHAPTERS

CHAPTER 1

Ultrasound-assisted extraction to obtain active extracts and cellulose fractions from rice straw. Application in food packaging systems

I. Application of ultrasound pre-treatment for enhancing extraction of bioactive compounds from rice straw

II. Applying ultrasound-assisted processing to obtain cellulose fibres from rice straw to be used as reinforcing agents

III. Valorisation of rice straw into cellulose microfibers for the reinforcement of thermoplastic corn starch films

IV. Antioxidant poly (lactic acid) films with rice straw extract for food packaging applications

V. Using rice straw fractions to develop reinforced, active PLA-starch bilayers for meat preservation

VI. Antioxidant starch composite films containing rice straw extract and cellulose fibres

CHAPTER 2

Application of subcritical water extraction to obtain active extracts and cellulose fractions from rice straw and comparison with the US treatment

VII. Active poly (lactic acid) films with rice straw aqueous extracts for meat preservation

VIII. Cellulose aerogels obtained from rice straw. Influence of the cellulose purification process

CHAPTER 1.I

Application of ultrasound pre-treatment for enhancing extraction of bioactive compounds from rice straw

Pedro A. V. Freitas, Chelo González-Martínez, Amparo Chiralt

Institute of Food Engineering for Development, Universitat Politècnica de València, 46022, Valencia, Spain

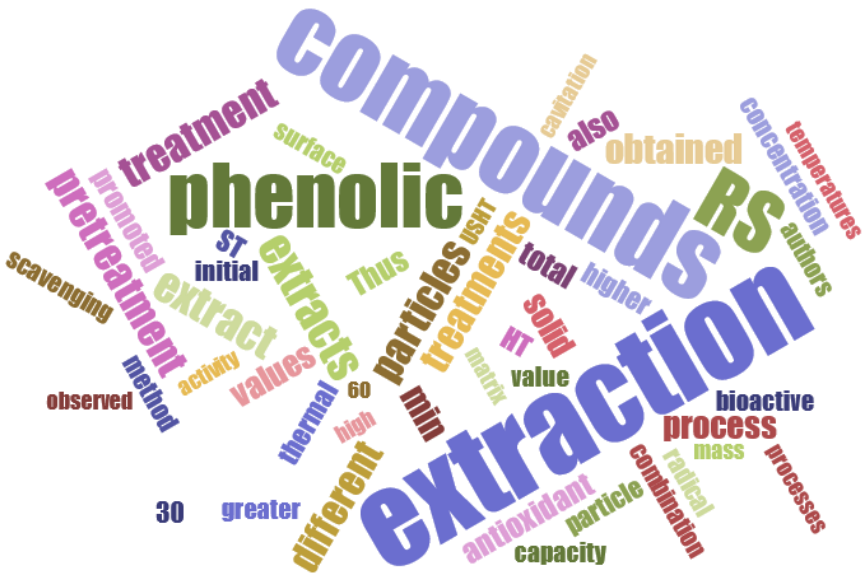

Foods (2020), 9(11), 1-15

ABSTRACT

The extraction of water-soluble bioactive compounds using different green methods is an eco-friendly alternative for valorising agricultural wastes such as rice straw (RS). In this study, aqueous extracts of RS (particles < 500 µm) were obtained using ultrasound (US), reflux heating (HT), stirring (ST) and a combination of US and ST (USST) or HT (USHT). The extraction kinetics was well fitted to a pseudo-second-order model. As regards phenolic compound yield, the US method (342 mg gallic acid (GAE). 100 g^{-1} RS) was more effective than the ST treatment (256 mg GAE.100 g^{-1} RS), reaching an asymptotic value after 30 min of process. When combined with HT (USHT), the US pre-treatment led to the highest extraction of phenolic compounds from RS (486 mg GAE.100 g^{-1} RS) while the extract exhibited the greatest antioxidant activity. Furthermore, the USHT extract reduced the initial counts of *Listeria innocua* by 1.7 logarithmic cycles. Therefore, the thermal aqueous extraction of RS applying the 30 min US pre-treatment, represents a green and efficient approach to obtain bioactive extracts for food applications.

Keywords: bioactive compounds; water extraction; antioxidant activity; pseudo-second-order law; antimicrobial activity; heating; combined methods

1. INTRODUCTION

A rising global population and limited natural resources have encouraged the food industries to seek new environmentally-friendly alternatives for agro-industrial waste management [1,2]. One of the primary agro-industrial wastes, rice straw (RS) is a by-product obtained from the rice grain (*Oryza sativa* L.) harvesting, which is considered one of the most important global food crops [3]. Indeed, the Food and Agriculture Organization of the United Nations reported that the annual world rice production was approximately 782 million tons, with 90 % production from the Asian continent [4]. Considering that one kilogram of rice grain provides 1.5 kg RS and the largest portion of RS is commonly burnt in the field, there is a continuous increase of air pollution associated with the release of dioxins, affecting human health and reducing the soil feasibility [3,5]. In this way, efforts have recently been made to find new alternatives for the reuse of RS, such as bioethanol production [6], silica extraction [7], paper production [8], cellulose isolation [9] or bioactive compound extraction [10,11].

RS contains about 35 % cellulose, 20 % lignin, 18 % hemicellulose and 15 % ashes (dry weight basis) [12]. Likewise, RS has been considered an excellent source of bioactive compounds, including phenolic compounds with antioxidant and antimicrobial potential. Menzel et al. [10] identified bioactive compounds from RS aqueous and alcoholic extracts using ultra-high-performance liquid chromatography coupled to high-resolution mass spectrometry. They found several types of compounds with excellent antioxidant properties, such as ferulic acid, protocatechuic acid, *p*-coumaric acid, caffeic acid, vanillic acid, tricin and vanillin. Some of these phenolic compounds, such as *p*-coumaric, and ferulic acid, have not been found in significant quantities in other vegetable and fruit matrices [13].

In recent years, new technologies have been applied in extraction methodologies in order to overcome problems related to traditional techniques, such as limitations in the extract yield and the fact that they consume a great deal of energy and time [14]. Ultrasound-assisted extraction (UAE) is an eco-friendly and efficient process that applies acoustic cavitation using an ultrasonic probe device in a closed flow-through mode in a determined matrix to extract target compounds. The ultrasound waves, ranging from 20 to 1000 kHz, have been applied to improve the extraction by the solvent acoustic cavitation. The shear forces promoted from the rupture of the bubbles disrupt the cell matrices, extracting higher amounts of compounds by means of different physical phenomena [14–16]. Many studies have shown the efficiency of UAE coupled with the greater antioxidant and antimicrobial activity of extracts from different vegetal matrices [17–21]. To the best of our knowledge, UAE has not been previously applied to extract phenolic compounds from the RS matrix to obtain bioactive extracts.

The aim of this study was to improve the water extraction effectiveness of bioactive compounds from rice straw by applying probe-based UAE. The performance of the UAE

treatments and their combination with conventional heating and stirring extraction methods was evaluated in terms of the extraction kinetics of phenolic compounds, as well as the antioxidant and antimicrobial activity of the obtained extracts. Likewise, the mass transfer phenomenon was correlated with the possible physical changes that occurred in the ground RS plant matrix.

2. MATERIAL AND METHODS

2.1. Chemicals

Gallic acid, Folin-Ciocalteau reagent (2N), methanol, and 2,2-Diphenyl-1-picrylhydrazyl (DPPH) were purchased from Sigma-Aldrich (USA). Sodium carbonate was obtained from PanReac Quimica S.L.U. (Castellar del Vallés, Barcelona, Spain). Tryptone soy broth, tryptone soy agar, phosphate-buffered saline, and peptone water were purchased from Scharlab (Barcelona, Spain). Strains of *Listeria innocua* (CECT 910) and *Escherichia coli* (CECT 101) were purchased from the Spanish Type Collection (CECT, University of Valencia, Valencia, Spain).

2.2. Plant material preparation

RS (*Oryza sativa* L., J. Sendra var) was obtained from L'Albufera rice fields, Valencia, Spain, and supply by the "Banco de Paja" (Valencia), from the harvest 2019. Samples were processed by drying the RS at 50 ± 2 °C under vacuum (0.5 mmbar) for 16 h. After that, the RS was milled using a milling machine (IKA, model M20, Germany) operating in 3 cycles of 90 s each. The ground RS was sieved to obtain particles of under 0.5 mm (representing 98 % wt. of the milled RS) (Figure 1) and stored in a desiccator at 20 ± 2 °C until further use.

2.3. Aqueous extraction of RS powder

The aqueous extracts of phenolic compounds were obtained using an RS: water ratio of 1:20 (m/v). As shown in Figure 1, different extraction approaches were used based on ultrasound (US), stirring (ST), heating under reflux condition (HT), and a combination. The US method was carried out using an ultrasonic homogenizer (Vibra CellTM VCX750, Sonics & Material, Inc., Newtown, CT, USA) equipped with a high-intensity probe operating in a continuous mode. RS and water were mixed and sonicated for 60 min at 25 °C (maintaining the sample in an ice bath to prevent heating), using 750 W power, 20 kHz frequency, and 40 % sonication amplitude. The ST extract was obtained by stirring the dispersion for 60 min at 350 rpm and 25 °C. The HT method consisted of heating the RS suspension at 100 °C for 60 min using a typical reflux device. Two combined extraction methods were carried out by successively applying 30 min US, as a pre-treatment, and ST for 60 min (USST) or HT for 60 min (USHT). The US pre-treatment time was established based on the results obtained for the US treatment.

In every process, the supernatant obtained after each treatment was filtered using a qualitative filter (Filterlab) and stored in a dark bottle at 4 ± 2 °C until used.

The extraction kinetics was evaluated in terms of the total phenolic content by sampling and analysing the extract after different process times: 2, 5, 10, 15, 20, 25, 30, 40, 50, and 60 min. To perform the other analyses, extracts obtained from the US method were characterized after 15, 30, and 60 min (US15, US30, and US60), and the ST and HT extracts were analysed after 60 min extraction time (ST60 and HT60). Likewise, combined USST60 and USHT60 treatments were also characterized. Each treatment was carried out in triplicate and analysed in terms of total solid yield (TSY), total phenolic content (TPC), antioxidant, and antibacterial activities. TSY was determined by drying the RS extracts at 70 ± 2 °C under vacuum for 6 h until constant weight. After extraction, the residues were collected, and their particle size distribution and microstructure were compared with those of the initial RS powder.

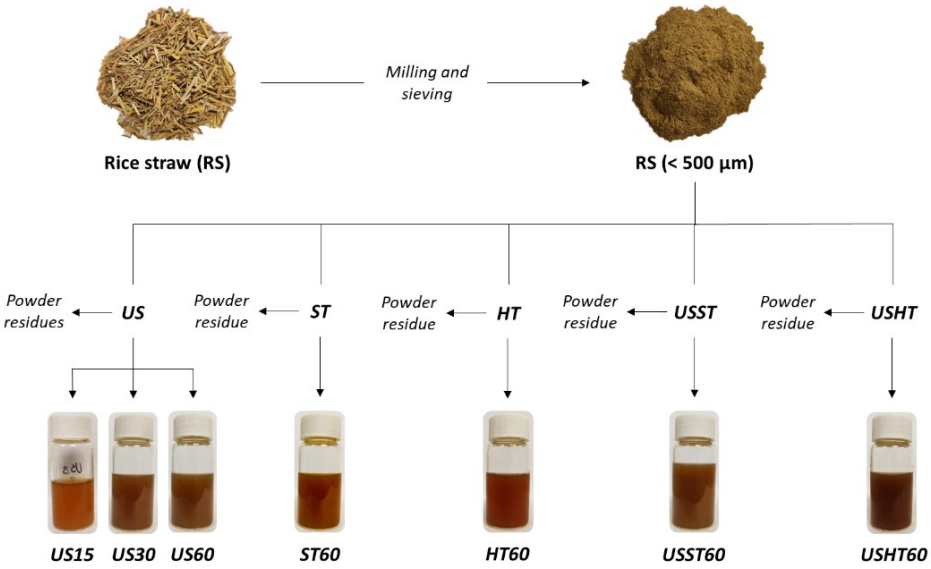

Figure 1. Schematic illustration and appearance of RS extracts obtained from different extraction processes: ultrasound (US), stirring (ST), heating under reflux condition (HT), and a combined treatment (USST and USHT). The number in the sample code indicates the processing time without considering the pre-treatment time.

2.4. Analysis of total phenolic content

TPC for the different extraction methods over time were determined according to the modified Folin-Ciocalteu method by Menzel et al. [10]. The TPC was determined from the absorbance values, using the linear equation fitted to the stand curve using gallic acid ($Abs_{725\ nm}$ = 0.099 [gallic acid] + 0.043; R^2 = 0.9991). The results were expressed as mg gallic acid equivalents (mg GAE) per 100 g of dried RS. All measurements were taken in triplicate.

2.5. Modelling extraction kinetics

A pseudo-second order rate law was applied to model the extraction kinetics, according to Ho et al. [22]. The dissolution rate of RS compounds, contained within the RS matrix, into water solution can be written as:

$$\frac{d(C_t)}{dt} = k(C_e - C_t)^2 \quad (1)$$

Where k is the second-order extraction rate constant (L.mg^{-1}.min^{-1}), C_e (mg.L^{-1}) and C_t (mg.L^{-1}) are the total phenol concentrations in the solvent phase at equilibrium and at any time t (min), respectively. Eq. 1 was integrated under the boundary conditions t = 0 to t and $C_t = C_0$ to C_t, thus obtaining Eq. 2.

$$C_t = \frac{ktC_e(C_e - C_0) + C_0}{kt(C_e - C_0) + 1} \quad (2)$$

When $C_0 = 0$, Eq. 2 can be linearized as Eq. 3 and the initial extraction rate, h (mg.L^{-1}.min^{-1}), can be obtained when t approaches 0 (Eq. 4):

$$\frac{t}{C_t} = \frac{1}{k(C_e)^2} + \frac{t}{C_e} \quad (3)$$

$$h = k(C_e)^2 \quad (4)$$

C_e, k, and h were determined from the linear fitting of the data in the plot t/C_t versus t, as inferred from Eq. 3 and Eq. 4. In the case of treatments applied after 30 min US pre-treatment, when $C_o \neq 0$, a non-linear fitting was applied, using the SOLVER tool from EXCEL to obtain k and C_e values.

The quality of fit for each extraction method was statistically evaluated by the determination coefficient (R^2) (Eq. 4), and the average absolute relative deviation (*AARD%*) (Eq. 5), which measure the model's predictive effectiveness.

$$R^2 = \frac{\sum_{i=1}^{N}(y_i^{cal} - y_i^{exp})^2}{\sum_{i=1}^{N}(y_i^{cal} - y_m)^2} \quad (5)$$

$$AARD\% = 100\ x\ \frac{1}{N}\sum_{i=1}^{N}\left|\frac{y_i^{cal} - y_i^{exp}}{y_i^{exp}}\right| \quad (6)$$

Where N is the number of the data set; y_i^{cal} is the predictive value of the model; y_i^{exp} is the experimental value; and y_m is the mean value.

2.6. Antioxidant activity by DPPH radical scavenging method

The antiradical activities of the different RS extracts were determined using the free radical 2,2-Diphenyl-1-pikryl-hydrazyl (DPPH) method, with some modifications [23]. For each RS extract, different concentrations were mixed with the 6.22 x 10^{-2} mM DPPH methanolic solution ($Abs_{515\ nm}$ = 0.7 ± 0.2) to a final volume of 4 mL. The initial DPPH concentration in the reaction medium was determined from a calibration curve ($Abs_{515\ nm}$ = 11.324 *[DPPH]* – 0.038; R^2 = 0.9992). The antiradical activity was evaluated by EC_{50}, which is defined as the amount of antioxidant necessary to reduce the initial DPPH concentration by 50% when reaction stability has been reached. The reaction stability times between the extract and DPPH solutions were 180 min for the US (15, 30, and 60 min), ST60, and their combined treatment (USST60), and 45 min for the HT60 and USHT60 treatments. To obtain the EC_{50} values, the plots $\%[DPPH]_{remaining}$ *vs.* mg solid extract/mg DPPH were obtained, where:

$$\%[DPPH]_{remaining} = \left(\frac{[DPPH]_t}{[DPHH]_{t=0}}\right) x\ 100 \quad (7)$$

$[DPPH]_t$ is the DDPH concentration value when the reaction was stable, and $[DPPH]_{t=0}$ is the DPPH initial concentration.

2.7. Antibacterial bioactivity

For both *Listeria innocua* and *Escherichia coli* strains (stored at -20 °C), a stock solution was obtained by transferring amounts of bacteria strain into 10 mL tryptic soy broth (TSB) using an inoculation loop twice. After incubation at 37 °C for 24 h, the working solution was prepared by pipetting 10 µl of the stock solution in 10 mL TSB and incubating at 37 °C for 24 h. The working solution was serially diluted in TSB to obtain 10^5 CFU.mL^{-1} (concentration was validated by incubation of 100 µL in tryptic soy agar at 37 °C for 24 h and counting).

The antimicrobial activity of the RS extract against *Listeria innocua* and *Escherichia coli* strains were analysed using previously described methods [24,25]. The analysis was carried out in standard 96-well microtiter plates (well volume of 200 µL). For each microorganism, 100 µL of 10^5 CFU.mL^{-1} bacteria solution was pipetted in each well together with different RS extract solution volumes. Then, the final volume in each well was completed to 200 µl with TSB and incubated at 37 °C for 24 h. The tested concentrations of freeze-dried RS extract dissolved in TSB were 96, 104, 112, 120, 128, 136, 144, 152, and 160 mg.mL^{-1}. Typically, the analysis controls were wells containing only bacterial suspension, extract solution and TSB solution. The final counts of each bacteria after incubation were determined in tryptic soy agar media for each well. Thus, 100 µL of each well was transferred in tryptic soy agar plates and incubated at 37 °C for 24 h to obtain the counts. The analysis was performed in duplicate.

2.8. Particle size distribution in RS powder

The particle size distributions of RS powders before and after the extraction processes were determined in triplicate using a laser-diffraction particle size analyser (Malvern Instruments, UK) coupled with a Scirocco 2000 dry dispersion unit. A refractive index of 1.520 and an absorption of 0.1 was considered. Samples were fed into the system at a feed rate of 60 % and a pressure of 2.5 bar until reaching an obscuration rate of 1.26 %. The parameter D_{43} and the mean particle size distribution curves were obtained.

2.9. High-resolution field emission scanning electron microscopy (FESEM)

The morphologies of the RS particles after the extraction processes were characterized using a High-Resolution Field Emission Scanning Electron Microscope (GeminiSEM 500, Zeiis, Oxford Instruments, UK). Before the microscopy observations, the samples were coated with platinum using an EM MED020 sputter coater (Leica Biosystems). The images were taken under vacuum and 2.0 kV acceleration voltage.

2.10. Statistical analysis

The data were submitted to analysis of variance (ANOVA), and Tukey's studentized range (HSD) test using a Minitab statistical program (version 17). This was performed to determine whether there were significant differences among the extraction methods, using the least significant difference (α) of 5 %.

3. RESULTS AND DISCUSSION

3.1. Extraction kinetics of phenolic compounds

The performance of the different aqueous extraction methods was compared in terms of the total phenolic content (TPC) reached after different process times (Fig. 2a, points). As previously observed by other authors [14,17,26,27] for extraction processes from plant matrices, the compound extraction rate was higher in the first stage of the process (10-15 min), progressively decreasing till the concentration reached an asymptotic value, considered as the equilibrium value (C_e). This is coherent with the greater driving force for mass transfer after short process times [28] while also reflecting the faster initial desorption of compounds from the surface of solid particles and the slower diffusion of compounds extracted from their more internal parts. For the combined USST treatment, the extraction rate was very low throughout the time due to the small difference between the initial TPC concentration (obtained during the 30 min US pre-treatment) and that reached at equilibrium, which indicates the limited capacity of simple stirring to improve phenol extraction after the US pre-treatment. However, in the USHT treatment, with the same initial TPC value, the equilibrium concentration increased with respect to that obtained in the USST process. Thus, different

treatments led to distinct asymptotic values of C_e, depending on the temperature and the application of the US step. Higher temperatures and the US pre-treatment promoted the extraction of the phenolic compounds, giving rise to higher TPC values at equilibrium (C_e).

Therefore, the US method was notably more efficient than the ST treatment (both at 25 °C), the former reaching a higher asymptotic value from practically 30 min extraction time. Thus, 30 min was chosen as the US pre-treatment time for combined processes. The combined USST method yielded higher final TPC values than the US, although these values were lower than those reached with a higher extraction temperature (100 °C) in the HT process. The HT extraction behaviour suggested that the high temperature significantly favours the release of phenolic compounds from the plant matrix into the extraction solvent, as previously reported by other authors [29,30]. The combination of 30 min US and 60 min HT (USHT process) gave rise to the highest yield in total phenolic content, which indicates the efficiency of the combination of US and thermal treatments as a means of favouring the extraction of phenolic compounds from the RS matrix. Phenolic compounds are linked through acetal, ether or ester covalent bonds with the lignocellulosic fraction of the plant matrix [31,32], and the debonding of phenolic compounds is promoted at high temperatures [33,34]. Thus, the combination of the structural effects provoked by sonication in the solid particles, and the cleavage of phenolic covalent bonds promoted by high temperatures, gave rise to the most efficient method with which to enhance the phenolic extraction yield. Other authors also found an increase in the extraction of phenolic compounds by applying heating or ultrasound to different plant matrices [17,30,33].

3.2. Extraction kinetics modelling

A pseudo-second order rate equation was adjusted to model the extraction kinetics. The kinetic parameters, the average absolute relative deviation (*AARD%*), and the determination coefficients (R^2) of the fitted model, are shown in Table 1. The goodness of model prediction can be seen in Fig. 2a, where the experimental points and fitted curves can be observed. Fig. 2b shows the fitting of the linearized model when C_o=0 (cases without US pre-treatment). Likewise, the values of statistical parameters, R^2 (> 0.98) and *AARD%* (< 10 %), also revealed the goodness of the fitted model, in agreement with other studies [27]. The pseudo-second order rate model is coherent with a two-step mass transfer process for the phenolic compounds: an initial and intensive washing-out of the solute on the RS particle surface, followed by a slow diffusion stage from the interior of the solid particles to the liquid solvent [14,22,28].

For treatments without US pre-treatment (C_o=0), the initial extraction rates were calculated (*h* values) and are shown in Table 1. The HT treatment presented the highest *h* value, followed by the US and ST treatments. This finding agrees with the phenol debonding action of high temperatures that promoted phenol extraction from the exposed surface of solid particles.

Ultrasonic cavitation at a lower temperature also promoted the fast extraction of phenolic compounds due to the US mechanical action that implied a greater solid surface exposure to the extraction process. However, this effect had a lower impact on the initial extraction rate than the high temperature. The ST treatment exhibited the lowest *h* value, due to the worse ability of low temperatures to debond phenols and the lack of enough mechanical energy to disrupt the particles and increase the extraction surface. The equilibrium concentration values were also positively affected by high temperatures and US application, coherently with their effects on the initial extraction rate (*h*). Thus, the US method increased the phenolic extraction by around 34 % with respect to the ST, but it was 24 % less extractive than the HT process.

The US pre-treatment (30 min) promoted the phenol extraction in both USST and USHT processes carried out at 25 and 100 °C, respectively. The phenolic equilibrium concentration was increased by around 54 % and 13 % with respect to that obtained in the ST and HT processes, respectively. Likewise, the C_e value obtained in the USHT treatment increased by around 40 % with respect to that obtained in the US treatment, but only by 12 % with respect to the HT. This finding agrees with the fact that high temperatures are more effective than ultrasonic cavitation at extracting phenolic compounds. Nevertheless, the combination of both effects in the USHT process produced the maximum extraction of phenolic compounds.

The constant rate values (*k*) were barely affected by either the temperature or the US effect but fell greatly in processes with a US pre-treatment (USST and USHT); this was due to the substantial reduction in the process driving force, since the initial concentration of the extract (170 $mg.L^{-1}$) was nearer the equilibrium value.

Table 1. Kinetic parameters obtained for the different extraction processes.

Extraction method[1]	k (x 10^{-3}) ($L.mg^{-1}.min^{-1}$)	C_e ($mg.L^{-1}$)	h ($mg.L^{-1}.min^{-1}$)	R^2	AARD%
US	2.12	178.6	67.60	0.998	4.89
ST	2.24	133.3	39.82	0.994	7.76
HT	1.91	222.2	94.32	0.992	4.08
USST	0.84	205.3	-	0.980	1.14
USHT	0.93	250.3	-	0.985	2.14

[1] ST: stirring, US: ultrasound, HT: heating, USST and UHHT: combination of 30 min US and ST or HT, respectively.

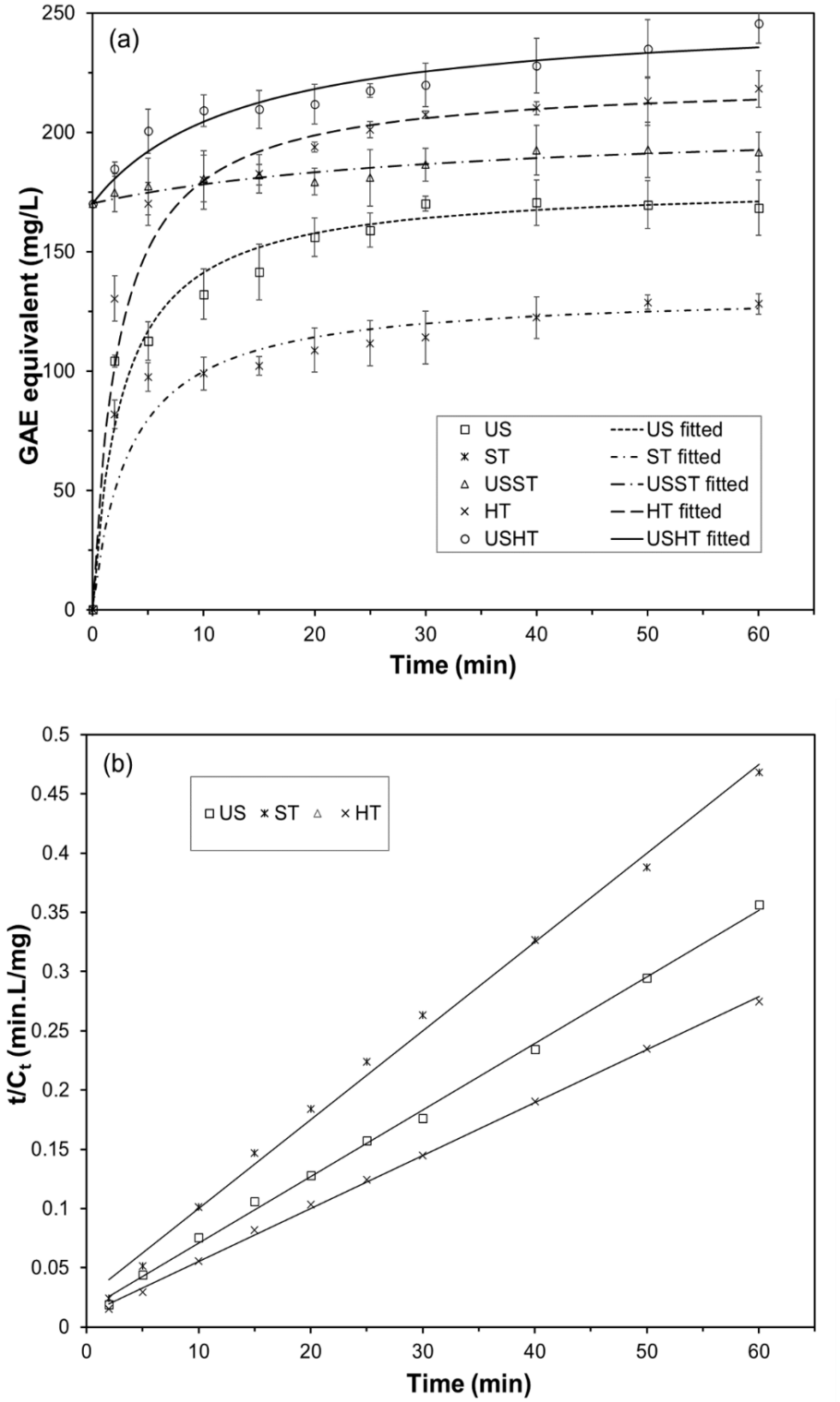

Figure 2. (a) Phenolic content of aqueous extracts obtained in the different processes as a function of time (points) and fitted kinetic model (lines). (b) Linearization of experimental points from the ST, US, and HT methods according to the pseudo-second order rate law. (US: ultrasound, ST: stirring, HT: heating, USST: stirring with 30 min of US pre-treatment, USHT: heating with 30 min of US pre-treatment).

3.3. Changes in the plant tissue produced by different extraction processes

Figure 3 shows the particle size distribution of the RS powder and the solid extraction residues after the different treatments: US at 15 (US15), 30 (US30) and 60 (US60) min, ST at 60 min (ST60), HT at 60 min (HT60), and the combined methods (with 30 min US pre-treatment) at 60 min (USST60 and USHT60). Before the extraction, the RS particles exhibited a monomodal distribution, with an average particle diameter (D_{43}) of 295 µm. As can be observed, the RS distribution showed fractions of the particles with mean diameters larger than the opening size of the used sieve (500 µm). Nevertheless, the RS particles are mostly rod-shaped, with a smaller diameter than length, as shown in Figure 4. Thus, these particles can pass through the mesh even if the length is longer than the opening size. In contrast, the laser diffraction method delivers a particle diameter corresponding to an equivalent sphere with the same diffraction pattern and the length of the particles mainly determines their mean radius of gyration and so, the equivalent sphere diameters.

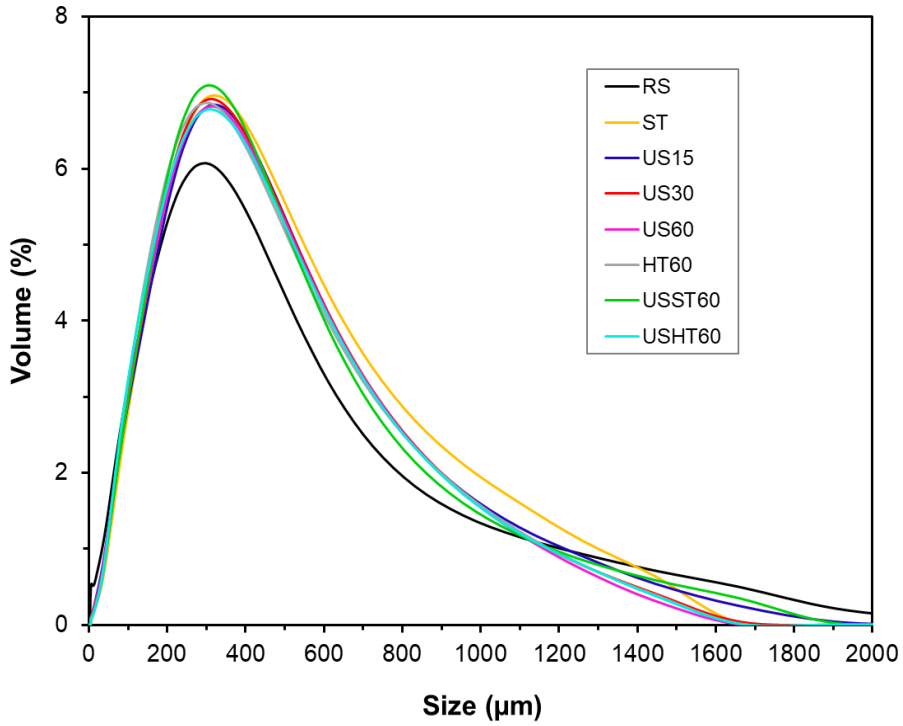

Figure 3. Particle size distribution obtained for the residual powder from the different extraction processes at a determined time (RS: rice straw, US: ultrasound, ST: stirring, HT: heating at reflux, USST, and USHT: combined treatments). The number in the sample code indicates the processing time.

The extraction processes provoked changes in the particle size distribution to a similar extent in every treatment. The distributions maintained the monomodal characteristic, exhibiting D_{43} values of 308 µm, but were slightly narrower, with a smaller presence of the biggest particles

(>1400 µm) and a greater one of particles with an intermediate diameter (300-1000 m). This behaviour was more marked in treatments where the US or high temperatures were applied, suggesting the particles become rounder during extraction. Compared with the other processes, however, it was not especially notable for the US treatments, in which more particle fragmentation would be expected due to the implosion of cavitation bubbles on the particle surface and the inter-particle collisions. Particle fragmentation was found by Machado et al. (2019) in the US extraction of trace metals from globe artichoke leaves and soybean seeds [35]. Nevertheless, US treatments in RS extraction processes could promote other physical changes than particle fragmentation, such as erosion, detexturation, sonocapillarity, or sonoporation, as described by other authors [36,37], which favoured the leaching of soluble compounds. Likewise, considering the limitations of the experimental method as a means of characterizing rod-shaped particles, the particle sizes obtained and their potential changes during extraction are not conclusive.

Microstructural changes in RS powders were also analysed by FESEM (Figure 4) to identify the potential effects of the different treatments on the particles that would explain the different mass transfer patterns. The untreated sample (Figure 4) showed the RS fragments with different dimensions that reveals the original structure of the RS tissue. This has numerous vascular bundles in different layers, consisting of a waxy cuticle, silicate epidermis, cortex (collenchyma), a thick lignified layer (sclerenchyma) and ground tissue (parenchyma) that contained cellulose microfibrils covered with lignin and hemicellulose [38]. Most of the particles resulting from the milling operation exhibit the fibrillar nature of the original tissue. These fibrillar fragments are mainly constituted by the cellulose-hemicellulose-lignin complex where phenolic compounds are bonded. Micrographs obtained at higher magnification were also shown in Figure 4 to better appreciate the morphology of the different particles before and after the extraction process.

From qualitative analyses of FESEM observations (Figure 4), a greater proportion of particles more laminar than tubular in shape appeared in micrographs corresponding to treatments in which US was applied. This suggests a certain degree of plane de-bonding in the fibril structures, resulting from the cavitation phenomena. This fibril destruction would contribute to the promotion of mass transfer during the extraction process in line with the increase of the surface exposed to the solvent action. Other effects, such as sonocapillarity or sonoporation, previously described [36,37], could also occur, but they are difficult to identify in the already unstructured ground tissue. In the thermal treatment without US application (HT60), the presence of flakes or de-bonded lamellas is less noticeable, but particles appeared more distorted, thus revealing the erosive thermal effect associated with the cleavage of phenolic structures from the carbohydrate-lignin complex. Moreover, the more planar particles would have a gyration radius, and thus a mean equivalent sphere diameter, similar to the corresponding original fibrils, which would explain the lack of notable differences in the

particle size distribution obtained by laser diffraction in the treatments submitted, or not, to US.

Then, the separation of different planes in the carbohydrate-lignin assemblies provoked by the US and phenol thermal de-bonding as a result of thermal treatment gave rise to the most effective extraction of phenolic compounds when combined in the USHT treatment.

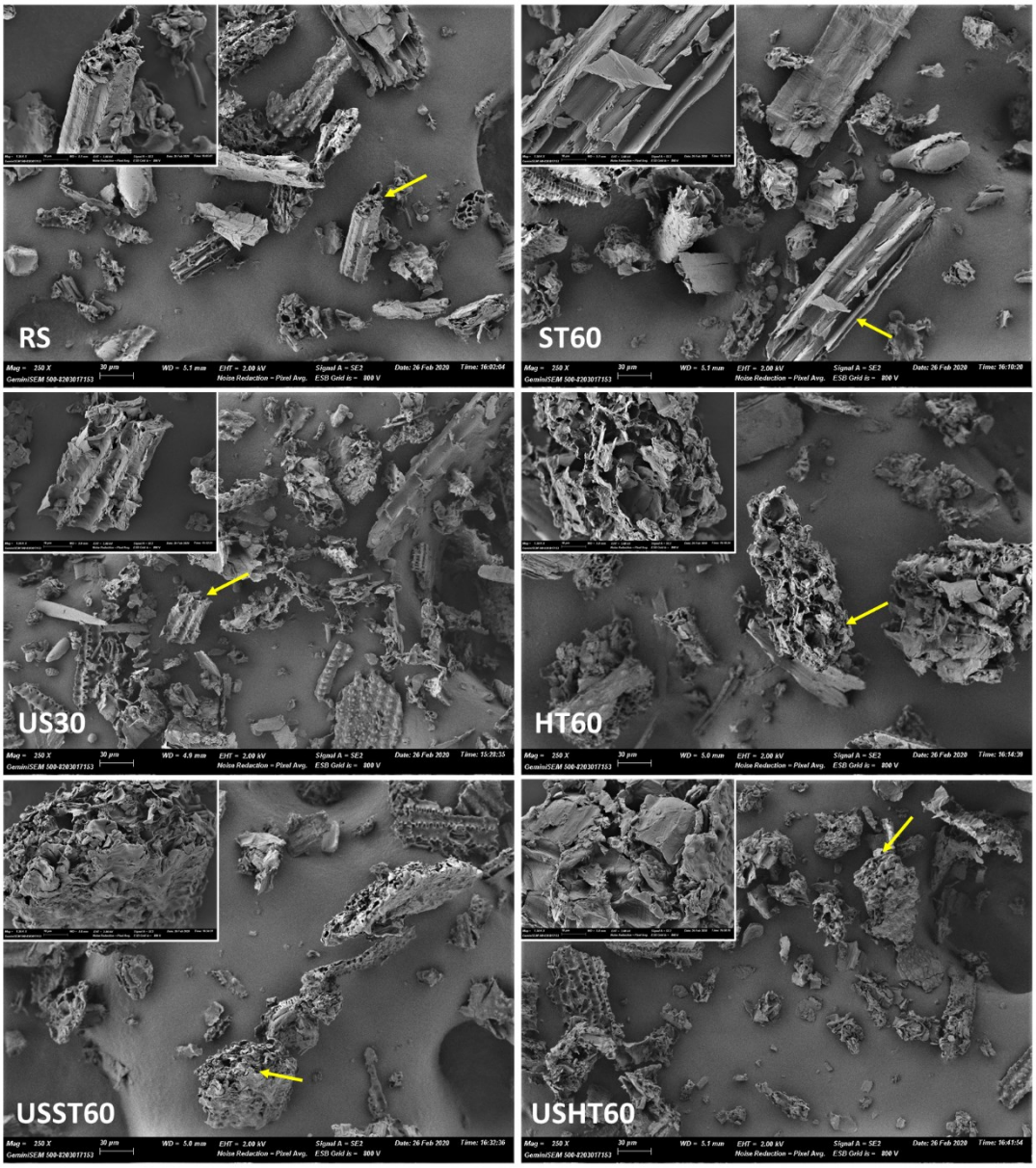

Figure 4. FESEM images of the particles from the residual powder and untreated RS (1300x magnification). (RS: rice straw, US: ultrasound, ST: stirring, HT: heating at reflux, USST, and USHT: combined treatments). The number in the sample code indicates the processing time. Micrographs of different particles (arrow marked) at higher magnification (x1300) were also included in each case.

3.4. Bioactive characterisation of the extracts

The RS extracts obtained from different extraction methods were characterized in terms of total solid yield (TSY), total phenolic content (TPC), antioxidant (Table 2), and antibacterial activities. RS contains a wide variety of compounds, such as lignin, cellulose, tannins, hemicellulose, sterols, flavonoids, phenolic aldehydes, and hydroxycinnamic acids, which may or not have bioactive properties [11,12,21]. The amount and proportion of these extracted compounds depend strictly on the extraction parameters, such as the method, type and proportion of extractor solvent, time, and temperature.

Table 2. Total solid yield (TSY), total phenolic content (TPC) and antioxidant capacity (EC_{50}) of the different extracts. Phenolic content and antioxidant capacity were expressed per mass unit of RS and dry extract.

Method[1]	TSY (g dry extract. 100 g^{-1} RS)	TPC_1 (mg GAE eq. 100 g^{-1} RS)	TPC_2 (mg GAE eq. g^{-1} dry extract)	$EC_{50(1)}$ (g RS. mg^{-1} DPPH)	$EC_{50(2)}$ (mg dry extract. mg^{-1} DPPH)
ST60	5.61 ± 0.07^{a}	256 ± 3^{a}	45.7 ± 0.1^{ab}	19.7 ± 0.6^{a}	11.0 ± 0.5^{a}
US15	5.7 ± 0.3^{a}	284 ± 17^{b}	49.2 ± 0.9^{a}	16.0 ± 1.3^{b}	9.2 ± 0.3^{b}
US30	7.48 ± 0.05^{b}	342 ± 10^{c}	45.7 ± 1.0^{ab}	12.5 ± 0.1^{c}	9.35 ± 0.18^{b}
US60	9.48 ± 0.17^{c}	354 ± 12^{c}	37.4 ± 1.9^{cd}	9.8 ± 0.3^{d}	9.3 ± 0.3^{b}
HT60	9.6 ± 0.6^{c}	459 ± 6^{d}	47.0 ± 3.0^{a}	7.8 ± 0.5^{e}	7.49 ± 0.05^{c}
USST60	9.0 ± 0.4^{c}	382 ± 6^{e}	42.3 ± 2.4^{bc}	10.4 ± 0.3^{f}	9.39 ± 0.10^{b}
USHT60	13.95 ± 0.13^{d}	486 ± 4^{f}	34.8 ± 0.5^{d}	4.6 ± 0.3^{g}	6.3 ± 0.4^{d}

[1] ST: stirring treatment, US: ultrasound treatment, HT: heating treatment, USST and UHHT: combination of 30 min US, and ST or HT, respectively. The number in the sample code indicates the process time. Means with different letters in the same column indicate significant differences (α = 0.05).

As shown in Table 2, non-statistical differences were found between the TSY values of ST60 and US15 treatments ($p > 0.05$) while the total solid extraction efficiency of the US treatment significantly increased ($p < 0.05$) when using longer sonication times, as has been previously observed by other authors [29]. No statistical differences were observed ($p > 0.05$) between the TSY of the US60 and HT60 treatments carried out at 25 and 100 °C, respectively. However, although the effects induced by ultrasonic cavitation and heating were comparable in terms of the total water solubilization capacity of the compounds present in the RS matrix, differences in the extract composition could provide distinct bioactive properties. The combination of US and heating (USHT60) yielded the highest solid leaching from RS ($p < 0.05$). Thus, as previously commented on, the US pre-treatment led to there being more points of the RS structure accessible to the solvent, thereby improving the mass transfer potential of

RS compounds. The US pre-treatment increased the total solid leaching by around 60% and 45% when used before the stirring and heating processes, respectively. Heat treatment provokes the softening of the plant tissue, weakening the cell wall integrity and the bond hydrolysis of the phenolic compounds linked to the carbohydrate-lignin complex, thus enhancing the solubility of phenols and other compounds [29,36,37].

The total phenolic content of the different extracts was expressed with respect to the RS mass (TPC_1) and to the total extracted solids (TPC_2). The former permits the observation of what treatment was more effective at extracting phenolic compounds from the raw material, whereas the latter supplies information on how rich in phenolic compounds the different extracts, which also contain other soluble compounds, are. Thermal treatments at 100 °C, with and without US pre-treatment, yielded the highest extraction of phenolic compounds from RS, according to what is described by other authors when analysing the temperature effect on the phenolic de-bonding from the cellular structure. The US pre-treatment enhanced this effect in line with the increase in the solid matrix surface available for the extraction, provoked by the cavitation phenomenon. The US pre-treatment improved the TSY of the ST treatment and the extraction of phenolic compounds from the RS matrix, but the extract's richness in phenols was slightly reduced due to the simultaneous promotion of the extraction of other components. In the same way, in the HT process, although the US pre-treatment enhanced the phenolic extraction, it led to the release of a greater quantity of other solids, thus implying an increase of 45 % in the total solid extraction, but of only 6 % in the phenolic compounds from the RS. The TPC values of the extracts (TPC_2) revealed that the greater total solid extraction does not guarantee a higher content of phenolic or active compounds in the extract. Thus, similar TPC_2 values were obtained for the US60 and HT60 treatments despite the different total solid yield. The poorest extract in phenols (lowest TPC_2 value) was that of the USHT60 treatment with the highest TSY. So, what this treatment promoted was the extraction of non-phenolic compounds as opposed to phenolic. The extracts from the US15 and US30 treatments had similar phenolic contents (TPC_2 values), however, longer US treatment times slightly decreased the phenolic richness of the extracts, thus indicating a greater promotion of the extraction of non-phenolic compounds. In this sense, other authors [39] indicated that 20 min of sonication time was enough to extract phenolic compounds from soy beverages.

A DPPH radical scavenging assay was used to analyse the antioxidant activities of the RS extracts obtained from different extraction methods. The results were expressed in terms of the EC_{50} parameter, referred to the mass of RS and extract ($EC_{50(1)}$ and $EC_{50(2)}$, respectively). Thus, $EC_{50(2)}$ indicates the radical scavenging capacity of the extracts, whereas $EC_{50(1)}$ reflects the ability of the extraction method to extract compounds with more radical scavenging capacity from the RS. A significant correlation was observed between the capacity of the extraction method to obtain phenolic compounds from RS (TPC_1) and the radical scavenging

capacity ($EC_{50(1)}$), with r values of -0.960. This indicates that the treatments that extracted a greater quantity of phenolic compounds from RS also extracted more compounds with radical scavenging capacity, which can be mainly attributed to the phenols. However, the parallel extraction of other compounds, as affected by the kind of treatment, determined the final ratio of the phenols in the extracts and their $EC_{50(2)}$ values. As can be observed in Table 2, the ST60 exhibited the lowest radical scavenging capacity (the highest EC_{50} values). Other authors [10] found a similar $EC_{50(2)}$ value (12.0 mg freeze-dried extract/mg DPPH) when extracting compounds from RS under similar conditions. Although the US treatments promoted the enrichment of the extracts in non-phenolic compounds when the extraction time lengthened, the extracts for 15, 30, and 60 min exhibited a similar radical scavenging capacity ($p > 0.05$), which was greater than that of the ST extract. The combination of the US with ST (USST60) did not imply extracts with more radical scavenging activity than that obtained by the US pre-treatment, nor was the extract enriched in phenolic compounds. In contrast, the thermal treatment produced the extracts with some of the highest radical scavenging capacities; this was enhanced by the US pre-treatment, despite the fact that US application more effectively promoted the extraction of non-phenolic compounds and, globally, the USHT60 extract had the lowest total phenolic content. This finding indicates that the thermal treatment promotes the extraction of the more active compounds (phenolic or not); this was enhanced when US pre-treatment was applied in line with the higher surface exposure in the solid particles due to the cavitation phenomenon. Other authors [30] also observed that the microwave and conventional oven heating pre-treatments promoted a significant increase in the antioxidant activity of extracts from fennel seeds, which was attributed to the promotion of flavonoid extraction. Flavonoid extraction from baobab seeds was also promoted when US treatments were carried out at higher temperatures [17]. Several compounds with proven antioxidant capacity, such as ferulic, protocatechuic, *p*-coumaric, caffeic, and vanillic acids, tricin, and vanillin have been identified in RS extracts by other authors [10,40].

In brief, the obtained results suggested that the combined ultrasound-heating method promoted a greater extraction of compounds from RS with antioxidant properties, diluted with other non-phenolic components, and, from a practical point of view, the obtained USHT60 extract exhibited the best potential to act as an efficient antioxidant material.

Considering the ability of the US and HT combination to extract bioactive compounds in terms of the radical scavenging capacity, the corresponding extract (USHT60) was also evaluated as to its antibacterial activity against *L. innocua* and *E. coli* strains. The extract obtained in the corresponding US30 pre-treatment (richer in phenolic compounds) was also analysed. Thus, different concentrations of freeze-dried extracts were applied in the well microtiter plates in order to determine the minimum inhibitory concentration. No total inhibition of bacterial growth was observed for the extract over the considered concentration range. However, the most heavily-concentrated USHT60 extract at 160 $mg.mL^{-1}$ reduced the initial counts of *L.*

innocua by 1.7 log CFU, although it was not effective at reducing the counts of *E. coli*. At the same concentration, the US30 extract was not effective at reducing the initial counts of *E. coli* or *L. innocua*, which suggests that the extraction of more active compounds was achieved during the thermal step of the extraction process. Although extracts obtained from RS contain antimicrobial compounds, such as ferulic and *p*-coumaric acids [10,21] with proven antibacterial activity against these strains, their concentration could not reach the minimal inhibitory concentration of the bacteria, or their interactions with other extract components could limit their effectiveness as antibacterial agents.

4. CONCLUSIONS

RS is an agro-industrial waste that contains a wide variety of bioactive compounds of technological interest for food application purposes, but the extraction conditions greatly influence the extraction efficiency of the target compounds. The application of ultrasound was notably more effective at extracting water-soluble phenolic compounds than simple stirring, as revealed by the higher extract yields and antioxidant activity of the extracts. Nevertheless, a high extraction temperature produced materials with improved antioxidant activities, in line with the promotion of the cleavage of covalent bonds between the phenolic compounds and the lignocellulosic fraction. This thermal effect was greatly enhanced when ultrasound pre-treatment was applied due to the increase in the substrate surface exposed to the extraction. Therefore, a combination of 30 min US plus 60 min thermal treatment in water reflux is recommended to obtain solid extracts with great antioxidant activity and notable anti-listerial effect, which could be used in the food or pharmaceutical industries.

5. ACKNOWLEDGEMENTS

The authors thank the Agencia Estatal de Investigación (Spain) for the financial support through projects PID2019-105207RB-I00/AEI/10.13039/501100011033 and Generalitat Valenciana [grant number GrisoliaP/2019/115].

6. REFERENCES

1. Sharma, B.; Vaish, B.; Monika; Singh, U.K.; Singh, P.; Singh, R.P. Recycling of Organic Wastes in Agriculture: An Environmental Perspective. *Int J Environ Res* **2019**, *13*, 409–429, doi:10.1007/s41742-019-00175-y.

2. Ng, H.-M.; Sin, L.T.; Tee, T.-T.; Bee, S.-T.; Hui, D.; Low, C.-Y.; Rahmat, A.R. Extraction of cellulose nanocrystals from plant sources for application as reinforcing agent in polymers. *Composites Part B: Engineering* **2015**, *75*, 176–200, doi:10.1016/j.compositesb.2015.01.008.

3. Peanparkdee, M.; Iwamoto, S. Bioactive compounds from by-products of rice cultivation and rice processing: Extraction and application in the food and pharmaceutical industries. *Trends in Food Science & Technology* **2019**, *86*, 109–117, doi:10.1016/j.tifs.2019.02.041.

4. FAOSTAT Available online: http://www.fao.org/faostat/en/#data/QC/visualize (accessed on Nov 4, 2020).

5. Sarkar, N.; Ghosh, S.K.; Bannerjee, S.; Aikat, K. Bioethanol production from agricultural wastes: An overview. *Renewable Energy* **2012**, *37*, 19–27, doi:10.1016/j.renene.2011.06.045.

6. Takano, M.; Hoshino, K. Bioethanol production from rice straw by simultaneous saccharification and fermentation with statistical optimized cellulase cocktail and fermenting fungus. *Bioresour. Bioprocess.* **2018**, *5*, 16, doi:10.1186/s40643-018-0203-y.

7. Krishania, M.; Kumar, V.; Sangwan, R.S. Integrated approach for extraction of xylose, cellulose, lignin and silica from rice straw. *Bioresource Technology Reports* **2018**, *1*, 89–93, doi:10.1016/j.biteb.2018.01.001.

8. Jani, S.M.; Rushdan, I. Mechanical properties of beating pulp and paper from rice straw. 8.

9. Elhussieny, A.; Faisal, M.; D'Angelo, G.; Aboulkhair, N.T.; Everitt, N.M.; Fahim, I.S. Valorisation of shrimp and rice straw waste into food packaging applications. *Ain Shams Engineering Journal* **2020**, S2090447920300101, doi:10.1016/j.asej.2020.01.008.

10. Menzel, C.; González-Martínez, C.; Vilaplana, F.; Diretto, G.; Chiralt, A. Incorporation of natural antioxidants from rice straw into renewable starch films. *International Journal of Biological Macromolecules* **2020**, *146*, 976–986, doi:10.1016/j.ijbiomac.2019.09.222.

11. Li, Y.; Qi, B.; Luo, J.; Khan, R.; Wan, Y. Separation and concentration of hydroxycinnamic acids in alkaline hydrolyzate from rice straw by nanofiltration. *Separation and Purification Technology* **2015**, *149*, 315–321, doi:10.1016/j.seppur.2015.06.006.

12. Barana, D.; Salanti, A.; Orlandi, M.; Ali, D.S.; Zoia, L. Biorefinery process for the simultaneous recovery of lignin, hemicelluloses, cellulose nanocrystals and silica from rice husk and Arundo donax. *Industrial Crops and Products* **2016**, *86*, 31–39, doi:10.1016/j.indcrop.2016.03.029.

13. Adom, K.K.; Liu, R.H. Antioxidant Activity of Grains. *J. Agric. Food Chem.* **2002**, *50*, 6182–6187, doi:10.1021/jf0205099.

14. Cheung, Y.-C.; Wu, J.-Y. Kinetic models and process parameters for ultrasound-assisted extraction of water-soluble components and polysaccharides from a medicinal fungus. *Biochemical Engineering Journal* **2013**, *79*, 214–220, doi:10.1016/j.bej.2013.08.009.

15. Ojha, K.S.; Aznar, R.; O'Donnell, C.; Tiwari, B.K. Ultrasound technology for the extraction of biologically active molecules from plant, animal and marine sources. *TrAC Trends in Analytical Chemistry* **2020**, *122*, 115663, doi:10.1016/j.trac.2019.115663.

16. Luque-García, J.L.; Luque de Castro, M.D. Ultrasound: a powerful tool for leaching. *TrAC Trends in Analytical Chemistry* **2003**, *22*, 41–47, doi:10.1016/S0165-9936(03)00102-X.

17. Ismail, B.B.; Guo, M.; Pu, Y.; Wang, W.; Ye, X.; Liu, D. Valorisation of baobab (Adansonia digitata) seeds by ultrasound assisted extraction of polyphenolics. Optimisation and comparison with conventional methods. *Ultrasonics Sonochemistry* **2019**, *52*, 257–267, doi:10.1016/j.ultsonch.2018.11.023.

18. Sumere, B.R.; de Souza, M.C.; dos Santos, M.P.; Bezerra, R.M.N.; da Cunha, D.T.; Martinez, J.; Rostagno, M.A. Combining pressurized liquids with ultrasound to improve the extraction of phenolic compounds from pomegranate peel (Punica granatum L.). *Ultrasonics Sonochemistry* **2018**, *48*, 151–162, doi:10.1016/j.ultsonch.2018.05.028.

19. Wang, L.; Boussetta, N.; Lebovka, N.; Vorobiev, E. Selectivity of ultrasound-assisted aqueous extraction of valuable compounds from flesh and peel of apple tissues. *LWT* **2018**, *93*, 511–516, doi:10.1016/j.lwt.2018.04.007.

20. Dias, A.L.B.; Arroio Sergio, C.S.; Santos, P.; Barbero, G.F.; Rezende, C.A.; Martínez, J. Ultrasound-assisted extraction of bioactive compounds from dedo de moça pepper (Capsicum baccatum L.): Effects on the vegetable matrix and mathematical modeling. *Journal of Food Engineering* **2017**, *198*, 36–44, doi:10.1016/j.jfoodeng.2016.11.020.

21. Karimi, E.; Mehrabanjoubani, P.; Keshavarzian, M.; Oskoueian, E.; Jaafar, H.Z.; Abdolzadeh, A. Identification and quantification of phenolic and flavonoid components in straw and seed husk of some rice varieties (*Oryza sativa* L.) and their antioxidant properties:

Identification and quantification of phenolic and flavonoid. *J. Sci. Food Agric.* **2014**, *94*, 2324–2330, doi:10.1002/jsfa.6567.

22. Ho, Y.S.; McKay, G. Sorption of dye from aqueous solution by peat. *Engineering Journal* **1998**, 10.

23. Brand-Williams, W.; Cuvelier, M.E.; Berset, C. Use of a free radical method to evaluate antioxidant activity. *LWT - Food Science and Technology* **1995**, *28*, 25–30, doi:10.1016/S0023-6438(95)80008-5.

24. Abdi, R.D.; Kerro Dego, O. Antimicrobial activity of Persicaria pensylvanica extract against Staphylococcus aureus. *European Journal of Integrative Medicine* **2019**, *29*, 100921, doi:10.1016/j.eujim.2019.05.007.

25. Requena, R.; Jiménez-Quero, A.; Vargas, M.; Moriana, R.; Chiralt, A.; Vilaplana, F. Integral Fractionation of Rice Husks into Bioactive Arabinoxylans, Cellulose Nanocrystals, and Silica Particles. *ACS Sustainable Chem. Eng.* **2019**, *7*, 6275–6286, doi:10.1021/acssuschemeng.8b06692.

26. Wang, Y.; Liu, J.; Liu, X.; Zhang, X.; Xu, Y.; Leng, F.; Avwenagbiku, M.O. Kinetic modeling of the ultrasoNic-assisted extraction of polysaccharide from Nostoc commune and physicochemical properties analysis. *International Journal of Biological Macromolecules* **2019**, *128*, 421–428, doi:10.1016/j.ijbiomac.2018.12.247.

27. González, N.; Elissetche, J.; Pereira, M.; Fernández, K. Extraction of polyphenols from and : Experimental kinetics, modeling and evaluation of their antioxidant and antifungical activities. *Industrial Crops and Products* **2017**, *109*, 737–745, doi:10.1016/j.indcrop.2017.09.038.

28. Dutta, R.; Sarkar, U.; Mukherjee, A. Pseudo-kinetics of batch extraction of Crotalaria juncea (Sunn hemp) seed oil using 2-propanol. *Industrial Crops and Products* **2016**, *87*, 9–13, doi:10.1016/j.indcrop.2016.04.006.

29. Tabaraki, R.; Heidarizadi, E.; Benvidi, A. Optimization of ultrasonic-assisted extraction of pomegranate (Punica granatum L.) peel antioxidants by response surface methodology. *Separation and Purification Technology* **2012**, *98*, 16–23, doi:10.1016/j.seppur.2012.06.038.

30. Hayat, K.; Abbas, S.; Hussain, S.; Shahzad, S.A.; Tahir, M.U. Effect of microwave and conventional oven heating on phenolic constituents, fatty acids, minerals and antioxidant potential of fennel seed. *Industrial Crops and Products* **2019**, *140*, 111610, doi:10.1016/j.indcrop.2019.111610.

31. Xu, G.; Ye, X.; Chen, J.; Liu, D. Effect of Heat Treatment on the Phenolic Compounds and Antioxidant Capacity of Citrus Peel Extract. *J. Agric. Food Chem.* **2007**, *55*, 330–335, doi:10.1021/jf062517l.

32. Purohit, A.J.; Gogate, P.R. Ultrasound-Assisted Extraction of β -Carotene from Waste Carrot Residue: Effect of Operating Parameters and Type of Ultrasonic Irradiation. *Separation Science and Technology* **2015**, *50*, 1507–1517, doi:10.1080/01496395.2014.978472.

33. Wanyo, P.; Meeso, N.; Siriamornpun, S. Effects of different treatments on the antioxidant properties and phenoliC compounds of rice bran and rice husk. *Food Chemistry* **2014**, *157*, 457–463, doi:10.1016/j.foodchem.2014.02.061.

34. Niwa, Y.; Miyachi, Y. Antioxidant action of natural health products and Chinese herbs. *Inflammation* **1986**, *10*, 79–91, doi:10.1007/BF00916043.

35. Machado, I.; Faccio, R.; Pistón, M. Characterization of the effects involved in ultrasound-assisted extraction of trace elements from artichoke leaves and soybean seeds. *Ultrasonics Sonochemistry* **2019**, *59*, 104752, doi:10.1016/j.ultsonch.2019.104752.

36. Chemat, F.; Rombaut, N.; Sicaire, A.-G.; Meullemiestre, A.; Fabiano-Tixier, A.-S.; Abert-Vian, M. Ultrasound assisted extraction of food and natural products. Mechanisms, techniques, combinations, protocols and applications. A review. *Ultrasonics Sonochemistry* **2017**, *34*, 540–560, doi:10.1016/j.ultsonch.2016.06.035.

37. Cravotto, G.; Cintas, P. Power ultrasound in organic synthesis: moving cavitational chemistry from academia to innovative and large-scale applications. *Chem. Soc. Rev.* **2006**, *35*, 180–196, doi:10.1039/B503848K.

38. Seo, D.-J.; Sakoda, A. Assessment of the structural factors controlling the enzymatic saccharification of rice straw cellulose. *Biomass and Bioenergy* **2014**, *71*, 47–57, doi:10.1016/j.biombioe.2014.10.027.

39. Rostagno, M.A.; Palma, M.; Barroso, C.G. Ultrasound-assisted extraction of isoflavones from soy beverages blended with fruit juices. *Analytica Chimica Acta* **2007**, *597*, 265–272, doi:10.1016/j.aca.2007.07.006.

40. Shi, J.; Wang, Y.; Wei, H.; Hu, J.; Gao, M.-T. Structure analysis of condensed tannin from rice straw and its inhibitory effect on Staphylococcus aureus. *Industrial Crops and Products* **2020**, *145*, 112130, doi:10.1016/j.indcrop.2020.112130

CHAPTER 1.II

Applying ultrasound-assisted processing to obtain cellulose fibres from rice straw to be used as reinforcing agents

Pedro A. V. Freitas, Chelo González-Martínez, Amparo Chiralt

Institute of Food Engineering for Development, Universitat Politècnica de València, 46022, Valencia, Spain

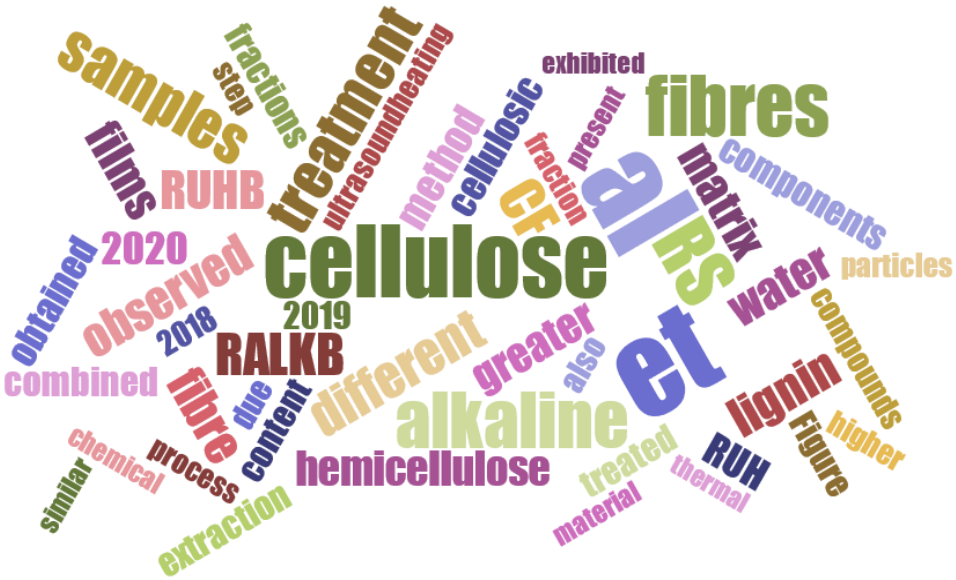

Innovative Food Science & Emerging Technologies (2022), 76, 102932

ABSTRACT

Rice straw (RS) is one of the most globally abundant agro-industrial residues. For its valorisation, a green combined ultrasound-reflux heating method was applied to obtain cellulose fibres (CF) from RS. The new method produced CF with a higher yield (37 %) than the alkaline process (29 %), more hydrophilic, and with a lower tendency to aggregate. Despite the slightly different degree of purification detected by the chemical and FTIR analysis, both fibres exhibited similar crystallinity, thermal behaviour, morphogeometric characteristics, and aspect ratio distributions (20-60). Both CF showed similar reinforcing capabilities in methylcellulose/gum Arabic films, enhancing the film stretchability and resistance to break by about 33 % and 20 %. Non-noticeable changes in water vapour permeability and the light internal transmission were observed, indicating good compatibility CF-polymer matrix. Therefore, using the ultrasound-heating method to obtain CF is an eco-friendlier process than the alkaline treatment, supplying suitable fibres as industrial reinforcing agents.

Keywords: green method, ultrasound-heating method, agro-industrial waste, cellulose microfibrils, reinforcing capacity, methylcellulose.

Industrial relevance: Ultrasound, an emerging technology in food processing, combined with reflux heating, can be a green alternative for obtaining cellulose microfibres for industrial applications. The new combined method was faster than the alkaline process (1.5 h *vs.* 6 h) and was more environmentally-friendly since it does not require a strong alkaline solution. Besides, both cellulose microfibres exhibited similar performances when incorporated into a polymer matrix. These results boost knowledge in the food packaging field, as well as the valorisation of agro-industrial wastes for industrial applications.

1. INTRODUCTION

Agricultural residues generated as wastes during or after the processing of agricultural crops are one example of a renewable resource that is available in huge amounts. Many of these agricultural residues are lignocellulose-rich, primarily containing cellulose, lignin, hemicellulose, and extractives, such as phenolic compounds (Saini et al., 2015). So, the agro-industrial waste derivatives could be used as value-added materials with antioxidant and antimicrobial properties (Freitas et al., 2020; Menzel et al., 2020; Prakash et al., 2018), biomass for fuel production (Casabar et al., 2020; Takano & Hoshino, 2018) or reinforcing fillers in polymeric materials useful in food packaging. The application of lignocellulosic agro-wastes in food packaging manufacturing processes is highly promising since these are renewable materials and their use contributes to boosting the management and valorisation of agro-industrial waste in the context of the circular economy (Collazo-Bigliardi et al., 2019; Freitas et al., 2020; Ng et al., 2015a; Sharma et al., 2019). Many studies have reported the isolation of different cellulose fractions from lignocellulosic by-products for different purposes. Residues, such as walnut shell, corncob and sugarcane bagasse (Harini & Chandra Mohan et al., 2020), pea and broad beans (Kassab et al., 2020), sugar palm (Ilyas et al., 2019), sugarcane bagasse (Saha & Ghosh, 2019), coffee and rice husk (Collazo-Bigliardi et al., 2018; Kargarzadeh, 2017; Requena et al., 2019) and rice straw (RS) (Boonterm et al., 2016), have been characterised as to their cellulose content and extraction.

Rice (*Oryza sativa* L.) is one of the most important global crops, with an annual world production of 780 million tons, which generates a large amount of RS (*FAOSTAT*, 2018; Peanparkdee & Iwamoto, 2019). RS, the leftover from rice production that includes stems, leaf blades, leaf sheaths, and the remains of the panicle after threshing, is one of the most abundant lignocellulosic waste materials in the world (Saini et al., 2015). After harvesting, the RS by-product is usually burned in the fields, which causes environmental and health problems in the population living near the rice paddies (Peanparkdee & Iwamoto, 2019; Sarkar et al., 2012). Considering that the lignocellulosic fraction represents approximately 70% of the RS dry matter (Barana et al., 2016), taking advantage of the cellulosic derivatives from this residual biomass is of great interest, as is their use as reinforcing agents in polymeric materials. Numerous studies can be found using nanocellulose (crystals of fibres) from different sources as reinforcement agents. In particular, micro or nanocrystals (CNC) from RS have been incorporated into different polymeric matrices, such as polyvinyl alcohol (PVA) (Ching et al., 2015), or cellulose acetate (Hassan et al., 2019). Nevertheless, few studies reported the use of cellulose fibres (CF). The use of CF instead of nanocrystals presents some advantages, such as a higher cellulose yield and a greater strength and elastic modulus, due to the higher aspect ratio of CF and fibre entanglements (Xu, 2013). The fibre entanglements play an important role in the force transferring from matrix to fibrils and from fibrils to fibrils.

The lignocellulosic fraction of RS consists of a complex matrix assembled by semicrystalline cellulose microfibrils, as the primary fibre component, linked to a cementing matrix composed of hemicellulose and lignin (Chen et al., 2011). Separating cellulose into its elemental form of nanofibrils, approximately 3-20 nm in width, is a difficult task. Among the chemical and physical treatments for obtaining cellulose fibres, the most common method focuses on treating biomass with a strongly alkaline sodium hydroxide solution. This alkaline treatment, also known as mercerisation, promotes the degradation of a substantial fraction of hemicellulose, lignin, and waxes present in the cellulosic material (Boonterm et al., 2016; Zhang et al., 2014). However, the alkaline treatment is associated with environmental problems due to the large amounts of contaminant alkaline solvent used and the need for a large quantity of water with which to wash the material after the extraction process (Boonterm et al., 2016). Moreover, the highly alkaline environment can induce the formation of stable bonds between hemicellulose and lignin, limiting the biomass delignification step (Salam et al., 2007). In this sense, some studies have been conducted to eliminate alkaline treatment in the cellulose purification, using steam explosion technique (Wang et al., 2018). Other more environmentally-friendly alternative treatments, such as combined ultrasound and heating processes, could also be used to replace the alkaline treatment in the extraction of hemicellulose and lignin from biomass. This combined process has been previously applied to obtain active extracts from RS with high extraction yield and antioxidant activity (Freitas et al. 2020). Being the extraction residue rich in cellulosic components, it has a great potential to be used as a source of cellulose fibres since it has been partially purified. Likewise, the US treated plant tissue could be more easily bleached due to the structural alterations provoked by the combined extraction process. In this sense, an integral process consisting of extraction of active compounds and obtaining cellulose fibres could be designed for a better valorisation of RS.

Ultrasound-assisted extraction (UAE) is an emerging, green operation that applies intense mechanical shear forces in a plant matrix to disrupt its primary structure and leach out target compounds (Cheung & Wu, 2013). The high shear rates stem from acoustic cavitation, a physical phenomenon characterised by the collapse of air or water vapour bubbles formed by the compression and rarefaction of ultrasonic waves propagating in the solvent (Ojha, 2020; Sumere et al., 2018). Likewise, another eco-friendly technique to extract compounds from lignocellulosic matrices is the heating of the aqueous dispersion of ground plant matrix at high temperatures (above 100 °C) (Wanyo et al., 2014). This promotes the cleavage of covalent bonds and Van der Waals forces present in the lignocellulosic fraction, extracting, or degrading, part of the hemicellulose, lignin, and other components (Korotkova et al., 2015). To enhance the water extraction efficiency of RS compounds, Freitas et al. (2020) applied ultrasound (US) as pre-treatment, followed by a reflux heating step. The extracts obtained by using US pre-treatment had the highest levels of phenolic compounds and total solid content, due to the greater extraction of hemicellulose and lignin fractions. To the best of our

knowledge, the combined ultrasound-reflux heating method has not yet been used as a step for obtaining cellulose fibres from RS.

Of the potential applications of cellulosic fibres, their reinforcing capacity may improve the functional properties of films aimed to food packaging. In this sense, Methylcellulose (MC), a biopolymer derived from cellulose, composed of methyl substitution groups linked to the native cellulose backbone (Nunes et al., 2018), is a biodegradable, non-toxic, with good adhesiveness, biocompatibility, and mechanical properties, with promising potential to be used as a food packaging material (Saha & Ghosh, 2019). Incorporation of cellulose fibre in this polymer matrix may improve its performance as packaging material. Likewise, the incorporation of other components such as gum Arabic (GA), a polysaccharide-protein complex, which can act as compatibilizer (Amalraj et al., 2020; Xu et al., 2018), could improve the fibre function in the film, promoting the reinforcing effect.

Therefore, the aim of this study was to obtain cellulose fibres (CF) from RS by applying the combined ultrasound-heating method plus a bleaching step. Ultrasounds were also applied to disaggregate fibre bundles in water medium and the fibrils were tested as reinforcing agents in Methylcellulose/Gum Arabic blend films. CF were characterised as to their different nano and microstructural characteristics, thermal behaviour and reinforcing capacity and compared with those obtained by applying the conventional alkaline treatment.

2. MATERIAL AND METHODS

2.1 Plant material and chemicals

RS (*Oryza sativa* L. var *J. Sendra*) was collected in a L'Albufera paddy field (Valencia, Spain), dried (50 ± 2 °C, 0.5 mmbar for 16 h), milled (3 cycles of 90 s each) using a grinding machine (IKA, model M20, Germany), and sieved to achieve particle sizes of under 0.5 mm. Methylcellulose (MC: viscosity of 15 cP), gum Arabic (GA), sodium chlorite, and sodium hydroxide were supplied by Sigma-Aldrich (United States). Glycerol, acetic acid, magnesium nitrate ($Mg(NO_3)_2$), and phosphorus pentoxide (P_2O_5) were purchased from Panreac Química (Spain). Sodium acetate trihydrate was supplied by FlukaTM (Germany).

2.2 Purification treatments of the cellulosic fraction from RS

2.2.1 Combined ultrasound-heating treatment

An alternative treatment based on a consecutive combination of ultrasound and heating was applied to extract hemicellulose and lignin fractions from RS. Firstly, a RS aqueous dispersion (5 %, w/v) was sonicated for 30 min with a probe-type high-intensity ultrasonic homogenizer (Vibra Cell^{TM} VCX750, Sonics & Material, United States), using 750 W power, 20 kHz frequency, and 40% sonication amplitude. During sonication, sample was immersed in an ice bath to

control the temperature that raised from 25 to 40 °C. The total ultrasonic power applied to the extraction system was calculated according to the calorimetric method (Kimura et al., 1996), with some modifications. To this end, the temperature increases of the system containing water was recorded every minute, by duplicate, and the applied acoustic power was calculated from the slope of the temperature-time curve. The obtained value was 31 ± 3 W, lower than the electric power of the equipment (750 W).

After sonication, the dispersion was heated at reflux temperature (100 °C) for 1 h, filtered and washed several times with distilled water to eliminate water soluble extract retained in the solid. The insoluble fraction from the combined (RUH) method was dried at 35 ± 2 °C for 48 h.

2.2.2 Alkali treatment

The alkali treatment was carried out following that described by Collazo-Bigliardi et al. (2018), using an RS: sodium hydroxide solution (4.5 %, w/v) at a ratio of 1:20 (w/v). The plant dispersion was heated at reflux temperature (100 °C) for 3 h. Afterwards, the insoluble material (RALK) was filtered, washed with distilled water until neutral pH to eliminate the alkali solution, and dried at 35 ± 2 °C for 48 h. Three RS samples were treated with alkaline solution twice.

2.2.3 Bleaching treatment

The samples obtained from those previously described treatments were bleached, following Requena et al. (2019), with some modifications. The bleaching solution was obtained by mixing equal parts of distilled water, acetate buffer solution (2 N), and sodium chlorite (1.7 %, w/v). Thus, the cellulosic material was mixed with the bleaching solution (5 %, w/v) and heated at reflux for 4 h. Afterwards, the dispersion was filtered and washed with distilled water until the complete removal of bleach solution residues. The bleached materials (RALK-B and RUH-B) were dried at 35 °C for 24 h. For each cellulosic sample, the bleaching process was performed four times while the process was repeated three times on different samples.

2.3 Characterisation of CF from RS

2.3.1 Moisture content

The equilibrium moisture content of cellulosic fractions was determined gravimetrically. Approximately 1.5-3 g of each cellulosic fraction was conditioned at 25 °C and different relative humidity (RH), in desiccators with different salt saturated solutions ($MgCl_2$: 53 %; NaCl: 75 %; and KCl: 84 %) for two weeks and then were dried at 60 ºC for 24h. Afterwards, the samples were placed in a desiccator at 25 °C with P_2O_5 for two weeks. The moisture contents were determined from the total weight loss of the conditioned samples and

expressed as percentage on dry basis. The analysis was performed in triplicate for each treatment. Samples of RS were conditioned at 53 % RH before their use and the equilibrium moisture content (5.1 ± 0.3 g/100 g d.b.) was obtained by the same procedure.

2.3.2 Chemical composition

The cellulose, hemicellulose, and lignin content of the untreated RS and each lignocellulosic fraction was performed according to the standard NREL method (NREL/TP-510-42618) (Sluiter, 2008b). In brief, the cellulosic materials were subjected to hydrolysis with sulfuric acid, and the lignin content was determined in the insoluble fraction. At the same time, the hydrolysed soluble fractions were used to quantify the sugar composition (typically glucose, xylose, and arabinose) by using high-performance liquid chromatography (HPLC, Agilent Technologies, model 1120 Compact LC, Germany). A HILIC Luna Omega Sugars column (150 x 4.6 mm, 3 µm) and an evaporative light scattering detector (ELSD Agilent Technologies 1200 Series, Germany) were used. The mobile phase was water: acetonitrile (25:75), in isocratic mode, at a flow rate of 0.8 $mL.min^{-1}$. The detector conditions were: 40 °C, 3.0 bars of gas pressure (N_2), and gain of 3. The software used was ChemStation program (Agilent Technologies, Germany). The cellulose content was expressed as % wt. of glucose in relation to the initial solid fraction, while the hemicellulose concentration was determined by the sum of the xylose and arabinose contents. Before the hydrolyses, the untreated RS and the insoluble fractions after ultrasound (RUS) and reflux heating (RUH) treatments were subject to a water extraction according to the standard NREL method to determine extractives in biomass (NREL/TP-510-42619) (Sluiter, 2008a). The ash content was determined thermogravimetrically using a thermogravimetric analyser (TGA 1 Stare System, Mettler-Toledo, Switzerland). Samples (3-4 mg) were heated from 25-700 °C under nitrogen flow (10 $mL.min^{-1}$) and a heating rate of 10 $°C.min^{-1}$. The residual mas was considered as ash content.

2.3.3 Morpho-geometric analyses

Both untreated samples and those obtained in each fibre isolation step were evaluated by using an optical microscope (Optika Microscope B-350, Italy) equipped with a camera (Optikam B2). The samples were prepared at 0.001 $mg.mL^{-1}$, placed on the glass slide, and observed at 10x and 40x magnification. Bleached fibre dispersions (0.001 $mg.mL^{-1}$) were sonicated using a probe-type high-intensity ultrasonic homogenizer (Vibra Cell^{TM} VCX750, 750 W power, 20 kHz frequency, Sonics & Material, United States) for 20 min before the microscopic observation.

The morphogeometric characteristics of sonicated CF dispersions were determined by measuring the particle length and width. For each sample, a minimum of 50 measurements were taken using the Optika Vision Lite program. The results were expressed in cumulative distributions for each parameter.

The particle size distributions of the water dispersed (0.001 mg.mL^{-1}) and sonicated bleached samples (0.001 mg.mL^{-1}, 20 min ultrasound) were also analysed by using a laser-diffraction particle size analyser (Mastersizer 3000, Malvern Instruments, UK) operating based on the Mie theory. The refractive and absorption indexes of 1.52 and 0.1, respectively, were considered. The samples were diluted, stirred at 1900 rpm, and fed into the system until an obscuration rate of 10 % was achieved. The size distribution plots were obtained using volume fraction of particles vs. size. The measurements were taken in triplicate.

2.3.4 Field emission scanning electron microscopy (FESEM)

The morphological characteristics of the cellulosic materials were analysed by using Field Emission Scanning Electron Microscope (ULTRATM 55, Zeiis, Oxford Instruments, UK). The samples were covered with platinum and the micrographs were obtained at an acceleration voltage of 2.00 kV.

2.3.5 Fourier transform infrared spectroscopy (FTIR)

A FTIR spectrometer (Vertex 80, Bruker AXS GmbH, Karlsruhe, Germany) equipped with microscopic (Hiperion) and attenuated total reflectance accessories was used to evaluate the vibrational profile of the functional groups present in the obtained CF. FTIR spectra were obtained at a resolution of 6 cm^{-1}, in the wavelength range of 4000-650 cm^{-1}, and performing 128 scans for each spectrum. The measurements were taken 5 times for each sample.

2.3.6 X-ray diffraction analysis (XRD)

The X-ray diffraction spectra of the cellulosic samples were obtained with an X-ray diffractometer (AXS/D8 Advance, Bruker, Karlsruhe, Germany) using Kα-Cu radiation (λ: 1.542 Å), 40 kV, 40 mA, step size of 2.0°.min^{-1}, and a 2θ scanning angle between 5° and 40°. The conditioned samples (25 °C and 53% relative humidity (RH)) were spread and compacted to cover the sample holder. For each treatment, the crystallinity index (CI, expressed as a percentage) was determined following the Seagal et al. (1959) method, which relates the maximum intensity of 200 lattice diffraction (I_{200}, crystalline peak) and the diffraction intensity at 2θ = 18° ($I_{2\theta\ 18°}$, amorphous phase valley). The data were obtained using XRD Commander software (Bruker AXS GmbH, Karlsruhe, Germany) and processed with DIFFRAC.EVA (Bruker AXS GmbH, Karlsruhe, Germany) and DRXWin (Windows, version 2.3) software.

$$CI\ (\%) = \frac{(I_{200} - I_{2\theta\ 18°})}{I_{200}} 100 \qquad (1)$$

2.3.7 Thermogravimetric analysis

A TGA analyser (TGA 1 Stare System analyser, Mettler-Toledo, Switzerland) was used to analyse the thermal behaviour of the cellulosic samples under nitrogen atmosphere (10 $mL.min^{-1}$). Samples of about 3-4 mg were weighed in an alumina pan and heated from 25 to 700 °C. Before the analysis, the samples were conditioned in desiccators with P_2O_5 at 25 °C for 2 weeks. The thermogravimetric and their derivatives curves were analysed using the STARe Evaluation Software (Mettler-Toledo, Switzerland) to obtain the initial temperature (T_{onset}), the temperature at the maximum degradation rate (T_{peak}), and the mass loss percentage in each detected thermal event. The measurements were taken in triplicate.

2.4 Reinforcing capacity and effect on physical properties in composite films

To evaluate the reinforcing capacity of the obtained fibres, films of Methylcellulose (MC) and Gum Arabic (GA), a polysaccharide-protein complex fully compatible with MC polymer (Amalraj et al., 2020; Xu et al., 2019), were obtained and characterised, using different ratios (1, 3 and 5 wt. % with respect to the total polymer mass) of cellulose fibres. These blends were chosen on the basis of the good fibre compatibility visually observed. Table 1 summarises the different composition of the obtained films.

Table 1. Mass fraction (g/g) of the different components (MC: methylcellulose; GA: gum Arabic; Gly: glycerol; CF: cellulose microfibres) present in the composite films.

Formulations	X_{MC}	X_{GA}	X_{Gly}	X_{CF}
Control	0.7500	0.0833	0.1667	-
USH-1	0.7438	0.0823	0.1653	0.0086
USH-3	0.7317	0.0813	0.1626	0.0244
USH-5	0.7200	0.0800	0.1600	0.0400
ALK-1	0.7438	0.0823	0.1653	0.0086
ALK-3	0.7317	0.0813	0.1626	0.0244
ALK-5	0.7200	0.0800	0.1600	0.0400

Aqueous dispersions of cellulose fibres at different concentrations were sonicated (Vibra Cell^{TM} VCX750, 750 W power, 20 kHz frequency, Sonics & Material, United States) at 25 °C (using an ice bath) for 20 min for the purposes of obtaining the films. Afterwards, MC (6% wt.) was added to the sonicated aqueous dispersions of cellulose fibres at 85 ± 2 °C and 700 rpm for 1 h (solution 1). Solution 2 was prepared by dispersing GA (2% wt.) in distilled water at 50 ± 2 °C and 700 rpm for 1 h. After that, a volume of solution 2 was mixed with solution 1 to reach the MC:GA mass ratio of 9:1. Later on, glycerol (20 % wt. with respect to the total polymer mass) was added, and the final solution was stirred at 50 ± 2 °C and 700 rpm for 1 h. The amount of dispersion equivalent to 2 g of MC/GA blend was poured onto 150 mm diameter Teflon plates and dried at 25 ± 2 °C for 72 h. The cast films were labelled as USH-1,

USH-3, USH-5, ALK-1, ALK-3, ALK-5, where the number indicates the wt. percentage of CF in the films, with respect to the polymers and USH or ALK indicate the method used to obtain the cellulose fibre prior to the bleaching process. As control samples, fibre-free MC/GA blended films were used. Before the characterisation, the composite films were conditioned at 53 % RH (using a $Mg(NO_3)_2$ over-saturated solution) for one week. The films were prepared in triplicate.

2.5 Film characterisation

The optical properties (transparency and colour) were analysed in composite films. A spectrocolorimeter (CM-3600d, Minolta Co., Japan) was used to determine the reflection spectra (R) of the films from 400 to 700 nm, obtained on white (R_g) and black (R_0) backgrounds. The internal transmittance (T_i) used to determine the transparency and the infinite reflectance (R_∞) were obtained, following the Kubelka-Munk theory of multiple scattering (Equations 2, 3, 4, and 5). Film colour coordinates L^* (lightness), a^* (redness-greenness), and b^* (yellowness-blueness) were obtained from the R_∞ spectra, using D65 illuminant and 10° observer. Chroma (C^*) and hue angle (h^*) were obtained following Equations 6 and 7, respectively. The measurements were taken six times for each sample (Andrade et al., 2020).

$$T_i = \sqrt{(a - R_0)^2 - b^2} \quad (2)$$

$$R_\infty = a - b \quad (3)$$

$$a = \frac{1}{2}\left[R + \left(\frac{R_0 - R + R_g}{R_0 \times R_g}\right)\right] \quad (4)$$

$$b = \sqrt{a^2 - 1} \quad (5)$$

$$C^* = \sqrt{a^{*2} + b^{*2}} \quad (6)$$

$$h^* = arctg\left(\frac{b^*}{a^*}\right) \quad (7)$$

The water vapour permeability (WVP) of films, expressed in $g.mm.kPa^{-1}h^{-1}.m^{-2}$, was determined gravimetrically, following ASTM E96/E96M (ASTM, 2005) with a modification proposed by McHugh et al. (1993). The samples were cut and placed in circular cups (Ø = 3.5 cm) containing 5 mL of distilled water (100 % RH). Then, the cups were put into desiccators at 25 °C and 53 % RH ($Mg(NO_3)_2$ over-saturated solution), which promoted a constant RH gradient of 47 % through the films. The systems were weighed every 1.5 h for 24 h, and the water vapour transmission rate was determined from the slope of the curve given by weight loss *vs.* time. The measurements were taken in triplicate.

The equilibrium water content of the films was determined gravimetrically following the method of Collazo-Bigliardi et al. (2019), with modifications. About 500 mg of each conditioned film (25 °C and 53 % RH for one week) was dried at 60 °C for 24 h and then placed in a dissector at 25 °C with P_2O_5 for two weeks. The moisture content was obtained from the mass loss of the film samples. The measurements were taken in triplicate.

The thickness of films was measured using a digital micrometer (Palmer, model COMECTA, Barcelona, accuracy of 0.001 mm) at ten random film positions.

According to ASTM D882 (ASTM, 2012), a universal testing machine (Stable Micro Systems, TA.XT plus, England) was used to determine the tensile properties of the films. The force-distance curves were obtained and transformed into stress-Hencky strain curves. The mechanical behaviour was analysed in terms of elastic modulus (EM), tensile strength (TS) and percentage of elongation at break (%E). The pre-conditioned (53 % RH) film samples (25 mm x 100 mm) were stretched at a crosshead speed of 12.5 $mm.min^{-1}$ by two grips initially separated by 50 mm. Eight samples for each treatment were evaluated in triplicate.

2.6 Statistical analysis

The experimental data were submitted to analysis of variance (ANOVA) using the Minitab statistical program (version 17), considering a confidence level of 95 %. Differences between the responses of the treatments were determined by Tukey's studentised range (HSD) test, using the least significant difference (α) of 5 %.

3. RESULTS AND DISCUSSION

3.1 Extraction and purification process of CF

Figure 1 shows the appearance of the products obtained in each step of the processes used for obtaining CF from RS: the alkaline treatment and the sequential combination of ultrasounds and reflux heating of the RS aqueous dispersion, both followed by a bleaching step. The appearance of the RUH-B fibres (Figure 1) suggests that the combined ultrasound-heating process was comparable to that performed with alkaline solution (RALK-B) since both products exhibited similar whiteness. The untreated RS particles and the cellulosic fractions were characterised as to their chemical composition, nano and microstructural characteristics and thermostability. The reinforcing capacity of cellulosic fibres was evaluated once incorporated into MC polymeric films.

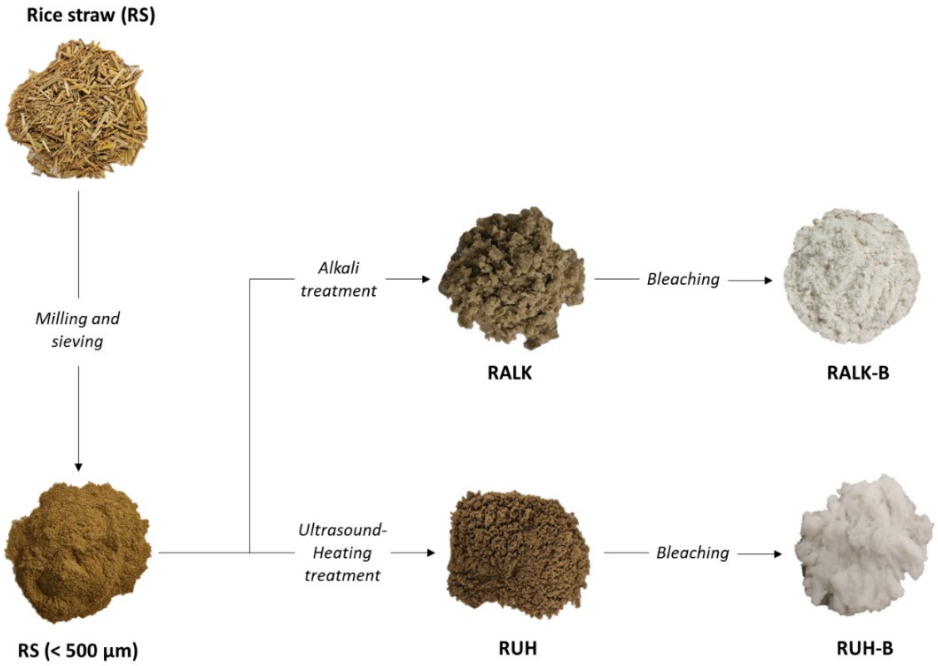

Figure 1. Different fractions obtained in the cellulose extraction process by applying a combined US-heating process or alkaline treatment before the bleaching step.

Table 2 summarizes the yield (referred to the initial dry RS) of the different solid fractions from each stage of obtaining process of the cellulose fibres, as well as water extractables and the chemical composition of raw RS and different fractions. The lower yields obtained at each stage (31.2 % and 29.5 % for RALK and RALK-B, respectively) suggested that the alkaline method was more effective at extracting non-cellulosic compounds than the RUH treatment, with greater yields in the insoluble material (85.5 %, 80.1 % and 37.4 % for RUS, RUH, and RUH-B, respectively). Thus, the alkaline process seems to promote greater tissue degradation with higher removal of hemicellulose, lignin, and waxes from RS (Faruk, 2012; Jones et al., 2017; Pickering et al., 2016), giving rise to a more purified cellulosic fraction. This was confirmed by the chemical composition analyses. The untreated RS showed cellulose, hemicellulose, and lignin contents of 36.7 %, 19.3 %, and 21.2 %, respectively, consistent with the values found by Singh et al. (2014). A progressive enrichment in cellulose content was observed for both treatments, according to the elimination of non-cellulosic components present in the raw RS. However, the samples submitted to the alkaline step (RALK-B) exhibited higher cellulose content and lower hemicellulose and lignin concentrations than those obtained by applying the combined ultrasound-heating method (RUH-B). Ultrasound (RUS) treatment step and combined method (RUH) only produced a slight, non-significant ($p>0.5$), decrease in the lignin content of the solid fraction while the hemicellulose content slightly increased due to the removal of other water-soluble compounds. However, the cellulose concentrations in the final fibres obtained from both purification methods (alkaline and

combined treatment) were more comparable after the bleaching step (73 % *vs.* 66 %, respectively). This result suggests that the main effect of the combined method was to disrupt the tissues of the RS, exposing the innermost tissue of the plant matrix, thus favouring the contact with the bleaching solvent. This is also coherent with the higher values of water extractables of RUS and RUH samples, compared with the raw RS sample. The extraction potential of the non-structural, water-soluble components from the solid plant tissue was promoted by RUS and RUH treatments (Table 2). Acoustic cavitation promoted by ultrasound is characterised by the implosion or explosion of water vapour or air bubbles, which generates high shear rates in the solvent (Ojha, 2020). This phenomenon transfers high amounts of energy to the dispersed material, causing the plant cell to rupture and extracting non-cellulosic compounds (Arruda et al., 2019; Cheung & Wu, 2013). Thus, US exposes tissues of the plant matrix and, when used in combination with heating, can increase the mass transfer efficiency. Freitas et al. (2020) observed that ultrasound promoted de-bonding in the RS fibrils, which increased the surface area of the plant material exposed to the extraction medium. These physical changes allowed greater accessibility of the solvent when the heating step was applied, enhancing the extraction levels of components, such as hemicelluloses, lignin, or waxes.

Table 2. Yield, chemical composition (% wt.), and the ashes content of RS and the cellulosic fractions at different treatment steps (mean values ± standard deviation of three replicates).

Sample	Yield (% wt.)	Water extractables (% wt.)	Cellulose* (% wt.)	Hemicellulose* (% wt.)	Lignin (% wt.)	Ashes (% wt.)
RS	-	9.3 ± 0.8^{a}	36.7 ± 0.4^{e}	19.3 ± 0.1^{a}	21.2 ± 0.5^{a}	17 ± 2^{a}
RUS	85.5	12.3 ± 0.2^{b}	37.3 ± 0.1^{de}	21.3 ± 0.2^{a}	20.5 ± 0.2^{a}	12 ± 1^{b}
RUH	80.1	14.8 ± 0.1^{c}	40.3 ± 0.8^{d}	20.1 ± 1.2^{a}	19.7 ± 1.4^{a}	11 ± 1^{b}
RALK	31.2	n/a	54.6 ± 3.1^{c}	8.2 ± 1.2^{c}	6.6 ± 1.7^{b}	8 ± 1^{c}
RUH-B	37.4	n/a	65.9 ± 0.7^{b}	15.6 ± 0.4^{b}	5.2 ± 0.2^{b}	5 ± 2^{cd}
RALK-B	29.5	n/a	73.4 ± 2.1^{a}	10.1 ± 0.8^{c}	2.6 ± 0.4^{c}	2 ± 3^{d}

*Cellulose was reported as % wt. of total glucose content in relation to the initial solid fraction; hemicellulose concentration was determined by the sum of the xylose and arabinose contents.

RS showed an ash content of approximately 17 % wt., which is mainly attributed to silica (Chen et al., 2011). The subsequent purification steps promoted a progressive reduction in the ash/silica content, suggesting the leaching out of these non-carbonaceous components. The fractions submitted to the alkaline treatment showed a lower ash content (RALK: 7.5 %) than those RUH treated (11 %) since the alkaline solution promoted the solubility of silica (Requena et al., 2019). Bleaching promoted the silica extraction from the lignocellulosic residue in both

RALK and RUH solids, but its final content was higher in cellulosic fractions obtained by the combined RUH treatment.

As concerns the water binding capacity of the fibres, Figure 2 shows the equilibrium water content of RALK-B and RUH-B fibres at different relative humidity. Significantly lower values were obtained for the RALK-B samples, which suggests the presence of a higher amount of exposed polar groups in the cellulosic materials coming from RUH-B treatment that promoted the fibre water affinity. This could be attributed to the higher purification of the cellulose chains in the RALK-B samples, which contributes to exposing the cellulosic OH groups that are able to establish hydrogen bonds between chains. The extensive hydrogen bonding between the cellulose chains decreases their capacity to interact/bond with water molecules (Bochek, 2003), thus reducing the hydrophilic nature of the fibre.

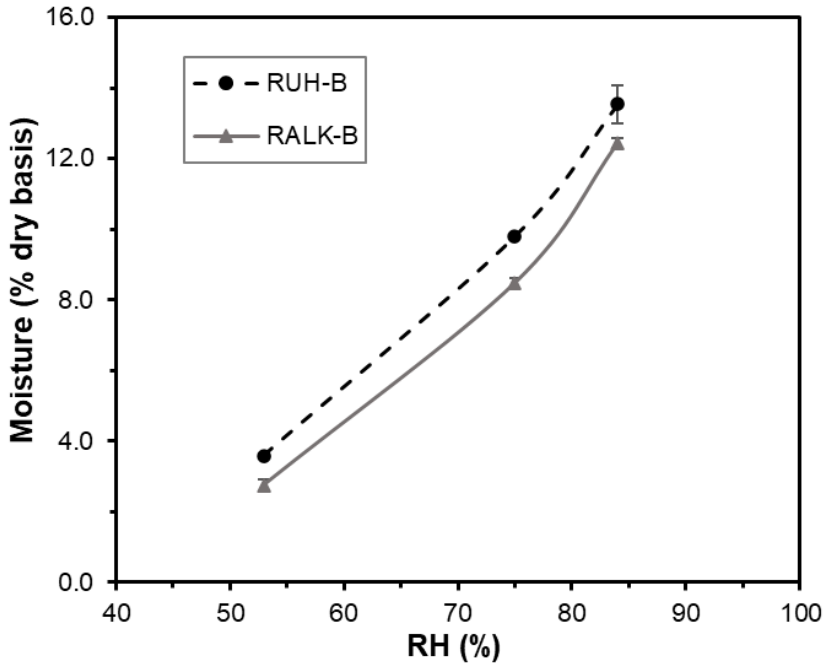

Figure 2. Equilibrium moisture content (% wt. dry basis) at 25 ºC at different relative humidity of the cellulose fibres obtained by applying the combined ultrasound-heating method (RUH-B) and the alkaline treatment (RALK-B).

3.2 Structural properties

The micro and nanostructural properties of the different cellulosic fractions were evaluated as to their microscopic characteristics, particle size distribution, FTIR analysis, and X-ray diffraction patterns. Figure 3 shows the FESEM micrographs in which the microstructural changes in the RS provoked by the CF extraction can be observed. The raw sample (RS) exhibited particles of different dimensions and sizes obtained after the milling and sieving

steps. The predominantly fibrillar rod-like shape of the particles reveals the RS tissue arrangement, which consists of a material with a high proportion of non-fibrous cells, such as the epidermis, parenchyma, and vessel cells (Jin & Chen, 2006). The innermost primary tissue, namely the sclerenchyma, is composed of CF embedded in a cementing matrix of hemicellulose and lignin (Seo & Sakoda, 2014). As shown in the micrograph of the RUH treated samples, the application of ultrasound followed by heating provoked the partial destruction of the original RS structures brought about by the different physical phenomena involved, such as detexturation, sonoporation and particle fragmentation (Chemat, 2017; Machado, 2019; Ojha, 2020). The RS tissue layers were observed to detach, leading to distorted and more planar particles, thus favouring the leaching out of non-cellulosic components, such as hemicellulose, lignin, and waxes. The observed disruption of the original RS structure facilitates the accessibility of the bleaching solvent to the solid matrix. It is worth mentioning that the removal of non-fibrous components from the cellulosic material was not evident at this stage. In contrast, the FESEM images from the RALK treated samples showed more intact particles than those RUH treated, despite being more distorted longitudinally, as also observed by (Moslemi, 2020). The observation of fibres aligned in the axial direction suggests the partial chemical removal of amorphous components, such as hemicellulose, lignin, and waxes (Zhang et al., 2014). This effect was more evident for RALK-B and RUH-B treated samples, which revealed smooth and homogeneous surface patterns due to an efficient surface washing of non-fibrous components, as also reported by other authors for the extraction of different plant matrices (Mohamad Haafiz et al., 2013; Rasheed et al., 2020). A certain degree of defibrillation was detected for the RUH-B samples at the edges of the fibre bundles (Figure 4), which suggests that the ultrasound-heating treatment disrupted the fibre bundle structure to a greater extent than the alkaline treatment.

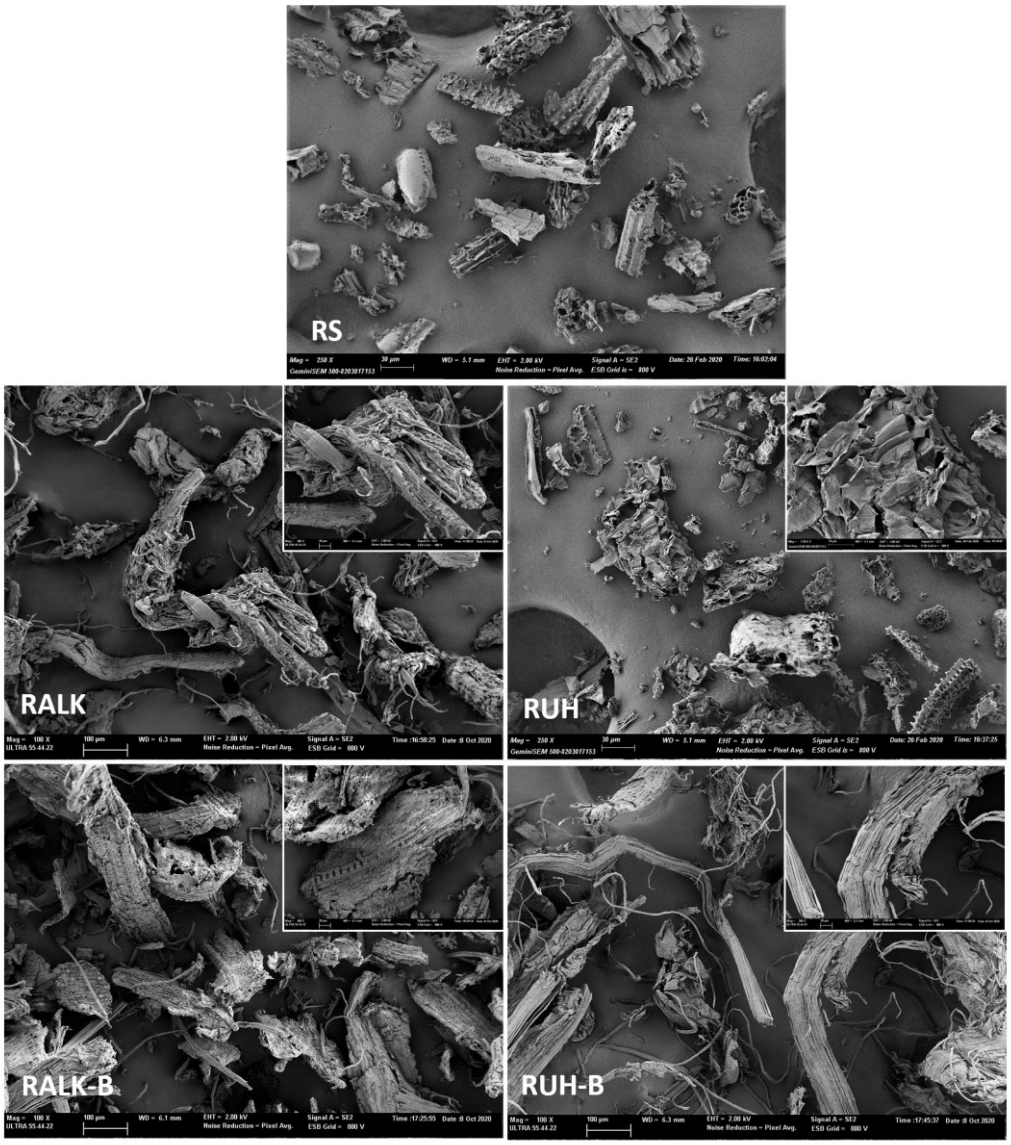

Figure 3. FESEM micrographs of cellulosic fractions before and after the bleaching step, in comparison with raw material (RS).

Figure 4 shows optical microscopy and FESEM observations of the CF obtained from RUH-B and RALK-B treatments after their aqueous dispersions and sonication for 20 min, before and after drying, respectively. Before drying, optical micrographs (10x magnification) revealed that the original fibre bundles were disrupted, and the defibrillated fibre bundles of varying lengths were dispersed in the aqueous medium, increasing the turbidity and dispersion consistency. At a greater magnification (40x magnification), detached cellulose fibrils can be observed at the edges of the fibres in the RUH-B samples (black arrows) but not in the samples treated with alkaline solution (RALK-B). This could be due to the effect of the alkaline treatment, which could eliminate these defibrillated fractions, or to the greater weakness of the fibril unions in the bundle provoked by the RUH treatment. These variations in the fibre structure could also

affect the hydrophilic nature of the different fibres, as demonstrated by the different equilibrium water content. In this sense, the alkaline treatment removes more compounds from the lignocellulosic fibre, promoting hydrogen bonds between cellulose chains, further reducing the interaction capacity with water molecules. What is remarkable is the large number of small fibre fragments, together with the largest fibres, in the RALK-B sample, which suggest the more aggressive effect of the alkaline treatment on the fibrous material. After drying the sonicated aqueous dispersions of fibres, the FESEM micrographs reveal that the fibres of the RUH-B treated samples remained mostly isolated, whereas those of the RALK-B treated samples exhibited aggregation with fibre entanglement. This reveals the different interaction forces between the two kinds of fibres, probably due to the different number of OH groups exposed on their surface due to the differences in the degree of cellulose purification. Greater attractive forces acted between the more hydrophobic RALK-B fibres, whereas repulsive interactions acted on the more hydrophilic RUH-B materials. These results ratify the different nature of the fibre's surface (more or less hydrophilic), as affected by the kind of treatment.

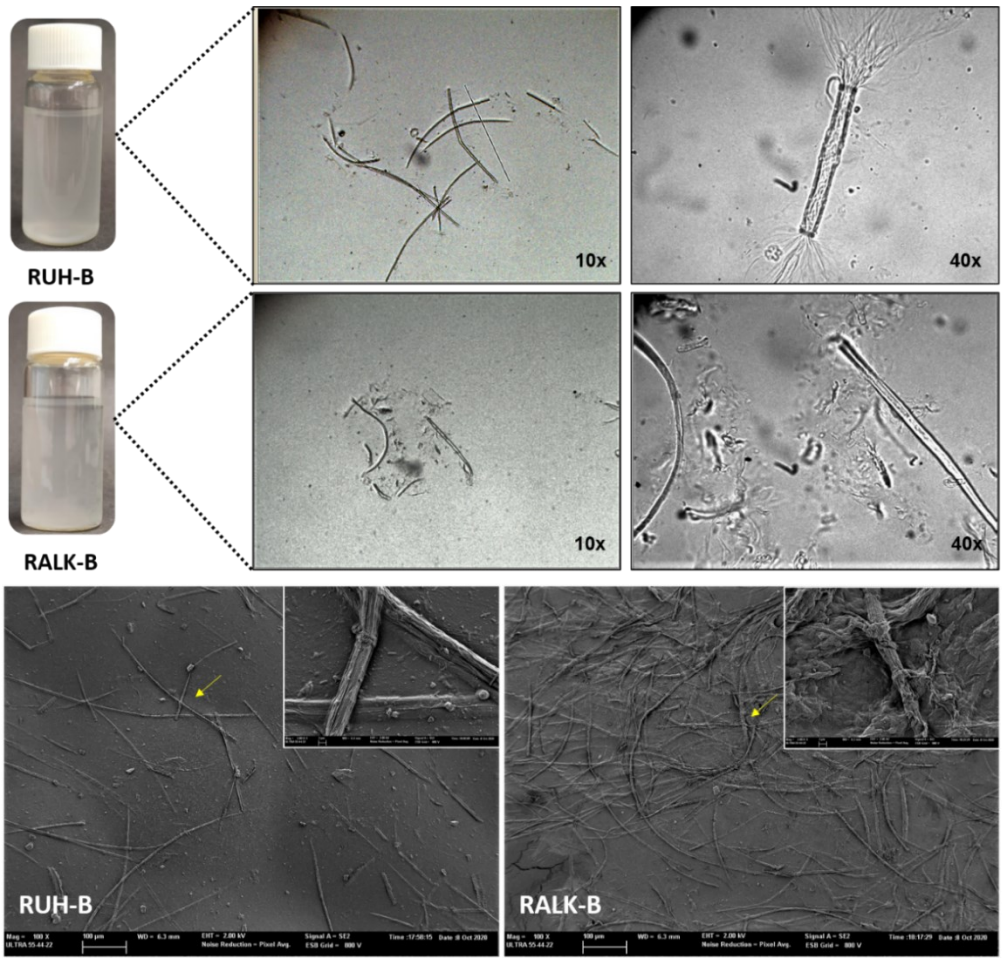

Figure 4. Optical and FESEM micrographs of the CF (RUH-B and RALK-B) sonicated aqueous dispersions before and after drying, respectively.

Laser diffraction was also used to investigate the morphogeometric properties of CF in terms of particle size distributions derived from their hydrodynamic volume. As can be observed in Figure 5a, the RUH-B and RALK-B samples exhibited an almost bimodal distribution, with two main peaks at about 15 and 70 µm. The RUH-B samples have a greater ratio of small particles (4.8 % volume fraction) than the RALK-B samples (4 %). So, the RUH treatment provoked a greater fraction of smaller particles (around 15 µm), or less aggregated particles, in comparison with the alkaline treatment. Nevertheless, it is remarkable that laser diffraction measurements provide the radius of gyration of the particles and so, the values are closer to the particle length. In this sense, the RALK-B treatment could give rise to longer fibres than the RUH-B, which could be due, in part, to the defibrillation effect observed at the edges of the fibrils (Figure 4).

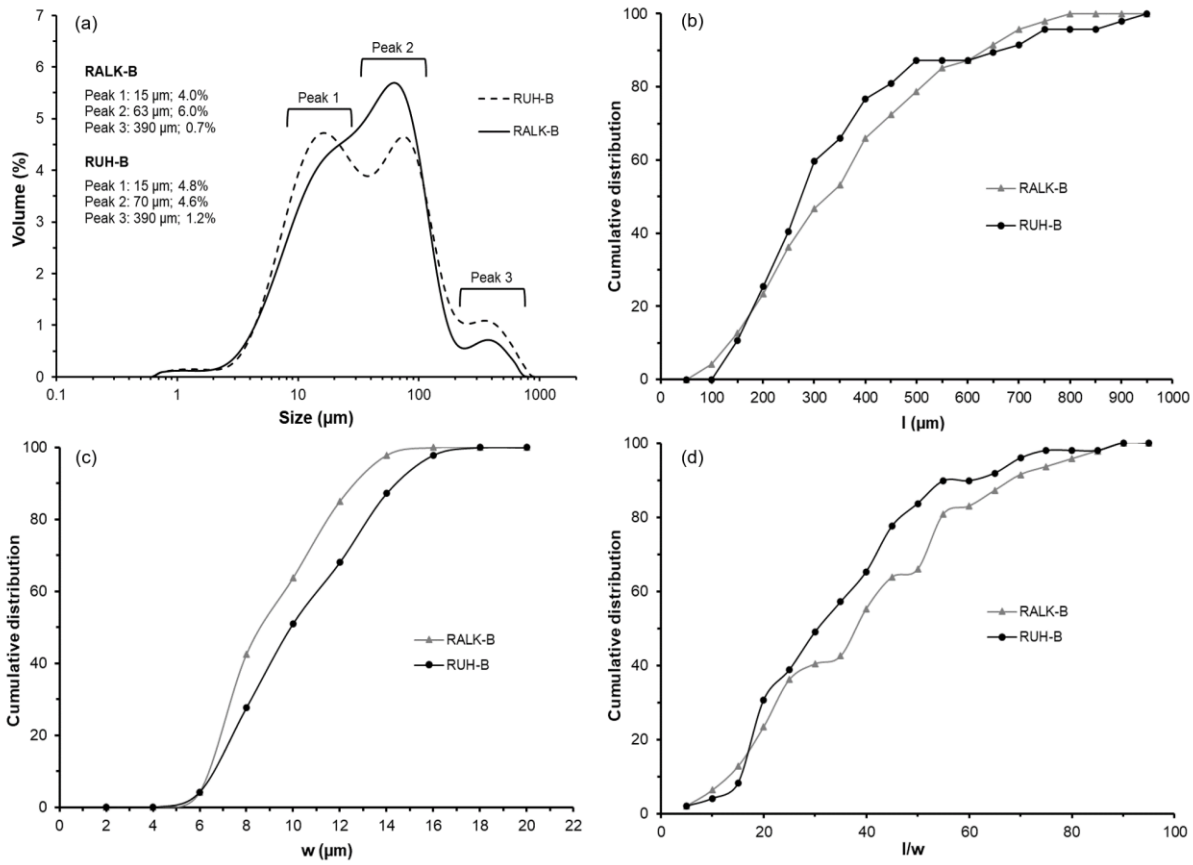

Figure 5. Particle size distributions of CF from laser diffraction (a) and cumulative distributions of CF (RALK-B and RUH-B) samples obtained from the image analyses of optical microscopy images (b: length (l); c: width (w); d: aspect ratio (l/w)).

Considering the CF rod-like shape, image analysis was applied to the optical micrographs in order to determine the cumulative distribution of the length (l), width (w), and the aspect ratio (l/w) of the CF (RUH-B and RALK-B) after water dispersion by sonication (Figures 5b, c, and d). A similar length distribution can be observed for the different particles, the maximum

frequency being for fractions of lengths of 200-350 µm. Nevertheless, as detected in laser diffraction analyses, a greater ratio of shorter particles can be observed for the RUH-B treatment, whereas the RALK-B particles exhibited a wider length distribution. In contrast, a remarkable reduction in the particle width may be observed for the sonicated fibres, which had values of under 20 µm (Figure 5c), as also shown in the FESEM images at a higher magnification (Figure 4). A greater fraction of thinner particles can be observed for the RALK-B samples; more than 60 % of the particles are thinner than 10 µm. This is coherent with the fact that the alkaline treatment removes a greater quantity of non-cellulosic components from the fibre. Consequently, the aspect ratio (l/w) of the RALK-B samples is slightly greater than that of the RUH-B samples, with a distribution ranging mainly between 10 and 50 (RUH-B) or 60 (RALK-B) (Figure 5d).

3.3 Fourier transform infrared spectroscopy (FTIR)

Figure 6 shows the FTIR spectra of untreated RS and unbleached (RUH and RALK) and bleached (RUH-B and RALK-B) cellulosic fractions. The spectrum of untreated RS showed a bell-shaped absorption band between 3690 and 2980 cm^{-1}, which is associated with the O-H stretching vibration (Chen et al., 2011). The O-H absorption band, present in cellulose, hemicellulose, and lignin, was slightly narrower and more intense for the bleached samples. This agrees with the cellulose concentration in the material (Table 2) since it has a higher ratio of OH groups than non-cellulosic components (hemicellulose and lignin) (Moslemi, 2020; Wang, 2018). The absorption bands at 2919 and 2852 cm^{-1} are associated with the C-H asymmetric and symmetrical vibration present in cellulose, hemicellulose, and lignin. These peaks shared more characteristics in RS and RUH treated samples, indicating a more similar composition, whereas there were greater differences between the both bleached samples (RUH-B and RALK-B), according to the greater elimination of non-cellulosic compounds by alkaline treatment. The absorption peak at 1730 cm^{-1} corresponds to the C=O stretching vibration of the carboxylic groups and esters present in phenolic and uronic acids, which are chemical structures constituting the lignin and hemicellulose fractions (Abraham, 2011; Chen et al., 2011). This peak disappeared partially in the RALK treated samples and totally in the RALK-B treated samples. However, it was present in the spectra of the bleached and non-bleached RUH treated samples, which indicates the presence of these kinds of compounds bonded to the cellulose structure, according to the chemical composition (Table 2). Wang et al. (2018) also observed the disappearance of this peak after the alkaline treatment of rice straw, whereas (Boonterm, 2016) detected the peak at 1730 cm^{-1} in cellulose obtained with the thermal steam explosion from rice straw. The different intensities of the bands at 1645 cm^{-1}, assigned to the O-H bending vibration of adsorbed water (Moslemi, 2020), coincides with the differences in the equilibrium moisture content of the samples; the samples coming from the RUH treatments exhibiting the higher intensity. Indeed, Chen et al. (2011) indicated that the lower intensity of this peak is related to a partial removal of hemicellulose. The thin peak at 1511

cm^{-1} corresponds to the C=C stretching vibration of the aromatic skeletons present in lignin rings (Elhussieny, 2020; Xu et al., 2006). This absorption band is absent in the spectra of the RALK treated samples and every bleached sample (RUH-B and RALK-B), thus indicating the efficiency of bleaching at eliminating a substantial fraction of lignin.

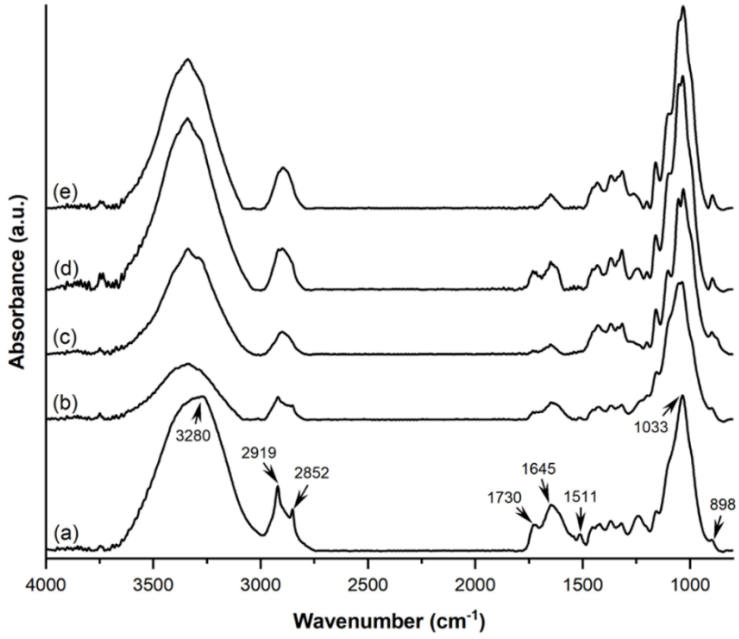

Figure 6. FTIR spectra of (a) untreated RS, RS treated with (b) ultrasound-heating and (c) alkaline solution, and bleached fibres from (d) the combined ultrasound-heating method and (e) the alkaline treatment.

Every spectrum showed an absorption band at 1033 cm^{-1}, related to the C-O-C-O-C stretching vibration of acetal linkage present in cellulose and hemicellulose. The 898 cm^{-1} band, associated with the C-O-C stretching vibration of the β-glycosidic bond present in the cellulose I structure, becomes more evident as the cellulose concentration increases in the bleached samples (RALK-B and RUH-B) (Pan & Sano, 2005; Wang, 2018). In brief, the obtained FTIR spectra suggested that, despite the alkaline method eliminating a greater fraction of hemicellulose and lignin from the plant matrix, the combined ultrasound-heating treatment produced similar fibres and could be alternatively applied to RS as a greener process.

3.4 Crystallinity analysis

The X-ray diffraction patterns of the raw powder and the different cellulosic fractions obtained at each stage of both processes are shown in Figure 7. Likewise, the crystalline nature of the materials was characterised in terms of the crystallinity index (CI). In every sample, four diffraction peaks were detected at 2θ = 15° ($1\bar{1}0$), 16° (110), 22° (200), and 34° (004), characteristic of the crystalline lattice of type I cellulose, as described by other authors (Junior,

2018; Nam et al., 2016). As the cellulose purification progressed, the diffraction peaks became more defined and slightly narrower, as corresponds to the progressive elimination of amorphous components (hemicellulose, lignin, and waxes).

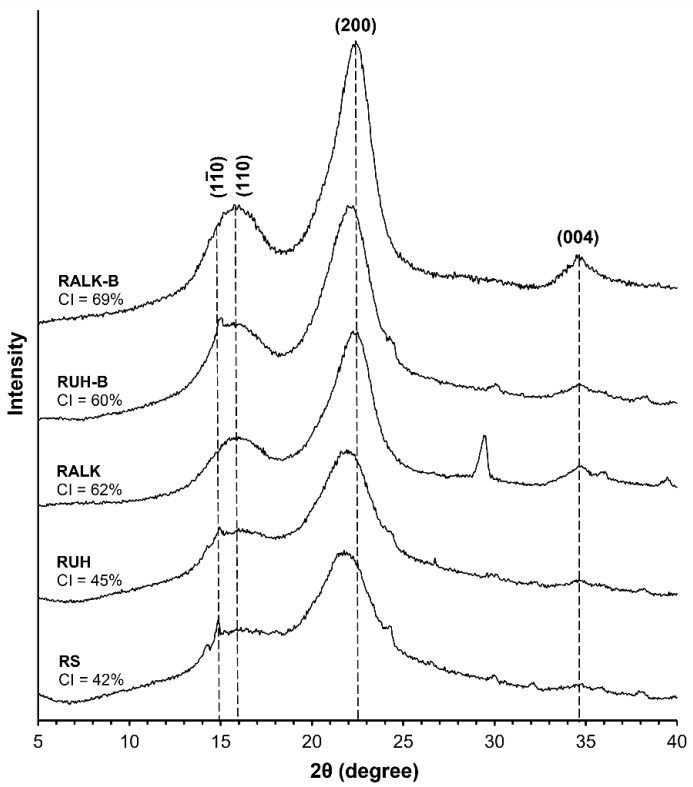

Figure 7. The X-ray diffractograms and crystallinity index (CI) of different cellulosic fractions from RS, before and after bleaching.

Compared to RS (CI: 42 %), the combined ultrasound-heating method (RUH) promoted a negligible increase in crystallinity (CI: 45 %), whereas a noticeable increase was observed for the cellulosic sample after the treatment with alkaline solution (CI: 62 %), similar to that obtained by Requena et al. (2019) for rice husk treated with alkaline solution. This agrees with what was deduced from chemical composition and FTIR analyses; the combined ultrasound-heating method was less efficient at extracting amorphous components from the plant matrix than the alkaline treatment. In addition to the chemical degradation and removal of amorphous components from the lignocellulosic matrix, NaOH solutions at low concentrations promote the swelling of interfibrillar regions, making them less rigid (Liu & Hu, 2009; Yue et al., 2012). This phenomenon allows for the rearrangement of the cellulose microfibrils, due to the penetration of Na ions into the crystalline network forming antiparallel crystalline soda-cellulose complexes, which change the crystallinity of the material (Budtova & Navard, 2016; Liu & Hu, 2009). From a determined NaOH concentration (e.g., 15 % for cotton fibre), a crystalline transition can occur, giving rise to the formation of cellulose II crystals (Yue et al.,

2012). This change was not clearly observed in the RS samples treated with the alkaline solution due to the low NaOH concentration used (4.5 %).

After the bleaching step, which focuses on removing lignin from the matrix (Ng et al., 2015b; Zainuddin, 2013), CI increased in both samples, but especially in the RUH-B samples. This suggests that, despite the ultrasound-heating combined method failing to eliminate a substantial fraction of lignin/hemicellulose components, the fibre delamination and the greater exposure of the RS tissue, observed by FESEM, seem to promote the bleaching solvent accessibility (Freitas et al., 2020). Thus, this produces cellulosic materials with similar crystalline characteristics to those produced by the conventional alkaline method, but containing other bonded compounds as revealed by chemical composition and FTIR analyses.

3.5 Thermogravimetric analysis

The thermal behaviour of the samples as the extraction progressed was evaluated by thermogravimetric analysis (TGA). Both the TGA and the derivative (DTGA) curves of the untreated, different cellulosic fractions are shown in Figure 8. Table 3 summarises the parameters (initial and maximum degradation temperatures and the mass loss percentage) of each detected thermal event. Each cellulosic sample exhibited three thermal degradation events. The first occurred in the temperature range of 30 to 140 °C, associated with the loss of water molecules bonded on cellulosic fractions and other small molecular weight volatiles (Theng et al., 2017; Wu et al., 2013). The second and third peaks are related to the thermal degradation of the lignocellulosic components, as reported by other authors (Requena et al., 2019). As can be observed, the second thermal event started at higher temperatures as the cellulose became more purified, in the following order: RS<RUH<RALK<RUH-B<RALK-B. The peak temperature ranged between 284 and 300 °C, depending on the sample. This agrees with the fact that the RALK/RUH and bleaching treatments eliminated hemicellulosic/lignin fractions to differing extents, as observed by the chemical composition, FTIR and XRD analyses, increasing the sample degradation temperature. The peak observed in the DTGA curve of the RALK-B sample was narrower and more intense than that of the RUH-B sample, in line with the greater purity and crystallinity of the cellulose fraction.

On the other hand, lignin is a group of polymers that exhibits a broad spectrum of thermal degradation starting at around 220 °C and continuing above 400 °C (Monteiro et al., 2012). In this sense, as reported by Theng et al. (2017), the last thermal event, observed between at 340-500 °C is attributed to the thermal degradation of the lignin and the products from the fragmentation of the organic structure. This peak, also found by El-Sakhawy & Hassan (2007) in microcrystalline cellulose from RS, was not expected in the thermograms of bleached fibres, which indicates the inability of either process to eliminate completely the lignin present in the inner structure of the fibre bundles. Indeed, the FESEM images (Figure 3) reveal some integral and compact fibre bundles, which could prevent the full access of the bleaching solvent.

According to Chen et al. (2011), the strong crystalline structure of cellulose in RS and the complexity of the structural configuration between cellulose, hemicellulose, and lignin are the limiting factors for the obtaining of accessible cellulose fibres.

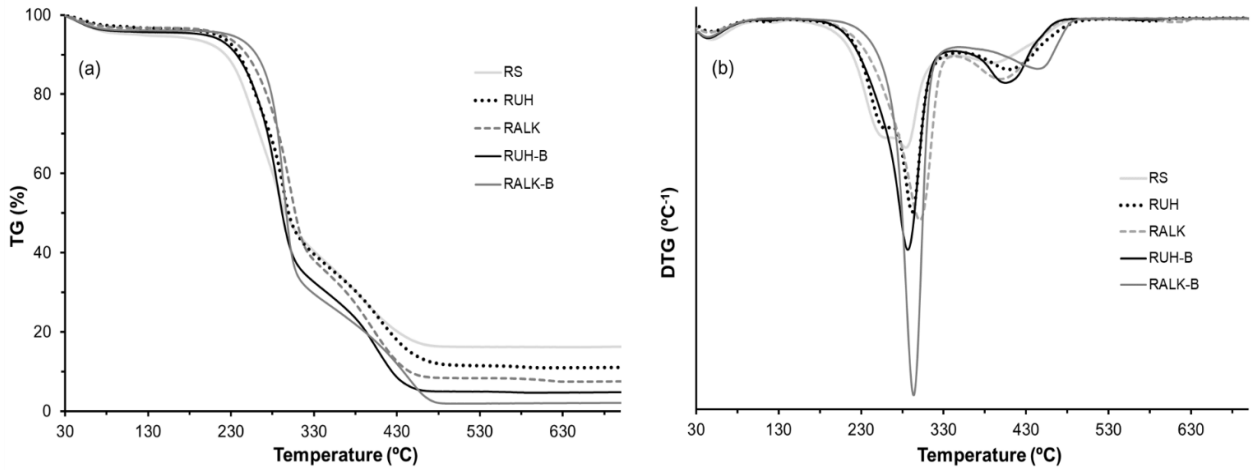

Figure 8. The TGA (a) and DTGA (b) curves of the RS samples before and after different treatments: RUH, RALK, RUH-B, and RALK-B.

Table 3. Thermal decomposition events detected for the cellulosic materials from RS (mean values ± standard deviation of two replicates).

Sample	[30-140] °C			[148-350] °C			[340-500] °C			Residue
	T_{onset}*	T_{peak}*	Mass loss (%)	T_{onset}*	T_{peak}*	Mass loss (%)	T_{onset}*	T_{peak}*	Mass loss (%)	Mass (%)
RS	33.19 ± 0.01	51.4 ± 2.0	1.7 ± 0.2	148 ± 5	284.2 ± 0.2	55.9 ± 1.5	345.5 ± 2.1	389 ± 2	20.7 ± 0.6	17 ± 2
RALK	33.0 ± 1.7	49.9 ± 1.5	0.9 ± 0.1	161 ± 1	301.3 ± 2.4	61.0 ± 2.2	341.7 ± 1.1	403 ± 7	26.8 ± 0.2	8 ± 1
RUH	32.3 ± 0.6	50.5 ± 1.3	1.2 ± 0.2	152 ± 2	292.4 ± 2.2	59.7 ± 0.9	349.0 ± 1.7	409 ± 3	23.8 ± 0.4	11 ± 1
RALK-B	33.7 ± 2.1	47.9 ± 2.1	1.1 ± 0.2	186 ± 7	294.0± 4.0	69.0 ± 7.0	349.0 ± 3.0	448 ± 8	24.0 ± 1.2	2 ± 3
RUH-B	33.3 ± 0.6	47.1 ± 2.3	1.3 ± 0.6	177 ± 2	286.0 ± 4.0	66.3 ± 2.3	344.0 ± 3.0	414 ± 15	27.0 ± 5.0	5 ± 2

3.6 Reinforcing properties in composite CMC/GA films

The reinforcement capacity of fibres obtained by means of the alternative (ultrasound-heating) and conventional (alkaline) methods was evaluated by measuring the tensile properties of MC/GA composite films incorporating different fibre ratios. The use of GA, a polysaccharide-protein complex (Maqbool, 2011; Xu et al., 2019), as a component of the MC polymer matrix was chosen to promote the compound compatibility, since GA exhibits excellent surfactant and encapsulating properties with other polymers and compounds (Amalraj et al., 2020; Xu et al., 2018). The reinforced capacity transfer from the CF to the polymer matrix is related to factors such as the microfibre entanglement, the intensity and type of microfibre-polymer interactions and the ratio between the water adsorption (which promotes plasticisation) and the filler rigidity. Thus, the mechanical properties of the composite films containing the different types and concentrations of CF were evaluated in terms of their tensile strength (TS) and elongation at break (%EB), as well as the elastic modulus (EM) (Table 4).

Table 4. Moisture content, WVP, and mechanical properties of the MC/GA blended films with or without different ratios of CMF from RS (mean values ± standard deviation of three replicates for moisture content and WVP; and eight replicates for thickness and mechanical parameters).

Formulation	Moisture (%)	*WVP** (*x10^3*) (g.mm.kPa^{-1}h^{-1}.m^{-2})	Thickness (μm)	EB* (%)	TS* (MPa)	EM* (MPa)
Control	9.8 ± 0.4^{a}	4.3 ± 0.2^{ab}	119 ± 8^{c}	9.1 ± 2.1^{e}	23.0 ± 3.0^{c}	156 ± 13^{a}
USH-1	8.8 ± 0.4^{bc}	4.2 ± 0.2^{ab}	121 ± 5^{bc}	13.7 ± 2.2^{bcd}	28.1 ± 1.2^{a}	161 ± 6^{a}
USH-3	8.0 ± 0.3^{cd}	4.3 ± 0.1^{ab}	129 ± 7^{ab}	12.0 ± 0.8^{cde}	28.0 ± 2.0^{a}	156 ± 13^{a}
USH-5	7.6 ± 0.4^{d}	4.6 ± 0.3^{a}	133 ± 8^{a}	11.8 ± 1.9^{de}	28.3 ± 1.4^{a}	152 ± 15^{a}
ALK-1	8.8 ± 0.3^{bc}	4.5 ± 0.3^{a}	127 ± 7^{abc}	16.1 ± 2.2^{ab}	27.0 ± 4.0^{ab}	157 ± 17^{a}
ALK-3	8.5 ± 0.4^{cd}	4.2 ± 0.2^{ab}	126 ± 4^{abc}	16.7 ± 2.1^{a}	24.2 ± 2.2^{bc}	127 ± 16^{b}
ALK-5	9.5 ± 0.2^{ab}	3.9 ± 0.1^{b}	124 ± 4^{bc}	14.7 ± 1.8^{ab}	24.2 ± 2.1^{bc}	122 ± 14^{b}

* *WVP*: water vapour permeability; EB: elongation at break; TS: tensile strength at break; EM: elastic modulus. Different letters in the same column indicate significant differences by the Tukey test (α = 0.05).

In general, all the composite films became mechanically more resistant to break and stretchable ($p<0.05$) after CF incorporation (greater TS and %EB values). So, films with 1 % and 3 % of RALK-B fibres exhibited a 77 % increase in EB, while the treatments incorporating RUH-B fibres in the same concentrations increased extensibility by about 33 %. The incorporation of a greater amount of fibres (5 %) reduced film stretchability, compared with the lower ratios. Cazón et al. (2018) also reported an increase in the stretchability for the films based on PVA/chitosan with 5% microcrystalline cellulose. As shown in Figure 4, the RUH-B and RALK-B

exhibited high aspect ratios, which enhanced the entanglement, interfacial interaction, and bondability between the cellulose microfibrils and the MC/GA matrix (Littunen et al., 2013; Ng et al., 2015b). Thus, CF incorporation promoted the force transferring from the microfibril to the polymer matrix. Nevertheless, a non-significant increase (p>0.05) in the EM values was observed for the CF reinforced films, as observed by other authors for cellulose acetate films with cellulose nanofibers from RS (Hassan et al., 2019). Even elastic modulus was reduced by about 20 % when 3 or 5 % of the CF from the ALK treatment was incorporated into the films. As concerns the resistance to break of the films (TS), CF from the RUH treatments increased the TS values by about 22 % at every tested ratio, whereas this effect was only observed in fibres from the ALK treatment at 1 %. Therefore, both kinds of fibres exhibited a reinforcing effect on the MC/GA films, which was reflected in different patterns: the RUH fibres promoted the film resistance to break to a greater extent, but were less effective at enhancing the film stretchability, whereas the RALK fibres made the films more stretchable. Likewise, 5 % of CF did not benefit the film tensile behaviour more than 1-3 %.

Table 4 also summarises the thickness, moisture content values and water vapour permeability (WVP) of the studied films. The equilibrium moisture content of the films decreased as the CF ratio rose, although 5 % of RALK fibres did not provoke this effect. The OH groups present in the cellulose microfibrils could interact with hydrophilic groups within the MC-GA-glycerol matrix, making these sites less available to interact with water molecules. Nevertheless, the lower water content of the films with CF did not lead to lower values of film thickness. In fact, the thickness of the films did not significantly change as a result of fibre addition, except when RUH fibres were incorporated at 3 and 5 %, in which case the films were slightly thicker, according to the increase in the surface solid density of the films. As concerns the WVP values, fibre addition only provoked a significant decrease (about 10 %) when obtained by means of the ALK treatment and incorporated at 5 %. Therefore, despite the expected increase in the tortuosity factor for mass transfer promoted by fibres, no improvement in the water barrier capacity of the films was obtained probably due to the hydrophilic nature of these fibres that favours water solubility in the matrix. Other authors have also found no improvement in the water vapour barrier capacity of the films when CF were incorporated into polymer matrices (Azmin et al., 2020; Cazón et al., 2018; Collazo-Bigliardi et al., 2019).

Figure 9 shows the appearance and the internal transmittance spectra of MC/GA-based films with different fibres and ratios. All of the composite films were similar in appearance to the control film, indicating good compatibility and entanglement of the CF in the polymer matrix. This was reflected in the small changes that occurred in the internal transmittance spectra (Figure 7) of the different samples provoked by fibre addition. As the fibre concentration rose, there was a slight decrease in the transparency of the films, due to the negligible light

scattering effect provoked by the CF dispersion in the polymer matrix, as also observed by other authors (Ching et al., 2015).

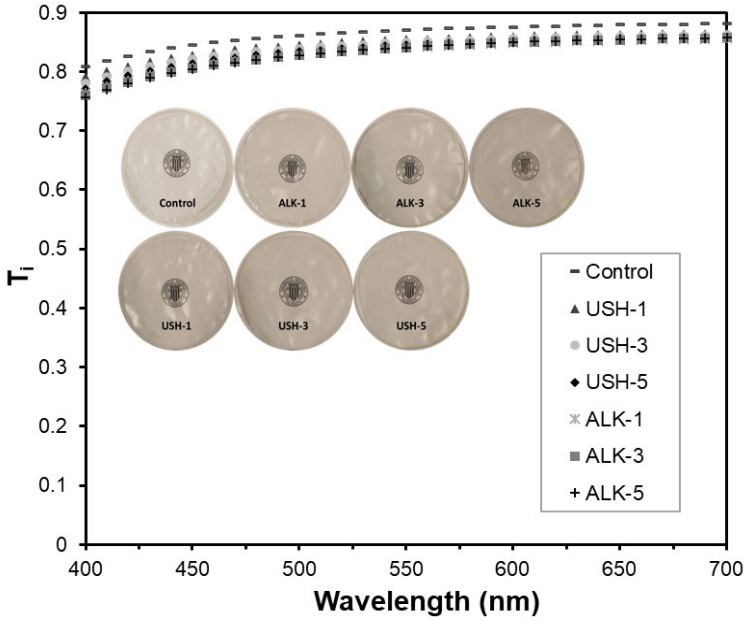

Figure 9. Internal transmittance of the MC/GA blended films with different types (RUH-B and RALK-B) and concentrations (0%, 1%, 3%, and 5% wt.) of CF.

4. CONCLUSIONS

Although alkaline treatment is the most common step in the process for obtaining CF, its substitution by an ultrasound-heating method has environmental advantages due to the elimination of alkaline solvents. This new method gave rise to cellulose fibre fractions with a slightly different degree of purification, but with a similar degree of crystallinity and aspect ratio, these being more hydrophilic in nature and with a lower tendency to aggregate. The reinforcing capacity of the fibres obtained with this new method was similar to those obtained using the alkaline treatment, enhancing the film stretchability by about 33%, and boosting the film resistance to break (by about 20 %) at 1, 3 or 5 %.

Therefore, the combined ultrasound-heating method can be a potential alternative for the purposes of obtaining CF from RS, avoiding the use alkaline solutions, is faster and presents a higher yield than the process with an alkaline step (37 *vs.* 29 %). Moreover, the ultrasound-heating method allows for obtaining active extracts rich in antioxidant compounds, which can be used for different applications in the food or pharmaceutical industries. Thus, a more integral valorisation of RS could be reached.

5. ACKNOWLEDGEMENTS

The authors thank the Agencia Estatal de Investigación (Spain) for the financial support through projects PID2019-105207RB-I00/AEI/10.13039/501100011033 and Generalitat Valenciana [grant number GrisoliaP/2019/115]. We also thank María del Sol Juan Borras (Institute of Food Engineering for Development), Universitat Politècnica de València for her assistance with chemical composition analysis.

6. REFERENCES

Abraham, E. (2011). Extraction of nanocellulose fibrils from lignocellulosic fibres: A novel approach. *Carbohydrate Polymers*, 86, 1468-1475.

ASTM. (2005). E96/E96M-05. Standard Test Methods for Water Vapor Transmission of Materials. American Society for Testing and Materials, 1-11.

ASTM. (2012). ASTM D882-12 Standard test method for tensile properties of thin plastic sheeting. American Society for Testing and Materials, 12.

Amalraj, A., Haponiuk, J. T., Thomas, S., & Gopi, S. (2020). Preparation, characterization and antimicrobial activity of polyvinyl alcohol/gum arabic/chitosan composite films incorporated with black pepper essential oil and ginger essential oil. *International Journal of Biological Macromolecules*, 151, 366-375. https://doi.org/10.1016/j.ijbiomac.2020.02.176

Andrade, J., González-Martínez, C., & Chiralt, A. (2020). The Incorporation of Carvacrol into Poly (vinyl alcohol) Films Encapsulated in Lecithin Liposomes. *Polymers*, 12(2), 497. https://doi.org/10.3390/polym12020497

Arruda, H. S. (2019). Effects of high-intensity ultrasound process parameters on the phenolic compounds recovery from araticum peel. *Ultrasonics - Sonochemistry*, 50, 82-95.

Azmin, S. N. H. M., Hayat, N. A. binti M., & Nor, M. S. M. (2020). Development and characterization of food packaging bioplastic film from cocoa pod husk cellulose incorporated with sugarcane bagasse fibre. *Journal of Bioresources and Bioproducts*, 5(4), 248-255. https://doi.org/10.1016/j.jobab.2020.10.003

Barana, D., Salanti, A., Orlandi, M., Ali, D. S., & Zoia, L. (2016). Biorefinery process for the simultaneous recovery of lignin, hemicelluloses, cellulose nanocrystals and silica from rice husk and Arundo donax. *Industrial Crops and Products*, 86, 31-39. https://doi.org/10.1016/j.indcrop.2016.03.029

Bochek, A. M. (2003). Effect of Hydrogen Bonding on Cellulose Solubility in Aqueous and Nonaqueous Solvents. *Russian Journal of Applied Chemistry*, 76(11), 1711-1719. https://doi.org/10.1023/B:RJAC.0000018669.88546.56

Boonterm, M. (2016). Characterization and comparison of cellulose fiber extraction from rice straw by chemical treatment and thermal steam explosion. *Journal of Cleaner Production*, 134, 592-599.

Budtova, T., & Navard, P. (2016). Cellulose in NaOH-water based solvents: A review. *Cellulose*, Springer Verlag, 2016, 23 (1), pp.5-55.

Casabar, J. T., Ramaraj, R., Tipnee, S., & Unpaprom, Y. (2020). Enhancement of hydrolysis with Trichoderma harzianum for bioethanol production of sonicated pineapple fruit peel. *Fuel*, 279, 118437. https://doi.org/10.1016/j.fuel.2020.118437

Cazón, P., Vázquez, M., & Velazquez, G. (2018). Novel composite films based on cellulose reinforced with chitosan and polyvinyl alcohol: Effect on mechanical properties and water vapour permeability. *Polymer Testing*, 69, 536-544. https://doi.org/10.1016/j.polymertesting.2018.06.016

Chemat, F., Rombaut, N., Sicaire, A., Meullemiestre, A., Fabiano-Tixier, A., Albert-Vian, M.(2017). Ultrasound assisted extraction of food and natural products. Mechanisms, techniques, combinations, protocols and applications. A review. *Ultrasonics Sonochemistry*, 540-560.

Chen, X.Yu, J., Lu, C. (2011). Study on structure and thermal stability properties of cellulose fibers from rice straw. *Carbohydrate Polymers*, 86, 245-250.

Cheung, Y.-C., & Wu, J.-Y. (2013). Kinetic models and process parameters for ultrasound-assisted extraction of water-soluble components and polysaccharides from a medicinal fungus. *Biochemical Engineering Journal*, 79, 214-220. https://doi.org/10.1016/j.bej.2013.08.009

Ching, Y. C., Rahman, A., Ching, K. Y., Sukiman, N. L., & Cheng, H. C. (2015). Preparation and Characterization of Polyvinyl Alcohol-Based Composite Reinforced with Nanocellulose and Nanosilica. *BioResources*, 10(2), 3364-3377. https://doi.org/10.15376/biores.10.2.3364-3377

Collazo-Bigliardi, S. (2018). Isolation and characterisation of microcrystalline cellulose and cellulose nanocrystals from coffee husk and comparative study with rice husk. *Carbohydrate Polymers*, 191, 205-215.

Collazo-Bigliardi, S., Ortega-Toro, R., & Chiralt, A. (2019). Improving properties of thermoplastic starch films by incorporating active extracts and cellulose fibres isolated from rice or coffee husk. *Food Packaging and Shelf Life*, 22, 100383. https://doi.org/10.1016/j.fpsl.2019.100383

Elhussieny, A. (2020). Valorisation of shrimp and rice straw waste into food packaging applications. *Ain Shams Engineering Journal*, 1-8.

El-Sakhawy, M., & Hassan, M. L. (2007). Physical and mechanical properties of microcrystalline cellulose prepared from agricultural residues. *Carbohydrate Polymers*, 1-10.

FAOSTAT. (2018). Recuperado 4 de noviembre de 2020, de http://www.fao.org/faostat/en/#data/QC/visualize

Faruk, O. (2012). Biocomposites reinforced with natural fibers: 2000–2010. *Progress in Polymer Science*, 45.

Freitas, P. A. V., González-Martínez, C., & Chiralt, A. (2020). Application of Ultrasound Pre-Treatment for Enhancing Extraction of Bioactive Compounds from Rice Straw. *Foods*, 9(11), 1657. https://doi.org/10.3390/foods9111657

Harini, K., & Chandra Mohan, C. (2020). Isolation and characterization of micro and nanocrystalline cellulose fibers from the walnut shell, corncob and sugarcane bagasse. *International Journal of Biological Macromolecules*, 163, 1375-1383. https://doi.org/10.1016/j.ijbiomac.2020.07.239

Hassan, M., Berglund, L., Abou-Zeid, R., Hassan, E., Abou-Elseoud, W., & Oksman, K. (2019). Nanocomposite Film Based on Cellulose Acetate and Lignin-Rich Rice Straw Nanofibers. *Materials*, 12(4), 595. https://doi.org/10.3390/ma12040595

Ilyas, R. A., Sapuan, S. M., Ibrahim, R., Abral, H., Ishak, M. R., Zainudin, E. S., Atikah, M. S. N., Mohd Nurazzi, N., Atiqah, A., Ansari, M. N. M., Syafri, E., Asrofi, M., Sari, N. H., & Jumaidin, R. (2019). Effect of sugar palm nanofibrillated cellulose concentrations on morphological, mechanical and physical properties of biodegradable films based on agro-waste sugar palm (Arenga pinnata (Wurmb.) Merr) starch. *Journal of Materials Research and Technology*, 8(5), 4819-4830. https://doi.org/10.1016/j.jmrt.2019.08.028

Jin, S., & Chen, H. (2006). Structural properties and enzymatic hydrolysis of rice straw. *Process Biochemistry*, 4.

Jones, D., Ormondroyd, G. O., Curling, S. F., Popescu, C.-M., & Popescu, M.-C. (2017). Chemical compositions of natural fibres. En Advanced High Strength Natural Fibre Composites in Construction (pp. 23-58). Elsevier. https://doi.org/10.1016/B978-0-08-100411-1.00002-9

Junior, M. G. (2018). Effect of the nano-fibrillation of bamboo pulp on the thermal, structural, mechanical and physical properties of nanocomposites based on starch/poly(vinyl alcohol) blend. *Cellulose*, 25, 1823-1849.

Kargarzadeh, H. (2017). Starch biocomposite film reinforced by multiscale rice husk fiber. *Composites Science and Technology*, 9.

Kassab, Z. (2020). Cellulosic materials from pea (Pisum Sativum) and broad beans (Vicia Faba) pods agro-industrial residues. *Materials Letters*, 4.

Kimura, T., Sakamoto, T., Leveque, J.-M., Sohmiya, H., Fujita, M., Ikeda, S., & Ando, T. (1996). Standardization of ultrasonic power for sonochemical reaction. *Ultrasonics Sonochemistry*, 3(3), S157-S161. https://doi.org/10.1016/S1350-4177(96)00021-1

Koda, S., Kimura, T., Kondo, T., & Mitome, H. (2003). A standard method to calibrate sonochemical efficiency of an individual reaction system. *Ultrasonics Sonochemistry*, 10(3), 149-156. https://doi.org/10.1016/S1350-4177(03)00084-1

Korotkova, E., Pranovich, A., Wärnå, J., Salmi, T., Murzin, D. Yu., & Willför, S. (2015). Lignin isolation from spruce wood with low concentration aqueous alkali at high temperature and pressure: Influence of hot-water pre-extraction. *Green Chemistry*, 17(11), 5058-5068. https://doi.org/10.1039/C5GC01341K

Littunen, K., Hippi, U., Saarinen, T., & Seppälä, J. (2013). Network formation of nanofibrillated cellulose in solution blended poly(methyl methacrylate) composites. *Carbohydrate Polymers*, 91(1), 183-190. https://doi.org/10.1016/j.carbpol.2012.08.032

Liu, Y., & Hu, H. (2009). X-ray Diffraction Study of Bamboo Fibers Treated with NaOH. *Fibers and Polymers*, 6, 735-739.

Machado, I. (2019). Characterization of the effects involved in ultrasound-assisted extraction of trace elements from artichoke leaves and soybean seeds. *Ultrasonics- Sonochemistry*, 59,104752.

Maqbool, M. (2011). Postharvest application of gum arabic and essential oils for controlling anthracnose and quality of banana and papaya during cold storage. *Postharvest Biology and Technology*, 62, 71-76.

Menzel, C., González-Martínez, C., Vilaplana, F., Diretto, G., & Chiralt, A. (2020). Incorporation of natural antioxidants from rice straw into renewable starch films. *International Journal of Biological Macromolecules*, 146, 976-986. https://doi.org/10.1016/j.ijbiomac.2019.09.222

Mohamad Haafiz, M. K., Eichhorn, S. J., Hassan, A., & Jawaid, M. (2013). Isolation and characterization of microcrystalline cellulose from oil palm biomass residue. *Carbohydrate Polymers*, 93(2), 628-634. https://doi.org/10.1016/j.carbpol.2013.01.035

Monteiro, S. N., Calado, V., Margem, F. M., & Rodriguez, R. J. S. (2012). Thermogravimetric Stability Behavior of Less Common Lignocellulosic Fibers—A Review. *Journal of Materials Research and Technology*, 1(3), 189-199. https://doi.org/10.1016/S2238-7854(12)70032-7

Moslemi, A. (2020). Addition of cellulose nanofibers extracted from rice straw to urea formaldehyde resin; effect on the adhesive characteristics and medium density fiberboard properties. *International Journal of Adhesion and Adhesives*, 6.

Nam, S., French, A. D., Condon, B. D., & Concha, M. (2016). Segal crystallinity index revisited by the simulation of X-ray diffraction patterns of cotton cellulose Iβ and cellulose II. *Carbohydrate Polymers*, 135, 1-9. https://doi.org/10.1016/j.carbpol.2015.08.035

Ng, H.-M., Sin, L. T., Tee, T.-T., Bee, S.-T., Hui, D., Low, C.-Y., & Rahmat, A. R. (2015a). Extraction of cellulose nanocrystals from plant sources for application as reinforcing agent in polymers. *Composites Part B: Engineering*, 75, 176-200. https://doi.org/10.1016/j.compositesb.2015.01.008

Nunes, M. R., de Souza Maguerroski Castilho, M., de Lima Veeck, A. P., da Rosa, C. G., Noronha, C. M., Maciel, M. V. O. B., & Barreto, P. M. (2018). Antioxidant and antimicrobial methylcellulose films containing Lippia alba extract and silver nanoparticles. *Carbohydrate Polymers*, 192, 37-43. https://doi.org/10.1016/j.carbpol.2018.03.014

Ojha, K. S. (2020). Ultrasound technology for the extraction of biologically active molecules from plant, animal and marine sources. *Trends in Analytical Chemistry*, 122, 1156633.

Pan, X., & Sano, Y. (2005). Fractionation of wheat straw by atmospheric acetic acid process. *Bioresource Technology*, 96(11), 1256-1263. https://doi.org/10.1016/j.biortech.2004.10.018

Peanparkdee, M., & Iwamoto, S. (2019). Bioactive compounds from by-products of rice cultivation and rice processing: Extraction and application in the food and pharmaceutical industries. *Trends in Food Science & Technology*, 86, 109-117. https://doi.org/10.1016/j.tifs.2019.02.041

Pickering, K. L., Efendy, M. G. A., & Le, T. M. (2016). A review of recent developments in natural fibre composites and their mechanical performance. *Composites Part A: Applied Science and Manufacturing*, 83, 98-112. https://doi.org/10.1016/j.compositesa.2015.08.038

Prakash, A., Vadivel, V., Banu, S. F., Nithyanand, P., Lalitha, C., & Brindha, P. (2018). Evaluation of antioxidant and antimicrobial properties of solvent extracts of agro-food by-products (cashew nut shell, coconut shell and groundnut hull). *Agriculture and Natural Resources*, 52(5), 451-459. https://doi.org/10.1016/j.anres.2018.10.018

Rasheed, M., Jawaid, M., Karim, Z., & Abdullah, L. C. (2020). Morphological, Physiochemical and Thermal Properties of Microcrystalline Cellulose (MCC) Extracted from Bamboo Fiber. Polymers, 13,465.

Requena, R., Jiménez-Quero, A., Vargas, M., Moriana, R., Chiralt, A., & Vilaplana, F. (2019). Integral Fractionation of Rice Husks into Bioactive Arabinoxylans, Cellulose Nanocrystals, and Silica Particles. *ACS Sustainable Chemistry & Engineering*, 7(6), 6275-6286. https://doi.org/10.1021/acssuschemeng.8b06692

Saha, S., & Ghosh, R. (2019). Cellulose Nanocrystals from lignocellulosic agro-waste: A comparative study on Conventional and Ultrasonic Assisted Preparation Methods. *Materials Today: Proceedings*, 11, 628-636. https://doi.org/10.1016/j.matpr.2019.03.020

Saini, J. K., Saini, R., & Tewari, L. (2015). Lignocellulosic agriculture wastes as biomass feedstocks for second-generation bioethanol production: Concepts and recent developments. *Biotech*, 5(4), 337-353. https://doi.org/10.1007/s13205-014-0246-5

Salam, A., Reddy, N., & Yang, Y. (2007). Bleaching of Kenaf and Cornhusk Fibers. *Industrial & Engineering Chemistry Research*, 46(5), 1452-1458. https://doi.org/10.1021/ie061371c

Sarkar, N., Ghosh, S. K., Bannerjee, S., & Aikat, K. (2012). Bioethanol production from agricultural wastes: An overview. *Renewable Energy*, 37(1), 19-27. https://doi.org/10.1016/j.renene.2011.06.045

Seo, D.-J., & Sakoda, A. (2014). Assessment of the structural factors controlling the enzymatic saccharification of rice straw cellulose. *Biomass and Bioenergy*, 71, 47-57. https://doi.org/10.1016/j.biombioe.2014.10.027

Sharma, B., Vaish, B., Monika, Singh, U. K., Singh, P., & Singh, R. P. (2019). Recycling of Organic Wastes in Agriculture: An Environmental Perspective. *International Journal of Environmental Research*, 13(2), 409-429. https://doi.org/10.1007/s41742-019-00175-y

Singh, R., Tiwari, S., Srivastava, M., & Shukla, A. (2014). Microwave Assisted Alkali Pretreatment of Rice Straw for Enhancing Enzymatic Digestibility. *Journal of Energy*, 2014, 1-7. https://doi.org/10.1155/2014/483813

Sluiter, A. (2008a). Determination of Extractives in Biomass: Laboratory Analytical Procedure (LAP); Issue Date 7/17/2005. *Technical Report*, 1-8.

Sluiter, A. (2008b). Determination of Structural Carbohydrates and Lignin in Biomass: Laboratory Analytical Procedure (LAP); Issue Date: April 2008; Revision Date: July 2011 (Version 07-08-2011). Technical Report, 18.

Sumere, B. R., de Souza, M. C., dos Santos, M. P., Bezerra, R. M. N., da Cunha, D. T., Martinez, J., & Rostagno, M. A. (2018). Combining pressurized liquids with ultrasound to improve the

extraction of phenolic compounds from pomegranate peel (Punica granatum L.). *Ultrasonics Sonochemistry*, 48, 151-162. https://doi.org/10.1016/j.ultsonch.2018.05.028

Takano, M., & Hoshino, K. (2018). Bioethanol production from rice straw by simultaneous saccharification and fermentation with statistical optimized cellulase cocktail and fermenting fungus. *Bioresources and Bioprocessing*, 5(1), 16. https://doi.org/10.1186/s40643-018-0203-y

Theng, D., Arbat, G., Delgado-Aguilar, M., Ngo, B., Labonne, L., Evon, P., & Mutjé, P. (2017). Comparison between two different pretreatment technologies of rice straw fibers prior to fiberboard manufacturing: Twin-screw extrusion and digestion plus defibration. *Industrial Crops and Products*, 107, 184-197. https://doi.org/10.1016/j.indcrop.2017.05.049

Wang, Z., Qiao, X., Sun, K. (2018). Rice straw cellulose nanofibrils reinforced poly(vinyl alcohol) composite films. *Carbohydrate Polymers*, 197, 442-450.

Wanyo, P., Meeso, N., & Siriamornpun, S. (2014). Effects of different treatments on the antioxidant properties and phenolic compounds of rice bran and rice husk. *Food Chemistry*, 157, 457-463. https://doi.org/10.1016/j.foodchem.2014.02.061

Wu, Q., Yao, F., Xu, X., Mei, C., & Zhou, D. (2013). Thermal degradation of rice straw fibers: Global kinetic modeling with isothermal thermogravimetric analysis. *Journal of Industrial and Engineering Chemistry*, 19(2), 670-676. https://doi.org/10.1016/j.jiec.2012.10.026

Xu, F., Liu, C. F., Geng, Z. C., Sun, J. X., Sun, R. C., Hei, B. H., Lin, L., Wu, S. B., & Je, J. (2006). Characterisation of degraded organosolv hemicelluloses from wheat straw. *Polymer Degradation and Stability*, 91(8), 1880-1886. https://doi.org/10.1016/j.polymdegradstab.2005.11.002

Xu, T., Gao, C., Feng, X., Yang, Y., Shen, X., & Tang, X. (2019). Structure, physical and antioxidant properties of chitosan-gum arabic edible films incorporated with cinnamon essential oil. *International Journal of Biological Macromolecules*, 7.

Xu, T., Gao, C., Yang, Y., Shen, X., Huang, M., Liu, S., & Tang, X. (2018). Retention and release properties of cinnamon essential oil in antimicrobial films based on chitosan and gum arabic. *Food Hydrocolloids*, 84, 84-92. https://doi.org/10.1016/j.foodhyd.2018.06.003

Xu, Y., Salmi, J., Kloser, E., Perrin, F., Grosse, S., Denault, J., Lau, P. (2013). Feasibility of nanocrystalline cellulose production by endoglucanase treatment of natural bast fibers. *Industrial Crops and Products*, 51, 381-384.

Yue, Y., Zhou, C., French, A. D., Xia, G., Han, G., Wang, Q., & Wu, Q. (2012). Comparative properties of cellulose nano-crystals from native and mercerized cotton fibers. *Cellulose*, 19(4), 1173-1187. https://doi.org/10.1007/s10570-012-9714-4

Zainuddin, S. Y. Z. (2013). Potential of using multiscale kenaf fibers as reinforcing filler in cassava starch-kenaf biocomposites. *Carbohydrate Polymers*, 92, 2299-2305.

Zhang, Z., Smith, C., & Li, W. (2014). Extraction and modification technology of arabinoxylans from cereal by-products: A critical review. *Food Research International*, 65, 423-436.

CHAPTER 1.III

Valorisation of rice straw into cellulose microfibres for the reinforcement of thermoplastic corn starch films

Pedro A. V. Freitas[1], Carla I. La Fuente Arias[2], Sergio Torres-Giner[1], Chelo González-Martínez[1], and Amparo Chiralt[1]

[1] Institute of Food Engineering for Development, Universitat Politècnica de València, 46022, Valencia, Spain

[2] Department of Agri-Food Industry, Food and Nutrition, Universidade de São Paulo, São Paulo, Brazil

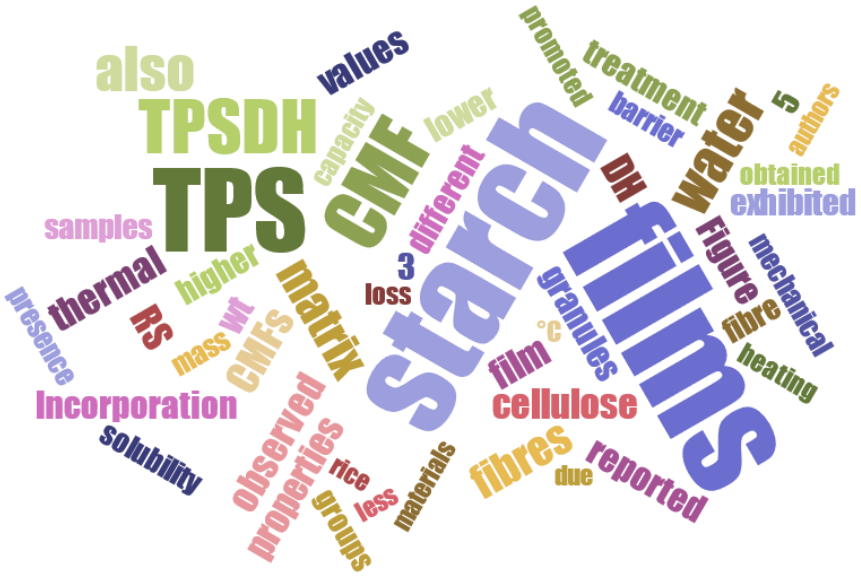

Applied Sciences (2021), 11, 8433

ABSTRACT

In the present study, agro-food waste derived rice straw (RS) was valorised into cellulose microfibres (CMFs) using a green process of combined ultrasound and heating treatments and were, thereafter, used to improve the physical properties of thermoplastic starch films (TPS). Mechanical defibrillation of the fibres gave rise to CMFs with cumulative frequencies of length and diameters below 200 and 5–15 µm, respectively. The resultant CMFs were successfully incorporated by melt mixing into TPS and also starch subjected to dry heating (DH) modification to yield TPS modified by dry heating (TPSDH) by thermo-compression and characterized. It was observed that both DH modification and fibre incorporation at 3 and 5 wt% loadings interfered with the starch gelatinization, leading to non-gelatinized starch granules in the biopolymer matrix. Thermo-compressed films prepared with both types of starches and reinforced with 3 wt % CMF were more rigid (per-centage increases of ~215% for TPS and ~207 % for the TPSDH), more resistant to break (~100 % for TPS and ~60 % for TPSDH), but also less extensible (~53 % for TPS and ~78 % for TPSDH). The incorporation of CMFs into the TPS matrix at both contents also promoted a decrease in water vapor (~15 %) and oxygen permeabilities (~30 %). Finally, the TPS composite films showed low changes in terms of optical properties and equilibrium moisture, being less soluble in water than the TPSDH films.

Keywords: waste valorisation, rice straw, thermoplastic starch, cellulose, thermal modification, microcomposites.

1. INTRODUCTION

Nowadays, the proper management of agro-industrial wastes is an essential socioeconomic and environmental issue. Most of these residues or by-products, generated in large quantities globally, are currently discarded or burned in the harvest fields [1]. In this sense, the use and valorisation of agro-industrial waste into added-value mate-rials are an emerging challenge that seeks to minimize environmental problems and promote the correct residue disposal. Agro-food and industrial waste derived biomass is essentially composed of lignocellulosic fractions, which are constituent biopolymers, such as cellulose, hemicellulose, and lignin [2,3]. Due to its renewability and biodegradability, the use of lignocellulosic-rich wastes can yield environmentally friendly materials through cost-effective processes with low environmental impact [4,5]. Several authors have reported the use of plant residues to obtain lignocellulosic fractions with potential application for biodiesel production [6], catalysts for biodiesel synthesis [7], antioxidant and antimicrobial materials [8,9] as well as reinforcing agents [10,11]. Particularly, cellulose and its derivatives extracted from biomass, such as cellulose microfibres (CMFs) and cellulose nanofibers, are highlighted renewable materials in the micro- and nanoscale, respectively, with low density, good compatibility, and excellent mechanical properties [12]. Thus, these lignocellulosic fractions can be used as rein-forcing fillers of biopolymers in green composites for food packaging applications.

After harvesting the rice grain (Oryza sativa L.), one of the most important primary crops, large quantities of rice straw (RS) are obtained worldwide. In fact, the annual rice production is estimated at 782 million tons and 1 kilogram of rice grain yields ap-proximately 1.5 kg of RS [13,14]. Generally, RS is directly burned in the paddies, which intensifies air pollution and damages soil feasibility and population health. Therefore, constant efforts are currently being made to propose different management approaches for this biomass waste [14,15]. Since RS is a lignocellulosic material that is composed of approximately 39 % cellulose, 20 % lignin, 23 % hemicellulose, and 15 % ashes, this waste derived biomass can be used to obtain several renewable added-value materials with interesting properties [16]. Among the most practical alternatives, RS can be valorised into CMF by different extraction methods. Typically, CMF from RS has a strong crystalline structure and low density, which can be used as reinforcing agent in biodegradable polymers instead to petroleum derived plastics [2,17].

Starch is a semicrystalline biopolymer consisting of linear and branched chains of □-D-glucopyranose units known as amylose and amylopectin, respectively [18]. The proportion of both constituents varies according to the source, from which the most common are cassava, maize, sweet potato, rice, oats, and peas [19,20]. Starch is widely investigated for several applications due to its renewability, biodegradability, low cost, availability, and biocompatibility [21–23]. In its native state, starch can be processed with a plasticizer in an extruder at temperatures between 140 and 160 °C and high pressure, giving rise to an

amorphous material with thermoplastic behaviour [21]. Although thermoplastic starch (TPS) films are excellent barriers to lipids, oxygen, and carbon dioxide, their use in food packaging is still limited since the barrier and mechanical properties are highly dependent on moisture content [18,24,25]. To overcome these shortcomings, the preparation of biodegradable TPS films reinforced with CMF obtained from agro-industrial wastes is an interesting alternative. Previous studies have reported that the incorporation of cellulosic materials in TPS-based green compo-site films exhibited enhanced mechanical properties [20,26], water vapor [27] and oxy-gen gas barrier [22], and thermal stability [28]. These recent advances indicate the significance and potential of green composites from starch and cellulose micro- and nanofibrils in the development of sustainable and cost-effective materials for food packaging [26,29] and other uses [30], from semistructural applications to biofoams or rein-forcing adhesives. Likewise, another strategy to modify and/or improve the properties of TPS films is pre-treating the starch in its native state by the dry heating (DH) meth-od. The so-called DH modification is a green physical pre-treatment that involves dry heating of native starch at temperatures between 110 and 150 °C for 1 to 4 h [31,32]. This method is very promising due to it is simple, fast, does not produce effluents, and can modify the original physicochemical properties of native starch to produce mate-rials with improved properties [32–34].

Thus, the objective of this work was to study the morphogeometric characteristics of CMF obtained from waste derived RS, before and after fibre grinding, and its subsequent incorporation by melt mixing into TPS. Prior to melt mixing, native starch was also subjected to DH modification to yield thermoplastic dried heated corn starch (TPSDH). The resultant doughs of TPS and TPSDH filled with CMFs were, thereafter, shaped into films by thermo-compression and characterized in terms of their morpho-logical characteristics, barrier properties, water solubility, water uptake, thermal behaviour, and mechanical performance to evaluate their potential application in food packaging.

2. MATERIAL AND METHODS

2.1 Materials

RS was obtained as waste of the rice industry that was collected in L'Albufera field (Valencia, Spain). It was supplied by the "Banco de Paja" (Valencia, Spain). The as-received fibres were dried under vacuum (50 ± 2 °C, 0.5 mmbar) for 16 h and milled (3 cycles of 90 s each, IKA, model M20, Germany), and sieved to < 0.5 mm particle size.

Corn starch was supplied by Roquette (Roquette Laisa, Benifaió, Spain). Glycerol, magnesium nitrate ($Mg(NO_3)_2$), phosphorus pentoxide (P_2O_5), dimethyl sulfoxide (DMSO), methanol, and acetic acid were all obtained from Panreac Quimica S.L.U. (Castellar del Vallés, Barcelona, Spain). Sodium acetate trihydrate was purchased by Fluka™ (Germany). Sodium chlorite and heptane were provided by Sigma-Aldrich S.A. (Madrid, Spain).

2.2 Extraction of cellulose microfibre

A combination of ultrasound and heating treatments are known lead to a certain degree of leaching out of hemicellulose and lignin present into the lignocellulosic RS matrix [8]. Based on this, CMF were extracted according to our previous methodology [35]. Briefly, an aqueous dispersion of RS particles with 5 % (w/v) solids was sonicated for 30 min at 25 °C (maintaining the temperature in an ice bath) using an ultrasonic homogenizer (750 W power, 20 kHz frequency, continuous mode) equipped with a high-intensity probe (Vibra CellTM VCX750, Sonics & Material, USA). After sonication, the RS dispersion was heated in a reflux heating apparatus at 100 °C for 1 h. Then, the plant dispersion was filtered using a qualitative filter (Filter Lab, Vidra Foc, Barcelona, Spain) and the solid fraction was dried at 40 °C for 48 h. Afterwards, the bleaching step of the cellulosic material was carried out by mixing the dry powder residue and the bleaching solution at 5 % (w/v). The bleaching solution consisted of equal parts of sodium hypochlorite solution (1.7 %, w/v), acetate buffer solution (2 N), and distilled water. The dispersion was treated under reflux heating for 4 cycles of 4 h each. The supernatant was filtered, and the residue was washed with distilled water several times to remove the residual bleach solution at each stage. Then, the bleached solid fraction was dried at 35 °C for 48 h and milled using a milling machine (pulses of 2 s for 20 min, model M20, IKA Werke GmbH & Co. KG, Staufen, Germany) to obtain the so-called CMF.

2.3 Dry Heating Treatment

Prior to melt mixing, corn starch was submitted to a DH pre-treatment, according to Maniglia et al. [33]. To this end, 50 g of starch were spread (1 mm thick layer) and compacted in an aluminium foil envelope. Then, the packaged sample was heated in a hot air oven (J.P. Selecta, S.A., Barcelona, Spain) at 130 °C for 4 h. Thereafter, the resultant starch was placed in a dark bottle and stored in a desiccator containing P_2O_5 at 6 ± 2 °C until further use.

2.4 Film Preparation

TPS and TPSDH films were prepared by melt blending and subsequent compression moulding using glycerol as plasticizer 30 wt % with respect to the total starch mass. Green composites were obtained by addition of CMF in concentrations of 1, 3, and 5 % wt. in relation to the starch content based on the optimization performed in our previous study [36]. Table 1 summarizes the different sample compositions used to produce the films. The film components were previously dry mixed in a beaker and then the melt-blended using an internal mini-mixer (HAAKETM PolyLabTM QC, Thermo Fisher Scientific, Karlsruhe, Germany) at 130 °C and 50 rpm for 10 min. The obtained dough was cold milled in the IKA's model and pre-conditioned at 25 °C and 53 % RH using an $Mg(NO_3)_2$ over-saturated solution for one week.

The obtained doughs were compression moulded in a hydraulic press (Model LP20, Labtech Engineering, Samut Prakan, Thailand). To this end, approximately 4 g of each dough was placed between two Teflon sheets and compressed in the hot plates. Control films (TPS) and those incorporating 1 (TPS1), 3 (TPS3), and 5 % wt. (TPS5) of CMF were preheated for 3 min at 160 °C in the plate press, then compressed at 160 °C for 2 min at 50 bars, followed by a second compression at 160 °C for 4 min at 130 bars, and finally cooled down to 80 °C. The processing conditions of the films obtained using modified DH starch with CMF (1 % wt.: TPSDH1, 3 % wt.: TPSDH3, and 5 % wt.: TPSDH5) or without CMF (TPSDH) were set as follows: preheating at 150 °C by 5 min, compression at 30 bars and 150 °C for 2 min, followed by 130 bars for 6 min, and then final cooling to 80 °C. All films were conditioned at 25 °C and 53 % RH ($Mg(NO_3)_2$) for one week before characterisations.

Table 1. Summary of compositions according to the mass fraction (g/g) of thermoplastic corn starch (TPS), thermoplastic dried heated corn starch (TPSDH), glycerol (Gly), and cellulose microfiber (CMF).

Sample	X_s	X_{Gly}	X_{CMF}
TPS	0.770	0.230	-
TPS1	0.763	0.229	0.008
TPS3	0.753	0.225	0.022
TPS5	0.741	0.222	0.037
TPSDH	0.770	0.230	-
TPSDH1	0.763	0.229	0.008
TPSDH3	0.753	0.225	0.022
TPSDH5	0.741	0.222	0.037

2.5 Material Characterization

2.5.1 Microscopy

An optical microscope (Optika Microscope B-350, OPTIKA S.r.l., Ponteranica, Italy) equipped with a camera (Optikam B2) was used to evaluate the morphology of the untreated RS and the resultant CMF samples before and after the milling process. To this end, the samples were extended with a water drop on the holder glass plate and the images were taken at 10x and 40x magnification. Morphogeometric properties of CMF, expressed as cumulative distributions, were obtained by measuring the particle length (*l*) in different regions of the sample, as shown in the imaging procedure of Figure 1. The Optika Vision Lite program was used to obtain a minimum of 60 measurements.

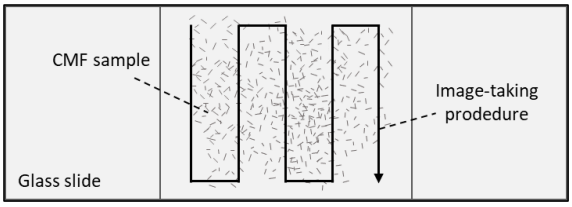

Figure 1. Image acquisition procedure to obtain the lengths of the cellulose microfibers (CMFs).

The morphologies of RS, CMF, and the cross-sections of the cryo-fractured films obtained by immersion in liquid nitrogen were evaluated using a Field Emission Scanning Electron Microscope (FESEM) equipped with focused ion gun (AURIGA Compact, Zeiss, Oxford Instruments). The conditioned samples (P_2O_5 at 25 ± 2 °C for 1 week) were covered with a platinum layer (EM MED020 sputter coater, Leica Biosystems, Barcelona, Spain), and the images were taken at 2.0 kV acceleration voltage. The SmartTiff program (version 2, Zeiss, Oxford Instruments, Abingdon, UK) was used to measuring the particle width (*w*) a minimum of 60 times.

2.5.2 Optical Evaluation

Optical properties of the films were obtained according to the Kubelka-Munk theory of multiple scattering to determine the film reflection spectra (*R*) using the black (R_0) and white (R_g) backgrounds. The internal transmittance (T_i) of the films ranging from 400 to 700 nm, the film colour coordinates *L** (lightness), *a** (redness-greenness), and *b** (yellowness-blueness) were determined using the Equations 1, 2, and 3, respectively. The colorimetric and transparency properties of the films were also evaluated in terms of hue angle (h_{ab}*) (Equation 4), chroma (C_{ab}*) (Equation 5), opacity (*O*) (Equation 6), and total colour difference (*ΔE**) (Equation 7). The measurements were performed in triplicate.

$$T_i = \sqrt{(a - R_0)^2 - b^2} \quad (1)$$

$$a = \frac{1}{2}\left[R + \left(\frac{R_0 - R + R_g}{R_0 \times R_g}\right)\right] \quad (2)$$

$$b = \sqrt{a^2 - 1} \quad (3)$$

$$h_{ab}{}^* = arctg\left(\frac{b^*}{a^*}\right) \quad (4)$$

$$C_{ab}{}^* = \sqrt{a^{*2} + b^{*2}} \quad (5)$$

$$O = A_{500} x\, l \quad (6)$$

In which A_{500}, and l are the absorbance at 500 nm, and the film thickness, respectively.

$$\Delta E^* = \sqrt{(\Delta L^*)^2 + (\Delta a^*)^2 + (\Delta b^*)^2} \quad (7)$$

Where $\Delta L^* = (L^* - L_0^*)$; $\Delta a^* = (a^* - a_0^*)$; $\Delta b^* = (b^* - b_0^*)$; and L_0^*, a_0^*, and b_0^* are the color coordinates of the control TPS film without fibres. The colour differences were evaluated according to the following criteria [37]: $\Delta E^* < 1$ indicate unnoticeable colour change; $1 \leq \Delta E^* \leq 2$ suggests that only an experienced observer can notice the difference; $2 \leq \Delta E^* \leq 3.5$ means that an inexperienced observer notices the difference; $3.5 \leq \Delta E^* \leq 5$ indicate clear noticeable difference; and $\Delta E^* \geq 5$ suggests that the observer notices different colours.

2.5.3 Equilibrium Moisture Content

The equilibrium moisture content of the films was determined by a gravimetric method. For this, film samples sizing 3 cm x 3 cm that were previously conditioned (25 °C and 53 % RH for two weeks) were dried at 60 °C for 24 h using a drying oven. Thereafter, the dried samples were placed in a dissector containing P_2O_5 at 25 °C for two weeks to eliminate bonded water. Moisture content was determined from the total mass loss of the conditioned film during the drying process. The measurements were carried out in triplicate.

2.5.4 Water Solubility

Water solubility was determined based on Talón et al. [38] methodology. A known mass of dry film sample (2 cm x 2 cm), conditioned in P_2O_5, were placed on a mesh, and immersed in a crucible with distilled water at 25 °C for 24 h. Afterward, the sample containing system was dried in an oven (J.P. Selecta, S.A.) at 60 °C for 48 h and, afterwards, conditioned in a desiccator with P_2O_5 at 25 °C for 1 week. The mass of residual film was weighed and compared with the initial mass of dry film. The measurements were carried out in triplicate and the results were expressed as g of solubilized film.100 g^{-1} film.

2.5.5 Barrier Measurements

Water vapor permeability (WVP) of the films was determined according to ASTM E96/E96M (ASTM, 2005) gravimetric methodology following the modifications proposed by McHUGH [35]. Film samples (Ø = 3.5 cm) were placed and sealed in Payne permeability cups filled with 5 mL of distilled water (100 % RH). Then, the cups were placed into desiccators containing $Mg(NO_3)_2$ over-saturated solution (53 % RH) and weighed periodically (ME36S, Sartorius, ± 0.00001 g, Fisher Scientific, Hampton, NH, USA) every 1.5 h for 25 h. For each treatment, the WVP was calculated considering the water vapor transmission rate (WVTR), which was determined from the slope of the weight loss *vs.* time. The measurements were performed in triplicate.

Oxygen permeability (OP) of the films was determined using an Ox-Tran equipment (Model 1/50, Mocon, Minneapolis, MN, USA) at 25 °C and 53 % of RH, according to ASTM D3985-05 (ASTM, 2010). The used area of films was 50 cm^2 and the oxygen transmission rate (OTR) was obtained every 15 min until equilibrium was reached. The measurements were carried out in triplicate.

2.5.6 Mechanical Characterization

The tensile properties of the films were obtained according to ASTM D882 (ASTM, 2012). A universal testing machine (Stable Micro Systems, TA.XT plus, Stable Micro Systems, Godalming, UK) was used to determine elongation at break (EB), tensile strength at break (TS), and elastic modulus (EM). Film samples with dimensions of 25 mm x 10 mm were grabbed by two grips initially separated by 50 mm and stretched at a crosshead speed of 50 $mm.min^{-1}$. Eight samples were evaluated for each formulation. Before the analysis, the films were conditioned at 53 % RH ($Mg(NO_3)_2$) and 25 °C for two weeks.

2.5.7 Thermal Analysis

The thermal stability of the films was determined by thermogravimetric analysis (TGA) using a thermogravimetric analyser (TGA 1 Star^e System analyser, Mettler-Toledo GmbH, Greifensee, Switzerland). Film samples, with a weight of 3–5 mg, were heated from 25 to 600 °C at a heating rate of 20 $°C.min^{-1}$ under nitrogen atmosphere (10 $mL.min^{-1}$). For each thermal event, the initial (T_{onset}) and final (T_{final}) degradation temperatures, temperature of maximum degradation rate (T_{peak}), and the residual mass were determined by analysing the TGA curves and their first derivative thermogravimetry (DTG) curves. The measurements were carried out in triplicate.

The phase transitions of the samples were investigated by differential scanning calorimeter (DSC) according to the method described by Collazo-Bigliardi et al. [40] with a DSC 1 Star^e System analyser (Mettler-Toledo GmbH) operating under a nitrogen atmosphere (10 $mL.min^{-1}$). Samples of about 5–6 mg were weighted in aluminium pans and heated from 25 to 160 °C, cooled to 25 °C, and then heated (second heating step) to 160 °C at 10 $°C.min^{-1}$ using, in all cases, rates of 10 $°C.min^{-1}$.

2.6 Statistical Analysis

The experimental data were submitted to multifactorial analysis of variance (ANOVA) at a confidence level of 95 % using Minitab Statistical Program (version 17). Tukey's studentized range (HSD) test, considering the least significant difference of 5 %, was applied to determine the influence of CMF on the properties of the starch-based films.

3. RESULTS AND DISCUSSION

3.1 Morphological characterization of CMFs

Figure 2 shows the FESEM micrographs of the untreated ground RS, the lignocellulosic residue after the combined ultrasound-heating treatment, the bleached cellulose fibres, and the resultant CMF obtained after the milling step.

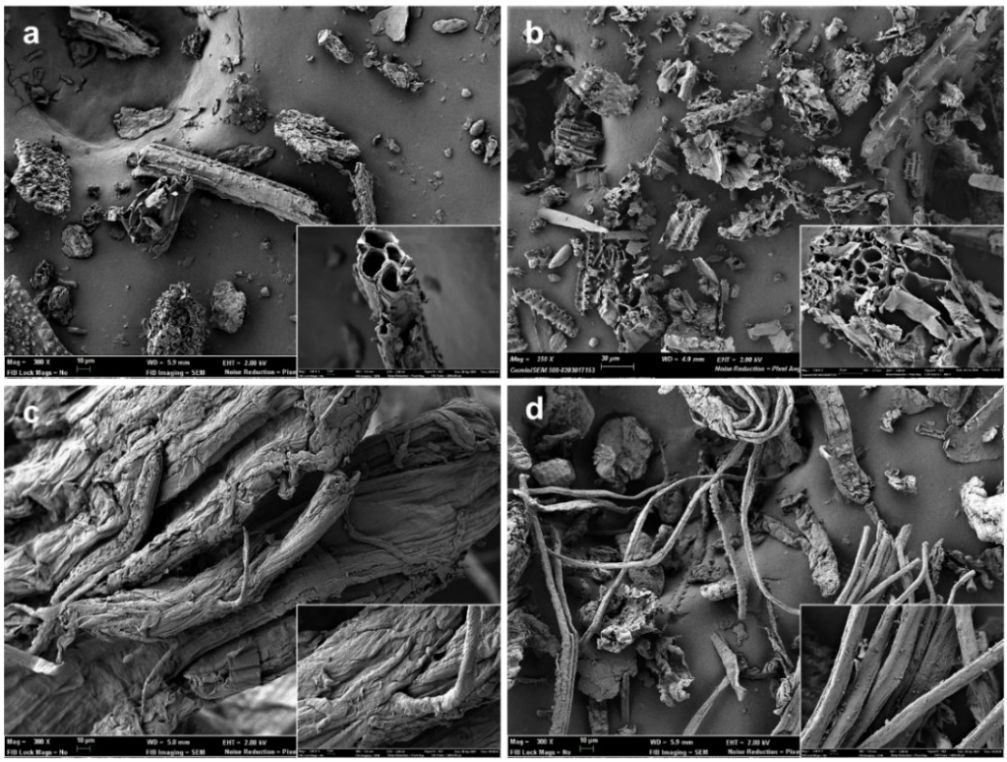

Figure 2. Field emission scanning electron microscope (FESEM) micrographs of untreated rice straw (RS) (a), RS treated with combined ultrasound-heating method (b), bleached cellulose microfibers (CMFs) before (c) and after (d) the milling step. Images were taken at 300x with insets at 2000x.

It can be observed that the untreated RS (Figure 2a) presented heterogeneous particle sizes, with a predominance of rod-like shape, as seen in the magnified FESEM image. The RS particles showed mean sizes of width and length in the 20–60 µm and 16–270 µm ranges, respectively. Prior to the RS fibre extraction, the grinding step was applied to improve the effectiveness of the combined ultrasound-heating method and the bleaching treatment. According to Chen et al. [2], RS has a strong crystalline structure, making the extraction and purification of cellulose fibres difficult. Likewise, RS presents a high proportion of non-fibrous cells, such as parenchyma, epidermis, and vessel cells [41]. The traditional alkaline pre-treatment, which aims to eliminate hemicellulose and lignin [42], was replaced by a more environmentally friendly aqueous treatment based on the application of ultrasounds, followed by reflux

heating. Figure 2b reveals that the application of ultrasound and heating promoted a certain degree of fibrillar plane de-bonding and distorted the RS particles, as previously reported [8]. The acoustic cavitation produced by the ultrasound waves, combined with the thermal erosion generated by reflux heating, promoted the disruption of the primary structure of RS and improved the leaching out of non-cellulosic components from the cellulosic matrix [43–45].

As shown in Figure 2c, the bleached cellulose fibres exhibited a swollen, rough, and unregular appearance. The removal of non-fibrous components from the lignocellulosic matrix, such as hemicellulose, lignin, and waxes, gave rise to an entangled material, as observed by other authors [46]. The lignocellulosic matrix comprises cellulose fibrils organized in fibres arranged in a longitudinal orientation and inserted in a cementing matrix consisted of hemicellulose and lignin [2]. Thus, after removing the amorphous components, the hydroxyl (–OH) groups of cellulose could establish extensive hydrogen (–H) bonds among their chains, leading to a more compact and disordered arrangement [47]. This phenomenon can be observed in Figure 2c in the FESEM image taken at higher magnification. Thereafter, the cellulose fibres were ground to break up the agglomerates and obtain thinner CMFs (Figure 2d). Image analysis using both optical microscopy and FESEM techniques served to determine the cumulative distributions of CMF lengths and widths, respectively shown in Figure 3. Therefore, the mechanical defibrillation of the cellulose fibre bundles was evident, which was considered to occur by detaching CMFs into long fibrils with a major cumulative frequency of lengths below 200 µm (Figure 3a). Likewise, there was a marked reduction in the CMF thickness, showing predominant values between 5-15 µm.

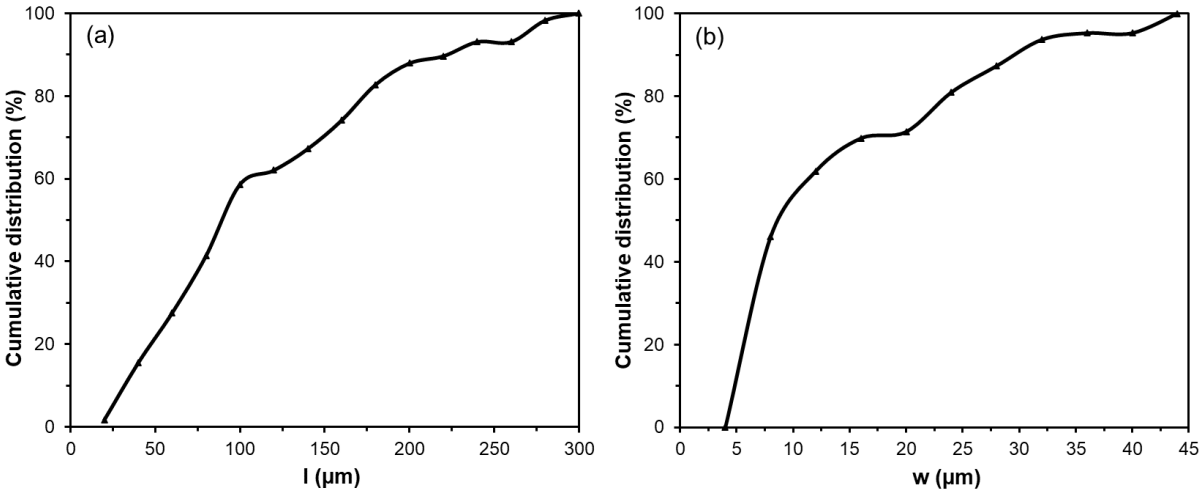

Figure 3. Cumulative distributions of cellulose microfiber (CMF) length (*l*) (a) and width (*w*) (b) obtained from image analyses of optical microscopy and field emission scanning electron microscopy (FESEM), respectively. A minimum of 60 measurements for each parameter was performed.

The magnified image of the ground material, shown in Figure 2d, revealed that CMF was isolated with a smooth surface pattern, confirming that the milling step was an efficient method to disrupt the tangled microfiber arrangement. In this regard, Jiang et al. [48] observed that mechanical defibrillation was effective at detaching cellulose fibrils from RS treated with the 2,2,6,6-tetramethylpiperidine-1-oxyl (TEMPO)-mediated oxidation method. The authors reported less uniform defibrillated particles, as also detected herein in Figure 2d. In this sense, the micrographs suggested that, due to the detachment of the fibre bundles into CMFs, the cellulosic material obtained could promote an efficient force transferring from the microfibers to polymer matrices, such as TPS [49].

3.2 Microstructure of the films

Figure 4 shows the FESEM micrographs of the cross-sections of the TPS-based films incorporating different CMF concentrations (1, 3, and 5 % wt.) obtained by cryo-fracture and their corresponding samples using DH-modified starch, that is, TPSDH. The TPS control film samples revealed a smooth and homogeneous cross-section surface pattern, indicating a good starch thermoplasticization, as also reported by other authors for starch films obtained in similar conditions [50,51]. In contrast, the TPSDH films exhibited remaining starch granules, which suggests changes in the starch thermoplasticization behaviour after the DH treatment. In this context, Chandanasree et al. [31] reported that the treatment of native starch by DH provokes partial damages in the semi-crystalline and crystalline regions of the granules, which prevents the granule swelling and delays its gelatinization. Furthermore, the DH treatment can oxidize and convert the –OH groups present in the starch chains to carbonyl (C=O) and carboxyl (–COOH) groups, which alters the gelatinization profile [52]. A progressive increase in the number of non-gelatinized starch granules was also observed in the cross-sections of the films of non-modified starch when the CMF concentration increased. However, this number increased in the samples prepared with DH-modified starch.

The starch thermoplasticisation occurs during heating, in the extruder or melt-mixing equipment, in the presence of a plasticizer, such as glycerol, at high temperatures (130 ℃) and pressures [21]. The microstructural features of the microcomposite films revealed that the CMF incorporation interfered the starch gelatinization with glycerol. This could be explained by the competitive interaction of the plasticizer with both CMF and starch through –H intermolecular bonds with the cellulose chains, decreasing their availability and subsequently provoking gelatinization of the granular structure of starch. This effect was mainly observed in the TPSDH samples, where the thermal treatment involved changes in its granular structure that already limits its gelatinization.

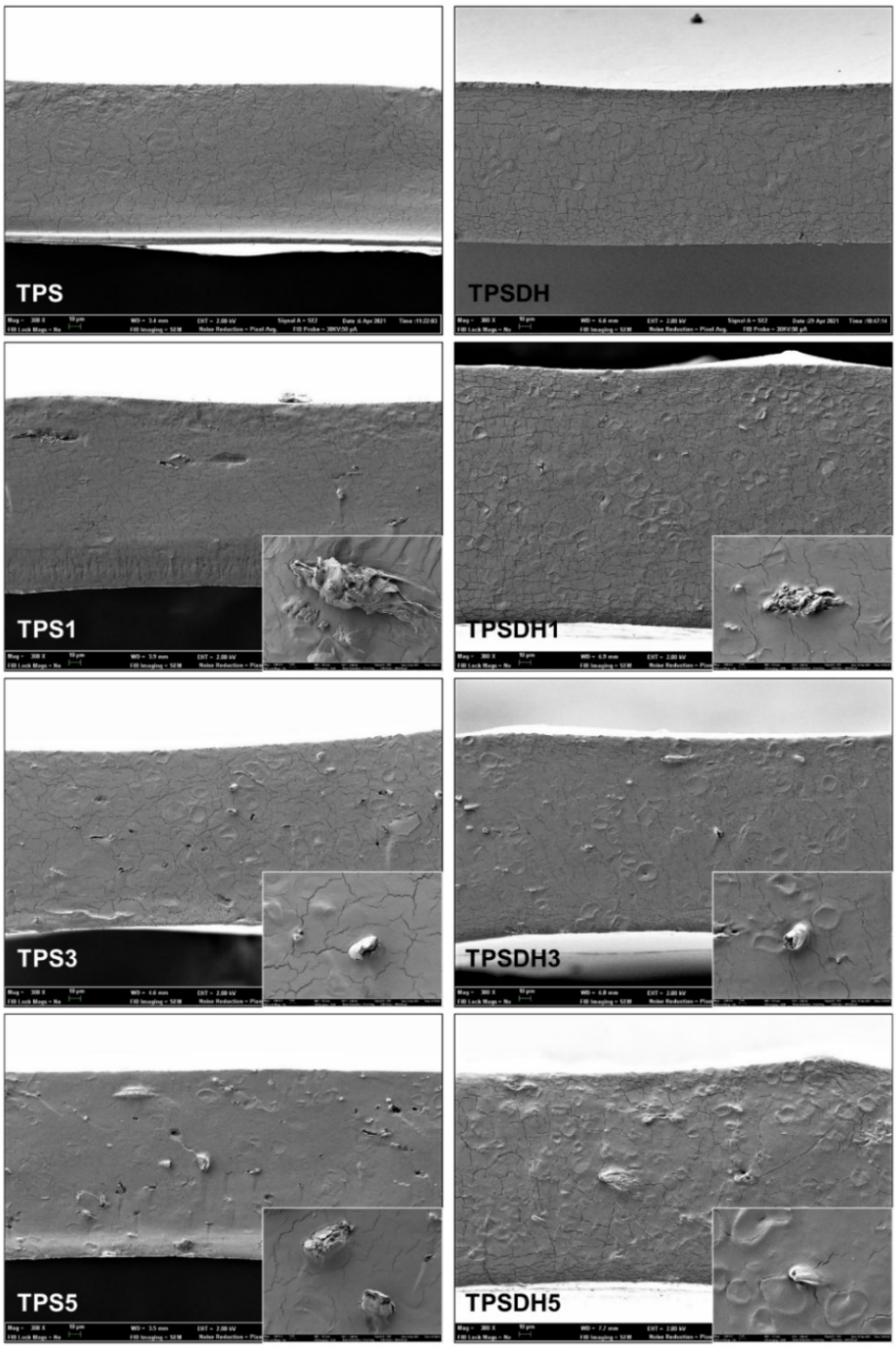

Figure 4. Field emission scanning electron microscope (FESEM) micrographs of the fracture surfaces of thermoplastic starch (TPS) and TPS modified by dry heating (TPSDH) films with contents of cellulose microfibers (CMFs) of 1 % wt. (TPS1, TPSDH1), 3 % wt. (TPS3, TPSDH3), and 5 % wt. (TPS5, TPSDH5). Images were taken at 300x with insets at 2000x.

Figure 4, which shows the fracture surfaces of film samples, revealed that the CMF incorporated into the films exhibited good compatibility with both types of TPS matrices, that is, non-modified and DH-modified starch This observation can be deduced from the good interfacial adhesion observed between the fibres and starch matrix due to the absence of gap between the fibre surface and the TPS matrix. Nevertheless, the film cryo-fracture does not seem to promote the breakage of the fibres, but their separation from the matrix, resulting in hollows that arise from the outgoing fibre during the fracture of the film samples. Similar findings were observed by Collazo-Bigliardi et al. [40] and Kargarzadeh et al. [28] in TPS films reinforced with CMFs from rice husk. The apparently good interfacial adhesion properties of fibres in the starch matrices could derive from the obtaining process of CMFs, without alkaline pre-treatment, which promoted the presence of exposed –OH groups on the surface of the fibres [53], thus enhancing the –H bond interactions with the –OH groups of starch.

3.3 Optical properties: colour and transparency

Film colour and transparency are not only important factors in food packaging designs, but also very useful for evaluating the filler-polymer matrix compatibility. Table 2 summarizes the colour coordinates in terms of L^*, C_{ab}^*, and h_{ab}^* as well as the total colour difference (ΔE^*) with respect to the neat TPS films without DH treatment and CMFs and the opacity coefficient of the different films. Likewise, the T_i spectra of the different films are shown in Figure 5. Both the CMF incorporation and starch DH modification significantly (p<0.05) affected the evaluated optical properties. Comparison of TPS and TPSDH films without fibres permits to elucidate that DH gave rise to slightly darker films with more saturated, that is, higher C_{ab}^* values, and a yellower colour, which suggest that Maillard or sugar caramelization reactions could occur during thermal treatment of native starch. Likewise, as the CMF concentration increased, both TPS and TPSDH films exhibited a slight decrease in their lightness (L^*) while colour saturation (C_{ab}^*) increased and hue tended to be more yellowish. This was reflected on the ΔE^* values, in which the colour coordinates L^*, a^*, and b^* of the TPS control film were used as a reference. In the TPS films without DH treatment, the ΔE^* values attained after the incorporation of low contents of CMF were below 1 indicating unnoticeable colour changes, whereas only in the microcomposite with 5 % wt. CMFs, that is, TPS5, an unexperienced observer can already observe colour differences ($2 \leq \Delta E^* \leq 3.5$). In the TPSDH films, as opposite, the combined effect of dispersed phases, that is, CMF and non-gelatinized starch granules, and coloured compounds formed during thermal modification of starch [31,54], gave rise to higher colour variations with respect to the neat TPS films. Thus, the TPSDH and its microcomposite with the lowest CMF content showed clear noticeable differences ($3.5 \leq \Delta E^* \leq 5$), whereas the samples with higher fibre contents yielded films with a noticeable different colour ($\Delta E^* \geq 5$).

Table 2. Optical properties in terms of lightness (L^*), chroma (C_{ab}^*), hue angle (h_{ab}^*), colour difference (ΔE*), and opacity (O) of thermoplastic starch (TPS) and TPS modified by dry heating (TPSDH) films with different contents of cellulose microfibers (CMFs).

Formulation	L^*	C_{ab}^*	h_{ab}^*	ΔE^*	O
TPS	88.5 ± 0.1^{a,1}	7.6 ± 0.1^{f}	92.6 ± 0.1^{a}	-	0.141 ± 0.001^{b}
TPS1	88.5 ± 0.1^{a,3}	7.5 ± 0.2^{f}	92.8 ± 0.1^{a}	0.07 ± 0.01e	0.146 ± 0.009^{b}
TPS3	88.1 ± 0.2^{b,5}	8.2 ± 0.3^{e}	92.6 ± 0.2^{a}	0.70 ± 0.02e	0.151 ± 0.005^{ab}
TPS5	87.6 ± 0.2^{c,7}	9.4 ± 0.3^{d}	91.5 ± 0.2^{b}	2.03 ± 0.01d	0.140 ± 0.005^{b}
TPSDH	86.0 ± 0.1^{d,2}	11.9 ± 0.5^{c}	89.2 ± 0.2^{cd}	4.76 ± 0.05^{c}	0.163 ± 0.001^{ab}
TPSDH1	86.2 ± 0.2^{d,4}	11.3 ± 0.2^{c}	89.5 ± 0.3^{c}	4.64 ± 0.10^{c}	0.163 ± 0.006^{ab}
TPSDH3	85.4 ± 0.1^{e,6}	12.4 ± 0.2^{b}	88.9 ± 0.1^{d}	6.24 ± 0.01^{b}	0.171 ± 0.007^{a}
TPSDH5	84.5 ± 0.1^{f,8}	14.2 ± 0.2^{a}	88.8 ± 01^{d}	7.88 ± 0.15^{a}	0.156 ± 0.007^{ab}

Different subscript letters indicate significant differences between samples of the same group (TPS or TPSDH films). Different numbers indicated significant differences between TPS and TPSDH samples with the same ratio of CMF (Tukey test, $p<0.05$).

The T_i spectra of the films within the wavelength range of 400–700 nm shown in Figure 5 revealed that the TPSDH films without CMF exhibited lower transparency that the TPS films, with lower values of T_i, mainly at the lowest wavelength. This can be explained by the presence of coloured compounds, formed during the starch DH modification process and the presence of dispersed starch granules in the films, which were non-completely gelatinized. These dispersed particles, having refractive indexes different from that of the starch continuous phase, promoted light scattering and film opacity. In both kind of films, a slight and progressive decrease in light transmission was observed as the CMF concentration increased. This result agrees with the observations reported by other authors for CMF-containing TPS samples [36,55,56], where the filler incorporation as dispersed phase also caused changes in the refractive index of the polymer matrix, promoting light scattering and opacity in the films. Therefore, opacity increased due to the presence of CMFs and the non-gelatinized starch granules. In particular, the opacity parameter, also included in Table 2, increased from 0.141 for the neat TPS film up to 0.171 for the TPSDH3 film.

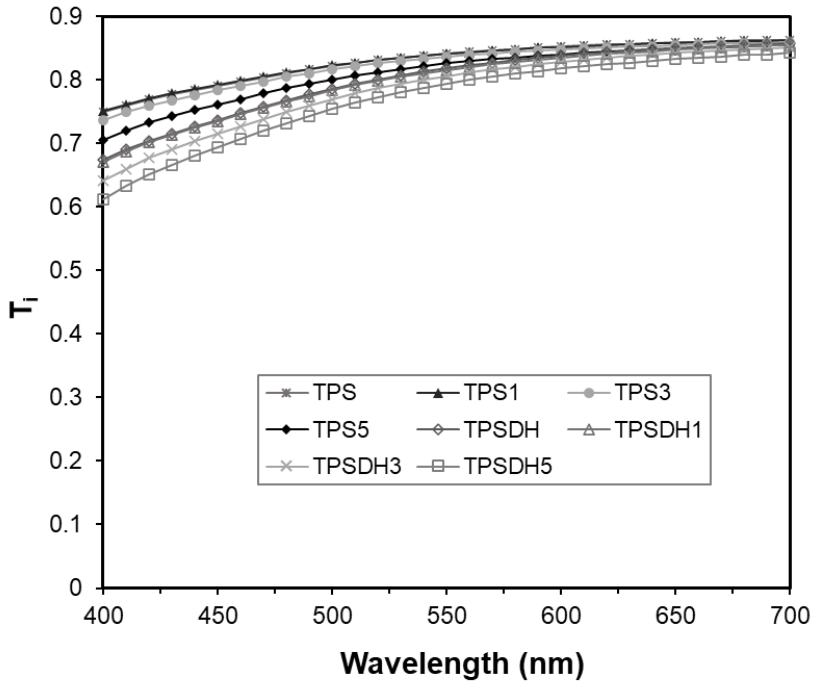

Figure 5. Internal transmittance (T_i) of thermoplastic starch (TPS) and TPS modified by dry heating (TPSDH) films with different contents of cellulose microfibers (CMFs).

3.4 Equilibrium moisture content and water solubility

Table 3 shows the equilibrium moisture content and water solubility of the different films prepared with TPS and TPSDH. One can observe that the DH treatment of starch slightly promoted water sorption capacity and water solubility of the films. In this sense, Lim et al. [57] reported that DH treatment of starch can damage its granular structure, which culminates in the exposure of its –OH groups, promoting the ability to interact with water molecules and water sorption capacity. Oh et al. [32] also reported an increase in water solubility of rice starch modified with the DH treatment. Furthermore, the CMF incorporation slightly decreased the water sorption capacity of both TPS and TPSDH films, whereas it provided different effects on water solubility for each kind of starch film, reducing solubility for the TPS films but increasing it in the case of the TPSDH films. The small changes in the water sorption capacity provoked by CMF can be explained in terms of the lower water affinity of the fibres in comparison with TPS [58], reflected on their low equilibrium water content (3 %) at 53 % RH [35]. In fact, the resulting water content of the microcomposites could be deduced from the mass balance considering the equilibrium water content of both starch matrix and fibres.

Table 3. Moisture, water solubility, water vapor permeability (WVP), and oxygen permeability (OP) of thermoplastic starch (TPS) and TPS modified by dry heating (TPSDH) films with different contents of cellulose microfibers (CMFs).

Formulation	Moisture (%)	Solubility (g soluble film·100 g^{-1} film)	WVP ($g.mm.kPa^{-1}.h^{-1}.m^{-2}$)	OP x 10^{14} ($cm^3.m^{-1}.s^{-1}.Pa^{-1}$)
TPS	$7.7 \pm 0.1^{a,1}$	$42 \pm 2^{a,2}$	$6.3 \pm 0.2^{ab,1}$	$9.0 \pm 0.3^{a,1}$
TPS1	$7.5 \pm 0.1^{a,1}$	$28 \pm 1^{b,2}$	$6.5 \pm 0.1^{a,1}$	$9.2 \pm 0.4^{a,1}$
TPS3	$7.7 \pm 0.1^{a,1}$	$37 \pm 4^{ab,2}$	$5.9 \pm 0.2^{b,1}$	$6.3 \pm 0.6^{b,2}$
TPS5	$7.1 \pm 0.2^{b,1}$	$36 \pm 5^{ab,2}$	$5.3 \pm 0.3^{c,1}$	$6.4 \pm 0.1^{b,2}$
TPSDH	$8.1 \pm 0.1^{a,2}$	$55 \pm 8^{b,1}$	$0.25 \pm 0.01^{a,2}$	$8.7 \pm 0.5^{a,1}$
TPSDH1	$7.9 \pm 0.1^{a,2}$	$80 \pm 8^{a,1}$	$0.33 \pm 0.05^{a,2}$	$8.8 \pm 0.4^{a,1}$
TPSDH3	$7.7 \pm 0.1^{b,1}$	$73 \pm 12^{ab,1}$	$0.31 \pm 0.02^{a,2}$	$7.7 \pm 0.4^{a,1}$
TPSDH5	$7.9 \pm 0.1^{a,2}$	$57 \pm 6^{ab,1}$	$0.31 \pm 0.01^{a,2}$	$8.4 \pm 0.1^{a,1}$

Different subscript letters indicate significant differences between samples of the same group (TPS or TPSDH films). Different numbers indicated significant differences between TPS and TPSDH samples with the same ratio of CMF (Tukey test, $p<0.05$).

The different effect of the fibres on water solubility of TPS and TPSDH films can be explained by the different interactions of CMF with both starch matrices. The –OH groups present in CMF could interact with the hydrophilic groups in starch, making it unavailable to interact with the water molecules [59]. This effect was evident for the water solubility of the TPS films, which decreased significantly (p<0.05) after the CMF incorporation, as previously reported by other authors [56,60,61]. Furthermore, the lower water solubility of these microcomposites due to the CMF presence could make starch less susceptible to hydrolysis, though this property mainly depends on its structural characteristics and modifications [62]. However, in the TPSDH films, the CMF incorporation promoted film water solubility, except for the samples containing 5 % wt. CMF. This different effect could be ascribed to a poorer integration and dispersion of the fibres in the starch matrix, having lower adhesion forces at the interface and, thus, favouring water penetration through the junction zones. The higher presence of non-gelatinized starch granules could also contribute to the higher solubility in the TPSDH films since this dispersed phase can reduce the cohesion forces of the matrix, which are related to the interchain bonds that depends on their interfacial adhesion in the continuous matrix.

3.5 Barrier properties to water vapor and oxygen gas

The values of WVP and OP of the TPS films are also shown in previous Table 3. The non-modified starch films exhibited WVP values ranging from 5.3 to 6.3 g.mm/kPa.h.m^2, close to the range reported by other authors for corn starch films [34,40]. Films of TPS with 3 and 5 % wt. CMF exhibited slightly lower but still significant (p<0.05) WVP values than the neat TPS

film, reaching percentages increases in the barrier performance of 6 % and 15 %, respectively. Since WVP of packaging materials is mainly affected by the solubility coefficient in the polymer matrix and also, but to a lesser extent, by the vapor diffusion rate [63], the permeability decrease attained in the film samples containing CMF can be ascribed to the chemical interaction by –H bonds of cellulose with hydrophilic groups of the starch-glycerol matrix described above [4,49,64]. Other authors also reported a decrease in WVP of TPS films from different sources incorporated with cellulosic fractions [61,65]. Furthermore, the CMF addition did not influence significantly (p>0.05) the WVP values of the TPSDH films, which already presented values remarkably lower (p<0.05) than the TPS samples. The latter lower permeability to water vapor of DH-modified starch can be ascribed to the large presence of intact starch granules, previously observed in the FESEM images, which would increase the tortuosity factor of the modified matrix, further limiting the diffusion of water molecules through the films. Other authors also reported lower values of VWP for DH-modified rice starch films [66].

As concerns the OP values, the incorporation of CMFs at contents of 3 and 5 % wt. promoted a significant (p<0.05) OP decrease of approximately 30 % with respect to the neat TPS film. This barrier enhancement can be attributed to the increase of tortuosity factor associated to fibre distribution along the TPS matrix, with a good compatibility and dispersion, which would limit the diffusion rate of oxygen molecules through the films. Other studies have also reported a decrease in the OP of starch-based films with cellulosic fractions [36,65], which are in agreement with the results reported herein. However, non-significant differences (p>0.05) in the OP values were observed for the TPSDH films after fibre incorporation. These films exhibited significantly (p<0.05) higher OP values than TPS microcomposite films with 3 and 5 % wt. CMF and similar to those observed for TPS films without and with 1 % wt. CMF. The lack of influence of the incorporated fibres on the barrier properties (both WVP and OP) of the TPSDH films suggests that the expected fibre promotion of the tortuosity factor is probably compensated by a lower adhesion force between the fibres and biopolymer matrix that promoted mass transfer through the union points. Moreover, the larger content of C=O and–COOH groups produced by depolymerization of heat-treated starch chains could promoted the solubility of oxygen molecules in the films, enhancing the transmission rate [67].

Therefore, incorporating CMF from RS in TPS films represents an adequate strategy to enhance the oxygen barrier capacity of the biopolymer films, being suitable to reduce or modulate oxidation reactions in packaged foods. In contrast, a very low effect of CMF on the barrier properties of the DH-modified starch films was observed, though these biopolymer films already exhibited better water vapor barrier capacity (90 % reduction of WVP with respect to untreated TPS films).

3.6 Mechanical Properties

The mechanical properties of the films, namely EB, TS, and EM were determined by tensile tests and summarized in Table 4. Both TPS and TPSDH films exhibited similar stiffness or elastic modulus, though the TPSDH films were slightly more rigid and remarkably more resistant to break but also less extensible. The TPS control film had an EB value of approximately 30 %, in line with that observed by Hernández-García et al. [50] for TPS films. Furthermore, the TPSDH film without fibres showed an EB value of 23 %, being lower than the neat TPS film. This mechanical embrittlement can be attributed to the changes occurred in the starch chains, such as short-chain amyloses produced by heat induced hydrolysis of starch [54] or the increase in the content of C=O and –COOH groups during the DH of starch [67]. Other authors [60,68] also suggested that the conversion of native –OH groups to C=O and –COOH ones in oxidized starch may promote –H bonds between amylose and amylopectin molecules, increasing the integrity of the biopolymer matrix and improving the tensile resistance of the films.

Table 4. Mechanical properties in terms of elongation at break (EB%), tensile strength at break (TS), and elastic modulus (EM) of thermoplastic starch (TPS) and TPS modified by dry heating (TPSDH) films with different contents of cellulose microfibers (CMFs).

Formulation	EB (%)	TS (MPa)	EM (MPa)
TPS	$30 \pm 4^{a,1}$	$3.4 \pm 0.6^{c,2}$	$180 \pm 50^{c,1}$
TPS1	$30 \pm 7^{a,1}$	$4.2 \pm 1.0^{bc,2}$	$140 \pm 30^{c,2}$
TPS3	$14 \pm 5^{b,1}$	$6.8 \pm 1.2^{a,2}$	$550 \pm 180^{a,1}$
TPS5	$18 \pm 4^{b,1}$	$4.6 \pm 0.9^{b,2}$	$300 \pm 100^{b,1}$
TPSDH	$23 \pm 4^{a,2}$	$6.4 \pm 0.4^{b,1}$	$190 \pm 30^{f,1}$
TPSDH1	$9 \pm 3^{bc,2}$	$6.9 \pm 0.5^{b,1}$	$320 \pm 70^{e,1}$
TPSDH3	$5 \pm 1^{c,2}$	$10.2 \pm 1.5^{a,1}$	$590 \pm 70^{d,1}$
TPSDH5	$10 \pm 3^{b,2}$	$7.2 \pm 1.2^{b,1}$	$290 \pm 100^{ef,1}$

Different subscript letters indicate significant differences between samples of the same group (TPS or TPSDH films). Different numbers indicated significant differences between TPS and TPSDH samples with the same ratio of CMF (Tukey test, $p<0.05$).

The incorporation of CMF at 3 % wt. increased notably film stiffness in both kind of films, being this effect less noticeable at other ratios of fibres. Several studies have also reported higher EM values of starch films containing cellulosic fractions from different sources [36,56,69]. In general, all the here-developed films became more resistant and less stretchable as higher loading of CMFs were incorporated. Higher fibre contents, of 3 and 5 % wt. CMF, decreased the TPS film stretchability by about 50 %, whereas a similar decrease was observed for the TPSDH film with only 1 % wt. CMFs. The lack of stretchability limits the overall extensibility of the films without markedly reducing the resistance to break. As shown in FESEM micrographs,

CMFs were strongly bonded to the polymer matrix, which restricted the movement of starch chains, decreasing their stretchability but also reinforcing the TPS matrix [70]. The highest reinforcing effect was observed for the 3 % wt. of CMF in both TPS and TPSDH films. These films particularly exhibited the highest EM (about 550 and 590 MPa for TPS and TPSDH, respectively) and resistance to break (approximately 7 and 10 MPa for TPS and TPSDH, respectively), but also with reduced elongation capacity (14 and 5 % for TPS and TPSDH, respectively). In this regard, Fazeli et al. [65] also observed a threshold concentration in cellulose nanofibers from henequen to reinforce starch films.

Therefore, the obtained results in tensile behaviour of TPS and TPSDH films demonstrated the reinforcing capacity of CMFs for starch films, which indicates good compatibility and dispersion along the TPS matrix. However, higher contents than 3 % wt. led to lower mechanical performances, which can be attributed to a loss of cohesion forces or a lower degree of dispersion and certain agglomeration of the fibres in the TPS matrix.

3.7 Thermal Properties

Figure 6 shows the TGA and first derivative (DTG) curves obtained for the TPS and TPSDH films and their microcomposites films prepared with CMFs. Table 5 gathers the thermal stability parameters, namely T_{onset}, T_{final}, and T_{deg} as well as the mass loss at T_{deg}. One can observe that fibre incorporation did not notably influence the thermal degradation properties of the TPS and TPSDH films. In particular, the TPS films showed the main degradation event ranging at approximately 150–455 °C, corresponding to a mass loss of nearly 80 % with a T_{deg} value of 341 °C. This event is associated with the thermal decomposition of glycerol [71], starch [28,72], and CMF. Figure 6a shows the thermal decomposition profile of the CMF fractions, showing the previously reported mass loss steps [35]: evaporation of bonded water (30–140 °C), cellulose and hemicellulose decomposition (177–350 °C) and lignin degradation (350–500 °C). The second thermal degradation step is referred as the “active pyrolysis zone” since mass loss rate is high, whereas the third one is called “passive pyrolysis zone” since the percentage of mass loss is smaller, and the mass loss rate is also much lower compared to that in the second zone [73]. In relation to the degradation profile of the TPS films, the sample containing 5 % wt. CMFs exhibited slightly higher mass loss from 180 to 280 °C, which can be attributed to the thermal degradation of the cellulose fractions, more noticeable due to its high content. However, this TPS5 sample was more stable than the other TPS films in the thermal range of 280–310 °C (see Figures 6a and 6c), suggesting that the CMF incorporation delayed the thermal degradation of the shortest chains of starch produced during its thermo-processing [74].

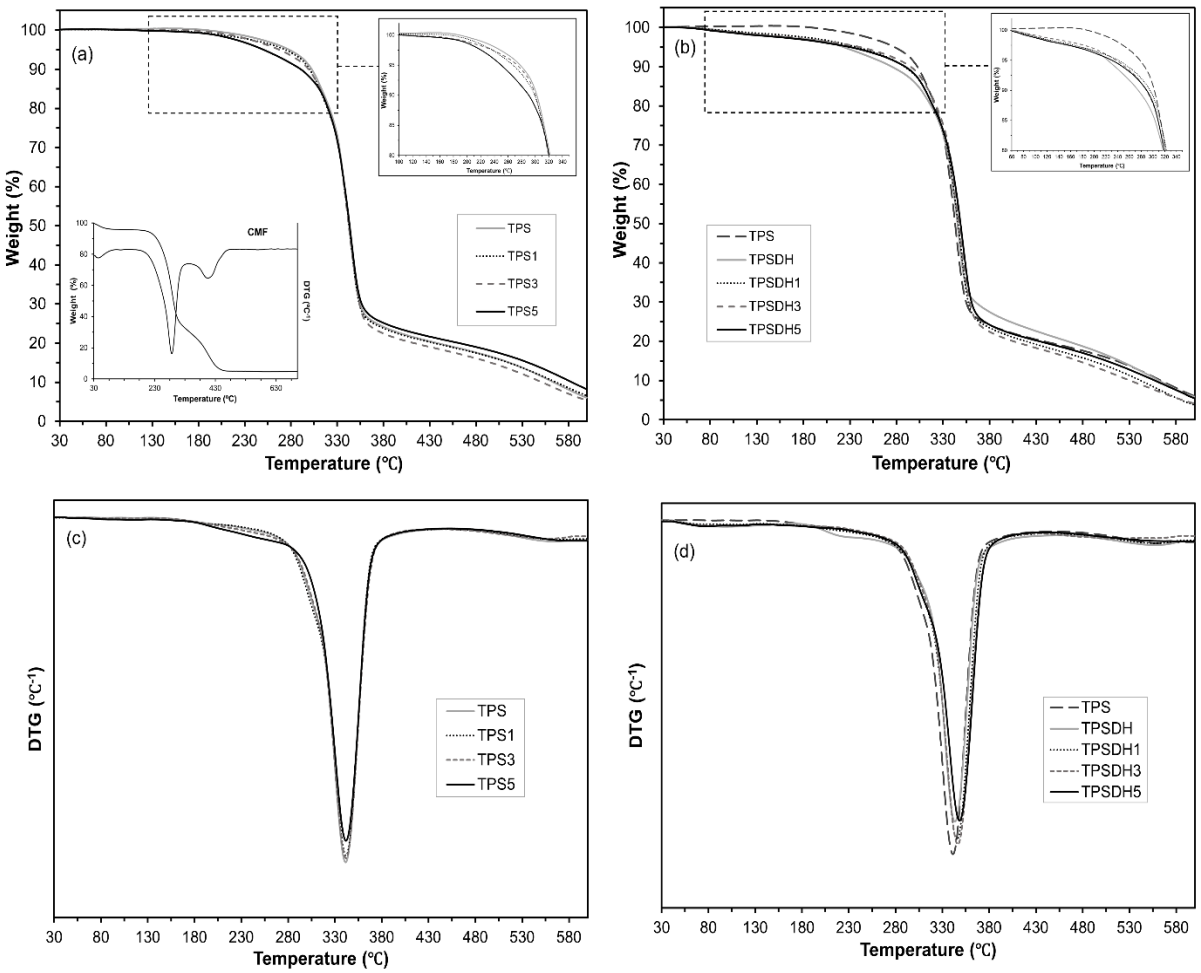

Figure 6. Thermogravimetric analysis (TGA) curves (a, b) and first derivative (DTG) curves (c, d) curves of thermoplastic starch (TPS) and TPS modified by dry heating (TPSDH) films with different contents of cellulose microfibers (CMFs).

Regarding the TPSDH films, these samples exhibited a slight initial mass loss (3–5 %) in the thermal range from approximately 50 to 150 °C, which is ascribed to evaporation of water adsorbed in the inner regions of the non-gelatinized starch granules and it may also derive from thermal decomposition of low-molecular weight (M_W) components produced during the DH treatment [54]. This mass loss can be observed in Figure 6b, where the mass loss curves of the TPS and TPSDH films were compared. As shown in Table 4 and also Figure 6d, TPSDH films exhibited slightly higher T_{deg} values than the TPS films. This thermal stability enhancement may be attributed to the presence of C=O and –COOH groups produced by the heat treatment of starch that allows for more –H bonds between the polymer chains [68]. Furthermore, the non-gelatinized starch granules, with more crystalline regions, could also contribute to the resultant thermal behaviour. In the TPSDH films, the concentration increases in CMF also implied a slight increase in the thermal stability, which could be due to the increasing presence of starch granules in the matrix.

Table 5. Onset, final, and peak temperatures (T_{onset}, T_{final}, and T_{deg}), and mass loss at T_{deg} (Δm%) obtained from thermogravimetric analysis (TGA) and glass transition temperature (T_g) obtained from differential scanning calorimetry (DSC) for thermoplastic starch (TPS) and TPS modified by dry heating (TPSDH) films with different contents of cellulose microfibres (CMFs).

	TGA				DSC
Formulation	**T_{onset} (°C)**	**T_{final} (°C)**	**T_{peak} (°C)**	**Δm (%)**	**T_g**
TPS	156 ± 1	455 ± 3	341 ± 1	80.7 ± 1.0	92 ± 4
TPS1	153 + 1	456 ± 1	343 ± 1	81.3 ± 0.7	86 ± 1
TPS3	152 ± 4	453 ± 1	342 ± 1	82 ± 1.0	85 ± 6
TPS5	154 ± 1	452 ± 3	343 ± 1	79.2 ± 0.2	82 ± 9
TPSDH	179 ± 2	455 ± 1	345 ± 1	80 ± 1	106 ± 1
TPSDH1	183 ± 1	454 ± 2	346 ± 2	78 ± 2	79 ± 2
TPSDH3	181 ± 1	449 ± 2	347 ± 1	80 ± 1	-
TPSDH5	182 ± 1	450 ± 1	349 ± 3	79 ± 3	124 ± 4

Finally, DSC analysis was also performed to evaluate the effect of the starch modification by DH and CMF incorporation on the thermal phase transitions of starch. The first heating scans, gathered in Figure 7, showed the typical endotherm of starch gelatinization associating peak temperatures in the 55–110 °C range for the film samples of TPSDH and TPS with the highest CMF loadings (TPS3 and TPS5). This agrees with the above-reported FESEM observations that revealed the presence of non-gelatinized starch granules in the starch matrix. It can also be observed that the gelatinization enthalpy increased with the CMF ratio due to the aforementioned higher presence of starch granules in the films. In the second heating scan, the TPS films also exhibited the glass transition (T_g) of the already gelatinized starch, being this transition less appreciable, that is, having a lower change in specific heat (ΔC_p), for TPSDH samples. The T_g values (midpoint) of the TPSDH sample was slightly higher than that of TPS, which is coherent with the stronger interactions promoted in the matrix when starch was DH modified. This result also agrees with the more resistance, but less ductile behaviour of the films attained during the mechanical characterization. As expected, the addition of CMF did not induce notable changes in the starch's T_g, when compared with the corresponding control sample, since the fibres are not miscible with starch. The small variations of T_g in the TPS composites with CMFs can be attributed to potential interactions between fibres or their remaining water contents and plasticizer that could modify the plasticization level of starch [31]. In this context, Collazo-Bigliardi et al. [40] found similar results for corn starch films filled with fibres derived from rice husk.

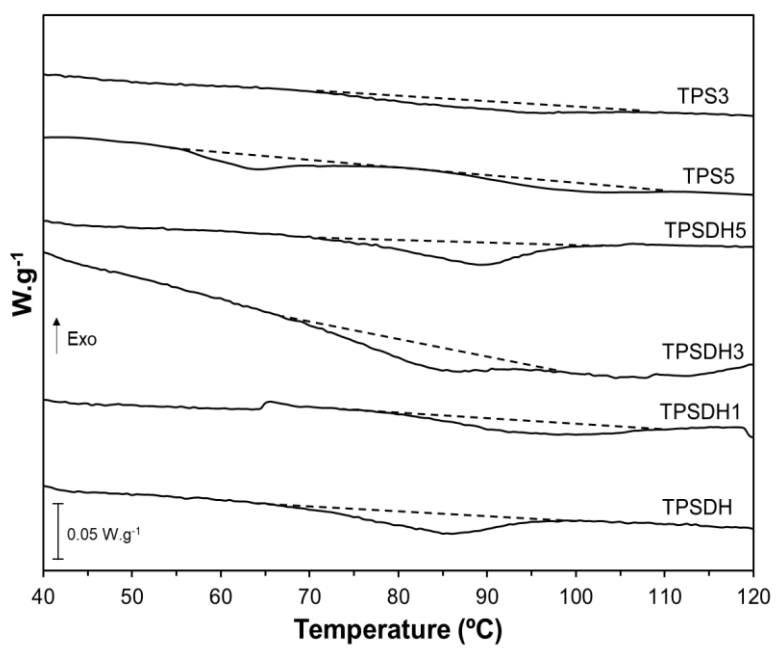

Figure 7. Differential scanning calorimetry (DSC) thermograms taken during first heating scan of thermoplastic starch (TPS) and TPS modified by dry heating (TPSDH) films with different contents of cellulose microfibres (CMFs).

4. CONCLUSIONS

CMFs with good reinforcing capacity for starch films were obtained from RS, a waste material derived from the agricultural and food industry, using a green process and mechanical defibrillation. Fibrils with a major cumulative frequency of lengths below 200 µm and 5–15 µm of thickness were obtained. Incorporation of CMF into starch matrices at 3 wt %, the most optimal content, led to stiffer and more resistance to break films for both non-modified and DH-modified corn starch films. Likewise, fibre at 3 and 5 wt % improved the oxygen and water vapor barrier capacity of TPS films but did not modify barrier properties of TPSDH films. Fibres interfered starch gelatinization during the starch-glycerol thermo-processing, more markedly in DH-modified starch with modified granular structure, giving rise to non-gelatinized starch granules into the film matrix. The dispersed phase (starch granules or fibres) also modified the optical properties of the TPS films, making them slightly less transparent. Therefore, it can be concluded that RS is a good source of CMF that can be used to improve properties of starch films with different purposes, such as their use as food packaging material. This contributes to the valorisation of the agricultural and food waste into added-value materials, useful at improving the performance of biodegradable food packaging material. Likewise, this study further confirms that the DH process of starch represents a green physical method to enhance the water barrier capacity and tensile strength of starch films.

5. ACKNOWLEDGEMENTS

The authors thank the Agencia Estatal de Investigación (Spain) for the financial support through projects PID2019-105207RB-I00/AEI/10.13039/501100011033 and Generalitat Valenciana [grant number GrisoliaP/2019/115]. C.L.F.A. acknowledges the São Paulo Research Foundation (FAPESP) for the Research Internships Abroad (BEPE) fellowship (2020/10498-0). S.T.-G. acknowledges MICI for his Ramón y Cajal contract (RYC2019-027784-I).

6. REFERENCES

1. Hafemann, E.; Battisti, R.; Marangoni, C.; Machado, R.A.F. Valorization of Royal Palm Tree Agroindustrial Waste by Isolating Cellulose Nanocrystals. *Carbohydrate Polymers* 2019, *218*, 188–198, doi:10.1016/j.carbpol.2019.04.086.

2. Chen, X. Study on Structure and Thermal Stability Properties of Cellulose Fibers from Rice Straw. *Carbohydrate Polymers*, 6. doi: 10.1016/j.carbpol.2011.02.022

3. Saini, J.K.; Saini, R.; Tewari, L. Lignocellulosic Agriculture Wastes as Biomass Feedstocks for Second-Generation Bioethanol Production: Concepts and Recent Developments. 3 *Biotech* 2015, 5, 337–353, doi:10.1007/s13205-014-0246-5.

4. Ng, H.-M.; Sin, L.T.; Tee, T.-T.; Bee, S.-T.; Hui, D.; Low, C.-Y.; Rahmat, A.R. Extraction of Cellulose Nanocrystals from Plant Sources for Application as Reinforcing Agent in Polymers. Composites Part B: Engineering 2015, 75, 176–200, doi:10.1016/j.compositesb.2015.01.008.

5. Sharma, B.; Vaish, B.; Monika; Singh, U.K.; Singh, P.; Singh, R.P. Recycling of Organic Wastes in Agriculture: An Environmental Perspective. *Int J Environ Res* 2019, 13, 409–429, doi:10.1007/s41742-019-00175-y.

6. Casabar, J.T.; Ramaraj, R.; Tipnee, S.; Unpaprom, Y. Enhancement of Hydrolysis with Trichoderma Harzianum for Bioethanol Production of Sonicated Pineapple Fruit Peel. *Fuel* 2020, 279, 118437, doi:10.1016/j.fuel.2020.118437.

7. Basumatary, B.; Basumatary, S.; Das, B.; Nath, B.; Kalita, P. Waste Musa Paradisiaca Plant: An Efficient Heterogeneous Base Catalyst for Fast Production of Biodiesel. *Journal of Cleaner Production* 2021, 305, 127089, doi:10.1016/j.jclepro.2021.127089.

8. Freitas, P.A.V.; González-Martínez, C.; Chiralt, A. Application of Ultrasound Pre-Treatment for Enhancing Extraction of Bioactive Compounds from Rice Straw. *Foods* 2020, 9, 1657, doi:10.3390/foods9111657.

9. Prakash, A.; Vadivel, V.; Banu, S.F.; Nithyanand, P.; Lalitha, C.; Brindha, P. Evaluation of Antioxidant and Antimicrobial Properties of Solvent Extracts of Agro-Food by-Products (Cashew Nut Shell, Coconut Shell and Groundnut Hull). *Agriculture and Natural Resources* 2018, 52, 451–459, doi:10.1016/j.anres.2018.10.018.

10. Ilyas, R.A.; Sapuan, S.M.; Ibrahim, R.; Abral, H.; Ishak, M.R.; Zainudin, E.S.; Atikah, M.S.N.; Mohd Nurazzi, N.; Atiqah, A.; Ansari, M.N.M.; et al. Effect of Sugar Palm Nanofibrillated Cellulose Concentrations on Morphological, Mechanical and Physical Properties of Biodegradable Films Based on Agro-Waste Sugar Palm (Arenga Pinnata (Wurmb.) Merr)

Starch. *Journal of Materials Research and Technology* 2019, 8, 4819–4830, doi:10.1016/j.jmrt.2019.08.028.

11. Kassab, Z. Cellulosic Materials from Pea (Pisum Sativum) and Broad Beans (Vicia Faba) Pods Agro-Industrial Residues. *Materials Letters* 2020, 4. doi: 10.1016/j.matlet.2020.128539

12. de Souza Lima, M.M.; Borsali, R. Rodlike Cellulose Microcrystals: Structure, Properties, and Applications. *Macromol. Rapid Commun*. 2004, 25, 771–787, doi:10.1002/marc.200300268.

13. FAOSTAT Available online: http://www.fao.org/faostat/en/#data/QC/visualize (accessed on 4 November 2020).

14. Peanparkdee, M.; Iwamoto, S. Bioactive Compounds from By-Products of Rice Cultivation and Rice Processing: Extraction and Application in the Food and Pharmaceutical Industries. *Trends in Food Science & Technology* 2019, 86, 109–117, doi:10.1016/j.tifs.2019.02.041.

15. Sarkar, N.; Ghosh, S.K.; Bannerjee, S.; Aikat, K. Bioethanol Production from Agricultural Wastes: An Overview. *Renewable Energy* 2012, 37, 19–27, doi:10.1016/j.renene.2011.06.045.

16. El-Tayeb, T.S.; Abdelhafez, A.A.; Ali, S.H.; Ramadan, E.M. Effect of Acid Hydrolysis and Fungal Biotreatment on Agro-Industrial Wastes for Obtainment of Free Sugars for Bioethanol Production. *Braz. J. Microbiol.* 2012, 43, 1523–1535, doi:10.1590/S1517-83822012000400037.

17. Neto, W.P.F.; Silvério, H.A.; Vieira, J.G.; da Costa e Silva Alves, H.; Pasquini, D.; de Assunção, R.M.N.; Dantas, N.O. Preparation and Characterization of Nanocomposites of Carboxymethyl Cellulose Reinforced with Cellulose Nanocrystals. *Macromol. Symp.* 2012, 319, 93–98, doi:10.1002/masy.201100194.

18. Galdeano, M.C.; Mali, S.; Grossmann, M.V.E.; Yamashita, F.; García, M.A. Effects of Plasticizers on the Properties of Oat Starch Films. *Materials Science and Engineering: C* 2009, 29, 532–538, doi:10.1016/j.msec.2008.09.034.

19. Forssell, P.; Lahtinen, R.; Lahelin, M.; MyllaÈrinen, P. Oxygen Permeability of Amylose and Amylopectin Fims. *Carbohydrate Polymers* 2002, 5. doi: 10.1016/S0144-8617(01)00175-8

20. Zainuddin, S.Y.Z. Potential of Using Multiscale Kenaf Fibers as Reinforcing Filler in Cassava Starch-Kenaf Biocomposites. *Carbohydrate Polymers* 2013, 7. doi: 10.1016/j.carbpol.2012.11.106

21. Carvalho, A.J.F. Starch: Major Sources, Properties and Applications as Thermoplastic Materials. In Monomers, Polymers and Composites from Renewable Resources; Elsevier, 2008; pp. 321–342 ISBN 978-0-08-045316-3.

22. González, K.; Retegi, A.; González, A.; Eceiza, A.; Gabilondo, N. Starch and Cellulose Nanocrystals Together into Thermoplastic Starch Bionanocomposites. *Carbohydrate Polymers* 2015, 117, 83–90, doi:10.1016/j.carbpol.2014.09.055.

23. Teixeira, E. de M.; Pasquini, D.; Curvelo, A.A.S.; Corradini, E.; Belgacem, M.N.; Dufresne, A. Cassava Bagasse Cellulose Nanofibrils Reinforced Thermoplastic Cassava Starch. *Carbohydrate Polymers* 2009, 78, 422–431, doi:10.1016/j.carbpol.2009.04.034.

24. Collazo-Bigliardi, S. Isolation and Characterisation of Microcrystalline Cellulose and Cellulose Nanocrystals from Coffee Husk and Comparative Study with Rice Husk. *Carbohydrate Polymers* 2018, 11. doi: 10.1016/j.carbpol.2018.03.022

25. Ghanbarzadeh, B.; Almasi, H.; Entezami, A.A. Improving the Barrier and Mechanical Properties of Corn Starch-Based Edible Films: Effect of Citric Acid and Carboxymethyl Cellulose. *Industrial Crops and Products* 2011, 33, 229–235, doi:10.1016/j.indcrop.2010.10.016.

26. Othman, S.H.; Majid, N.A.; Tawakkal, I.S.M.A.; Basha, R.K.; Nordin, N.; Shapi'I, R.A. Tapioca Starch Films Reinforced with Microcrystalline Cellulose for Potential Food Packaging Application. *Food Sci. Technol* 2019, 39, 605–612, doi:10.1590/fst.36017.

27. Chen, J.; Wang, X.; Long, Z.; Wang, S.; Zhang, J.; Wang, L. Preparation and Performance of Thermoplastic Starch and Microcrystalline Cellulose for Packaging Composites: Extrusion and Hot Pressing. *International Journal of Biological Macromolecules* 2020, 165, 2295–2302, doi:10.1016/j.ijbiomac.2020.10.117.

28. Kargarzadeh, H. Starch Biocomposite Film Reinforced by Multiscale Rice Husk Fiber. *Composites Science and Technology* 2017, 9. doi: 10.1016/j.compscitech.2017.08.018

29. Syafri, E.; Jamaluddin; Wahono, S.; Irwan, A.; Asrofi, M.; Sari, N.H.; Fudholi, A. Characterization and Properties of Cellulose Microfibers from Water Hyacinth Filled Sago Starch Biocomposites. *International Journal of Biological Macromolecules* 2019, 137, 119–125, doi:10.1016/j.ijbiomac.2019.06.174.

30. Abdul Khalil, H.P.S.; Bhat, A.H.; Ireana Yusra, A.F. Green Composites from Sustainable Cellulose Nanofibrils: A Review. *Carbohydrate Polymers* 2012, 87, 963–979, doi:10.1016/j.carbpol.2011.08.078.

31. Chandanasree, D.; Gul, K.; Riar, C.S. Effect of Hydrocolloids and Dry Heat Modification on Physicochemical, Thermal, Pasting and Morphological Characteristics of Cassava (Manihot Esculenta) Starch. *Food Hydrocolloids* 2016, 52, 175–182, doi:10.1016/j.foodhyd.2015.06.024.

32. Oh, I.K.; Bae, I.Y.; Lee, H.G. Effect of Dry Heat Treatment on Physical Property and in Vitro Starch Digestibility of High Amylose Rice Starch. *International Journal of Biological Macromolecules* 2018, 108, 568–575, doi:10.1016/j.ijbiomac.2017.11.180.

33. Maniglia, B.C.; Lima, D.C.; Matta Junior, M.D.; Le-Bail, P.; Le-Bail, A.; Augusto, P.E.D. Preparation of Cassava Starch Hydrogels for Application in 3D Printing Using Dry Heating Treatment (DHT): A Prospective Study on the Effects of DHT and Gelatinization Conditions. *Food Research International* 2020, 128, 108803, doi:10.1016/j.foodres.2019.108803.

34. Sun, Q.; Xu, Y.; Xiong, L. Effect of Microwave-Assisted Dry Heating with Xanthan on Normal and Waxy Corn Starches. *International Journal of Biological Macromolecules* 2014, 68, 86–91, doi:10.1016/j.ijbiomac.2014.04.032.

35. Freitas P.A.V.; González-Martínez, C.; Chiralt, A. Applying ultrasound-assisted processing to obtain cellulose fibers from rice straw to be used as reinforcing agents. *Innovative Food Science and Emerging Technology* 2021, In Press.

36. Collazo-Bigliardi, S.; Ortega-Toro, R.; Chiralt Boix, A. Reinforcement of Thermoplastic Starch Films with Cellulose Fibres Obtained from Rice and Coffee Husks. *Journal of Renewable Materials* 2018, 6, 599–610, doi:10.32604/JRM.2018.00127.

37. Rojas-Lema, S.; Quiles-Carrillo, L.; Garcia-Garcia, D.; Melendez-Rodriguez, B.; Balart, R.; Torres-Giner, S. Tailoring the Properties of Thermo-Compressed Polylactide Films for Food Packaging Applications by Individual and Combined Additions of Lactic Acid Oligomer and Halloysite Nanotubes. *Molecules* 2020, 25, 1976, doi:10.3390/molecules25081976.

38. Talón, E.; Trifkovic, K.T.; Nedovic, V.A.; Bugarski, B.M.; Vargas, M.; Chiralt, A.; González-Martínez, C. Antioxidant Edible Films Based on Chitosan and Starch Containing Polyphenols from Thyme Extracts. *Carbohydrate Polymers* 2017, 157, 1153–1161, doi:10.1016/j.carbpol.2016.10.080.

39. McHUGH, T.H.; Avena-Bustillos, R.; Krochta, J.M. Hydrophilic Edible Films: Modified Procedure for Water Vapor Permeability and Explanation of Thickness Effects. *J Food Science* 1993, 58, 899–903, doi:10.1111/j.1365-2621.1993.tb09387.x.

40. Collazo-Bigliardi, S.; Ortega-Toro, R.; Chiralt, A. Improving Properties of Thermoplastic Starch Films by Incorporating Active Extracts and Cellulose Fibres Isolated from Rice or Coffee Husk. *Food Packaging and Shelf Life* 2019, 22, 100383, doi:10.1016/j.fpsl.2019.100383.

41. Jin, S.; Chen, H. Structural Properties and Enzymatic Hydrolysis of Rice Straw. *Process Biochemistry* 2006, 4. doi: 10.1016/j.procbio.2005.12.022

42. Zhang, Z.; Smith, C.; Li, W. Extraction and Modification Technology of Arabinoxylans from Cereal By-Products: A Critical Review. *Food Research International* 2014, 14. doi: 10.1016/j.foodres.2014.05.068

43. Cheung, Y.-C.; Wu, J.-Y. Kinetic Models and Process Parameters for Ultrasound-Assisted Extraction of Water-Soluble Components and Polysaccharides from a Medicinal Fungus. *Biochemical Engineering Journal* 2013, 79, 214–220, doi:10.1016/j.bej.2013.08.009.

44. Hayat, K.; Abbas, S.; Hussain, S.; Shahzad, S.A.; Tahir, M.U. Effect of Microwave and Conventional Oven Heating on Phenolic Constituents, Fatty Acids, Minerals and Antioxidant Potential of Fennel Seed. *Industrial Crops and Products* 2019, 140, 111610, doi:10.1016/j.indcrop.2019.111610.

45. Machado, I. Characterization of the Effects Involved in Ultrasound-Assisted Extraction of Trace Elements from Artichoke Leaves and Soybean Seeds. *Ultrasonics- Sonochemistry* 2019, 7. doi: 10.1016/j.ultsonch.2019.104752

46. Moslemi, A. Addition of Cellulose Nanofibers Extracted from Rice Straw to Urea Formaldehyde Resin; Effect on the Adhesive Characteristics and Medium Density Fiberboard Properties. *International Journal of Adhesion and Adhesives* 2020, 6. doi: 10.1016/j.ijadhadh.2020.102582

47. Bochek, A.M. Effect of Hydrogen Bonding on Cellulose Solubility in Aqueous and Nonaqueous Solvents. *Russian Journal of Applied Chemistry* 2003, 76, 1711–1719, doi:10.1023/B:RJAC.0000018669.88546.56.

48. Jiang, F.; Han, S.; Hsieh, Y.-L. Controlled Defibrillation of Rice Straw Cellulose and Self-Assembly of Cellulose Nanofibrils into Highly Crystalline Fibrous Materials. RSC Ad*v.* 2013, 3, 12366, doi:10.1039/c3ra41646a.

49. Littunen, K.; Hippi, U.; Saarinen, T.; Seppälä, J. Network Formation of Nanofibrillated Cellulose in Solution Blended Poly(Methyl Methacrylate) Composites. *Carbohydrate Polymers* 2013, 91, 183–190, doi:10.1016/j.carbpol.2012.08.032.

50. Hernández-García, E.; Vargas, M.; Chiralt, A. Thermoprocessed Starch-Polyester Bilayer Films as Affected by the Addition of Gellan or Xanthan Gum. *Food Hydrocolloids* 2021, 113, 106509, doi:10.1016/j.foodhyd.2020.106509.

51. Menzel, C.; González-Martínez, C.; Vilaplana, F.; Diretto, G.; Chiralt, A. Incorporation of Natural Antioxidants from Rice Straw into Renewable Starch Films. *International Journal of Biological Macromolecules* 2020, 146, 976–986, doi:10.1016/j.ijbiomac.2019.09.222.

52. Oladebeye, A.O.; Oshodi, A.A.; Amoo, I.A.; Karim, A.A. Functional, Thermal and Molecular Behaviours of Ozone-Oxidised Cocoyam and Yam Starches. *Food Chemistry* 2013, 141, 1416–1423, doi:10.1016/j.foodchem.2013.04.080.

53. Abraham, E. Extraction of Nanocellulose Fibrils from Lignocellulosic Fibres: A Novel Approach. *Carbohydrate Polymers* 2011, 8. doi: 10.1016/j.carbpol.2011.06.034

54. Hung, P.V.; My, N.T.H.; Phi, N.T.L. Impact of Acid and Heat-Moisture Treatment Combination on Physicochemical Characteristics and Resistant Starch Contents of Sweet Potato and Yam Starches. *Starch - Stärke* 2014, 66, 1013–1021, doi:10.1002/star.201400104.

55. Benito-González, I.; López-Rubio, A.; Martínez-Sanz, M. High-Performance Starch Biocomposites with Celullose from Waste Biomass: Film Properties and Retrogradation Behaviour. *Carbohydrate Polymers* 2019, 216, 180–188, doi:10.1016/j.carbpol.2019.04.030.

56. Fourati, Y.; Magnin, A.; Putaux, J.-L.; Boufi, S. One-Step Processing of Plasticized Starch/Cellulose Nanofibrils Nanocomposites via Twin-Screw Extrusion of Starch and Cellulose Fibers. *Carbohydrate Polymers* 2020, 229, 115554, doi:10.1016/j.carbpol.2019.115554.

57. S. Lim, H.; Han, J.-A.; N. BeMiller, J.; Lim, S.-T. Physical Modification of Waxy Maize Starch by Dry Heating with Ionic Gums. *J. Appl. Glycosci*. 2006, 53, 281–286, doi:10.5458/jag.53.281.

58. Ma, X.; Yu, J.; Kennedy, J.F. Studies on the Properties of Natural Fibers-Reinforced Thermoplastic Starch Composites. *Carbohydrate Polymers* 2005, 62, 19–24, doi:10.1016/j.carbpol.2005.07.015.

59. Avérous, L.; Fringant, C.; Moro, L. Plasticized Starch–Cellulose Interactions in Polysaccharide Composites. *Polymer* 2001, 42, 6565–6572, doi:10.1016/S0032-3861(01)00125-2.

60. El Halal, S.L.M.; Colussi, R.; Deon, V.G.; Pinto, V.Z.; Villanova, F.A.; Carreño, N.L.V.; Dias, A.R.G.; Zavareze, E. da R. Films Based on Oxidized Starch and Cellulose from Barley. *Carbohydrate Polymers* 2015, 133, 644–653, doi:10.1016/j.carbpol.2015.07.024.

61. Muller, C.M.O.; Laurindo, J.B.; Yamashita, F. Effect of Cellulose Fibers Addition on the Mechanical Properties and Water Vapor Barrier of Starch-Based Films. *Food Hydrocolloids* 2009, 6. doi: 0.1016/j.foodhyd.2008.09.002

62. Cornejo-Ramírez, Y.I.; Martínez-Cruz, O.; Del Toro-Sánchez, C.L.; Wong-Corral, F.J.; Borboa-Flores, J.; Cinco-Moroyoqui, F.J. The Structural Characteristics of Starches and Their Functional Properties. CyTA - *Journal of Food* 2018, 16, 1003–1017, doi:10.1080/19476337.2018.1518343.

63. Talja, R.A.; Helén, H.; Roos, Y.H.; Jouppila, K. Effect of Various Polyols and Polyol Contents on Physical and Mechanical Properties of Potato Starch-Based Films. *Carbohydrate Polymers* 2007, 67, 288–295, doi:10.1016/j.carbpol.2006.05.019.

64. Hedenqvist, M.S. Barrier Packaging Materials. In Handbook of Environmental Degradation of Materials; Elsevier, 2012; pp. 833–862 ISBN 978-1-4377-3455-3.

65. Fazeli, M.; Keley, M.; Biazar, E. Preparation and Characterization of Starch-Based Composite Films Reinforced by Cellulose Nanofibers. *International Journal of Biological Macromolecules* 2018, 116, 272–280, doi:10.1016/j.ijbiomac.2018.04.186.

66. Li, Y.; Shoemaker, C.F.; Ma, J.; Shen, X.; Zhong, F. Paste Viscosity of Rice Starches of Different Amylose Content and Carboxymethylcellulose Formed by Dry Heating and the Physical Properties of Their Films. *Food Chemistry* 2008, 109, 616–623, doi:10.1016/j.foodchem.2008.01.023.

67. Reyes, I.; Hernandez-Jaimes, C.; Vernon-Carter, E.J.; Bello-Perez, L.A.; Alvarez-Ramirez, J. Air Oxidation of Corn Starch: Effect of Heating Temperature on Physicochemical Properties and In Vitro Digestibility. *Starch - Stärke* 2021, 73, 2000237, doi:10.1002/star.202000237.

68. Zamudio-Flores, P.B.; Vargas-Torres, A.; Pérez-González, J.; Bosquez-Molina, E.; Bello-Pérez, L.A. Films Prepared with Oxidized Banana Starch: Mechanical and Barrier Properties. *Starch - Stärke* 2006, 58, 274–282, doi:10.1002/star.200500474.

69. Adeyi, A.J.; Durowoju, M.O.; Adeyi, O.; Oke, E.O.; Olalere, O.A.; Ogunsola, A.D. Momordica Augustisepala L. Stem Fibre Reinforced Thermoplastic Starch: Mechanical Property Characterization and Fuzzy Logic Artificial Intelligent Modelling. *Results in Engineering* 2021, 10, 100222, doi:10.1016/j.rineng.2021.100222.

70. Lu, Y.; Weng, L.; Cao, X. Biocomposites of Plasticized Starch Reinforced with Cellulose Crystallites from Cottonseed Linter. *Macromol. Biosci.* 2005, 5, 1101–1107, doi:10.1002/mabi.200500094.

71. Maria V, D.; Bernal, C.; Francois, N.J. Development of Biodegradable Films Based on Chitosan/Glycerol Blends Suitable for Biomedical Applications. *J Tissue Sci Eng* 2016, 07, doi:10.4172/2157-7552.1000187.

72. Merci, A.; Marim, R.G.; Urbano, A.; Mali, S. Films Based on Cassava Starch Reinforced with Soybean Hulls or Microcrystalline Cellulose from Soybean Hulls. *Food Packaging and Shelf Life* 2019, 20, 100321, doi:10.1016/j.fpsl.2019.100321.

73. Melendez-Rodriguez, B.; Torres-Giner, S.; Aldureid, A.; Cabedo, L.; Lagaron, J.M. Reactive Melt Mixing of Poly(3-Hydroxybutyrate)/Rice Husk Flour Composites with Purified Biosustainably Produced Poly(3-Hydroxybutyrate-Co-3-Hydroxyvalerate). *Materials* 2019, 12, 2152, doi:10.3390/ma12132152.

74. Menzel, C.; González-Martínez, C.; Chiralt, A.; Vilaplana, F. Antioxidant Starch Films Containing Sunflower Hull Extracts. *Carbohydrate Polymers* 2019, 214, 142–151, doi:10.1016/j.carbpol.2019.03.022.

CHAPTER 1.IV

Antioxidant poly (lactic acid) films with rice straw extract for food packaging applications

Pedro A. V. Freitas, Nuria Julia Bas Gil, Chelo González-Martínez, Amparo Chiralt

Institute of Food Engineering for Development, Universitat Politècnica de València, 46022, Valencia, Spain

Submitted to Food Packaging and Shelf Life

ABSTRACT

Antioxidant PLA films incorporating 2, 4 and 6 % of phenol-rich extract from rice straw (RS) were obtained by melt blending and compression-moulding. Aqueous RS extract was obtained by a combined ultrasound-reflux heating method and characterised as to its total phenolic content (TPC) and antioxidant capacity. The effect of the extract ratio on the functional properties of the films was analysed, as well as the release kinetics of antioxidants in food simulants (ethanol 10 % and 50 %). Extract incorporation slightly reduced the strength of the polymer matrix, stretchability, resistance to break, barrier capacity and thermostability, while films became brownish and gained antioxidant capacity. Phenolic compounds from the extract were effectively released into food simulants, depending on the extract concentration, the food simulant and contact time. The radical scavenging capacity of the films reached asymptotic values from about 150 h contact time, and films with 6 % of the extract exhibited similar values for both simulants. So, PLA films with approximately 6 % of extract could be used as biodegradable active packaging material with antioxidant capacity in both aqueous foods (simulant A) and more fatty products (simulant D1). Further studies are required to verify the antioxidant efficiency of the films in real foods.

Keywords: phenolic compounds, active food packaging, bioactive extract, release kinetics, ultrasound extraction, heating method.

1. INTRODUCTION

Oxidative reactions, microbial growth, and metabolism are the main factors that lead to a loss of quality and the deterioration of foodstuffs, producing waste (Han et al., 2018). Food spoilage through oxidative processes occurs when food is exposed to air, heat or light, producing reactive oxygen species that damage chemical structures, such as proteins, lipids and vitamins (Marzlan et al., 2022; Lourenço et al., 2019). Oxidative reactions can promote food discoloration and lead to a decrease in nutritional value, as well as produce off-odours and off-flavours (Han et al., 2018; Moreno et al., 2018). To overcome these problems, and despite their potential adverse effects on human health, the food industry often uses synthetic antioxidants due to their stability, availability and low cost (Botterweck et al., 2000; Randhawa & Bahna, 2009). The application of non-synthetic antioxidants for food preservation purposes is a current growing trend since consumers increasingly demand healthier and safer food products incorporating natural substances. Of the natural plant antioxidants, phenolic extracts obtained from agri-food residues or by-products represent an interesting alternative. Obtaining active extracts from these residues contributes to proper environmentally-friendly waste management, produces added-value materials and boosts the circular bioeconomy (Arun et al., 2020). Several studies have been reported to obtain plant extracts from agri-food residues with bioactive properties, such as spinach by-products (Derrien et al., 2017), berry leaves (Ziemlewska et al., 2021), winemaking by-products (Troilo et al., 2021; Jara-Palacios et al., 2020), saffron stigma (Lahmass et al., 2018), rice and coffee husks (Collazo-Bigliardi et al., 2019), and rice straw (Freitas, et al., 2020; Menzel et al. 2020).

Of the agro-industrial residues worldwide, the second most widely-produced is rice straw (RS) (*Oryza sativa* L.). The Food and Agriculture Organization of the United Nations (FAO) concluded that global rice production reached approximately 782 million tons, 90 % of which was from the Asian continent (FAOSTAT, 2018). Considering that one kilogram of rice grain provides 1.5 kg of RS (Peanparkdee & Iwamoto, 2019), around 1,173 million tons of problematic waste, without any monetary value that is difficult to manage, is produced every year. This leads to a continuous increase in air pollution, as the primary destination of this by-product is to be burnt on the paddies, releasing harmful dioxins, such as polychlorinated dibenzo-*p*-dioxins, dibenzofurans, and greenhouse gas emissions (CH_4, CO_2, and N_2O), thus promoting global warming and affecting human health (Yang et al., 2006). Since RS is a lignocellulosic-rich material (39 % cellulose, 20 % lignin, 23 % hemicellulose, and 15 % ashes), alternative waste management can be applied with a focus on waste valorisation and the minimisation of environmental impacts (El-Tayeb et al., 2012).

Obtaining phenolic-rich extracts from RS is a promising alternative for the valorisation of RS since the extracted phenolic compounds have been shown to exhibit high antioxidant capacity and antimicrobial activity (Barana et al., 2016; Karimi et al., 2014). Likewise, it is imperative to

optimise the main extraction parameters, such as type of solvent, pre-treatments, temperature, time, and pressure. In fact, the processing factors directly affect the extraction efficiency of phenolic compounds, originally esterified or etherified with the lignocellulosic matrix, especially hemicellulose and lignin. Freitas et al. (2020) reported that the ultrasound pre-treatment of RS water dispersion, followed by water reflux extraction, promoted significant damage to the RS cell tissue, giving rise to an aqueous extract with high phenolic content and antioxidant capacity. These phenolic-rich RS extracts can be used for food formulation or can be incorporated into biodegradable food packaging materials to minimise or delay oxidative processes in foods, as well as to replace synthetic antioxidants.

Biodegradable, economic, and sustainable packaging systems are being proposed to induce more efficient and eco-friendly alternatives to the use of non-biodegradable petroleum-based plastics (Balaji et al., 2018). Poly (lactic acid) (PLA) is a bio-based biodegradable polyester currently ranked in first place in the bioplastics market with a percentage of 18.7 % of the total production of bioplastics (European bioplastics, 2020). PLA is included in the group of thermoplastic biopolymers with good barrier and mechanical properties, such as a high resistance to break. Furthermore, PLA has a relatively hydrophobic structure compared with other biopolymers, dissolves fairly easily in solvents such as chloroform, and does not dissolve in water, alcohols, or alkanes (Avérous et al., 2001). PLA has been studied for the purposes of applying it in active food packaging with antioxidant (Jamshidian et al. 2012a,b; Bassani et al., 2019) and antimicrobial properties (Muller et al., 2017a; Vasile et al., 2019; Llana-Ruiz-Cabello et al., 2015). Different processing methods have been used to incorporate bioactive compounds into polymer matrices to provide them with active properties, including solvent casting, electrospinning, supercritical impregnation, or spin coating, (Velásquez et al., 2021). However, the incorporation of active compounds into the polymer master batch, by melt blending with thermoplastic polymers, represents a cheaper approach with respect to the other techniques, leading to a good standardization of the active material and being more applicable at industrial scale. The challenge with this method is to maintain bioactivity of the usually thermolabile compounds.

The aim of this study was to obtain PLA-based bioactive films, incorporating phenolic-rich aqueous extract from RS obtained by the combined ultrasound-reflux heating method. PLA films were characterised as to their functional properties; typically, their microstructural, optical, thermal, and barrier properties. Likewise, the release kinetics of phenolic compounds from the PLA active films and their radical scavenging capacity were analysed in two food simulants (aqueous ethanol solutions at 10 % and 50 %).

2. MATERIAL AND METHODS

2.1 Materials

Amorphous PLA 4060D, density 1.24 g/cm^3, an average molecular weight of 106,226 D, with 40% low molecular weight fraction (275 D), was purchased from Natureworks (U.S.A). Ethanol and methanol were supplied by Sigma-Aldrich (Sigma-Aldrich Chemie, Steinheim, Germany). Folin-Ciocalteu reagent, 2,2-Diphenyl-1-pikryl-hydrazyl (DPPH) and Poly (ethylene glycol) (PEG1000) were purchased from Sigma-Aldrich (St. Louis, MO, USA). Sodium carbonate (Na_2CO_3) and magnesium nitrate ($Mg(NO_3)_2$) were obtained from PanReac Química S.L.U (Castellar del Vallés, Barcelona, Spain). di-Phosphorous pentoxide (P_2O_5) was obtained from VWR Chemicals (Belgium).

2.2 Extract preparation

The plant extract was obtained using a previously described method (Freitas et al., 2020). RS (*Oryza sativa L.*), supplied by the straw bank of Valencia (Spain) and obtained from L'Albufera rice fields, was dried at 50 ± 2 °C, under vacuum (0,8 mmbar) for 20 h. Afterwards, the dried RS was milled using a milling machine (IKA, model M20, Germany) and sieved to obtain particles of under 0.5 mm. RS aqueous extract was obtained by ultrasound pre-treatment, followed by a heating reflux step (Freitas et al., 2020). A probe high-intensity ultrasonic homogeniser (Vibra CellTM VCX750, Sonics & Material, Inc., Newtown, CT, USA) was used to sonicate the RS: a distilled water suspension, with a ratio of 1:20 (m/v), at 25 °C (using an ice bath to prevent excessive heating) for 30 min, applying a frequency of 20 kHz, 750 W power, and 40 % sonication amplitude. After that, the plant suspension was heated using a typical reflux device at 100 °C for 1 h. The RS extract was obtained by vacuum filtration using a vacuum pump (MZ 2C NT, 7.0 mbar, Vacuubrand, Germany) with a Buncher funnel and qualitative filter (Filterlab). Then, the RS dry extract was obtained by freeze drying (Telstar, model LyoQuest-55) at -60 ℃, 0.8 mbar for 72 h, and stored in a dark glass bottle at 4 ± 2 °C until further use. A total volume of about 750 mL of aqueous extract was freeze-dried in each cycle. The total solid yield obtained after freeze drying process was 14 g dried extract.100 g^{-1} RS.

2.3 Preparation of films

PLA pellets was initially conditioned in a desiccator containing P_2O_5 for 2 days to remove residual water. PLA films were obtained both with and without RS freeze-fried extract using PEG1000 (at 8% wt. with respect to the polymer mass), as plasticiser, by melt blending and compression moulding. As summarised in Table 1, the incorporation of the active extracts in the films was performed by adding percentages of 2, 4, and 6% wt. of RS extract (with respect to the total polymer mass) to the control mixture (PLA/PEG1000). The mixing process was

performed in an internal mixer (HAAKE^{TM} PolyLab^{TM} QC, Thermo Fisher Scientific, Germany) at 160 °C and 50 rpm for 6 min. After cold milling the solid blend, the compression-moulding process was performed using a hydraulic press (Model LP20, Labtech Engineering, Thailand). To this end, 3 g of the pellets were put onto Teflon sheets and placed into the hydraulic press to obtain the films by preheating at 160 °C for 3 min, compressing at 160 °C and 100 bars for 3 min and cooling for 5 min to 70 °C.

Table 1. Mass fractions of the different formulations: PLA (0% wt. RS extract), PLARS2 (2% wt. RS extract), PLARS4 (4% wt. RS extract), PLARS6 (6% wt. RS extract).

Formulation	X_{PLA}	$X_{PEG1000}$	$X_{RS\ extract}$
PLA	0.926	0.074	-
PLARS2	0.909	0.073	0.018
PLARS4	0.893	0.071	0.036
PLARS6	0.877	0.070	0.053

2.4 Film characterisation

2.4.1 Microstructural properties

High resolution Field Emission Scanning Electron Microscopy (FESEM) was performed to study the structure of the film cross-sections. The films were cryo-fractured by immersion in liquid nitrogen, covered with platinum using an EM MED020 sputter coater (Leica BioSystems, Barcelona, Spain) and the images were taken with a Field Emission Scanning Electron microscope equipped with focused ion gun (Auriga Compact, Zeiis, Oxford Instruments), at ×400 magnification (with inserts at ×2000), using an acceleration voltage of 2.0 kV.

2.4.2 Optical properties

A spectro-colorimeter CM-3600d (Minolta Co. Tokyo, Japan) was used to measure the transparency by means of the internal transmittance (T_i) parameter. The Kubelka-Munk theory of multiple scattering, using the film reflection spectra obtained on black and white backgrounds, was used to find T_i at a light wavelength range of 400 to 700 nm. The measurements were taken six times for each formulation. A D65 illuminant and 10º observer were used to obtain the film's colour coordinates *L** (lightness), *a** (redness-greenness), and *b** (yellowness-blueness) from the infinite reflectance (Freitas et al., 2022).

The film's colour was analysed by means of the psychometric coordinates, Chroma, or saturation (C_{ab}*) (Equation 1), hue angle (h_{ab}*) (Equation 2):

$$C_{ab}^{*} = \sqrt{a^{*2} + b^{*2}} \quad (1)$$

$$h_{ab}^{*} = arctg\left(\frac{b^{*}}{a^{*}}\right) \quad (2)$$

The colour difference between the films containing extract and the extract-free film was also determined though the Total Colour Difference parameter (*ΔE**) (Equation 3).

$$\Delta E^{*} = \sqrt{(\Delta L^{*})^{2} + (\Delta a^{*})^{2} + (\Delta b^{*})^{2}} \quad (3)$$

Where *ΔL**, *Δa** and *Δb** correspond to the differences between the colour parameters of the active and the control films.

2.4.3 Mechanical properties

The thickness of the films was measured using a digital micrometer (Palmer, model COMECTA, Barcelona, accuracy of 0.001 mm) at ten random film positions.

Tensile strength (TS), elastic modulus (EM) and the elongation at break (EB) of the films were determined using a universal test machine (TA.XTplus model, Stable Micro Systems, Haslemere, England) following the standardised ASTM D882 method (ASTM, 2012). The control and active films were cut (2.5 x 10 cm), mounted in the film-extension grips of the testing machine and lengthened at a crosshead speed of 12.5 mm/min until breaking. Eight samples per formulation were evaluated.

2.4.4 Thermal behaviour

A thermogravimetric analyser (TGA 1 Star^{e} System, Mettler-Toledo Inc., Switzerland) was used to measure the thermal stability of the films. The samples (3-5 mg) were placed in an alumina crucible and heated in a single-step thermal program from 25 °C to 700 °C at a heating rate of 10 °C.min^{-1} under a nitrogen flow (10 mL.min^{-1}). The derivative curves (DTGA) of the thermograms were obtained using the STAR^{e} Evaluation Software (Mettler-Toledo, Switzerland). The initial degradation temperature, the temperature at maximum degradation rate and the mass loss percentage in each detected thermal event were determined. The analysis was performed in triplicate for the extract, PEG1000 and PLA films.

Differential scanning calorimetry (DSC) analysis was performed in a differential scanning calorimeter (Star^{e} System, Mettler-Toledo Inc., Switzerland). The film samples (5-7 mg) were placed in aluminium-sealed pans and a five-step thermal program was performed under a nitrogen flow (30 mL.min^{-1}). The samples were heated from -25 to 200 °C at a heating rate of 10 °C.min^{-1}, maintained at 200 °C for 5 min, cooled down to -10 °C at -50 °C.min^{-1}, maintained at -10 °C for 5 min, and heated up again to 200 ºC at a heating rate of 10 °C.min^{-1}. The analysis was performed in triplicate for each film formulation.

2.4.5 Barrier properties

According to ASTM E96/E96M (ASTM, 2005), a gravimetric method, using the modification of McHUGH et al. (1993), was used to determine the water vapour permeability (WVP). The 3.5 cm diameter films were placed on Payne permeability cups (Elcometer SPRL, Hermelle/s Argenteau, Belgium) filled with 5 ml of distilled water (100% relative humidity) and sealed. The cups were placed in a desiccator at 25 °C with $Mg(NO3)_2$ to maintain the relative humidity at 53%. A fan was placed on top of each cup to decrease the resistance to water vapour transport. The cups were weighed every 1.5 hours for 25 h with an analytical balance (± 0.0001 g) and the WVP was calculated from the slope of the weight loss-time curves (Freitas et al., 2021). The analysis was performed in triplicate for each formulation.

The oxygen permeability (OP) was determined following a modified version of the ASTM Standard Method D3985-05 (2010). Three replicates per formulation were measured using an OX-TRAN Model 2/21 ML (Mocon Lippke, Neuwied, Germany) at 25 °C and 53% of RH. The film samples (50 cm^2) were exposed to an oxygen flow and the oxygen transmission was obtained every 15 min until equilibrium was reached. The OP values were calculated by dividing the oxygen transmission by the difference in partial pressure of oxygen between the two sides of the film, and then multiplying by the average film thickness.

2.5 Antioxidant activity of the RS extract and films

The RS extract, and the amount of it released from the films into food simulants, were characterised as to the total phenolic content (TPC) and antioxidant activity. For this, an aqueous solution of freeze-dried extract was prepared at 2.5 $mg.mL^{-1}$. The TPC analysis was carried out in triplicate using a modified version of the Folin-Ciocalteu method (Menzel et al., 2020) and the results were expressed as mg gallic acid equivalent (mg GAE) per g of solid extract.

The antioxidant capacity of the dry RS extract was determined by using the DPPH (2,2-Diphenyl-1-pikryl-hydrazyl) radical scavenging method (Brand-Williams et al., 1995), with some modifications (Freitas et al., 2020). The antiradical activity was evaluated in triplicate by obtaining the EC_{50} parameter, defined as the amount of sample required to reduce the DPPH concentration by 50 % when the reaction stability is reached.

2.6 Release kinetics of antioxidant compounds in food simulants

The release kinetics of the RS extract compounds from the films to different food simulants (A: ethanol 10 % (v/v) and D1: ethanol 50 % (v/v) was analysed following the methodology proposed by Requena et al. (2017), with some modifications. Approximately 2 g of control and active films were cut (1x1 cm squares) and immersed in the corresponding simulant at a ratio of 1:10 and maintained under stirring at 20 °C for 24, 72, 144 and 240 h. After each time, the

liquid was filtered (Filter-Lab, 0.45 µm) and analysed as to TPC and the radical scavenging activity (EC_{50}), as described in section 2.5. All of the experiments were carried out in duplicate. The EC_{50} values were referred per mass unit of extract incorporated into the film (mg of dry extract/mg DPPH).

Peleg´s equation (Equation 4) (Peleg, 1988) was used to model the release kinetics, in terms of percentage of phenolic content released with respect to the total content incorporated into the films (M_t), as a function of time. The initial release rate ($1/k_1$) and the maximum release ratio at equilibrium (EV: $1/k_2$) were obtained from model fitting. This was carried out by non-linear optimisation mode, using the solver tool from Excel.

$$M_t = \frac{t}{k_1 + k_2 t} \quad (4)$$

In order to elucidate the mass transfer mechanisms involved in the extract compound release into each food simulant, the Korsmeyer-Peppas model (Equation 5) (Peppas & Peppas, 1994) was also fitted to the experimental data.

$$\frac{Mt}{M\infty} = kt^n \quad (5)$$

Where M_t/M_∞ is the released ratio at time t with respect to the equilibrium value, k is the release rate constant, involving the diffusion coefficient, and *n* is the transport exponent related to the mass transfer mechanisms.

2.7. Statistical analysis

The statistical analysis was carried out using Minitab 17 Statistical Software. The analysis of variance (ANOVA) and Tukey's studentised range HSD (honestly significant difference) tests were used to check the significant differences between the film treatments, using the least significant difference (α) of 5%. Multifactorial regression models were fitted to describe the release of phenolic compounds and antioxidant activity in different food simulants, considering the extract concentration in PLA films and the contact time with the simulants and interactions between both factors. The goodness of fitted models was verified by the lack-of-fit test, the significance of the coefficients by the Student's t-test (α = 0.05), and the determination coefficient (R^2).

3. RESULTS AND DISCUSSION

3.1 Film characterisation

3.1.1 Microstructural properties

Figure 1 shows the FESEM images of the cross section of the cryo-fractured PLA films incorporating or not the active extract at different concentrations. The control PLA film exhibited a smooth and homogeneous surface pattern, showing brittle and rubbery domains in the polymer matrix, as previously observed by other authors for similar PLA films (Muller et al., 2017b). The plastic fracture observed in the PLA film is characteristic of plasticised amorphous polymers, as previously observed by other authors (Hernández-García et al., 2021; Muller et al., 2017a).

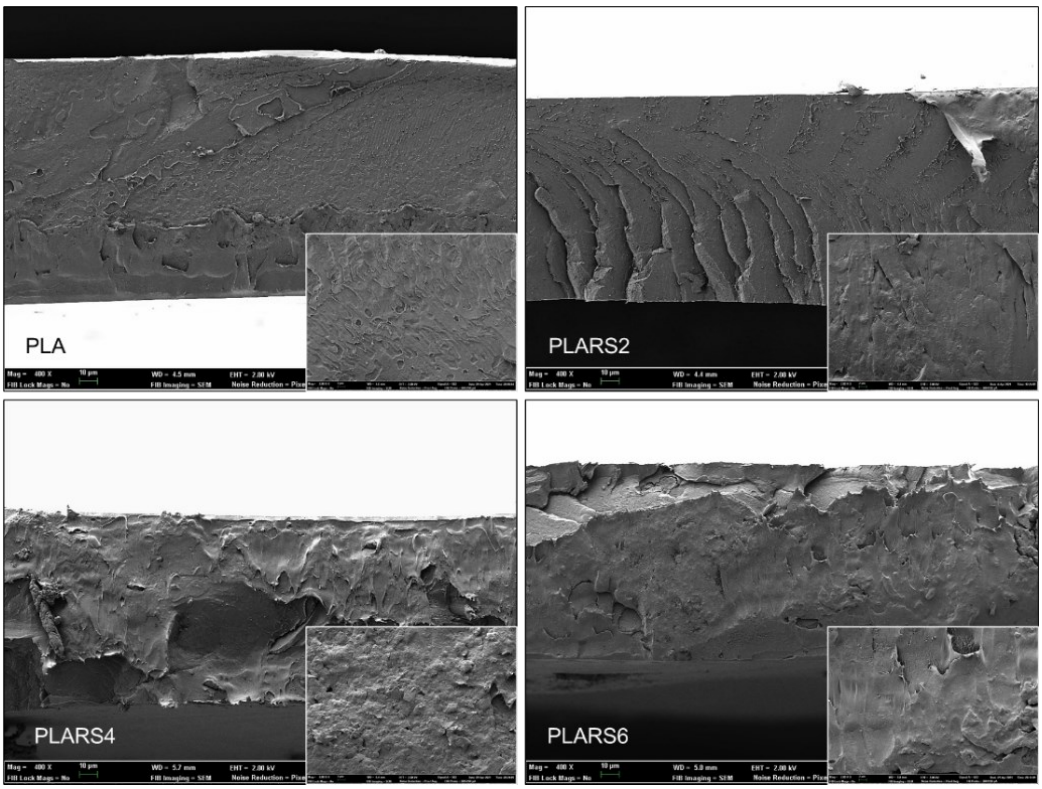

Figure 1. FESEM images of the cross section of PLA films without extract and with different concentrations of RS extract: 2 % wt. (PLARS2), 4 % wt. (PLARS4), and 6 % wt. (PLARS6).

When the RS extract was incorporated into the films, small changes in the internal microstructure were revealed by their different cryo-fracture behaviour, which exhibited areas with a more brittle fracture, as observed by other authors when tannic acid was incorporated into starch-chitosan films (Talón et al., 2017). This suggests the possible establishment of interactions between some of the RS extract components and the PLA/PEG1000 matrix. Menzel et al. (2020) identified several phenolic compounds in the

aqueous RS extract, such as *p*-coumaric, protocatechuic, ferulic, caffeic, vanilinic, tricine, and vanillin acids, which can establish hydrogen bonds with the carbonyl group of PLA chains (Figure 2c). Moreover, as the extract concentration rose in the films, changes in the cross-section appearance were observed along with an increase in the surface roughness. The presence of non-miscible compounds within the polymer matrix produced small aggregates dispersed in the matrix, while both miscible and non-miscible compounds modified the film cryofracture pattern. These differences in the microstructural arrangement in the active films, compared with the control, could affect their physical properties.

3.1.2 Optical properties - Colour and internal transmittance of the active films

The visual appearance of the PLA films is shown in Figure 2a. Observation with the naked eye showed no marked differences in the transparency of the films, whereas the colourless PLA films became more yellow-brown as the RS extract concentration increased, exhibiting small dot-like shapes with a slightly darker colour due to the dispersed solid fraction of the extract, more visible in the most concentrated films. The presence of the coloured compounds and small solid particles affected the colour properties of the samples: typically, the internal transmittance spectrum (T_i) (Figure 2a) and the colour coordinates of the PLA films (Table 2).

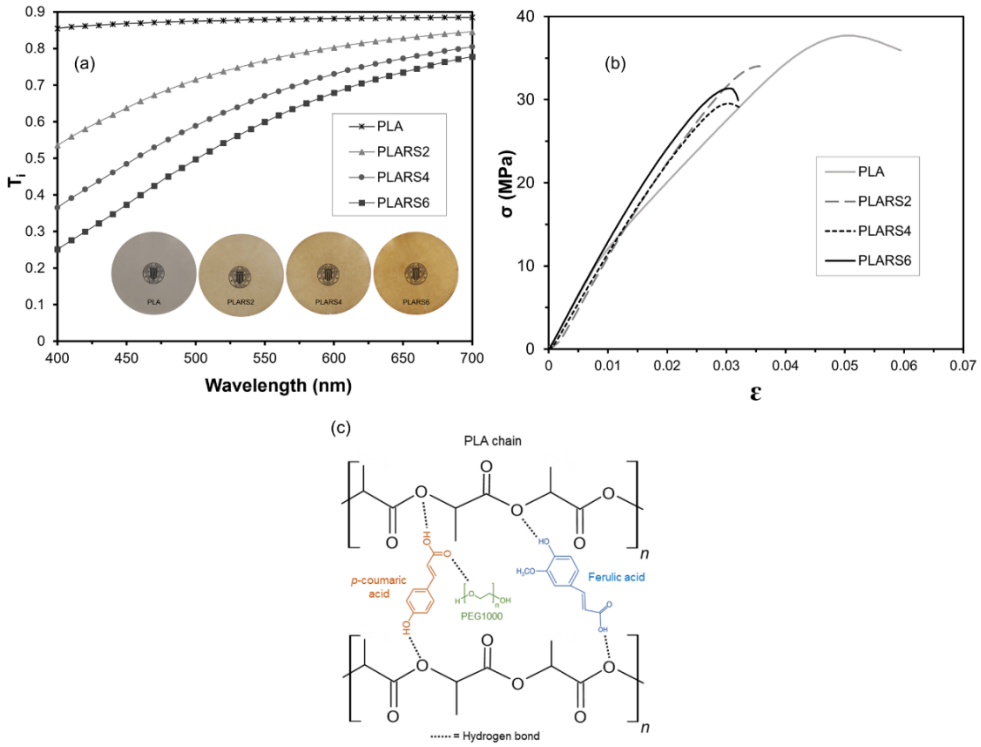

Figure 2. (a) Visual appearance and internal transmittance spectra of films; (b) Stress-strain curves of PLA films with different RS extract concentrations (PLA: control; PLARS2: 2 % wt.; PLARS4: 4 % wt.; PLARS6: 6 % wt.); (c) Possible hydrogen bonds among the phenolic compounds present in the RS extract and polymer chains.

T_i is closely related to the internal microstructure of the polymer matrix and the component arrangement, which will determine the degree of light scattering and the film transparency (Muller et al., 2017a). As shown in Figure 2a, neat PLA films exhibited the highest transmittance values, in coherence with the high film transparency and homogeneity. A gradual decrease in the T_i values was observed when the concentration of the extract rose, in agreement with that observed by other authors when plant extracts were incorporated into polymer matrices (Collazo-Bigliardi et al., 2019; Freitas et al., 2020b). Differences in the T_i values must be attributed to the selective light absorption of the incorporated coloured compounds as well as to the light scattering effect provoked by non-miscible particles in the matrix, thus reducing the light transmission at the corresponding wavelengths.

Table 2 shows the values of colour coordinates for the different films, lightness (L^*), Chroma (C_{ab}^*), hue angle (h_{ab}^*) and the total colour difference (ΔE^*) with respect to the extract free PLA film. The L^* and h^* values progressively decreased ($p<0.05$) as the RS extract rose in the film, whereas the Chroma and total colour difference (ΔE^*) significantly increased. This agrees with the fact that the extract made the films darker and more saturated in a reddish colouration. Menzel et al. (2019) also observed this tendency when incorporating aqueous extracts from sunflower hulls into starch-based films.

Table 2. Optical properties of PLA-based films with different RS extract concentrations (0, 2, 4 or 6 % wt.). L^*: luminosity; C_{ab}^*: chroma; h_{ab}^*: hue; ΔE^*: colour difference. Mean values and standard deviations.

Formulation	L^*	C_{ab}^*	h_{ab}^*	ΔE^*
PLA	90.7 ± 0.2^a	2.50 ± 0.13^a	99.6 ± 0.8^a	-
PLARS2	81.5 ± 0.4^b	18.31 ± 0.50^b	85.6 ± 0.2^b	18.4 ± 0.6
PLARS4	73.8 ± 0.3^c	27.31 ± 0.26^c	80.5 ± 0.1^c	30.1 ± 0.4
PLARS6	67.6 ± 0.7^d	34.70 ± 0.65^d	77.1 ± 0.3^d	39.7 ± 0.6

Different letters in the same column indicate significant differences between films by the Tukey test ($\alpha = 0.05$).

3.1.3 Mechanical properties

Figure 2b shows the typical stress-strain curves of PLA films with and without differing ratios of RS extract. From the curves, the film's mechanical parameters, namely elastic modulus (EM), tensile strength at break (TS), and elongation at break (E%), were obtained and shown in Table 3. As can be observed in Figure 2b, the samples exhibited the typical plastic behaviour, where the most resistant and stretchable sample prior to fracture was the control film without a RS extract. These mechanical parameters slightly worsened in active films, which became more brittle (less extensible with lower resistance to break). This indicates that the

compounds of the RS extract modify the chain interactions in the polymer matrix, regardless of their concentration. Table 3 summarises the values of E%, TS and EM obtained for the different film formulations as well as their thickness. The thicknesses of the different films were not significantly different (*p<0.05*), having an average value of 0.145 mm, in the range of those obtained by Muller et al. (2017b) for the same polymer and process conditions. The addition of the active extract in the polymer matrix provoked a decrease in the E% values of the films (*p<0.05*), regardless of the extract concentration used. Thus, the active films were less stretchable (about 43%) than the control film. This effect was also observed by Jamshidian et al. (2012a) for antioxidant PLA-based films with ascorbyl palmitate and can be attributed to several factors. The potential hydrogen bonds established between the extract phenolic compounds (Figure 2c) and both PEG1000 and PLA chains could reduce the polymer matrix stretchability, while the inter-chain forces could be reduced by the interruptions caused by the presence of other molecules/particles, thus giving rise to less resistant and more brittle matrices. Non-significant differences in the TS values (*p>0.05*) were observed when up to 2 % of the extract was incorporated, while higher concentrations provoked a slight decrease (about 13 %), leading to less resistant films. The interactions between the extract compounds and PLA and PEG1000 chains and the small, dispersed particles could reduce the cohesion forces in the polymer matrix due to steric hindrance for inter-chain forces. The presence of the small particles (compound aggregates) within the polymer matrix, as observed in the FESEM micrographs (Figure 1), could act as stress concentrators, thus decreasing the TS values. Similar results were found by Vilarinho et al. (2021) when incorporating green tea extract into PLA films reinforced with cellulose nanocrystals. In contrast, no notable differences were found between the EM values of the active and control films.

Table 3. Thicknesses, tensile properties (TS, E%, EM), oxygen permeability (OP), and water vapour permeability (WVP) of PLA films containing different RS extract concentrations (PLA: control; PLARS2: 2 % wt.; PLARS4: 4 % wt.; PLARS6: 6 % wt.). Mean values and standard deviations.

Formulation	Thickness (mm)	E (%)	TS (MPa)	EM (MPa)	OP (x10^{12}) ($cm^3.m^{-1}.s^{-1}.Pa^{-1}$)	WVP ($mm.g.kPa^{-1}.h^{-1}.m^{-2}$)
PLA	0.146 ± 0.009^{a}	6.0 ± 0.7^{a}	34 ± 3^{a}	1255 ± 36^{ab}	1.66 ± 0.01^{a}	0.111 ± 0.008^{a}
PLARS2	0.148 ± 0.006^{a}	3.4 ± 0.2^{b}	34.0 ± 1.4^{a}	1288 ± 34^{ab}	1.56 ± 0.04^{a}	0.128 ± 0.005^{ab}
PLARS4	0.145 ± 0.007^{a}	3.4 ± 0.3^{b}	29 ± 3^{b}	1232 ± 25^{b}	1.56 ± 0.03^{a}	0.147 ± 0.004^{bc}
PLARS6	0.142 ± 0.006^{a}	3.1 ± 0.2^{b}	30.7 ± 2.2^{b}	1315 ± 76^{a}	1.53 ± 0.06^{a}	0.151 ± 0.014^{c}

* E%: elongation at break; TS: tensile strength at break; EM: elastic modulus. Different letters in the same column indicate significant differences between films by the Tukey test (α = 0.05).

3.1.4 Barrier properties – Water vapour and oxygen permeability

The WVP and OP values of the different PLA films are summarised in Table 3. The extract-free PLA film exhibited WVP and OP values of 3.14 x 10^{-14} kg.m.Pa^{-1}.s^{-1}.m^{-2} and 1.66 x10^{-18} m^3.m.m^{-2}.s^{-1}.Pa^{-1}, respectively, similar to those found in previous studies (Hosseini et al., 2016; Muller et al., 2017b). The incorporation of the RS extract slightly decreased the barrier capacity of the films to both water vapour and oxygen, although the OP values were not significantly affected. This can be attributed to the decrease in the matrix cohesion forces provoked by the extract, as deduced from the mechanical behaviour. The hydrophilic nature of the RS extract could also contribute to the lower water vapour barrier capacity of the films, promoting the film's water affinity and the permeation of water molecules. Other studies also reported higher WVP values in PLA-based films with bioactive compounds (Vilarinho et al, 2021; Roy & Rhim, 2020; Srisa & Harnkarnsujarit, 2020). Nevertheless, despite the slight worsening in their water vapour barrier capacity, the films incorporating bioactive extracts present interesting properties with the potential to protect packaged foods from oxidation and microbial spoilage.

3.1.5 Thermal behaviour

Figure 3 (a and b) shows the TGA curves and their derivatives (DTGA), obtained for the different films and RS extract and Table 4 summarises the parameters of the thermal degradation events detected for each film formulation: onset (T_o), peak (T_p) and end temperature (T_f), percentage of mass variation (Δm) and residual mass. The thermal degradation of the RS extract was also analysed to better understand its behaviour during the film thermoprocessing and its potential effect on the thermal behaviour of PLA films. As shown in Figure 3 (a and b), the RS extract showed several thermodegradation steps, coherently with its complex composition: a first step, between 45 and 130 °C, that can be mainly attributed to water loss (mass loss of around 6 %) and several steps above 130 °C, which can be attributed to the degradation of the different components present in the extract. These results suggested that a fraction of the extract is likely degraded during the film manufacturing process (160 ºC) in agreement with that reported by other authors (Menzel et al., 2019). The great residual mass of the extract (around 20 %) suggested that it contains a high percentage of silica and other minerals from RS (Chen et al., 2011).

As concerns the TGA analysis of the films (Figure 3a), all of the samples exhibited a single degradation step starting at about 190 °C in the extract-free PLA and 235 °C in films with the RS extract, with a total mass loss of over 95-98 %. The temperature at which the maximum degradation rate may be found (T_p in Table 4) is significantly reduced when the RS extract is present in the films. This indicates that the RS extract compounds affect the thermodegradation of PLA, which could be attributed to their interference with the interchain forces affecting the matrix cohesion and compactness, as deduced from the tensile and barrier

properties. Likewise, the presence of several types of phenolic acids in the RS extract (Menzel et al. 2020; Elzaawely et al., 2017) could favour the partial hydrolysis of PLA into low molecular weight compounds, thermally less stable, thus lowering the degradation temperatures. In contrast, the thermal degradation of the extract-free PLA film started earlier (lower T_o) than the films with the RS extract (Figure 3b). This could be attributed to the initial thermal degradation of the plasticiser PEG1000 (T_o: 160 °C, T_p: 300 °C), as observed in its TGA and DTGA curves embedded into Figure 3a, which seems not to occur in films containing the RS extract. This suggests that PEG could also interact with the extract components, promoting its thermal stability and delaying its degradation at higher temperatures. There was no significant difference in the residual mass of the films (< 1 %) despite the different RS extract concentration with notable residual mass. This can be explained by the relatively low amount of RS extract present in every formulation, which not significantly affect the overall residue of the films.

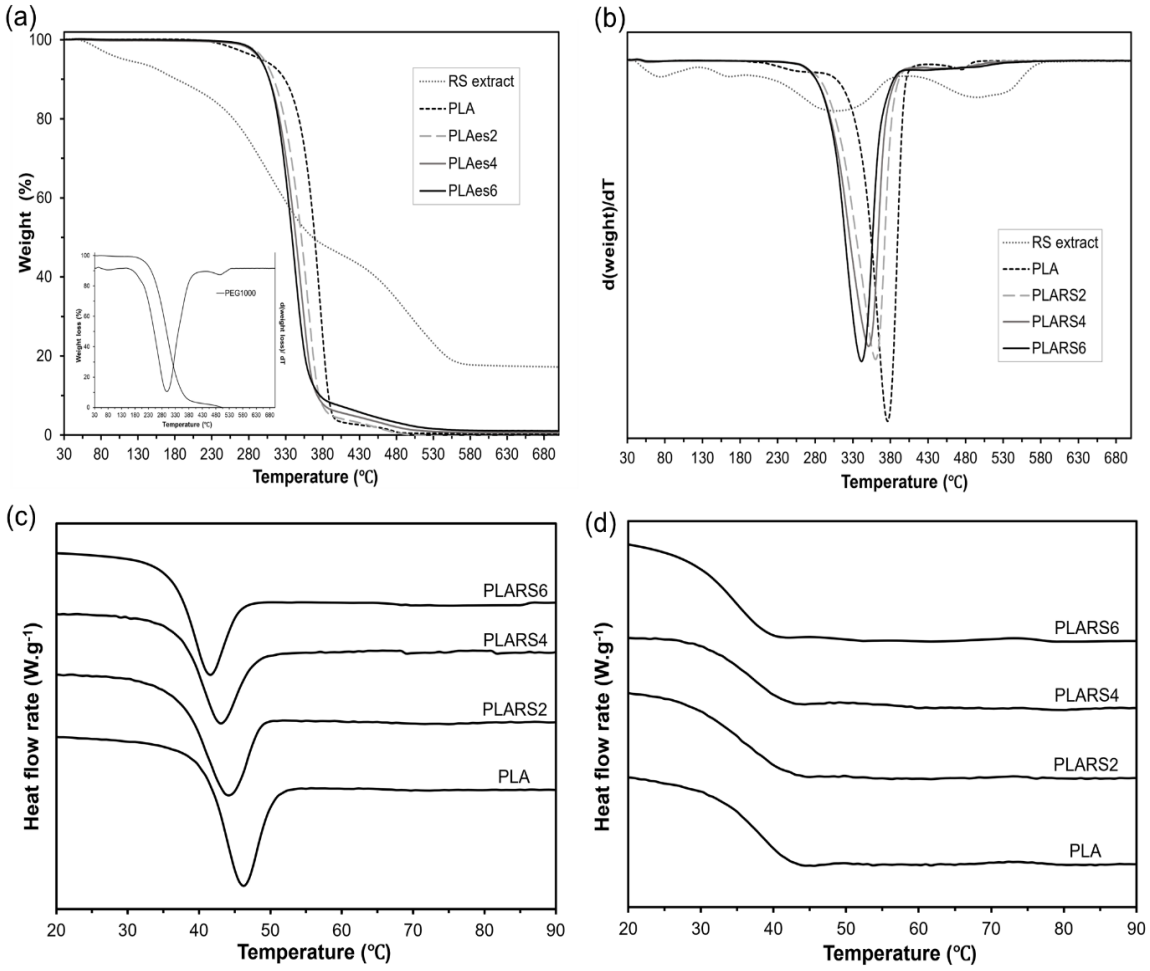

Figure 3. TGA curves (a), DTGA derivative curves (b), and DSC (c: first heating, d: second heating) thermograms of PLA films with different RS extract concentrations (PLA: control; PLARS2: 2 %; PLARS4: 4 %; PLARS6: 6 % wt.).

The glass transition temperature (T_g) of the PLA in every film was analysed by DSC. Thermograms of the first and second heating scans of the different films are shown in Figures 3c and 3d, respectively, where the relaxation endotherms, associated with the ageing of the polymer, can be observed in the first scan in the glass transition region. Table 4 shows the values of T_g obtained from the second heating scan, where thermal history is erased, and the relaxation enthalpy obtained from the first heating scan. The PLA control film showed a T_g value of 37.7 °C, similar to that reported by other authors for PEG 1000 plasticised amorphous PLA (Muller et al., 2017b). The T_g values of active films tended to decrease slightly when the RS extract rose in the films, although the differences were not statistically significant. Likewise, as the extract concentration increased, the polymer relaxation enthalpy (expressed per gram of polymer) significantly decreased ($p<0.05$), which suggests that extract compounds also inhibited the degree of PLA chain reassociation during ageing to some extent.

Therefore, the incorporation of the RS extract into PLA films, at the concentration levels used, partially limits the interchain forces in the PLA matrix, making the polymer matrix slightly less cohesive, as reflected in the decrease in the film's mechanical resistance, extensibility and barrier capacity, and the small changes in the thermal behaviour. Nevertheless, the observed changes were no remarkable to compromise the food packaging requirements of films, including thermal, barrier, and mechanical performance. In this sense, besides exhibiting suitable functionality for packaging purposes, the potential antioxidant capacity of the films can be considered an important improvement for food preservation purposes.

Table 4. Thermal degradation parameters (onset (T_o), end (T_e) and peak (T_p) temperatures, mass loss (ΔM), and residual mass) of the films and DSC parameters (relaxation enthalpy -ΔH_{relax}- from the first heating scan, and glass transition temperature (T_g) from the second heating scan). (PLA: control; PLARS2: 2 % wt..; PLARS4: 4 % wt.; PLARS6: 6 % wt.).

	TGA					DSC	
Formulation	**T_o (°C)**	**T_e (°C)**	**T_p (°C)**	**Δm (%)**	**Residue (%)**	**ΔH_{relax} (J/g)**	**T_g**
PLA	190 ± 6^{b}	495 ± 1^{a}	376 ± 1^{a}	97.3 ± 0.1^{a}	0.4 ± 0.2^{a}	5.4 ± 0.1^{a}	38 ± 3^{a}
PLARS2	237 ± 2^{a}	511 ± 1^{b}	361 ± 2^{b}	96.4 ± 0.2^{b}	0.5 ± 0.1^{a}	4.3 ± 0.8^{ab}	36 ± 2^{a}
PLARS4	239 ± 4^{a}	535 ± 4^{c}	351 ± 1^{c}	94.2 ± 0.1^{c}	0.6 ± 0.6^{a}	3.1 ± 0.1^{b}	36 ± 2^{a}
PLARS6	234 ± 1^{a}	566 ± 3^{d}	342 ± 1^{d}	98.5 ± 0.2^{d}	1.1 ± 0.3^{a}	3.4 ± 0.1^{b}	34 ± 2^{a}

Different letters in the same column indicate significant differences between films by the Tukey test (α = 0.05).

3.2 Antioxidant properties of the PLA films containing RS extract

The antioxidant capacity of the films was analysed through the release study of potentially active compounds of RS extracts into food simulants of differing polarities that can emulate

foods systems with different fat contents (Requena et al. 2017). The antioxidant capacity of the RS extract was first analysed through its TPC and DPPH radical scavenging capacity. Afterwards, these activities were analysed in the simulants in contact with the films for different times, where differing extents of the potentially active compounds were released.

3.2.1 Content of phenolic compounds and DPPH radical scavenging capacity of RS

The RS extract obtained via aqueous extraction by reflux heating for 1 h after 30 min US pre-treatment was selected on the basis of a previous study where these conditions gave rise to a phenolic-rich extract with high DPPH radical scavenging capacity (Freitas et al. 2020). The value of TPC obtained in the dry extract was 37.1 ± 0.4 mg GAE/g. This value is higher than that obtained by Menzel et al (2020) in rice straw, using aqueous extraction at room temperature (29 mg GAE/g dry extract). These authors reported that the most abundant phenolic compounds analysed in the rice straw extract were ferulic, protocatechuic and *p*-coumaric acids.

As concerns the DPPH radical scavenging capacity of the RS extract, the EC_{50} value obtained was 6.3 ± 0.3 mg freeze-dried extract/mg DPPH, in agreement with that previously reported for the same extraction conditions (Freitas et al., 2020). This value was a great deal lower (greater antioxidant activity) than that found by Menzel et al., (2020) for the RS extracts obtained at room temperature using water, methanol and ethanol as solvents (12, 20 and 19 mg freeze-dried extract/mg DPPH, respectively). This indicates that the use of US and high temperatures in water extraction promoted the release of highly antioxidant phenolic compounds with potential applications as food antioxidants. Ultrasound provokes an increase in the contact points between the RS matrix and the solvent, caused by collisions between the particles and the shock waves created by the collapse of cavitation bubbles in the liquid, consequently increasing the solid transfer from the RS to the solvent (Cheung & Wu, 2013; Hayat et al., 2019). Furthermore, when heat treatment is applied, the plant tissue becomes softened, which reduces its integrity and weakens the bonds between phenolics and the plant matrix, enhancing the extraction yield. Indeed, Li et al. (2015) stated that extracting phenolic compounds from a plant matrix is achieved when there is a disruption of the ester and ether bonds between the analyte and the lignocellulosic fraction.

3.2.2 Release kinetics of antioxidant compounds into food simulants

The release of these active compounds is needed for them to exert the protective action in the target substrate. The analyses of TPC and antioxidant capacity at different times of film immersion in two food simulants (A: 10 % ethanol, and D1: 50 % ethanol) would permit the prediction of the antioxidant capacity of the different films when applied as packaging systems on different foods. Figure 4 shows the percentage of TPC released in both simulants, with respect to the TPC present in the film with the incorporated RS extract. As expected, the total

amount of released phenolic increased as the contact times lengthened and it was higher when the extract concentration in the films rose, according to the higher driving force for mass transfer (greater concentration gradient).

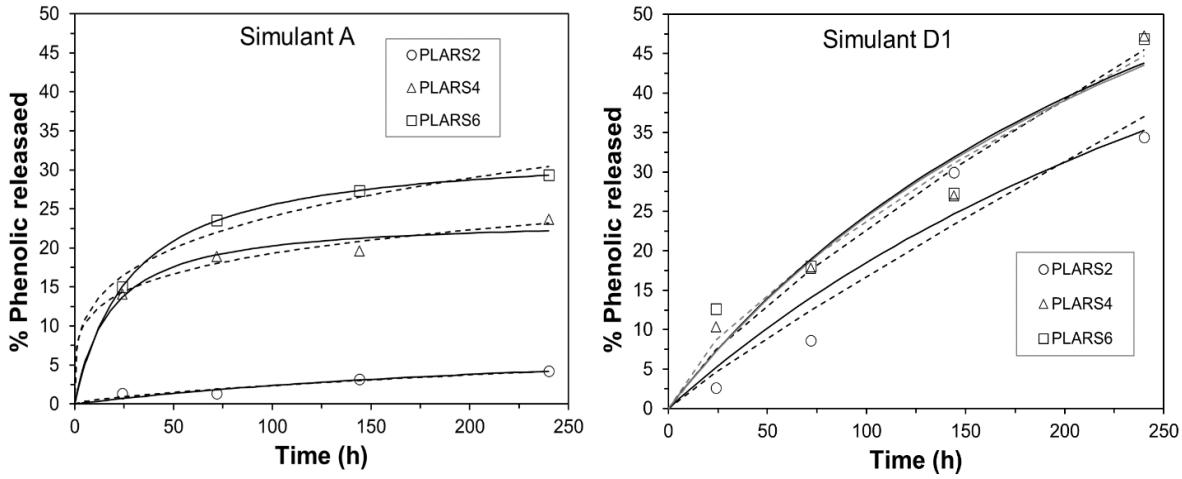

Figure 4. Percentage of total phenolic released from active films as a function of time for simulants A and D: experimental data (points) and the Peleg (continuous lines) and Korsmeyer-Peppas (dashed lines) fitted models.

The release pattern was also affected by the type of simulant. Thus, the phenolic compounds were released faster and at a higher ratio into simulant D1, whereas in the more polar simulant A, the process was more limited, almost reaching a plateau level after 2 contact days, with a very low percentage of compounds released, especially in the case of the films with the lowest extract ratio. In contrast, simulant D1 (50 % ethanol) favoured the release of greater amounts of phenolic compounds, with scarcely any differences between films with differing extract ratios. This variation in release behaviour is coherent with that observed by other authors analysing the release behaviour of different antioxidants from PLA, which was greatly promoted by the ethanol ratio in the food simulant (Jamshidian et al., 2012b). The compound's chemical affinity with the polymer matrix and its solubility in the simulant define the partition coefficient at equilibrium. In this sense, the main phenolic compounds of aqueous RS extract, as determined by Menzel et al, (2020) are ferulic, *p*-coumaric and protocatechuic acids, which are more soluble in ethanol than in water. Thus, the increase of ethanol ratio in the simulant will promote the solubility of these phenolic acids. It is worth mentioning that the nature of the phenolic compounds released in each simulant could be different, being the phenolic compounds released in simulant A more polar than in simulant D1. Likewise, the distinct profiles of phenolic compounds released would lead to different bioactivity of the material due to both the total amount and nature of the released compounds. In addition to the differences in compound solubility, changes in the polymer matrix in contact with the liquid phase also affected the release behaviour. Thus, the higher ethanol ratio of simulant D1 permitted the penetration of ethanol into the matrix, provoking

swelling and the relaxation of the hydrophobic PLA matrix (Sato et al., 2013), which could favour the release of the compound into the simulant, attaining higher percentages of released phenolics. In contrast, the high polarity of simulant A (10 % ethanol) makes it difficult for the hydrophobic film to swell, leading to reduced release rates.

The parameters obtained by fitting the Peleg's equation are shown in Table 5, where the values of the determination coefficient (R^2) were also included. As expected, the initial release rate ($1/k_1$) increased when the extract concentration rose in the film and was similar for 4 and 6 % of extract in both simulants. The lowest release rate was obtained for films with 2% of RS extract, especially in simulant A. The equilibrium values (EV=1/k2) in simulant A also increased when the extract concentration rose (9-33 % release), whereas a complete release was estimated at infinite time (EV value) in simulant D1. In fact, this value must be limited to 100 % in the optimisation process of the model parameters. The obtained results point to an enhancement in both the release ratio and rate when the extract concentration was higher than 2 %, which can also be attributed to the more open PLA matrix (weaker interchain forces) promoted by the presence of higher extract ratio in the matrix.

The parameters obtained by fitting the Korsmeyer-Peppas model in each food simulant, are also shown in Table 5. The values of n coefficient were equal to or lower than 0.5 for data obtained in simulant A, thus indicating that Fickian or quasi-Fickian diffusion mechanisms are involved in the release of the phenolic compounds from the PLA matrix. Nevertheless, films in the simulant that is richer in ethanol (D1) exhibited n values of over 0.5, attributed to anomalous transport where the compound diffusion is coupled with the polymer relaxation brought about by the effect of the solvent (Peppas & Brannon-Peppas, 1994). This confirms the hypothesised role of ethanol penetrating and swelling the PLA matrix, thus favouring the mass transfer rate by an anomalous mass transport mechanism where the polymer relaxation enhances the compound diffusion. Additionally, the hydrolytic degradation of the PLA matrix in the presence of ethanol has been described by other authors (Iñiguez-Sancho et al., 2016), which will also contribute to the promotion of mass transfer processes. This hydrolysis has been found to be much faster in 50 % ethanol-aqueous solutions than in 95% ethanol or pure water. The creation of free volume due to the penetration of ethanol provoked the polymer swelling, thus allowing for more water molecules to diffuse into the PLA matrix, which accelerates the polymer hydrolysis rate up to 3.7 times in comparison with pure water (Tsuji, 2010; Iñiguez-Sancho et al., 2016). Nevertheless, all the films maintained their physical integrity throughout the entire experiment, despite changing their appearance, depending on the PLA matrix alteration.

Therefore, the different chemical interactions of the extract compounds with the PLA matrix and the degree of relaxation of the polymeric matrix in contact with the solvent affected the release kinetic parameters. Thus, the amount released at equilibrium was higher in simulant

D1, which contains a higher proportion of ethanol, as also observed by other authors (Jamshidian et al., 2012b) studying PLA films containing different antioxidants. So, the maximum percentage of phenolic released was found in simulant D1 for films with higher extract concentrations. In real food systems, different food-PLA interactions could be expected, which would also affect the compound's release and the antioxidant's effectiveness.

The antioxidant capacity of the films was also analysed through the EC_{50} parameter. This indicates the DPPH radical scavenging capacity of the films, representing the amount of sample required to reduce the DPPH concentration by 50 % when the reaction stability is reached; so, the lower the value, the higher the radical scavenging capacity. To compare the EC_{50} values obtained at different contact times in both simulants with the value of pure extract, the EC_{50} was expressed as equivalent mg extract/mg DPPH, considering the amount of extract incorporated in each film. Figure 5 shows the EC_{50} values of the films *vs.* contact time, where the progressive decrease in EC_{50} was obtained as the release progressed. Therefore, the radical scavenging capacity increased in line with the release of the extract compound; however, in no case did the values reach those of the pure extract, always showing higher EC_{50} values (Figure 5). However, as the contact time lengthened in simulant A, the films with 6 % extract exhibited similar EC_{50} values to the films in simulant D1, in the range of 15 mg extract/mg DPPH. In contrast, the films with 2 and 4 % of extract in simulant A reached asymptotic values of about 30 mg extract/mg DPPH, which even rose at final times when the extract content was 2 %, probably due to the oxidative degradation of the released compounds. Therefore, the radical scavenging capacity of the films with 6 % RS extract was similar at relatively short contact times (150 h), regardless of the type of substrate in contact. The obtained results indicate that the compounds responsible for the radical scavenging capacity were not completely released from the films or were partially degraded during thermal processing, although there was notable activity (EC_{50} = 12 mg incorporated extract/mg DPPH) after about 150 h contact time in different simulated food systems when the films contained 6 % of extract. Differences in the amount of phenolic compounds released did not explain the almost constant radical scavenging capacity, which suggests that this capacity was not only related with the total phenolic compounds estimated by the Folin-Ciocalteu method. For comparison purposes, the EC_{50} values of typical strong antioxidants, such as ascorbic acid or α-tocopherol, are 0.12 and 0.26 mg compound /mg DPPH, respectively (Brand-Williams et al., 1995).

Table 5. Parameters of the Peleg and Korsmeyer-Peppas models obtained for simulants A (10 % ethanol aqueous solution) and D1: (50 % ethanol aqueous solution) for the films with differing concentrations of RS extract.

	Peleg Model						Korsmeyer-Peppas Model					
	Simulant A			Simulant D1			Simulant A			Simulant D1		
Treatment	k_1	*EV*	R^2	k_1	*EV*	R^2	*n*	*k*	R^2	*n*	*k*	R^2
PLARS2	31.5	9.4	0.936	4.4	100	0.937	0.66	0.012	0.950	0.91	0.003	0.933
PLARS4	0.74	23.9	0.985	3.1	100	0.964	0.21	0.307	0.992	0.79	0.006	0.982
PLARS6	0.86	32.8	0.999	3.1	100	0.951	0.27	0.212	0.989	0.71	0.009	0.971

The antioxidant capacity of the films was also analysed through the EC_{50} parameter. This indicates the DPPH radical scavenging capacity of the films, representing the amount of sample required to reduce the DPPH concentration by 50 % when the reaction stability is reached; so, the lower the value, the higher the radical scavenging capacity. To compare the EC_{50} values obtained at different contact times in both simulants with the value of pure extract, the EC_{50} was expressed as equivalent mg extract/mg DPPH, considering the amount of extract incorporated in each film. Figure 5 shows the EC_{50} values of the films *vs.* contact time, where the progressive decrease in EC_{50} was obtained as the release progressed. Therefore, the radical scavenging capacity increased in line with the release of the extract compound; however, in no case did the values reach those of the pure extract, always showing higher EC_{50} values (Figure 5). However, as the contact time lengthened in simulant A, the films with 6 % extract exhibited similar EC_{50} values to the films in simulant D1, in the range of 15 mg extract/mg DPPH. In contrast, the films with 2 and 4 % of extract in simulant A reached asymptotic values of about 30 mg extract/mg DPPH, which even rose at final times when the extract content was 2 %, probably due to the oxidative degradation of the released compounds.

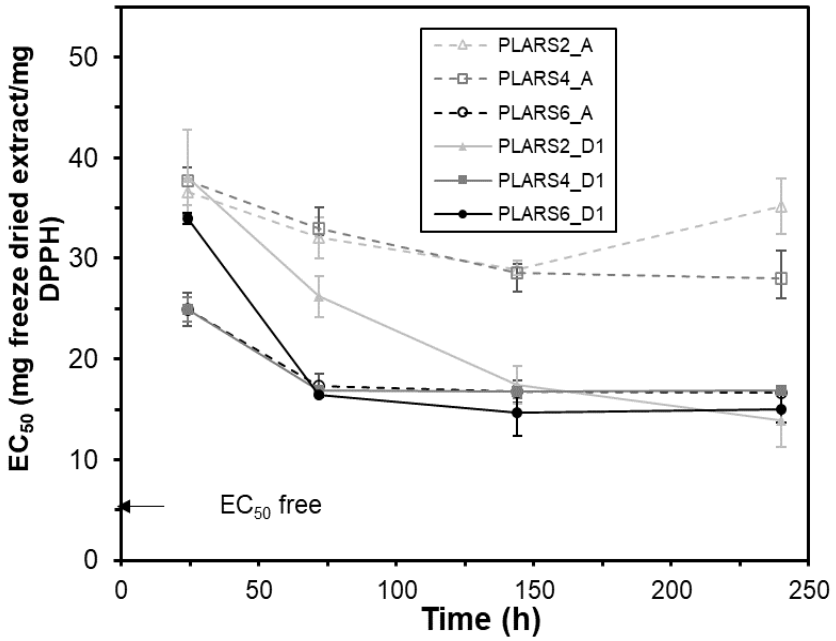

Figure 5. EC_{50} values for the active films in simulants A and D1 over time. An arrow in the bottom right-hand corner of the graph shows the value of EC_{50} for the free extract (6.3 ± 0.3 mg dry extract/ mg DPPH).

Therefore, the radical scavenging capacity of the films with 6 % RS extract was similar at relatively short contact times (150 h), regardless of the type of substrate in contact. The obtained results indicate that the compounds responsible for the radical scavenging capacity were not completely released from the films or were partially degraded during thermal

processing, although there was notable activity (EC_{50} = 12 mg incorporated extract/mg DPPH) after about 150 h contact time in different simulated food systems when the films contained 6 % of extract. Differences in the amount of phenolic compounds released did not explain the almost constant radical scavenging capacity, which suggests that this capacity was not only related with the total phenolic compounds estimated by the Folin-Ciocalteu method. For comparison purposes, the EC_{50} values of typical strong antioxidants, such as ascorbic acid or α-tocopherol, are 0.12 and 0.26 mg compound /mg DPPH, respectively (Brand-Williams et al., 1995).

3.2.3. Surface response for the antioxidant capacity of the films

In order to obtain a practical model that allows for estimating the released phenolic ratio and the radical scavenging capacity (EC_{50}) as a function of both contact time and extract concentration in the film, multifactorial regression models were also obtained, and the corresponding surface response (Figure 6). The regression equations 7 and 8 explained 98 % and 93 % of the variation in %GAE for simulants A and D1, respectively. Likewise, the radical scavenging capacity of the released compounds (EC_{50} parameter), expressed as mg film/mg DPPH were described by Equations 9 and 10, explaining 97 % and 91 %, respectively, in A and D1 simulants, of total EC_{50} variation.

$$\hat{Y}_{\%GAE}(Simulant\ A) = 0.040t - 0.0002t^2 + 15.745x - 1.478x^2 + 0.011xt - 26.87 \quad (7)$$

$$R^2 = 0.98$$

$$\hat{Y}_{\%GAE}(Simulant\ D1) = 0.162t + 7.940x - 0.763x^2 - 13.340 \quad (8)$$

$$R^2 = 0.93$$

The radical scavenging capacity of the released compounds determined by the EC_{50} parameter, expressed as mg film/mg DPPH, were described by Equations 9 and 10 in the different simulants, in terms of contact time and extract concentration in the film.

$$\hat{Y}_{EC50}(Simulant\ A) = -6.030t - 0.020t^2 - 768.7x + 50.30x^2 + 3459 \quad (9)$$

$$R^2 = 0.97$$

$$\hat{Y}_{EC50}(Simulant\ D1) = -13.780t - 0.023t^2 - 1015x + 80.10x^2 + 1.241xt + 3889 \quad (10)$$

$$R^2 = 0.91$$

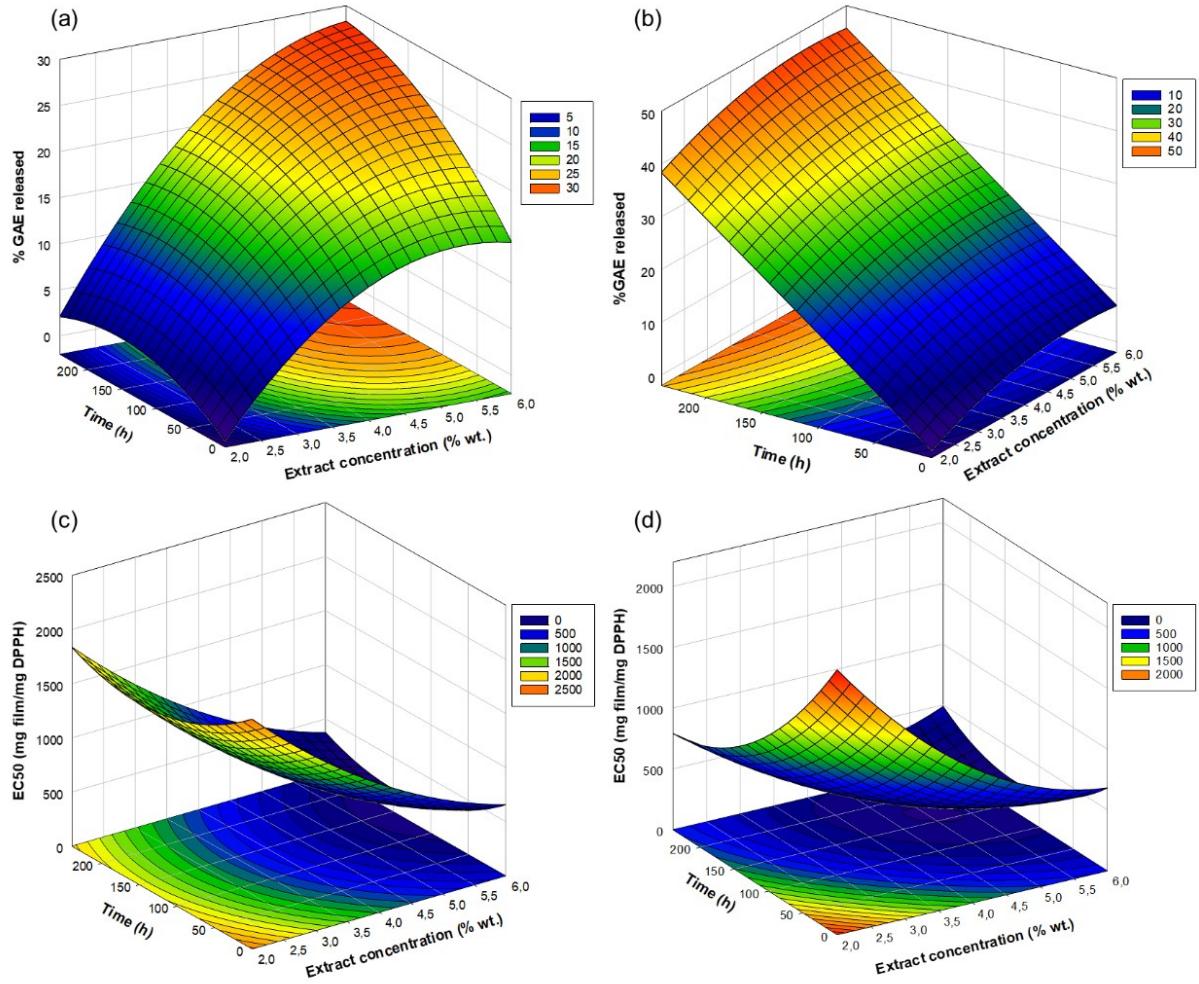

Figure 6. Response surface plots from the fitted regression models for %GAE released in simulant A (a) and D1 (b), and EC_{50} of the PLA films in the simulants A (c) and D1 (d).

Figure 6 clearly shows that, from 150 h contact time onwards, the films with the highest extract concentration in simulant A exhibited antioxidant capacity similar to that in contact with simulant D1, as commented on above. This indicates that, despite the greater release of total phenolics in simulant D1, the phenolics released in simulant A exhibited high antioxidant potential; the greater the amount of extract incorporated into the polymer matrix, the greater the degree of similarity between the antioxidant potential of the films in both simulants.

The maximum release of phenolic compounds and the minimum value of EC_{50} (maximum radical scavenging capacity) were obtained from the obtained functions. Thus, in simulant A, the optimal film formulation was that containing 6 % wt. extract, with a maximum phenolic release of 30.4 % of GAE at the final time (240 h), exhibiting the maximum radical scavenging capacity (EC_{50} = 209 mg film/ mg DPPH) at 148 h contact time. In simulant D1, the optimal films would contain 5.1 % extract, which released 46.1 % GAE at the final time (240 h), exhibiting the maximum radical scavenging capacity (EC_{50} = 201 mg film/mg DPPH) at 159 h

contact time. Therefore, films with an extract concentration of nearly 6 % exhibited a very similar radical scavenging capacity in both simulants after approximately 150 h contact time; this suggests that this extract concentration in the films ensures their potential antioxidant capacity in food systems regardless of their polar nature, despite the fact that the release of phenolic compounds would be greater in less polar substrates. To sum up, both time and extract concentration in the film affected the amount of phenolic compounds released and the potential radical scavenging capacity of films, but the latter reached an almost constant value from about 150 h contact time onwards for films with an extract concentration of nearly 6 %. So, these PLA films could be used as biodegradable active packaging materials with antioxidant capacity in both aqueous foods (simulant A) or more fatty foods, such as oil-in water emulsions (simulant D1).

4. CONCLUSIONS

The rice straw aqueous extract obtained by an ultrasound-assisted and reflux-heating process had remarkable phenolic content and radical scavenging capacity. Its incorporation into PLA films turned them a little brown while slightly modifying the polymer chain arrangement and strength of the matrix, which promoted a small loss in the film stretchability, resistance to break, barrier capacity and PLA thermostability. However, the films gained antioxidant capacity when the extract was incorporated. The phenolic components incorporated into the extract were able to be released, depending on the extract concentration in the films, the food simulant polarity and contact time. In the ethanol-rich simulant (D1), the total content of phenolics could be released at equilibrium, whereas only 33 % at most could be released in the most aqueous simulant (A). The radical scavenging capacity of the films, referred per mass unit of incorporated dry extract, reach asymptotic values from about 150 h contact time onwards; these were lower than those of the pure extract, but films with an extract concentration of nearly 6 % exhibited very similar values in both simulants. This suggests that this extract concentration in the films ensures their potential antioxidant capacity in food systems regardless of their polar nature. No good correlation between the amount of phenolic compounds released and the radical scavenging capacity was found, which suggests that other extract compounds contributed to this capacity of the films. So, PLA films incorporating about 6 % of rice straw extract could be used as biodegradable active packaging material with interesting antioxidant capacity in both aqueous foods (simulant A) and more fatty products, such as oil-in water emulsions (simulant D1). Further studies will be carried out to verify their potential antioxidant efficiency in different real food systems.

5. ACKNOWLEDGEMENTS

The authors thank the Agencia Estatal de Investigación (Spain) for the financial support through projects PID2019-105207RB-I00/AEI/10.13039/501100011033 and Generalitat Valenciana [grant number GrisoliaP/2019/115].

6. REFERENCES

ASTM. (2005). E96/E96M-05. Standard Test Methods for Water Vapor Transmission of Materials. American Society for Testing and Materials, 1-11.

ASTM. (2010). D3985-05 Oxygen Gas Transmission Rate Through Plastic Film and Sheeting Using a Coulometric Sensor. Annual Book of ASTM Standards, C, 1–7. https://doi.org/10.1520/D3985-05.2

ASTM. (2012). ASTM D882-12 Standard test method for tensile properties of thin plastic sheeting. American Society for Testing and Materials, 12.

Abbasi-Parizad, P., De Nisi, P., Scaglia, B., Scarafoni, A., Pilu, S., & Adani, F. (2021). Recovery of phenolic compounds from agro-industrial by-products: Evaluating antiradical activities and immunomodulatory properties. *Food and Bioproducts Processing*, 127, 338–348. https://doi.org/10.1016/j.fbp.2021.03.015

Avérous, L., Fringant, C., & Moro, L. (2001). Plasticized starch–cellulose interactions in polysaccharide composites. *Polymer*, 42(15), 6565–6572. https://doi.org/10.1016/S0032-3861(01)00125-2

Balaji, A. B., Pakalapati, H., Khalid, M., Walvekar, R., & Siddiqui, H. (2018). Natural and synthetic biocompatible and biodegradable polymers. In Biodegradable and Biocompatible Polymer Composites (pp. 3–32). Elsevier. https://doi.org/10.1016/B978-0-08-100970-3.00001-8

Barana, D., Salanti, A., Orlandi, M., Ali, D. S., & Zoia, L. (2016). Biorefinery process for the simultaneous recovery of lignin, hemicelluloses, cellulose nanocrystals and silica from rice husk and Arundo donax. *Industrial Crops and Products*, 86, 31–39. https://doi.org/10.1016/j.indcrop.2016.03.029

Bassani, A., Montes, S., Jubete, E., Jesus, P., Sanjuán, A. P., Spigno, G. (2019). Incorporation of waste orange peels extracts into PLA films. *Chemical Engineering transactions*, 74, 1063-1068. https://doi.org/10.3303/CET1974178

Botterweck, A. A. M., Verhagen, H., Goldbohm, R. A., Kleinjans, J., & van den Brandt, P. A. (2000). Intake of butylated hydroxyanisole and butylated hydroxytoluene and stomach cancer risk: Results from analyses in the Netherlands Cohort Study. *Food and Chemical Toxicology*, 38(7), 599–605. https://doi.org/10.1016/S0278-6915(00)00042-9

Brand-Williams, W., Cuvelier, M. E., & Berset, C. (1995). Use of a free radical method to evaluate antioxidant activity. *LWT - Food Science and Technology*, 28(1), 25–30. https://doi.org/10.1016/S0023-6438(95)80008-5

Chen, X. (2011). Study on structure and thermal stability properties of cellulose fibers from rice straw. *Carbohydrate Polymers*, 6.

Cheung, Y.-C., & Wu, J.-Y. (2013). Kinetic models and process parameters for ultrasound-assisted extraction of water-soluble components and polysaccharides from a medicinal fungus. *Biochemical Engineering Journal*, 79, 214–220. https://doi.org/10.1016/j.bej.2013.08.009

Collazo-Bigliardi, S., Ortega-Toro, R., & Chiralt, A. (2019). Improving properties of thermoplastic starch films by incorporating active extracts and cellulose fibres isolated from rice or coffee husk. *Food Packaging and Shelf Life*, 22, 100383. https://doi.org/10.1016/j.fpsl.2019.100383

Delgado-Ospina, J., Lucas-González, R., Viuda-Martos, M., Fernández-López, J., Pérez-Álvarez, J. Á., Martuscelli, M., & Chaves-López, C. (2021). Bioactive compounds and techno-functional properties of high-fiber co-products of the cacao agro-industrial chain. Heliyon, 7(4), e06799. https://doi.org/10.1016/j.heliyon.2021.e06799

Derrien, M., Badr, A., Gosselin, A., Desjardins, Y., & Angers, P. (2017). Optimization of a green process for the extraction of lutein and chlorophyll from spinach by-products using response surface methodology (RSM). *LWT - Food Science and Technology*, 79, 170–177. https://doi.org/10.1016/j.lwt.2017.01.010

El-Tayeb, T. S., Abdelhafez, A. A., Ali, S. H., & Ramadan, E. M. (2012). Effect of acid hydrolysis and fungal biotreatment on agro-industrial wastes for obtainment of free sugars for bioethanol production. *Brazilian Journal of Microbiology*, 43(4), 1523–1535. https://doi.org/10.1590/S1517-83822012000400037

Elzaawely, A. A., Maswada, H. F., El-Sayed, M. E. A., & Ahmed, M. E. (2017). Phenolic Compounds and Antioxidant Activity of Rice Straw Extract. *International Letters of Natural Sciences*, 64, 1–9. https://doi.org/10.18052/www.scipress.com/ILNS.64.1

European Bioplastics, nova-Institute (2020). Bioplastics market data. [Web page] Recovered 1st April of 2021 from https://www.european-bioplastics.org/market/

FAOSTAT. (n.d.). Retrieved November 4, 2020, from http://www.fao.org/faostat/en/#data/QC/visualize

Freitas, P. A. V., de Oliveira, T. V., Silva, R. R. A., Fialho e Moraes, A. R., Pires, A. C. dos S., Soares, R. R. A., Junior, N. S., & Soares, N. F. F. (2020). Effect of pH on the intelligent film-forming solutions produced with red cabbage extract and hydroxypropylmethylcellulose. *Food Packaging and Shelf Life*, 26, 100604. https://doi.org/10.1016/j.fpsl.2020.100604

Freitas, P. A. V., González-Martínez, C., & Chiralt, A. (2020). Application of Ultrasound Pre-Treatment for Enhancing Extraction of Bioactive Compounds from Rice Straw. *Foods*, 9(11), 1657. https://doi.org/10.3390/foods9111657

Freitas, P. A. V., La Fuente Arias, C. I., Torres-Giner, S., González-Martínez, C., Chiralt, A. (2021). Valorization of Rice Straw into Cellulose Microfibers for the Reinforcement of Thermoplastic Corn Starch Films. *Applied Sciences*, 11, https://doi.org/10.3390/app11188433

Freitas, P. A. V., González-Martínez, C., & Chiralt, A. (2022). Applying ultrasound-assisted processing to obtain cellulose fibres from rice straw to be used as reinforcing agents. *Innovative Food Science & Emerging Technologies*, 76, https://doi.org/10.1016/j.ifset.2022.102932

Han, J.-W., Ruiz-Garcia, L., Qian, J.-P., & Yang, X.-T. (2018). Food Packaging: A Comprehensive Review and Future Trends: Food packaging: Review and future trend. *Comprehensive Reviews in Food Science and Food Safety*, 17(4), 860–877. https://doi.org/10.1111/1541-4337.12343

Hayat, K., Abbas, S., Hussain, S., Shahzad, S. A., & Tahir, M. U. (2019). Effect of microwave and conventional oven heating on phenolic constituents, fatty acids, minerals and antioxidant potential of fennel seed. *Industrial Crops and Products*, 140, 111610. https://doi.org/10.1016/j.indcrop.2019.111610

Hernández-García, E., Vargas, M., & Chiralt, A. (2021). Thermoprocessed starch-polyester bilayer films as affected by the addition of gellan or xanthan gum. *Food Hydrocolloids*, 113, 106509. https://doi.org/10.1016/j.foodhyd.2020.106509

Hosseini, S. F., Javidi, Z., & Rezaei, M. (2016). Efficient gas barrier properties of multi-layer films based on poly(lactic acid) and fish gelatin. *International Journal of Biological Macromolecules*, 92, 1205–1214. https://doi.org/10.1016/j.ijbiomac.2016.08.034

Lahmass, I., Ouahhoud, S., Elyoubi, M., Benabbas, R., Sabouni, A., Asehraou, A., Saalaoui, E. (2018). Evaluation of antioxidant activities of saffron stigma and spath as by-product of Crocus sativus L. *MOJ Biology and Medicine*, 3(4), 154–158. https://doi.org/10.15406/mojbm.2018.03.00091

Jamshidian, M., Tehrany, E. A., Imran, M., Akhtar, M. J., Cleymand, F., & Desobry, S. (2012a). Structural, mechanical and barrier properties of active PLA–antioxidant films. *Journal of Food Engineering*, 110(3), 380–389. https://doi.org/10.1016/j.jfoodeng.2011.12.034

Jamshidian, M., Tehrany, E. A., & Desobry, S. (2012b). Release of synthetic phenolic antioxidants from extruded poly lactic acid (PLA) film. *Food Control*, 28(2), 445–455. 475 https://doi.org/10.1016/j.foodcont.2012.05.005

Jara-Palacios, M. J., Gonçalves, S., Heredia, F. J., Hernanz, D., & Romano, A. (2020). Extraction of Antioxidants from Winemaking Byproducts: Effect of the Solvent on Phenolic Composition, Antioxidant and Anti-Cholinesterase Activities, and Electrochemical Behaviour. *Antioxidants*, 9(8), 675. https://doi.org/10.3390/antiox9080675

Karimi, E., Mehrabanjoubani, P., Keshavarzian, M., Oskoueian, E., Jaafar, H. Z., & Abdolzadeh, A. (2014). Identification and quantification of phenolic and flavonoid components in straw and seed husk of some rice varieties (Oryza sativa L.) and their antioxidant properties: Identification and quantification of phenolic and flavonoid. *Journal of the Science of Food and Agriculture*, 94(11), 2324–2330. https://doi.org/10.1002/jsfa.6567

Li, Y., Qi, B., Luo, J., Khan, R., & Wan, Y. (2015). Separation and concentration of hydroxycinnamic acids in alkaline hydrolyzate from rice straw by nanofiltration. *Separation and Purification Technology*, 149, 315–321. https://doi.org/10.1016/j.seppur.2015.06.006

Llana-Ruiz-Cabello, M., Pichardo, S., Baños, A., Núñez, C., Bermúdez, J. M., Guillamón, E., Aucejo, S., Cameán, A. M. (2015). Characterisation and evaluation of PLA films containing an extract of Allium spp. to be used in the packaging of ready-to-eat salads under controlled atmospheres. *LWT - Food Science and Technology*, 64, 1354-1361. https://doi.org/10.1016/j.lwt.2015.07.057

Lourenço, S. C., Moldão-Martins, M., & Alves, V. D. (2019). Antioxidants of Natural Plant Origins: From Sources to Food Industry Applications. *Molecules*, 24(22), 4132. https://doi.org/10.3390/molecules24224132

McHUGH, T. H., Avena-Bustillos, R., & Krochta, J. M. (1993). Hydrophilic Edible Films: Modified Procedure for Water Vapor Permeability and Explanation of Thickness Effects. *Journal of Food Science*, 58(4), 899–903. https://doi.org/10.1111/j.1365-2621.1993.tb09387.x

Menzel, C., González-Martínez, C., Chiralt, A., & Vilaplana, F. (2019). Antioxidant starch films containing sunflower hull extracts. *Carbohydrate Polymers*, 214, 142–151. https://doi.org/10.1016/j.carbpol.2019.03.022

Menzel, C., González-Martínez, C., Vilaplana, F., Diretto, G., & Chiralt, A. (2020). Incorporation of natural antioxidants from rice straw into renewable starch films. *International Journal of Biological Macromolecules*, 146, 976–986. https://doi.org/10.1016/j.ijbiomac.2019.09.222

Muller, J., González-Martínez, C., & Chiralt, A. (2017b). Poly(lactic) acid (PLA) and starch bilayer films, containing cinnamaldehyde, obtained by compression moulding. *European Polymer Journal*, 95, 56–70. https://doi.org/10.1016/j.eurpolymj.2017.07.019

Nerín, C., Tovar, L., & Salafranca, J. (2008). Behaviour of a new antioxidant active film versus oxidizable model compounds. *Journal of Food Engineering*, 84(2), 313–320. https://doi.org/10.1016/j.jfoodeng.2007.05.027

Ng, H.-M., Sin, L. T., Tee, T.-T., Bee, S.-T., Hui, D., Low, C.-Y., & Rahmat, A. R. (2015). Extraction of cellulose nanocrystals from plant sources for application as reinforcing agent in polymers. *Composites Part B: Engineering*, 75, 176–200. https://doi.org/10.1016/j.compositesb.2015.01.008

Peanparkdee, M., & Iwamoto, S. (2019). Bioactive compounds from by-products of rice cultivation and rice processing: Extraction and application in the food and pharmaceutical industries. *Trends in Food Science & Technology*, 86, 109–117. https://doi.org/10.1016/j.tifs.2019.02.041

Peppas, N. A., Brannon-Peppas, L. B. Water Diffusion and sorption in amorphous macromolecular systems and foods. (1994). *Journal of Food Engineering*, 22, 189-210. https://doi.org/10.1016/B978-1-85861-037-5.50015-1

Peleg, M. (1988). An Empirical Model for the Description of Moisture Sorption Curves. *Journal of Food Science*, 53(4), 1216–1217. https://doi.org/10.1111/j.1365-2621.1988.tb13565.x

Randhawa, S., & Bahna, S. L. (2009). Hypersensitivity reactions to food additives. *Current Opinion in Allergy & Clinical Immunology*, 9(3), 278–283. https://doi.org/10.1097/ACI.0b013e32832b2632

Requena, R., Vargas, M., & Chiralt, A. (2017). Release kinetics of carvacrol and eugenol from poly(hydroxybutyrate-co-hydroxyvalerate) (PHBV) films for food packaging applications. *European Polymer Journal*, 92, 185–193. https://doi.org/10.1016/j.eurpolymj.2017.05.008

Rojas-Lema, S., Quiles-Carrillo, L., Garcia-Garcia, D., Melendez-Rodriguez, B., Balart, R., & Torres-Giner, S. (2020). Tailoring the Properties of Thermo-Compressed Polylactide Films for Food Packaging Applications by Individual and Combined Additions of Lactic Acid Oligomer and Halloysite Nanotubes. *Molecules*, 25(8), 1976. https://doi.org/10.3390/molecules25081976

Roy, S., & Rhim, J.-W. (2020). Preparation of bioactive functional poly(lactic acid)/curcumin composite film for food packaging application. *International Journal of Biological Macromolecules*, 162, 1780–1789. https://doi.org/10.1016/j.ijbiomac.2020.08.094

Sato, S., Gondo, D., Wada, T., Kanehashi, S., & Nagai, K. (2013). Effects of various liquid organic solvents on solvent-induced crystallization of amorphous poly(lactic acid) film. *Journal of Applied Polymer Science*, 129(3), 1607–1617. https://doi.org/10.1002/app.38833

Setford, P. C., Jeffery, D. W., Grbin, P. R., & Muhlack, R. A. (2017). Factors affecting extraction and evolution of phenolic compounds during red wine maceration and the role of process modelling. *Trends in Food Science & Technology*, 69, 106–117. https://doi.org/10.1016/j.tifs.2017.09.005

Sibhatu, H. K., Anuradha Jabasingh, S., Yimam, A., & Ahmed, S. (2021). Ferulic acid production from brewery spent grains, an agro-industrial waste. *LWT*, 135, 110009. https://doi.org/10.1016/j.lwt.2020.110009

Srisa, A., & Harnkarnsujarit, N. (2020). Antifungal films from trans-cinnamaldehyde incorporated poly (lactic acid) and poly(butylene adipate-co-terephthalate) for bread packaging. *Food Chemistry*, 333, 127537. https://doi.org/10.1016/j.foodchem.2020.127537

Talón, E., Trifkovic, K. T., Nedovic, V. A., Bugarski, B. M., Vargas, M., Chiralt, A., & González-Martínez, C. (2017). Antioxidant edible films based on chitosan and starch containing polyphenols from thyme extracts. *Carbohydrate Polymers*, 157, 1153–1161. https://doi.org/10.1016/j.carbpol.2016.10.080

Vasile, C., Stoleru, E., Darie-Nita, R. N., Dumitriu, R. P., Pamfil, D., Tartau, L. (2019). Biocompatible Materials Based on Plasticized Poly(lactic acid), Chitosan and Rosemary Ethanolic Extract I. Effect of Chitosan on the Properties of Plasticized Poly(lactic acid) Materials. *Polymers*, 11(6), 1-28. https://doi.org/10.3390/polym11060941

Vilarinho, F., Stanzione, M., Buonocore, G. G., Barbosa-Pereira, L., Sendón, R., Vaz, M. F., & Sanches Silva, A. (2021). Green tea extract and nanocellulose embedded into polylactic acid film: Properties and efficiency on retarding the lipid oxidation of a model fatty food. *Food Packaging and Shelf Life*, 27, 100609. https://doi.org/10.1016/j.fpsl.2020.100609

Yang, H.-H., Tsai, C.-H., Chao, M.-R., Su, Y.-L., & Chien, S.-M. (2006). Source identification and size distribution of atmospheric polycyclic aromatic hydrocarbons during rice straw burning period. *Atmospheric Environment*, 40(7), 1266–1274. https://doi.org/10.1016/j.atmosenv.2005.10.032

Ziemlewska, A., Zagórska-Dziok, M., & Nizioł-Łukaszewska, Z. (2021). Assessment of cytotoxicity and antioxidant properties of berry leaves as by-products with potential application in cosmetic and pharmaceutical products. *Scientific Reports*, 11(1), 3240. https://doi.org/10.1038/s41598-021-82207-2

CHAPTER 1.V

Using rice straw fractions to develop reinforced, active PLA-starch bilayers for meat preservation

Pedro A. V. Freitas, Chelo González-Martínez, Amparo Chiralt

Institute of Food Engineering for Development, Universitat Politècnica de València, 46022, Valencia, Spain

Submitted to Food Chemistry

ABSTRACT

Bilayers from thermoplastic corn starch (TPS) and PLA were obtained, incorporating or not RS valorised fractions: active extract (es) into PLA and cellulose fibres (cf) into TPS films. The films were obtained by melt blending and compression moulding while the bilayers were obtained by thermocompression of the different monolayers (TPS-PLA, TPScf-PLA, TPS-PLAes and TPScf-PLAes). TPS conferred oxygen barrier capacity to the laminates, which was improved by the cf incorporation. The extract slightly reduced the PLA resistance but improved their oxygen barrier capacity. The tensile and barrier properties of the bilayers revealed changes in the performance of each layer associated with the interlayer compound migration. The TPScf-PLAes bags exhibited noticeable antioxidant capacity when used in meat packaging and reduced microbial counts throughout cold storage. Therefore, these bilayers have considerable potential to extend the shelf-life of meat samples, preserving their quality and safety for longer, while using RS fractions permits its valorisation.

Keywords: active food packaging, phenolic compounds, antioxidant activity, ultrasound-assisted extraction, fresh pork meat.

1. INTRODUCTION

Foods are highly susceptible to processing and storage conditions which directly affect their quality and safety. Each year, it is estimated that microbiological spoilage and oxidative reactions are responsible for more than 25 % of food losses (Baghi et al., 2022; Chawla et al., 2021;). In this sense, food packaging plays an essential role in maintaining integrity, quality, and food safety, as well as in extending the shelf-life of food during the distribution chain and storage (Topuz & Uyar, 2020). Beyond the traditional purposes, such as cost-effective food protection, with an adequate barrier capacity for oxygen and water vapour, the packaging industries are currently focusing on the development of packaging materials using an environmentally-friendly approach, from renewable, biodegradable, and/or recyclable sources (Topuz & Uyar, 2020). Likewise, the incorporation of active compounds, such as antioxidants and antimicrobial agents, into these biodegradable materials comprises a new and constant challenge in the field of packaging.

Active food packaging is a well-known technology that incorporates additives into packaging materials to preserve or improve the quality of packaged foods as well as to reduce the risk of contamination and foodborne illness (Baghi et al., 2022). The strategy followed by this kind of packaging is based on the release of the active compounds from the packaging to the headspace or the food surface, thus preserving or improving their shelf life throughout storage. Of the active agents, extracts obtained from lignocellulosic-rich agro-industrial waste represent an interesting alternative to synthetic additives. These extracts are made up of a wide variety of phenolic compounds, exhibiting excellent antioxidant and/or antimicrobial properties.

Rice straw (RS) is an agro-industrial residue obtained after harvesting the rice grain, where large amounts of RS are obtained since 1 kg of rice grain generates approximately 1.5 kg of RS (Peanparkdee & Iwamoto, 2019). RS is a lignocellulosic material composed of approximately 37 % cellulose, 20 % hemicellulose, 20 % lignin and 17 % ash (Freitas et al., 2022a). The aqueous extraction of RS permitted the obtaining of phenolic-rich fractions (225-486 mg gallic acid equivalent.100 g^{-1} RS) (Menzel et al. 2020; Freitas et al., 2020) with high antioxidant capacity, and cellulose fibres (Freitas et al., 2022a) which are high added-value products, useful for application in different fields, such as the development of more sustainable and effective packaging materials.

Overall, biodegradable materials exhibit worsened functional properties than those of petrochemical plastics and the use of a single polymer does not meet the packaging requirements of many foods. To overcome these drawbacks, both the incorporation of reinforcing agents and additives from renewable resources into the polymer matrices and the obtaining of biodegradable multilayer systems represent feasible alternatives for developing sustainable packaging materials for food systems (Anukiruthika et al., 2020; Wang et al.,

2022). Multilayer systems consists of combinations of two or more layers of materials with complementary properties to act as an effective barrier to environmental conditions that cause food spoilage (Kaiser et al., 2017). The laminates should be materials with improved functional properties with respect to the individual layers, such as enhanced mechanical properties, good oxygen and water vapour barrier properties, sealability, and machinability (Anukiruthika et al., 2020; Kaiser et al., 2017). Combining hydrophilic biodegradable polymers with hydrophobic ones could provide the laminates with improved functional performance (Wang et al., 2022). In this sense, starch is a semicrystalline biopolymer hydrophilic in nature that gives rise to thermoplastic films with excellent barrier properties to lipids, carbon dioxide, and oxygen, but with high permeability to water vapour and water solubility (Galdeano et al., 2009). In contrast, poly (lactic acid) (PLA) is a bio-based, biodegradable polyester, hydrophobic in nature, that has good mechanical properties, water vapour barrier capacity and heat sealability, but exhibits low barrier capacity to oxygen (Avérous et al., 2001). Thus, starch and PLA films can be combined to produce laminates with improved functional properties for food applications, in which the PLA layer should be the contact face in the case of moist foods.

The aim of this study was to produce biodegradable bilayer films based on PLA and corn starch incorporating bioactive extract and cellulose fibres obtained from RS. The films were characterised as to their barrier, mechanical and optical properties, as well as to their microstructure and thermal behaviour. Likewise, the effectiveness of this packaging material was validated in a real foodstuff, by evaluating the development of the quality parameters (pH, colour, oxidation, and microbial counts) of packaged fresh pork meat throughout 16 days of cold storage.

2. MATERIAL AND METHODS

2.1 Materials

Amorphous PLA 4060D, with an average molecular weight of 106,226 D and density 1.24 g/cm^3 was supplied by Natureworks (U.S.A). Corn starch (27 % amylose) was purchased from Roquette (Roquette Laisa, Spain). Poly (ethylene glycol) (PEG1000) and sodium chlorite were obtained by Sigma-Aldrich (St. Louis, MO, USA). Glycerol, acetic acid, sodium carbonate (Na_2CO_3), di-phosphorus pentoxide (P_2O_5), and magnesium nitrate ($Mg(NO_3)_2$) were supplied by PanReac Quimica S.L.U. (Castellar del Vallés, Spain). Gallic acid, Folin-Ciocalteau reagent (2 N), methanol (> 99.9 purity), 2,2-Diphenyl-1-picrylhydrazyl (DPPH), sodium chlorite, 2-thiobarbituric acid (> 98 % purity), and 1,1,3,3-tetramethoxypropane were supplied by Sigma-Aldrich (St. Louis, MO, USA). Iodine (99.5 % purity) was purchased from Acros Organics® (Geel, Belgium). For microbiological tests, Violet red bile agar (VRB) was purchased from Scharlab S.L. (Sentmenat, Spain). Buffered peptone water, Trypticasein soy broth (TSB), Man, Rogosaand Sharpe agar (MRS) was supplied by Labkem (Barcelona, Spain).

2.2. Obtaining Rice Straw fractions

RS (Oryza sativa L.), J. Sendra var., was provided by L'Albufera rice fields (Valencia, Spain) and vacuum dried (0.8 mmbar, 50 ± 2 °C, 16 h), ground and sieved (particles of under 0.5 mm), before the extraction process. The aqueous extract and cellulose fibres were obtained from rice straw (RS), as described in previous studies (Freitas et al., 2020 and 2022a).

The aqueous RS extract was obtained as described by Freitas et al. (2020) by applying a combined ultrasound-reflux heating method, with a RS: distilled water ratio of 1:20 (w/v). The total phenolic content (TPC) of the extract was quantified as 37.1 ± 0.4 mg gallic acid equivalent (GAE) per g of freeze-dried extract, by the Folin-Ciocalteu method (Freitas et al. 2020). Likewise, the antioxidant capacity of the extract, evaluated by the 2,2-Diphenyl-1-pikryl-hydrazyl (DPPH) radical scavenging method (Brand-Williams et al., 1995; Menzel et al., 2019), and expressed as EC_{50} value, was 6.3 ± 0.3 mg freeze-dried extract.mg^{-1} DPPH. The EC_{50} value is defined as the ratio of the sample to the DPPH required to reduce the DPPH concentration by 50 % when the reaction stabilises.

The cellulose fibres (CF) were obtained from the RS water insoluble residue as reported by Freitas et al. (2022a). The chemical composition of the CF, analysed following the NREL/TP-510-42,618 method (Sluiter, 2008), was 66 % cellulose, 10 % hemicellulose, 5 % lignin, and 5 % ashes (Freitas et al. 2022a) and their morpho-geometric characteristics, evaluated by FESEM image analyses, showed major cumulative frequencies of lengths and thicknesses of below 200 µm and 5-15 µm, respectively (Freitas et al., 2021).

2.3 The preparation of films

2.3.1 PLA monolayers

Amorphous PLA pellets were first conditioned at P_2O_5 for 2 days to eliminate residual water. PLA active films (PLAes), plasticised with PEG1000 at 8 % wt. (with respect to the polymer mass), were obtained by incorporating the freeze-dried RS extract at 6 % wt. with respect to the polymer mass. The PLA/PEG1000 monolayer films without RS extract were prepared as the control formulation (PLA). The film components were previously mixed in a beaker and then melt-blended using an internal mixer (HAAKETM PolyLabTM QC, Thermo Fisher Scientific, Karlsruhe, Germany) at 160 °C and 50 rpm for 6 min. Thereafter, the solid blend was milled using a gridding machine (IKA, model M20, Germany) and compression-moulded using a hydraulic press (Model LP20, Labtech Engineering, Thailand). The milled pellets (3 g) were put onto Teflon sheets and thermoformed by preheating at 160 °C for 3 min, compression at 100 bars at 160 °C for 3 min, and final cooling to 80 °C.

2.3.2 TPS monolayers

Pre-conditioned starch (in P_2O_5 at 25 °C for 5 days) was first-hand mixed with glycerol, as plasticiser, at 30 % wt. with respect to the polymer mass. The composite blend (TPScf) was obtained by incorporating CF into the control mixture (TPS) at 3 % wt. Then, the dispersion was melt-blended in the internal mixer at 130 °C and at 50 rpm for 10 min. The doughs obtained were milled and pre-conditioned at 25 °C and 53 % RH for one week. Afterwards, the milled pellets (4 g per film) were compression-moulded in the hydraulic press by preheating at 160 °C for 3 min, compression at 30 bars and 160 °C for 2 min, followed by 130 bars and 160 °C for 6 min, and final cooling to 80 °C. The TPS and TPScf films were conditioned at 25 °C and 53 % RH (in a chamber with an oversaturated solution of $Mg(NO_3)_2$) for at least one week before characterisation.

2.3.3 Bilayer assembly of PLA and starch monolayers

Bilayer films were prepared by thermocompression of the PLA or PLAes and TPS or TPScf monolayers. The films were preheated at 120 °C for 2 min, compressed at 10 bars and 120 °C for 3 min, and a final cooling to 70 °C. The bilayers obtained were conditioned at 25 °C and 53 % RH at least one week before characterisation.

2.4 Characterisation of films

2.4.1 Microstructural properties and film thickness

Monolayer and bilayer films were immersed in liquid nitrogen and cryo-fractured to observe their cross-section surface by means of a Field Emission Scanning Electron Microscope (ULTRATM 55, Zeiis, Oxford Instruments, UK). Before the microscopic observation, the samples were platinum coated using an EM MED020 sputter coater (Leica BioSystems, Barcelona, Spain). The micrographs were taken under vacuum and 2.0 kV acceleration voltage.

A digital micrometer (Palmer, model COMECTA, Barcelona, accuracy of 0.001 mm) was used to measure the thicknesses of the films at ten random film positions.

2.4.2 Equilibrium moisture content

The equilibrium moisture content of the films was determined gravimetrically by triplicate. To this end, conditioned films (at 25 °C and 53 % RH for two weeks) of about 3 cm x 3 cm were weighed and dried at 60 °C for 24 h. Afterward, the samples were placed in a dissector at 25 °C with P_2O_5 for two weeks, to ensure dry conditions, and weighed. The moisture content was expressed as the total weight loss of the samples during the drying process with respect to their dry weight.

The water solubility of the films was determined according to Talón et al., (2017). Film samples (3 cm x 3 cm) were previously conditioned in P_2O_5 at 25 °C for two weeks to ensure dry conditions. The results were expressed as g of solubilised film/100 g dry film. The analysis was performed in triplicate.

2.4.3 Optical properties

The optical properties of the films were analysed following the Kubelka-Munk theory of multiple scattering using a spectrocolorimeter (CM-3600d, Minolta Co., Japan) (Freitas et al., 2021). Briefly, the reflection spectra were determined from 400 to 700 nm using white and black backgrounds to determine the internal transmittance (Ti) and the infinite reflectance (R_∞). Then, the film colour coordinates *L** (lightness), *a** (redness-greenness), and *b** (yellowness-blueness) were obtained from the R_∞ spectra, using D65 illuminant and 10° observer. Chroma (*C**) and hue angle (*h**) were obtained from the colour coordinates *a** and *b**. The measurements were taken six times for each sample.

2.4.4 Thermal properties

The thermal behaviour of the films was determined by thermogravimetric analysis (TGA) using a thermogravimetric analyser (TGA 1 Stare System analyser, Mettler-Toledo, Switzerland). Conditioned film samples (P_2O_5 at 25 °C for 2 weeks) were weighed (3-5 mg) in alumina pans and heated from 25 to 700 °C under nitrogen atmosphere (10 mL.min^{-1}) at a heating rate of 10 °C.min^{-1}. For each thermal event, the thermogravimetric curves (TGA) and their derivatives (DTGA) were analysed to obtain the initial degradation temperature (T_{on}), the temperature at the maximum degradation rate (T_p), the final degradation temperature (T_{end}), and the mass loss percentage (Δm). The measurements were taken in duplicate.

Differential scanning calorimetry (DSC) was used to determine the phase transitions of the films using a DSC Stare System analyser (Mettler-Toledo GmbH, Switzerland), operating under nitrogen flow (30 mL.min^{-1}). For the PLA films, aluminium-sealed pans containing film samples (5-7 mg) were heated from -25 to 200 °C at a heating rate of 10 °C.min^{-1}, maintained at 200 °C for 5 min, cooled down to -10 °C at -50 °C.min^{-1}, maintained at -10 °C for 5 min, and heated up again to 200 °C at a heating rate of 10 °C.min^{-1}. The starch films were analysed following the Collazo-Bigliardi et al. (2019) method. Film samples (5-9 mg) were heated from 25 to 160 °C, cooled to 25 °C, and then heated (second heating step) to 160 °C at a heating rate of 10 °C.min^{-1}. All measurements were taken in duplicate.

2.4.5 Barrier properties

The water vapour permeability (WVP) of the films was determined gravimetrically based on the ASTM E96/E96M (ASTM, 2005), following the modification proposed by (McHUGH et al.,

1993). The film samples were cut (Ø = 3.5 cm), placed and sealed in circular Payne permeability cups (Elcometer SPRL, Hermelle/s Argenteau, Belgium) containing 5 mL of distilled water (100 % RH). Afterward, the cups were put into desiccators at 25 °C and 53 % RH (using $Mg(NO_3)_2$ over-saturated solution), thus maintaining a constant RH gradient of 100-53 % through the films, and weighed periodically (ME36S, Sartorius, ± 0.00001 g, Fisher Scientific, Hampton, NH, USA), every 1.5 h for 27 h. The WVP of films, expressed in $g.mm.kPa^{-1}h^{-1}.m^{-2}$, was determined from the water vapour transmission rate, which was obtained from the slope of the weight loss *vs.* time curve at the steady state. The analysis was carried out in triplicate.

The oxygen permeability (OP) of the films was obtained using Ox-Tran equipment (Model 1/50, Mocon, Minneapolis, MN, USA) at 25 °C and 53 % RH, according to ASTM D3985-05 (ASTM, 2010). For this, the oxygen transmission rate through the films (50 cm^2) was determined every 15 min until equilibrium was reached. For each treatment, the measurements were taken in triplicate.

2.4.6 Tensile properties

ASTM D882 (ASTM, 2012) was used to obtain the stress-strain curves of the films and to determine the elastic modulus (EM), tensile strength at break (TS), and elongation at break (E) of the films, using a universal test machine (TA.XTplus model, Stable Micro Systems, Haslemere, England). Conditioned film samples (53 % RH at 25 °C for 2 weeks) were cut (25 mm x 100 mm) and stretched at a crosshead speed of 50 $mm.min^{-1}$ by two grips initially separated by 50 mm. Eight samples for each treatment were evaluated.

2.5 Preservation capacity of the bilayer films for fresh pork meat

Fresh pork meat was purchased from the local market and fillets were cut into 22 ± 1 g pieces, in an aseptic environment, and packaged in thermo-sealed bags of bilayer films (Fig. 3). To this end, laminates of PLA and CF reinforced starch, selected with and without active extract in the PLA sheet (PLA-TPScf and PLAes-TPScf laminates), were chosen on the basis of their better functional properties. The films were cut to 12 cm x 7 cm and sealed using a vacuum sealer (Vacio Press, Saeco) to obtain bags that were thermo-sealed after the meat sample was placed inside. Samples were packaged in duplicate for the analyses at each time. Likewise, meat samples wrapped in a commercial film were used as a control treatment. The packaged samples were stored at 4 °C for 16 days, and the meat quality parameters were evaluated atfter 0, 3, 7, 13, and 16 days of storage in the samples packaged in the different bags.

2.5.1 pH measurement

The pH of the pork meat was determined as described by (Moreno et al., 2018),by direct immersion of the glass electrode probe (Mettler-Toledo GmbH, Schwerzenbach, Switzerland) into the fillets. For each sample, five measurements were taken.

2.5.2 Colour measurement

The meat colour coordinates *L**, *a**, *b**, C_{ab}***, and h_{ab}*** were determined with a spectrocolorimeter (CM-3600d, Minolta Co., Japan), using a D65 illuminant and 10º observer. The total colour difference (*ΔE**) of the fillets after each storage time with respect to the initial time was determined according to Equation 1.

$$\Delta E^* = \sqrt{(\Delta L^*)^2 + (\Delta a^*)^2 + (\Delta b^*)^2} \quad (1)$$

Where $\Delta L^* = (L^* - L_0^*)$; $\Delta a^* = (a^* - a_0^*)$; $\Delta b^* = (b^* - b_0^*)$; and L_0^*, a_0^*, and b_0^* are the colour coordinates of the fillets at initial time.

2.5.3 2-thiobarbituric acid reactive substances (TBARS) assay

The lipid oxidation in the packaged meat was determined by the TBARS assay following the (Siu & Draper, 1978) methodology. Briefly, 10 g of meat was homogenised with 50 mL of distilled water and 50 mL of 10 % trichloroacetic acid and homogenised (ULTRA-TURRAX®, Model T 25 D, IKA®, Germany) for 3 min. The dispersion was then filtered and 8 mL of the filtrate was mixed with 2 mL of 2-thiobarbituric acid (0.06 mol.L^{-1}) and heated at 80 °C for 90 min. Afterward, the mixture was cooled to room temperature, and the absorbance at 532 nm was recorded. TBARS values were expressed as mg malonaldehyde (MDA) per kg of meat using 1,1,3,3-tetramethoxypropane as standard.

2.5.4 Microbiological analysis

A microbiological analysis of the packaged meat after different storage times was performed to quantify total viable counts (TV), psychrotrophic bacteria (PB), total coliforms (TC), and lactic acid bacteria (LA). Briefly, 10 g of meat sample was aseptically taken, mixed with 90 mL of 0.1 % peptone water in sterile bag, and homogenised using a Masticator paddle blender (IUL Instruments, Barcelona, Spain) for 3 min. The resulting dispersion was serially diluted by transferring 1 mL of each dilution into 9 mL of tryptic soy broth (TSB), thus obtaining a 10^{-2} dilution. From this, serial dilutions were obtained, and 1 mL of each dilution tube was mixed with the appropriate medium to quantify the corresponding microorganism. TC was quantified in the chromogenic medium Brilliance *E. coli*/Coliforms Selective Agar by incubation at 37 °C for 24 h. The LA was determined using MRS agar after incubation at 30 °C for 72 h. Finally, the TV and PB were quantified in PCA plates by incubation at 37 °C or 4 °C for 48 or 7

days, respectively. For each treatment, plates with 25 to 250 colonies were selected to determine the bacterial counts, which were expressed as log colony-forming units per gram of meat (log CFU.g^{-1}).

2.6 Statistical analysis

The experimental data were analysed through an analysis of variance (ANOVA) using the Minitab Statistical Program (version 17) with a confidence level of 95 %. Tukey's studentised range (HSD) test was performed to determine whether there were significant differences between the formulations, using 5 % least significant difference (α).

3. RESULTS AND DISCUSSION

3.1 Structure and appearance of films

Fig. 1a-d shows the FESEM micrographs of the cross-sections of the different bilayer films made up of thermoplastic starch and PLA with and without CF (in TPS films) or RS extract (in PLA films). Micrographs of the different monolayers at higher magnifications before and after their thermoassembly were also shown in Fig. 1e-l. Both TPS and PLA layers without additive exhibited the typical homogeneous microstructure previously described for glycerol plasticised corn starch (Collazo et al., 2019) and PEG plasticised amorphous PLA (Muller et al. 2017). The good interfacial compatibility between the starch and PLA monolayers was deduced from the non-delamination or detachment that occurs despite the cryo-fracture mechanical stress, as also reported by other authors (Muller et al., 2017). In the studied laminates, PLA is an amorphous polymer, containing a fraction of low molecular oligomers, which may contribute to the increase in its polarity and chemical affinity with starch molecules at the interface (Muller et al., 2017). Nevertheless, changes in the microstructure of the respective monolayers after the thermoadhesion process (Fig. 1e-l) could be attributed to the interlayer compound migration and the subsequent changes in the compound arrangement in the final bilayer. Thus, low molecular weight compounds, such as water and glycerol, could migrate from the starch layer to PLA and PEG1000 or extract compounds could migrate from the PLA to the starch sheet.

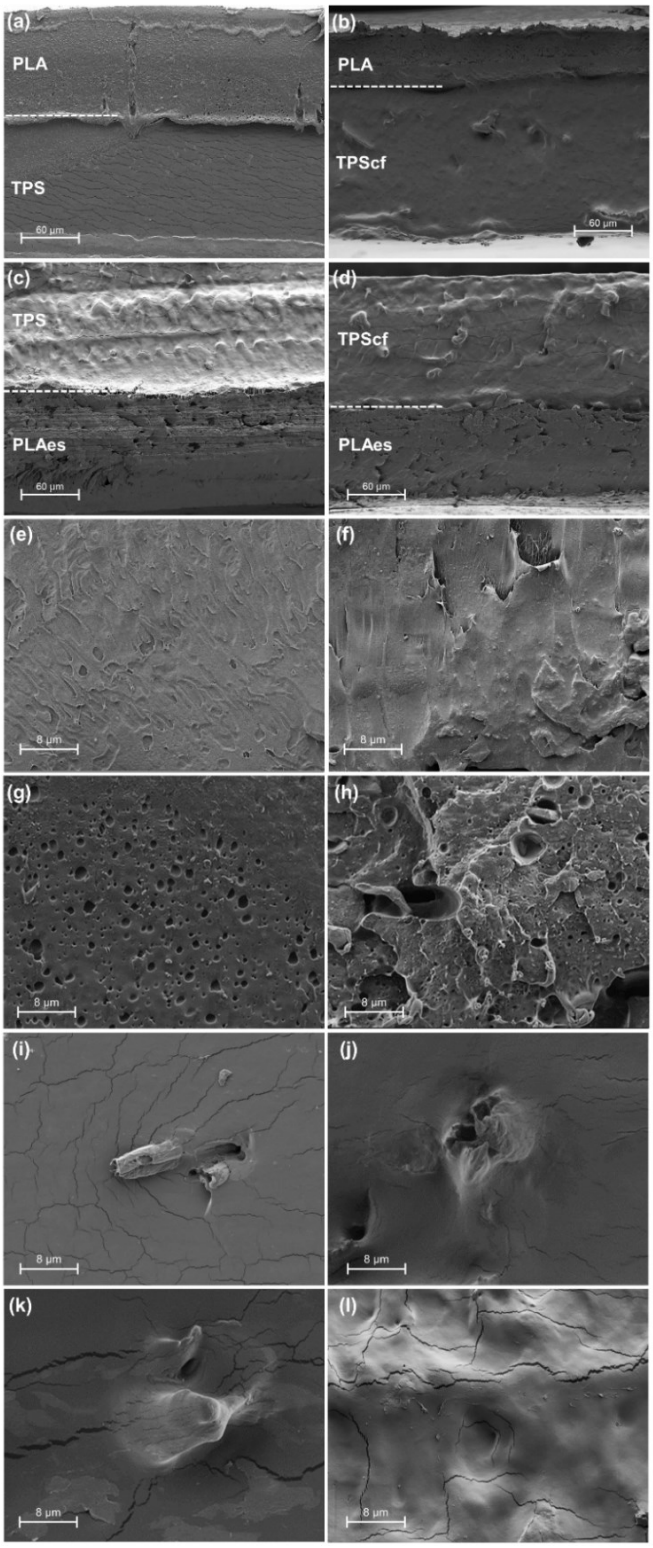

Fig. 1. Fig. 1. FESEM images of the cross-section of PLA/starch bilayers (a: PLA-TPS, b: PLA-TPScf, c: PLAes-TPS and d: PLAes-TPScf), showing the interface (dashed line) between sheets, and micrographs at higher magnification of the monolayers before and after thermo-adhesion in the different bilayers (e: PLA: before; f: PLAes before; g: PLA after, in PLA-TPS; h: PLAes after, in PLAes-TPScf; i: TPScf: before; j: TPScf after, in PLA-TPScf; k: TPScf after, in PLAes-TPScf; l: TPS after, in PLAes-TPS).

In Fig. 1e-l, the microstructural changes occurring in the PLA layer due to the incorporation of the RS extract before and after the thermosealing step can be observed. The incorporation of the RS extract promoted differences in the cryofracture behaviour, also exhibiting a small proportion of fine dispersed particles in the PLA matrix. This suggests a partial compatibility of the extract compounds with the polymer matrix. Some extract components could be homogeneously integrated into the polymer network, but some others aggregated, forming a finely dispersed phase. Some authors (Menzel et al. 2019; Karimi et al., 2014) identified several phenolic compounds in the aqueous RS extracts, such as *p*-coumaric, protocatechuic, ferulic, caffeic and vanillic acids, which could establish hydrogen bonds with the carbonyl group of PLA chains or with the end chain hydroxyls. The presence of miscible and non-miscible compounds within the polymer matrix modified the films cryofracture pattern, which can also affect the physical properties of the films.

The CF particles in TPS films may be clearly appreciated in Fig. 1i-k. The composite structure did not show any cracks or gaps between the CF and TPS matrices, which suggested good interfacial compatibility and entanglement, as observed in previous studies (Freitas et al., 2021). After the thermosealing of the bilayers, CF appeared even better integrated in the starch matrix, thus indicating the promotion of the chemical affinity between the polymer matrix and CF in the bilayers. Likewise, the cryofractured surface of the starch matrix in the bilayers (Fig. 1j-l) revealed changes in the component arrangement which can be attributed to the interlayer component migration.

Table 2 shows the thickness of the different films, where the PLA monolayers were thinner than the TPS monolayers. This agrees with the lower mass (3 g) of the PLA sheets when compared to the TPS (4 g), but also with the slower creep of starch during thermocompression. This flow was reduced even more when CFs were present in the blend, which can be attributed to the glycerol interactions with CF that weakened its plasticising effect (Freitas et al. 2021). As can be inferred from Fig. 1 and Table 2, none of the bilayer films were as thick as those estimated from the sums of the thicknesses of the separated monolayers, which suggests the radial flow of the polymer layers during the thermadhesion step. The reduction was about 12, 18, 15, and 20 % for PLA-TPS, PLA-TPScf, PLAes-TPS, and PLAes-TPScf bilayers, respectively. In every case, the PLA layers showed the greatest thinning, whereas the TPScf was thicker than the TPS layer. Differerences between the thicknesses of the layers can be attributed to the interlayer migration of low molecular compounds (water and glycerol) and the different flowability of the polymer matrices during the thermoadhesion step. These effects were also observed by other authors (Andrade et al., 2022) studying multilayer films based on PLA/poly(vinyl alcohol)/PLA laminates.

The internal transmittance (T_i) of all films and their psychometric colour coordinates (L^*, C_{ab}^*, and h_{ab}^*) are shown in Fig. 2, and Table 1, respectivelly. The neat PLA monolayer exhibited

the highest T_i and L^* values, coherent with the higher degree of homogeneity and transparency of the polymer matrix. The incorporation of the RS extract turned the PLAes film a yellowish-brown and made it darker, characterised by the higher values of C_{ab}^* and the lower values of L^* and h_{ab}^*, while the films exhibited a noticeable decrease in the T_i values. This was due to the presence of coloured compounds of the RS extract, which promoted selective light absorption and scattering. However, no significant changes in either the T_i or colour coordinates were observed after the incorporation of CF into the TPScf film. Similar results were found by Fourati et al. (2020) when analysing starch films reinforced with different cellulosic fractions.

The colour and appearance of the bilayer films were greatly influenced by the corresponding monolayers, as observed in the T_i spectra (Fig. 2) and colour coordinates (Table 1). The bilayer films without the extract (PLA-TPS and PLA-TPScf) exhibited optical properties that were similar to those of starch films, while the bilayers with the RS extract (PLAes-TPS and PLAes-TPScf) were more similar to the PLAes film. Nevertheless, there were differences in the bilayers that could be associated with the structural changes promoted by thermoadhesion, as previously commented on. It was the bilayer assembly of PLAes with TPS or TPScf in particular that promoted internal transmittance with respect to the PLAes monolayer, mainly when CF were not present in the starch layer, and the films exhibited a higher degree of lightness and less colour saturation. Therefore, the starch layer attenuated the colour effects of the RS extract, mainly when it did not contain CF. Likewise, the bilayers of PLA without the RS extract with TPScf were less transparent than the TPS, exhibiting a darker and more saturated colour. Therefore, differences in the light interactions in the bilayers affected their colour and transparency that were also affected by the structural changes promoted by thermoadhesion.

Table 1. Colour parameters, lightness (L^*), chroma (C_{ab}^*), and hue angle (h_{ab}^*) of the monolayer and bilayer films. Mean values and standard deviations.

Formulation	L^*	C_{ab}^*	h_{ab}^*
PLA	90.7 ± 0.2^{a}	2.51 ± 0.13^{e}	99.6 ± 0.8^{a}
PLAes	67.6 ± 0.7^{f}	34.57 ± 0.65^{a}	77.1 ± 0.3^{f}
TPS	88.5 ± 0.1^{b}	7.57 ± 0.10^{d}	92.5 ± 0.1^{b}
TPScf	88.1 ± 0.2^{b}	8.25 ± 0.35^{cd}	92.6 ± 0.2^{b}
PLA-TPS	87.3 ± 0.3^{b}	7.58 ± 0.11^{d}	92.2 ± 0.3^{b}
PLA-TPScf	86.0 ± 0.5^{c}	9.50 ± 0.31^{c}	90.9 ± 0.4^{c}
PLAes-TPS	76.9 ± 1.2^{d}	27.92 ± 2.06^{b}	83.4 ± 0.7^{d}
PLAes-TPScf	72.2 ± 0.9^{e}	34.41 ± 1.22^{a}	81.0 ± 0.6^{e}

Different subscript letters in the same column indicate significant differences via the Tukey test ($p < 0.05$).

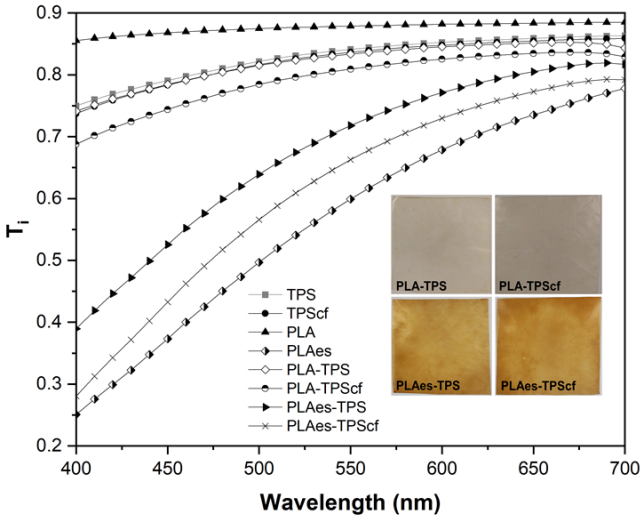

Fig. 2. The internal transmittance (Ti) of the monolayers (TPS, TPScf, PLA, PLAes) and bilayer films (PLA-TPS, PLA-TPScf, PLAes-TPS, and PLAes-TPScf) and the visual appearance of the bilayer films.

Table 2. Thickness, moisture content, water solubility, water vapour permeability (WVP), oxygen permeability (OP), and tensile properties (E: elongation at break; TS: tensile strength; EM: elastic modulus) of monolayer and bilayer films. Mean values and standard deviations.

Formulation	Experimental thickness (mm)	Moisture (%)	Solubility (g soluble solids/100 g film)	WVP ($g.mm.kPa^{-1}.h^{-1}.m^{-2}$)	OP ($x10^{14}$) ($cm^3.m^{-1}.s^{-1}.Pa^{-1}$)	E (%)	TS (MPa)	EM (MPa)
PLA	0.146 ± 0.008^{c}	0.7 ± 0.1^{c}	1.2 ± 0.4^{c}	0.11 ± 0.01^{e}	165.9 ± 1.1^{a}	6.0 ± 0.7^{e}	34.2 ± 0.5^{a}	1255 ± 36^{a}
PLAes	0.144 ± 0.007^{c}	0.9 ± 0.1^{c}	1.9 ± 0.8^{c}	0.15 ± 0.01^{e}	154.3 ± 5.3^{b}	3.2 ± 0.2^{f}	30.5 ± 1.6^{b}	1315 ± 76^{a}
TPS	0.171 ± 0.026^{bc}	8.3 ± 0.2^{a}	42.4 ± 1.6^{a}	6.32 ± 0.19^{a}	9.0 ± 0.5^{d}	30.4 ± 3.5^{a}	3.4 ± 1.0^{g}	175 ± 53^{c}
TPScf	0.185 ± 0.025^{b}	8.0 ± 0.6^{a}	36.9 ± 4.1^{a}	5.94 ± 0.17^{b}	6.6 ± 0.7^{e}	12.3 ± 5.0^{cd}	6.8 ± 1.2^{f}	551 ± 150^{b}
PLA-TPS	0.278 ± 0.033^{a}	6.9 ± 0.3^{b}	18.3 ± 3.8^{b}	0.42 ± 0.06^{de}	16.8 ± 0.7^{c}	19.4 ± 4.7^{b}	11.7 ± 1.0^{cd}	555 ± 22^{b}
PLA-TPScf	0.273 ± 0.012^{a}	6.7 ± 0.4^{b}	18.3 ± 1.3^{b}	0.24 ± 0.09^{e}	9.4 ± 1.0^{d}	16.1 ± 3.0^{bc}	12.4 ± 1.2^{c}	611 ± 16^{b}
PLAes-TPS	0.269 ± 0.013^{a}	6.7 ± 0.3^{b}	17.9 ± 0.8^{b}	0.87 ± 0.12^{c}	10.3 ± 0.8^{d}	13.7 ± 3.2^{c}	7.82 ± 1.4^{ef}	507 ± 23^{b}
PLAes-TPScf	0.262 ± 0.007^{a}	6.6 ± 0.1^{b}	18.1 ± 0.6^{b}	0.61 ± 0.07^{cd}	9.6 ± 1.2^{d}	8.4 ± 2.5^{de}	9.6 ± 1.0^{de}	574 ± 38^{b}

Different subscript letters in the same column indicate significant differences via the Tukey test ($p < 0.05$).

Table 3. Thermal degradation events, with the onset (T_{on}) and peak (T_p) temperatures, mass loss (Δm) and final residue obtained from the TGA curves, and glass transition temperature (mid-point: T_g) obtained from the second heating scan of DSC, for the PLA and TPS layers before (monolayers) and after (bilayers) thermocompression. Mean values and standard deviations.

Formulation	TGA										DSC	
	[35-120] ℃			[150-460] ℃			[435-665] ℃			Residue	T_{gPLA}	$T_{gStarch}$
	T_{on}*	T_p*	Δm (%)	T_{on}*	T_p*	Δm (%)	T_{on}*	T_p*	Δm (%)			
PLA	-	-	-	190 ± 6^{b}	376 ± 1^{a}	97.3 ± 0.1^{a}	-	-	-	0.4 ± 0.2^{c}	37.7 ± 2.5^{ab}	-
PLAes	-	-	-	234 ± 1^{a}	342 ± 1^{b}	98.5 ± 0.2^{a}	-	-	-	1.1 ± 0.3^{b}	34.2 ± 1.5^{bc}	-
TPS	44 ± 2^{b}	67 ± 2^{a}	1.8 ± 0.1^{b}	156 ± 1^{c}	333 ± 1^{bc}	80.7 ± 1.0^{c}	432 ± 2^{c}	548 ± 3^{e}	16.5 ± 1.2^{a}	0.7 ± 0.2^{c}	-	92.4 ± 4.1^{a}
TPScf	50 ± 2^{a}	65 ± 1^{ab}	1.4 ± 0.5^{b}	152 ± 4^{c}	332 ± 1^{c}	82 ± 1.0^{c}	448 ± 3^{b}	564 ± 2^{c}	15.3 ± 1.5^{a}	1.3 ± 0.1^{b}	-	85.2 ± 6.4^{a}
PLA-TPS	36 ± 1^{c}	58 ± 1c	2.5 ± 0.3^{a}	153 ± 3^{c}	334 ± 2^{bc}	85.3 ± 1.6^{b}	461 ± 2^{a}	589 ± 9^{ab}	10.6 ± 1.1^{b}	2.1 ± 0.6^{a}	37.2 ± 0.6^{ab}	68.8 ± 5.4^{b}
PLA-TPScf	41 ± 2^{b}	64 ± 1^{ab}	1.8 ± 0.3^{ab}	154 ± 8^{c}	335 ± 1^{bc}	87.4 ± 0.5^{b}	462 ± 3^{a}	554 ± 1^{d}	10.2 ± 1.1^{b}	2.3 ± 0.4^{a}	37.8 ± 0.3^{a}	62.2 ± 0.5^{bc}
PLAes-TPS	35 ± 1^{c}	62 ± 2^{b}	1.9 ± 0.2^{ab}	152 ± 1^{c}	338 ± 1^{bc}	83.8 ± 0.5^{bc}	465 ± 1^{a}	600 ± 3^{a}	11.2 ± 2.1^{b}	2.0 ± 0.2^{a}	35.4 ± 0.5^{abc}	66.0 ± 1.5^{bc}
PLAes-TPScf	46 ± 3^{b}	66 ± 6^{ab}	1.1 ± 0.4^{b}	158 ± 3^{c}	338 ± 3^{bc}	84.2 ± 0.4^{bc}	459 ± 1^{a}	566 ± 8^{c}	13.7 ± 0.6^{ab}	2.2 ± 0.4^{a}	31.7 ± 1.0^{c}	58.3 ± 0.5^{c}

Different subscript letters in the same column indicate significant differences via the Tukey test ($p < 0.05$).

3.2 Water relations and barrier and tensile properties of the films

Table 2 gives the equilibrium moisture content and water solubility of the different mono- and bilayers. The incorporation of the RS extract into the PLA matrix or CF into the starch matrix did not affect ($p > 0.05$) the moisture content or the water solubility with respect to their corresponding control monolayer. The hydrophobic PLA matrix had markedly lower water sorption capacity and water solubility than starch films, which makes it desirable for wet food contact applications. As expected, although the bilayers exhibited intermediate equilibrium moisture content values compared to the PLA and starch monolayers, they were higher than what was expected from the mass balance in the bilayer (3:4 mass ratio in PLA:TPS layers). This suggests that the water binding capacity of the PLA increased in the bilayer assembly, probably due to the interlayer migration of water from the starch sheet and the subsequent progress of PLA hydrolysis involved in the thermosealing step. This effect was similar in the four bilayers, suggesting similar changes during the thermosealing step in every case. In contrast, the bilayer water solubility was in the range of that expected from the individual solubility of each layer and its mass fraction in the bilayer.

Table 2 shows the values of WVP, OP, and the tensile properties of the different monolayer and bilayer films. The PLA films exhibited a good water vapour barrier capacity that was slighlty worsened by the RS extract, whereas the starch films exhibited a better oxygen barrier capacity that was enhanced by CF incorporation. The incorporation of RS extract into the PLA monolayer (PLAes) and CF into the starch film (TPScf) provoked a decrease of 7 and 26 %, respectively, in the OP values with respect to their corresponding controls. The presence of hydrophilic components from the extract in the PLA matrix could reduce the solubility of oxygen molecules, while the presence of CF increases the tortuosity factor for the mass transfer of the starch films, thus limiting the diffusion rate of oxygen through the matrix (Freitas et al., 2021). It is worth mentioning that the presence of antioxidant phenolic compounds could promote the oxygen scavenging effect, as an additional oxygen barrier effect of the films.

The bilayers exhibited WVP values similar to those of the PLA monolayers, while the OP values were closer to those of the starch films. This is coherent with the lamination theory, which states that the barrier properties of a multilayer system are closer to those of the monolayer with the highest barrier capacity (Siracusa, 2012). In fact, the theoretical values of OP and WVP determined according to the perpendicular mass transfer model with parallel assembled resistances, were very similar (predicted range of WVP values: 0.20-0.27 $g.mm.kPa^{-1}.h^{-1}.m^{-2}$, and OP values: 9.0-14.0 $cm^3.m^{-1}.s^{-1}.Pa^{-1}$) to the experimental values for both WVP and OP. Thus, the WVP of the PLA-TPS and PLA-TPScf bilayers did not differ ($p>0.05$) from that of the PLA film with or without extract, while the incorporation of the extract into the PLA films led to a slight increase in the WVP values for PLAes-TPS and PLAes-TPScf bilayers. The differences

with respect to the theoretical values were greater in the case of WVP than in that of OP, which suggests greater changes in the PLA limiting layer for water transfer during thermoadhesion. The phenolic acids from the RS extract could promote the partial hydrolysis of PLA chains, mainly during thermocompression, which would alter the interchain forces of the polymer network, favouring the diffusion of water vapour through the films.

As concerns the oxygen barrier, the presence of the RS extract (in PLAes-TPS) or CF (in PLA-TPScf) in the bilayers had a similar decreasing effect on the OP values, with respect to the PLA-TPS laminate, (about 41 % and 46 %, respectively) while a non-additive effect was observed for the PLAes-TPScf bilayer.

Therefore, the lamination of PLA and starch films was effective at obtaining bilayer assemblies with an improved water vapour and oxygen barrier capacity, although the improvement was affected by the potential interlayer migration of low molecular compounds. From the point of view of the barrier capacity, the best combination was PLA-TPScf, although PLAes-TPScf also exhibited the best oxygen barrier capacity.

The PLA and TPS monolayer exhibited values of tensile parameters (Table 2) in the range of previously reported values (Vilarinho et al., 2021; Collazo-Bigliardi et al., 2019; Freitas et al., 2021). The incorporation of the RS extract reduced the TS and E values of the PLA film by about 11 and 46 %, respectively. This implied a weakening effect in the matrix due to the reduction in the inter-chain forces with the newly established molecular interactions with the extract components. In contrast, CF greatly promoted the stiffness and resistance to break of TPS films, as previously reported (Freitas et al. 2021). In general, all bilayers became markedly less resistant and stiff than PLA films, as well as less stretchable than TPS films. These noticeable changes in the tensile properties with respect to what is expected from the PLA monolayer (the most resistant and less extensible) is coherent with the previously mentioned interlayer compound migration that altered the initial properties of the layers. The partial hydrolysis of PLA chains promoted by the water diffusion from TPS could affect the PLA mechanical resistance with the subsequent effect on the bilayer tensile behaviour. Lim et al. (2010) suggest that a moisture content in PLA resin above 250 ppm can lead to severe hydrolytic degradation during the thermal treatment, which provokes a molecular weight drop and alters the functional properties of PLA-based materials. The active bilayers (PLAes-TPS and PLAes-TPScf) were the least resistant to break and least stretchable ($p<0.05$), which suggests that phenolic acids could also contribute to the partial hydrolysis of the PLA matrix. Muller et al. (2017) also found this effect in PLA/starch bilayer films containing cinnamaldehyde. Although the incorporation of CF into the starch film increased the TS and EM values by approximately 100 % and 300 %, respectively, this reinforcing effect was not observed ($p < 0.05$) in the corresponding bilayers (PLA-TPScf and PLAes-TPScf) since the properties of the assembled PLA

film were of superior strength, thus masking the improvement in the starch film resulting from the incorporation of CF.

3.3 Thermal behaviour

TGA and DSC analyses were performed to evaluate potential changes in the thermal behaviour of polymers associated with the thermoassembly step. Table 3 gathers the thermogravimetric parameters of each thermal degradation event, as well as the glass transition temperature (T_g) of the polymers in the films before and after thermocompression. Except for the PLA and PLAes monolayers, all films exhibited a first thermodegradation step ranging between 35-120 °C, corresponding to the loss of bonded water present in the starch matrix. The neat and active PLA monolayers exhibited a single thermodegradation step, with a Δm of about 97-98 %, as also reported by other authors (Rasheed et al., 2020). The incorporation of RS extract markedly decreased the T_p of the PLA film (from 376 to 342 °C), which also suggests that the extract components weakened the intermolecular forces of the PLA/PEG 1000 matrix, as commented above. Nonetheless, the active PLA films exhibited higher T_{on} than the control PLA, which could be related to the establishment of interactions between the extract's compounds and the polymer matrix, thereby delaying its initial degradation.

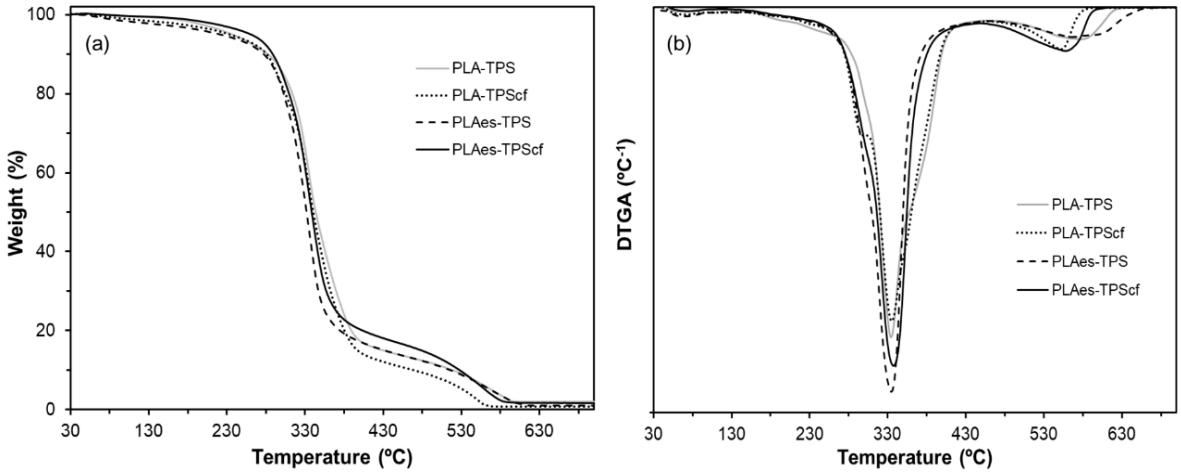

Fig. 3. TGA (a) and DTGA (b) curves of bilayers films based on PLA with or without RS extract and starch with or without CF.

The second thermodegradation stage of the bilayers is related to the thermal decomposition of both the starch/glycerol (Kargarzadeh, 2017) and PLA/PEG 1000 (Rasheed et al., 2021) matrices, with and without CF (Freitas et al., 2021) or RS extract. As shown in Fig. 3 and Table 3, the bilayers did not exhibit noticeable differences, showing similar values of T_{on} (152-158 °C), T_p (334-338 °C), and Δm (84-87 %). The PLA-TPS sample exhibited a slightly faster mass change at the beginning of the second thermal event (Fig. 3b) than the other bilayers, which may be due to the molecular interactions, either of the extract compounds or the CF, with the low molecular weight polymer chains, which delayed their thermodegradation to some

extent. The active bilayers exhibited a retarded degration at the end of this step, which could be attributed to the contribution of extract components in terms of their own thermodegradation or their interactions with the degradation mechanisms of the polymers. The third and last stage of degradation (435-665 °C) occurred for the starch monolayers and every bilayer and corresponds to the degradation of the first step fragmentation products of the starch films (Danilovas et al. 2014). Of the bilayers, the laminates with the RS extract exhibited higher Δm, which could be due to the degradation of the lignin fraction present in the extract.

The T_g values (obtained from the second heating step of the DSC analyses) of all films are shown in Table 3. The T_g for PLA was similar to that previously reported for the polymer plasticised with PEG (Muller et al., 2017), while glycerol-plasticised TPS also exhibited T_g in the previously described range (Collazo-Bigliardi et al., 2019). The presence of the RS extract did not significantly change (*p>0.05*) the T_g of the PLA matrix, although a decreasing trend was observed, thus indicating a plasticising effect. As deduced from the tensile behaviour, the extract components reduced the interchain forces of the PLA/PEG1000 matrix, resulting in lower strength matrices, as also observed in PLA films when ferulic or cinnamic acids were incorporated (Ordoñez et al., 2022). The T_g value of starch was not affected by the incorporation of CF, although Averous et al. (2001) reported an increase in T_g determined by DMA in reinforced TPS matrices with CFs. As concerns the bilayers, submitted to thermocompression, a marked reduction in the T_g values of starch was observed, mainly when CFs were present, which could be attributed to the interlayer migration of low molecular weight compounds that provoked changes in the layers' composition, thus affecting their initial properties. The incorporation of CF into the starch matrix modifies the water interactions with the components (Averous et al., 2001), which could promote the migration of the hydrophilic components present in the RS extracts. This would lead to a decrease in the cohesiveness of the starch network, either by weakening the interchain forces or even through the partial hydrolysis of the polymer. Menzel et al. (2020) reported the depolymerisation of amylose by thermal processing, which was reduced by the protective effect of glycerol and enhanced in the presence of RS extracts. Therefore, the migration of glycerol from the starch sheet and RS extract phenolic acids from PLA could lead to amylose depolymerisation during thermocompression and T_g reduction. In contrast, no significant changes in the T_g values of the PLA layers was observed with respect to the corresponding monolayers, except when these contained extract and were in contact with the TPScf layer. The migration of both water and glycerol molecules from the starch to the PLA layer could enhance the effect of the extract within the PLA matrix. These greater changes were also observed in the mechanical behaviour of the bilayer, with a reduction in TS and E.

The thermal behaviour also confirmed the migration of low MW compounds between layers during their thermoadhesion, which modified the initial properties of the monolayers.

However, even accounting for this effect, the bilayers exhibited global properties that better meet food packaging requirements in terms of their water vapour and oxygen barrier capacity, maintaining mechanical resistance and flexibility, and, with potential antioxidant and antibacterial capacity, in the case of active laminates.

3.4 Pork meat preservation with bilayer bags

The obtained bilayers, both CF-reinforced and with and without RS extract, were used to evaluate their capacity to preserve fresh pork meat. Fig. 4 shows the changes in the different quality parameters of fresh pork meat packaged with the PLA-TPScf and PLAes-TPScf bilayers, as compared with samples wrapped in a commercial film, throughout 16 days of cold storage (4 °C).

The pH is an important indicator of meat quality since it affects its water retention capacity, colour, and flavour (Kim et al., 2016). As shown in Fig. 4a, the initial pH value of the meat was 5.5, in line with values found for fresh pork meat (Yang et al., 2019). The storage time and the type of packaging significantly affected the pH values of the samples ($p<0.05$). Overall, the meat exhibited an increase in pH values throughout storage, which is characteristic of the enzymatic and/or microbiological deterioration of proteins that give rise to alkaline substances, such as amines (Pacquit et al., 2006). Although statistically different over time, the samples packed with the PLAes-TPScf bilayer did not exhibit a marked increase in pH (5.5 to 5.6), suggesting that the active film was more efficient than the other treatments at maintaining the pH of the meat. Furthermore, as compared with the control sample, the PLA-TPScf control bilayer was more efficient at maintaining the pH of the sample. This may be due to their water vapour and oxygen barrier properties, affecting the microbial metabolism and the oxidative and enzymatic reactions.

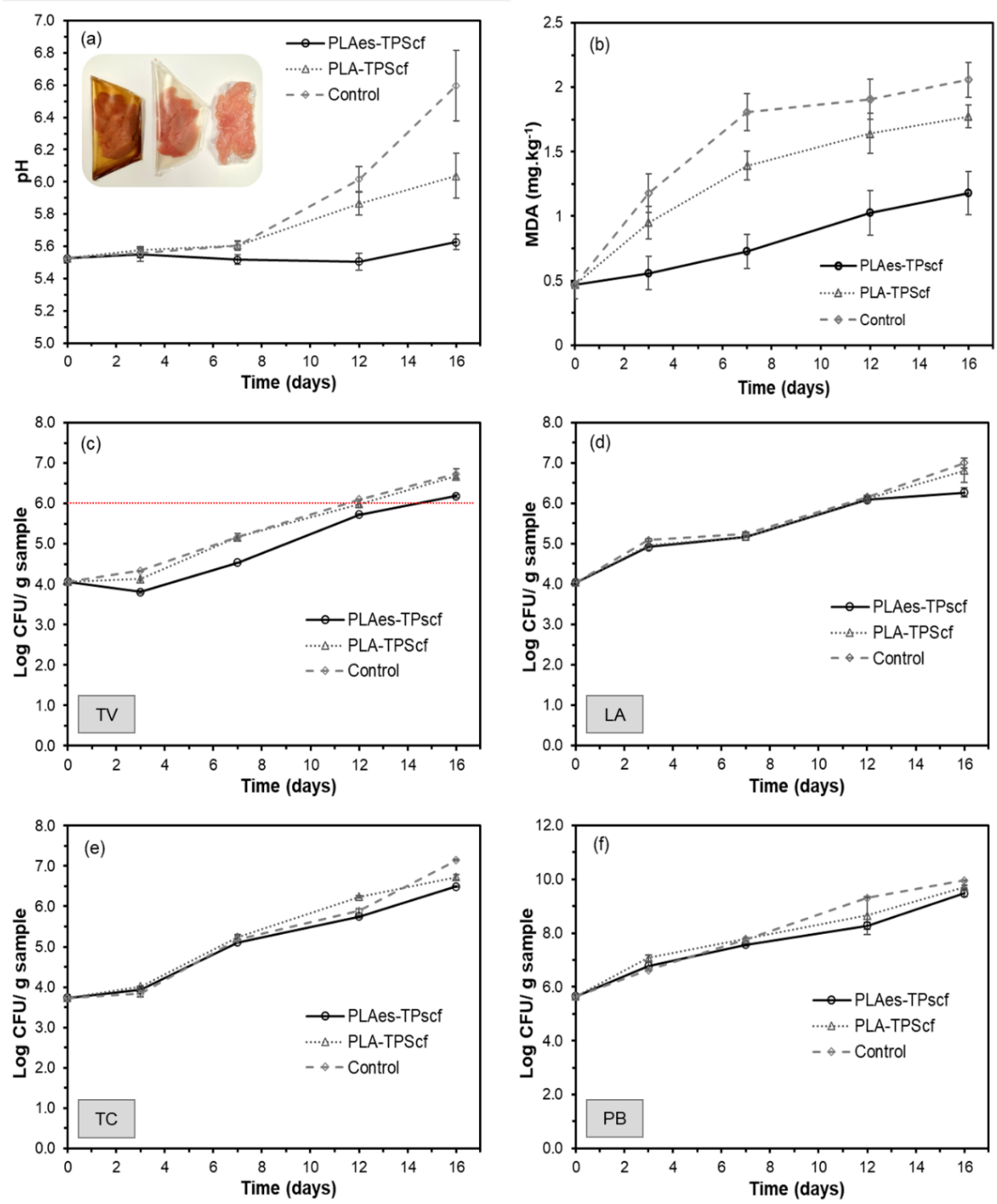

Fig. 4. Development of pH values (a), TBARS index (b), and microbial counts (c, d, e, f) (total viable counts (TV), psychrotrophic bacteria (PB), total coliforms (TC), and lactic acid bacteria (LA)) of pork meat samples packed with bilayer (PLAes-TPScf and PLA-TPScf) thermosealed bags and control sample wrapped with a commercial film, stored at 4 °C for 16 days.

Fig. 4b shows the MDA levels, expressed as mg MDA/kg sample, in the meat throughout storage, where the continuous increase of MDA levels can be observed. Nonetheless, the

samples packaged with the active bilayer exhibited the lowest rate of increase in the TBARS values, indicating a retarded meat oxidation, compared to the bilayer without the RS extract and control sample. This may be attributed to the radical scavenging capacity of the extract compounds that would be released on the surface of the meat. The reduced OP values of the bilayers, enhanced by the starch layer, also contributed to their oxidation inhibition capacity (Hernández-García et al., 2022a). In fact, samples packaged with the PLA-TPScf bag exhibited lower oxidation levels than the control sample. This film had similar OP values to the PLAes-TPScf film, but a lower inhibition capacity of oxidative reactions. This demonstrates the active role of the antioxidant compounds of the RS extract in meat preservation. Likewise, the light barrier capacity of the active bilayer could also provide the bags with antioxidant effect, protecting the meat against undesirable photoreactions, such as the photooxidation of lipids, vitamins, and pigments. Other studies reported that the RS extracts exhibited great antioxidant activity due to a set of several phenolic acids extracted from the lignocellulosic matrix, such as ferulic, *p*-coumaric, and protocatechuic acids (Freitas et al., 2022b; Menzel et al., 2020). The antioxidant ability of phenolic acids is mainly due to the hydroxyl phenolics that act as hydrogen donors, affected by the other substituents in the aromatic ring, whose positions and number influence their antioxidant activity (Topuz & Uyar, 2020). Therefore, the incorporation of active extract, as well as the use of cellulosic fractions from RS in multilayer PLA-starch systems, showed itself to have potential application to delay the oxidation of fresh pork meat.

The microbial counts in the pork meat for TV, PB, TC, and LA bacteria are shown in Fig. 4c-f. The meat samples exhibited a continuous microbial growth throughout storage, regardless of the packaging, as also reported by other authors (Andrade et al., 2022; Kim et al., 2016). In general, no marked differences were observed between samples packaged with different films and the control sample, despite the low OP values of the bilayers that limit the amount of oxygen available for bacteria. This suggests that at the low storage temperature, oxygen availability was not limiting for microbial growth. Nevertheless, samples packaged with the active PLAes-TPScf bilayers exhibited the lowest count values throughout storage, the differences being significant for TV counts ($p<0.05$) from the third storage day onwards. This indicates a certain antibacterial effect of the released RS extract compounds on the meat surface. In fact, samples packed with the PLAes-TPScf film reached the TV count acceptability limit (10^6-10^7 CFU/g sample, depending on the country (Kim & Jang, 2018)), 3 days later than the other treatments (Fig. 4c). Similar effects were observed by Hernández-García et al. (2022a) for pork meat packaged with starch-polyester bilayer films with ferulic, *p*-coumaric, and protocatechuic acids, which are also present in the RS extract. These authors observed a slow and limited release of the phenolic acids from the polyester layer to polar simulants, which could limit the antimicrobial action of the active compound, since the minimal inhibitory concentration of the bacteria could not be reached soon enough on the food surface.

As concerns meat colour development, all of the samples exhibited a decrease in *L** values over time, becoming darker (Fig. 5a), which could be attributed to the sample water loss that promotes the pigment concentrations and refractive index near the surface, provoking light absorption (Hernández-García et al., 2022b). This effect was slightly more pronounced for meat samples packed with the PLAes-TPScf film, which exhibited a lower water vapour barrier capacity than the PLA-TPScf film. Additionally, the potential release of coloured compounds from the extract to the meat surface could contribute to the fact that these meat samples are darker while also showed the lowest colour saturation (C_{ab}*) at the end of storage. However, this sample also exhibited the mildest changes in the h_{ab}* values throughout storage, suggesting the smallest changes in the oxymyoglobin related with the antioxidant effect of the extract.

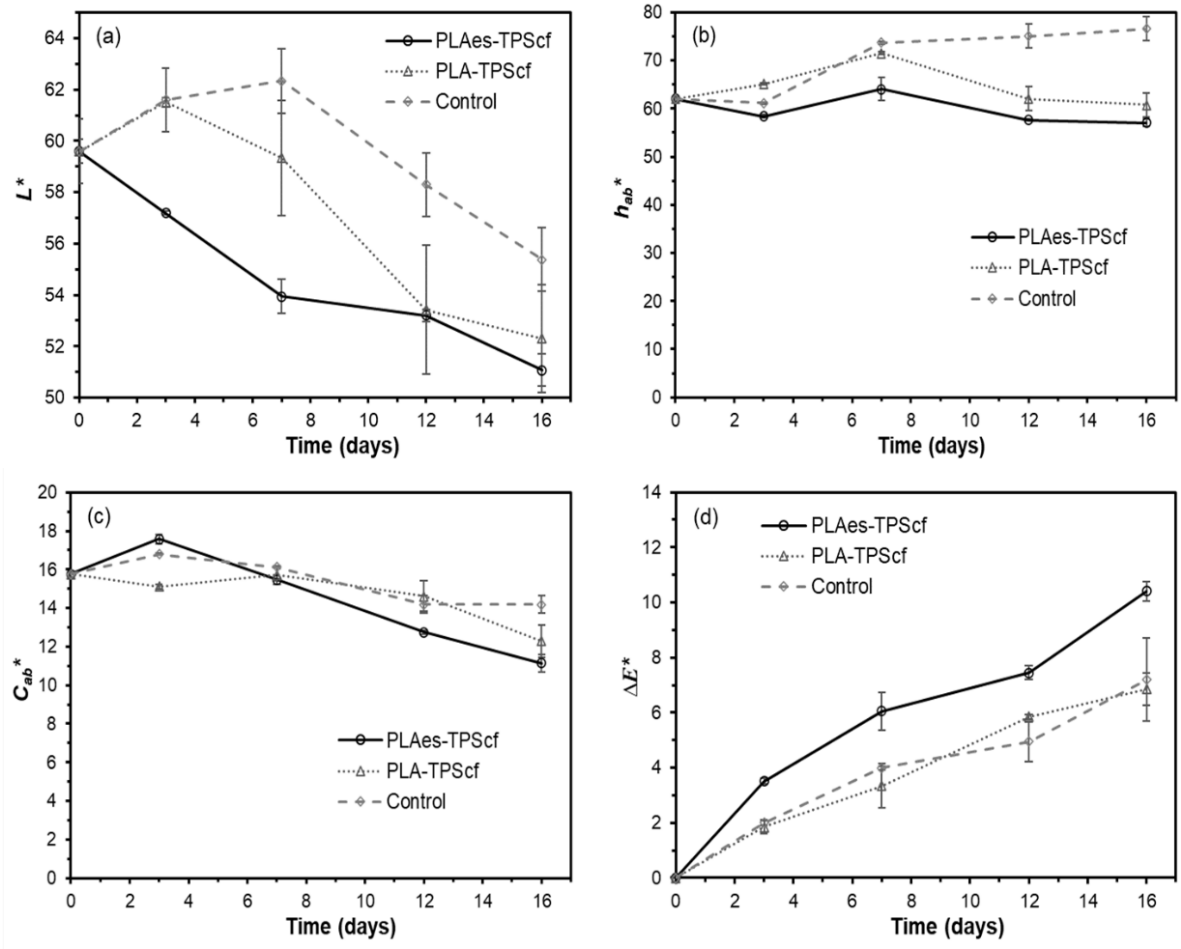

Fig. 5. Colour parameters *L**, C_{ab}*, h_{ab}*, and *ΔE** of the pork meat packed in the thermosealed bilayer (PLAes-TPScf and PLA-TPScf) bags and the control sample wrapped with a commercial film, throughout cold storage at 4 °C for 16 days.

Due to the greater change in both the C_{ab}* and *L** values, the samples packed with PLAes-TPScf present the highest values of the *ΔE** parameter throughout storage. Nevertheless, the

active PLAes-TPScf film was effective at maintaining the global colour of the meat, whereas the non-packaged samples became more yellowy-brown, which is characteristic of myoglobin oxidation. These results coincided with the lowest degree of lipid oxidation, as deduced from the TBARS analysis. Lipid and myoglobin oxidation are linked; the oxidation of one of these leads to the formation of chemicals that promotes the oxidation of the other. Several studies reported the preservation of the fresh meat colour because of the incorporation of antioxidant compounds (Faustman et al., 2010). Thus, the starch-PLA bilayer with RS extract and CF could be applied for the purposes of meat preservation, the PLA loaded with the RS extract being the food contact layer.

4. CONCLUSIONS

The PLA-TPS bilayer films containing RS extract (into PLA) and CF (into TPS) exhibited improved functional properties for food preservation with respect to the monolayer films. TPS conferred oxygen barrier capacity to the laminates, while PLA offered a wet food contact option with water vapour barrier capacity. CF incorporation into TPS reinforced the strength of the films and improved their barrier capacity. The RS extract slightly reduced the PLA resistance and elongation at break but improved their oxygen barrier capacity. The tensile and barrier properties of bilayer films revealed changes in the performance of each layer associated with the interlayer migration of the low molecular weight compounds present in each monolayer. The bilayers with CF in the TPS sheet exhibited the lowest values of oxygen permeability while the RS extract in the PLA sheet slightly promoted the WVP and reduced resistance and elongation at break of the bilayers.

On the basis of their low oxygen permeability, the bilayers with CF reinforced TPS and PLA with and without RS antioxidant extract were used to evaluate the preservation capacity of pork meat, using PLA as the food contact layer in thermo-sealed bags. A noticeable antioxidant capacity of the RS extract was observed in the meat samples packaged with the TPScf-PLAes bags, while the microbial counts were also reduced throughout the cold storage time. Therefore, these bilayers had great potential to extend the shelf-life of meat samples, maintaining quality parameters and safety for longer, while using fractions of the RS waste which permit its valorisation.

5. ACKNOWLEDGEMENTS

The authors thank the Agencia Estatal de Investigación (Spain) for the financial support through projects PID2019-105207RB-I00/AEI/10.13039/501100011033 and Generalitat Valenciana [grant number GrisoliaP/2019/115].

6. REFERENCES

ASTM. (2005). E96/E96M-05. Standard Test Methods for Water Vapor Transmission of Materials. American Society for Testing and Materials, 1-11.

ASTM. (2010). D3985-05 Oxygen Gas Transmission Rate Through Plastic Film and Sheeting Using a Coulometric Sensor. Annual Book of ASTM Standards, C, 1–7. https://doi.org/10.1520/D3985-05.2

ASTM. (2012). ASTM D882-12 Standard test method for tensile properties of thin plastic sheeting. American Society for Testing and Materials, 12.

Andrade, J., González-Martínez, C., & Chiralt, A. (2022). Antimicrobial PLA-PVA multilayer films containing phenolic compounds. *Food Chemistry*, 375, 131861. https://doi.org/10.1016/j.foodchem.2021.131861

Anukiruthika, T., Sethupathy, P., Wilson, A., Kashampur, K., Moses, J. A., & Anandharamakrishnan, C. (2020). Multilayer packaging: Advances in preparation techniques and emerging food applications. *Comprehensive Reviews in Food Science and Food Safety*, 19(3), 1156–1186. https://doi.org/10.1111/1541-4337.12556

Avérous, L., Fringant, C., & Moro, L. (2001). Plasticized starch–cellulose interactions in polysaccharide composites. *Polymer*, 42(15), 6565–6572. https://doi.org/10.1016/S0032-3861(01)00125-2

Baghi, F., Gharsallaoui, A., Dumas, E., & Ghnimi, S. (2022). Advancements in Biodegradable Active Films for Food Packaging: Effects of Nano/Microcapsule Incorporation. *Foods*, 11(5), 760. https://doi.org/10.3390/foods11050760

Chawla, R., Sivakumar, S., & Kaur, H. (2021). Antimicrobial edible films in food packaging: Current scenario and recent nanotechnological advancements- a review. *Carbohydrate Polymer Technologies and Applications*, 2, 100024. https://doi.org/10.1016/j.carpta.2020.100024

Collazo-Bigliardi, S., Ortega-Toro, R., & Chiralt, A. (2019). Improving properties of thermoplastic starch films by incorporating active extracts and cellulose fibres isolated from rice or coffee husk. *Food Packaging and Shelf Life*, 22, 100383. https://doi.org/10.1016/j.fpsl.2019.100383

Fourati, Y., Magnin, A., Putaux, J.-L., & Boufi, S. (2020). One-step processing of plasticized starch/cellulose nanofibrils nanocomposites via twin-screw extrusion of starch and cellulose fibers. *Carbohydrate Polymers,* 229, 115554. https://doi.org/10.1016/j.carbpol.2019.115554

Freitas, P. A. V., Arias, C. I. L. F., Torres-Giner, S., González-Martínez, C., & Chiralt, A. (2021). Valorization of Rice Straw into Cellulose Microfibers for the Reinforcement of Thermoplastic Corn Starch Films. *Applied Sciences*, 11(18), 8433. https://doi.org/10.3390/app11188433

Freitas, P. A. V., González-Martínez, C., & Chiralt, A. (2020). Application of Ultrasound Pre-Treatment for Enhancing Extraction of Bioactive Compounds from Rice Straw. *Foods*, 9(11), 1657. https://doi.org/10.3390/foods9111657

Freitas, P. A. V., González-Martínez, C., & Chiralt, A. (2022a). Applying ultrasound-assisted processing to obtain cellulose fibres from rice straw to be used as reinforcing agents. *Innovative Food Science & Emerging Technologies*, 76, 102932. https://doi.org/10.1016/j.ifset.2022.102932

Freitas, P. A. V., González-Martínez, C., & Chiralt, A. (2022b). Antioxidant starch composite films containing rice straw extract and cellulose fibres. *Food Chemistry*, 400, 134073. https://doi.org/10.1016/j.foodchem.2022.134073

Galdeano, M. C., Mali, S., Grossmann, M. V. E., Yamashita, F., & García, M. A. (2009). Effects of plasticizers on the properties of oat starch films. *Materials Science and Engineering: C*, 29(2), 532–538. https://doi.org/10.1016/j.msec.2008.09.034

Hernández-García, E., Vargas, M., & Chiralt, A. (2022a). Starch-polyester bilayer films with phenolic acids for pork meat preservation. *Food Chemistry*, 385, 132650. https://doi.org/10.1016/j.foodchem.2022.132650

Hernández-García, E. Vargas, M., & Chiralt, A. (2022b). Biodegradable multilayer films for active food packaging, based on starch and polyesters with phenolic acids. Doctoral Thesis. Accessed September 05, 2022. <https://riunet.upv.es/bitstream/handle/10251/181473/Hernandez%20-%20Biodegradable%20multilayer%20films%20for%20active%20food%20packaging%20based%20on%20starch%20and%20polyeste....pdf?sequence=1&isAllowed=y>

Kaiser, K., Schmid, M., & Schlummer, M. (2017). Recycling of Polymer-Based Multilayer Packaging: A Review. *Recycling*, 3(1), 1. https://doi.org/10.3390/recycling3010001

Kargarzadeh, H., Johar, N., Ahmad, I. (2017). Starch biocomposite film reinforced by multiscale rice husk fiber. Composites Science and Technology, 151, 147-155.

Kim, H. W., Jeong, J. Y., Seol, K.-H., Seong, P.-N., & Ham, J.-S. (2016). Effects of Edible Films Containing Procyanidin on the Preservation of Pork Meat during Chilled Storage. *Korean Journal for Food Science of Animal Resources*, 36(2), 230–236. https://doi.org/10.5851/kosfa.2016.36.2.230

Mchugh, T. H., Avena-Bustillos, R., & Krochta, J. M. (1993). Hydrophilic Edible Films: Modified Procedure for Water Vapor Permeability and Explanation of Thickness Effects. *Journal of Food Science*, 58(4), 899–903. https://doi.org/10.1111/j.1365-2621.1993.tb09387.x

Menzel, C., González-Martínez, C., Vilaplana, F., Diretto, G., & Chiralt, A. (2020). Incorporation of natural antioxidants from rice straw into renewable starch films. *International Journal of Biological Macromolecules*, 146, 976–986. https://doi.org/10.1016/j.ijbiomac.2019.09.222

Moreno, O., Atarés, L., Chiralt, A., Cruz-Romero, M. C., & Kerry, J. (2018). Starch-gelatin antimicrobial packaging materials to extend the shelf life of chicken breast fillets. *LWT*, 97, 483–490. https://doi.org/10.1016/j.lwt.2018.07.005

Muller, J., González-Martínez, C., & Chiralt, A. (2017). Poly(lactic) acid (PLA) and starch bilayer films, containing cinnamaldehyde, obtained by compression moulding. *European Polymer Journal*, 95, 56–70. https://doi.org/10.1016/j.eurpolymj.2017.07.019

Pacquit, A., Lau, K., Mclaughlin, H., Frisby, J., Quilty, B., & Diamond, D. (2006). Development of a volatile amine sensor for the monitoring of fish spoilage. *Talanta*, 69(2), 515–520. https://doi.org/10.1016/j.talanta.2005.10.046

Peanparkdee, M., & Iwamoto, S. (2019). Bioactive compounds from by-products of rice cultivation and rice processing: Extraction and application in the food and pharmaceutical industries. *Trends in Food Science & Technology*, 86, 109–117. https://doi.org/10.1016/j.tifs.2019.02.041

Rasheed, M., Jawaid, M., Karim, Z., & Abdullah, L. C. (2020). Morphological, Physiochemical and Thermal Properties of Microcrystalline Cellulose (MCC) Extracted from Bamboo Fiber. *Polymers*, 13, 465.

Rasheed, M., Jawaid, M., Parveez, B., Hussain Bhat, A., & Alamery, S. (2021). Morphology, Structural, Thermal, and Tensile Properties of Bamboo Microcrystalline Cellulose/Poly(Lactic Acid)/Poly(Butylene Succinate) Composites. *Polymers*, 13(3), 465. https://doi.org/10.3390/polym13030465

Siracusa, V. (2012). Food Packaging Permeability Behaviour: A Report. *International Journal of Polymer Science*, 2012, 1–11. https://doi.org/10.1155/2012/302029

Siu, G. M., & Draper, H. H. (1978). A survey of the malonaldehyde content of retail meats and fish. Journal of Food Science, 43(4), 1147–1149. https://doi.org/10.1111/j.1365-2621.1978.tb15256.x

Sung, S.-Y., Sin, L. T., Tee, T.-T., Bee, S.-T., Rahmat, A. R., Rahman, W. A. W. A., Tan, A.-C., & Vikhraman, M. (2013). Antimicrobial agents for food packaging applications. *Trends in Food Science & Technology*, 33(2), 110–123. https://doi.org/10.1016/j.tifs.2013.08.001

Talón, E., Trifkovic, K. T., Nedovic, V. A., Bugarski, B. M., Vargas, M., Chiralt, A., & González-Martínez, C. (2017). Antioxidant edible films based on chitosan and starch containing polyphenols from thyme extracts. *Carbohydrate Polymers*, 157, 1153–1161. https://doi.org/10.1016/j.carbpol.2016.10.080

Topuz, F., & Uyar, T. (2020). Antioxidant, antibacterial and antifungal electrospun nanofibers for food packaging applications. *Food Research International*, 130, 108927. https://doi.org/10.1016/j.foodres.2019.108927

Wang, Q., Chen, W., Zhu, W., McClements, D. J., Liu, X., & Liu, F. (2022). A review of multilayer and composite films and coatings for active biodegradable packaging. *Npj Science of Food*, 6(1), 18. https://doi.org/10.1038/s41538-022-00132-8

Yang, W., Xie, Y., Jin, J., Liu, H., & Zhang, H. (2019). Development and Application of an Active Plastic Multilayer Film by Coating a Plantaricin BM-1 for Chilled Meat Preservation. *Journal of Food Science*, 84(7), 1864–1870. https://doi.org/10.1111/1750-3841.14608

CHAPTER 1.VI

Antioxidant starch composite films containing rice straw extract and cellulose fibres

Pedro A. V. Freitas, Chelo González-Martínez, Amparo Chiralt

Institute of Food Engineering for Development, Universitat Politècnica de València, 46022, Valencia, Spain

Food Chemistry (2023), 400, 134073

ABSTRACT

Antioxidant aqueous rice straw (RS) extract was obtained by a combined ultrasound-reflux heating process and cellulose fibres (CF) were purified by bleaching the extraction residue. Both fractions were incorporated into corn starch to obtain films by melt blending and compression moulding. CF (at 3% wt.) greatly increased the elastic modulus (by 200 %) and tensile strength at break (by 100%) while reducing film stretchability. Films with CF exhibited the greatest barrier capacity to water vapour and oxygen. The incorporation of RS extract (at 4, 6 and 8% wt.) plasticised the film's amorphous phase, but also reinforced the matrix to a certain extent. The active films showed a high degree of UV absorption and DPPH radical scavenging capacity. Mono-dose sunflower oil bags were obtained with films with CF and RS extracts that, to a great extent, prevent oil oxidation in an accelerated oxidative test under UV radiation throughout 50 days.

Keywords: bioactive constituents, active extracts, thermoplastic starch films, valorisation of residues, green extraction methods, circular economy.

1. INTRODUCTION

The valorisation of agricultural waste is of growing interest in the context of the circular economy. One potential use of the fractions obtained from lignocellulosic residues is that of the development of packaging materials with circulating resources (Mochane et al., 2021), thus helping to limit the disposal of waste in landfills and to eliminate greenhouse gas emissions while valorising the vegetal residues (Mak et al., 2020). One potential application of these residues is based on both their cellulosic content and bioactive phytochemicals, which could be used for producing packaging materials with improved functions, such as reinforced mechanical properties and antioxidant or antimicrobial activity. Of the agricultural waste, rice straw (RS) is the third-largest residue from agriculture after sugarcane bagasse and maize straw, presenting problematic waste management and non-economic value. Due to its high cellulose content (37 %, Freitas et al. (2022a)), RS is a good source of cellulosic components (microfibres, nanocrystals), which could be used as reinforcing materials for enhancing the film´s mechanical and barrier properties (Freitas et al. 2021 and 2022a). The lignocellulosic fraction consists of a complex matrix made up of crystalline cellulose microfibrils as the primary fibre component linked to a cementing matrix composed of hemicellulose and lignin (Chen et al., 2011), which have to be removed to obtain the purified cellulose. Several authors (Perumal et al., 2018; Freitas et al., 2022a) incorporated nanocrystals or cellulose fibres (CF) from RS into different polymer matrices, such as polyvinyl alcohol/chitosan, or starch/methylcellulose/gum Arabic blended films, to analyse their reinforcing capacity. Their incorporation into the polymeric matrix led to films which are stronger and have greater elastic modulus due to the fibre entanglement , which plays an important role in the force transferring from the matrix to fibrils and from fibrils to fibrils (Balakrishnan et al., 2018). Moreover, the RS has been shown to be a valuable source of phenolic compounds, such as ferulic, *p*-coumaric, protocatechuic or caffeic acids, tricin, pyrogallol or vanillin, among others (Menzel et al., 2020). Most of these phenolic compounds exhibited antioxidant and/or antimicrobial activity and can be obtained from RS by water extraction, leading to aqueous extracts with proven antioxidant capacity (Menzel et al., 2020; Freitas et al. 2020). These active extracts could be incorporated into biodegradable polymers for the purposes of obtaining sustainable active packaging materials for food packaging applications. These active packages could contribute to enhancing food preservation by adding new functionalities to the materials, such as antioxidant and antimicrobial activities, which could extend the shelf-life and enhance the safety of the foodstuff.

Starch is a biodegradable polymer, thermoplastic in nature, and considered a valuable material for food packaging. The major disadvantages of the starch-based films are related to their low mechanical resistance, water sensitivity and solubility and limited water vapour barrier properties. Nevertheless, these films exhibit a great oxygen barrier capacity, which is essential for the prevention of oxidative processes in foodstuffs. This can be enhanced by

incorporating both natural antioxidant compounds, which can act as oxygen or radical scavenging agents, and cellulose fibres (CF) (Talón et al., 2019). Therefore, it is possible to address a new strategy to develop sustainable packaging materials by using biodegradable polymers, such as starch, and lignocellulosic waste fractions, such as cellulose components and bioactive extracts. This is aligned with the circular bioeconomy, reusing agricultural waste, and the Sustainable Development Goals as defined by the United Nations (Economic & Affairs, 2018). The use of these RS fractions in starch-based films could extend the shelf-life of perishable products that are highly susceptible to lipid oxidation, such as unsaturated sunflower oils (with 70 % unsaturated fatty acids), while enhancing the barrier and mechanical properties of the packaging material. This strategy is also in line with the current consumer demand for non-synthetic additives and contributes to proper environmentally-friendly waste management, producing added-value materials, reducing food losses, and boosting the circular bioeconomy (Ng et al., 2015).

Very few studies incorporating both cellulose and bioactive fractions from agricultural waste have been carried out to the best of our knowledge. Menzel (2020) studied the improvement of starch film properties by using a three-principle approach: antioxidants, cross-linking, and reinforcement, and obtained films with valuable phenolic compounds and cellulose fibres from sunflower hulls, and citric acid as the crosslinker. Films had inherent antioxidant activity and a better mechanical performance, in terms of stress resistance and extensibility, while an increase in the branch-chain length of citric acid cross-linked starch was observed. Sá et al. (2020) developed films based on bacterial cellulose produced from cashew apple juice and lignin and cellulose nanocrystals from the cashew tree pruning fibre. Lignin and cellulose nanocrystals enhanced the tensile and barrier properties of the films, while lignin provided films with UV-absorbing and antioxidant properties.

Therefore, the aims of this study were to use valorised fractions of RS (antioxidant aqueous extract and CF) to improve the functional properties of starch-based films and to evaluate how well they prevent sunflower oil oxidation. To this end, films were obtained by melt blending and compression moulding and characterised as to their microstructure, mechanical, optical, and barrier properties, as well as their thermal behaviour and antioxidant activity. Finally, the performance of the films in the prevention of sunflower oil oxidation was evaluated in mono-dose oil bags submitted to an accelerated oxidation test.

2. MATERIAL AND METHODS

2.1 Chemicals

Corn starch (27 % amylose) was supplied by Roquette (Roquette Laisa, Spain). Glycerol, acetic acid, sodium carbonate (Na_2CO_3) (99.5 % purity), di-phosphorus pentoxide (P_2O_5), and magnesium nitrate ($Mg(NO_3)_2$) were supplied by PanReac Quimica S.L.U. (Castellar del Vallés,

Spain). Gallic acid, Folin-Ciocalteau reagent (2 N), methanol (> 99.9 purity), 2,2-Diphenyl-1-picrylhydrazyl (DPPH), sodium chlorite, 2-thiobarbituric acid (> 98 % purity), and 1,1,3,3-tetramethoxypropane were purchased from Sigma-Aldrich (St. Louis, MO, USA). Iodine (99.5 % purity) was obtained by Acros Organics® (Geel, Belgium).

2.2. Obtaining Rice Straw fractions

Aqueous extract and cellulose fibres were obtained from rice straw (RS), as described in previous studies (Freitas et al., 2020 and 2022a). RS (*Oryza sativa* L.), J. *Sendra var.*, was obtained from L'Albufera rice fields (Valencia, Spain) and was vacuum dried (0.8 mmbar, 50 ± 2 °C, 16 h), ground using a grinding machine (IKA, model M20, IKA Werke GmbH & Co. KG, Staufen, Germany), and sieved (particles of under 0.5 mm) before the extraction process.

2.2.1 Aqueous extract

Aqueous RS extract was obtained according to Freitas et al. (2020), by applying a sequential combination of ultrasound followed by a reflux heating step, using a RS: distilled water ratio of 1:20 (w/v). The aqueous dispersion was sonicated at 25 °C (using an ice bath) for 30 min using a probe high-intensity ultrasonic homogeniser (Vibra CellTM VCX750, 750 W power, Sonics & Material, Inc., Newtown, CT, USA), operating at a frequency of 20 kHz, 40 % sonication amplitude. Afterwards, the plant suspension was heated at 100 °C for 1 h using a typical reflux heating device. The suspension was filtered with a qualitative filter (Filterlab), and the filtrate was freeze-dried (Telstar, model LyoQuest-55) at -65 °C and 0.8 mbar for 72 h. The freeze-dried RS extract was stored in a dark bottle at 4 ± 2 °C until further use. The total phenolic content (TPC) of the RS extract was 37.1 ± 0.4 mg gallic acid equivalent (GAE) per g of freeze-dried extract, according to the Folin-Ciocalteu method (Freitas et al. 2020). The antioxidant capacity of the extract, evaluated by the 2,2-Diphenyl-1-pikryl-hydrazyl (DPPH) radical scavenging method (Brand-Williams et al., 1995; Menzel et al., 2019), and expressed as EC_{50} value, was 6.3 ± 0.3 mg freeze-dried extract/mg DPPH. The EC_{50} value is defined as the ratio of sample to DPPH required to reduce the DPPH concentration by 50 % when reaction stability is achieved.

2.2.2 Cellulose fibres

The insoluble residue from the aqueous extraction of RS (section 2.2.1) was dried (40 °C for 48 h), and used to obtain cellulose fibres (CF), as reported by Freitas et al. (2022a). Briefly, the bleaching step was performed by mixing the lignocellulosic residue and the bleaching solution at 5 % (w/v), which consisted of a solution of equal parts of sodium chlorite solution (1.7 %, w/v), acetate buffer solution (2 N), and distilled water. The mixture was heated at reflux for 4 cycles of 4 hours each. After the bleaching cycles, the bleached cellulose fraction was dried at 35 °C for 48 h and ground using a milling machine (pulses of 2 s for 20 min, model M20, IKA

Werke GmbH & Co. KG, Staufen, Germany) to obtain the CF. The chemical composition of the CF, analysed according to the NREL/TP-510-42,618 method (Sluiter, 2008), was 66 % cellulose, 10 % hemicellulose, 5 % lignin, and 5 % ashes (Freitas et al. 2022a). Likewise, the morpho-geometric characteristics of CF evaluated by FESEM showed major cumulative frequencies of lengths and thicknesses below 200 µm and 5-15 µm, respectively (Freitas et al., 2021).

2.3 Film preparation

Thermoplastic starch-based films were obtained with and without CF at 3 % (wt.) with respect to the total starch mass, since this was the CF ratio that gave rise to the maximum reinforcing capacity in a previous study (Freitas et al., 2021). Likewise, RS extract at 0, 4, 6, and 8 % wt. (with respect to the total starch mass) was incorporated into TPS films with and without CF. Films were obtained by melt blending of the components and subsequent compression moulding, using glycerol as plasticiser at 30 % wt. with respect to the total starch mass. Pre-conditioned starch (P_2O_5 at 25 °C for 7 days) was firstly mixed with the other film components and melt-blended in an internal mixer (HAAKETM PolyLabTM QC, Thermo Fisher Scientific, Karlsruhe, Germany) at 130 °C and 50 rpm for 10 min. For each treatment, the obtained solid mixture was milled and conditioned at 25 °C and 53 % relative humidity (RH) (using $Mg(NO_3)_2$ saturated solution) for one week. Thereafter, the milled pellets (4 g) were put onto Teflon sheets and compression-moulded in a heat plates hydraulic press (Model LP20, Labtech Engineering, Thailand) as follows: preheating at 160 °C for 3 min, compression at 30 bars and 160 °C for 2 min, followed by 130 bars for 6 min (160 °C), and then a final cooling to 80 °C. All films were conditioned at 25 °C and 53 % RH for one week before their characterisation.

2.4 Film characterisation

2.4.1 Film microstructure

A Field Emission Scanning Electron Microscope (ULTRATM 55, Zeiis, Oxford Instruments, UK) was used to observe the morphologies of the cross-sections of the films. The conditioned samples (P_2O_5 for 1 week at 25 °C) were cryo-fractured by immersion in liquid nitrogen and then covered with platinum using an EM MED020 sputter coater (Leica BioSystems, Barcelona, Spain). The micrographs were taken under vacuum and at 2.0 kV acceleration voltage.

2.4.2 Thermal analysis

A TGA analyser (TGA 1 Stare System analyser, Mettler-Toledo, Switzerland) was used to perform the thermogravimetric analysis (TGA) of the films. Conditioned film samples (P_2O_5 for 1 week at 25 °C) of about 3-5 mg were weighed in alumina pans and heated from 25 to 700 °C at a heating rate of 10 °C.min^{-1} under a nitrogen atmosphere (10 mL.min^{-1}). The thermal stability for each treatment was evaluated in terms of the initial (T_{on}) and maximum

degradation rate (T_p) temperatures, and the residual mass by analysing the TGA curves and their first derivative (DTGA). The measurements were taken in duplicate.

The phase transitions of the films were analysed by differential scanning calorimetry (DSC) using a DSC Stare System analyser (Mettler-Toledo GmbH, Switzerland). Dry conditioned samples (5-7 mg) were sealed in aluminium pans and heated from 25 to 160 °C, then cooled to 25 °C, and subsequently heated again to 160 °C at a heating rate of 10 °C.min^{-1} under nitrogen atmosphere (10 mL.min^{-1}). The analyses were performed in duplicate.

2.4.3 Equilibrium water content and water solubility

The equilibrium water content of the films, conditioned at 53% RH and 25°C for two weeks, was determined as described by Freitas et al. (2021). Film samples (3 cm x 3 cm) were dried at 60 °C for 24 h, and then placed into desiccators containing P_2O_5 at 25 °C for two weeks. For each treatment, the moisture content was determined from the total mass loss of the film after the drying process. The measurements were taken in triplicate.

The water solubility of the films was determined according to the methodology described by Talón et al. (2017). Conditioned film samples (P_2O_5 at 25 °C for two weeks) of about 2 cm x 2 cm were placed on a mesh and immersed in a crucible containing 30 mL of distilled water at 25 °C for 24 h. Thereafter, the crucibles were dried in an oven (J. P. Selecta, S. A., Spain) at 60 °C for 48 h and then placed in desiccators containing P_2O_5 at 25 °C for one week. The water solubility of the films was expressed as the mass of solubilised film per 100 g of dry film. The measurements were taken in triplicate.

2.4.4 Tensile properties

The tensile properties of the films, typically tensile strength at break (TS), elongation at break (E), and elastic modulus (EM), were determined according to ASTM D882 (ASTM, 2012) using a universal test machine (TA.XTplus model, Stable Micro Systems, Haslemere, England). Before the analysis, the films were conditioned at 25 °C and 53 % RH for two weeks. The film samples (25 mm x 100 mm) were grabbed by two grips initially separated by 50 mm and stretched at a crosshead speed of 50 mm.min^{-1}. Eight samples were evaluated for each formulation.

2.4.5 Barrier properties

The oxygen permeability (OP) of the films was determined according to ASTM D3985-05 (ASTM, 2010) methodology using an Oxygen Permeation Analyser (Model 8101e, Systech Illinois, Illinois, USA) at 25 °C and 53 % RH. The area of the films was 50 cm^2 and the oxygen transmission rate (OTR) was obtained every 15 min until equilibrium was reached. The measurements were taken in duplicate.

The water vapour permeability (WVP) of the films, expressed as g.mm.kPa^{-1}h^{-1}.m^{-2}, was obtained gravimetrically according to ASTM E96/E96M (ASTM, 2005), with modifications described by McHugh et al. (1993). Conditioned film samples (at 53 % RH and 25 °C, for two weeks) were cut (Ø = 3.5 cm), sealed in Payne permeability cups (Elcometer SPRL, Hermelle/s Argenteau, Belgium) containing 5 mL of distilled water (100 % RH), and placed into desiccators at 25 °C and 53 % RH ($Mg(NO_3)_2$). The cups were weighed periodically (ME36S, Sartorius, ± 0.00001 g, Fisher Scientific, Hampton, NH, USA) every 1.5 h for 27 h. The WVP of the films were determined from the water vapour transmission rate, which was determined from the slope of the weight loss *vs.* time curve. For each treatment, the analysis was performed in triplicate.

2.4.6 Optical properties

The optical properties of the films were obtained based on the Kubelka-Munk theory of multiple scattering using a spectrocolorimeter (CM-3600d, Minolta Co., Japan). The reflection spectra (R) of the films from 400 to 700 nm were obtained on white (R_g) and black (R_0) backgrounds. The internal transmittance (T_i) and the infinite reflectance (R_∞) were obtained according to Eqs. 1-4. The film colour coordinates *L** (lightness), *a** (redness-greenness), and *b** (yellowness-blueness) were obtained from the R_∞ spectra, considering observer 10º and illuminant D65. Finally, the psychometric colour coordinates were obtained: chroma (C_{ab}^*) (Eq. 5), hue angle (h_{ab}^*) (Eq. 6), and total colour difference (ΔE^*) (Eq. 7).

The light barrier properties of the films were evaluated by measuring the UV-vis spectra ranging from 200 to 900 nm using a UV-visible spectrophotometer (Evolution 201, Thermo Scientific) operating in light transmission mode.

$$T_i = \sqrt{(a - R_0)^2 - b^2} \quad (1)$$

$$R_\infty = a - b \quad (2)$$

$$a = \frac{1}{2}\left[R + \left(\frac{R_0 - R + R_g}{R_0 \times R_g}\right)\right] \quad (3)$$

$$b = \sqrt{a^2 - 1} \quad (4)$$

$$C_{ab}^* = \sqrt{a^{*2} + b^{*2}} \quad (5)$$

$$h^{**}_{ab} = arctg\left(\frac{b^*}{a^*}\right) \quad (6)$$

$$\Delta E^* = \sqrt{(\Delta L^*)^2 + (\Delta a^*)^2 + (\Delta b^*)^2} \quad (7)$$

Where $\Delta L^* = (L^* - L_0^*)$; $\Delta a^* = (a^* - a_0^*)$; $\Delta b^* = (b^* - b_0^*)$; and L_0^*, a_0^*, and b_0^* are the colour coordinates of the fillets at initial time.

2.4.7 Phenolic content and antioxidant properties of the films

The total content of phenolic compounds in the processed films was determined by dissolving a determined mass of films in distilled water and quantifying the total phenolic compounds released into the aqueous media and their corresponding antioxidant capacity as described by (Collazo-Bigliardi et al., 2019), with some modifications. Conditioned film samples (P_2O_5 at 25 °C for two weeks) of about 1.5 g were immersed in 100 mL of distilled water and stirred in dark bottles for 16 h at 20 ± 2 °C. Afterwards, the samples were filtered (Filter-Lab, 0.45 µm) and the filtrate analysed as to the TPC and the radical scavenging activity (EC_{50}), as described in section 2.2.1. All measurements were taken in triplicate.

2.4.8 Prevention of sunflower oil oxidation with mono-dose film bags

The antioxidant properties of the films with RS extracts were validated by packaging sunflower oil in thermo-sealed mono-dose bags of the films and storing it for 50 days under accelerated oxidation conditions. To this end, TPS-8 and TPScf-8 films, and their corresponding black samples without RS extract, TPS and TPScf, were selected, based on their antioxidant content and oxygen barrier capacity. Film samples, 7 cm x 11 cm in size, were previously thermo-sealed using a vacuum sealer (Vacio Press, Saeco) to obtain rectangular bags. Then, 7 mL of commercial sunflower oil was placed into the bags and thermo-sealed (Fig. 3). To validate the oxidation conditions, open Petri dishes containing 7 mL of sunflower oil was used as sample control. The bags were stored in a chamber at 30 °C, 53 % RH, and exposed to fluorescent light (intensity of 1000-1500 lux) at 30 cm from the samples for 50 days. The oxidative stability of the packaged oil samples was evaluated in terms of the peroxide index and the 2-thiobarbituric acid reactive substance (TBARS) index on days 0, 10, 20, 35, and 50 of storage. The oil samples from two bags of each film were analysed at each storage time.

2.2.1.1. Peroxide index

The peroxide index of the sunflower oil was determined according to the titrimetric method (IUPAC - International Union of Pure & Applied Chemistry). For this purpose, oil samples of about 1 g were dissolved with 10 mL organic solvent consisting of glacial acetic acid: decan-1-ol in a ratio of 3:2 (v/v). 200 µL of saturated potassium iodide solution was added and kept in the dark for 1 min. Afterwards, 50 mL distilled water was added, and the dispersion was titrated using an automatic titrator (Titrando, Metrohm Ion Analysis, Switzerland) with 0.01 or 0.001 M sodium thiosulfate, depending on the expected peroxide concentration. The procedure was performed in duplicate for each treatment.

2.2.1.2. The 2-thiobarbituric acid reactive substance (TBARS) assay

The TBARS index of the oil samples was performed according to the method previously described by Papastergiadis et al. (2012). Briefly, 1 g of sample was mixed with 5 mL distilled water, vortexed for 2 min, and centrifuged at 5000*g* for 5 min. Subsequently, the aqueous phase was separated and collected, and the procedure was repeated twice. 2 mL of the aqueous extract was mixed with 2 mL of 2-thiobarbituric acid solution (46 mM) in a test tube and heated at 100 °C for 35 min. Afterward, the tubes were cooled to room temperature and the absorbance was obtained at 532 nm. The TBARS index was expressed as mg malonaldehyde (MDA) per kg of sunflower oil, using 1,1,3,3-tetramethoxypropane as standard (0.5 – 12 μM).

2.5 Statistical analysis

The experimental data were analysed through a multifactorial analysis of variance at a 95 % confidence level using the Minitab Statistical Program (version 17). Tukey's studentised range (HSD) test, considering the least significant difference (α) of 5 %, was applied to determine whether there were significant differences among the samples.

3. RESULTS AND DISCUSSION

3.1. Film microstructure and appearance

The microstructure of the obtained films can be observed in Fig. 1, where the FESEM micrographs of the different samples are shown. The typical homogeneous matrix of the starch film was obtained when no cellulosic fibre or extract was incorporated into the formulation, as reported by other authors (Tavares et al., 2019). The incorporation of the RS extract in different ratios provoked slightly more heterogeneous films, in which small particle aggregates appeared dispersed in the starch matrix (arrows in Fig. 1). The number of particles increased as the extract ratio rose in the films, which suggests that the RS extract compounds were only partially compatible with the starch matrix and separated from the starch continuous phase during the melt blending process. Some compounds were homogeneously incorporated, but some separated as visible aggregates in the FESEM micrographs. Similar behaviour was observed in PLA films which incorporated RS extract (Freitas et al. 2022b). The incorporation of 3 % CF into the films also produced a heterogenous structure (Fig. 1), showing the large fibres embedded in the starch matrix. A good interfacial adhesion can be observed between CF particles and the polymer matrix, as deduced from the micrographs in which no CF separation can be seen to have occurred during the film cryofracture, both in films with and without RS extract.

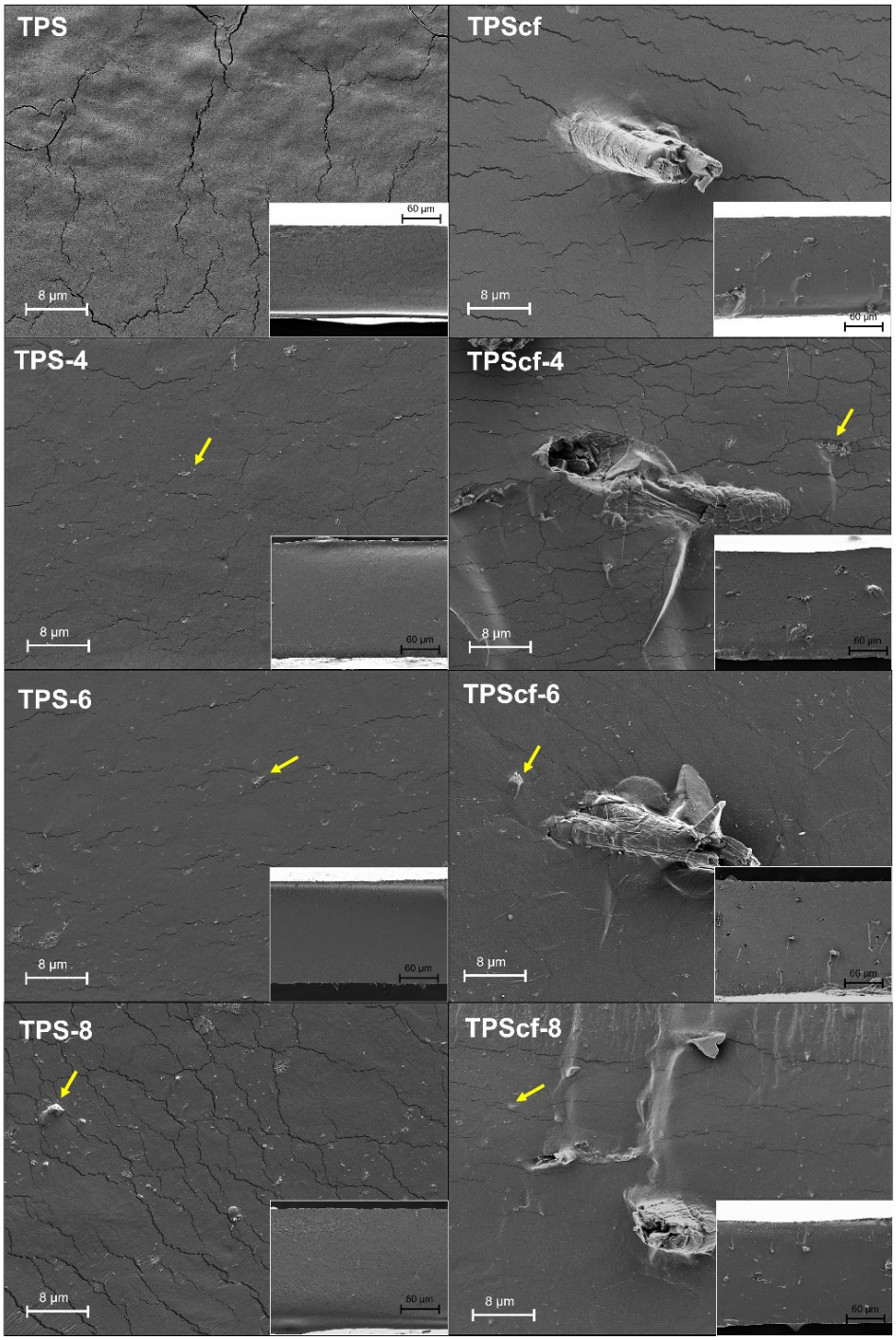

Fig. 1. FESEM micrographs (2000x magnification) of films with different RS extract ratios (0, 4, 6 and 8 % w/w) with (right) and without (left) cellulose fibres (CF). Arrows marked the RS extract aggregates formed in the starch matrix. Embedded micrographs (400x magnification) show a complete image of the film's cross section.

Incorporating both RS fractions provoked notable changes in the film-light interactions that were reflected in the differences of the internal transmittance and colour between the films. Fig. 2a shows the film transmittance in the UV-Vis wavelength range, where these differences

can be appreciated for the films with CF and RS extracts with respect to the TPS film. As expected, CF led to a decrease in the transmittance of the TPS films, in the complete wavelength range, whereas the RS extract absorbed UV radiation (λ < 400 nm) and low wavelength VIS radiation intensely, giving rise to the appearance of colour. Films containing both CF and RS extracts had the lowest transmittance values, which represents a good light barrier able to protect foods sensitive to light induced oxidative processes. Both light dispersions provoked by the dispersed particles and selective absorption due to the coloured compounds of the RS extract contributed not only to the film's appearance but also to their light barrier capacity.

The colour parameters (Lightness: L^*, Chrome: C_{ab}^* and hue: h_{ab}^*) of the films are shown in Table 1, in which the impact of light interactions with the films on their appearance may be quantified through the total colour difference with respect to the TPS films without RS components. The greatest colour difference was observed for films with 8 % RS extract with and without CF; this, however, decreased when the ratio of RS extract was reduced, in line with the lower content of coloured compounds from the RS extract. The incorporation of CF did not provoke relevant colour differences in the films, only promoting a slightly more vivid colour (higher C_{ab}^* values) due to the enhancement of light scattering by the dispersed fibres. Nevertheless, this effect was completely attenuated in films containing RS extract, where the presence of CF did not imply significant colour changes with respect to the corresponding film without fibres, despite the small differences observed in the transmittance spectra. In contrast, the RS extract led to a reduction in the film's lightness, an increase in colour saturation (C_{ab}^*) and a displacement of the hue value (h_{ab}^*) towards a redder colour, proportionally to the extract ratio in the films.

Table 1. Colour parameters (Lightness: L^*, Chrome: C_{ab}^* and hue: h_{ab}^*) and total global difference (ΔE^*) of TPS films with different RS extract ratios (0, 4, 6, and 8 % wt.) with and without CF.

Formulation	L^*	C_{ab}^*	h_{ab}^*	ΔE^*
TPS	$88.5 \pm 0.1^{a,1}$	$7.57 \pm 0.10^{a,2}$	$92.5 \pm 0.1^{a,1}$	-
TPS-4	$68.9 \pm 1.4^{b,1}$	$43.2 \pm 1.4^{c,1}$	$80.6 \pm 0.1^{b,1}$	40.4 ± 2.0^{d}
TPS-6	$60.4 \pm 0.7^{c,1}$	$48.7 \pm 0.5^{d,1}$	$74.3 \pm 1.2^{c,1}$	50.1 ± 0.7^{bc}
TPS-8	$55.5 \pm 2.0^{d,1}$	$47.7 \pm 0.9^{d,1}$	$70.0 \pm 1.8^{d,1}$	52.5 ± 0.6^{a}
TPScf	$88.1 \pm 0.2^{a,1}$	$8.3 \pm 0.5^{b,1}$	$92.6 \pm 0.3^{a,1}$	0.8 ± 0.4^{e}
TPScf-4	$67.9 \pm 1.2^{b,1}$	$42.8 \pm 0.8^{d,1}$	$80.1 \pm 0.8^{b,1}$	40.8 ± 1.2^{d}
TPScf-6	$60.5 \pm 0.8^{c,1}$	$47.7 \pm 0.2^{d,1}$	$74.3 \pm 0.7^{c,1}$	49.2 ± 0.6^{c}
TPScf-8	$59.3 \pm 0.7^{c,1}$	$49.4 \pm 0.6^{d,1}$	$72.9 \pm 0.8^{c,1}$	51.4 ± 0.3^{ab}

Different subscript letters indicate significant differences between samples of the same group (TPS or TPScf films). Different numbers indicate significant differences between TPS and TPScf samples with the same ratio of RS extract (Tukey test, $p < 0.05$).

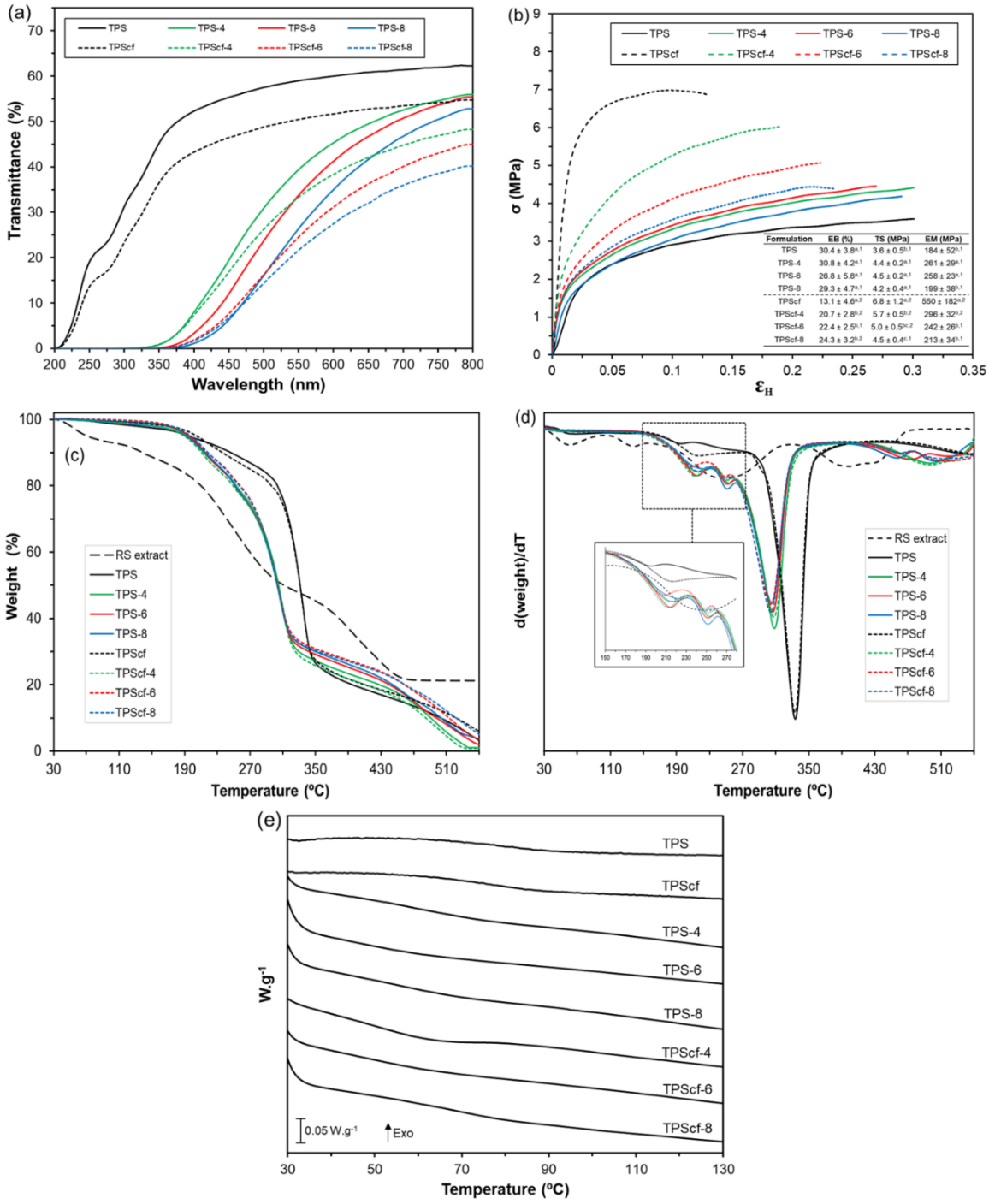

Fig. 2. (a) UV-Vis spectra, (b) Stress-strain curves and tensile properties (inserted table) (EB, TS, and EM), (c) TGA curves, (d) DTGA first derivative curves, and (e) second heating DSC thermograms of thermoplastic starch films with different contents of RS extract (0, 4, 6, and 8 % wt.) with (continuous lines) and without (dashed lines) CF. For the mechanical properties, different subscript letters indicate significant differences between samples of the same group (TPS or TPScf films). Different numbers indicate significant differences between TPS and TPScf samples with the same ratio of RS extract (Tukey test, $p < 0.05$).

3.2. Thermal behaviour of the films

The DSC thermograms (second heating step) of different samples showed the glass transition of starch (Fig. 2e). The T_g midpoint values are shown in Table 2, where the plasticising effect of the RS extract on the TPS matrix may be observed, whereas no significant changes in the T_g were provoked by the addition of CF. The observed T_g values of TPS are in the range reported by other authors (Collazo-Bigliardi et al. 2019; Ordoñez et al., 2021), whereas the incorporation of the RS extract (at 4-8 %) reduced T_g by about 15 °C. This suggests that the extract compounds provoked a reduction in the mean molecular weight of the starch matrix, increasing the free-volume of the polymer chains and promoting their molecular mobility (Dalnoki-Veress et al., 2001). Other studies (Menzel et al., 2020) also reported the plasticising effect of the RS aqueous extract on thermoprocessed potato starch films. In this study, lower molar mass and shorter amylose branches were determined in the glycerol plasticised starch films, which explained the reduction in the glass transition of the starch matrix. The presence of phenolic acids in the extract promoted the degradation of starch during the melt-blending process, whereas glycerol was observed to exert a protective effect, in agreement with what has been reported by other authors (Carvalho et al., 2003).

Fig. 2c shows the TGA curves of both the different films and of the RS extract. The TGA curves of all the films exhibited the typical degradation behaviour of glycerol-plasticised starch with a first mass loss step, before the main degradation peak, corresponding to the loss of bonded water and glycerol (2 % wt.). The thermal stability of the starch matrix was also affected by the presence of the RS extract, but it was not notably affected by the incorporation of CF. This incorporation (mass fraction 0.02) hardly modified the TGA curve of the TPS films, only slightly delaying the loss of glycerol in the first mass loss step, probably due to the enhanced retention of glycerol brought about by fibre interactions. The mechanism proposed for starch thermo-degradation is a non-oxidative process, which starts first with a scission of glycosidic bonds and the formation of the glycosidic radicals; the starch macromolecules are not directly converted into low molecular weight volatile products, char and levoglucosan, but undergo intermediate physical and chemical changes (Yang et al., 2013). Thus, the depolymerisation of the starch macromolecules takes place with the formation of β-(1,6) anhydro d-glucopyranose (levoglucosan), 2-furaldehyde (furfural) and a range of lower molecular-weight volatile and gaseous fragmentation products (Danilovas et al., 2014). The typical temperature at which the main polymer degradation occurs is in the range of 250-350 °C (Danilovas et al., 2014), as also observed in the film samples. Nevertheless, although all the films with extracts exhibited the main thermo-degradation peak at a temperature about 30 °C lower than that of the extract-free films, this difference was not significantly dependent on the concentration of the extract in the matrix. Both the onset and peak temperatures were affected. The thermo-degradation temperature falls when the molecular weight of the polymer or its degree of crystallisation decreases. In general, the greater the polymer molar mass and cohesion forces of the matrix,

the higher the degradation temperature (Danilovas et al., 2014). Therefore, the reduction in the thermal stability of the starch polymers provoked by the extract compounds could be attributed to the starch depolymerising during thermal processing, which is enhanced when there is extract present in the blend, as reported by Menzel et al. (2020), and commented on above. The different ratio of extract in the blend did not significantly affect the thermal stability of the starch films, which suggests that depolymerising occurred to a similar degree in every case. A similar response was also observed for the T_g values of the starch matrix, as a function of the extract concentration, which also points to a similar degree of polymer hydrolysis, regardless of the concentration of extract in the blend. The last degradation step of the starch films, at between 400-600 °C, was attributed to the degradation of the first step fragmentation products (Danilovas et al. 2014) and the small differences between samples may be due to the contribution of the most thermostable fractions of the incorporated extract.

The TGA curve of the pure extract revealed the different steps of weight loss prior to and after the main polymer degradation step. The observed peaks in the DTGA curves allow for a better identification of the four mass loss steps: the first (up to about 125 °C) could be attributed to the loss of bounded water (6 % mass loss), the second (125-195 °C) could be assigned to the degradation of low molecular compounds, such as sugars and phenolic compounds (6 % mass loss), the third broad event (46 % mas loss), at between 195-400 °C, could be mainly attributed to the degradation of the hemicellulose fractions, which degrade at between 150-350 °C, and the fourth step, at between 400-600 °C, (25 % mass loss), may be ascribed to the residual lignin fraction that undergoes gradual decomposition in the range of 250–500 °C (Collazo-Bigliardi et al., 2018). The residual mass, 17.3 %, must be mainly attributed to the silica, present in large quantities in rice straw (17 %, Freitas et al., 2021) in which the extract was enriched. The thermal degradation of the cellulose fraction was previously reported (Freitas et al., 2022a), and exhibited two degradation steps; the main first peak at 286 °C, attributed to the cellulose and residual hemicellulose degradation, and the second at 340–500 °C, attributed to the degradation of the residual lignin and the fragmentation products formed in the first step (Theng et al., 2017).

Therefore, thermal analysis revealed changes in the amorphous phase of the starch films associated with the partial hydrolysis of starch polymers by the action of the RS extract that favoured film plasticisation while reducing the thermal stability of the polymeric matrix.

Table 2. Onset (T_{on}) and peak (T_p) temperatures and mass loss (%Δm) of the different thermodegradation steps and final residual mass of the starch-based films with and without CF and different RS extract ratios. The DSC glass transition temperature (T_g) from the second heating scan was also included.

	TGA							DSC
	[100-400] °C			[400-600] °C			Residue (%)	T_g
Formulation	T_{on}	T_p	%Δm	T_{on}	T_p	%Δm		
TPS	$156 \pm 1^{a,1}$	$333 \pm 1^{a,1}$	$81 \pm 1^{a,1}$	$432 \pm 2^{a,2}$	$548 \pm 3^{a,1}$	17 ± 2^{c}	$2.1 \pm 0.1^{a,1}$	$92 \pm 5^{a,1}$
TPS-4	$129 \pm 1^{b,1}$	$308 \pm 1^{b,1}$	$76 \pm 1^{b,1}$	$401 \pm 1^{b,1}$	$499 \pm 2^{b,1}$	21 ± 1^{a}	$1.4 \pm 0.5^{a,1}$	$64 \pm 3^{b,1}$
TPS-6	$128 \pm 3^{b,1}$	$306 \pm 2^{b,1}$	$74 \pm 1^{bc,1}$	$397 \pm 3^{bc,1}$	$476 \pm 1^{c,2}$	23 ± 1^{ab}	$1.8 \pm 0.2^{a,2}$	$61 \pm 1^{b,1}$
TPS-8	$128 \pm 3^{b,1}$	$305 \pm 2^{b,1}$	$72 \pm 1^{c,1}$	$393 \pm 4^{c,1}$	$515 \pm 9^{b,1}$	24 ± 1^{a}	$1.7 \pm 1^{a,1}$	$63 \pm 1^{b,1}$
TPScf	$152 \pm 4^{a,1}$	$332 \pm 1^{a,1}$	$82 \pm 1^{a,1}$	$448 \pm 3^{a,1}$	$564 \pm 2^{a,1}$	15 ± 1^{c}	$1.6 \pm 0.1^{b,2}$	$85 \pm 3^{a,1}$
TPScf-4	$126 \pm 2^{b,1}$	$308 \pm 2^{b,1}$	$78 \pm 1^{b,1}$	$402 \pm 1^{b,1}$	$499 \pm 2^{c,1}$	20 ± 1^{b}	$0.7 \pm 0.5^{b,2}$	$61 \pm 1^{b,1}$
TPScf-6	$128 \pm 4^{b,1}$	$305 \pm 2^{b,1}$	$73 \pm 2^{c,1}$	$401 \pm 1^{b,1}$	$519 \pm 2^{b,1}$	24 ± 2^{a}	$2.5 \pm 0.3^{a,1}$	$63 \pm 4^{b,1}$
TPScf-8	$127 \pm 7^{b,1}$	$305 \pm 1^{b,1}$	$74 \pm 1^{c,1}$	$398 \pm 4^{b,1}$	$517 \pm 4^{b,1}$	23 ± 1^{a}	$1.5 \pm 0.4^{b,1}$	$66 \pm 7^{b,1}$

Different subscript letters indicate significant differences between samples of the same group (TPS or TPScf films). Different numbers indicate significant differences between TPS and TPScf samples with the same ratio of RS extract (Tukey test, $p < 0.05$).

3.3. Water relations, and mechanical and barrier properties of the films

The incorporation of CF and RS extracts into TPS films affected water relations (water sorption and solubility), tensile behaviour and the barrier capacity of the TPS films, which would, in turn, affect their functionality as packaging materials. Table 3 shows the equilibrium moisture content and water solubility of the films, where the promoted changes can be observed. Other authors (Avérous et al., 2001a; Freitas et al., 2021; Wang et al., 2018) reported that cellulose fibres decreased the moisture diffusion coefficient and sorption capacity of starch composites as the fibre content increased. These effects were attributed to the hydrogen bonds formed between the matrix phase and the fibre phase within the composite, which blocks part of the active sites of the matrix for water interactions and adsorption. However, at the low ratio of fibres incorporated into the films, no significant differences in the equilibrium moisture content were observed for the extract-free films. The incorporation of extracts into fibre-free TPS films did not produce any significant changes in their equilibrium moisture content either. In contrast, the incorporation of extracts into TPS films containing fibre decreased the equilibrium water content, which suggests a notable reduction in the number of active points for water adsorption in the films, probably due to the enhancement of internal hydrogen bonding within the matrix.

The water solubility of the films was only significantly reduced in the films with CF. This reduction has also been reported by other authors (Avérous et al., 2001; Fourati et al., 2020) and can be explained by the insoluble nature of CF and its bonding to the starch matrix through -OH groups, reducing the availability of the starch chains to interact with the water molecules. In contrast, the incorporation of a RS extract tends to slightly enhance the film's solubility, regardless of its concentration. This can be explained by the water solubility of the extract compounds, as well as by the partial hydrolyses of amylose chains, deduced from the thermal analyses, which would promote the starch matrix solubility.

As concerns the barrier capacity of the films, the RS extract enhanced the oxygen barrier capacity but worsened the water vapour barrier of the films, regardless of its concentration (Table 3). Nevertheless, when films contained CF, the OP values of the films decreased, and these lower values were maintained when the RS extract was incorporated in different ratios. CF also reduced the WVP values that were enhanced when the RS extract was added. Therefore, CF improved the water vapour and oxygen barrier capacities of the films regardless of whether they contain RS extract or not, although slightly higher values of WVP were obtained when the films did contain RS extract. The permeability values of the matrix depended on both permeant solubility and diffusion within the matrix. The incorporation of CF promoted the tortuosity factor for mass transfer purposes and thus reduced the diffusion coefficient. Likewise, the new molecular interactions within the matrix when CF and RS extracts were incorporated could affect the permeant solubility parameter. In the case of films with CF, the permeation of both water and oxygen molecules was inhibited, as reflected in the

reduction in the OP and WVP. For films with a RS extract, the permeability of water molecules was enhanced probably due to the plasticisation of the matrix that promoted molecular mobility and diffusion-controlled processes. In contrast, when both RS extract and CF were present in the films, the OP values did not significantly increase with respect to what was obtained for TPScf films; the WVP values, however, were higher, although still lower than the corresponding values of the films without CF. Oun et al. (2022) also found a marked WVP reduction when they incorporated cellulose nanocrystals and aronia (*Aronia melanocarpa*) extract in polyvinyl alcohol/chitosan-based films. The authors reported that the presence of nanocrystals increased the tortuosity factor, while the aronia extract favoured the interchain interactions between polymers, thus also reducing the WVP of the films.

Table 3. Moisture, water solubility, oxygen permeability (OP), and water vapour permeability (WVP) of thermoplastic starch films with different contents of CF (0% and 3% wt.) and RS extract (0, 4, 6, and 8 % wt.).

Film	Moisture content (%, d.b.)	Solubility (g soluble film/100 g film)	OP (x10^{14}) ($cm^3.m^{-1}.s^{-1}.Pa^{-1}$)	WVP ($mm.g.kPa^{-1}.h^{-1}.m^{-2}$)
TPS	$8.3 \pm 0.2^{a,1}$	$42.4 \pm 1.6^{a,1}$	$8.6 \pm 0.2^{a,1}$	$6.3 \pm 0.2^{b,1}$
TPS-4	$8.2 \pm 0.2^{a,1}$	$45.2 \pm 1.2^{a,1}$	$7.8 \pm 0.1^{b,1}$	$7.9 \pm 0.3^{a,1}$
TPS-6	$8.5 \pm 0.2^{a,1}$	$44.8 \pm 3.7^{a,1}$	$7.4 \pm 0.1^{c,1}$	$7.8 \pm 0.3^{a,1}$
TPS-8	$8.1 \pm 0.1^{a,1}$	$45.2 \pm 0.6^{a,1}$	$7.7 \pm 0.2^{bc,1}$	$7.6 \pm 0.1^{a,1}$
TPScf	$8.3 \pm 0.1^{a,1}$	$38.6 \pm 1.2^{b,2}$	$6.3 \pm 0.1^{a,2}$	$5.9 \pm 0.2^{b,2}$
TPScf-4	$7.7 \pm 0.2^{b,2}$	$47.6 \pm 2.6^{a,1}$	$6.9 \pm 0.1^{a,2}$	$7.2 \pm 0.2^{a,2}$
TPScf-6	$7.7 \pm 0.1^{b,2}$	$45.6 \pm 0.7^{a,1}$	$6.8 \pm 0.5^{a,2}$	$7.1 \pm 0.2^{a,2}$
TPScf-8	$7.8 \pm 0.1^{b,2}$	$42.7 \pm 3.1^{ab,1}$	$6.7 \pm 0.2^{a,2}$	$6.8 \pm 0.1^{a,2}$

Different subscript letters indicate significant differences between samples of the same group (TPS or TPScf films). Different numbers indicate significant differences between TPS and TPScf samples with the same ratio of RS extract (Tukey test, $p < 0.05$).

Fig. 2b shows the typical stress-strain curves of the different film formulations with the characteristic tensile parameters (embedded table): elastic modulus (EM) and tensile (TS) and elongation (EB) at break. As observed in previous studies analysing starch-fibre composites (Adeyi et al., 2021; Collazo-Bigliardi et al., 2019), the incorporation of CF into the TPS films led to a significant reinforcement effect, greatly promoting the strength of the films. Although the EM values increased by almost 200 % and the TS by about 100 %, the films became less extensible (EB decreased by almost 60 %) ($p < 0.05$). This reinforcing effect was previously observed in the TPS matrices with the same CF concentration, thus demonstrating the good properties of CF as a reinforcing agent for starch films (Freitas et al., 2021). A slight reinforcement capacity was also observed for the RS extract in TPS films, but to a much lesser extent than that of fibres. However, this effect was not observed for the highest extract concentration. Thus, films with 4 and 6 % of RS extracts exhibited EM values that were 40 %

higher ($p < 0.05$) than those of TPS films, whereas the EM value of films with 8 % extract did not significantly differ from that of TPS films. As concerns the resistance to break (TS values), all the extract concentrations increased the TS values by about 20 %, without there being any significant changes in the film's stretchability. In films containing CF, the incorporation of the extract promoted the films extensibility by about 60 %, while reducing the resistance to break (slightly) and the EM (by about 45-60 % depending on the extract concentration). This behaviour reflects the fact that the extract compounds were able to interact with the starch chains, probably through induced interchain cross-linking, thus hindering the intermolecular motion, enhancing the cohesion forces of the matrix, and promoting film stiffness. In this sense, the RS extract is rich in phenolic acids, mainly ferulic and *p*-cumaric acids (Menzel et al., 2019), that can form interchain hydrogen bonds, enhancing the strength of the starch matrices. A great number of studies reported the cross-linking activity of ferulic acid with different polysaccharides and proteins (Hadrich et al., 2020; Li et al., 2019; Yerramathi et al., 2021). Nevertheless, when the extract solids reach a limit in the film, the cohesion forces could weaken, probably due to the excess of the non-film-forming material that interferes with the chain association.

In contrast, the RS extract seems to inhibit the reinforcing capacity of fibres in the films with CF. This seems to point to the bonding of extract compounds to the cellulosic hydroxyls or to the starch hydroxyls, thus limiting the starch-cellulose bonding ability and, therefore, the fibre reinforcing capacity. Hydrogen bonding between fibres and the polymer represents a key factor in the reinforcement of fibre composites. Avérous et al. (2001) demonstrated the different reinforcing effects of leafwood cellulose fibres on LDPE (no fibre-polymer interactions) and TPS (hydrogen bond formation) films. The ratios of EM and TS of the composites with respect to the fibre-free polymers were notably higher in the case of starch than for LDPE composites. Therefore, it can be assumed that the presence of the RS extract in the films inhibited the fibre-polymer interactions, thus reducing the reinforcing effect. Cellulose fibres at 3 % with respect to starch had a notable reinforcing capacity in the starch matrix, as deduced in a previous study (Freitas et al., 2021). Nevertheless, in the presence of extract, this capacity was undermined, which suggests that fibres also interact with the extract compounds, limiting their capacity to reinforce the polymer matrix.

3.4. Antioxidant capacity of the films and prevention of sunflower oil oxidation

Table 4 shows the quantity of total phenolic compounds (TPC) released from the different films in the aqueous medium, and their corresponding DPPH radical scavenging capacity. The results reflected the TPC released per mass unit of film and the corresponding percentage with respect to what was initially incorporated into the film, considering both the extract content and its TPC value. In no case was the total delivery of the incorporated phenolics achieved; however, higher percentages were obtained from the films with 8 % extract without

CF and from every film with CF. The incomplete delivery could be attributed to the partial degradation of these compounds during the thermal processing of the films.

As expected, the radical scavenging capacity of the films, expressed as the ratio of film to DPPH necessary to inhibit the radical activity by 50 % (EC_{50}) increased as the extract ratio rose in the film, since lower amounts of EC_{50} were obtained. When this parameter was referred to the respective mass of extract in the different films, no absolutely constant values were obtained, these being lower than what was determined in the pure extract (6.3 ± 0.3). This indicates that the radical scavenging capacity of the extract after the film processing was enhanced (lower EC_{50} values than the initial extract: 3.95 as mean value) probably due to the formation of more active compounds either during the film thermoprocessing (at 130 and 160 ^{o}C, respectively, for melt blending and compression moulding) in which new antioxidant compounds could be released from the lignin fraction of the extract (Wanyo et al., 2014) or in the thermo-formation of new antioxidant compounds through Maillard or caramelisation reactions during the melt blending step, as reported by other authors (Plaza et al., 2010) for different plant extracts when submitted to high temperature processes. Therefore, although no total recovery of phenolics was achieved from the thermoprocessed films, their radical scavenging capacity was enhanced, and so was their antioxidant activity.

Table 4. Total phenolic content (mg GAE / g film) and DPPH scavenging capacity (EC_{50}) of the films containing different ratios of RS extract (0, 4, 6, and 8% wt.) with and without CF. %GAE recovered with respect to what was initially incorporated into the film and EC_{50} referred per mg of the extract incorporated into the films were also included.

Formulation	TPC (mg GAE/g film)	TPC (%GAE released)	EC_{50} (mg film/mg DPPH)	EC_{50} (mg extract/mg DPPH)
TPS	n.d.	n.d.	n.d.	n.d.
TPS-4	$1.10 \pm 0.02^{c,1}$	$74.4 \pm 1.7^{b,1}$	$85.4 \pm 4.3^{a,1}$	$3.4 \pm 0.2^{c,1}$
TPS-6	$1.63 \pm 0.02^{b,1}$	$73.3 \pm 1.0^{b,1}$	$75.0 \pm 0.2^{b,1}$	$4.5 \pm 0.1^{b,1}$
TPS-8	$2.63 \pm 0.14^{a,1}$	$89.0 \pm 5.0^{a,2}$	$50.5 \pm 1.1^{c,1}$	$4.0 \pm 0.1^{a,1}$
TPScf	n.d.	n.d.	n.d.	n.d.
TPScf-4	$1.22 \pm 0.06^{c,2}$	$83.0 \pm 4.0^{b,2}$	$113.0 \pm 4.0^{a,2}$	$4.5 \pm 0.1^{a,2}$
TPScf-6	$2.14 \pm 0.03^{b,2}$	$96.2 \pm 1.2^{a,2}$	$69.0 \pm 4.0^{b,2}$	$4.1 \pm 0.2^{a,1}$
TPScf-8	$2.40 \pm 0.04^{a,2}$	$80.8 \pm 1.5^{b,1}$	$40.3 \pm 1.1^{c,2}$	$3.2 \pm 0.1^{b,2}$

Different subscript letters indicate significant differences between samples of the same group (TPS or TPScf films). Different numbers indicate significant differences between TPS and TPScf samples with the same ratio of RS extract (Tukey test, $p < 0.05$).

To validate the antioxidant capacity in real foods, the ability of the films containing extracts to prevent sunflower oil oxidation was analysed in an accelerated oxidation test (Talón et al., 2019). To this end, film bags of TPS with 8 % extract with and without CF (TPS-8 and TPScf-8

formulations) were selected to obtain mono-dose oil samples based on their higher antioxidant capacity and lower oxygen permeability. For comparison purposes, mono-dose bags of the corresponding films without extract were also prepared and analysed as to their peroxide index and TBARS value as a function of the storage time under oxidation conditions with UV light. Fig. 3 shows the development of the controlled oxidation parameters for these four oil samples and the control sample in an open plate. The peroxide index (Fig. 3a) increased very quickly in the open samples, demonstrating the oxidative conditions of the test, whereas in packaged oil the peroxide formation was much slower since the bag material limited the oxygen transfer, since all the films exhibited relatively low values of OP. Likewise, the bags with RS extracts delayed the peroxide formation even more, which must be attributable to the antioxidant effect of the extract compounds. Consequently, the TBARS index values (Fig. 3b), from the secondary oxidation phase, were lower in packaged oil samples and notably reduced when the bags contained RS extracts. When the RS extract was present in the films, it was not possible to observe significant differences between the films with CF and those without, but TPS bags with CF were more efficient at limiting oil oxidation than TPS without CF. This can be attributed to the reduction in OP brought about by CF incorporation, as well as the lower light transmittance of the TPScf films, which protect oil from light induced oxidation. In the case of films with RS extract, the high capacity of the extract to limit oil oxidation masked the possible differences associated with the lower OP of TPScf-8 films, compared to TPS-8. Likewise, both films with extracts exhibited a high degree of UV light absorption, which will also contribute to the antioxidant capacity of the material. Therefore, the incorporation of both CF and active extract from the RS agri-food residue into starch mono-dose bags constituted efficient protection for the purposes of delaying the oxidation of sunflower oil throughout storage.

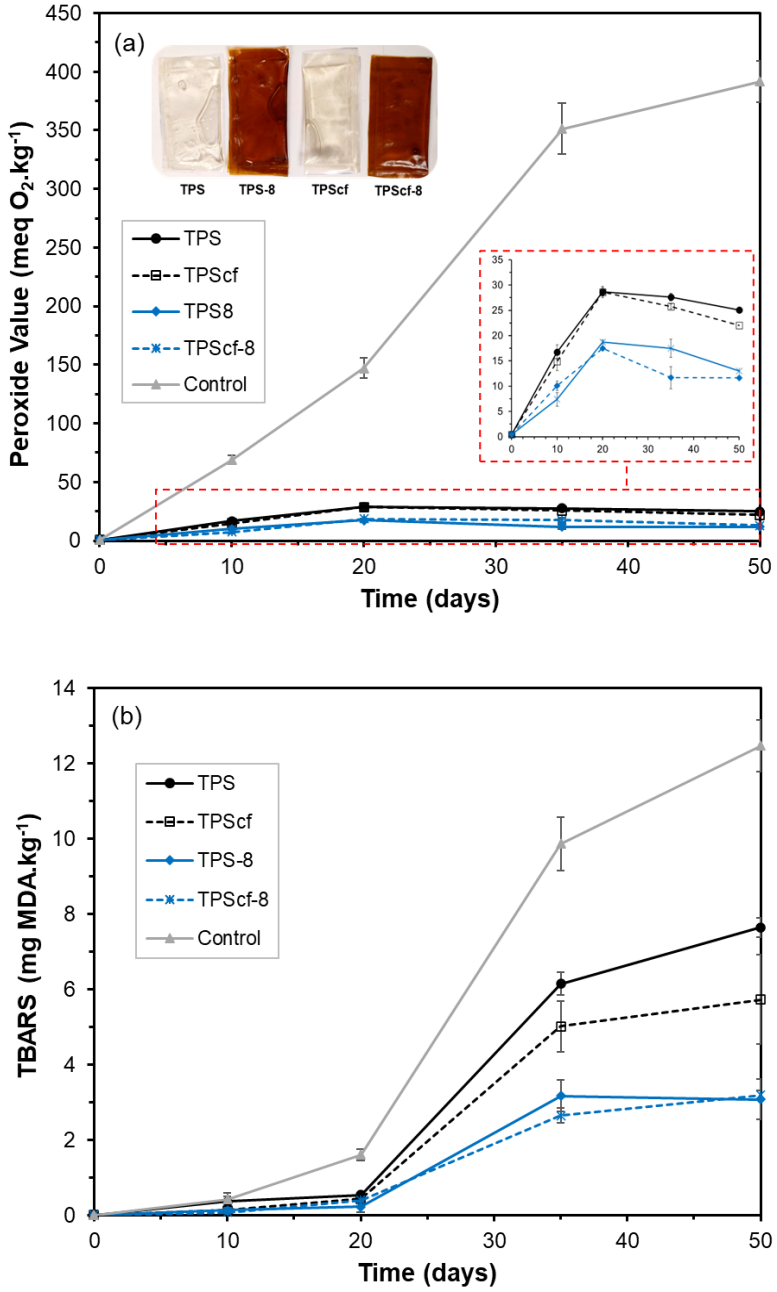

Fig. 3. Peroxide index and TBARs values of sunflower oil packaged in starch films containing or not RS extract (at 8 % wt.) and CF, compared to the open control samples, throughout 50 days of storage.

4. CONCLUSIONS

New functionalities of thermoplastic TPS films were achieved when RS fractions were incorporated. CF promoted the film strength and is an effective reinforcing agent at 3 % with respect to thermoplastic starch. The incorporation of RS aqueous extract into both TPS and reinforced TPS films, produced more plasticised, less thermostable matrices, but provided

them with strong antioxidant and UV absorption capacity, which permits the prevention of sunflower oil oxidation. CF enhanced the oxygen and water vapour barrier capacity of the films with and without RS extracts, while reinforcing their mechanical resistance and elastic modulus. Therefore, obtaining fractions from RS that are useful for the purposes of improving food packaging materials, such as starch films, represents a good strategy for the valorisation of this waste, while at the same time opening up new windows in the development of active biodegradable materials for food packaging and preservation.

5. ACKNOWLEDGEMENTS

The authors thank the Agencia Estatal de Investigación (Spain) for the financial support through projects PID2019-105207RB-I00/AEI/10.13039/501100011033 and Generalitat Valenciana [grant number GrisoliaP/2019/115].

6. REFERENCES

ASTM. (2005). E96/E96M-05. Standard Test Methods for Water Vapor Transmission of Materials. American Society for Testing and Materials, 1-11.

ASTM. (2010). D3985-05 Oxygen Gas Transmission Rate Through Plastic Film and Sheeting Using a Coulometric Sensor. Annual Book of ASTM Standards, C, 1–7. https://doi.org/10.1520/D3985-05.2

ASTM. (2012). ASTM D882-12 Standard test method for tensile properties of thin plastic sheeting. American Society for Testing and Materials, 12.

Adeyi, A. J., Durowoju, M. O., Adeyi, O., Oke, E. O., Olalere, O. A., & Ogunsola, A. D. (2021). Momordica augustisepala L. stem fibre reinforced thermoplastic starch: Mechanical property characterization and fuzzy logic artificial intelligent modelling. *Results in Engineering*, *10*, 100222. https://doi.org/10.1016/j.rineng.2021.100222

Avérous, L., Fringant, C., & Moro, L. (2001a). Plasticized starch–cellulose interactions in polysaccharide composites. *Polymer*, *42*(15), 6565–6572. https://doi.org/10.1016/S0032-3861(01)00125-2

Balakrishnan, P., Gopi, S., Geethamma, V. G., Kalarikkal, N., & Thomas, S. (2018). Cellulose Nanofiber vs Nanocrystals From Pineapple Leaf Fiber: A Comparative Studies on Reinforcing Efficiency on Starch Nanocomposites. *Macromolecular Symposia*, *380*(1), 1800102. https://doi.org/10.1002/masy.201800102

Brand-Williams, W., Cuvelier, M. E., & Berset, C. (1995). Use of a free radical method to evaluate antioxidant activity. *LWT - Food Science and Technology*, *28*(1), 25–30. https://doi.org/10.1016/S0023-6438(95)80008-5

Carvalho, A. J. F., Zambon, M. D., Curvelo, A. A. S., & Gandini, A. (2003). Size exclusion chromatography characterization of thermoplastic starch composites 1. Influence of plasticizer and fibre content. *Polymer Degradation and Stability*, *79*(1), 133–138. https://doi.org/10.1016/S0141-3910(02)00265-3

Chen, X., Yu, J., Zhang, Z., & Lu, C. (2011). Study on structure and thermal stability properties of cellulose fibers from rice straw. *Carbohydrate Polymers*, *85*(1), 245–250. https://doi.org/10.1016/j.carbpol.2011.02.022

Collazo-Bigliardi, S. (2018). Isolation and characterisation of microcrystalline cellulose and cellulose nanocrystals from coffee husk and comparative study with rice husk. *Carbohydrate Polymers*, 11.

Collazo-Bigliardi, S., Ortega-Toro, R., & Chiralt, A. (2019). Improving properties of thermoplastic starch films by incorporating active extracts and cellulose fibres isolated from rice or coffee husk. *Food Packaging and Shelf Life*, *22*, 100383. https://doi.org/10.1016/j.fpsl.2019.100383

Dalnoki-Veress, K., Forrest, J. A., Murray, C., Gigault, C., & Dutcher, J. R. (2001). Molecular weight dependence of reductions in the glass transition temperature of thin, freely standing polymer films. *Physical Review E*, *63*(3), 031801. https://doi.org/10.1103/PhysRevE.63.031801

Danilovas, P. P., Rutkaite, R., & Zemaitaitis, A. (2014). Thermal degradation and stability of cationic starches and their complexes with iodine. *Carbohydrate Polymers*, *112*, 721–728. https://doi.org/10.1016/j.carbpol.2014.06.038

Fourati, Y., Magnin, A., Putaux, J.-L., & Boufi, S. (2020). One-step processing of plasticized starch/cellulose nanofibrils nanocomposites via twin-screw extrusion of starch and cellulose fibers. *Carbohydrate Polymers*, *229*, 115554. https://doi.org/10.1016/j.carbpol.2019.115554

Freitas, P. A. V., Arias, C. I. L. F., Torres-Giner, S., González-Martínez, C., & Chiralt, A. (2021). Valorization of Rice Straw into Cellulose Microfibers for the Reinforcement of Thermoplastic Corn Starch Films. *Applied Sciences*, *11*(18), 8433. https://doi.org/10.3390/app11188433

Freitas, P. A. V., González-Martínez, C., & Chiralt, A. (2020). Application of Ultrasound Pre-Treatment for Enhancing Extraction of Bioactive Compounds from Rice Straw. *Foods*, *9*(11), 1657. https://doi.org/10.3390/foods9111657

Freitas, P. A. V., González-Martínez, C., & Chiralt, A. (2022a). Applying ultrasound-assisted processing to obtain cellulose fibres from rice straw to be used as reinforcing agents. *Innovative Food Science & Emerging Technologies*, *76*, 102932. https://doi.org/10.1016/j.ifset.2022.102932

Freitas, P. A. V., Nuria J. B. Gil., González-Martínez, C., & Chiralt, A. (2022b). Antioxidant poly (lactic acid) films with rice straw extract for food packaging applications. *Food Packaging and Shelf Life*. In press.

Hadrich, A., Dulong, V., Rihouey, C., Labat, B., Picton, L., & Le Cerf, D. (2020). Biomimetic hydrogel by enzymatic crosslinking of pullulan grafted with ferulic acid. *Carbohydrate Polymers*, *250*, 116967. https://doi.org/10.1016/j.carbpol.2020.116967

Li, K., Zhu, J., Guan, G., & Wu, H. (2019). Preparation of chitosan-sodium alginate films through layer-by-layer assembly and ferulic acid crosslinking: Film properties, characterization, and

formation mechanism. *International Journal of Biological Macromolecules*, *122*, 485–492. https://doi.org/10.1016/j.ijbiomac.2018.10.188

Mak, T. M. W., Xiong, X., Tsang, D. C. W., Yu, I. K. M., & Poon, C. S. (2020). Sustainable food waste management towards circular bioeconomy: Policy review, limitations and opportunities. *Bioresource Technology*, *297*, 122497. https://doi.org/10.1016/j.biortech.2019.122497

Menzel, C. (2020). Improvement of starch films for food packaging through a three-principle approach: Antioxidants, cross-linking and reinforcement. *Carbohydrate Polymers*, *250*, 116828. https://doi.org/10.1016/j.carbpol.2020.116828

Menzel, C., González-Martínez, C., Chiralt, A., & Vilaplana, F. (2019). Antioxidant starch films containing sunflower hull extracts. *Carbohydrate Polymers*, *214*, 142–151. https://doi.org/10.1016/j.carbpol.2019.03.022

Menzel, C., González-Martínez, C., Vilaplana, F., Diretto, G., & Chiralt, A. (2020). Incorporation of natural antioxidants from rice straw into renewable starch films. *International Journal of Biological Macromolecules*, *146*, 976–986. https://doi.org/10.1016/j.ijbiomac.2019.09.222

Mochane, M. J., Magagula, S. I., Sefadi, J. S., & Mokhena, T. C. (2021). A Review on Green Composites Based on Natural Fiber-Reinforced Polybutylene Succinate (PBS). *Polymers*, *13*(8), 1200. https://doi.org/10.3390/polym13081200

Ng, H.-M., Sin, L. T., Tee, T.-T., Bee, S.-T., Hui, D., Low, C.-Y., & Rahmat, A. R. (2015). Extraction of cellulose nanocrystals from plant sources for application as reinforcing agent in polymers. *Composites Part B: Engineering*, *75*, 176–200. https://doi.org/10.1016/j.compositesb.2015.01.008

Ordoñez, R., Atarés, L., & Chiralt, A. (2021). Physicochemical and antimicrobial properties of cassava starch films with ferulic or cinnamic acid. *LWT*, *144*, 111242. https://doi.org/10.1016/j.lwt.2021.111242

Oun, A. A., Shin, G. H., & Kim, J. T. (2022). Antimicrobial, antioxidant, and pH-sensitive polyvinyl alcohol/chitosan-based composite films with aronia extract, cellulose nanocrystals, and grapefruit seed extract. *International Journal of Biological Macromolecules*, *213*, 381–393. https://doi.org/10.1016/j.ijbiomac.2022.05.180

Papastergiadis, A., Mubiru, E., Van Langenhove, H., & De Meulenaer, B. (2012). Malondialdehyde Measurement in Oxidized Foods: Evaluation of the Spectrophotometric Thiobarbituric Acid Reactive Substances (TBARS) Test in Various Foods. *Journal of Agricultural and Food Chemistry*, *60*(38), 9589–9594. https://doi.org/10.1021/jf302451c

Perumal, A. B., Sellamuthu, P. S., Nambiar, R. B., & Sadiku, E. R. (2018). Development of polyvinyl alcohol/chitosan bio-nanocomposite films reinforced with cellulose nanocrystals isolated from rice straw. *Applied Surface Science*, *449*, 591–602. https://doi.org/10.1016/j.apsusc.2018.01.022

Plaza, M., Amigo-Benavent, M., del Castillo, M. D., Ibáñez, E., & Herrero, M. (2010). Facts about the formation of new antioxidants in natural samples after subcritical water extraction. *Food Research International*, *43*(10), 2341–2348. https://doi.org/10.1016/j.foodres.2010.07.036

Sá, N. M. S. M., Mattos, A. L. A., Silva, L. M. A., Brito, E. S., Rosa, M. F., & Azeredo, H. M. C. (2020). From cashew byproducts to biodegradable active materials: Bacterial cellulose-lignin-cellulose nanocrystal nanocomposite films. *International Journal of Biological Macromolecules*, *161*, 1337–1345. https://doi.org/10.1016/j.ijbiomac.2020.07.269

Sluiter, A. (2008). Determination of Structural Carbohydrates and Lignin in Biomass: Laboratory Analytical Procedure (LAP); Issue Date: April 2008; Revision Date: July 2011 (Version 07-08-2011). *Technical Report*, 18.

Talón, E., Trifkovic, K. T., Nedovic, V. A., Bugarski, B. M., Vargas, M., Chiralt, A., & González-Martínez, C. (2017). Antioxidant edible films based on chitosan and starch containing polyphenols from thyme extracts. *Carbohydrate Polymers*, *157*, 1153–1161. https://doi.org/10.1016/j.carbpol.2016.10.080

Talón, E., Vargas, M., Chiralt, A., & González-Martínez, C. (2019). Antioxidant starch-based films with encapsulated eugenol. Application to sunflower oil preservation. *LWT*, *113*, 108290. https://doi.org/10.1016/j.lwt.2019.108290

Tavares, K. M., Campos, A. de, Mitsuyuki, M. C., Luchesi, B. R., & Marconcini, J. M. (2019). Corn and cassava starch with carboxymethyl cellulose films and its mechanical and hydrophobic properties. *Carbohydrate Polymers*, *223*, 115055. https://doi.org/10.1016/j.carbpol.2019.115055

Theng, D., Arbat, G., Delgado-Aguilar, M., Ngo, B., Labonne, L., Evon, P., & Mutjé, P. (2017). Comparison between two different pretreatment technologies of rice straw fibers prior to fiberboard manufacturing: Twin-screw extrusion and digestion plus defibration. *Industrial Crops and Products*, *107*, 184–197. https://doi.org/10.1016/j.indcrop.2017.05.049

Wang, Z., Qiao, X., & Sun, K. (2018). Rice straw cellulose nanofibrils reinforced poly(vinyl alcohol) composite films. *Carbohydrate Polymers*, *197*, 442–450. https://doi.org/10.1016/j.carbpol.2018.06.025

Wanyo, P., Meeso, N., & Siriamornpun, S. (2014). Effects of different treatments on the antioxidant properties and phenolic compounds of rice bran and rice husk. *Food Chemistry*, *157*, 457–463. https://doi.org/10.1016/j.foodchem.2014.02.061

Yang, Z., Liu, X., Yang, Z., Zhuang, G., Bai, Z., Zhang, H., & Guo, Y. (2013). Preparation and formation mechanism of levoglucosan from starch using a tubular furnace pyrolysis reactor. *Journal of Analytical and Applied Pyrolysis*, *102*, 83–88. https://doi.org/10.1016/j.jaap.2013.03.012

Yerramathi, B. B., Kola, M., Annem Muniraj, B., Aluru, R., Thirumanyam, M., & Zyryanov, G. V. (2021). Structural studies and bioactivity of sodium alginate edible films fabricated through ferulic acid crosslinking mechanism. *Journal of Food Engineering*, *301*, 110566. https://doi.org/10.1016/j.jfoodeng.2021.1105

CHAPTER 2.VII

Active poly (lactic acid) films with rice straw aqueous extracts for meat preservation purposes

Pedro A. V. Freitas, Chelo González-Martínez, Amparo Chiralt

Institute of Food Engineering for Development, Universitat Politècnica de València, 46022, Valencia, Spain

Submitted to Food Packaging and Shelf Life

ABSTRACT

Aqueous extracts from rice straw, using ultrasound-assisted reflux heating extraction (USHT) and Subcritical Water Extraction (SWE), under two process conditions (160 °C, 7 bars; and 180 °C, 11 bars), were obtained and characterised as to their phenolic content and antioxidant and antimicrobial capacities. These extracts were incorporated (6 % wt.) into PLA films by melt blending and compression moulding that were characterised as to their structural and functional properties and their capacity to preserve fresh pork meat, as vacuum thermo-sealed bags, throughout 16 days of cold storage. The extracts slightly reduced the extensibility, resistance to break and water barrier capacity of the PLA films but enhanced their oxygen barrier capacity and the UV light-blocking effect. The films with RS extracts were effective at preserving meat quality parameters, inhibiting microbial growth, meat oxidation, discolouration, and weight loss, thus extending the meat shelf life. The SWE extract obtained at 180 °C was the most effective at obtaining active films for meat preservation, exhibiting the greatest antioxidant and antibacterial activity. Therefore, the green SWE technique is useful for obtaining active extracts from RS, allowing for its valorisation in the development of biodegradable active materials useful to extend the food shelf life.

Keywords: subcritical water extraction, ultrasound-reflux heating method, antimicrobial extracts, antioxidant compounds, meat preservation, agro-industrial valorisation.

1. INTRODUCTION

Active food packaging improves food preservation by maintaining its quality and safety for longer , thus extending the food shelf-life (Baghi et al., 2022; Sung et al., 2013). To this end, it is necessary to release active compounds into the food or headspace in order to inhibit, minimize, or delay undesirable reactions, such as oxidation, discolouration or microbial growth, that cause food spoilage (Han et al., 2018; Nerín et al., 2008). Of the different strategies to obtain active packaging materials, the direct incorporation of active compounds into the polymer matrix for their subsequent release into the food system is the most common practice (Almasi et al. 2021). Specifically, antioxidant and antimicrobial compounds are frequently used in the development of active materials for food packaging since oxidation and microbial attack are the most common spoilage processes in food products (Sofi et al. 2018). In this sense, naturally-ocurring antioxidant/antimicrobial compounds are highly appreciated by consumers since these are seen as safer. Many plant extracts contain compounds with antioxidant or antimicrobial capacity (Zazharskyi et al. 2019; Saeed et al. 2012; Lee et al. 2033) that can be used as active ingredients for the formulation of active films. In this sense, the plant tissue from different agri-food waste could be valorised as sources of active extracts for different uses in the area of food preservation (Makris et al. 2007; Torres-Valenzuela et al. 2020; Panzella et al. 2020). Specifically, different active extracts obtained from agri-food wastes, such as pink pepper (Merlo et al., 2019), hops (Almeida et al., 2022), grape seed (Zhao et al., 2022), coffee and rice husks (Collazo-Bigliardi et al., 2019) or rice straw (RS) (Menzel et al., 2020), have been incorporated into polymer matrices to obtain active materials for food packaging or coating.

The use of biodegradable polymer matrices to obtain active food packaging materials is a highly recommended means of reducing the environmental impact of plastics while the active properties add value to the more expensive biodegradable polymers. Thus, the valorisation of agro-industrial wastes and by-products into value-added products, useful for developing biodegradable, active packaging materials represents an interesting practice in the reduction of ecological and environmental problems while boosting the circular economy (Bhat, 2021).

One of the most produced agro-industrial residues worldwide, rice straw (RS) is one of the leftovers generated after the rice harvest that has no direct economic value, and is usually burned in the rice paddies (Peanparkdee & Iwamoto, 2019; Saini et al., 2015). Given its renewability, availability, cheapness, and richness in lignocellulosic fractions (~70 % dry matter), several environmentally-friendly approaches have been proposed to valorise and exploit its potential (Goodman, 2020). Obtaining bioactive extracts from RS, using green and sustainable extraction processes, is of great interest given the notable antioxidant and antimicrobial properties (Menzel, 2020; Freitas et al., 2021) of some of its components, such as ferulic, gallic, protocatechuic or *p*-coumaric acids (Karimi et al., 2014; Menzel et al., 2020).

The process extraction efficiency and the profile of active extract compounds depend on factors, such as temperature and time, kind of solvent, pressure or sample pre-treatments (Alara et al., 2021; Herrero et al., 2012). Likewise, the extraction process must be green, fast, scalable, toxic solvent-free, and economically profitable. To this end, different technologies have been applied, such as supercritical extraction, microwave-assisted extraction, ultrasound-assisted extraction, or subcritical water extraction, using green solvents. (Torres-Valenzuela et al. 2020).

Freitas et al. (2020) applied ultrasound pre-treatment and reflux heating water extraction to obtain RS antioxidant extracts that contain a notable content in polyphenols and antioxidant capacity. Application of high shear rates caused by acoustic cavitation promoted the extraction of the target compounds from the plant matrix due to the intense disruption of the plant structure and the exposure of the innermost cell tissues (Cheung & Wu, 2013; Luque-García & Luque de Castro, 2003; Ojha et al., 2020), thus facilitating solvent accessibility in the subsequent heating step that promotes the debonding of phenolic compounds from the plant matrix.

Subcritical water extraction (SWE), also known as pressurized hot water extraction, is a green, innovative extraction technique that uses water under subcritical conditions, i.e., temperatures above the boiling point of water and pressures high enough to keep the liquid water below its critical point (~374 °C and 218 atm) (Castro-Puyana et al., 2013). SWE has been applied in the green extraction of a wide range of components from different plant sources (Collazo-Bigliardi et al., 2019; Requena et al., 2019; Moirangthemet al. 2021), improving the mass transfer of non-polar compounds due to changes in the water solvent properties, such as the decrease in surface tension or dielectric constant, as a function of the pressure/temperature (Ong et al., 2006; Plaza et al., 2010; Ong et al., 2006). Therefore, SWE at a different processing temperature/pressure will give rise to extracts with different composition profiles and bioactivity.

Of the compostable polymers that are used to obtain active packaging materials for food preservation purposes, poly (lactic acid) (PLA) is recognized as safe and has already been used as a food packaging material (Södergard, 2000), fulfilling functions of mechanical protection, barrier to moisture, fats, and gases (Haugaard, 2000). The development of biodegradable PLA-based films incorporating active extracts obtained from agro-industrial waste, has great potential to extend the shelf-life of packaged foods. These materials would contribute to a reduction in food residues and plastic contamination, and to the valorisation of agro-industrial waste, boosting the circular economy.

In this study, aqueous extracts from rice straw, using US assisted reflux heating extraction (USHT) and SWE under two extraction conditions (160 °C, 7 bars; and 180 °C, 11 bars), were obtained and characterised as to their phenolic content and antioxidant and antimicrobial

capacity. These extracts were incorporated into PLA films obtained by melt blending and compression moulding that were analysed as to their structural and functional properties (mechanical, optical, thermal and barrier properties). Likewise, the capacity of the films to preserve fresh pork meat, as vacuum thermo-sealed bags, was analysed through the control of the meat quality parameters (pH, colour, weight loss, microbial counts, and oxidation) throughout 16 days of cold storage.

2. MATERIAL AND METHODS

2.1 Materials

RS (*Oryza sativa* L var. *J. Sendra*) was obtained as waste from the rice industry and collected in a L'Albufera paddy field (Valencia, Spain). The RS was dried at 50 ± 2 °C under vacuum (0.5 mmbar) for 16 h, milled using a grinding machine (IKA, model M20, IKA Werke GmbH & Co. KG, Staufen, Germany) operating at 3 cycles of 90 s each, sieved to obtain RS particle sizes lower than 0.5 mm, and then stored at 20 ± 2 °C until further use.

Amorphous PLA 4060D, with an average molecular weight of 106,226 D and density 1.24 g/cm^3 was purchased from Natureworks (U.S.A). Trichloroacetic acid (> 99 % purity), magnesium nitrate ($Mg(NO_3)_2$), and di-Phosphorous pentoxide (P_2O_5) were supplied by PanReac Química S.L.U (Castellar del Vallés, Barcelona, Spain). 2-thiobarbituric acid (> 98 % purity), ethanol (98 % purity), and methanol (> 99.9 purity) were obtained from Sigma-Aldrich (St. Louis, MO, USA). For microbiological tests, buffered peptone water, Trypticasein soy broth (TSB) and Man Rogosaand Sharpe agar (MRS) were purchased from Labkem (Barcelona, Spain). Violet red bile agar (VRB) was supplied by Scharlab S.L. (Sentmenat, Spain). Strains of *Listeria innocua* (CECT 910) and *Escherichia coli* (CECT 101) were purchased from the Spanish Type Collection (CECT, University of Valencia, Valencia, Spain).

2.2. Obtaining and characterisation of RS aqueous extracts

Three aqueous RS extracts were obtained, by applying a previously optimised combined ultrasound-reflux heating treatment (USHT) (Freitas et al. 2020) and subcritical water extraction (SWE) at 160 (SWE160) and 180 (SWE180) ^{o}C. For the USHT process, an aqueous suspension of RS particles was prepared at 5 % (w/w) in distilled water and sonicated for 30 min, using a high-intensity ultrasonic homogenizer probe (Vibra CellTM VCX750, Sonics & Material, Inc., Newtown, CT, USA) operating at a frequency of 20 kHz, 750 W power and 40 % sonication amplitude, in continuous mode, maintaining the temperature at about 25 °C (using an ice bath to prevent excessive heating). Thereafter, the RS suspension was heated in a typical reflux heating apparatus at 100 °C for 1 h.

For SWE processes, the RS particles were dispersed in distilled water at a ratio of 1:10 (w/w) and submitted to extraction in a Pressure Reactor (Model 1-T-A-P-CE, 5 L capacity, Amar Equipaments PVT.LTD, Mumbai, India) under two extraction conditions: 160 °C, 7 bars, 150 rpm for 30 min, and 180 °C, 11 bars, 150 rpm for 30 min.

After each extraction step, the RS dispersion was filtered (Filterlab) to obtain the liquid extracts, which were freeze-dried (Telstar, model LyoQuest-55) at -60 °C, 0.8 mbar for 72 h. The obtained freeze-dried extracts were stored in a dark bottle at 0 % relativity humidity (RH) (with P_2O_5) and at 4 ± 2 °C until further use.

The dried extracts were characterised as to their total phenolic content (TPC) and antioxidant capacity. TPC was determined in triplicate for each extract, by using the modified Folin-Ciocalteu method, as described by Menzel et al. (2020). The TPC was determined through the absorbance values and the standard curve of gallic acid. The results were expressed as mg GAE per g of dry extract.

The antioxidant activity of the extracts was determined through the ABTS and DPPH radical scavenging capacity. The ABTS assay was carried out as reported by Re et al. (1999). To prepare the ABTS radical cation (ABTS**•+**), ABTS and $K_2S_2O_5$ were dissolved in distilled water to a final concentration of 7 mM and 2.45 mM, respectively. These solutions were mixed and maintained for 16 h in darkness at 4 °C. Different volumes of diluted extracts in distilled water were mixed with the ABTS**•+** solution (diluted to absorbance at 734 nm equals 0.7 ± 0.2) and the absorbance reduction was measured at 734 nm. Each extract was analysed in duplicate. The standard curve was prepared using different concentrations of Trolox and the results were expressed as Trolox equivalent antioxidant capacity (TEAC), in µmol Trolox/mg extract.

The 2,2-Diphenyl-1-pikryl-hydroxyl (DPPH) method (Brand-Williams et al., 1995), with some modifications, was also used to quantify the antioxidant capacity of the extracts, as described by Freitas et al. (2020). Each extract was mixed with the DPPH methanolic solution (Abs_{515nm} = 0.7 ± 0.2) at different concentrations to a final volume of 4 mL. A calibration curve was used to determine the initial DPPH concentration in the reaction medium. The antioxidant activity of the different extract was reported as the EC_{50} value, which is the concentration required to reduce the DPPH concentration by 50 % when the reaction is stable. The time to achieve reaction stability was 12 h for all cases.

The minimal inhibitory concentration (MIC) of the extracts for a Gram + (*Lysteria innocua*) and a Gram – (*Escherichia coli*) bacteria was analysed in order to assess the potential antibacterial effect of the extracts, as described by Requena et al. (2019), using a 96-well disposable sterile microtiter plate (well volume of 200 µL). Stock solutions of each extract and different dilutions, ranging between 20 and 200 $mg.mL^{-1}$ (with 10 $mg.mL^{-1}$ intervals) were obtained with the TSB broth medium. Aliquots (100 µL) of each dilution were placed in the corresponding wells.

Wells were inoculated with 100 µL of 10^5 CFU.mL^{-1} bacterial dispersion and incubated at 37 °C for 24 h. The bacterial counts in the wells were determined by inoculation of 100 µL of each well content in tryptic soy agar media, for 24 h at 37 °C. The MIC value of each extract was considered as the lowest concentration of the extracts in which the bacterial count on the plate was zero. Each extract was analysed in duplicate.

2.3. Film preparation and characterisation

PLA films with the different RS extracts were prepared by melt blending and compression moulding. The amorphous PLA pellets were preconditioned in P_2O_5 for 2 days to eliminate residual water. On the basis of previous studies (Freitas et al. 2022), PLA samples were hand-mixed with the dried extracts, at 6 % with respect to the polymer mass, and melt-blended, using an internal mini-mixer (HAAKETM PolyLabTM QC, Thermo Fisher Scientific, Karlsruhe, Germany), at 160 °C and 50 rpm for 6 min. PLA films without RS extract were also prepared as control films. All films were thermoformed by thermocompression of 3 g of the blend, previously milled (IKA, model M20, Germany), using a heat plate hydraulic press (Model LP20, Labtech Engineering, Thailand) by applying: preheating at 160 °C for 3 min, compression at 100 bars and 160 °C for 3 min, and final cooling to 80 °C. The films were labelled as PLA (control), PLA-USHT, PLA-SWE160, and PLA-SWE180, which indicate the type of active extract incorporated in the PLA film.

2.3.1. Film microstructure

The morphologies of the cross-sections of films were evaluated using a Field Emission Scanning Electron Microscope (ULTRA^{TM} 55, Zeiis, Oxford Instruments, UK). The film samples were cryo-fractured by immersion in liquid nitrogen and then platinum coated, using an EM MED020 sputter coater (Leica BioSystems, Barcelona, Spain). The micrographs were taken at 2.0 kV acceleration voltage.

2.3.2 Colour and transparency

A Spectro-colorimeter (CM-3600d, Minolta Co. Tokyo, Japan) was used to measure the optical properties of the films according to the Kubelka-Munk theory of multiple scattering. The infinite reflectance spectra were obtained from the film reflectance on black and white backgrounds, in the range of 400 to 700 nm, as previously described (Freitas et al., 2023). The CIEL*a*b* colour coordinates of the films were obtained from the infinite reflectance spectra, using D65 illuminant and 10° observer and the psychometric coordinates, chroma (C_{ab}*) and hue angle (h_{ab}*), were calculated (Freitas et al., 2023). The measurements were taken in triplicate for each film and three films were measured for each sample.

A UV-visible spectrophotometer (Evolution 201, Thermo Scientific) operating in light transmission mode was used to determine the UV-vis spectra of the films. For each formulation, the spectra were obtained between 200 to 900 nm, in triplicate.

2.3.3 Tensile properties

Tensile strength at break (TS), elastic modulus (EM), and elongation at break (E) were determined following the ASTM D882 method (ASTM, 2001) using a universal test machine (TA.XTplus model, Stable Micro Systems, Haslemere, England). Film samples (2.5 x 10 cm) were grabbed by two grips, initially separated by 50 mm, and stretched at a crosshead speed of 12.5 $mm.min^{-1}$ until break. Before the analysis, a digital micrometer (Palmer, model COMECTA, Barcelona, accuracy of 0.001 mm) was used to measure the thicknesses of the films at ten random film positions. Eight samples were evaluated per treatment.

2.3.4 Barrier properties

The water vapour permeability (WVP) of the films was determined following the gravimetric method ASTM E96/E96M (ASTM, 2005) applying the modification proposed by McHugh et al., (1993). Film samples (3.5 cm diameter) were cut, placed, and sealed on Payne permeability cups (Elcometer SPRL, Hermelle/s Argenteau, Belgium) filled with 5 mL of distilled water (100 % RH). The cups were placed into desiccators at 25 °C and 53 % RH ($Mg(NO_3)_2$ over-saturated solution) containing a fan placed on top of each cup to decrease the resistance to water vapour transport. The cups were weighed every 1.5 hours with an analytical balance (± 0.0001 g) throughout 48 h. Finally, the WVP was calculated from the slope of the weight loss-time curves (Freitas et al., 2021). For each formulation, the analysis was carried out in triplicate.

An Oxygen Permeation Analyser (Model 8101e, Systech Illinois, Illinois, USA) was used to determine the oxygen permeability (OP) of the films at 25 °C and 53 % RH, following the ASTM D3985-05 methodology (ASTM, 2010). The oxygen transmission rate through the film samples (50 cm^2) was measured every 15 min until equilibrium was reached (difference between the last 4 measurements of less than 1 %). The OP of the films was calculated by dividing the oxygen transmission rate by the difference in partial pressure of oxygen between the two sides of the film and multiplying it by the average film thickness. The measurements were taken in duplicate for each film.

2.3.5 Thermal behaviour of the films

Differential scanning calorimetry (DSC) and thermogravimetric analysis (TGA) of the films was carried out to analyse the effect of extracts on phase transitions and thermal stability of PLA. Film samples (5-7 mg) in aluminium-sealed pans were analysed in the calorimeter (Stare System, Mettler-Toledo Inc., Switzerland), under a nitrogen flow (30 $mL.min^{-1}$), by applying a

heating scan from -25 to 200 °C at 10 °C.min^{-1}, maintaining at 200 °C for 5 min, cooling down to -10 °C at -50 °C.min^{-1}, maintaining at -10 °C for 5 min, and heating up to 200 °C at a 10 °C.min^{-1}. The analysis was performed in triplicate for each film formulation. For TGA, film samples (3-5 mg) placed in an alumina crucible were analysed in the equipment (TGA 1 Stare System, Mettler-Toledo Inc., Switzerland) from 25 °C to 700 °C at a heating rate of 10 °C.min^{-1}, under a nitrogen flow (10 mL.min^{-1}). The derivative curves (DTGA) of the thermograms were obtained using the STARe Evaluation Software (Mettler-Toledo, Switzerland). The initial degradation temperature, the temperature at maximum degradation rate and the mass loss were determined. The analysis was performed in duplicate for each sample.

2.4 Pork meat preservation capacity of the films

The capacity of the films with different active extracts to preserve fresh pork meat during cold storage was evaluated. To this end, fresh pork meat was obtained from the local market and aseptically cut into fillets of about 22 g. Previously, the control and active films (12 cm x 7 cm) were thermo-sealed using a vacuum sealer (Vacio Press, Saeco) to obtain bags. Then, the fillets were put into the film bags, and thermo-sealed. The packaged samples were stored for 16 days at 4 °C. The meat quality parameters, typically pH, mass loss, colour, microbial count, and 2-thiobarbituric acid reactive substances (TBARS) index, were evaluated on days 0, 7, and 16 days of storage, using two different sample bags for each time.

2.4.1. Colour measurement

The meat CIEL*a*b* colour coordinates were obtained with a Spectro-colorimeter (CM-3600d, Minolta Co., Japan) using a D65 illuminant and at 10º observer. The meat colour parameters at initial time (L_0^*, a_0^*, b_0^*) was used to determine the total colour difference of the samples (ΔE^*) throughout the storage, by applying Eq. 1.

$$\Delta E^* = \sqrt{(\Delta L^*)^2 + (\Delta a^*)^2 + (\Delta b^*)^2} \quad (1)$$

Where $\Delta L^* = (L^* - L_0^*)$; $\Delta a^* = (a^* - a_0^*)$; $\Delta b^* = (b^* - b_0^*)$.

2.4.2 Mass loss and pH measurement

The pH analysis was performed by immersing an electrode probe (Mettler-Toledo GmbH, Schwerzenbach, Switzerland) into the pork meat fillets (five measurements per sample). In addition, the sample weight loss was determined by weighing each fillet at 0, 7 and 16 days of storage.

2.4.3 2-thiobarbituric acid reactive substances (TBARS) assay

The antioxidant capacity of the active films was evaluated by measuring the TBARS index of the meat following the methodology previously described by (Siu & Draper, 1978). An amount of 10 g of meat was mixed with 50 mL of distilled water and 50 mL of 10 % trichloroacetic acid (w/v), and then homogenized using an Ultra-turrax homogenizer (ULTRA-TURRAX®, Model T 25 D, IKA®, Germany) for 2 min. Later on, the suspension was vacuum filtered using qualitative filter (Filterlab) and 8 mL of the filtrate was mixed with 2 mL of 2-thiobarbituric acid (0.06 mol.L^{-1}) and heated at 80 °C for 90 min. Thereafter, the absorbance at 532 nm was measured and the TBARS index were expressed as mg malonaldehyde (MDA) per kg of meat using 1,1,3,3-tetramethoxypropane as standard (0.5 – 12 µM). The measurements were performed in triplicate.

2.4.4 Microbiological analysis

Microbial counts, typically total viable (TV), psychrotrophic bacteria (PB), total coliforms (TC), and lactic acid bacteria (LA) were determined in packaged meat throughout storage. Briefly, meat samples (10 g) were aseptically weighed and mixed with 90 mL of 0.1% peptone water in sterile bags and homogenised in Stomacher for 3 min, obtaining a 10^{-1} dilution. Afterwards, the obtained suspension was serially diluted by transferring 1 mL of each dilution into 9 mL of tryptic soy broth (TSB), and then 1 mL of each dilution tube was mixed with the appropriate medium to quantify the corresponding tested microorganism. LA bacteria were quantified in MRS agar by incubation at 30 °C for 72 h, TC were determined using the chromogenic medium Brilliance *E. coli*/Coliforms Selective Agar, after incubation at 37 °C for 24 h. TV and PB bacteria were determined in PCA plates by incubation at 37 °C or 4 °C for 48 and 7 days, respectively. For each microorganism and treatment, plates with 25-250 colonies were selected to determine the bacterial count and expressed as log colony-forming units per gram of meat (log CFU.g^{-1} sample).

2.5 Statistical analysis

Analysis of variance (ANOVA) and Tukey's HSD (honestly significant difference) test, considering the least significant difference (α) of 5 %, were applied to determine whether there were significant differences between the active extracts and or the film formulations. The statistical analysis was carried out using Minitab Statistical Software (version 17).

3. RESULTS AND DISCUSSION

3.1. Active properties of the RS extracts.

Table 1 shows the phenolic content, antioxidant parameters, and MIC values of each active extract. A different phenolic content and antioxidant capacity were obtained via the different

extraction processes. SWE was more effective than USHT process at phenolic extraction, the efficiency increasing when the temperature rose. The phenolic content of the extracts was linearly correlated with their ABTS radical scavenging capacity (r=0.996), but a poor correlation was observed between EC_{50} values and TPC (r =-0.828). The higher the TPC, the lower the EC_{50} values (a smaller extract amount was required to reduce the DDPH radical activity by 50 %), although SWE extracts seem to exhibit a different tendency with respect to TPC. This suggests that phenolic compounds detected from the Folin-Ciocalteu assay in the extracts did not have the same composition profile in USHT extract as in the SWE extracts and exhibited different DPPH scavenging capacity. In this sense, other antioxidant compounds neo-formed through Maillard and caramelisation reactions at the highest SWE temperature could also contribute to the EC_{50} values, as described by other authors as regards the SWE of different plant matrices (Plaza et al., 2010a). Plaza et al. (2010b) studied the formation of Maillard and caramelisation products during SWE using glycation model systems with amino acids and glucose, as a function of temperature, and found that the extent of non-enzymatic browning reactions was higher when the temperature increased. Therefore, SWE180 extracts could contain a greater ratio of these kinds of brown compounds.

Table 1. Total solid yield (TSY), total phenolic content (TPC), antioxidant capacity (EC_{50} and Trolox equivalent antioxidant capacity (TEAC)), and minimum inhibitory concentration (MIC) for *L. innocua* and *E. coli* of the bioactive extracts obtained with different extraction methods.

	USHT*	**SWE160***	**SWE180***
TSY (g dry extract. 100 g^{-1} RS)	13.95 ± 0.13^{b}	23.1 ± 0.3^{a}	23.4 ± 1.1^{a}
TPC (mg GAE. g^{-1} dry extract)**	37.1 ± 0.4^{c}	51.1 ± 2.4^{b}	82.5 ± 3.2^{a}
EC_{50} (mg dry extract. mg^{-1} DPPH)	6.3 ± 0.3^{a}	2.0 ± 0.1^{b}	1.2 ± 0.1^{c}
TEAC (µmol Trolox.mg^{-1} dry extract)	0.59 ± 0.02^{c}	0.67 ± 0.01^{b}	0.94 ± 0.02^{a}
MIC *L. innocua* (mg.mL^{-1})	>200	50 ± 3^{a}	30 ± 3^{b}
MIC *E. coli* (mg.mL^{-1})	>200	>200	182 ± 3

*Different letters in the same column indicate significant differences between films by the Tukey test (α = 0.05).

**GAE: gallic acid equivalent.

For comparison purposes, the EC_{50} values of potent antioxidant compounds, such as ascorbic acid or α-tocopherol, are 0.12 and 0.26 mg compound /mg DPPH, respectively (Brand-Williams et al., 1995), which indicates that the SWE extracts, especially SWE180, exhibited a high DPPH radical scavenging capacity, nearer to that of the strong antioxidants.

As concerns the antimicrobial capacity of the extracts, the MIC values of the extracts for both Gram+ and Gram- bacteria also suggested greater antibacterial activity of the SWE extracts, since lower MIC values were obtained for these extracts. Although in no case were the MIC values of USHT extracts reached at the maximum concentration (200 mg.mL^{-1}) used, SWE

extracts reached the MIC value of *L. innocua* at 30 and 50 mg/mL^{-1} for SWE160 and SWE180 extracts, respectively. *E coli* was less sensitive to these extracts, exhibiting higher MIC values (over 200 mg.mL^{-1}, for SWE160 extract). Previous studies with phenolic acids also pointed to the differences as regards the effectiveness against each bacterium (Ordoñez et al., 2021), which are the main phenolic compounds in RS aqueous extracts (Menzel et al. 2020). Ferulic acid, one of the main constituents of rice straw aqueous extract (Menzel et al. 2020) was also more effective against *L. innocua* than against *E. coli*, as observed by other authors (Takahashi et al. 2013; Andrade et al. 2022). Gram-negative bacteria, such as *E. coli,* are expected to be more resistant to antimicrobials, as their outer membrane limits the crossing of small molecules to a greater degree (Liu et a. 2020).

3.2. Properties of the films

3.2.1 Microstructure and optical properties of the films

Fig. 1 shows the cross-sections of PLA films with and without RS extracts obtained by different extraction methods (USHT, SWE160 and SWE180). The control PLA films exhibited a plastic cryofracture, with brittle and rubbery domains, characteristic of this amorphous polymer, as observed by other authors (Muller et al., 2017; Sanyang et al., 2016). The incorporation of RS extracts promoted appreciable differences in the microstructure of the films, according to the new interactions established between the extract components and PLA chains. The phenolic-rich composition of the extracts, including ferulic acid, *p*-coumaric acid, protocatechuic acid, and caffeic acid (Menzel et al., 2020), may imply the extensive formation of hydrogen bonds between the phenol OH groups and carbonyl of the PLA chains or with the end chain hydroxyl, which could promote a new interchain entanglement. Likewise, the presence of small aggregates, or small holes, in the polymer matrix, depending on the extract incorporated, suggested the lack of total compatibility of the extract compounds and polymer, giving rise to phase separation and a more heterogenous structure. The PLA-USHT film showed a high proportion of small aggregates that were well adhered to the polymer matrix, whereas films with SWE extracts showed small holes that, in some cases, contained loose particles. This suggests a different affinity of non-miscible compounds of the extracts with the polymer, giving rise to differing adhesion forces of dispersed particles with the matrix, depending on their composition. A rough surface pattern of the cross-section of PLA films was also reported by Díaz-Galindo et al. (2020) when the a greater concentration of grapevine cane extract was incorporated (5-15 % wt.). The SWE promotes the extraction of less polar compounds, such as phenolic acids, (Ong et al., 2006; Plaza et al., 2010) but also favours the extraction of hemicellulose (Requena et al. 2019), which could be less compatible with the PLA chains, given their polymeric, hydrophilic nature. Therefore, interchain interactions with miscible compounds of the extracts and dispersion of the non-compatible fractions provoked a

structural modification in the PLA matrix that can affect its functional properties as a packaging material, such as its optical, barrier or mechanical properties.

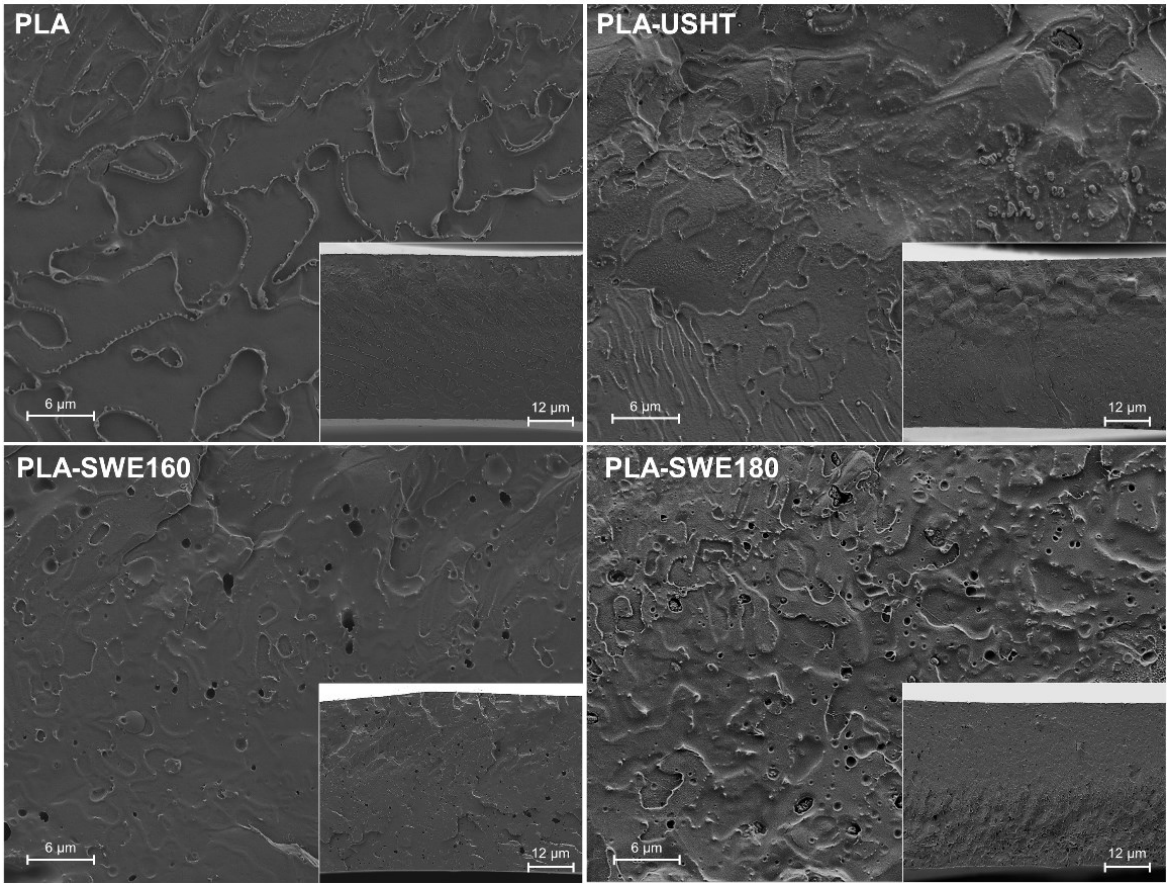

Fig. 1. FESEM micrographs of the cryo-fracturated PLA films with and without different RS active extracts. The images were taken at ×600 magnification (with inserts at ×2000).

As concerns the optical characteristics of the films, their visual appearance, colour coordinates and UV-vis transmittance spectra are shown in Fig. 2a. The incorporation of extracts promoted marked changes in the film colour that becomes reddish, more vivid, and darker than the control PLA film. Active films exhibited a notable decrease in lightness (L^*: from 90.7 to 61.0), with a pronounced increase in colour saturation (C_{ab}^*: from 2.7 to 49.2), and a significant change in the hue angle (h_{ab}^*: from 99.0 to 75.2), in which the extract SWE180 promoted the highest changes. The total colour difference (ΔE^*) of the active films with respect to the control PLA film was higher for PLA-SWE180 films (55.7) than PLA-SWE160 (45.1), while the lowest value was obtained for PLA-USHT films (36.7). This is coherent with a higher ratio of coloured compounds in the extracts, since many chemicals present in the lignin fraction are responsible for the dark colour in plant matrices (Do et al., 2020). Likewise, the high temperatures and pressures applied in the SWE process could promote browning reactions, such as Maillard and caramelisation reactions, giving rise to more coloured/more intensely coloured extracts, mainly at 180 °C, as previously reported (Plaza et al. 2010b).

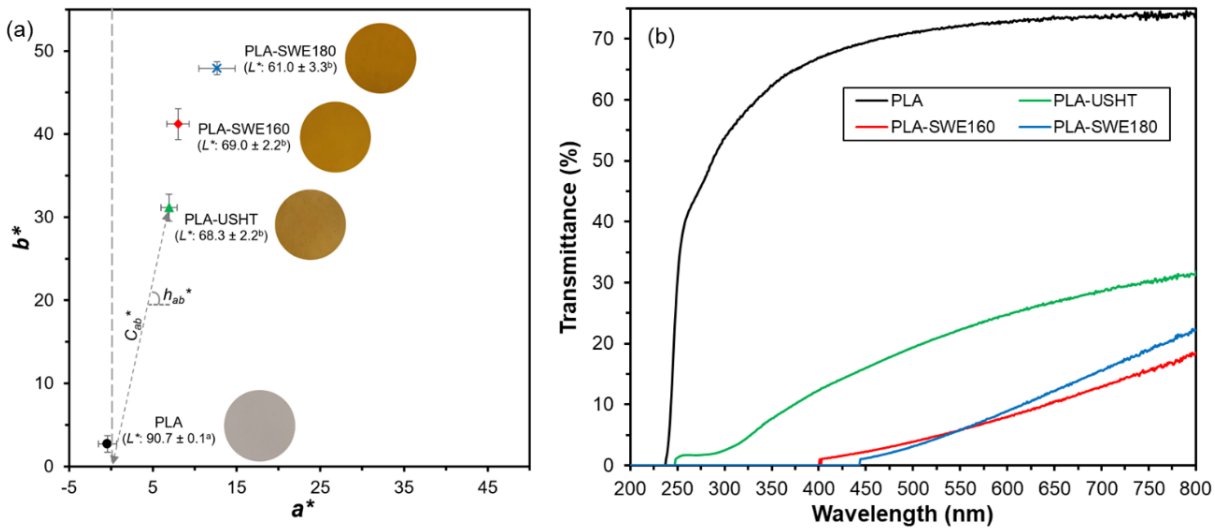

Fig. 2. (a) Visual appearance and colour coordinates (mean values and standard deviations), and (b) UV-vis spectra of the PLA films with different RS extracts.

As concerns the UV-vis transmittance spectra, the net PLA film was highly transparent, with 70-80 % transmittance in the visible wave-length range, with a slight light-blocking effect in the UV region (400-250 nm). In contrast, the active films exhibited a marked decrease in light transmission in both the visible and UV ranges, due to the presence of the extract compounds in the polymer matrix with the ability to absorb UV light. In fact, phenolic compounds are considered as photo-protective compounds due to their molecular structure, with conjugated double bonds and aromatic rings (Woo et al., 2011). The most intense UV-vis light blocking effect was achieved for the films with SWE extracts (SWE160 and SWE180). These transmitted approximately 20 % in the visible light range and exhibited a total blocking effect between 400-450 nm. The PLA-USHT film was slightly more transparent than the other active films, especially in the UV region. Wen et al. (2020) also reported an excellent light-blocking effect of poly (vinyl alcohol) films with green tea extract. Thus, the presence of active RS extracts, especially those obtained by SWE, prevented the UV light transmission, which is responsible for promoting the photo-oxidation of the components present in foods, such as vitamins, fatty acids, or pigments.

3.2.2 Thermal, mechanical and barrier properties of the films.

Thermal analysis of the films obtained by DSC (second heating to delete the polymer thermal history) (Fig. 3b and c) showed the typical glass transition of the amorphous PLA at 55.8 °C, in the previously reported range by other authors (Ordoñez et al., 2022). The incorporation of RS extracts provoked a plasticizing effect, reducing the T_g values by about 5 °C, regardless of the kind of extract (Table 2).

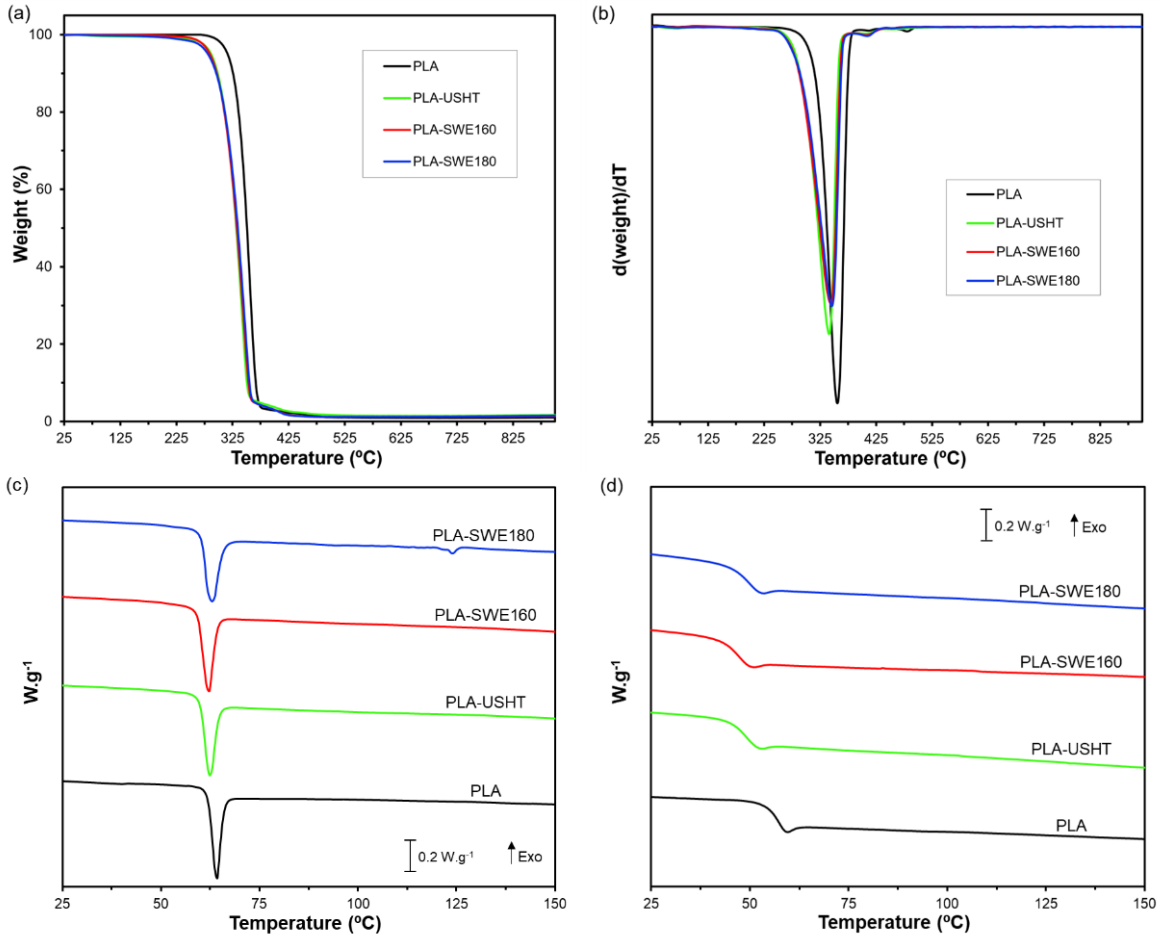

Fig. 3. (a) TGA curves, (b) DTGA first derivative curves, (c) first and (d) second heating DSC thermograms of PLA films with different RS active extracts.

Table 2. Thermal parameters of the PLA films obtained from DSC (glass transition temperature (T_g)) and TGA (initial temperature (T_o), peak temperature (T_p), and residue).

	TGA*			DSC*
Formulation	**T_o (°C)**	**T_p (°C)**	**Residue (%)**	**T_g (°C)**
PLA	269 ± 6^a	357 ± 1^a	1.1 ± 0.5^a	55.8 ± 0.4^a
PLA-USHT	218 ± 4^b	342 ± 1^b	1.7 ± 0.4^a	49.6 ± 2.5^b
PLA-SWE160	214 ± 2^b	344 ± 1^b	1.4 ± 0.5^a	47.7 ± 2.2^b
PLA-SWE180	216 ± 3^b	345 ± 1^b	1.8 ± 0.4^a	48.5 ± 1.5^b

* Different letters in the same column indicate significant differences between films by the Tukey test ($\alpha = 0.05$).

Likewise, TGA also revealed the effect of RS extracts on thermal stability of PLA (Fig. 3a and b). The typical degradation curve of amorphous PLA was obtained, with a single thermal event starting at 269 °C (T_o) and maximum degradation rate at 357 °C (T_p), as reported by other

authors (Ordoñez et al. 2022). The incorporation of RS extracts provoked a decrease in both T_o and T_p of about 50 and 15 °C, respectively, regardless of the extract incorporated, as shown in Table 2. These effects reflected the structural changes in the PLA matrix due to action of some extract components, such as phenolic acids or bonded water. These compounds could promote the partial hydrolyses of PLA during thermal processing, with the subsequent formation of shorter chains. The low molecular weight chains would contribute to a reduction in the T_g and thermal stability of the matrix, whose degradation started at a lower temperature. Similar effects on T_g of PLA matrices have been observed when plant extracts were incorporated (Khakestani et al. 2017).

Figure 4a shows the typical stress-strain curves of the films, whose mean thickness was 0.140 mm, with no significant differences between formulations. The embedded table in Figure 4a gives the values of the film tensile parameters, typically TS, E, and EM.

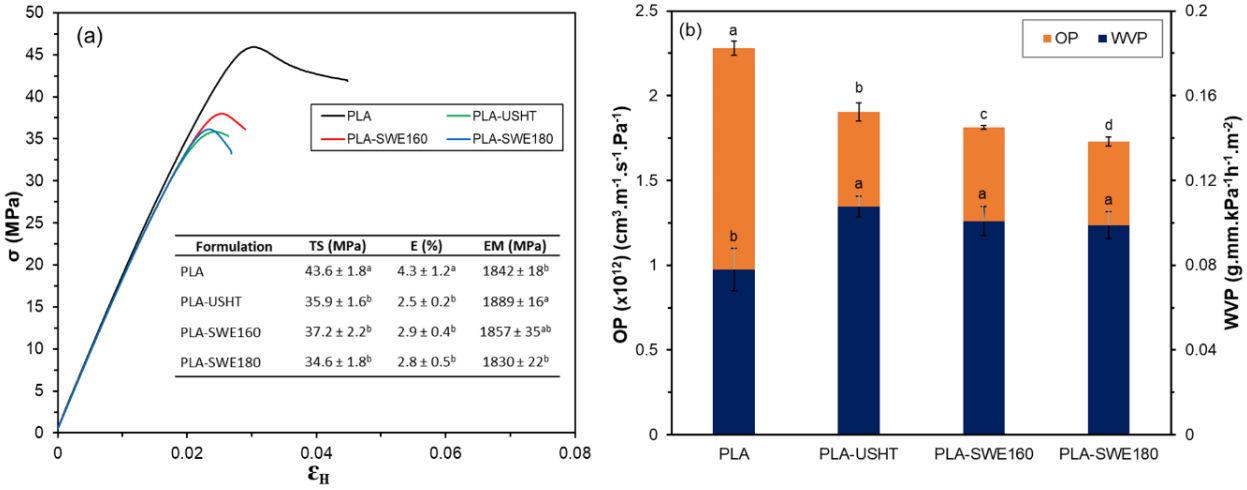

Fig. 4. (a) Stress–strain curves and tensile properties (inserted table) (TS, E, and EM) (different subscript letters in the same column indicate significant differences between samples by Tukey test), and (b) oxygen permeability (OP), and water vapour permeability (WVP) of the PLA films with different RS extracts (for each property, different letters indicate significant differences).

The control PLA films showed TS, E, and EM values in the range found by other authors for PLA films of similar characteristics (Muller et al. 2017; Cvek et al., 2022). Nevertheless, the incorporation of active extracts markedly affected the tensile behaviour of the films, making them less extensible and reducing their resistance to break, as shown in Figure 2a. Therefore, the active films exhibited a slightly worsened mechanical performance with respect to the neat PLA film, with reductions of about 18 and 36 %, respectively, in the TS and E values. This behaviour reflected the weakening effect provoked by the extract compounds in the polymer matrix resulting from the compound interactions with the PLA chains that globally reduced

the interchain forces and matrix cohesiveness, as previously observed in PLA films when molecular compounds of different characteristics, such as phenolic acids (Ordoñez et al. 2022) or other antioxidant compounds (Bassani et al. 2019; Freitas et al., 2023) were incorporated. Additionally, the phenolic acids present in the extracts could promote the hydrolysis of the PLA chains during the film thermo-manufacturing steps to a certain degree, as deduced from the thermal analysis. This would also contribute to the weakening of the PLA network. Nevertheless, the described interactions did not significantly affect the film stiffness since no notable changes were observed in the elastic modulus of the films with extracts.

Fig. 4b shows the WVP and OP values of the control PLA film and those containing different RS extracts. The extract-free film exhibited a WVP value of 0.077 $g.mm.kPa^{-1}.h^{-1}.m^{-2}$, similar to that reported by other authors for PLA films (Díaz-Galindo et al., 2020; Jamshidian et al., 2012). Nevertheless, the incorporation of the active extract slightly worsened the water vapour barrier capacity of the films, leading to an increase in the WVP values of about 30 % ($p < 0.05$). This could be associated with the presence of hydrophilic components from the RS extracts in the matrix, which would enhance the solubility of water molecules through the polymer network, and with the weakening effect of the compound extracts in the polymer network cohesion forces that enhances molecular mobility and diffusion.

The OP values of the films were also greatly influenced by the incorporation of the active extracts ($p < 0.05$). All of the active films showed a decrease in the OP values with respect to the control PLA film, which could be attributed to several reasons: 1) the promotion of the hydrophilic nature of the polymer matrix when RS extracts were present that enhances the oxygen solubility in the matrix, and 2) the oxygen scavenging capacity of the extract compounds that limits the oxygen transfer in the active films (Bonilla et al., 2013). The PLA-USHT, PLA-SWE160, PLA-SWE180 films exhibited reductions in the OP values of approximately 16, 20, and 24 %, respectively, which correlate with the respective antioxidant capacity of the present extracts. The greater the radical scavenging capacity of the extracts, the more significant the OP reduction in the films. This points to a greater impact of the antioxidant power on the oxygen transfer through the films.

Therefore, despite the slightly worse mechanical properties and water vapour permeability of the films with RS extracts, their oxygen and light barrier capacity as well as their potential active properties could represent a significant improvement in terms of their food packaging potential, as a means of preventing food oxidation reactions during storage.

3.2.3 Pork meat preservation capacity of the films

The active and control PLA films were used to evaluate their ability to package and preserve fresh pork meat during storage. For this purpose, the quality parameters of packaged meat, namely weight loss, pH, TBARS index, microbial count, and colour were analysed throughout

16 days of cold storage. Fig. 5a shows the weight loss of the meat fillets packaged in the active and control film bags. The samples packaged with the control PLA films exhibited the greatest weight loss, reaching values of about 10 % after 16 storage days, in the range reported by other authors (Hernández-García et al., 2022). The active film bags were more effective at preventing the sample weight loss (~ 4 % after 6 storage days), with no significant differences between active bags. The meat water retention capacity may be affected by different processing factors, such as cutting, temperature, salt addition or grinding, and by the intrinsic characteristics of the meat, such as the pH value that directly affects the water retention capacity of meat proteins (Haque et al., 2016).

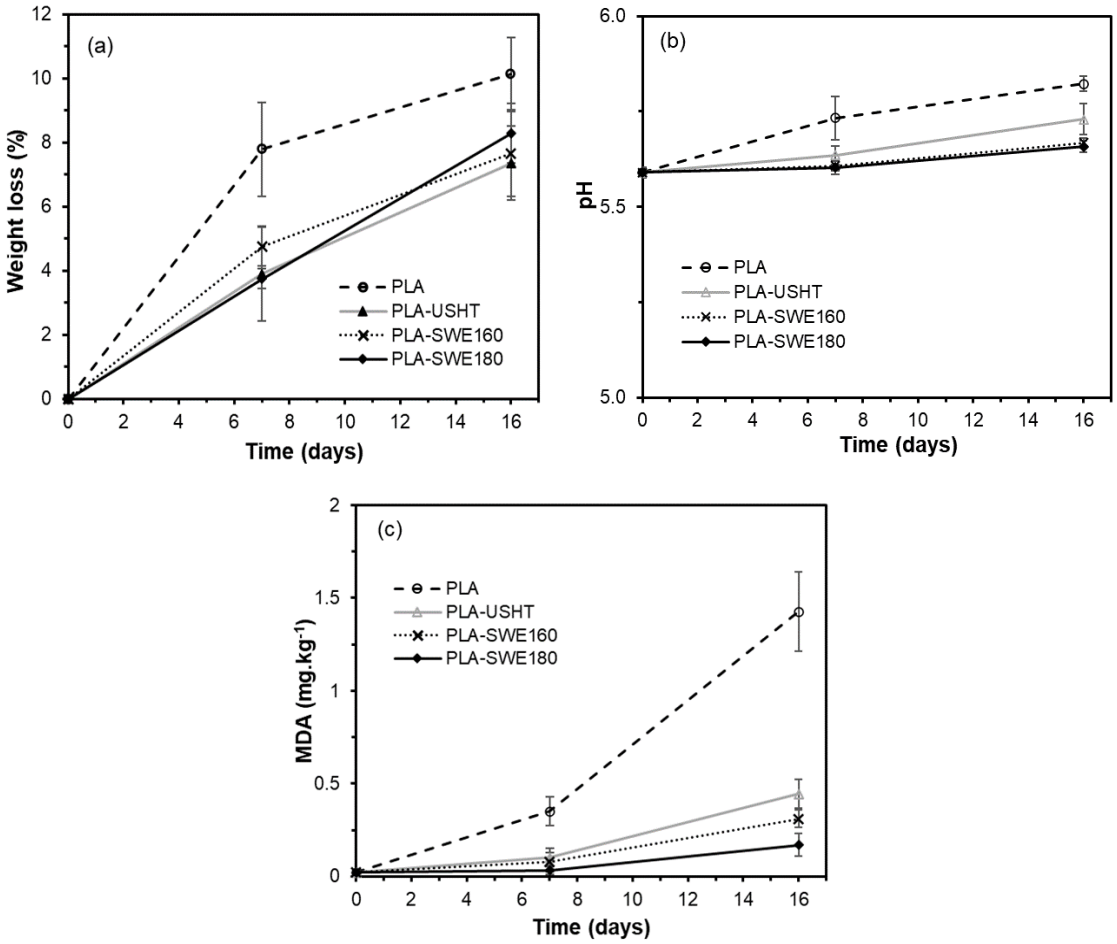

Fig. 5. Weight loss (a), pH (b), and TBARS (c) values of the pork meat packaged in the PLA film bags with different extracts stored at 4 °C for 16 days.

Fig. 5b shows the pH values of the meat as a function of storage time, where the expected increase can be observed in every sample. The pH increase is associated with the deterioration of proteins through enzymatic reactions or the metabolism of microorganisms that leads to the production of alkaline compounds, such as biogenic amines. The initial pH value of the

meat was 5.59, consistent with the values reported by other studies for fresh pork meat (Yang et al., 2019). The meat packaged in the control film bag exhibited a greater increase in pH, (pH final value of 5.70) than the samples packaged in active bags, which also coincides with the higher weight loss value of this sample. Meat samples packaged with PLA-SWE160 and PLA-SWE180 films showed the smallest changes in the pH values throughout time, which could be attributed to the active properties of the films, as discussed below for the other quality parameters.

As concerns meat oxidation, the development of malondialdehyde (MDA) levels, one of the end-products originating from hydroperoxide decomposition, as a function of storage time is shown in Fig. 4c for the different treatments. Initially, the meat exhibited a TBARS index of 0.1 mg MDA.kg^{-1} sample, typical of fresh pork meat (Kaczmarek et al., 2017). The storage time and the type of packaging significantly affected the TBARS values. All of the meat samples showed a progressive increase in the TBARS index, but the samples packaged with the control film had a much higher oxidation rate. This indicates that the extracts incorporated into PLA films were efficient at retarding meat oxidation during storage. The ability to slow down the oxidative processes in meat could be associated with the release of antioxidant compounds from the films to the meat surface. Likewise, the lower OP values and the significant UV-light barrier of the active films could produce additional antioxidant effects, since the lower oxygen and UV light exposure of the meat samples prevent meat photo-oxidation. The antioxidant effects were mainly appreciated after 16 storage days and were aligned with the different antioxidant activity of the extracts incorporated into the films (PLA-SWE180 >PLA-SWE160 >PLA-USHT). Therefore, the films with a SWE180 extract with the lowest oxygen permeability, more intense UV light blocking effect and the highest antioxidant capacity of the extract were the most effective at preserving the meat samples from oxidative deterioration.

Fig. 6 shows the microbial counts in the packaged meat, in terms of the TV, LA, TC, and PB bacteria, at the different storage times. As reported by other authors (Kim et al., 2016), all the microorganisms tested in the meat samples exhibited progressive microbial growth . The microbial counts in the control sample (packaged in an extract-free PLA bag) were higher than those of the samples packaged in active films, which indicates the capacity of these films to inhibit microbial growth. Of the active films, the PLA-USHT was the least efficient at reducing microbial counts, especially in the case of TV and PB bacteria, with the samples exhibiting similar counts to the control sample. In fact, the samples packaged in PLA and PLA-USHT bags exceeded the acceptability limit of the total viable count in pork meat (6 log CFU.g^{-1}, Commission Regulation No 2073/2005) on day 16 of cold storage, whereas the samples packaged in SWE160 and SWE180 films remained below this limit throughout the entire period tested. The PLA-SWE180 film was the most effective at inhibiting microbial growth, exhibiting a log reduction of TV, LA, TC, and PB bacteria of about 1.9, 0.9, 1.1, and 1.4, respectively, after 16 storage days with respect to the control sample . This is coherent with

the different antibacterial activity of the extracts deduced from the MIC values obtained for Gram+ and Gram- bacteria. The antibacterial effect of the released phenolic compounds is associated with their ability to inhibit bacterial virulence factors, such as enzymes and toxins, interact with the cytoplasmic membrane, and suppress the formation of bacterial biofilms (Miklasińska-Majdanik et al., 2018).

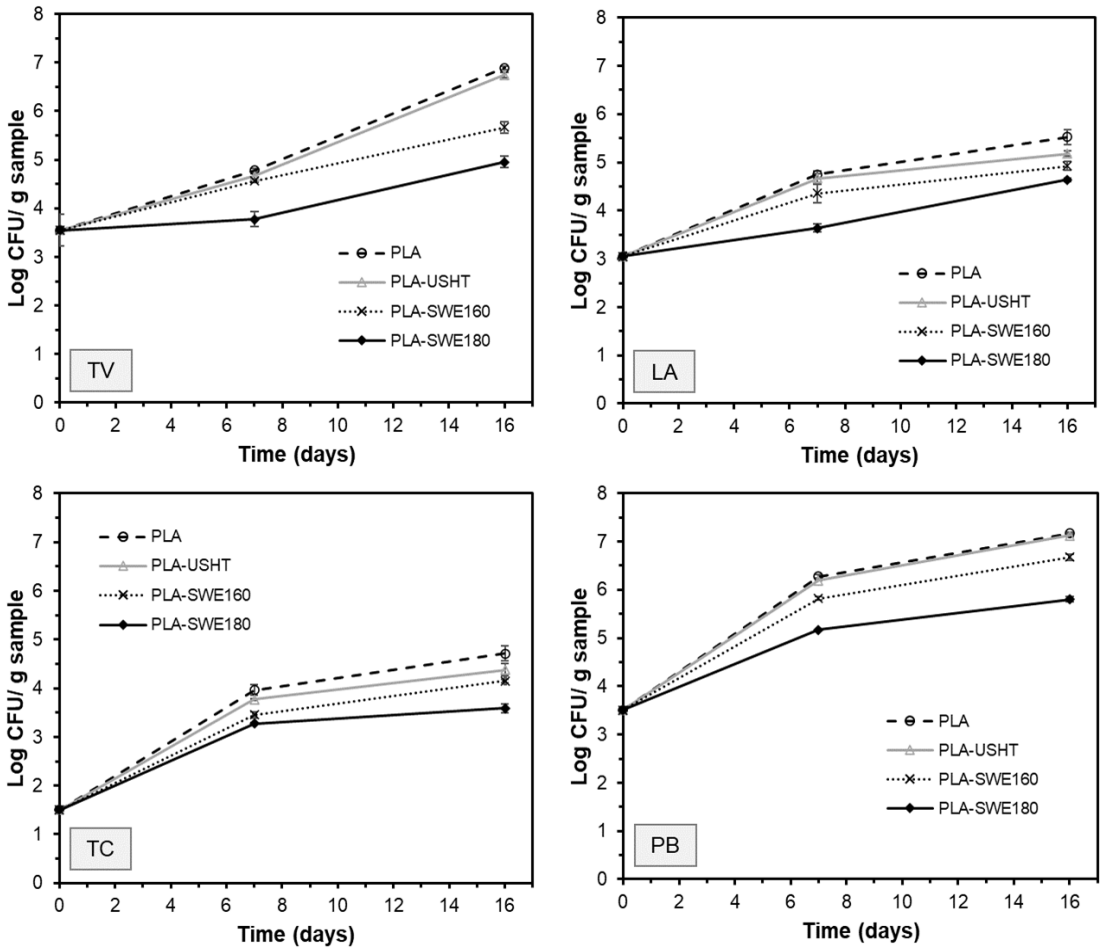

Fig. 6. Development microbial counts (total viable counts (TV), lactic acid bacteria (LA), total coliforms (TC), and psychrotrophic bacteria (PB) of pork meat packed with PLA films stored at 4 °C for 16 days.

The colour changes of packaged meat, in terms of the L^*, C_{ab}^*, h_{ab}^* coordinates, and the total colour difference (ΔE^*) with respect to the initial coordinates are shown in Fig. 7, as a function of storage time at 4 °C. All of the meat samples became darker (L^* decrease) and less vivid in colour (C_{ab}^*) decrease), with small changes in hue, throughout storage (Fig. 7). However, the samples packaged in the extract-free film exhibited the most significant changes in the colour coordinates, which was reflected in the higher values of ΔE^* at each storage time. The colour changes are associated with water loss and pigment oxidation during storage. Water loss modifies the sample surface reflectance and pigment concentration, which affect sample

colour (Hernández-García et al., 2022). Myoglobin is the heme protein responsible for meat colour, and the oxidation of the central iron atom within the heme group is responsible for discoloration, producing changes from red OxyMb to brownish MetMb. This oxidation has been linked to lipid oxidation since the oxidation of one of these compounds produces chemical species that can promote the oxidation of the others. Therefore, previous studies reported that meat colour was preserved by the incorporation of antioxidant compounds (Faustman et al., 2010). In fact, active films with antioxidant extracts better preserved the colour of the meat samples, leading to smaller colour differences throughout storage. The colour development was coherent with the sample oxidation pattern reflected in the TBARS analysis and indicates the key role played by the antioxidant extracts in delaying the oxidative decay of the samples that produces both rancidity and colour degradation.

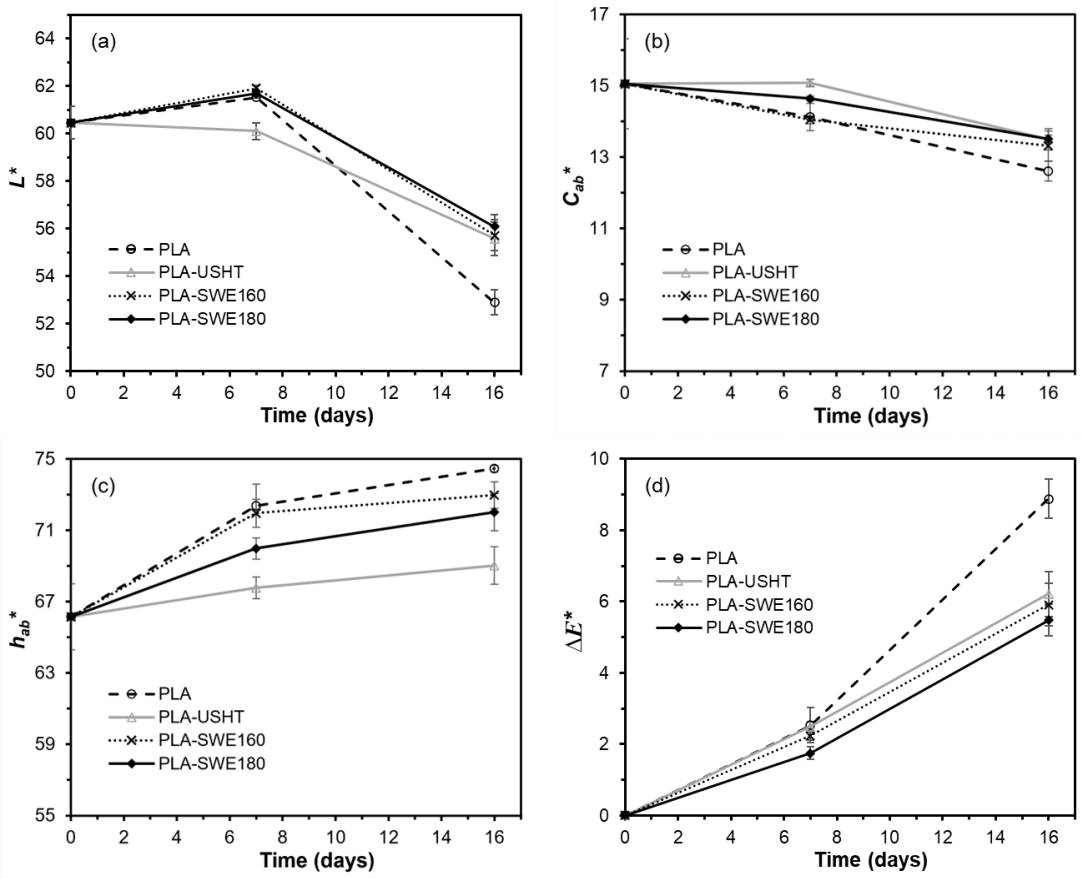

Fig. 7. Colour parameters *L** (a), C_{ab}* (b), h_{ab}* (c), and *ΔE** (d) of the pork meat packaged in the PLA films bags added with different extracts stored at 4 °C for 16 days.

Active PLA films with RS extracts exhibited good preservation capacity to package fresh pork meat, compared to extract free PLA films, maintaining the quality paremeters throughout longer times and extending the product shelf life. SWE (especilly a 180 °C) produced extracts with greater antioxidant and antibacterial activity, which were reflected in a greater

efectiveness of the films containing these extracts to preserve meat from oxidative and microbial spoilage.

4. CONCLUSIONS

Aqueous RS extracts obtained by combined US-reflux heating and SWE exhibited antioxidant and antibacterial activity; this was greater in the SWE extracts, especially at 180 °C. These extracts slightly reduced the extensibility, resistance to break and water barrier capacity of the PLA films when incorporated at 6 % wt. Nonetheless, they enhanced the oxygen barrier capacity and the UV light blocking effect of the films. The films with RS extracts were effective at preserving meat quality parameters for longer, inhibiting meat oxidation, discolouration, and weight loss, so extending the meat shelf life. The SWE extract obtained at 180 °C was the most effective at obtaining active films for meat preservation. Therefore, the green SWE technique permits active extracts to be obtained from RS, which is useful for producing active PLA films to extend the meat shelf life. These results represent a sustainable alternative to valorise the RS waste for developing biodegradable active materials to extend the shelf life of food products sensitive to oxidative and microbial deterioration.

5. ACKNOWLEDGMENTS

The authors thank the Agencia Estatal de Investigación (Spain) for the financial support through projects PID2019-105207RB-I00/AEI/10.13039/501100011033 and Generalitat Valenciana [grant number GrisoliaP/2019/115].

6. REFERENCES

ASTM. (2005). E96/E96M-05. Standard Test Methods for Water Vapor Transmission of Materials. American Society for Testing and Materials, 1-11.

ASTM. (2010). D3985-05 Oxygen Gas Transmission Rate Through Plastic Film and Sheeting Using a Coulometric Sensor. Annual Book of ASTM Standards, C, 1–7. https://doi.org/10.1520/D3985-05.2

ASTM. (2012). ASTM D882-12 Standard test method for tensile properties of thin plastic sheeting. American Society for Testing and Materials, 12.

Alara, O. R., Abdurahman, N. H., & Ukaegbu, C. I. (2021). Extraction of phenolic compounds: A review. *Current Research in Food Science*, 4, 200-214. https://doi.org/10.1016/j.crfs.2021.03.011

Almasi, H., Jahanbakhsh Oskouie, M., & Saleh, A. (2021). A review on techniques utilized for design of controlled release food active packaging. *Critical reviews in food science and nutrition*, 61(15), 2601-2621.

Almeida, A. da R., Brisola Maciel, M. V. de O., Machado, M. H., Sganzerla, W. G., Teixeira, G. L., da Rosa, C. G., Block, J. M., Nunes, M. R., & Barreto, P. L. M. (2022). Production of chitosan and poly (vinyl alcohol) films functionalized with hop extract (Humulus lupulu L. var. Cascade) for food packaging application. *Food Packaging and Shelf Life*, 32, 100833. https://doi.org/10.1016/j.fpsl.2022.100833

Andrade, A.; González-Martínez, C., & Chiralt. A. Physical and active properties of poly (vinyl alcohol) films with phenolic acids as affected by the processing method. *Food Packaging and Shelf Life*, 2022, 33, 100855. https://doi.org/10.1016/j.fpsl.2022.100855.

Baghi, F., Gharsallaoui, A., Dumas, E., & Ghnimi, S. (2022). Advancements in Biodegradable Active Films for Food Packaging: Effects of Nano/Microcapsule Incorporation. *Foods*, 11(5), 760. https://doi.org/10.3390/foods11050760

Barana, D., Salanti, A., Orlandi, M., Ali, D. S., & Zoia, L. (2016). Biorefinery process for the simultaneous recovery of lignin, hemicelluloses, cellulose nanocrystals and silica from rice husk and Arundo donax. *Industrial Crops and Products*, 86, 31-39. https://doi.org/10.1016/j.indcrop.2016.03.029

Bassani, A., Montes, S., Jubete, E., Palenzuela, J., Sanjuán, A. P., & Spigno, G. (2019). Incorporation of waste orange peels extracts into PLA films. *Chemical Engineering Transactions*, 74(A), 1063-1068.

Bhat, R. (2021). Sustainability challenges in the valorization of agri-food wastes and by-products. *Valorization of Agri-Food Wastes and By-Products* (pp. 1-27). Elsevier. https://doi.org/10.1016/B978-0-12-824044-1.00022-2

Bonilla, J., Talón, E., Atarés, L., Vargas, M., & Chiralt, A. (2013). Effect of the incorporation of antioxidants on physicochemical and antioxidant properties of wheat starch–chitosan films. *Journal of food Engineering*, 118(3), 271-278.

Brand-Williams, W., Cuvelier, M. E., & Berset, C. (1995). Use of a free radical method to evaluate antioxidant activity. *LWT - Food Science and Technology*, 28(1), 25-30. https://doi.org/10.1016/S0023-6438(95)80008-5

Castro-Puyana, M., Herrero, M., Mendiola, J. A., & Ibáñez, E. (2013). Subcritical water extraction of bioactive components from algae. *Functional Ingredients from Algae for Foods and Nutraceuticals* (pp. 534-560). Elsevier. https://doi.org/10.1533/9780857098689.3.534

Cheung, Y.-C., & Wu, J.-Y. (2013). Kinetic models and process parameters for ultrasound-assisted extraction of water-soluble components and polysaccharides from a medicinal fungus. *Biochemical Engineering Journal*, 79, 214-220. https://doi.org/10.1016/j.bej.2013.08.009

Collazo-Bigliardi, S., Ortega-Toro, R., & Chiralt, A. (2019). Improving properties of thermoplastic starch films by incorporating active extracts and cellulose fibres isolated from rice or coffee husk. *Food Packaging and Shelf Life*, 22, 100383. https://doi.org/10.1016/j.fpsl.2019.100383

Cvek, M., Paul, U. C., Zia, J., Mancini, G., Sedlarik, V., & Athanassiou, A. (2022). Biodegradable Films of PLA/PPC and Curcumin as Packaging Materials and Smart Indicators of Food Spoilage. *ACS Applied Materials & Interfaces*, 14(12), 14654-14667. https://doi.org/10.1021/acsami.2c02181

Díaz-Galindo, E. P., Nesic, A., Cabrera-Barjas, G., Dublan-García, O., Ventura-Aguilar, R. I., Vázquez-Armenta, F. J., Aguilar-Montes de Oca, S., Mardones, C., & Ayala-Zavala, J. F. (2020). Physico-Chemical and Antiadhesive Properties of Poly(Lactic Acid)/Grapevine Cane Extract Films against Food Pathogenic Microorganisms. *Polymers*, 12(12), 2967. https://doi.org/10.3390/polym12122967

Do, N. H., Pham, H. H., Le, T. M., Lauwaert, J., Diels, L., Verberckmoes, A., Do, N. H. N., Tran, V. T., & Le, P. K. (2020). The novel method to reduce the silica content in lignin recovered from black liquor originating from rice straw. *Scientific Reports*, 10(1), 21263. https://doi.org/10.1038/s41598-020-77867-5

Faustman, C., Sun, Q., Mancini, R., & Suman, S. P. (2010). Myoglobin and lipid oxidation interactions: Mechanistic bases and control. *Meat science*, 86(1), 86-94.

Freitas, P. A. V., Arias, C. I. L. F., Torres-Giner, S., González-Martínez, C., & Chiralt, A. (2021). Valorization of Rice Straw into Cellulose Microfibers for the Reinforcement of Thermoplastic Corn Starch Films. *Applied Sciences*, 11(18), 8433. https://doi.org/10.3390/app11188433

Freitas, P. A. V., Gil, N. J. B., & González-Martínez, C. (2022). Antioxidant poly (lactic acid) films with rice straw extract for food packaging applications. *Food packaging and shelf life*, In press.

Freitas, P. A. V., González-Martínez, C., & Chiralt, A. (2020). Application of Ultrasound Pre-Treatment for Enhancing Extraction of Bioactive Compounds from Rice Straw. *Foods*, 9(11), 1657. https://doi.org/10.3390/foods9111657

Freitas, P. A., González-Martínez, C., & Chiralt, A. (2023). Antioxidant starch composite films containing rice straw extract and cellulose fibres. *Food Chemistry*, 400, 134073.

Haque, M. A., Timilsena, Y. P., & Adhikari, B. (2016). Food Proteins, Structure, and Function. *Reference Module in Food Science*. https://doi.org/10.1016/B978-0-08-100596-5.03057-2

Goodman, B. A. (2020). Utilization of waste straw and husks from rice production: A review. *Journal of Bioresources and Bioproducts*, 5(3), 143-162.

Han, J.-W., Ruiz-Garcia, L., Qian, J.-P., & Yang, X.-T. (2018). Food Packaging: A Comprehensive Review and Future Trends: Food packaging: Review and future trends. *Comprehensive Reviews in Food Science and Food Safety*, 17(4), 860-877. https://doi.org/10.1111/1541-4337.12343

Hernández-García, E., Vargas, M., & Chiralt, A. (2022). Starch-polyester bilayer films with phenolic acids for pork meat preservation. *Food Chemistry*, 385, 132650. https://doi.org/10.1016/j.foodchem.2022.132650

Herrero, M., Plaza, M., Cifuentes, A., & Ibáñez, E. (2012). Extraction Techniques for the Determination of Phenolic Compounds in Food. *Comprehensive Sampling and Sample Preparation* (pp. 159-180). Elsevier. https://doi.org/10.1016/B978-0-12-381373-2.00132-0

Jamshidian, M., Tehrany, E. A., Imran, M., Akhtar, M. J., Cleymand, F., & Desobry, S. (2012). Structural, mechanical and barrier properties of active PLA–antioxidant films. *Journal of Food Engineering*, 110(3), 380-389. https://doi.org/10.1016/j.jfoodeng.2011.12.034

Kaczmarek, A. M., Muzolf-Panek, M., Rudzi, M., Szablewski, T., & Cegielska-Radziejewska, R. (2017). The effect of plant extracts on pork quality during storage. *Italy Journal of Food Science*, 29, 644-656.

Karimi, E., Mehrabanjoubani, P., Keshavarzian, M., Oskoueian, E., Jaafar, H. Z., & Abdolzadeh, A. (2014). Identification and quantification of phenolic and flavonoid components in straw and seed husk of some rice varieties (Oryza sativa L.) and their antioxidant properties: Identification and quantification of phenolic and flavonoid. *Journal of the Science of Food and Agriculture*, 94(11), 2324-2330. https://doi.org/10.1002/jsfa.6567

Khakestani, M., Jafari, S. H., Zahedi, P., Bagheri, R., & Hajiaghaee, R. (2017). Physical, morphological, and biological studies on PLA/n HA composite nanofibrous webs containing E quisetum arvense herbal extract for bone tissue engineering. *Journal of Applied Polymer Science*, 134(39), 45343.

Kim, H. W., Jeong, J. Y., Seol, K.-H., Seong, P.-N., & Ham, J.-S. (2016). Effects of Edible Films Containing Procyanidin on the Preservation of Pork Meat during Chilled Storage. *Korean Journal for Food Science of Animal Resources*, 36(2), 230-236. https://doi.org/10.5851/kosfa.2016.36.2.230

Lee, S. E., Hwang, H. J., Ha, J. S., Jeong, H. S., & Kim, J. H. (2003). Screening of medicinal plant extracts for antioxidant activity. *Life sciences*, 73(2), 167-179.

Li, B., Akram, M., Al-Zuhair, S., Elnajjar, E., & Munir, M. T. (2020). Subcritical water extraction of phenolics, antioxidants and dietary fibres from waste date pits. *Journal of Environmental Chemical Engineering*, 8(6), 104490. https://doi.org/10.1016/j.jece.2020.104490

Liu, Y.; Jia, Y.; Yang, K.; Li, R.; Xiao, X., & Wang, Z. Anti-HIV agent azidothymidine decreases Tet(X)-mediated bacterial resistance to tigecycline in Escherichia coli. Commun. Biol., 2020, 3 (162). https://doi.org/10.1038/s42003-020-0877-5

Luque-García, J. L., & Luque de Castro, M. D. (2003). Ultrasound: A powerful tool for leaching. *Trends in Analytical Chemistry*, 22(1), 41-47. https://doi.org/10.1016/S0165-9936(03)00102-X

Makris, D. P., Boskou, G., & Andrikopoulos, N. K. (2007). Polyphenolic content and in vitro antioxidant characteristics of wine industry and other agri-food solid waste extracts. *Journal of Food Composition and Analysis*, 20(2), 125-132.

Mchugh, T. H., Avena-Bustillos, R., & Krochta, J. M. (1993). Hydrophilic Edible Films: Modified Procedure for Water Vapor Permeability and Explanation of Thickness Effects. *Journal of Food Science*, 58(4), 899-903. https://doi.org/10.1111/j.1365-2621.1993.tb09387.x

Menzel, C., González-Martínez, C., Vilaplana, F., Diretto, G., & Chiralt, A. (2020). Incorporation of natural antioxidants from rice straw into renewable starch films. *International Journal of Biological Macromolecules*, 146, 976-986. https://doi.org/10.1016/j.ijbiomac.2019.09.222

Merlo, T. C., Contreras-Castillo, C. J., Saldaña, E., Barancelli, G. V., Dargelio, M. D. B., Yoshida, C. M. P., Ribeiro Junior, E. E., Massarioli, A., & Venturini, A. C. (2019). Incorporation of pink pepper residue extract into chitosan film combined with a modified atmosphere packaging: Effects on the shelf life of salmon fillets. *Food Research International*, 125, 108633. https://doi.org/10.1016/j.foodres.2019.108633

Miklasińska-Majdanik, M., Kępa, M., Wojtyczka, R., Idzik, D., & Wąsik, T. (2018). Phenolic Compounds Diminish Antibiotic Resistance of Staphylococcus Aureus Clinical Strains. *International Journal of Environmental Research and Public Health*, 15(10), 2321. https://doi.org/10.3390/ijerph15102321

Moirangthem, K., Ramakrishna, P., Amer, M. H., & Tucker, G. A. (2021). Bioactivity and anthocyanin content of microwave-assisted subcritical water extracts of Manipur black rice (Chakhao) bran and straw. *Future Foods*, 3, 100030.

Muller, J., González-Martínez, C., & Chiralt, A. (2017). Poly(lactic) acid (PLA) and starch bilayer films, containing cinnamaldehyde, obtained by compression moulding. *European Polymer Journal*, 95, 56-70. https://doi.org/10.1016/j.eurpolymj.2017.07.019

Nerín, C., Tovar, L., & Salafranca, J. (2008). Behaviour of a new antioxidant active film versus oxidizable model compounds. *Journal of Food Engineering*, 84(2), 313-320. https://doi.org/10.1016/j.jfoodeng.2007.05.027

Ojha, K. S., Aznar, R., O'Donnell, C., & Tiwari, B. K. (2020). Ultrasound technology for the extraction of biologically active molecules from plant, animal and marine sources. *Trends in Analytical Chemistry*, 122, 115663. https://doi.org/10.1016/j.trac.2019.115663

Ong, E. S., Cheong, J. S. H., & Goh, D. (2006). Pressurized hot water extraction of bioactive or marker compounds in botanicals and medicinal plant materials. *Journal of Chromatography* A, 1112(1-2), 92-102. https://doi.org/10.1016/j.chroma.2005.12.052

Ordoñez, R., Atarés, L., & Chiralt, A. (2021). Physicochemical and antimicrobial properties of cassava starch films with ferulic or cinnamic acid. *Lwt*, 144, 111242.

Ordoñez, R., Atarés, L., & Chiralt, A. (2022). Effect of ferulic and cinnamic acids on the functional and antimicrobial properties in thermo-processed PLA films. *Food Packaging and Shelf Life*, 33, 100882.

Panzella, L., Moccia, F., Nasti, R., Marzorati, S., Verotta, L., & Napolitano, A. (2020). Bioactive phenolic compounds from agri-food wastes: An update on green and sustainable extraction methodologies. *Frontiers in nutrition*, 7, 60.

Peanparkdee, M., & Iwamoto, S. (2019). Bioactive compounds from by-products of rice cultivation and rice processing: Extraction and application in the food and pharmaceutical industries. *Trends in Food Science & Technology*, 86, 109-117. https://doi.org/10.1016/j.tifs.2019.02.041

Plaza, M., Amigo-Benavent, M., del Castillo, M. D., Ibáñez, E., & Herrero, M. (2010a). Facts about the formation of new antioxidants in natural samples after subcritical water extraction. *Food Research International*, 43(10), 2341-2348. https://doi.org/10.1016/j.foodres.2010.07.036

Plaza, Merichel, Miryam Amigo-Benavent, María D. del Castillo, Elena Ibáñez and Miguel Herrero (2010b). Neoformation of antioxidants in glycation model systems treated under subcritical water extraction conditions. *Food Research International*, 43: 1123-1129. doi: https://doi.org/10.1016/j.foodres.2010.02.005

Requena, R., Jiménez-Quero, A., Vargas, M., Moriana, R., Chiralt, A., & Vilaplana, F. (2019). Integral Fractionation of Rice Husks into Bioactive Arabinoxylans, Cellulose Nanocrystals, and Silica Particles. *ACS Sustainable Chemistry & Engineering*, 7(6), 6275-6286. https://doi.org/10.1021/acssuschemeng.8b06692

Requena, R., Vargas, M., & Chiralt, A. (2019). Study of the potential synergistic antibacterial activity of essential oil components using the thiazolyl blue tetrazolium bromide (MTT) assay. *Lwt*, 101, 183-190.

Saeed, N., Khan, M. R., & Shabbir, M. (2012). Antioxidant activity, total phenolic and total flavonoid contents of whole plant extracts Torilis leptophylla L. *BMC complementary and alternative medicine*, 12(1), 1-12.

Saini, J. K., Saini, R., & Tewari, L. (2015). Lignocellulosic agriculture wastes as biomass feedstocks for second-generation bioethanol production: Concepts and recent developments. 3 *Biotech*, 5(4), 337-353. https://doi.org/10.1007/s13205-014-0246-5

Sanyang, M. L., Sapuan, S. M., Jawaid, M., Ishak, M. R., & Sahari, J. (2016). Development and characterization of sugar palm starch and poly(lactic acid) bilayer films. *Carbohydrate Polymers*, 146, 36-45. https://doi.org/10.1016/j.carbpol.2016.03.051

Siu, G. M., & Draper, H. H. (1978). A survey of the malonaldehyde content of retail meats and fish. *Journal of Food Science*, 43(4), 1147-1149. https://doi.org/10.1111/j.1365-2621.1978.tb15256.x

Sofi, S. A., Singh, J., Rafiq, S., Ashraf, U., Dar, B. N., & Nayik, G. A. (2018). A comprehensive review on antimicrobial packaging and its use in food packaging. *Current Nutrition & Food Science*, 14(4), 305-312.

Sumere, B. R., de Souza, M. C., dos Santos, M. P., Bezerra, R. M. N., da Cunha, D. T., Martinez, J., & Rostagno, M. A. (2018). Combining pressurized liquids with ultrasound to improve the extraction of phenolic compounds from pomegranate peel (Punica granatum L.). *Ultrasonics Sonochemistry*, 48, 151-162. https://doi.org/10.1016/j.ultsonch.2018.05.028

Sung, S.-Y., Sin, L. T., Tee, T.-T., Bee, S.-T., Rahmat, A. R., Rahman, W. A. W. A., Tan, A.-C., & Vikhraman, M. (2013). Antimicrobial agents for food packaging applications. *Trends in Food Science & Technology*, 33(2), 110-123. https://doi.org/10.1016/j.tifs.2013.08.001

Takahashi, H.; Kashimura, M.; Koiso, H.; Kuda, T., & Kimura, B. Use of ferulic acid as a novel candidate of growth inhibiting agent against Listeria monocytogenes in ready-to-eat food. *Food Control*, 2013, 33 (1), 244-248. https://doi.org/10.1016/j.foodcont.2013.03.013

Torres-Valenzuela, L. S., Ballesteros-Gómez, A., & Rubio, S. (2020). Green solvents for the extraction of high added-value compounds from agri-food waste. *Food Engineering Reviews*, 12(1), 83-100.

Wen, H., Hsu, Y.-I., Asoh, T.-A., & Uyama, H. (2020). Antioxidant activity and physical properties of pH-sensitive biocomposite using poly(vinyl alcohol) incorporated with green tea extract. *Polymer Degradation and Stability*, 178, 109215. https://doi.org/10.1016/j.polymdegradstab.2020.109215

Woo, K. K., Ngou, L. S., Soong, W. K., Tang, P. Y. (2011). Stability of Betalain Pigment from Red Dragon Fruit (Hylocereus polyrhizus). *American Journal of Food Technology*, 6 (2), 140-148. https://doi.org/10.3923/ajft.2011.140.148

Yang, W., Xie, Y., Jin, J., Liu, H., & Zhang, H. (2019). Development and Application of an Active Plastic Multilayer Film by Coating a Plantaricin BM-1 for Chilled Meat Preservation. Journal of *Food Science*, 84(7), 1864-1870. https://doi.org/10.1111/1750-3841.14608

Zakaria, S. M., Kamal, S. M. M., Harun, M. R., Omar, R., & Siajam, S. I. (2017). Subcritical Water Technology for Extraction of Phenolic Compounds from Chlorella sp. Microalgae and Assessment on Its Antioxidant Activity. *Molecules*, 22(7), 1105. https://doi.org/10.3390/molecules22071105

Zazharskyi, V. V., Davydenko, P., Kulishenko, O., Borovik, I. V., & Brygadyrenko, V. V. (2019). Antimicrobial activity of 50 plant extracts. *Biosystems Diversity*, 27(2), 163-169.

Zhao, X., Tian, R., Zhou, J., & Liu, Y. (2022). Multifunctional chitosan/grape seed extract/silver nanoparticle composite for food packaging application. *International Journal of Biological Macromolecules*, 207, 152-160. https://doi.org/10.1016/j.ijbiomac.2022.02.180

CHAPTER 2.VIII

Influence of the cellulose purification process on the properties of aerogels obtained from rice straw

Pedro A. V. Freitas, Chelo González-Martínez, Amparo Chiralt

Institute of Food Engineering for Development, Universitat Politècnica de València, 46022, Valencia, Spain

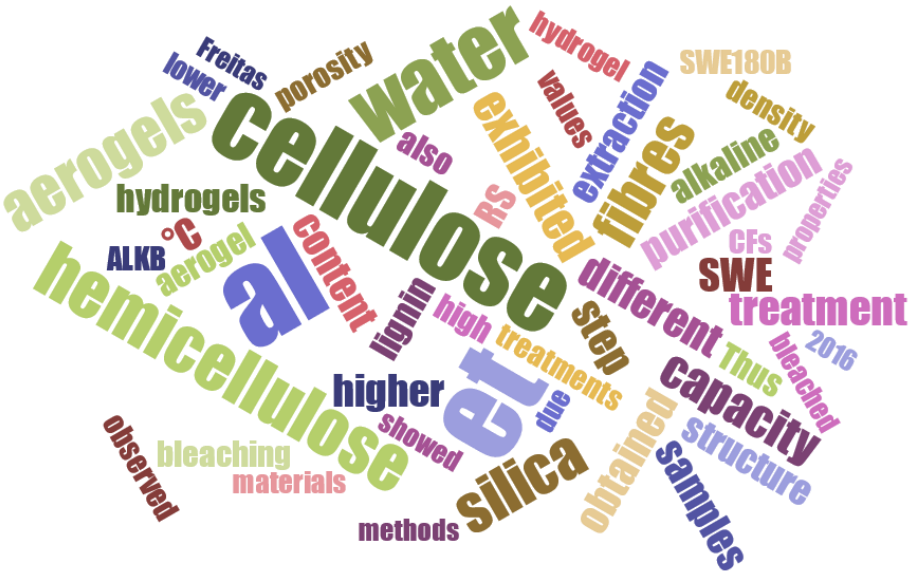

Submitted to Food Hydrocolloids

ABSTRACT

Cellulose aerogels were obtained from purified rice straw cellulose fibres (CF) by applying different extraction methods: the conventional alkaline treatment (ALK) and alternative aqueous extraction based on the ultrasound combined with reflux heating (USHT) and subcritical water extraction (SWE) (160 and 180 °C). The purified CF were characterised by their composition, colour, microstructure, and hydrogel-forming capacity. Aerogels were obtained from the CF aqueous dispersion and characterised by their microstructure, porosity, density, water adsorption, water absorption (WAC), and retention (WRC) capacities. The composition and properties of the CFs were significantly affected by the purification process. After bleaching, the alkaline process exhibited the lowest yields since it was the most effective at eliminating non-cellulosic components from RS. The USHT treatment was as efficient as the ALK at eliminating the silica content, but the fibres maintained a notable ratio of hemicellulose (~16 %). The SWE treatments were not so effective at removing silica (15 %) but greatly promoted the selective extraction of hemicellulose, especially at 180 °C (3 %). The CF compositional differences affected their hydrogel formation capacity and the properties of aerogels. A higher hemicellulose content in the CF led to better-structured hydrogels with better water-holding capacity, while the aerogels exhibited a more cohesive structure with thicker walls, higher porosity (99 %) and water vapour sorption capacity, but lower liquid water retention capacity (0.2 g/g). The residual silica content also interfered with the hydrogel and aerogel formation, giving rise to less structured hydrogels and more fibrous aerogels, with lower porosity (97-98 %).

Keywords: water absorbing material, subcritical water extraction, ultrasound-reflux heating, alkaline treatment, sorption isotherm

1. INTRODUCTION

Aerogel consists of ultralightweight materials with outstanding physical and chemical properties, such as high porosity (80-99.8 %), low density (0.003-0.500 g.cm-3) and a large surface area (100-1600 m2.g-1), as well as excellent optical and acoustic properties (Kistler, 1932; Long et al., 2018). Due to their unique properties, aerogels have great potential applications in different fields, including in the development of medical materials, optoelectronics, drug carriers, sensors, adsorption catalysis, acoustic and thermal insulation, aerospace materials, and superabsorbents for different applications (Jiang & Hsieh, 2014; Long et al., 2018; Zaman et al., 2020). A wide range of materials can be used for producing aerogels, such as synthetic polymers, carbon derivatives, inorganic compounds, macromolecules, and celluloses (Long et al., 2018). Cellulose aerogels in particular have been the subject of great interest in different research areas and for industrial applications, since they are highly porous materials with low density and a highwater-absorption capacity and are mechanically more resistant than other types of aerogels, such as those based on silica or metal oxides (Budtova, 2019; Jiang & Hsieh, 2014; Long et al., 2018). Likewise, cellulose aerogels have advantages when compared to other materials due to their biodegradability, renewability, non-toxicity, low cost, ready availability, and biocompatibility (Henschen et al., 2016; Wang et al., 2016). The process for manufacturing cellulose aerogels comprises dispersing or dissolving the cellulosic material to form wet cellulose hydrogels, followed by the solvent exchange, and then the drying step to remove the solvent and maintain the three-dimensional cellulosic structure (Zaman et al., 2020).

Cellulose is the most naturally abundant polymer and has long been a major renewable source of materials. In the native forms, the long poly(β-1,4-glucopyranose) chains are organised into highly crystalline 1.5–3.5 nm wide nanofibrils with intramolecular and intermolecular hydrogen bonds as part of larger microfibrils and macroscopic fibres (Habibi et al., 2010, Klemm et al., 2005). Globally, Rice straw (RS) is the largest crop residue with relatively high cellulose content (about 40 %, Barana et al., 2016; Freitas et al., 2022) that could be used as a non-wood cellulose source. Cellulose fibres from mechanically ground rice straw were 12–35 nm wide and several micrometres long, with very similar crystal structures and mechanical properties to those obtained from grinding wood (Abe & Yano, 2009). Therefore, obtaining cellulose from rice straw to transform it into high-value-added products is an interesting alternative in the context of the circular economy, while the use of a sustainable and eco-friendly process for this transformation is necessary. Different green alternatives and approaches for the valorisation of RS have been proposed, such as obtaining bioactive extracts (Freitas et al., 2020a), paper production (Nagpal et al., 2021), biodiesel (Sahu, 2021), active packaging (Freitas et al., 2022), and cellulose fibres and nanofibres as reinforcing agents (Freitas et al., 2021). Fontes-Candia et al. (2019) produced cellulose aerogels from A. donax

waste biomass, with different degrees of purification, which exhibited a low density and excellent water and oil absorption and retention capacities.

Cellulose purification from the lignocellulosic rice straw complex is difficult (Chen et al., 2011) and requires the extraction of hemicellulose, lignin, and silica from the plant matrix. The most common step in the cellulose purification process is alkaline extraction, using KOH or NaOH solutions. This treatment chemically eliminates a substantial fraction of the hemicellulose, lignin, silica, and waxes present in the biomass (Zhang et al., 2014). After the alkaline treatment, a bleaching step is applied, until the colour of the cellulose fibre became off-white. The alkaline treatment presents two drawbacks: the use of non-environmentally-friendly solutions that need effluent processing and large amounts of washing water after treatment. More eco-friendly extraction methods, such as subcritical water extraction (SWE) or ultrasound-assisted aqueous extraction (UAE), could be used to replace the alkaline treatment of biomass.

SWE is an eco-friendly and cost-effective extraction technique based on the use of liquid water at high temperatures and at a pressure below the critical point (Castro-Puyana et al., 2013). In these subcritical processing conditions, an improved mass transfer is achieved, with greater solubilisation of compounds, due to the changes in the water properties. Water under subcritical conditions exhibits a decrease in dielectric constant, surface tension, density, and viscosity, as a function of temperature, which enhances its ability to penetrate into the solid matrix and solubilise less polar compounds (Ong et al., 2006; Plaza et al., 2010), which lends great potential in the extraction of non-cellulosic components from lignocellulosic residues.

The application of a combined ultrasound-reflux heating treatment to extract compounds from the lignocellulosic plant tissue was also very effective at purifying the cellulose fraction of rice straw (Freitas et al. 2022). The acoustic cavitation phenomena provoked by the ultrasound step led to the disruption of the plant cell structure, exposing the innermost plant tissues, and thereby improving the accessibility of the extracting solvent. Consequently, the extraction efficiency was enhanced by weakening intermolecular interactions between the plant matrix and non-cellulosic components. The fibres obtained were richer in hemicellulose but exhibited a similar reinforcing capacity in different polymer films (Freitas et al. 2022; Freitas et al. 2021) to those obtained by alkaline extraction.

The aim of this study was to produce cellulose aerogels with CF obtained from RS by applying different purification methods before the bleaching step: the combined ultrasound-reflux heating method (USHT), and SWE at two processing temperatures (160 and 180 °C). The fibres were characterised as to their chemical composition, structural characteristics, and hydrogel-forming capacity. Likewise, cellulose aerogels were obtained by the freeze-drying of hydrogels and evaluated as to their microstructure, density and porosity, moisture sorption and water absorption and retention capacity.

2. MATERIAL AND METHODS

2.1 Materials and plant preparation

RS (*Oryza sativa L.*), *J. Sendra* var. was collected in the L'Albufera rice paddy (Valencia, Spain) and dried at 50 ± 2 °C under vacuum (0.8 mmbar) for 16 h. Afterwards, the plant material was ground (IKA, model M20, IKA Werke GmbH & Co. KG, Staufen, Germany) for 3 cycles of 90 s each, sieved (particles of under 0.5 mm), and then stored at 20 ± 2 °C until further use.

Acetic acid, magnesium nitrate ($Mg(NO_3)_2$), and di-phosphorus pentoxide (P_2O_5) were purchased from PanReac Quimica S.L.U. (Castellar del Vallés, Spain). Sodium acetate trihydrate was purchased from FlukaTM (Germany). Sulfuric acid (98 % purity), sodium hydroxide, glucose, arabinose, and sodium chlorite were supplied by Sigma-Aldrich (St. Louis, MO, USA). D(+)-Xylose was supplied by Merck KGaA (Darmstadt, Germany).

2.2 Obtaining cellulosic fractions

Three alternative treatments were applied before the bleaching step to the ground RS for removing hemicellulose and lignin components: 1) the traditional alkaline treatment, as a control; 2) the combined ultrasound-reflux heating method; and 3) subcritical water extraction.

2.2.1 Alkaline treatment

The alkaline extraction of RS was performed as previously described by Collazo-Bigliardi et al., (2018). A dispersion consisting of RS (5 % wt.) and sodium hydroxide solution (4.5 % wt.) was heated to 100 °C using a typical reflux device for 2 cycles of 3 h each. At the end of each cycle, the solid material was filtered and washed with abundant water to remove the alkaline solution. Finally, the insoluble residue obtained (ALK) was dried at 35 °C for 24 h to determine the step yield.

2.2.2 Combined ultrasound-reflux heating method

A sequential method consisting of a combination of ultrasound and reflux heating was performed according to Freitas et al. (2022). Briefly, a 5 % (w/v) aqueous dispersion of RS was first sonicated at 25 °C (by immersion in an ice bath) for 30 min, using a probe high-intensity ultrasonic homogeniser (Vibra Cell^{TM} VCX750, 750 W power, Sonics & Material Inc., Newtown, CT, USA) operating at a frequency of 20 kHz, 40 % sonication amplitude, in continuous mode. Afterwards, the plant dispersion was heated at reflux (100 °C) for 1 h, filtered and washed with water three times and the insoluble fraction (USHT) was dried at 35 °C for 24 h to determine the step yield.

2.2.3 Subcritical water extraction

The subcritical water extraction (SWE) of the RS was carried out using an RS: distilled water ratio of 1:10 (w/v). The SWE process was performed using a Pressure Reactor (Model 1-T-A-P-CE, 5 L capacity, Amar Equipment PVT. LTD, Mumbai, India) under two extraction conditions: 160 °C, 7 bars, 150 rpm, for 30 min; and 180 °C, 11 bars, 150 rpm for 30 min. Afterwards, the plant dispersion was cooled to 30 °C, filtered with a qualitative filter (Filterlab), and washed with water to eliminate the soluble fraction retained in the solid residue. Then, the insoluble fractions (named as SWE-160 and SWE-180) were dried at 35 °C for 24 h to determine the step yield.

2.2.4 Bleaching treatment

The solid residues (ALK, USHT, SWE-160, and SWE-180) were bleached according to Freitas et al. (2022). The dry samples were mixed at 5 % wt. with a bleaching solution prepared by mixing equal parts of distilled water, acetate buffer solution (2 N), and sodium chlorite (1.7 %, w/v). The suspension was treated under reflux heating at 100 °C for 4 h. Thereafter, the solid fraction was filtered and washed with distilled water to remove the residual bleaching solution. The procedure was repeated three times. Then, the bleached samples were dried at 35 °C for 48 h and milled using a milling machine (model M20, IKA Werke GmbH & Co. KG, Staufen IKA, Germany), applying pulses of 2 s for 20 min. The bleached solid residues were labelled as ALK-B, USHT-B, SWE-160-B, and SWE-180-B.

2.3 Characterisation of cellulosic fractions

2.3.1 Chemical composition

The chemical composition of the different lignocellulosic fractions, typically cellulose, hemicellulose, and lignin were determined following the standard NREL methodology (NREL/TP-510-42,618) (Sluiter, 2008b). Before the hydrolysis, the raw RS and the non-bleached solid residues from the different treatments were submitted to water extraction following the standard NREL method to determine water extractives of biomass (NREL/TP510-42,619) (Sluiter, 2008a). After the two-step sulfuric acid hydrolysis, the Klason lignin content was determined gravimetrically as the acid-insoluble fraction, while the sugar composition in terms of glucose, xylose, and arabinose was quantified in the acid-soluble fractions by high-performance liquid chromatography (HPLC). To this end, a liquid chromatograph (Agilent Technologies, model 1120 Compact LC, Germany) equipped with a HILIC Luna Omega Sugars column (150 mm × 4.6 mm, 3 µm) and an evaporative light scattering detector (ELSD Agilent Technologies 1200 Series, Germany) was used. The mobile phase was water: acetonitrile (25:75), in isocratic mode, at a flow rate of 0.8 $mL.min^{-1}$. The detector conditions were: 40 °C, 3.0 bars of nitrogen pressure, and a gain of 5. The data were analysed by the software

ChemStation Program (Agilent Technologies, Germany). The hemicellulose content was calculated by the sum of the xylose and arabinose contents with respect to the initial solid fraction, and the cellulose content was obtained from the glucose concentration. The ash content of the cellulosic fractions was determined from the thermogravimetric analyses, described below.

2.3.2 Colour properties

Colour properties of the bleached CFs were obtained by evaluating the colour coordinates of cellulosic films (section 2.4) in order to avoid the porosity effect, according to the Kubelka-Munk theory of multiple scattering using a spectrocolorimeter (CM-3600d, Minolta Co., Japan) (Freitas et al., 2021). The reflection spectra of the films were obtained from 400 to 700 nm using white and black backgrounds. Then, the colour coordinates *L** (lightness), *a** (redness-greenness), and *b** (yellowness-blueness) were calculated from the infinite reflectance spectra, using D65 illuminant and 10° observer. The psychometric coordinates, (C_{ab}*) (Eq. 1) and hue angle (h_{ab}*) (Eq. 2) were calculated from *a** and *b** values. The whiteness index (*WI*) of the samples was also determined according to Eq. 3. The measurements were performed in triplicate for each sample and three times for each replicate.

$$C^* = \sqrt{a^{*2} + b^{*2}} \quad (1)$$

$$h^* = arctg\left(\frac{b^*}{a^*}\right) \quad (2)$$

$$WI = 100 - \sqrt{(100 - L^*)^2 + a^{*2} + b^{*2}} \quad (3)$$

2.3.3 Microstructure

A Field Emission Scanning Electron Microscope (ULTRATM 55, Zeiis, Oxford Instruments, UK) was used to evaluate the morphologies of the raw RS and the different cellulosic fractions obtained in the cellulose extraction steps. Conditioned samples (P_2O_5 at 25 °C for two weeks) were previously covered with a platinum layer using an EM MED020 sputter coater (Leica BioSystems, Barcelona, Spain) for 30 s, and the images were taken at 2.0 kV acceleration voltage.

2.3.4 Thermogravimetric analysis

The thermal behaviour of the different lignocellulosic fractions was evaluated by thermogravimetric analysis (TGA) using a thermogravimetric analyser (TGA 1 Stare System analyser, Mettler-Toledo, Switzerland) under nitrogen flow (10 mL.min-1). Samples (conditioned in P_2O_5 at 25 °C for two weeks) of about 3-5 mg were weighed in alumina pans

and heated from 25 to 700 °C at 10 °C.min^{-1}. The thermogravimetric curves and their derivatives (DTGA) were analysed to obtain the initial (T_{on}) and the maximum thermo-degradation rate (T_p) temperatures and the residual mass for each observed thermal event, as well as the final residue. These measurements were taken in duplicate.

2.3.5 Fourier transformed infrared spectroscopy (FTIR)

FTIR spectra of the lignocellulosic fractions at different purification steps were evaluated using an FTIR spectrometer (Vertex 80, Bruker AXS GmbH, Karlsruhe, Germany) equipped with microscopic (Hiperion) and attenuated total reflectance accessories. Spectra were obtained at a resolution of 6 cm^{-1}, in the wavelength range of 4000–650 cm^{-1}, performing 128 scans for each spectrum.

2.3.6 X-ray diffraction analysis (XRD)

An X-ray diffractometer (AXS/D8 Advance, Bruker, Karlsruhe, Germany) was used to evaluate the X-ray diffraction pattern spectra of the different cellulosic fractions. Conditioned samples were compacted to cover the sample holder and the analysis was performed using Kα-Cu radiation (λ: 1.542 Å), 40 kV, 40 mA, step size of 2.0°. min^{-1}, and a 2ϑ scanning angle between 5° and 40°. Crystallinity index (*CI*), expressed as percentage, was determined from the maximum intensity of 200 lattice diffraction (I_{200}, crystalline peak) and the diffraction intensity at 2θ = 18° ($I_{2\theta\ 18°}$, amorphous phase valley) using the empirical equation (Eq. 4) proposed by Seagal et al. (1959).

$$CI\ (\%) = \frac{(I_{200} - I_{2\theta\ 18})}{I_{200}} \times 100 \qquad (4)$$

2.3.7 Hydrogel formation capacity

The ability of each cellulosic fraction to form hydrogels through cyclic freezing-thawing (FT) was also evaluated. To this end, CF samples (0.075 g) were dispersed with 15 mL of distilled water and ultrasonicated (Vibra CellTM VCX750, Sonics & Material, Inc., Newtown, CT, USA), operating in a continuous mode, at a frequency of 20 kHz, 40 % sonication amplitude, and at 25 °C (using an ice bath to prevent heating), for 20 min. Then, CF dispersions were placed in polycarbonate centrifuge tubes (Beckman Coulter Inc, USA) and submitted to three cycles of FT. Each cycle consisted of freezing at -20 °C for 16 h and subsequent thawing at room temperature for 9 h. After each FT cycle, the morphology (consistency and syneresis) of the formed hydrogels was visually analysed and photographs were taken.

2.4 Production of aerogels

Cellulosic aerogels were obtained following Fontes-Candia et al. (2019), with some modifications. Briefly, water dispersions of CF samples were prepared as described in section 2.3.7 and poured into a Petri dish 6 cm in diameter, frozen at -40 °C for 16 h, and then freeze-dried (Telstar, model LyoQuest-55) at -60 °C, 0.8 mbar for 72 h. The aerogels obtained were labelled as USHT-B, ALK-B, SWE-160-B, and SWE-180-B, according to the respective extraction process applied.

In order to determine the porosity of the aerogels and the colour of the CFs, the same CF aqueous dispersions were also used to produce films, by casting 15 mL of the cellulose dispersions in Petri dishes (6 cm diameter) and drying at 25 °C for 72 h.

Before characterisations, both aerogels and films were conditioned in a desiccator containing P_2O_5 (0 % RH) at 25 °C.

2.5 Characterisation of aerogels

2.5.1 Density and porosity

The density of the different aerogels and films was determined considering the mass and volume of each sample. The sample dimensions were measured using a digital calliper (Palmer, model COMECTA, Barcelona, accuracy of 0.001 mm) at six different positions in each replicate (four samples per treatment). The theoretical and measured porosity of the aerogels were determined according to Eqs. 5 and 6, respectively, where ρ_a is the aerogel density, ρ_c is the theoretical density of cellulose (1600 mg.cm^{-3}), and ρ_f is the density of the cellulosic films.

$$Theoretical\ Porosity\ (\%) = \left(1 - \frac{\rho_a}{\rho_c}\right) \times 100\% \quad (5)$$

$$Measured\ Porosity\ (\%) = \left(1 - \frac{\rho_a}{\rho_f}\right) \times 100\% \quad (6)$$

2.5.2 Microstructure

Micrographs of the aerogels were obtained as described in section 2.3.5 on samples sizing 1 cm x 1 cm, coated with platinum for 1 min. The images were taken at 2.0 kV acceleration voltage.

2.5.3 Sorption isotherms

Conditioned (0 % RH at 25 °C) aerogel samples were placed in desiccators at 25 °C containing different over-saturated salt solutions (LiCl, CH_3COOK, $MgCl_2$, K_2CO_3, KI, NaCl, and KCl) with

water activities (a_w) of 0.113, 0.2251, 0.3278, 0.4316, 0.6886, 0.7529, and 0.8434, respectively. When samples reached constant weight, the equilibrium moisture content was determined by drying them at 60 °C for 48 h until a constant weight was reached, and later on maintaining them under P_2O_5 atmosphere to ensure dry conditions. The sorption experimental data were fitted to the Guggenheim-Anderson-de Böer (GAB) (Eq. 7) model using the Excel and the OriginPro programs (Version 2021, OriginLab Corporation, Northampton, MA, USA).

$$\omega_e = \frac{\omega_0 \cdot C \cdot k \cdot a_w}{(1 - k \cdot a_w) \cdot [1 + (C - 1) \cdot k \cdot a_w]} \quad (7)$$

Where ω_e is the equilibrium moisture content (dry basis), ω_0, the monolayer moisture content, a_w, the water activity and k and C are the equation parameters, which are temperature dependent and related to the water sorption enthalpy.

2.5.4 Water absorption and retention capacities

The water absorption capacity (WAC) of the aerogels, expressed as g absorbed water. g^{-1} aerogel, was measured according to that previously described by Jiang & Hsieh (2014), with some modifications. Briefly, conditioned aerogel samples (P_2O_5 at 25 °C) sizing 1 cm x 1 cm were placed on a mesh and immersed in a Petri dish containing distilled water (30 mL) at 20 °C for 15 min (enough time to saturate). Afterwards, the excess of water contained in the mesh was removed with absorbent paper and the system was weighed. The measured WAC was determined by applying Eq. 8, where w_s and w_o are the mass of the aerogel fully water-saturated and dried aerogels, respectively. The theoretical WAC was also calculated, assuming a constant aerogel volume and considering the determined porosity and the aerogel and water densities (ρ_w= 0.9982 $g.cm^{-3}$ at 20 °C) (Eq. 9). To determine the water retention capacity (WRC), the system containing the saturated aerogel was placed on absorbent paper and periodically weighed until reaching a constant weight. The WRC was expressed as the mass of water retained per mass unit of aerogel. All these analyses were performed in quintuplicate for each aerogel.

$$Measured\ WAC\ = \frac{(w_s - w_o)}{w_o} \quad (8)$$

$$Theoretical\ WAC\ = \frac{Porosity \times \rho_{water}}{\rho_a} \quad (9)$$

2.6 Statistical analysis

The obtained experimental data were analysed through analysis of variance at a confidence level of 95 % using Minitab Statistical Program (version 17). Tukey's HSD (honestly significant

difference), considering the least significant difference (α) of 5 %, was performed to determine whether there were significant differences between the formulations.

3. RESULTS AND DISCUSSION

3.1 Properties of cellulosic fractions

3.1.1 Yield, composition, appearance, and colour properties

Fig. 1 shows the samples obtained during the cellulose purification processes by applying the different pre-treatments before and after the bleaching step. The bleached CFs obtained with the alkaline treatment and the combined ultrasound-reflux heating method exhibited similar appearance and whiteness, as also reported by Freitas et al. (2022), whereas the CFs from the SWE method had a more yellowish appearance, especially the sample obtained at 180 °C that exhibited a more vivid and intense colour. This was also reflected in the colour coordinates and whiteness index (*WI*) of cellulosic films (Table 1) obtained from the bleached samples, which were used to evaluate colour instead of cellulose fibres to avoid the porosity effects. ALK-B fibre gave rise to films that were whiter, less saturated in colour and with higher lightness values than the other cellulose fractions. Films prepared with the USHT-B fibres exhibited intermediate colour coordinates and *WI*, while those prepared with the SWE fibres were more yellowish with the most saturated colour and the lowest *WI* ($p<0.05$), especially in the case of the treatment at 180 °C. The presence of coloured compounds in the SWE fibres suggested that the cellulose purification process could not be as efficient as the other methods. The partially degraded compounds of residual lining can contribute to the colour of the cellulose, since these are responsible for the dark colour of the extracted black liquor (Do et al., 2020). Nonetheless, the high temperatures used in the subcritical extraction step could partially depolymerise cellulose and hemicellulose chains, which could favour browning reactions, such as caramelisation or Maillard reactions, as described by other authors (Plaza et al. 2010a,b). This agrees with the appearance of the solid residues after the SWE step (SWE-160-B and SWE-180-B; Fig. 1), which were darker than those obtained with the alkaline or the combined ultrasound-reflux heating treatments.

To investigate the differences between the cellulose purification processes, the yields (with respect to the dried RS), water extractables, as well as chemical composition in terms of cellulose, hemicellulose, klason lignin, and ashes, were analysed and shown in Table 2. The obtained composition of raw RS was coherent with those found by other authors (Barana et al., 2016). In general, an enrichment in cellulose content was observed after each purification step, especially after the bleaching treatment (Table 2), which points to the different extent to which hemicellulose and lignin are eliminated and the solubilisation/hydrolysis of silica, which is present in large quantities in the raw RS (~17 % wt., Zhang et al., 2014). The fractions from the alkaline treatment (ALK and ALK-B) exhibited the lowest yields, thus indicating that

this treatment was the most efficient at removing the non-cellulosic components from RS. This was also reflected in the fact that the fractions had the lowest hemicellulose, lignin, and silica content. The USHT and SWE treatments led to samples with a similar cellulose content (36-40 %), which significantly increased ($p<0.05$) after the bleaching step (62-69 %).

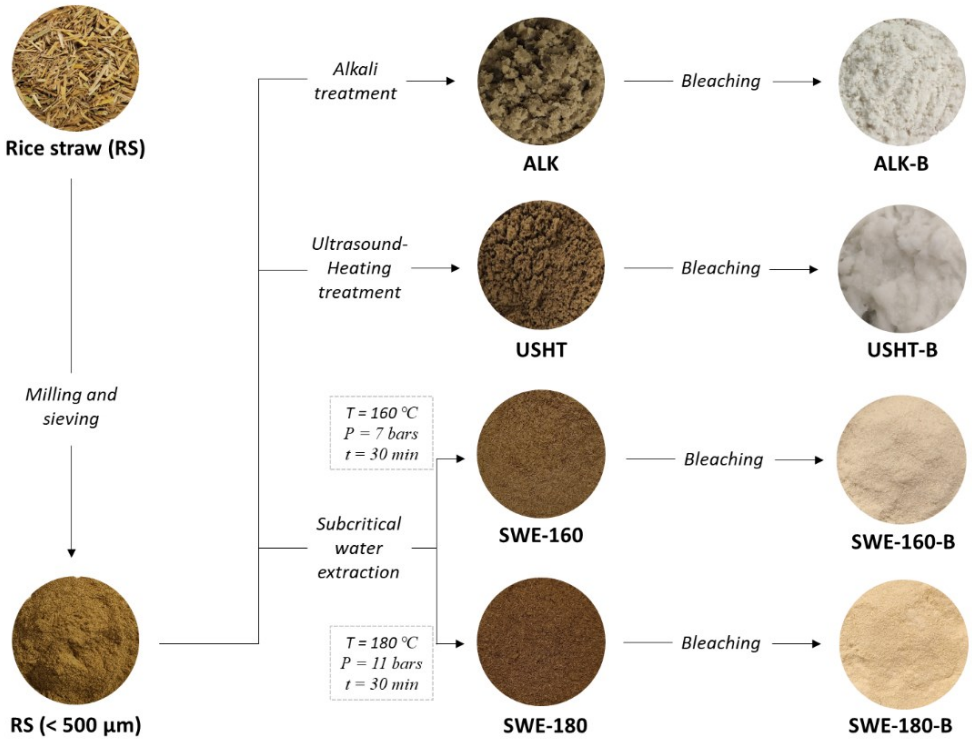

Fig. 1. Flow chart and samples obtained in the purification process steps (extraction and bleaching) applied on RS.

Table 1. Colour coordinates and whiteness index (*WI*) of the cellulosic fibres obtained by the different purification treatments (determined in the casted films to avoid the porosity effects).

Treatment	*L**	*C**	*h**	*WI*
ALK-B	93.0 ± 1.4^{a}	2.8 ± 0.4^{d}	75 ± 3^{c}	92.4 ± 1.2^{a}
USHT-B	88.5 ± 0.7^{b}	4.4 ± 0.4^{c}	98 ± 1^{a}	87.7 ± 0.5^{b}
SWE-160-B	88.2 ± 0.7^{b}	5.8 ± 0.1^{b}	95 ± 1^{ab}	86.8 ± 0.6^{bc}
SWE-180-B	87.8 ± 0.2^{b}	6.5 ± 0.4^{a}	94 ± 1^{b}	86.1 ± 0.5^{c}

Different subscript letters in the same column indicate significant differences by the Tukey test ($p < 0.05$).

Table 2. Yield (with respect to the initial mass of RS), water extractables, and composition of the untreated RS and the cellulosic fractions at the different purification steps (mean values ± standard deviation).

Sample	Yield (% wt.)	Water extractables (% wt.)	Cellulose (% wt.)	Hemicellulose (% wt.)	Klason Lignin (% wt.)	Ashes (% wt.)
RS	-	9.3 ± 0.8^{c}	36.7 ± 0.4^{f}	19.3 ± 0.1^{a}	21.2 ± 0.5^{bc}	17 ± 2
ALK	31.2	2.4 ± 0.4^{d}	54.6 ± 3.1^{d}	8.2 ± 1.2^{c}	6.6 ± 1.7^{d}	8 ± 1
USHT	80.1	14.8 ± 0.1^{a}	40.3 ± 0.8^{e}	20.1 ± 1.2^{a}	19.7 ± 1.4^{c}	11 ± 1
SWE-160	79.5	15.5 ± 0.4^{a}	36.0 ± 0.2^{f}	14.2 ± 2.3^{b}	22.6 ± 0.2^{ab}	15 ± 1
SWE-180	75.2	12.3 ± 0.1^{b}	38.1 ± 2.0^{ef}	2.7 ± 0.1^{d}	23.7 ± 1.5^{a}	13 ± 5
ALK-B	29.5	n/a	73.4 ± 2.1^{a}	10.1 ± 0.8^{c}	2.6 ± 0.4^{e}	2 ± 3
USHT-B	37.4	n/a	65.9 ± 0.7^{b}	15.6 ± 0.4^{b}	5.2 ± 0.2^{d}	5 ± 2
SWE-160-B	35.0	n/a	61.6 ± 0.1^{c}	9.7 ± 1.3^{c}	4.7 ± 0.6^{de}	15 ± 1
SWE-180-B	39.2	n/a	68.7 ± 1.4^{b}	3.4 ± 0.4^{d}	5.1 ± 1.1^{d}	15 ± 3

Different subscript letters in the same column indicate significant differences by the Tukey test ($p<0.05$).

SWE promoted a selective extraction of hemicellulose, especially at 180 °C, but a high ratio of ash/silica (~15 %) was maintained even after the bleaching step. In fact, the SWE-180 treatment was more effective at eliminating hemicellulose than the alkaline treatment (3 % *vs.* 10 % in the bleached fibres). This could be related to a better capacity of the SWE to partially solubilise or hydrolyse the hemicellulose chains, with the formation of arabinoxylan oligomers, as reported by other authors (Ong et al., 2006; Plaza et al., 2010). In contrast, the solubilisation of silica did not occur quantitatively in SWE processes. This is highly dependent on temperature and pH, solubilising at high temperatures and pH above 9.0 (Le et al., 2015). At the neutral pH of SWE conditions, silica was not extracted, whereas it was almost completely eliminated during the alkaline treatment. The USHT-B samples had a similar ash content to that ALK-B, which indicates that this treatment was mechanically efficient at removing silica (~35 % wt. reduction). In fact, the sonication of plant suspensions has been proposed as an effective method in biomass desilification to avoid the operational problems that silica particles present in biorefineries (Le et al., 2015; Yunus et al., 2010).

Of the proven alternative methods, SWE at 180 °C was the most efficient at purifying the cellulose fibres since this exhibited a cellulose content closer to that of the alkaline method. This was due to its greater hemicellulose extractive power, despite its inability to remove the silica.

3.1.2 Microstructure of CFs

The morphological changes in the insoluble RS fractions provoked by the different CF purification methods are shown in Fig. 2. Rod-shaped RS fragments demonstrate the typical morphological nature of the plant tissue, a porous material composed of highly silicified epidermis, parenchyma and vascular tissues, and lumen (Jiang & Hsieh, 2014; Le et al., 2015).

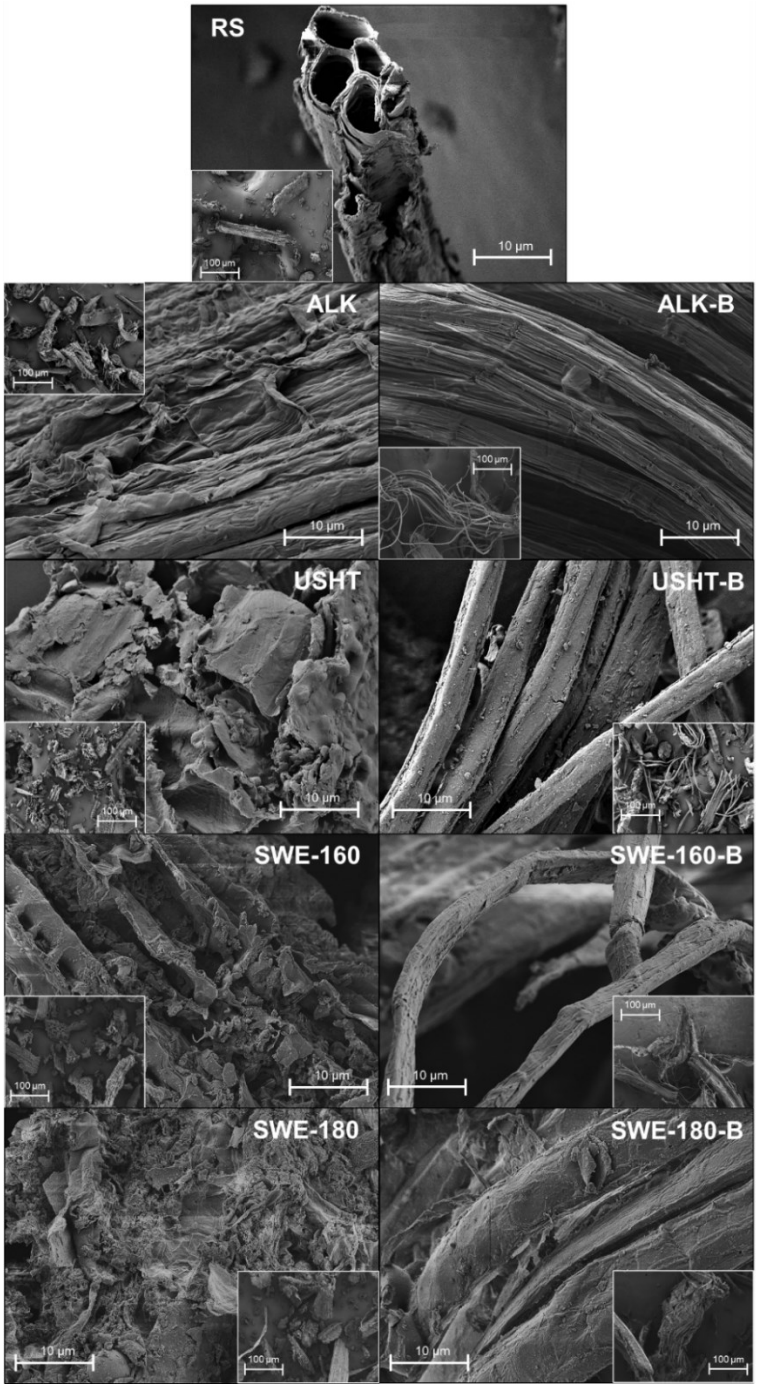

Fig. 2. FESEM micrographs of the raw RS and the different lignocellulosic fractions obtained before and after the bleaching step.

After the alkaline treatment of the raw RS, distorted particles (inserts at 100x magnification in Fig. 2, ALK) with a homogeneous surface could be observed, which can be related to the elimination of hemicellulose, silica, and waxes. Micrographs of RS treated with the USHT combined method revealed disrupted and deformed structures caused by sonication, thus exposing the innermost parts of the RS matrix. Quite a similar effect was observed in the micrographs of the SWE fractions, although these showed a rougher surface, with the presence of small particles, indicating that the silica or lignin were still present in the ligno-cellulosic structure (Abd-Talib et al., 2020). The morphology of bleached fibres revealed a smoother structure due to the removal of a substantial fraction of the lignin, thus better exposing the cellulose fibre bundles. The appearance of the CFs was similar, with diameters of less than 5 µm, as also reported by Jiang et al. (2013). Defibrillated CFs were observed in the bleached samples for all of the treatments, thus indicating the effectiveness of the combined ultrasound-reflux heating and SWE methods at eliminating non-cellulosic components. A smaller quantity of defibrillated fibres was detected in the SWE-180-B samples, which may be related to the large amount of hemicellulose removed; this leads to more cellulose OH groups available for the establishment of hydrogen bonds, giving rise to more aggregated CF (Bocheck, 2003).

3.1.3 TGA analysis

The changes in the thermal stability of the cellulosic fractions as the purification progressed were analysed by thermogravimetric analysis. Fig. 3 shows the mass loss and derivative curves of untreated RS and bleached fibres. The thermogravimetric parameters for each purification step, including the initial (T_{on}) and maximum degradation rate (T_p) temperatures, the weight loss at each step (Δm), as well as the final residual mass, are gathered in Table 3. All of the insoluble fractions showed a weight loss (4-5 %) below 150 °C, which is associated with the loss of adsorbed water, as also reported by other authors (Wu et al., 2013). In similar lignocellulosic materials, such as rice husk, hemicellulose, cellulose and lignin fractions exhibited typical thermal degradation patterns in temperature ranges of 150-350 °C, 275-350 °C, and 250-500 °C, respectively (Collazo-Bigliardi, 2018; Mansaray & Ghaly, 1998), but other studies reported a wider temperature rage in the case of lignin degradation (160-900 °C) with high residual mass (Yang et al. 2007) The degradation profile of the raw RS showed a broadened peak, with a marked shoulder, between 170 and 400 °C, mainly associated with the cellulose and hemicellulose degradation, followed by the final degradation of the lignin fraction from 400 to 550 °C. As the insoluble fractions became richer in cellulose, mainly after the bleaching step, the second event started at higher temperatures and the main peak narrowed while the initial shoulder disappeared, in agreement with the greater cellulose purity. Yang et al. (2007) reported that cellulose pyrolysis occurred between 315–400 °C, with the maximum weight loss rate at 355 °C and very little solid residue. The mass loss of the thermo-degradation step of the samples associated within cellulose degradation (170-400 °C

in Table 3) significantly increased after the bleaching step due to the removal of other compounds and enrichment in cellulose while the peak temperature was barely modified. Thus, the ALK-B fibre, with the highest cellulose content (Table 2), exhibited the highest mass loss (Δm of 73 %) in this step, whereas the SWE-B samples presented the lowest values (Δm of 64 %) with the highest final residual mass, in agreement with the final cellulose, hemicellulose and silica contents of the samples.

All of the treatments exhibited a broadened peak between 380 and 660 °C, which is associated with either the final decomposition of lignin, which occurs at a very low mass rate, or with the final thermal degradation of hemicellulose, since no contribution of cellulose at T > 400 °C has been found (Yang at al., 2007). Thus, these results coincide with the composition data of the fibres and the lack of total efficiency of the purification methods to completely remove lignin, as also reported by El-Sakhawy & Hassan (2007).

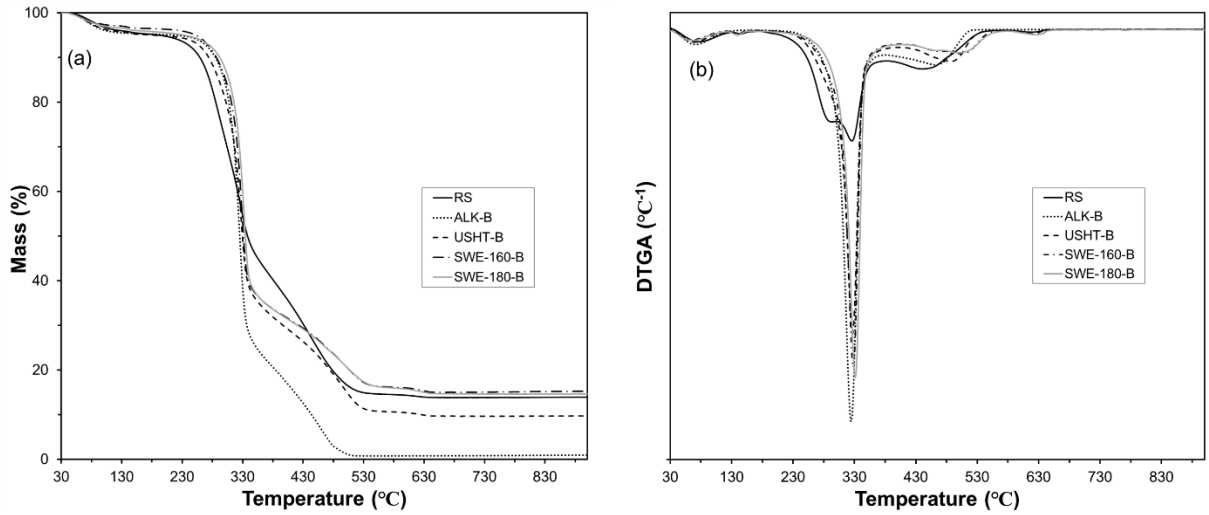

Fig. 3. TGA and DTGA curves of the raw RS samples and cellulosic fractions obtained with the different purification methods after the bleaching step.

Table 3. Onset (T_{on}) and peak (T_p) temperatures and mass loss (%Δm) of the different thermodegradation steps and final residual mass of cellulosic materials obtained with different purification pre-treatments (mean values ± standard deviation of two replicates).

Treatment	[40-180] °C			[160-400] °C			[380-660] °C			Residue (%)
	T_{on}*	T_p*	Δm (%)	T_{on}*	T_p*	Δm (%)	T_{on}*	T_p*	Δm (%)	
RS	39 ± 1^{b}	79 ± 7^{ab}	5 ± 1^{a}	171 ± 7^{cd}	327 ± 1^{b}	57 ± 1^{d}	391 ± 9^{ab}	446 ± 4^{cd}	13 ± 1^{ab}	17 ± 2
ALK	44 ± 1^{a}	66 ± 5^{c}	5 ± 1^{a}	179 ± 1^{c}	301 ± 3^{c}	57 ± 3^{cd}	372 ± 1^{c}	427 ± 11^{e}	25 ± 4^{ab}	8 ± 1
USHT	38 ± 1^{b}	81 ± 5^{a}	5 ± 2^{a}	178 ± 1^{c}	323 ± 4^{b}	62 ± 1^{bc}	379 ± 6^{bc}	444 ± 4^{de}	26 ± 2^{a}	11 ± 1
SWE-160	45 ± 1^{a}	72 ± 5^{abc}	5 ± 1^{a}	170 ± 1^{cd}	322 ± 4^{b}	54 ± 2^{d}	387 ± 5^{b}	461 ± 3^{c}	25 ± 1^{ab}	15 ± 1
SWE-180	43 ± 2^{a}	70 ± 4^{bc}	4 ± 2^{a}	167 ± 6^{d}	327 ± 2^{ab}	56 ± 3^{d}	392 ± 4^{ab}	460 ± 2^{cd}	27 ± 1^{a}	13 ± 5
ALK-B	41 ± 1^{ab}	70 ± 5^{c}	4 ± 2^{a}	203 ± 6^{a}	324 ± 1^{b}	73 ± 1^{a}	368 ± 6^{c}	477 ± 11^{b}	22 ± 2^{bc}	2 ± 3
USHT-B	43 ± 3^{ab}	73 ± 2^{abc}	4 ± 1^{a}	192 ± 6^{b}	327 ± 1^{ab}	66 ± 1^{b}	401 ± 1^{a}	495 ± 11^{a}	19 ± 1^{cd}	5 ± 2
SWE-160-B	45 ± 1^{a}	66 ± 2^{c}	4 ± 1^{a}	196 ± 1^{ab}	327 ± 1^{ab}	64 ± 1^{b}	393 ± 10^{ab}	504 ± 6^{a}	16 ± 1^{d}	15 ± 1
SWE-180-B	42 ± 4^{ab}	70 ± 4^{bc}	4 ± 2^{a}	192 ± 3^{b}	331 ± 1^{a}	64 ± 2^{b}	401 ± 1^{a}	501 ± 1^{a}	16 ± 2^{d}	15 ± 3

Different subscript letters in the same column indicate significant differences by the Tukey test ($p < 0.05$).

3.1.4 FTIR and X-ray analysis

The vibrational pattern of the functional groups present in each cellulosic fraction and the changes induced by the different purification treatments were analysed by FTIR in the 4000-800 cm^{-1} region (Fig. 4a). The broad bell-shaped absorption band between 3000 and 3800 cm^{-1} is assigned as O-H stretching vibrations, when involved in hydrogen bonds (Do et al., 2020). In general, this band becomes more intense and narrower as the purification progresses, which is related to the removal of amorphous components, such as hemicellulose, lignin, and waxes (Freitas et al., 2022; Wang et al., 2018). This behaviour was mainly detected for the fraction treated with the alkaline solution and the corresponding bleached ALK-B fibre. The band at 1730 cm^{-1} is attributed to the stretching of the C=O present in phenolic acids and uronic acids from the lignin and hemicellulose components, respectively (Chen et al., 2011; Esteves et al., 2013). Except for the ALK fraction (bleached or not), this peak is present in ever treatments, indicating the greater efficiency of the alkaline method at eliminating non-cellulosic components. The peak at 1511 cm^{-1} in the FTIR spectra of the untreated RS and USHT, SWE-160, and SWE-180 fractions is associated with the C=C stretching vibration of aromatic rings present in the lignin structure (Xu et al., 2006). This band disappeared in all of the spectra of the bleached samples, coherent with the reduction in lignin content (Table 2).

For the treatments submitted to SWE, the absorption band at 1033 cm^{-1}, related to the stretching of the acetal groups C-O-C-O-C found in the structure of cellulose and hemicellulose, becomes more intense when compared to the other purification methods. This could be due to the overlapping of the asymmetric stretching vibration of Si-O-Si present in amorphous silica, which exhibits a characteristic band at 1100 cm^{-1} (Do et al., 2020; Le et al., 2015). The typical stretching vibration of the β-glycosidic bond (C-O-C) present in the cellulose appeared at 898 cm^{-1} becoming more defined and intense as the purification process progressed.

Fig. 4b shows the XRD patterns and crystallinity index (*CI*) of the untreated RS and the fractions obtained with the different purification treatments before and after the bleaching step. All of the samples showed the same typical crystalline profile of cellulose Iβ, with diffraction peaks at 2θ = 15° ($1\bar{1}0$), 16° (110), 22° (200), and 34° (004) (Chen et al., 2011; Freitas et al., 2022). The maintenance of the most abundant allomorphic form of cellulose found in nature suggested that none of the treatments tested, even the alkaline, altered its crystalline arrangement (Nam et al., 2016). In general, the diffraction peaks were sharper (mainly the one corresponding to (200)) and CI increased after the bleaching treatment, coherently with the elimination of amorphous components, including hemicellulose, lignin, waxes, and silica, thereby realigning the cellulose chains (Li et al., 2009; Zainuddin et al., 2013). Fibres obtained with the alkaline treatment exhibited the greatest CI values before and after the bleaching process (62 and 69 %, respectively) whereas the USHT treatment produced the fibres with the

lowest *CI* (45 and 60 %, respectively, before and after bleaching), probably due to the fact that they had the highest content in amorphous hemicellulose (Table 2). On the other hand, a slight shift of the peak corresponding to the plane (200) was observed for the ALK samples, before and after bleaching. This behaviour could be explained by the rearrangement of cellulose chains caused by the penetration of Na+ ions in the crystalline network to form antiparallel crystalline soda-cellulose complexes, as described by Budtova & Navard (2016), Liu & Hu (2009), and Freitas et al. (2022).

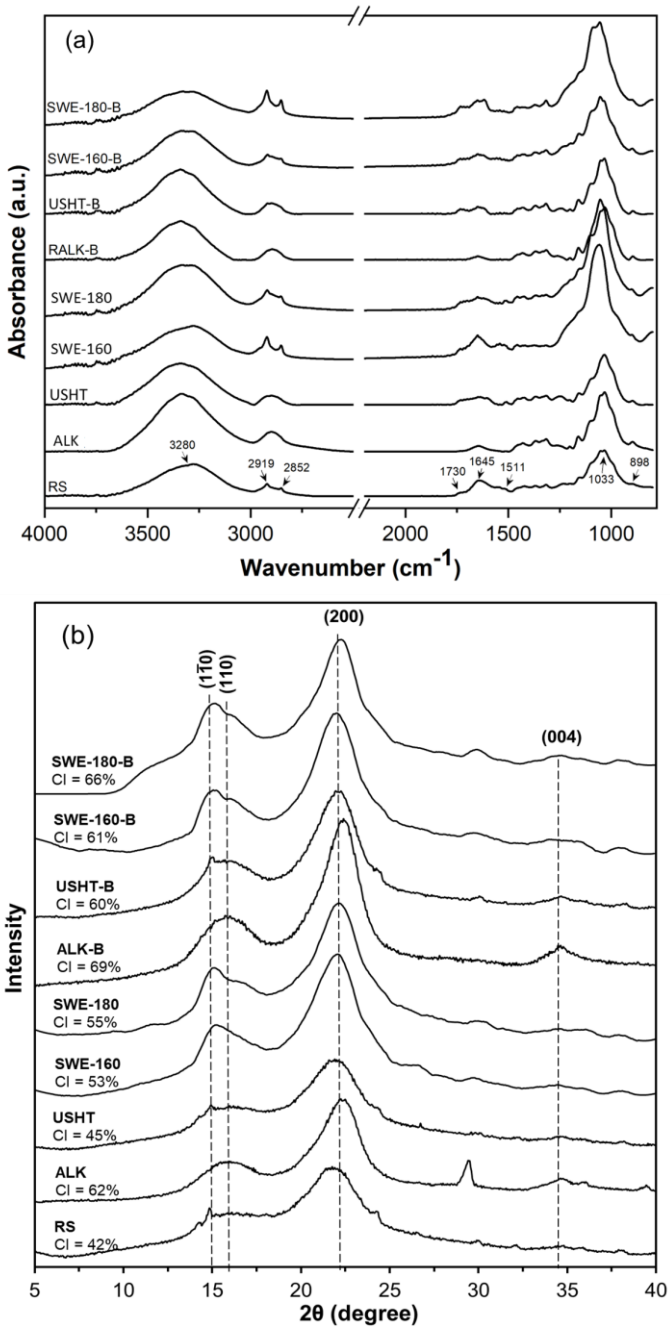

Fig. 4. FTIR (a) and XRD (b) spectra of the untreated RS and the cellulosic fractions purified by different treatments before and after bleaching step.

3.1.5 Hydrogel formation capacity

The ability of the different bleached CFs to form hydrogels through cyclic freezing-thawing (FT) was evaluated. Thus, Fig. 5 shows the aqueous suspensions of different CFs obtained after the sonication step and their changes after each FT.

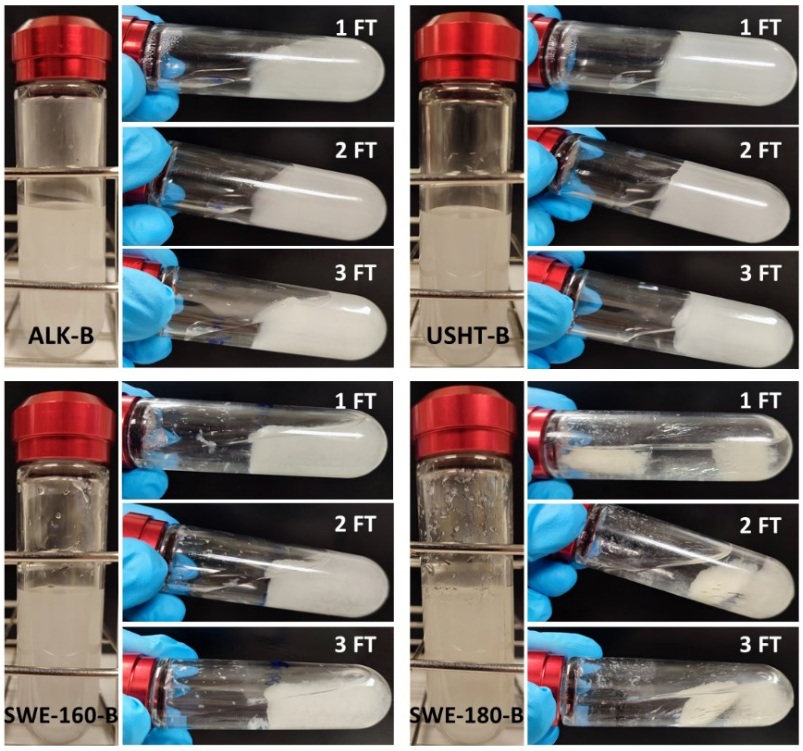

Fig. 5. Photographs of the sonicated bleached CF suspensions (vertical tubes) and their respective hydrogels (horizontal tubes) after each freezing-thawing (FT) cycles.

All of the fibres gave rise to homogeneous and viscous suspensions, indicating that the sonication step was effective at both defibrillating the CF bundles and dispersion. However, marked differences were observed between the hydrogels produced with the different CFs. The hydrogel from the USHT-B fibres showed the best physical integrity, with a similar appearance after the three FT cycles. A slight degree of hydrogel compaction and syneresis was observed after each FT cycle, due to the progressive association of the CFs, which provoked the decrease in the water holding capacity of the CF three-dimensional network (Jiang & Hsieh, 2014). These changes were more noticeable for the hydrogels obtained by treatments other than USHT-B, with a slight increase in visual compactness and syneresis for the ALK-B hydrogel, followed by SWE-160-B hydrogel. The SWE-180-B fibre produced much weaker hydrogels with a low water holding capacity, even after the first FT cycle. As reported by Abdel-Mohsen et al. (2011) and Figueroa-Pizano et al. (2020), three-dimensional network arrangements of hydrogels, obtained by the FT method, are markedly influenced by the freezing temperature and the rate, time and number of FT cycles, the nature of the polymer,

and the polymer: solvent ratio. The formation of hydrogels via the FT method is due to the cryoconcentration of the water solution containing the polymers during water crystallisation, which provokes the association of the polymer chains to form polymeric domains surrounding the nuclei of ice crystals, thus becoming hydrogels when the system thaws (Abdel-Mohsen et al., 2011; Jiang & Hsieh, 2014). The type and concentration of polymers influence the strength and degree of interaction between their chains under each FT condition, granting physical integrity for the three-dimensional polymer network. The differences between the gelling capacity observed in the samples could be related to their different composition. The hemicellulose content of CFs could play an important role in the hydrogel structure due to its greater water solubility. There was a greater amount of hemicellulose in the USHT-B fibres, followed by ALK-B, SWE-160-B, and SWE-180-B. So, this could favour the polymer association, together with the cellulose fibrils, thus contributing to the formation of a more cohesive hydrogel structure. In fact, in the SWE-180-B hydrogel with the lowest content of hemicellulose (~3 %), an inhomogeneous hydrogel with a poor water holding capacity was obtained. Likewise, in the case of the hydrogels with intermediate hemicellulose contents (~10 % in the ALK-B and SWE-160-B samples), they also exhibited intermediate visual firmness and water holding capacity. Nevertheless, the presence of silica could also affect the hydrogel formation, since, with similar hemicellulose contents, ALK-B hydrogels presented a more cohesive structure than the silica-rich SWE-160-B hydrogels, at every FT cycle. This could be attributed to the hydrogen bond formation between silica particles and hydroxyl groups of polymers that interfere with the polymer association in the cryoconcentrated domains. Hydrogen bonds of amorphous silica particles and hydroxyl groups have been observed by Cabrera et al., (2016) through the use of NMR and FTIR techniques.

3.2 Properties of aerogels

3.2.1 Appearance and microstructure

Fig. 6 shows the visual appearance and FESEM micrographs of aerogels prepared with the different bleached CFs. Observation with the naked eye showed unnoticeable differences between the ALK-B and USHT-B aerogels, which exhibited a cohesive spongy structure with a smooth surface. A more fibrillar arrangement and a rough surface were observed for the aerogels obtained from SWE fibres, which was more marked for the SWE-180-B sample.

FESEM micrographs revealed no marked structural differences between the ALK-B, USHT-B, and SWE-160-B aerogels, which showed irregularly dispersed micrometric pores, with film-like lamellas surrounding the cellulose fibres. The formation of these lamellas could be attributed to the presence of hemicellulose and other water-soluble compounds, which were aggregated during the cryoconcentration of the water fibre dispersions, in line with the ice crystal formation, wrapping the cellulose fibres and generating the interconnected lamellas in the freeze-dried material. Aerogels obtained with the SWE-180-B CFs with very low

hemicellulose content, exhibited a more filamentous structure with a less evident interconnecting lamellar structure.

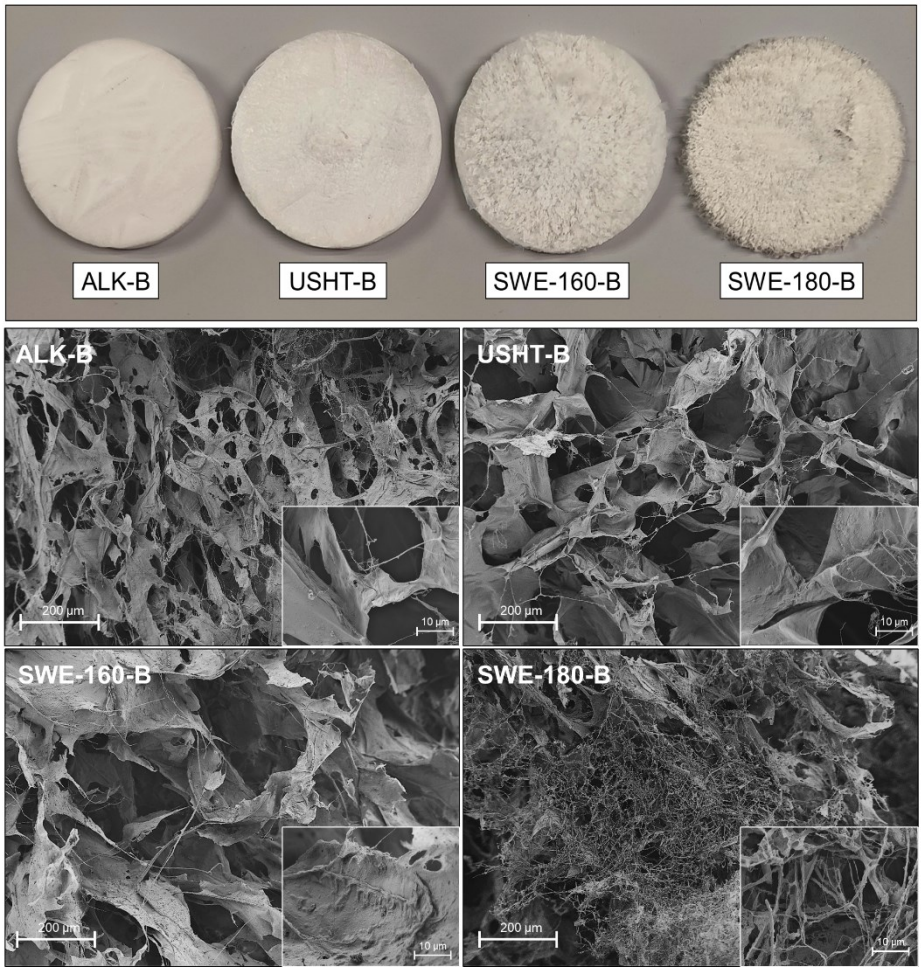

Fig. 6. Visual appearance and FESEM micrographs (x100 magnification with embedded micrographs at x2000 magnification) of cellulose aerogels prepared with bleached CF obtained with different purification processes: alkaline treatment, combined ultrasound-reflux heating, and subcritical water extraction at 160 °C and 180 °C.

The pore sizes in the aerogels depend on the ice crystal growth that occurred during the freezing step. This is affected by the sample cooling rate that determines the nucleation rate and nuclei propagation, which is greatly affected by the solution viscosity and molecular diffusion (Jiang and Hsieh, 2014). Soluble hemicellulose may increase the solution viscosity, thus affecting the final crystal size and consequently the pore sizes in the aerogel after the ice sublimation. Jiang & Hsieh (2014) observed changes in the aerogel pore sizes and wall thickness depending on the rate of ice formation in RS cellulose nanocrystal suspensions. The higher the cooling rate, the greater the number of nuclei formed and the smaller the crystal sizes, which gave rise to smaller pores in the aerogel structure. Likewise, as ice crystals grow more slowly and larger, more solids are cryo-concentrated to assemble into ordered domains

around larger crystals resulting in thicker walls in the aerogel. The poorer physical integrity of the aerogels from SWE-180-B fibres, as also observed in the corresponding hydrogel, could be related with the lower ratio of soluble polymer, such as hemicellulose, which contributes to the wall formation. Mandin et al. (2021) obtained cellulose nanofibre aerogels with and without xyloglucan, a hemicellulose fraction extracted from tamarind seed, and found structural differences associated with the presence of xyloglucan.

On the other hand, as previously observed for the hydrogels, the presence of a high silica ratio could also affect the aerogel microstructure. Hydrogen bonds between silica particles and polymers or fibres could reduce the interchain forces in the solid domains, thus contributing to a weakening of the cohesion forces in the aerogel three-dimensional network. Thus, both SWE-160-B and SWE-180-B silica-rich aerogels exhibited poorer physical integrity which could be, in part, attributed to the silica interactions with the chemical groups present in the cellulose and hemicellulose chains (Cabrera et al., 2016; Do et al., 2020; Le et al., 2015).

3.2.2 Water sorption isotherms

All of the cellulose aerogels exhibited type III isotherms, which reflects a slow increase in the equilibrium moisture content at low water activity values followed by a marked increase at intermediate and high-water activity values. This behaviour indicates that water molecules adsorb irregularly in multilayers with no prevalent monolayer adsorption, and there was no water capillary condensation in the pores in the studied range, since this phenomenon would occur at higher water activity (a_w>0.95) (Aviara, 2020). The experimental data were modelled by fitting the GAB equation, which is applicable over a wide range of a_w values (Baptestini et al., 2020). Fig. 7 shows the experimental points and the GAB fitted model (R^2 > 0.97) for the different aerogels, as well as the GAB parameters (embedded table in the figure). The water sorption levels at each a_w value was in the range of what has previously been reported for fibres from different cellulosic derivatives, with sorption properties correlated to the accessibility and the amount of sorption sites and also to the degree of crystallinity of the fibres (Simon et al., 2022). The differences in the water sorption behaviour of the different materials over the studied a_w range must be attributed to compositional differences (Table 2) and degree of crystallinity (Fig. 4). The samples from the USHT treatment exhibited a greater moisture sorption capacity, which could be attributed to the higher content of amorphous hemicellulose and the lower level of crystallinity of the material (60 %), which promotes water binding capacity, as previously described (Ioelovich & Leykin, 2010). In contrast, samples from the ALK treatment with a higher cellulose content and greater crystallinity exhibited a poorer water binding capacity. Nevertheless, the high silica content in samples from the SWE treatments could also interfere with the water sorption behaviour of the material due to the silica interactions with the hydroxyl groups that make them unavailable for water molecules, reducing the water binding capacity of the material. Hydrogen bonds of amorphous silica

particles with hydroxyl groups have been demonstrated through NMR and FTIR analyses (Cabrera et al. 2016). In fact, the SWE-180-B sample, with a high degree of crystallinity (66 %) and a high silica content (15 %), exhibited the lowest water sorption capacity within the a_w range.

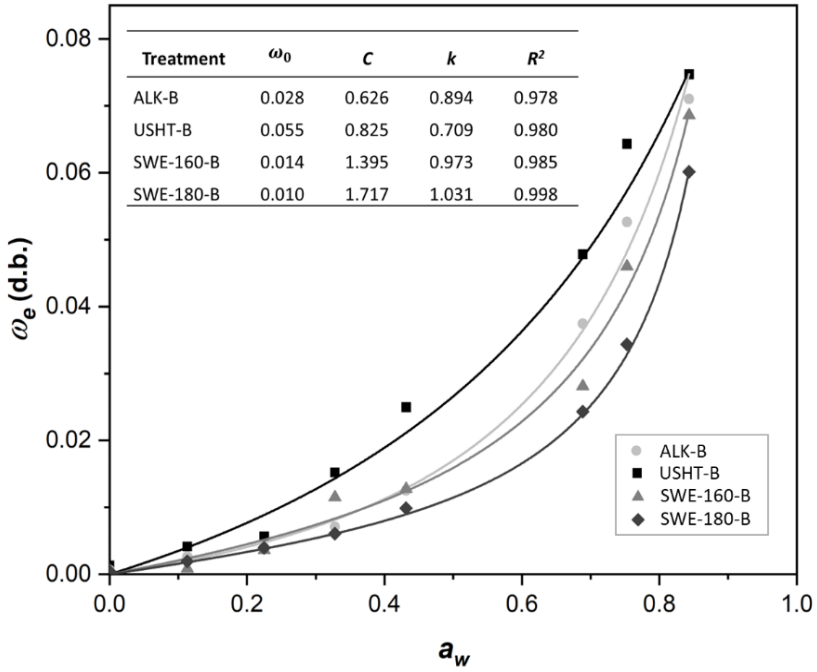

Fig. 7. Sorption isotherms of the cellulosic aerogels obtained from the cellulose fractions purified by the different treatments. Experimental points, GAB fitted model (lines), and parameters of the fitted GAB model obtained for the different aerogels (inserted table).

3.2.3 Porosity and water absorption and retention capacities of aerogels

The effects of the purification treatments of CFs on the properties of cellulose aerogels were also evaluated in terms of density, porosity, water absorption, and water retention capacity (Table 3). Very lowdensity (5.3-6.1 g.cm^{-3}) and high porosity (98.8-99.1 %) values were observed for ALK-B, USHT-B, and SWE-160-B aerogels, typical of ultralightweight and porous materials. These values are comparable to graphene and silica aerogels, which exhibited density and porosity values of about 4 mg.cm^{-3} and 98.2 % (Ngoc Hong, 2017; Xie et al., 2016), and 70-150 mg.cm^{-3} and 80-93 % (Amirjan et al., 2012; Buratti & Moretti, 2013), respectively. Nonetheless, the SWE-180-B aerogel exhibited higher density (16.8 mg.cm^{-3}) and lower porosity ($p<0.05$), in coherence with the marked structural differences observed by the FESEM analysis. The measured porosity values were always lower than the theoretical, since the film density was lower than the theoretical density value of crystalline cellulose (1600 mg.cm^{-3}, Diddens et al. (2008)). This means that the fibre packing in the films was more open than in crystalline cellulose, including non-removed compounds and bonded water, which reduces

the real density of the cellulosic material. Likewise, the density of cellulose films was greatly affected by the previous purification and homogenisation method due to the presence of empty spaces or pores among the fibrils (Spence et al., 2010). The samples richer in silica (SWE-160-B and SWE-180-B) exhibited lower film density, which points to the contribution of this compound to the fibre arrangement in the films, forming a less compact, lighter structure, despite the higher density of silica.

All of the aerogels exhibited very high water absorption capacities (WAC values), ranging from 49 to 56 g water.g^{-1} aerogel. These WAC values, typical of superabsorbent materials, are within the range found for some nanocellulose aerogels (Alakalhunmaa et al., 2016; Mandin et al., 2021; Yang & Cranston, 2014; W. Zhang et al., 2012). The theoretical WAC, determined from the porosity values, was higher in every sample than the determined WAC. This is explained by the partial collapse of the aerogel structure when it swells in contact with water, which leads to a loss in water absorption capacity with respect to that predicted from the air volume. The SWE-180-B aerogel exhibited the smallest difference between the real and theoretical WAC values, thus indicating that its structure collapses less during the wetting process. The structural collapse would be related with the ability of water to dissolve components relevant in the three-dimensional building of aerogel, such as hemicellulose.

Table 3. Density, porosity, water sorption, and water retention capacity values of the different cellulose aerogels. Mean values and standard deviation.

	ALK-B	USHT-B	SWE-160-B	SWE-180-B
Density (mg.cm^{-3})	6.1 ± 0.7^{b}	5.5 ± 0.3^{b}	5.3 ± 0.1^{b}	16.8 ± 1.6^{a}
Measured porosity (%)	98.9 ± 0.1^{ab}	99.1 ± 0.1^{a}	98.8 ± 0.1^{b}	96.7 ± 0.4^{c}
Theoretical porosity (%)	99.6 ± 0.1^{a}	99.7 ± 0.2^{a}	99.7 ± 0.1^{a}	98.9 ± 0.1^{b}
Film density (mg.cm^{-3})	554 ± 63^{a}	587 ± 26^{a}	463 ± 7^{b}	435 ± 5^{c}
Theoretical WAC (g.g^{-1} aerogel)	182 ± 11^{a}	183 ± 11^{a}	188 ± 5^{a}	59 ± 5^{b}
Measured WAC (g.g^{-1} aerogel)	55.6 ± 1.6^{a}	52.3 ± 2.9^{ab}	45 ± 4^{b}	49 ± 4^{ab}
WRC (g.g^{-1} aerogel)	1.0 ± 0.3^{a}	0.2 ± 0.1^{c}	0.2 ± 0.1^{bc}	0.5 ± 0.2^{b}

WAC: water absorption capacity; WRC: water retention capacity. Different subscript letters in the same line indicate significant differences by the Tukey test ($p<0.05$).

As concerns the water retention capacity (WRC), the ALK-B aerogel exhibited the highest WRC value ($p<0.05$), followed by the SWE-180-B samples, while the other treatments exhibited similar values ($p>0.05$). The higher WRC of ALK-B could be related to its higher proportion of cellulose, which may contribute to the structural strength of the aerogel, as well as to the immobilisation of more water molecules through extensive hydrogen bonds. Fontes-Candia et al. (2019) found similar levels of water retention by aerogels produced from *Arundo donax* sugarcane biomass.

4. CONCLUSIONS

The USHT and SWE alternative extraction methods were effective at eliminating non-cellulosic compounds, but to a different degree compared to the commonly-used ALK treatment. The SWE treatment at 180 °C was more effective at eliminating hemicelluloses, while the ALK and USHT methods gave rise to fibres richer in hemicellulose with the lowest silica content.

The final composition of the bleached CFs markedly affected the structure and properties of the cellulose-based hydrogels and aerogel obtained. Thus, a higher hemicellulose content in the CF led to more consistent hydrogels with a greater water holding capacity and to aerogels with thicker walls and higher porosity and water vapour sorption capacity. In contrast, the presence of silica gave rise to weaker hydrogels and fibrous aerogels, with lower porosity and poorer water absorption capacity.

Therefore, RS can be valorised to obtain high added value cellulosic materials, such as aerogels, using aqueous extraction, by applying ultrasounds or subcritical conditions to favour cellulosic purification. The different extraction methods provide the materials with modulated properties, depending on their final composition.

5. ACKNOWLEDGMENTS

The authors thank the Agencia Estatal de Investigación (Spain) for the financial support through projects PID2019-105207RB-I00/AEI/10.13039/501100011033 and Generalitat Valenciana [grant number GrisoliaP/2019/115].

6. REFERENCES

Abe, K., Yano, H. (2009). Comparison of the characteristics of cellulose microfibril aggregates of wood, rice straw, and potato tuber. *Cellulose*, 16, 1017-1023.

Abdel-Mohsen, A. M., Aly, A. S., Hrdina, R., Montaser, A. S., & Hebeish, A. (2011). Eco-Synthesis of PVA/Chitosan Hydrogels for Biomedical Application. *Journal of Polymers and the Environment*, 19(4), 1005-1012. https://doi.org/10.1007/s10924-011-0334-0

Abd-Talib, N., Mohd-Setapar, S. H., Asli, U. A., Pa'ee, K. F., Len, K. Y. T., & Mohd-Nasir, H. (2020). Silica removal by alkaline hydrogen peroxide treatment to enhance the conversion of rice straw to sugars. *Materials Today: Proceedings*, 31, 145-149. https://doi.org/10.1016/j.matpr.2020.01.397

Alakalhunmaa, S., Parikka, K., Penttilä, P. A., Cuberes, M. T., Willför, S., Salmén, L., & Mikkonen, K. S. (2016). Softwood-based sponge gels. *Cellulose*, 23(5), 3221-3238. https://doi.org/10.1007/s10570-016-1010-2

Amirjan, E., Mirzaee, O., Soleimani Dorcheh, M. R., & Dorcheh, A. S. (2012). Preparation and Characterization of Nanoporous Silica Aerogel Granules on The Basis of Water Glass Via Ambient Pressure Drying Method. *Jurnal Teknologi*, 59(2). https://doi.org/10.11113/jt.v59.2598

Aviara, N. (2020). Moisture Sorption Isotherms and Isotherm Model Performance Evaluation for Food and Agricultural Products. G. Kyzas & N. Lazaridis (Eds.), Sorption in 2020s. IntechOpen. https://doi.org/10.5772/intechopen.87996

Baptestini, F. M., Corrêa, P. C., Ramos, A. M., Junqueira, M. da S., & Zaidan, I. R. (2020). GAB model and the thermodynamic properties of moisture sorption in soursop fruit powder. *Revista ciência agronômica*, 51(1). https://doi.org/10.5935/1806-6690.20200006

Barana, D., Salanti, A., Orlandi, M., Ali, D. S., & Zoia, L. (2016). Biorefinery process for the simultaneous recovery of lignin, hemicelluloses, cellulose nanocrystals and silica from rice husk and Arundo donax. *Industrial Crops and Products*, 86, 31-39. https://doi.org/10.1016/j.indcrop.2016.03.029

Bochek, A. M. (2003). Effect of hydrogen bonding on cellulose solubility in aqueous and nonaqueous solvents. *Russian Journal of Applied Chemistry*, 76(11), 1711-1719.

Boonterm, M., Sunyadeth, S., Dedpakdee, S., Athichalinthorn, P., Patcharaphun, S., Mungkung, R., & Techapiesancharoenkij, R. (2016). Characterization and comparison of

cellulose fiber extraction from rice straw by chemical treatment and thermal steam explosion. *Journal of Cleaner Production*, 134, 592-599. https://doi.org/10.1016/j.jclepro.2015.09.084

Bragam, E. S., & Poletto, M. (2020). Preparation and Characterization of Hemicellulose Films from Sugarcane Bagasse. *Materials*, 13, 1-10.

Budtova, T., & Navard, P. (2016). Cellulose in NaOH-water based solvents: A review. *Cellulose*, 23(1). https://doi.org/10.1007/s10570-015-0779-8

Buratti, C., & Moretti, E. (2013). Silica nanogel for energy-efficient windows. En Nanotechnology in Eco-Efficient Construction (pp. 207-235). Elsevier. https://doi.org/10.1533/9780857098832.2.207

Cabrera, Y., Cabrera, A., Larsen, F. H., & Felby, C. (2016). Solid-state 29Si NMR and FTIR analyses of lignin-silica coprecipitates. *Holzforschung*, 70(8), 709-718. https://doi.org/10.1515/hf-2015-0165

Castro-Puyana, M., Herrero, M., Mendiola, J. A., & Ibáñez, E. (2013). Subcritical water extraction of bioactive components from algae. *Functional Ingredients from Algae for Foods and Nutraceuticals* (pp. 534-560). Elsevier. https://doi.org/10.1533/9780857098689.3.534

Chen, X., Yu, J., Zhang, Z., & Lu, C. (2011). Study on structure and thermal stability properties of cellulose fibers from rice straw. *Carbohydrate Polymers*, 85(1), 245-250. https://doi.org/10.1016/j.carbpol.2011.02.022

Collazo-Bigliardi, S. Ortega-Toro, R., & Chiralt Boix, A. (2018). Isolation and characterisation of microcrystalline cellulose and cellulose nanocrystals from coffee husk and comparative study with rice husk. *Carbohydrate Polymers*, 11.

Collazo-Bigliardi, S., Ortega-Toro, R., & Chiralt Boix, A. (2018). Reinforcement of Thermoplastic Starch Films with Cellulose Fibres Obtained from Rice and Coffee Husks. *Journal of Renewable Materials*, 6(7), 599-610. https://doi.org/10.32604/JRM.2018.00127

Do, N. H., Pham, H. H., Le, T. M., Lauwaert, J., Diels, L., Verberckmoes, A., Do, N. H. N., Tran, V. T., & Le, P. K. (2020). The novel method to reduce the silica content in lignin recovered from black liquor originating from rice straw. *Scientific Reports*, 10(1), 21263. https://doi.org/10.1038/s41598-020-77867-5

Diddens, I.; Murphy, B.; Krisch, M.; Müller, M. Anisotropic Elastic Properties of Cellulose Measured Using Inelastic X-ray Scattering. *Macromolecules* 2008, 41, 9755– 9759 DOI: 10.1021/ma801796u.

El-Sakhawy, M., & Hassan, M. L. (2007). Physical and mechanical properties of microcrystalline cellulose prepared from agricultural residues. *Carbohydrate Polymers*, 10.

Esteves, B., Velez Marques, A., Domingos, I., & Pereira, H. (2013). Chemical changes of heat treated pine and eucalypt wood monitored by FTIR. *Maderas. Ciencia y Tecnología*, 245-258. https://doi.org/10.4067/S0718-221X2013005000020

Figueroa-Pizano, M. D., Vélaz, I., & Martínez-Barbosa, M. E. (2020). A Freeze-Thawing Method to Prepare Chitosan-Poly(vinyl alcohol) Hydrogels Without Crosslinking Agents and Diflunisal Release Studies. *Journal of Visualized Experiments*, 155, 59636. https://doi.org/10.3791/59636

Fontes-Candia, C., Erboz, E., Martínez-Abad, A., López-Rubio, A., & Martínez-Sanz, M. (2019). Superabsorbent food packaging bioactive cellulose-based aerogels from Arundo donax waste biomass. *Food Hydrocolloids*, 96, 151-160. https://doi.org/10.1016/j.foodhyd.2019.05.011

Freitas, P. A. V., Arias, C. I. L. F., Torres-Giner, S., González-Martínez, C., & Chiralt, A. (2021). Valorization of Rice Straw into Cellulose Microfibers for the Reinforcement of Thermoplastic Corn Starch Films. *Applied Sciences*, 11(18), 8433. https://doi.org/10.3390/app11188433

Freitas, P. A. V., Gil, N. J. B., González-Martínez, C., Chiralt, A. (2022). Antioxidant poly (lactic acid) films with rice straw extract for food 2 packaging applications. *Food Packaging and Shelf Life*, 30.

Freitas, P. A. V., González-Martínez, C., & Chiralt, A. (2020). Application of Ultrasound Pre-Treatment for Enhancing Extraction of Bioactive Compounds from Rice Straw. *Foods*, 9(11), 1657. https://doi.org/10.3390/foods9111657

Freitas, P. A. V., González-Martínez, C., & Chiralt, A. (2022). Applying ultrasound-assisted processing to obtain cellulose fibres from rice straw to be used as reinforcing agents. *Innovative Food Science & Emerging Technologies*, 76, 102932. https://doi.org/10.1016/j.ifset.2022.102932

Henschen, J., Illergård, J., Larsson, P. A., Ek, M., & Wågberg, L. (2016). Contact-active antibacterial aerogels from cellulose nanofibrils. *Colloids and Surfaces B: Biointerfaces*, 146, 415-422. https://doi.org/10.1016/j.colsurfb.2016.06.031

Ioelovich, M., & Leykin, A. (2010). Study of sorption properties of cellulose and its derivatives. *BioResources*, 6(1), 178-195. https://doi.org/10.15376/biores.6.1.178-195

Jiang, F., Han, S., & Hsieh, Y.-L. (2013). Controlled defibrillation of rice straw cellulose and self-assembly of cellulose nanofibrils into highly crystalline fibrous materials. *RSC Advances*, 3(30), 12366. https://doi.org/10.1039/c3ra41646a

Jiang, F., & Hsieh, Y.-L. (2014). Super water absorbing and shape memory nanocellulose aerogels from TEMPO-oxidized cellulose nanofibrils via cyclic freezing–thawing. *J. Mater. Chem.* A, 2(2), 350-359. https://doi.org/10.1039/C3TA13629A

Kistler, S. S. (1932). Coherent Expanded Aerogels. *The Journal of Physical Chemistry*, 36, 52-64.

Krishania, M., Kumar, V., & Sangwan, R. S. (2018). Integrated approach for extraction of xylose, cellulose, lignin and silica from rice straw. *Bioresource Technology Reports*, 1, 89-93. https://doi.org/10.1016/j.biteb.2018.01.001

Kumar, P., Kumar, S., & Joshi, L. (2015). Socioeconomic and Environmental Implications of Agricultural Residue Burning. Springer India. https://doi.org/10.1007/978-81-322-2014-5

Le, D. M., Sørensen, H. R., Knudsen, N. O., & Meyer, A. S. (2015). Implications of silica on biorefineries—Interactions with organic material and mineral elements in grasses. *Biofuels, Bioproducts and Biorefining*, 9(1), 109-121. https://doi.org/10.1002/bbb.1511

Li, R., Fei, J., Cai, Y., Li, Y., Feng, J., & Yao, J. (2009). Cellulose whiskers extracted from mulberry: A novel biomass production. *Carbohydrate Polymers*, 76(1), 94-99. https://doi.org/10.1016/j.carbpol.2008.09.034

Liu, Y., & Hu, H. (2008). X-ray Diffraction Study of Bamboo Fibers Treated with NaOH. *Fibers and Polymers*, 9(6), 735-739.

Long, L.-Y., Weng, Y.-X., & Wang, Y.-Z. (2018). Cellulose Aerogels: Synthesis, Applications, and Prospects. *Polymers*, 10(6), 623. https://doi.org/10.3390/polym10060623

Mandin, S., Moreau, S., Talantikite, M., Novalès, B., Maigret, J.-E., Cathala, B., & Moreau, C. (2021). Cellulose Nanofibrils/Xyloglucan Bio-Based Aerogels with Shape Recovery. *Gels*, 7(1), 5. https://doi.org/10.3390/gels7010005

Mansaray, G., & Ghaly, A. E. (1998). Thermal degradation of rice husks in nitrogen atmosphere. *Bioresource Technology*, 65, 13-20.

Nagpal, R., Bhardwaj, N. K., Mishra, O. P., & Mahajan, R. (2021). Cleaner bio-pulping approach for the production of better strength rice straw paper. *Journal of Cleaner Production*, 318, 128539. https://doi.org/10.1016/j.jclepro.2021.128539

Nam, S., French, A. D., Condon, B. D., & Concha, M. (2016). Segal crystallinity index revisited by the simulation of X-ray diffraction patterns of cotton cellulose Iβ and cellulose II. *Carbohydrate Polymers*, 135, 1-9. https://doi.org/10.1016/j.carbpol.2015.08.035

Ngoc Hong, P. (2017). Carbon Nanotube and Graphene Aerogels – The World's 3D Lightest Materials for Environment Applications: A Review. *International Journal of Materials Science and Applications*, 6(6), 277. https://doi.org/10.11648/j.ijmsa.20170606.12

Ong, E. S., Cheong, J. S. H., & Goh, D. (2006). Pressurized hot water extraction of bioactive or marker compounds in botanicals and medicinal plant materials. *Journal of Chromatography* A, 1112(1-2), 92-102. https://doi.org/10.1016/j.chroma.2005.12.052

Plaza, M., Amigo-Benavent, M., del Castillo, M. D., Ibáñez, E., & Herrero, M. (2010). Facts about the formation of new antioxidants in natural samples after subcritical water extraction. *Food Research International*, 43(10), 2341-2348. https://doi.org/10.1016/j.foodres.2010.07.036

Ruthes, A. C., Martínez-Abad, A., Tan, H.-T., Bulone, V., & Vilaplana, F. (2017). Sequential fractionation of feruloylated hemicelluloses and oligosaccharides from wheat bran using subcritical water and xylanolytic enzymes. *Green Chemistry*, 19(8), 1919-1931. https://doi.org/10.1039/C6GC03473J

Sahu, O. (2021). Characterisation and utilization of heterogeneous catalyst from waste rice-straw for biodiesel conversion. *Fuel*, 287, 119543. https://doi.org/10.1016/j.fuel.2020.119543

Salam, A., Reddy, N., & Yang, Y. (2007). Bleaching of Kenaf and Cornhusk Fibers. *Industrial & Engineering Chemistry Research*, 46(5), 1452-1458. https://doi.org/10.1021/ie061371c

Seagal, J. J., Creely, A. E. Martin, J. Conrad, C. M. An Empirical Method for Estimating the Degree of Crystallinity of Native Cellulose Using the X-Ray Diffractometer. *Textile Research Journal*, 1, 786-794.

Simon, M., Fulchiron, R., & Gouanvé, F. (2022). Water Sorption and Mechanical Properties of Cellulosic Derivative Fibers. *Polymers*, 14(14), 2836. https://doi.org/10.3390/polym14142836

Sluiter, A. (2008a). Determination of Extractives in Biomass: Laboratory Analytical Procedure (LAP); Issue Date 7/17/2005. *Technical Report*, 12.

Sluiter, A. (2008b). Determination of Structural Carbohydrates and Lignin in Biomass: Laboratory Analytical Procedure (LAP); Issue Date: April 2008; Revision Date: July 2011 (Version 07-08-2011). *Technical Report*, 18.

Spence, K. L., Venditti, R. A., Rojas, O. J., Habibi, Y., & Pawlak, J. J. (2010). The effect of chemical composition on microfibrillar cellulose films from wood pulps: water interactions and physical properties for packaging applications. *Cellulose*, 17(4), 835-848.

Wang, X., Zhang, Y., Jiang, H., Song, Y., Zhou, Z., & Zhao, H. (2016). Fabrication and characterization of nano-cellulose aerogels via supercritical CO2 drying technology. *Materials Letters*, 183, 179-182. https://doi.org/10.1016/j.matlet.2016.07.081

Wang, Z., Qiao, X., & Sun, K. (2018). Rice straw cellulose nanofibrils reinforced poly(vinyl alcohol) composite films. *Carbohydrate Polymers*, 197, 442-450. https://doi.org/10.1016/j.carbpol.2018.06.025

Wu, Q., Yao, F., Xu, X., Mei, C., & Zhou, D. (2013). Thermal degradation of rice straw fibers: Global kinetic modeling with isothermal thermogravimetric analysis. *Journal of Industrial and Engineering Chemistry*, 19(2), 670-676. https://doi.org/10.1016/j.jiec.2012.10.026

Xie, Y., Xu, S., Xu, Z., Wu, H., Deng, C., & Wang, X. (2016). Interface-mediated extremely low thermal conductivity of graphene aerogel. *Carbon*, 98, 381-390. https://doi.org/10.1016/j.carbon.2015.11.033

Xu, F., Liu, C. F., Geng, Z. C., Sun, J. X., Sun, R. C., Hei, B. H., Lin, L., Wu, S. B., & Je, J. (2006). Characterisation of degraded organosolv hemicelluloses from wheat straw. *Polymer Degradation and Stability*, 91(8), 1880-1886. https://doi.org/10.1016/j.polymdegradstab.2005.11.002

Yang, X., & Cranston, E. D. (2014). Chemically Cross-Linked Cellulose Nanocrystal Aerogels with Shape Recovery and Superabsorbent Properties. *Chemistry of Materials*, 26(20), 6016-6025. https://doi.org/10.1021/cm502873c

Yang H., Yan R., Chen H., Lee, D.H., Zheng, C. (2007). Characteristics of hemicellulose, cellulose and lignin pyrolysis. *Fuel,* 86, 1781–1788.

Yunus, R., Salleh, S. F., Abdullah, N., & Biak, D. R. A. (2010). Effect of ultrasonic pre-treatment on low temperature acid hydrolysis of oil palm empty fruit bunch. *Bioresource Technology*, 101(24), 9792-9796. https://doi.org/10.1016/j.biortech.2010.07.074

Zainuddin, S. Y. Z., Ahmad, I., Kargarzadeh, H., Abdullah, I., & Dufresne, A. (2013). Potential of using multiscale kenaf fibers as reinforcing filler in cassava starch-kenaf biocomposites. *Carbohydrate Polymers*, 92(2), 2299-2305. https://doi.org/10.1016/j.carbpol.2012.11.106

Zaman, A., Huang, F., Jiang, M., Wei, W., & Zhou, Z. (2020). Preparation, Properties, and Applications of Natural Cellulosic Aerogels: A Review. *Energy and Built Environment*, 1(1), 60-76. https://doi.org/10.1016/j.enbenv.2019.09.002

Zhang, W., Zhang, Y., Lu, C., & Deng, Y. (2012). Aerogels from crosslinked cellulose nano/microfibrils and their fast shape recovery property in water. *Journal of Materials Chemistry*, 22(23), 11642. https://doi.org/10.1039/c2jm30688c

Zhang, Z., Smith, C., & Li, W. (2014). Extraction and modification technology of arabinoxylans from cereal by-products: A critical review. *Food Research International*, 14.

GENERAL DISCUSSION

The extensive and increasing use of petrochemical-based polymers to produce food packaging materials contributes to the plastics current environmental issue. Although conventional plastics are cheaper and have suitable functional properties for protecting food against spoilage and contamination, the enormous amount of plastic waste generated worldwide coupled with their high stability to biodegradation has negatively affected the environment. Greenhouse gas emissions (N_2O, CH_4, CO_2), accumulated and inadequately landfilled plastics, as well as micro- and nano-plastics found in marine and freshwater ecosystems, are some of the severe consequences that the world's wildlife and population are increasingly facing today. In this context, the development of biodegradable food packaging materials, with a claim towards minimising environmental impact, represents a green alternative to partially replace non-degradable plastics. Biodegradable biopolymers, such as starch and PLA, are being successfully used and investigated for food packaging purposes due to their availability, renewability, economic competitiveness, and food contact compatibility. Nevertheless, the use of these biopolymers as packaging materials may be limited due to their functional performance and lack of fitting the packaging requirements for different food matrices. For instance, starch materials are highly sensitive to moisture which modifies their properties. In contrast, PLA has a limited oxygen barrier capacity, which can compromise its application in oxidation-sensitive products. Of the different strategies to improve the functional properties of these materials, the incorporation of cellulose fibres, as reinforcing agents, and active extracts, with antioxidant/antibacterial capacity, represents an interesting alternative, since both components could be obtained from agro-wastes, such as rice straw (RS), which, in turn, could be valorised, contributing to boosting the waste management and circular economy.

RS is one of the most generated agro-industrial residues worldwide, which is considered biomass without direct economic value and is usually burned in the fields after the rice harvest. Due to its high availability, biodegradability, renewability, low cost, and lignocellulosic composition, including cellulose, hemicellulose, and lignin (~70 % dry matter), RS can be used as a source of bioactive extracts, with antioxidant and antimicrobial activity, as well as cellulosic reinforcing materials to be applied in biodegradable packaging materials.

This Doctoral thesis focused on obtaining cellulosic fractions and bioactive extracts from RS by applying different extraction and purification techniques, and their incorporation into starch and PLA-based films, as well as into starch-PLA multilayers, in order to obtain active packaging materials useful for extending the shelf life of different food matrices. Different extraction methods, using water as a green solvent, have been studied to obtain active extracts from rice straw while the extract residue was purified to obtain cellulose fibres.

Active extracts from rice straw

Different aqueous extraction methods were studied, described in **Chapters 1.I** and **2.I**, in order to improve the extraction yield of bioactive compounds from RS, by using ultrasound-assisted extraction (as treatment and pre-treatment), stirring method at 60 °C, heating under reflux condition, combined methods (ultrasound-stirring; ultrasound-heating) (**Chapter 1.I**), and subcritical water extraction (**Chapter 2.VII**). **Table 1** summarises the bioactive extracts obtained with their total solid yield and the analysed antibacterial activity. The obtained results in **Chapter 1.I** demonstrated that the extraction kinetics of phenolic compounds from RS were well fitted to a pseudo-second-order model, which is characterised by a two-step mass transfer process: an initial washing out of phenolics present at the RS particle surface, followed by a slow diffusion step from the innermost zones of the plant particles to the extracting solvent. The application of ultrasound pre-treatment (up to 30 min) improved the extraction yield of phenolic compounds with respect to both the stirring and reflux heating methods, being more effective when combined with the reflux heating method. The extract obtained by applying the combined ultrasound-reflux heating method exhibited the highest solid yield, the greatest DPPH radical scavenging capacity, and antimicrobial activity against Listeria *innocua*, although did not have the highest phenolic content from the Folin-Ciocalteu method. This revealed the different profile of antioxidant compounds, depending on the extraction method, as can be clearly observed in the correlation maps (**Figure 1**) between the total phenolic content (TPC) and the DPPH radical capacity (EC_{50}) of the extracts referred per mass unit of dry extracts (**Figure 1a**) or dried RS (**Figure 1b**). EC_{50} values quantify the amount of antioxidant per mg DPPH necessary to reduce by 50 % its initial concentration when the stability of the reaction is reached. **Figure 1a** reflects the antioxidant capacity of the compounds present in the dried extracts, whereas **Figure 1b** shows the ability of each extraction method to obtain different antioxidants from RS. Differences between both plots are related to the total solid process yield. A high extraction yield could lead to the presence of non-active compounds in the extract, such as some hemicellulose or silica, although the process could recover a greater amount of these compounds from RS. As shown in **Figure 1b**, the combined ultrasound-reflux heating method was more effective to extract phenolics and compounds with DPPH radical scavenging capacity from the RS, although the total extracted solids contain lower concentration of phenolics. Based on these results, the extract obtained by a sequential combination of ultrasound and reflux heating was selected to develop active films based on PLA and starch for different studies in this Doctoral Thesis (**Chapters 1.IV, 1.V, 1.VI, 2.VII**).

In **Chapter 2.VII**, bioactive extracts from RS were obtained by applying subcritical water extraction (SWE) or pressurized hot water extraction at 160 and 180 °C. **Table 1** also shows the process yields and antibacterial capacity of the extracts compared with the other extraction methods studied in **Chapter 1.I**. The different subcritical conditions did not affect

the process solid yield (~23 g dried extract. 100 g^{-1} RS) but enriched the extracts in phenolics and other bioactive compounds with DPPH radical scavenging activity, mainly when performed at 180 °C and 11 bars (**Figure 1a**). This process was also more effective at recovering active compounds from the RS (**Figure 1b**). The higher temperature and pressure increased the solubility of less polar compounds, such as phenolics, and gave rise to possible neoformed compounds from Maillard, caramelisation, and thermoxidation reactions (with antioxidant and antimicrobial character) (Plaza et al., 2010). Under subcritical conditions, the water gained penetrating power, reduction of viscosity and dielectric constant, and ability to break interactions between the target active compounds and the RS matrix, thus increasing the extraction yield of potentially active compounds. The active extracts obtained at 160 and 180 °C were markedly more antioxidant than those evaluated in **Chapter 1.I**, in terms of total phenolic content (TPC) and EC_{50} values, as shown in **Figure 1a**. The obtained EC_{50} values were nearer to those of pure compounds found in RS aqueous extracts (table inserted in **Figure 1a**). Moreover, the extract obtained at 180 °C exhibited antibacterial activity against *E. coli* and *L. innocua* whereas that obtained at 160 °C exhibited anti-listerial effect. Therefore, the challenge of improving the effectiveness of extraction of bioactive compounds from RS was achieved with SWE, which triggered a subsequent investigation in order to evaluate the effect of incorporating these extracts on the functional properties of PLA-based films, as well as their potential application to preserve fresh pork meat (**Chapter 2.VII**).

Table 1. Different active extracts studied in this Doctoral Thesis. Extraction process yield and antibacterial properties of the extracts.

Chapter	Extraction method	TSY (g dried AE.100 g^{-1} RS)*	Antimicrobial activity*	Notation
1.I	Stirring (60 min, 25 °C)	5.6 ± 0.1	-	ST60
	Probe-ultrasound (15 min, 25 °C)	5.7 ± 0.3	-	US15
	Probe-ultrasound (30 min, 25 °C)	7.5 ± 0.1	-	US30
	Probe-ultrasound (60 min, 25 °C)	9.5 ± 0.2	-	US60
	Heating (60 min, 100 °C)	9.6 ± 0.6	-	HT60
	Probe ultrasound (30 min) + Stirring (60 min)	9.0 ± 0.4	-	USST60
	Probe ultrasound (30 min) + heating (60 min)	14.0 ± 0.1	*L. innocua* (1.7 logarithmic reduction at 200 mg/mL^{-1})	USHT60
2.VII	Subcritical water extraction (160 °C, 30 min, 7 bars)	23.1 ± 0.3	*L. innocua* (MIC: 50 $mg.mL^{-1}$)	SWE 160
	Subcritical water extraction (180 °C, 30 min, 11 bars)	23.4 ± 1.1	*L. innocua* (MIC: 30 $mg.mL^{-1}$) and *E. coli* (MIC: 182 $mg.mL^{-1}$)	SWE 180

* TSY: total solid yield; AE: active extract; RS: rice straw; MIC: minimal inhibitory concentration.

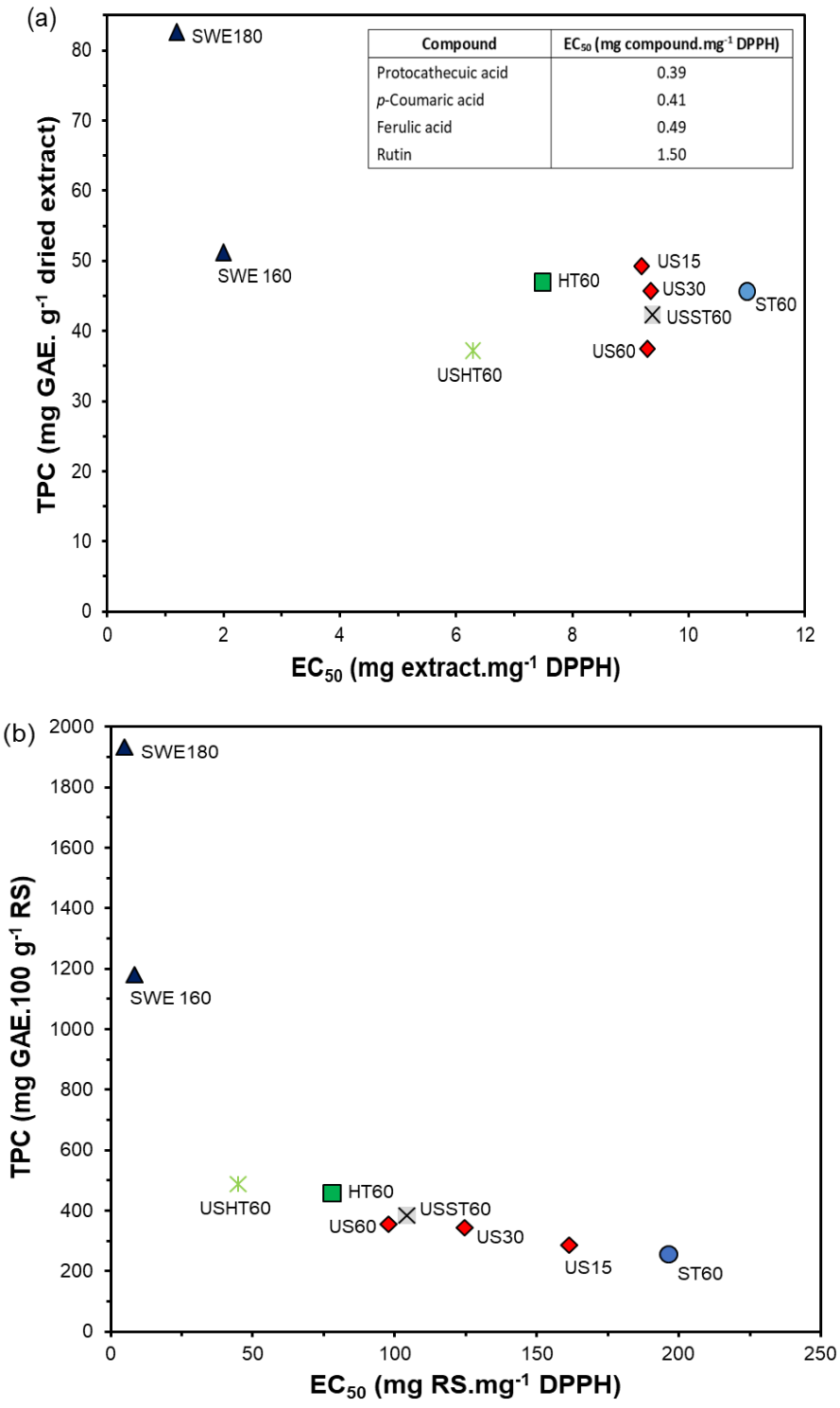

Figure 1. Correlation map between TPC, expressed as mg GAE. g^{-1} dried extract (**a**) or mg GAE. 100 g^{-1} RS (**b**), and EC_{50} (mg.mg^{-1} DPPH, of dried extract (**a**) or RS (**b**)), of the different aqueous RS active extracts obtained by applying different extraction techniques. The inserted table shows the EC_{50} values for the main phenolic compounds found in RS extract: protocathecuic acid, *p*-coumaric acid, ferulic acid, and rutin (Brand-Williams et al., 1995).

Cellulose fibres from rice straw

In order to exploit the full capacity of RS as an eco-friendly source of value-added materials, the insoluble fractions obtained after the extraction processes were used to isolate cellulose fibres (CF) in **Chapters 1.II** and **2.VIII**. In general, obtaining CFs involves their extraction from the plant material with an alkaline solution, where a substantial fraction of hemicellulose, waxes, and silica are eliminated, followed by a bleaching step for the final elimination of the lignin fraction. Since some of the extraction techniques evaluated in **Chapters 1.I** and **2.VII** could be effective in extracting water-soluble components from the plant matrix, including hemicellulose and lignin fractions, the challenge was to obtain CF by replacing the alkaline treatment by the proven most effective extraction methods: combined ultrasound-reflux heating and SWE, prior the bleaching stage. The results in **Chapter 1.II** showed that the combined ultrasound-reflux did not eliminate a substantial fraction of amorphous components from the cellulosic matrix but exposed the innermost regions of the plant tissue and allowed for a better access of the bleaching solvent, giving rise to a cellulosic material comparable to that obtained by applying the conventional alkaline method. Although the fibres from the new method showed slightly lower cellulose content (66 % *vs.* 73 %), both CFs exhibited similar morpho-geometric characteristics, aspect ratio (20-60), crystallinity, thermal behaviour, as well as reinforcement capacity in methylcellulose/gum Arabic-based films (**Table 2**). Being more hydrophilic and with less tendency to aggregate than the fibres derived from the alkaline method, the CF obtained with the proposed alternative method was selected to improve the functional properties of thermoplastic starch films in subsequent studies (**Chapters 1.III**, **V**, **VI**).

Results shown in **Chapter 2.VIII** demonstrated that the application of SWE to the RS, especially at 180 °C for 30 min, was more effective in the selective elimination of hemicellulose fractions in the extraction residue than the conventional alkaline method (3 % *vs.* 8 % hemicellulose in the residue) but were not so effective at eliminating lignin and ash (silica) fractions. Nevertheless, the subsequent bleaching step led to a notable separation of lignin from the cellulose fraction, while the silica remained linked to the bleached residue. Therefore, the SWE could be used to obtain cellulosic fractions from RS with a residual load of silica, which can modulate their properties for different uses.

All fibres obtained with the different purification methods were used to produce cellulose aerogels, ultralight, superabsorbent biodegradable materials with low density and high porosity, with potential application in different fields, such as food and pharmaceutical industries. The differences in the chemical composition of the CFs gave rise to cellulose aerogels with different morphological characteristics, porosity, density, water absorption and retention capacity, and moisture sorption. In general, the aerogels obtained with the fibres from the combined and alkaline method exhibited a more cohesive three-dimensional

structure, which could be related to the higher hemicellulose content and low proportion of silica. In contrast, the SWE (especially at 180 °C) cellulose fibres, with low hemicellulose content and high proportion of silica, exhibited a less cohesive structure. However, these CFs could have interesting properties as reinforcing agents in different polymer matrices, thus improving the force transferring from the fibres to the polymer matrix.

Methylcellulose/ Gum Arabic, Starch, and PLA films with rice straw fractions

Different biodegradable polymeric films were obtained and analysed in the present study using corn starch and amorphous PLA, incorporating RS fractions to modulate the film properties, intending to valorise this waste in packaging materials. The most active aqueous extracts from RS (USHT, SWE160 and SWE180) were used to obtain starch and PLA active films. In contrast, cellulose fibres obtained by applying the USHT method were incorporated into methylcellulose/ gum Arabic and starch matrices to verify their reinforcing capacity. Likewise, lamination of PLA and starch films by thermocompression was carried out to obtain bilayer films with improved barrier capacity, incorporating or not CF into the starch layer and the active USHT extract into the PLA sheet, which would be the food contact layer. Tables 2 and 3 show the different film formulations studied in the Thesis. The effect of the incorporated components into the polymer matrices on their properties was analysed. For comparison purposes, Figures 2, 3 and 4 showed the plots of tensile, barrier and optical properties, respectively, where the different films are located, allowing to compare them together.

Table 2. Composition of film formulations obtained by casting, based on blends of methyl cellulose (MC), gum Arabic (GA), glycerol (Gly), and cellulose fibres (CF) (obtained from different purification treatments), studied in the Chapter II of this Doctoral Thesis.

Chapter	Description	Film composition Mass fraction				Notation	Sample code (Fig. 2 & 3)
		MC	GA	Gly	CF		
1.II	Methylcellulose/gum Arabica (9:1) blend films reinforced with different CF ratios (1, 3, 5% wt.) obtained by different purification methods (US – ultrasound-reflux heating method; AL – alkaline treatment)	0.7500	0.0833	0.1667	-	MGA	1
		0.7438	0.0823	0.1653	0.0086	MGA-US-1	2
		0.7317	0.0813	0.1626	0.0244	MGA-US-3	3
		0.7200	0.0800	0.1600	0.0400	MGA-US-5	4
		0.7438	0.0823	0.1653	0.0086	MGA-AL-1	5
		0.7317	0.0813	0.1626	0.0244	MGA-AL-3	6
		0.7200	0.0800	0.1600	0.0400	MGA-AL-5	7

The reinforcing properties of the CF from the USHT method, in comparison with those from the alkaline method, was firstly analysed in glycerol plasticised methylcellulose/ gum Arabica (9:1) blend films, obtained by casting **(Chapter 1.II)**. As previously commented, both CFs

showed good compatibility with the polymer matrix and similar reinforcing capacity in these films, enhancing the film stretchability and resistance to break by about 33 % and 20 %, as can be observed in **Figure 2**. CFs did not promote significant changes in water vapour permeability and the light internal transmission of the films.

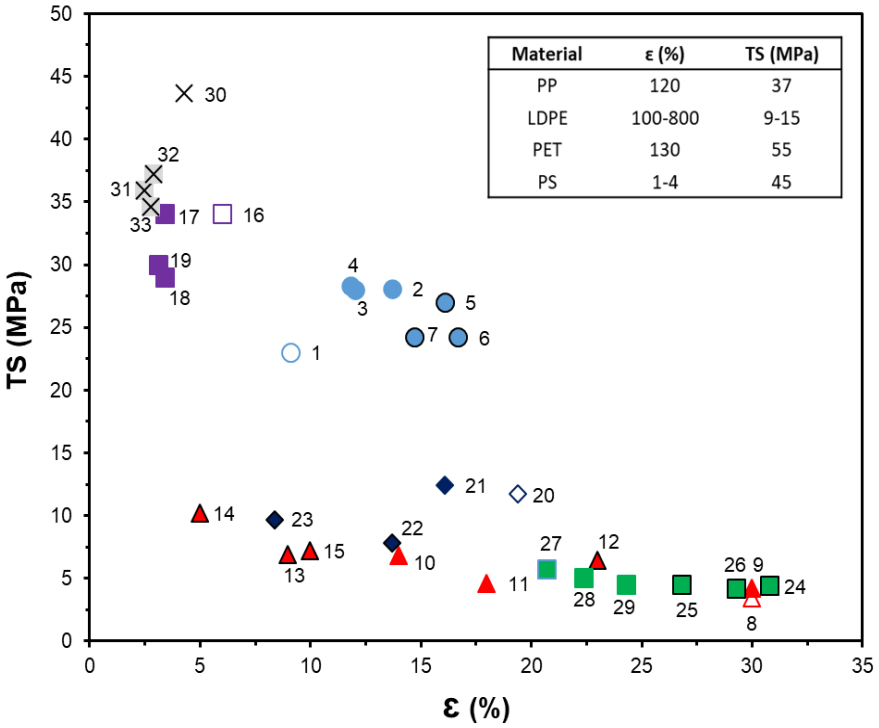

Figure 2. Correlation map of tensile properties (Tensile Strength at break *vs.* Elongation at break) of all formulations obtained in this Doctoral Thesis. The values for some conventional plastics used in food packaging are shown in the inserted table (PP, LDPE, PET, PS, Zhao et al. (2008); Mark et al. (1999)).

In **Chapter 1.III,** the effect of CF on the functional properties of starch-based films was analysed. For this purpose, 1, 3, and 5 % wt. of CF were successfully incorporated into films of glycerol plasticised corn starch and corn starch-modified by dry heating treatment, obtained by melt blending and compression moulding (**Table 3**). The fibres exhibited good interfacial adhesion within the composite materials, and their incorporation into starch matrices at 3 % wt., the most optimal content, led to stiffer, less extensible, and more resistant to break films (**Figure 2**). Likewise, fibres at 3 and 5 % wt. improved the oxygen and water vapour barrier capacity of starch films but did not significantly change the barrier properties of modified starch films, which were less permeable to water vapour (**Figure 3**). CFs interfered with the starch gelatinisation during the starch–glycerol thermo-processing, more markedly in modified starch, giving rise to non-gelatinised starch granules into the film matrix. The dispersed phase (starch granules or fibres) also modified the optical properties of the TPS films, making them slightly less transparent. Taking these results into account, 3 % wt. of CFs

were incorporated into starch matrices in further studies aimed to developing bilayer films with PLA layers (**Chapter 1.V**), or to obtain active starch films by incorporating different ratios of the USHT extract (**Chapter 1.VI**).

Table 3. Composition of film formulations obtained by melt blending and compression moulding, studied in **Chapters 1.III**, **IV**, **V**, **VI**, and **2.VII** of this Doctoral Thesis.

Chapter	Description	Film composition Mass fraction						Notation	Sample code (Fig. 2-4)
		Starch	Gly	PLA	PEG1000	CF	AE		
1.III	Starch films (TPS) and Modified (dry heating treatment) starch films (TPSdh) reinforced with different USHT CF ratios (1, 3, 5% wt.)	0.770	0.230	-	-	-	-	TPS	8
		0.763	0.229	-	-	0.008	-	TPScf-1	9
		0.753	0.225	-	-	0.022	-	TPScf-3	10
		0.741	0.222	-	-	0.037	-	TPScf-5	11
		0.770	0.230	-	-	-	-	TPSdh	12
		0.763	0.229	-	-	0.008	-	TPSdh-cf-1	13
		0.753	0.225	-	-	0.022	-	TPSdh-cf-3	14
		0.741	0.222	-	-	0.037	-	TPSdh-cf-5	15
1.IV	PLA (with PEG 1000) films with different ratios (2, 4 and 6 % wt.) of active extract obtained by the USHT method.	-	-	0.926	0.074		-	PLAp	16
		-	-	0.909	0.073		0.018	PLAus-2	17
		-	-	0.893	0.071		0.036	PLAus-4	18
		-	-	0.877	0.070		0.053	PLAus-6	19
1.V	Bilayer films of PLA (with PEG 1000), and 0 or 6 % wt. of USHT active extract, and starch (with and without 3 % wt. of USHT CF)	0.770	0.230	0.926	0.074	-	-	PLA-TPS	20
		0.753	0.225	0.926	0.074	0.022	-	PLA-TPScf	21
		0.770	0.230	0.877	0.070	-	0.053	PLAes-TPS	22
		0.753	0.225	0.877	0.070	0.022	0.053	PLAes-TPScf	23
1.VI	Starch films (TPS) reinforced with 3 % wt. of USHT CF (TPSCF) and with different USHT active extract ratios (4, 6, 8 % wt.) (TPSus-X).	0.770	0.230	-	-	-	-	TPS	8
		0.746	0.224	-	-	-	0.030	TPSus-4	24
		0.735	0.220	-	-	-	0.045	TPSus-6	25
		0.724	0.217	-	-	-	0.059	TPSus-8	26
		0.753	0.225	-	-	0.022	-	TPSCF	10
		0.730	0.218	-	-	0.022	0.030	TPSCFus-4	27
		0.719	0.216	-	-	0.021	0.044	TPSCFus-6	28
		0.709	0.213	-	-	0.021	0.057	TPSCFus-8	29
2.VII	PLA films with 6 % of active extracts, obtained by different extraction methods: USHT, SWE180 and SWE 160	-	-	1.0	-	-	-	PLA	30
		-	-	0.944	-	-	0.056	PLA-US	31
		-	-	0.944	-	-	0.056	PLA-S160	32
		-	-	0.944	-	-	0.056	PLA-S180	33

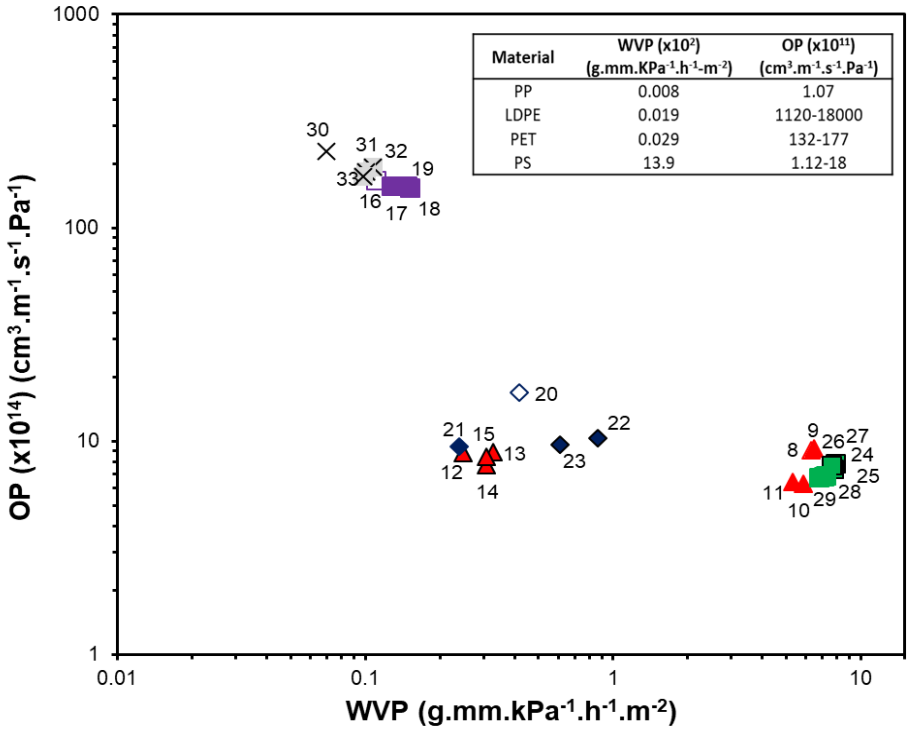

Figure 3. Barrier properties map (OP *vs.* WVP) showing the location of all formulations obtained in this Doctoral Thesis. The values for some conventional plastics used in food packaging are shown in the inserted table (PS, PET, PP, LDPE, Ortega-Toro et al. (2017)).

Of the different strategies to obtain active packaging materials, the direct incorporation of active compounds into the polymer matrix for their subsequent release into food systems is the most common practice. Different factors affect the effectiveness of the material, such as the nature and concentration of the active substances incorporated and their effectiveness for a determined function, their release kinetics from the polymer matrix and their solubility in the food system. Likewise, the compound-polymer interactions affect both the release kinetics and the final properties of the material for packaging purposes. Therefore, the purpose of **Chapter 1.IV** was to produce and characterise active PLA-based films incorporating different ratios (2, 4, and 6 % wt. with respect to the PLA mass) of the active USHT RS extract obtained in **Chapter 1.I** (combined ultrasound-reflux heating method) (**Table 3**). The active films, obtained by melt blending and compression moulding, were characterised as to their microstructure and thermal behaviour, mechanical, optical and barrier properties. Likewise, the release kinetics of antioxidant compounds in two food simulants (simulant A (10 % aqueous ethanol solution), and simulant D1 (50 % aqueous ethanol solution)) were investigated. The extract incorporation into PLA films slightly modify their microstructure and appearance, as well as barrier and tensile properties, as shown in **Figures 2** and **3**. PLA films with extract became darker and yellow-brown (**Figure 4**), with slightly reduced stretchability, resistance to break, water vapour barrier and thermostability. However, the films maintained

the oxygen barrier capacity and gained antioxidant capacity. The antioxidant compounds of the incorporated extract were released in the food simulants, depending on the extract concentration in the films, the food simulant polarity and contact time. In the ethanol-rich simulant (D1), the total content of phenolic compounds incorporated with the extract could be released at equilibrium. In contrast, only 33 % of them could be released in the most aqueous simulant (A). The DPPH radical scavenging capacity of the films referred, per mass unit of incorporated dry extract, reached asymptotic values from about 150 h contact time onwards. However, films with extract concentration of nearly 6 % exhibited very similar values in both simulants. This suggests that this extract concentration in the films ensures their potential radical scavenging capacity in food systems regardless of their polar nature. So, PLA films incorporating about 6 % of RS extract could be used as biodegradable active packaging material with remarkable antioxidant capacity in both aqueous foods (simulant A) and more fatty products, such as oil-in water emulsions (simulant D1).

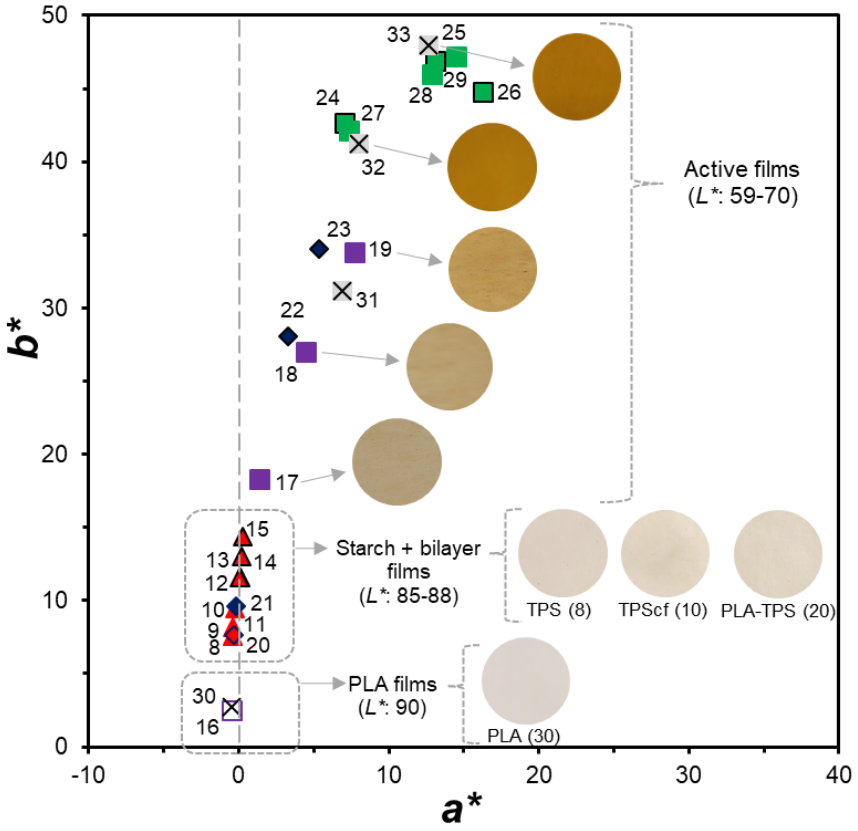

Figure 4. Chromatic plane *a*b** showing the *locust* of the different film formulations based on PLA, starch, and PLA-starch bilayers without active extracts, and with RS active extracts obtained with different extraction methods (USHT, SWE-160, and SWE-180).

Supported by the results found in **Chapters 1.III** and **1.IV**, the strategy studied in **Chapter 1.V** was to develop bilayer films by laminating polymer monolayers with complementary barrier

capacity, such as starch and PLA. Starch gives rise to thermoplastic films with excellent oxygen, lipid, and carbon dioxide barrier properties, although it is highly soluble in water and exhibits low water vapour barrier capacity. Meanwhile, PLA is a polyester with good mechanical properties and water vapour barrier capacity but a limited oxygen barrier. In this context, starch films were produced with and without CFs (3 % wt.), while PLA films plasticised with PEG1000 were obtained with and without RS active extract (6 % wt.). Four bilayer films were obtained by thermocompression of all possible combinations of PLA and starch films (**Table 3**). The starch-PLA laminates were characterised as to their functional properties as packaging material and tested in their ability to extend the shelf life of fresh pork meat during cold storage. The oxygen and water vapour barrier properties of the bilayer films were significantly improved in the laminates. These exhibited an oxygen barrier capacity similar to the starch monolayers and water vapour permeability values closer to that of PLA films, in coherence with the lamination theory. When compared with the control bilayer (PLA-TPS), the presence of active extract or CF in the PLA and starch layers, respectively, had similar effects to those observed in the respective monolayers, decreasing the oxygen permeability values of the bilayers (PLAes-TPS: ~41 % and PLA-TPScf: ~46 %). However, all bilayers became less stiff and resistance to break than the most resistant PLA monolayers (**Figure 2**). This suggests that the interlayer compound migration during the thermocompression step negatively affected the mechanical performance of bilayers. Specifically, the water migration from the starch film to PLA sheet could promote the partial hydrolyses of PLA chains, giving rise to a weakening effect of the polymer matrix and also decreasing its water vapour barrier capacity with respect to the PLA films. The optical properties of the bilayer films were markedly affected by the presence of extract in the PLA sheet due to the coloured nature of the extract compounds (**Figure 4**).

Both valorised fractions from RS, active extract (**Chapter 1.I**) and CFs (**Chapter 1.II**), were used to improve the functional and active properties of thermoplastic starch-based films in **Chapter 1.VI**. As shown in **Table 3**, the films were obtained by melt blending and compression moulding, with and without CFs at 3 % wt. and with different ratios of USHT active extract (0, 4, 6, and 8 % wt.). As expected, the incorporation of CFs, with or without extract, played an essential role in the reinforcement of the films, making them more resistant to break, stiffer and less extensible (**Figure 2**), while decreasing the water vapour and oxygen permeability. When the extract was incorporated into both starch and reinforced starch matrices, the films were more stretchable and less thermo-resistant. Nevertheless, the incorporation of RS extract gave rise to films with marked antioxidant capacity and light absorption, especially in the UV region, exhibiting notable colour differences with respect to free extract films (**Figure 4**). Due to the coloured nature of the RS extract, films became reddish-brown as a function of the extract concentration.

Given the excellent bioactivity of the extracts obtained by applying SWE (**Chapter 2**), the approach used in **Chapter 2.VII** was to explore the usefulness of these materials to produce active films based on amorphous PLA. As shown in **Table 3**, PLA films with 6 % wt. of the most active extracts (USHT, SWE160 and SWE180) were obtained by melt blending and compression moulding and characterised as to their structural and functional properties. The different extracts produce slight microstructural changes in the PLA matrix, suggesting different degrees of compatibility, according to the nature of each extract. All extracts weakened the PLA matrix, resulting in a small decrease of the film stiffness and resistance to break (**Figure 2**) and water vapour barrier capacity (**Figure 3**). However, films with extracts were less permeable to oxygen, especially with SWE extracts, as a result of their improved antioxidant capacity (OP reduction: PLA-S160: ~20 %; PLA-S180: ~25 %). Likewise, the active films exhibited strong UV light absorption, especially those prepared with SWE extracts, which could prevent UV light induced oxidative reactions in foods. The optical properties of the PLA matrix was, therefore, modified by the incorporation of extracts, which promoted the film colouration depending on the extracts components (**Figure 4**).

By comparing the properties of the different obtained films several groups can be observed in both correlation maps of tensile (**Figure 2**) and barrier (**Figure 3**) properties, depending on the polymeric matrix. As concerns tensile behaviour, all PLA films were grouped, these being more resistant and less stretchable than starch and methylcellulose films. The incorporation of RS fractions (extracts or cellulose fibres) modulates the tensile properties of each polymeric matrix, widening their characteristic *locust* in the map. The highest changes induced by the RS fractions were produced in starch films, especially in ε (%) values, with also notable modification in the TS, depending on the type of starch and the reinforcing effect of CF or plasticizing effect of the active extract. PEG 1000 plasticization of PLA films reduced the TS and increase ε (%), whereas the extract incorporation provoked similar effects in both PEG plasticised and non-plasticised PLA films. These exhibited a resistance to break in the range of some conventional plastics used in food packaging, although these are less extensible than PP, LDPE, or PET. In contrast, starch films are much less resistant that the usual plastics, although could exhibited comparable extensibility, depending on the film formulation. It is remarkable that the PLA-starch bilayer films were mechanically closer to starch films than PLA films due to the changes occurred in the PLA during the thermocompression step. These changes are related with the interlayer compound migration, such as the water transfer from starch films, which could promote hydrolytic changes in the PLA chain, as previously commented. PLA is extremely thermosensitive in the presence of moisture; a moisture content above 250 ppm can promote severe hydrolytic degradation upon thermal treatment, which leads to a molecular weight drop and then a change in the film's functional properties (Lim et al., 2010).

Regarding barrier properties, all studied films exhibited lower water vapour barrier capacity than conventional plastics but had better oxygen barrier capacity, mainly starch-based films or bilayers containing starch sheets. These bilayers exhibited high oxygen barrier and lower water vapour permeability than the starch monolayers, which supposed to be a notable improvement in their adequacy for food packaging purposes. The oxygen barrier capacity was enhanced when the antioxidant extract was incorporated into the films by oxygen-scavenging effect. This points to their ability to preserve foods against oxidative reactions responsible for the spoilage of many foods, such as fatty products. Nevertheless, the obtained films would be less appropriate for foods whose quality is highly susceptible to water gain or losses, such as crispy products.

Concerning the optical properties and appearance of the films (**Figure 4**), the main changes were promoted by adding RS extracts to obtain active films, depending on the extract and concentration and interactions with the polymer matrix. All active films became darker and reddish-brown, as shown in **Figure 4**, which supposes advantages or disadvantages, depending on their target use. In any case, the extracts provide the films with UV light-blocking effect, representing an additional protection capacity for many foods preservation.

Taking these considerations into account, as well as de high moisture sensitivity of starch films, PLA could be used for packaging moist foods as a contact layer, whereas starch films could be used to obtain packaging materials for oil or fats. In this sense, different studies with real foods were carried out to validate the adequacy of some of the studied active films to preserve food quality during storage under different conditions, as discussed below.

Capacity of active films to extend food shelf life

Different active films based on starch, PLA or their bilayers, containing active extracts from RS, were tested as to their ability to extend the shelf life of fatty (sunflower oil) and moist (fresh pork meat) foods. Starch-based films were used to obtain mono-dose bags for packaging sunflower oil, while PLA and starch-PLA bilayers were used for wrapping meat samples, using PLA as the food contact layer. Oil bags were submitted to an accelerated oxidation test, and meat bag samples were cold storage. In all cases, sample analyses were carried out throughout storage in order to evaluate the changes in the product quality parameters to assess the product shelf extension in the active package, compared with control samples (films without active extract).

Starch films reinforced or not with cellulose fibres (3 % wt.), containing 8 % wt. of USHT extract, were highly effective at preventing sunflower oil oxidation in an accelerated oxidation test for 50 days. The active films delayed both the peroxide formation and secondary oxidative

reactions (TBARS) with respect to the corresponding control packaged samples with extract. No significant differences in the protection capacity were observed for films with and without fibres, despite the lower oxygen permeability of the reinforced films. Therefore, the inhibition of the oil oxidative deterioration in the TPS bags must be mainly attributed to the high UV light-blocking effect and antioxidant action of the extract in the bags. Based on these results, biodegradable starch films containing CF and RS extract are proposed for their use in mono-dose packaging of oxidation sensitive oils, due to their higher mechanical resistance, barrier properties, and antioxidant capacity.

Regarding the shelf-life studies of packaged meat, the incorporation of USHT extract into the PLA food contact layer of bilayers was a successful strategy to prevent meat oxidation, pH changes, and colour changes throughout 16 cold storage days. The active bilayers effectively mitigated the microbial growth along the time. The established limit for total viable counts (10^6 CFU.g^{-1} sample) was reached on 12 storage days for the control packaged samples and the extract-free bilayers and on 14 days for samples packaged in the active bilayer.

Considering the greater antioxidant and antibacterial activity of SWE extracts, other shelf-life study in fresh pork meat was carried out using non-plasticised PLA film bags with 6 % wt. of the different extracts (USHT, SWE160 and SWE180). The films with SWE extracts, especially SWE180, were more effective than USHT extract at maintaining the meat quality parameters, typically pH, weight loss, colour, oxidation indexes, and microbial counts throughout cold storage, in agreement with their higher antioxidant and antibacterial capacity. Therefore, PLA bags with SWE extracts are proposed to extend the meat shelf life, since microbial counts and oxidation limits were not reached on 16 storage days in samples packaged with these materials, being the extract obtained a 180 °C more effective than that 160 °C.

As a global conclusion, using lignocellulosic rice straw to obtain valorised fractions, such as active extracts and cellulosic fibres, for developing food packaging materials, represents a useful approach to improving the functionality of biodegradable polymers for food packaging purposes, while boosting the circular economy. Incorporating active extracts from RS provided biodegradable films with antioxidant and antimicrobial properties. Likewise, the use of cellulose fractions from RS could provide the starch films with improved functional performance, all this adding value to these polymeric materials to replace synthetic plastics. The integral fractionation of RS, obtaining active extracts and purified cellulose fibres, using green and innovative extraction processes, allowed for the whole valorisation of RS waste in the developed materials while opening new windows for other industrial uses. In this sense, RS, an agro-industrial residue often burned after rice harvesting, can be considered a highly versatile material that gives rise to different valorised fractions with high applicability in the pharmaceutical, food, and food packaging fields.

References

Brand-Williams, W., Cuvelier, M. E., & Berset, C. (1995). Use of a free radical method to evaluate antioxidant activity. *LWT - Food Science and Technology*, 28(1), 25–30.

Lim, L., Cink, K., Vanyo, T. (2010). Processing of Poly (lactic acid). In Rafael Auras, Loong-Tak Lim, Susan E. M. Selke, Hideto Tsuji (Eds.), *Poly (lactic acid). Synthesis, Structures, Properties, Processing, and Applications* (pp. 203-227).

Mark, E. J. (Ed.) (1999). *Polymer Data Handbook*. New York: Oxford university press.

Ortega-Toro, R., Bonilla, J., Talens, P., & Chiralt, A. (2017). Starch-based materials in food packaging. In M. A. Villar, S. E. Barbosa, M. A. García, L. A. Castillo, & O. V. López (Eds.), *Future of starch-based materials in food packaging* (pp. 257-312). Aspen Publishers.

Plaza, Merichel, Miryam Amigo-Benavent, María D. del Castillo, Elena Ibáñez and Miguel Herrero (2010). Neoformation of antioxidants in glycation model systems treated under subcritical water extraction conditions. Food Research International, 43, 1123-1129.

Zhao, R., Torley, P., Halley, P. J. Emerging biodegradable materials: starch- and protein-based bio-nanocomposites (2008). *Journal of Materials Science*, 43, 3058-3071.

CONCLUSIONS

1. Rice straw contains a wide variety of bioactive compounds of technological interest for food application purposes, but the extraction conditions greatly influence the extraction efficiency of the target compounds. The application of ultrasound was notably more effective at extracting water-soluble phenolic compounds than simple stirring, as revealed by the higher extract yields and antioxidant activity of the extracts. Nevertheless, a high extraction temperature produced materials with improved antioxidant activities, in line with the promotion of the cleavage of covalent bonds between the phenolic compounds and the lignocellulosic fraction. This thermal effect was greatly enhanced when ultrasound pre-treatment was applied due to the increase in the substrate surface exposed to the extraction. Therefore, a combination of 30 min ultrasound plus 60 min thermal treatment in water reflux is recommended to obtain solid extracts with great antioxidant activity and notable anti-listerial effect, which could be used in the food or pharmaceutical industries.

2. Application of the combined ultrasound-heating method to purify the cellulose fraction of rice straw gave rise to cellulose fibres with a slightly different degree of purification than the alkaline extraction, but with a similar degree of crystallinity and aspect ratio, these being more hydrophilic in nature and with a lower tendency to aggregate. The reinforcing capacity of the fibres obtained with this new method, in methyl-cellulose based films, was similar to those obtained using the alkaline treatment, enhancing the film stretchability by about 33 %, and boosting the film resistance to break (by about 20 %) at 1, 3 or 5 %. Therefore, the combined ultrasound-heating method can be a potential alternative for the purposes of obtaining cellulose fibres from rice straw, avoiding the use alkaline solutions, is faster and presents a higher yield than the process with an alkaline step (37 *vs.* 29 %). Moreover, the ultrasound-heating method allows for obtaining active extracts rich in antioxidant compounds, which can be used for different applications in the food or pharmaceutical industries. Thus, a more integral valorisation of rice straw could be reached.

3. Cellulose fibres obtained from rice straw, by applying ultrasound-heating method and mechanical defibrillation had a major cumulative frequency of lengths below 200 µm and 5–15 µm of thickness and exhibited good reinforcing capacity for starch films. Incorporation of the fibres into starch matrices at 3 % wt., the most optimal content, led to stiffer and more resistance to break films for both non-modified and dry heating-modified corn starch films. Likewise, fibre at 3 and 5 % wt. improved the oxygen and water vapour barrier capacity of strach films but did not modify barrier properties of films based on modified starch. Fibres interfered starch gelatinization during the starch-glycerol thermo-processing, more markedly in modified starch, giving rise to non-gelatinized starch granules into the film matrix. The dispersed phase (starch granules or fibres) also modified the optical properties of the starch films, making them slightly less transparent. Therefore, these fibres can be used to improve the properties of starch films with different purposes, such as their use as food packaging material.

4. Incorporation of the rice straw aqueous extract obtained by combined ultrasound-reflux-heating process (with high phenolic content and radical scavenging capacity) into PLA films turned them a little brown while slightly modifying the polymer chain arrangement and strength of the matrix, which promoted a small loss in the film stretchability, resistance to break, barrier capacity and PLA thermostability. However, the films gained antioxidant capacity when the extract was incorporated. The phenolic components incorporated into the extract were able to be released, depending on the extract concentration in the films, the food simulant polarity and contact time. In the ethanol-rich simulant (D1), the total content of phenolics could be released at equilibrium, whereas only 33 % at most could be released in the most aqueous simulant (A). The radical scavenging capacity of the films, referred per mass unit of incorporated dry extract, reach asymptotic values from about 150 h contact time onwards; these were lower than those of the pure extract, but films with an extract concentration of nearly 6 % exhibited very similar values in both simulants. Therefore, this extract concentration in the films ensures their potential antioxidant capacity in food systems regardless of their polar nature. So, PLA films incorporating about 6 % of rice straw extract could be used as biodegradable active packaging material with antioxidant capacity in both aqueous foods (simulant A) and more fatty products, such as oil-in-water emulsions (simulant D1).

5. The PLA-TPS bilayer films containing rice extract (into PLA) and cellulose fibres (into TPS) exhibited improved functional properties for food preservation with respect to the monolayer films. TPS conferred oxygen barrier capacity to the laminates, while PLA offered a wet food contact option with water vapour barrier capacity. CF incorporation into TPS reinforced the strength of the films and improved their barrier capacity. The RS extract slightly reduced the PLA resistance and elongation at break but improved their oxygen barrier capacity. The tensile and barrier properties of bilayer films revealed changes in the performance of each layer associated with the interlayer migration of the low molecular weight compounds present in each monolayer. The bilayers with cellulose fibres in the TPS sheet exhibited the lowest values of oxygen permeability while the extract in the PLA sheet slightly promoted the water vapour permeability and reduced resistance and elongation at break of the bilayers. Bilayers with fibre-reinforced TPS and PLA with the antioxidant extract (with the lowest oxygen permeability) were useful to preserve fresh pork meat, using PLA as the food contact layer in thermo-sealed bags. A noticeable antioxidant capacity of the extract was observed in the meat samples, while the microbial counts were also reduced throughout the cold storage time. Therefore, these bilayers had great potential to extend the shelf-life of meat samples, maintaining quality parameters and safety for longer, while using fractions of the rice straw which permit its valorisation.

6. New functionalities of thermoplastic starch films were achieved when rice straw fractions were incorporated. Cellulose fibres at 3 % promoted the film strength with respect to

thermoplastic starch while the incorporation of the extract into both reinforced and non-reinforced films produced more plasticised, less thermostable matrices, but provided them with strong antioxidant and UV absorption capacity. This permitted the prevention of sunflower oil oxidation. Cellulose fibres enhanced the oxygen and water vapour barrier capacity of the films with and without extracts while reinforcing their mechanical resistance and elastic modulus. Therefore, obtaining fractions from rice straw that are useful for the purposes of improving food packaging materials, such as starch films.

7. Aqueous extracts from rice straw obtained by combined ultrasound-reflux heating (USHT) and subcritical water extraction (SWE) exhibited antioxidant and antibacterial activity, this being greater in the SWE extracts, especially at 180 °C. These extracts slightly reduced the extensibility, resistance to break and water barrier capacity of the PLA films when incorporated at 6 % wt. Nonetheless, they enhanced the oxygen barrier capacity and the UV light-blocking effect of the films. The films with RS extracts were effective at preserving meat quality parameters for longer times, inhibiting meat oxidation, discolouration, and weight loss, so extending the meat shelf life. The SWE extract obtained at 180 °C was the most effective in obtaining active films for meat preservation. Therefore, the SWE technique allows for obtaining active extracts from RS, which are useful for obtaining active PLA films to extend the meat shelf life.

8. The USHT and SWE alternative extraction methods were effective at eliminating non-cellulosic compounds from rice straw to a different extent compared to the common ALK treatment. SWE treatment at 180 °C was more effective at eliminating hemicelluloses, while ALK and USHT methods gave rise to hemicellulose-richer fibres with the lowest silica content. The final composition of the bleached fibres markedly affected the structure and properties of the cellulose-based hydrogels and aerogel obtained. Thus, higher hemicellulose content in the fibres led to more consistent hydrogels with higher water holding capacity and aerogels with thicker walls and higher porosity and water vapour sorption capacity. In contrast, the presence of silica gave rise to weaker hydrogels and fibrous aerogels, with lower porosity and water absorption capacity. Therefore, rice straw can be valorised to obtain high-added-value cellulosic materials, such as aerogels, using aqueous extraction, by applying ultrasounds or subcritical conditions to favour cellulosic purification. The different extraction methods provide the materials with modulated properties, depending on their final composition.

As a global conclusion, using lignocellulosic rice straw to obtain valorised fractions, such as active extracts and cellulosic fibres, for developing food packaging materials, represents a useful approach to improving the functionality of biodegradable polymers for food packaging purposes, while boosting the circular economy. Incorporating active extracts from rice straw provided biodegradable films with antioxidant and antimicrobial properties. Likewise, the use of cellulose fractions could provide the starch films with improved functional performance, all

this adding value to these polymeric materials to replace synthetic plastics. The integral fractionation of RS, obtaining active extracts and purified cellulose fibres, using green and innovative extraction processes, allowed for the whole valorisation of rice straw in the developed materials while opening new windows for other industrial uses. In this sense, rice straw, an agro-industrial residue often burned after rice harvesting, can be considered a highly versatile material that gives rise to different valorised fractions with high applicability in the pharmaceutical, food or food packaging fields.